



**HAL**  
open science

# Nouvelles molécules et cibles thérapeutiques dans le traitement des infections causées par les mycobactéries non-tuberculeuses

Matthéo Alcaraz

► **To cite this version:**

Matthéo Alcaraz. Nouvelles molécules et cibles thérapeutiques dans le traitement des infections causées par les mycobactéries non-tuberculeuses. Sciences du Vivant [q-bio]. Université de Montpellier, 2023. Français. NNT: . tel-04842135

**HAL Id: tel-04842135**

**<https://hal.science/tel-04842135v1>**

Submitted on 17 Dec 2024

**HAL** is a multi-disciplinary open access archive for the deposit and dissemination of scientific research documents, whether they are published or not. The documents may come from teaching and research institutions in France or abroad, or from public or private research centers.

L'archive ouverte pluridisciplinaire **HAL**, est destinée au dépôt et à la diffusion de documents scientifiques de niveau recherche, publiés ou non, émanant des établissements d'enseignement et de recherche français ou étrangers, des laboratoires publics ou privés.

# THÈSE POUR OBTENIR LE GRADE DE DOCTEUR DE L'UNIVERSITÉ DE MONTPELLIER

En Microbiologie

École doctorale CBS2

Unité de recherche : Institut de Recherche en Infectiologie de Montpellier  
Equipe : Pathogénie Mycobactérienne et Nouvelles Cibles Thérapeutiques

## Nouvelles molécules et cibles thérapeutiques dans le traitement des infections causées par les mycobactéries non-tuberculeuses

Présentée par Matthéo ALCARAZ

Le 22 Novembre 2023

Sous la direction de Laurent KREMER

Devant le jury composé de

Pr Alexandra AUBRY, PU-PH, Sorbonne Université, CIMI, Paris

Dr Jean-François CAVALIER, DR2 CNRS, LISM, Marseille

Dr Hédia MARRAKCHI, CRCN CNRS, IPBS, Toulouse

Pr Edouard TUAILLON, PU-PH, CHU Montpellier

Dr Laurent KREMER, DR Inserm, IRIM, Montpellier

Rapportrice

Rapporteur

Examinatrice

Examineur

Directeur de thèse



UNIVERSITÉ  
DE MONTPELLIER





# Remerciements

Je voudrais, dans un premier temps, remercier les membres de mon jury qui m'ont fait l'honneur d'avoir accepté de juger mes travaux de thèse. C'est avec plaisir et fierté que je vous présente ce manuscrit de thèse illustrant la majeure partie des travaux de recherche que j'ai pu effectuer ces trois dernières années. Je remercie le Pr Alexandra Aubry et le Dr Jean-François Cavalier d'avoir accepté d'évaluer mon travail en tant que rapporteurs. Mes remerciements sont également adressés à mes examinateurs, le Dr Hédia Marrakchi et le Pr Edouard Tuillon.

Je tiens à remercier également les membres de mon comité de suivi de thèse, le Pr Jean-Philippe Lavigne, le Dr Stéphane Canaan et le Dr Laurent Marsollier, pour les nombreux conseils lors de nos réunions annuelles, que ce soit sur un plan professionnel ou personnel.

Les travaux de thèse de ces trois dernières années ne seraient rien sans mon directeur de thèse, le Dr Laurent Kremer, à qui j'adresse un remerciement tout particulier pour m'avoir fait confiance dans la multitude de projets qu'il m'a confiés et que nous avons pu mener à bien ensemble. Merci à lui pour m'avoir guidé tout au long de ces projets et pour m'avoir poussé dans mes retranchements quand cela était nécessaire, dans le but de développer mon esprit critique et scientifique.

D'un point de vue général, je tiens à remercier toute l'équipe « Pathogénie mycobactérienne et nouvelles cibles thérapeutiques » dans laquelle j'ai pu faire mes armes pendant plus de 3 ans à travers mon stage de master 2 ainsi que cette thèse.

Je tiens à remercier, dans un premier temps, les anciens que j'ai pu connaître en commençant par Matt Johansen, ou encore Clément Raynaud qui ont eu la patience de me former à de nombreuses techniques de base de bactériologie durant mon stage de master 2 alors que le temps leur était compté et grâce à qui j'ai pu mener à bien la plupart de mes projets futurs.

Je remercie également Mickael Blaise pour l'ensemble de nos discussions, qu'elles aient été au sein de l'équipe ou au milieu d'un couloir, et tous ses conseils avisés.

Je me dois également de remercier chaleureusement Yves-Marie Boudehen, *aka* BYM, de passage dans l'équipe pour deux ans, sans lequel la vie dans le bureau aurait été beaucoup moins animée. Merci à toi pour ta disponibilité à toute épreuve quand il s'agissait de biologie moléculaire, ou de n'importe quelle autre question scientifique sur un coin de paillasse. Merci à toi pour tous ces montages photos, ces blagues, et cette bonne humeur pendant nos heures de travail, mais aussi à l'extérieur de l'institut. A tous ces apéros, ces sorties et ces conseils de vie, je suis fier de te compter aujourd'hui parmi mes amis, enfin collègues.

Merci également à ceux que j'ai vu arriver dans l'équipe pendant ces dernières années, merci à Yara pour ses discussions et conseils sur n'importe quel sujet, et merci à John pour cette curiosité scientifique à toute épreuve, à tous tes conseils et aux idées complémentaires que tu as pu apporter à mes projets grâce à nos discussions.



Je tiens aussi à remercier Claire, la poissonnière, pour la formation complète à l'expérimentation animale et à la gestion des zebrafish, ainsi que pour tes conseils pour les présentations orales au cours de ces années.

Mes remerciements vont bien sûr également à Françoise, toi qui m'as accompagné depuis le début sur l'ensemble de mes projets, toi qui m'as formé à la plupart des techniques de bactériologie et à l'évaluation des antibiotiques. Une pensée à toutes nos matinées sous la hotte à compter nos boîtes de CMI ou à étaler, mais jamais sans faire la course.

Et bien entendu, comment ne pas te remercier toi Morgane, toi qui m'as épaulé tout au long de cette thèse, au quotidien et dans n'importe quel moment. J'ai découvert une collègue en or, une très bonne scientifique, mais surtout une personne formidable avec des valeurs et une vision comparable à la mienne. Merci d'avoir toujours été là dans les moments difficiles, à n'importe quelle heure et pour n'importe quelle raison, mais je repense aussi à tous nos moments de rigolade, de fou rire, qu'ils soient au P2, au bureau, sur la terrasse ou à l'extérieur. Merci pour tous ces conseils, toutes ces discussions sérieuses, toutes nos conneries verbales ou matérielles ; à tous les tapas de Montpellier testés avec toi, tous ces restaurants, tous ces verres et toutes ces sorties. Même si la fin de la thèse n'a pas été des plus faciles, je sais qu'on a forgé quelque chose de fort, et je suis honoré et heureux de pouvoir te compter parmi mes amis les plus proches aujourd'hui. Je suis de tout cœur avec toi pour la suite, et j'espère que tu seras là encore de nombreuses années pour que je puisse te raconter encore ma vie, mes doutes, mes jugements divers et mes blagues souvent douteuses ; mais bien entendu que je puisse aussi entendre et écouter tes histoires, tes jugements, tes projets et tes blagues tout aussi douteuses.

Je tiens également à remercier tout particulièrement l'ensemble des personnes travaillant à l'IRIM et avec qui j'ai pu avoir de nombreuses discussions tout aussi bien très sérieuses que très légères. Je vous remercie tous pour faire de l'IRIM un cadre de travail agréable et stimulant. J'en oublierai certainement beaucoup, mais merci à Pascale et à nos cafés matinaux, toi qui as toujours le mot qui motive et qui as toujours été là si besoin, que ce soit professionnellement ou humainement. Merci à toute la team beer hour, je ne pourrai citer tout le monde mais vous vous reconnaîtrez, mais merci pour ces moments hors du travail au sein de l'institut. Merci à Yonis, Pauline, Marie, Fabien, Emma et la fameuse équipe de beer pong, avec Dylan et Baptiste, sans qui nous n'aurions pas pu ramener la coupe à la maison deux fois consécutives. Enfin, merci à Arthur, depuis le master on se suit, et même depuis le stage de L3, tu as toujours été là au détour d'un couloir ou en dehors de l'institut, je te souhaite que de bonnes choses pour ton aventure américaine.

Enfin, je tiens à remercier tout particulièrement toutes les personnes de mon entourage qui ne sont pas de ce monde IRIMien et qui sont très importantes à mes yeux.

Je commencerai par remercier Jason, toi qui connais la vie de thésard, tu as toujours été là également dans les moments difficiles mais surtout dans les bons moments, à toutes nos soirées et nos débriefs sur nos vies, très heureux de te compter comme mon ami.

Merci à toi Théo pour ta joie de vivre, ton optimisme et tes folles histoires. Mais aussi pour ton soutien dans les moments difficiles, mais surtout à nos bonnes rigolades autour d'une bière bien fraîche.



Je remercierai bien sûr aussi Lina, ma petite canadienne. Loin des yeux, mais près du cœur, tu comptes énormément pour moi, et je te souhaite tout le bonheur dans cette étape difficile qu'est la thèse. Je suis heureux que lorsqu'on se voit, même si c'est très bref et trop rare, que les choses n'aient absolument pas changé, et que notre complicité reste la même après toutes ces années et ces kilomètres. J'espère pouvoir venir te voir dans ton nouvel environnement froid et hostile très vite pour continuer à rire, juger et n'avoir que des photos ratées de nous.

Comment ne pas remercier mon plus vieil ami, cet énergumène d'Enzo, toi qui m'as vu grandir et murir, comme moi qui ai pu te voir évoluer au fil des deux dernières décennies. Toi qui as toujours été là dans n'importe quel moment, heureux ou malheureux. Je repense à toutes nos sorties CoJ, tous ces débriefs de vie des dernières années même si on ne partage plus la même ville, les mêmes activités ou le même quotidien. Toi qui dis à tout le monde que tu as un pote en thèse, toi qui as toujours été fier de mon parcours, je t'en suis extrêmement reconnaissant, et sache que même si je ne le dis pas, je suis très fier de l'homme que tu es devenu, et très heureux de te compter parmi mes plus fidèles amis, et sans aucun doute pour de très nombreuses années encore.

J'ai une pensée également pour toi Zoé, merci à toi d'être qui tu es, ma petite parisienne sudiste. Comment ne pas penser à nos moments passés ensemble, à tous nos appels ragots et débriefs que je ne remplacerai pour rien au monde. On ne soit pas si souvent, mais je sais que tu es quelqu'un qui compte énormément pour moi, et qui reste un modèle d'abnégation, d'acharnement et de générosité à toute épreuve. Tu es une amie fidèle, que j'ai aimé apprendre à connaître au fil de ces dernières années et que je souhaite encore voir évoluer dans la vie.

Puis j'adresserai mes remerciements également à toi Maëva. Toi qui as toujours cru en moi et mes choix. Merci d'avoir été non loin de moi depuis le début de cette aventure, mais même avant ça, qu'importe la situation tu m'as soutenu et encouragé. Même si tu ne comprenais pas toujours mes cours, mes projets, ou mes discussions scientifiques, tu t'es intéressée à ce que je faisais, ou du moins à l'esthétisme de mes diapos, et tu as toujours su que je réussirai, même si le chemin n'est pas encore fini. J'espère encore pouvoir te casser la tête avec mes antibiotiques pendant encore quelques temps.

Pour finir, je tiens à remercier toute ma famille pour leur éternel soutien depuis le début de mes études. Merci à mes grands-parents de m'avoir toujours encouragé dans mes décisions professionnelles et de croire en mes rêves. Merci à mon frère Titouan, d'être qui tu es et de t'intéresser de plus en plus à ce que je vis. Ces dernières années nous ont rapproché à travers les différents voyages qu'on a pu faire, hâte de nos prochaines destinations ensemble. Et comment ne pas remercier mes parents, vous qui avez tout mis en œuvre pour me permettre de faire les études que je voulais, et de croire en moi depuis petit. Je ne vous ai jamais vraiment remercié mais je suis conscient des choses que vous avez faites pour moi depuis toutes ces années.

Merci à vous tous.



# Sommaire

<b>Abréviations</b> .....	<b>11</b>
<b>Index des figures</b> .....	<b>15</b>
<b>INTRODUCTION</b> .....	<b>19</b>
<b>Chapitre I : Le genre <i>Mycobacterium</i></b> .....	<b>21</b>
<b>1. Généralités</b> .....	<b>23</b>
<b>1.1. Classification</b> .....	<b>23</b>
<b>1.1.1. Classification de Runyon</b> .....	<b>23</b>
<b>1.1.2. Classification selon la pathogénicité</b> .....	<b>25</b>
<b>1.1.3. Mycobactéries à croissance lente ou rapide</b> .....	<b>25</b>
<b>1.2. Phylogénie</b> .....	<b>27</b>
<b>2. Différentes espèces du complexe des mycobactéries</b> .....	<b>27</b>
<b>2.1. Mycobactéries à croissance lente : l'exemple de <i>Mycobacterium tuberculosis</i></b> .....	<b>27</b>
<b>2.2. Mycobactéries à croissance rapide : <i>Mycobacterium fortuitum</i> et <i>Mycobacterium abscessus</i></b> .....	<b>29</b>
<b>2.2.1. <i>Mycobacterium fortuitum</i></b> .....	<b>31</b>
<b>2.2.2. <i>Mycobacterium abscessus</i></b> .....	<b>33</b>
<b>2.2.2.1. Présentation générale du complexe et différents morphotypes</b> .....	<b>33</b>
<b>2.2.2.2. Physiopathologie de l'infection chez l'Homme</b> .....	<b>37</b>
<b>a. Épidémiologie et symptômes des infections extra-pulmonaires à <i>M. abscessus</i></b> .....	<b>37</b>
<b>b. Épidémiologie et symptômes des infections pulmonaires à <i>M. abscessus</i></b> .....	<b>39</b>
<b>c. Facteurs de risques environnementaux et humains aux infections à <i>M. abscessus</i></b> .....	<b>41</b>
<b>2.2.2.3. Modèles d'étude expérimentaux</b> .....	<b>45</b>
<b>Chapitre II : Antibiothérapie et mécanismes de résistances chez <i>M. abscessus</i></b> .....	<b>51</b>
<b>1. L'antibiothérapie conventionnelle contre <i>M. abscessus</i></b> .....	<b>53</b>
<b>1.1. Les macrolides</b> .....	<b>55</b>
<b>1.2. Les β-lactamines</b> .....	<b>57</b>
<b>1.3. Les aminoglycosides</b> .....	<b>59</b>
<b>1.4. Les tétracyclines</b> .....	<b>61</b>
<b>1.5. Les fluoroquinolones</b> .....	<b>63</b>
<b>1.6. Nouvelles classes d'antibiotiques et alternatives</b> .....	<b>65</b>
<b>1.6.1. Les phénazines</b> .....	<b>65</b>
<b>1.6.2. Les oxazolidinones</b> .....	<b>67</b>
<b>1.6.3. Les diarylquinolines</b> .....	<b>69</b>
<b>1.6.1. Les autres classes d'antibiotiques</b> .....	<b>71</b>
<b>1.6.2. Les bactériophages : une alternative aux antibiotiques</b> .....	<b>75</b>
<b>2. Mécanismes de résistance aux antibiotiques chez <i>M. abscessus</i></b> .....	<b>77</b>
<b>2.1. Polymorphisme génétique et mutations acquises</b> .....	<b>77</b>
<b>2.1. Enzymes modifiant / inactivant les antibiotiques</b> .....	<b>81</b>
<b>2.1.1. β-lactamines</b> .....	<b>81</b>
<b>2.1.2. Aminoglycosides</b> .....	<b>83</b>
<b>2.1.3. Tétracyclines</b> .....	<b>85</b>
<b>2.1.4. Rifamycines</b> .....	<b>85</b>





2.2.	Enzymes protégeant la cible des antibiotiques : Erm41 .....	87
2.3.	Export actif <i>via</i> des pompes à efflux.....	89
<b>Chapitre III :97 Paroi et acides mycoliques .....</b>		<b>97</b>
1.	<i>La paroi mycobactérienne, une structure atypique .....</i>	<i>99</i>
1.1.	Paroi des Gram positive et Gram négative.....	99
1.2.	La paroi mycobactérienne .....	99
1.2.1.	Membrane plasmique .....	101
1.2.2.	Périplasme, peptidoglycane et arabinogalactane .....	103
1.2.3.	La mycomembrane .....	103
2.	<i>Les acides mycoliques.....</i>	<i>105</i>
2.1.	Description, structure et propriétés .....	105
2.2.	Voie de synthèse des acides mycoliques .....	111
2.2.1.	Synthèse de malonyl-CoA et carboxyacyl-CoA.....	111
2.2.2.	FAS I.....	113
2.2.3.	FAS II.....	115
2.2.4.	Modification de la chaîne méromycolique et condensation.....	119
2.3.	Transport et transfert à la paroi .....	121
3.	<i>L'énoyl ACP réductase InhA .....</i>	<i>123</i>
3.1.	Description et fonction d'InhA .....	123
3.2.	Inhibiteurs d'InhA .....	125
3.2.1.	Inhibiteurs indirects d'InhA.....	125
3.2.2.	Inhibiteurs directs d'InhA.....	127
<b>OBJECTIFS.....</b>		<b>131</b>
<b>RESULTATS .....</b>		<b>137</b>
<i>Article 1 : “Designing quinoline-isoniazid hybrids as potent anti-tubercular agents inhibiting mycolic acid biosynthesis”.....</i>		<i>139</i>
<i>Article 2 : “Efficacy and mode of action of a direct inhibitor of Mycobacterium abscessus InhA”..</i>		<i>187</i>
<i>Article 3 : “In vitro and in vivo efficacy of NITD-916 against Mycobacterium fortuitum” .....</i>		<i>215</i>
<i>Discussion Générale et Perspectives .....</i>		<i>235</i>
<i>Références.....</i>		<i>267</i>
<b>ANNEXES.....</b>		<b>295</b>
<i>Annexe 1 : “Mycobacterium abscessus, un modèle de résistance aux différentes classes d'antibiotiques” .....</i>		<i>297</i>
<i>Annexe 2 : “Silencing essential gene expression in Mycobacterium abscessus during infection” ..</i>		<i>307</i>
<i>Annexe 3 : “Mycobacteriophage-antibiotic therapy promotes enhanced clearance of drug-resistant Mycobacterium abscessus” .....</i>		<i>344</i>



# Abréviations

<b>AAC(2')</b> : Aminoglycoside 2'-Acétyltransférase	<b>DIB</b> : Dibécacine
<b>ACC</b> : Acyl-CoA Carboxylase	<b>DOX</b> : Doxycycline
<b>ACP</b> : Acyl Carrier Protein	<b>Eis</b> : Enhanced Intracellular Survival
<b>ADN</b> : Acide Désoxyribonucléique	<b>EMB</b> : Ethambutol
<b>Ag85</b> : Antigène 85	<b>ER</b> : Enoyl Réductase
<b>AMK</b> : Amikacine	<b>ERS</b> : European Respiratory Society
<b>AG</b> : Arabinogalactane	<b>ESCMID</b> : European Society of Clinical Microbiology and Infectious Diseases
<b>AT</b> : AcylTransférase	<b>ETH</b> : Éthionamide
<b>ATS</b> : American Thoracic Society	<b>FAS</b> : Fatty Acid Synthase
<b>AZM</b> : Azithromycine	<b>FDA</b> : Food and Drug Administration
<b>BC</b> : Biotine Carboxylase	<b>GEN</b> : Gentamycine
<b>BCG</b> : Bilié de Calmette et Guérin	<b>GMSCF-KO</b> : Granulocyte-Macrophage Colony-Stimulating Factor Knock Out
<b>BDQ</b> : Bédaquiline	<b>GPLs</b> : Glycopeptidolipides
<b>BPCO</b> : Broncho-Pneumopathies Chroniques Obstructives	<b>HYG</b> : Hygromycine
<b>CAP</b> : Capréomycine	<b>IDSA</b> : Infectious Diseases Society of America
<b>CCCP</b> : Carbonyl Cyanide 3-ChloroChenylhydrazone	<b>ILI</b> : Inclusions Lipidiques Intracellulaires
<b>CIP</b> : Ciprofloxacine	<b>IMP</b> : Imipénème
<b>CFTR</b> : Cystic Fibrosis Transmembrane conductance Regulator	<b>INH</b> : Isoniazide
<b>CFX</b> : Céfoxitine	<b>KAN</b> : Kanamycine
<b>CFZ</b> : Clofazimine	<b>KR</b> : $\beta$ -Ketoacyl Réductase
<b>CLR</b> : Clarithromycine	<b>KS</b> : $\beta$ -Ketoacyl Synthase
<b>CMI</b> : Concentration Minimale Inhibitrice	<b>LAM</b> : LipoArabinoMannane
<b>CoA</b> : Coenzyme A	<b>LDTs</b> : L,D-transpeptidases
<b>CT</b> : Carboxyltransférase	<b>LM</b> : Lipomannane
<b>DAT</b> : Diacyl tréhalose	<b>LNZ</b> : Linézolide
<b>DDTs</b> : D,D-transpeptidases	<b>LPS</b> : Lipopolysaccharide
<b>DH</b> : Déshydratase	<b>MCL</b> : Mycobactéries à Croissance Lente
	<b>MCR</b> : Mycobactéries à Croissance Rapide



**MmpL** : Mycobacterial membrane protein  
Large  
**MmpS** : Mycobacterial membrane protein  
Small  
**MNC** : Minocycline  
**MNT** : Mycobactéries Non-Tuberculeuses  
**MOX** : Moxifloxacine  
**MPT** : Malonyl/Palmitoyl Transférase  
**MQ** : Ménaquinone  
**NAG** : N-acétylglucosamine  
**NAM** : acide N-acétylmuramique  
**NGM** : acide N-glycolylmuramique  
**OMS** : Organisation Mondiale de la Santé  
**PA $\beta$ N** : Phenylalanine-Arginine  $\beta$ -  
Naphtylamide  
**PBP** : Penicillin-Binding Proteins  
**PIM** : Phosphatidyl-*myo*-inositol-mannosides  
**PIM<sub>2</sub>** : Phosphatidyl-*myo*-inositol  
dimmannosides  
**PG** : Peptidoglycane  
**PMA** : Phorbol 12-myristate 13-acetate  
**PTH** : Prothionamide  
**PZA** : Pyrazinamide  
**R** : Rugueux - « rough »  
**RFB** : Rifabutine

**RFP** : Rifapentine  
**RIF** : Rifampicine  
**ROS** : “Reactive Oxygen Species”  
**S** : Lisse - « smooth »  
**SAM** : S-adénosyl-méthionine  
**SCID** : Severe Combined ImmunoDeficiency  
**SDR** : « Short chain  
Dehydrogenase/Reductase »  
**STR** : Streptomycine  
**TAC** : Thiacétazone  
**TAG** : Triacylglycérol  
**TCS** : Triclosan  
**TDM** : Tréhalose Dimycolate  
**TDZ** : Tédizolide  
**TET** : Tétracycline  
**TGC** : Tigécycline  
**Th1** : Lymphocytes CD4+ T-helper  
**THP** : Tétrahydropyridine  
**TLR-2** : « Toll-Like Receptor 2 »  
**TMM** : Tréhalose Monomycolate  
**TNF- $\alpha$**  : Tumor Necrosis Factor  $\alpha$   
**TOB** : Tobramycine  
**VIH** : Virus de l’Immunodéficience Humaine  
**VP** : Verapamil



# Index des figures

FIGURE 1 : CLASSIFICATION DES MYCOBACTERIES PRINCIPALES SELON LEUR TEMPS DE CROISSANCE ET LEUR VIRULENCE .....	24
FIGURE 2 : ARBRE PHYLOGENETIQUE DU GENRE <i>MYCOBACTERIUM</i> OBTENU PAR COMPARAISON DES GENOMES ENTIERS .....	26
FIGURE 3 : REGIME D'ANTIBIOTHERAPIE DE PREMIERE INTENTION REQUIS DANS LE CADRE D'INFECTIONS PULMONAIRES A UNE SOUCHE SENSIBLE DE <i>M. TUBERCULOSIS</i> .....	28
FIGURE 4 : DIFFERENTS REGIMES D'ANTIBIOTHERAPIE RECOMMANDES CONTRE UNE INFECTION A <i>M. FORTUITUM</i> SELON LE TYPE D'INFECTION .....	30
FIGURE 5 : MODIFICATION DE LA CLASSIFICATION TAXONOMIQUE ET DE LA NOMENCLATURE DU COMPLEXE <i>M. ABSCESSUS</i> DEPUIS SA DISTINCTION EN TANT QU'ESPECE EN 1992 JUSQU'EN 2013 .....	30
FIGURE 6 : DIFFERENTES CARACTERISTIQUES DIFFERENCIANT LE MORPHOTYPE LISSE DE MORPHOTYPE RUGUEUX DE <i>M. ABSCESSUS</i>	32
FIGURE 7 : STRUCTURE DES GLYCOPEPTIDOLIPIDES SYNTHETISES PAR <i>M. ABSCESSUS</i> .....	32
FIGURE 8 : REPRESENTATION DE CORDES FORMEES PAR LE MORPHOTYPE RUGUEUX DE <i>M. ABSCESSUS</i> .....	34
FIGURE 9 : COLONISATION DE <i>M. ABSCESSUS</i> , RECRUTEMENT DU SYSTEME IMMUNITAIRE ET ECHAPPEMENT DU GRANULOME .....	36
FIGURE 10 : SYMPTOMES EXTRA-PULMONAIRES VISIBLES SUITE A UNE INFECTION A <i>M. ABSCESSUS</i> .....	38
FIGURE 11 : DIFFERENTES CATEGORIES DE FACTEURS DE RISQUES AUX INFECTIONS AUX MNT ET NOTAMMENT A <i>M. ABSCESSUS</i> ..	40
FIGURE 12 : DIFFERENTS MODELES D'ETUDES EXPERIMENTALES PRECLINIQUES ( <i>IN VITRO</i> , <i>EX VIVO</i> ET <i>IN VIVO</i> ) POUR L'ETUDE DE LA PATHOGENESE DE <i>M. ABSCESSUS</i> ET L'ACTIVITE DE MOLECULES CANDIDATS .....	44
FIGURE 13 : REGIME THERAPEUTIQUE RECOMMANDE DANS LE CADRE D'UNE INFECTION A <i>M. ABSCESSUS</i> .....	52
FIGURE 14 : STRUCTURE DES MACROLIDES, DONT CEUX UTILISES DANS LE TRAITEMENT CONTRE <i>M. ABSCESSUS</i> ET LEUR MODE D'ACTION SUR LA SYNTHESE DES PROTEINES PROCARYOTES .....	54
FIGURE 15 : STRUCTURE DES B-LACTAMINES (CEFOXITINE ET IMPENEME) ET LEUR MODE D'ACTION SUR LES TRANSPEPTIDASES DU PEPTIDOGLYCANE DE <i>M. ABSCESSUS</i> .....	56
FIGURE 16 : STRUCTURE DE L'AMIKACINE ET MECANISMES D'INHIBITION DE LA SYNTHESE PROTEIQUE BACTERIENNE ASSOCIES.....	58
FIGURE 17 : STRUCTURE DES TETRACYCLINES, ET NOTAMMENT DE LA TIGECYCLINE UTILISEE CONTRE LES INFECTIONS A <i>M. ABSCESSUS</i> ET SON MODE D'INHIBITION DE L'ELONGATION DE LA TRADUCTION MYCOBACTERIENNE .....	60
FIGURE 18 : LIAISON DE LA TIGECYCLINE A L'ARNr 16S DU RIBOSOME BACTERIEN .....	62
FIGURE 19 : STRUCTURE ET MODE D'ACTION DE LA MOXIFLOXACINE .....	64
FIGURE 20 : STRUCTURE ET MODE D'ACTION DE LA CLOFAZIMINE .....	66
FIGURE 21 : STRUCTURE ET MODE D'ACTION DU LINEZOLIDE .....	68
FIGURE 22 : STRUCTURE ET MODE D'ACTION DE LA BEDAQUILINE .....	70
FIGURE 23 : STRUCTURE ET MODE D'ACTION DE LA RIFABUTINE .....	72
FIGURE 24 : MODE D'ACTION ET INHIBITION DU TRANSPORTEUR MmpL3.....	74
FIGURE 25 : STRUCTURES DE DIFFERENTS INHIBITEURS DE MmpL3 DECRITS CHEZ <i>M. ABSCESSUS</i> .....	76
FIGURE 26 : CYCLE D'INFECTION DES BACTERIOPHAGES LYTICIQUES ET LYSOGENIQUES .....	78





FIGURE 27 : MECANISME D'HYDROLYSE DE L'IMIPENEME PAR LA $\beta$ -LACTAMASE $BLA_{MAB}$ .....	80
FIGURE 28 : INACTIVATION ENZYMATIQUE DE L'AMIKACINE PAR L'ACETYLTRANSFERASE $EIS2$ ET SA STRUCTURE CRISTALLOGRAPHIQUE .....	82
FIGURE 29 : MECANISME DE RESISTANCE A LA TETRACYCLINE VIA LA MONOOXYGENASE $FAD$ -DEPENDANTE $MAB_{TETX}$ .....	84
FIGURE 30 : INACTIVATION DE LA RIFABUTINE PAR $ARR_{MAB}$ .....	86
FIGURE 31 : METHYLATION DE L'ARNr 23S PAR $ERM41$ .....	88
FIGURE 32 : MECANISME DE RESISTANCE AUX DERIVES DU THIACTAZONE .....	90
FIGURE 33 : MECANISME DE RESISTANCE A LA CLOFAZIMINE ET LA BEDAQUILINE .....	92
FIGURE 34 : MECANISMES DE RESISTANCE, INNES OU ACQUIS, A DIVERSES CLASSES D'ANTIBIOTIQUES CHEZ <i>M. ABSCESSUS</i> .....	95
FIGURE 35 : STRUCTURE DE LA PAROI DES BACTERIES A GRAM NEGATIVE ET A GRAM POSITIVE .....	98
FIGURE 36 : REPRESENTATION SCHEMATIQUE DE LA PAROI MYCOBACTERIENNE DE <i>M. ABSCESSUS</i> .....	102
FIGURE 37 : STRUCTURE GENERALE DES ACIDES MYCOLIQUES .....	106
FIGURE 38 : ACIDES MYCOLIQUES DE <i>M. TUBERCULOSIS</i> .....	106
FIGURE 39 : ACIDES MYCOLIQUES DE <i>M. ABSCESSUS</i> .....	108
FIGURE 40 : STRUCTURE DES ACIDES MYCOLIQUES EPOXY .....	108
FIGURE 41 : SYNTHESE DE MALONYL-CoA A PARTIR D'ACETYL-CoA .....	112
FIGURE 42 : ORGANISATION DU SYSTEME MULTIFONCTIONNEL $FAS I$ .....	114
FIGURE 43 : VOIE DE BIOSYNTHESE DES ACIDES MYCOLIQUES CHEZ LES MYCOBACTERIES .....	116
FIGURE 44 : CONDENSATION MYCOLIQUE FINALE FORMANT LES ACIDES MYCOLIQUES MATURES .....	120
FIGURE 45 : SCHEMA DE LA REACTION DE REDUCTION DU SUBSTRAT ENOYL-ACP EN ACYL-ACP CATALYSEE PAR LA PROTEINE $INH A$ .....	122
FIGURE 46 : MECANISME CATALYTIQUE DE REDUCTION OPEREE PAR $INH A$ ET REPRESENTATION DES RESIDUS DETERMINANTS DANS CELUI-CI .....	124
FIGURE 47 : STRUCTURE DE DIFFERENTS INHIBITEURS INDIRECTS D' $INH A_{MTB}$ .....	124
FIGURE 48 : MECANISME D'ACTIVATION ET D'ACTION DE L'ISONIAZIDE CHEZ <i>M. TUBERCULOSIS</i> .....	126
FIGURE 49 : STRUCTURE DE DIVERS INHIBITEURS DIRECTS D' $INH A_{MTB}$ .....	128
FIGURE 50 : REPRESENTATION DES DIFFERENTES STRATEGIES MISES EN EVIDENCE PAR CES TRAVAUX ET EXPLOITABLES DANS DE FUTURES ETUDES ENVERS LES INFECTIONS MYCOBACTERIENNES .....	264



# INTRODUCTION



# Chapitre I :

## Le genre *Mycobacterium*



## 1. Généralités

Le genre des mycobactéries, nommé pour la première fois en 1896 par Lehmann et Neumann [1], appartient au phylum des *Actinobacteria*. Ces bacilles acido-alcoolo résistants sont des microorganismes saprophytes retrouvés principalement dans l'environnement tel que l'eau et le sol. Les actinobactéries, notamment les mycobactéries, possèdent un génome riche en Guanine-Cytosine [2]. Ces dernières appartiennent à la famille des *Mycobacteriaceae*, provenant du sous-ordre des *Corynebacterineae* au sein de l'ordre des *Actinomycetales* et de la classe des Actinomycètes. Les mycobactéries se démarquent des autres bactéries car elles ne répondent pas à la coloration de Gram classiquement utilisée. Elles sont cependant discriminées grâce à la coloration de Ziehl-Neelsen spécifique de ce genre bactérien en raison de la richesse en lipides particulière de la paroi mycobactérienne, capable de retenir le colorant rose de la fuschine après un lavage acido-alcoolique [3].

### 1.1. Classification

Le genre *Mycobacterium* regroupe près de 200 espèces validées, renfermant une grande diversité morphologique, physiologique ou encore biochimique qui a poussé la communauté scientifique à classer les espèces selon différents critères.

#### 1.1.1. Classification de Runyon

L'une des premières classifications en date est la classification de Runyon qui repose sur des observations phénotypiques et temporelles de différentes mycobactéries [4]. Cette classification a permis de différencier les mycobactéries à croissance lente (MCL) des mycobactéries à croissance rapide (MCR). Ce temps de croissance ainsi que la pigmentation des mycobactéries ont permis à Ernest Runyon de les distinguer en quatre groupes :

- I- Les photochromogènes qui se pigmentent après exposition à la lumière, croissance lente (ex : *Mycobacterium kansasii*, *Mycobacterium marinum*)
- II- Les scotochromogènes qui sont toujours pigmentées d'orange à jaune, croissance lente (ex : *Mycobacterium gordonae*, *Mycobacterium scrofulaceum*)



**Figure 1 : Classification des mycobactéries principales selon leur temps de croissance et leur virulence**

adapté de Johansen MD, *et al.* 2020 [5]

Mycobactéries non-tuberculeuses		
Mycobactéries à croissance rapide	Mycobactéries à croissance lente	
<i>M. chelonae-abscessus</i> complex • <i>M. abscessus</i> subsp. <i>abscessus</i> • <i>M. abscessus</i> subsp. <i>bolletii</i> • <i>M. abscessus</i> subsp. <i>massiliense</i> • <i>M. chelonae</i> <i>M. fortuitum</i>	<i>M. marinum</i> <i>M. ulcerans</i>	<i>M. tuberculosis</i> complex
<i>M. smegmatis</i> <i>M. vaccae</i>	<i>M. avium</i> complex • <i>M. avium</i> • <i>M. intracellulare</i> • <i>M. chimaera</i> <i>M. haemophilum</i> <i>M. xenopi</i> <i>M. kansasii</i> <i>M. simiae</i>	<i>M. leprae</i>
	<i>M. terrae</i> complex <i>M. goodii</i>	

Pathogènes stricts  
 Pathogènes opportunistes  
 Saprophytes

III- Les non photochromogènes qui ne sont jamais pigmentées, croissance lente (ex : *Mycobacterium tuberculosis*, *Mycobacterium avium*)

IV- Les mycobactéries à croissance rapide (ex : *Mycobacterium smegmatis*, *Mycobacterium fortuitum*, *Mycobacterium abscessus*).

#### 1.1.2. Classification selon la pathogénicité

Une autre classification existante repose sur la pathogénicité des espèces mycobactériennes. On vient distinguer le genre en 3 grands groupes (**Figure 1**) [5] :

I- Les mycobactéries pathogènes stricts pour l'Homme ou l'animal. On y retrouve les espèces du complexe *M. tuberculosis* et *Mycobacterium leprae*, respectivement responsables de la tuberculose et de la lèpre. Ces deux pathogènes s'opposent aux Mycobactéries Non-Tuberculeuses (MNT), comprenant d'autres pathogènes stricts tels que *Mycobacterium marinum* ou *Mycobacterium ulcerans*. Ces MNT, ou mycobactéries atypiques, englobent toutes les autres espèces mycobactériennes telles que :

II- Les mycobactéries pathogènes opportunistes. Au sein de ce groupe, on retrouve des espèces qui peuvent causer des infections chez l'Homme sous certaines conditions, notamment le complexe *Mycobacterium abscessus-chelonae*, *M. avium* ou encore *M. fortuitum*.

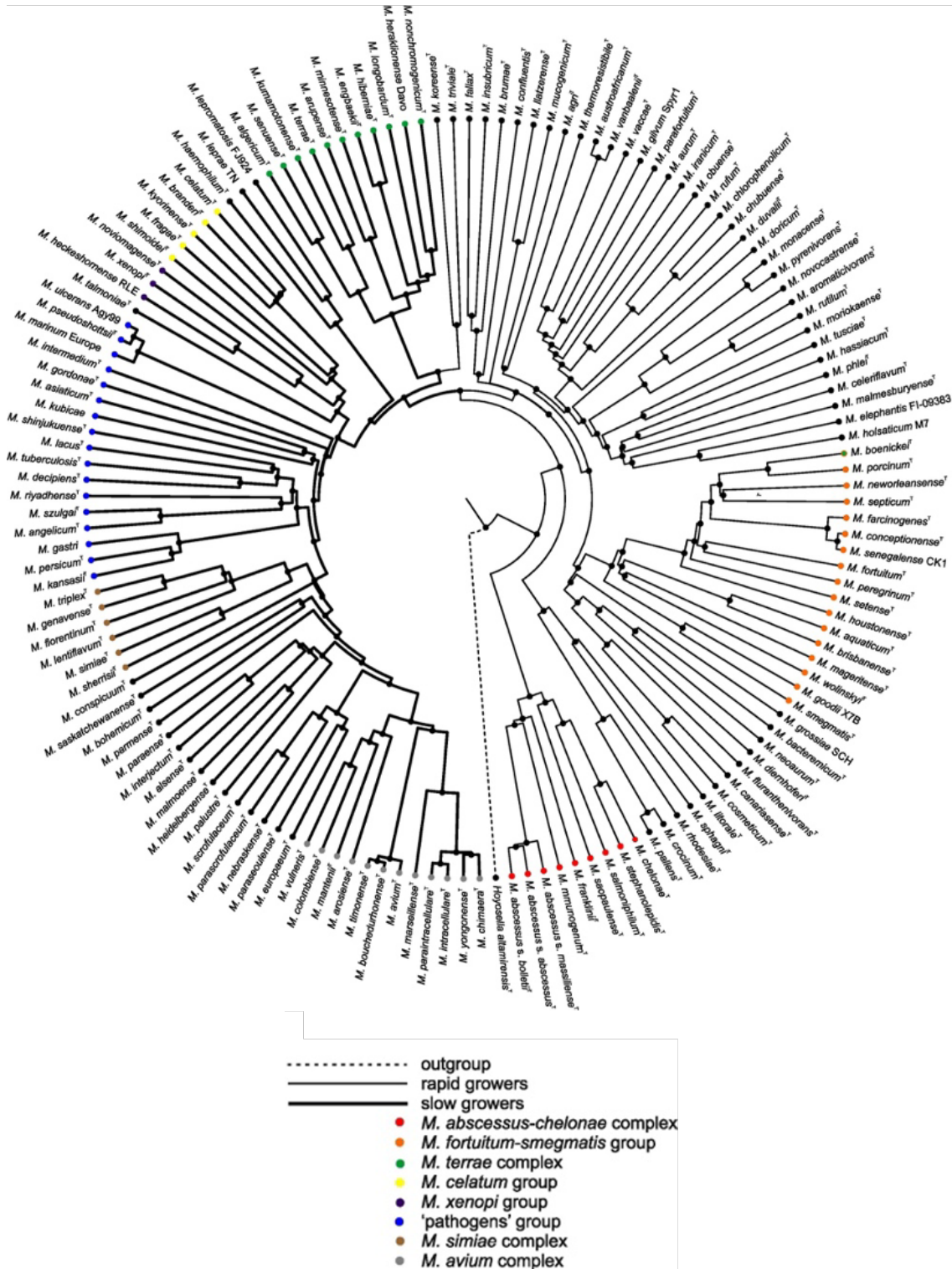
III- Les mycobactéries non-pathogènes telles que *M. smegmatis*, *M. gordonae* ou encore *Mycobacterium vaccae*.

#### 1.1.3. Mycobactéries à croissance lente ou rapide

Même si l'ensemble des classifications se rejoignent pour décrire une espèce mycobactérienne, le temps de croissance de ces espèces reste une caractéristique couramment utilisée. Les MCL forment des colonies en milieu solide après 7 jours d'incubation, contre moins de 7 jours pour les MCR. Le complexe des mycobactéries tuberculeuses regroupe des espèces à croissance lente, avec par exemple un temps de génération d'environ 20 heures pour *M. tuberculosis* [6]. Aujourd'hui, l'espèce ayant la croissance la plus lente est *M. leprae* avec un temps de génération compris entre 12 et 14 jours [7]. Enfin parmi les MNT, on retrouve les deux types de croissance, lente (*M. marinum*, *M. ulcerans* ou *M. avium*) et rapide (*M. smegmatis*, *M. fortuitum* ou *M. abscessus*).

Figure 2 : Arbre phylogénétique du genre *Mycobacterium* obtenu par comparaison des génomes entiers

Tortoli E, *et al.* 2017, [8]



## 1.2. Phylogénie

Ces classifications ont ensuite été consolidées par de nombreuses études phylogénomiques et de nouvelles techniques de génétique et de séquençage. En effet, le séquençage de l'ARNr 16S et de 6 autres gènes conservés (*hsp65*, *rpoB*, *smpB*, *sodA*, *tmRNA* et *tuf*) [9], ainsi que la comparaison des génomes entiers [10] ont confirmé la distinction initialement phénotypique entre MCL et MCR. Néanmoins, la taxonomie et la phylogénie des mycobactéries ont subi certaines modifications ces dernières années. En effet, en 2018 l'étude de Gupta *et al.* basée sur la comparaison de protéines conservées a suggéré l'existence de cinq groupes monophylétiques distincts : *Tuberculosis-Simiae*, *Terrae*, *Triviale*, *Fortuitum-Vaccae* et *Abscessus-Chelonae* [11]. Cette nouvelle nomenclature a souligné le risque d'une certaine confusion en clinique lors du diagnostic et du traitement des infections mycobactériennes [12]. Plus récemment, une étude a utilisé de nombreuses méthodes différentes permettant de définir les limites d'un genre tels que le séquençage et la similarité de séquence de l'ARNr 16S, le pourcentage d'identité protéique et nucléotidique, l'alignement de fractions de génome et le pourcentage de protéines conservées. Ainsi, ces travaux ont confirmé l'affiliation des mycobactéries en un genre *Mycobacterium* unique [13]. Enfin, d'un point de vue plus phylogénique et évolutif, certaines analyses ont montré que parmi les MCR, le complexe *M. abscessus-chelonae* était le cluster le plus ancestral du genre *Mycobacterium* avec une liaison étroite à un ancêtre commun (**Figure 2**) [8].

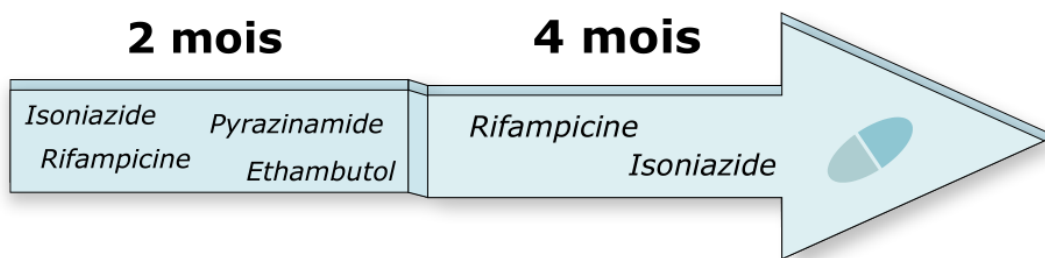
## 2. Différentes espèces du complexe des mycobactéries

### 2.1. Mycobactéries à croissance lente : l'exemple de *Mycobacterium tuberculosis*

Approximativement la moitié des espèces du genre *Mycobacterium* sont des MCL et comporte l'ensemble des mycobactéries strictement pathogènes (*M. tuberculosis*, *M. leprae*, *M. marinum* ou *M. ulcerans*). On y retrouve également des pathogènes opportunistes tel que le complexe *M. avium* ou encore *M. kansasii*. On associe le phénotype de croissance lente à un mode de vie intracellulaire et à la pathogénicité, contrairement aux MCR qui sont majoritairement environnementales et qui incluent seulement un nombre limité de pathogènes opportunistes. La MCL la plus décrite aujourd'hui est *M. tuberculosis*, un pathogène humain obligatoire, et l'agent étiologique de la tuberculose. Ce bacille a été identifié et isolé pour la première fois par Robert Koch en 1882 [14], prouvant l'aspect infectieux et transmissible de la tuberculose. Cette affection est considérée comme l'une des plus

**Figure 3 : Régime d'antibiothérapie de première intention requis dans le cadre d'infections pulmonaires à une souche sensible de *M. tuberculosis***

Le régime antibiotique classique traitant les infections pulmonaires à une souche de *M. tuberculosis* sensible est divisé en deux phases, une première phase de 2 mois comprenant de l'isoniazide (INH), de la rifampicine (RIF), de l'éthambutol (EMB) et de la pyrazinamide (PZA) par voie orale. Cette première période est suivie d'une seconde phase de 4 mois où l'INH et l'EMB sont maintenus.



anciennes touchant l'Homme, avec des représentations de la pathologie dans la littérature et l'art égyptien [15]. L'ancienneté de ce syndrome a été démontrée par la mise en évidence de signes physiopathologiques caractéristiques de la tuberculose et d'ADN mycobactérien sur des squelettes datant de plusieurs millénaires [16,17]. C'est une infection hautement contagieuse, principalement pulmonaire, parfois extra-pulmonaire, transmise *via* les aérosols et les sécrétions respiratoires. Bien que les traitements cliniques curatifs et préventifs aient permis de ralentir l'épidémie, la tuberculose n'en reste pas pour autant éradiquée à travers le monde. La stratégie curative dans le cadre d'infections pulmonaires à une souche sensible de *M. tuberculosis* comprend deux phases, une première phase de 2 mois de traitement incluant la prise d'isoniazide (INH), de rifampicine (RIF), d'éthambutol (EMB) et de pyrazinamide (PZA) par voie orale. Puis l'INH et l'EMB sont conservés pendant quatre mois supplémentaires (**Figure 3**). La stratégie préventive, mise en place depuis 1924 basée sur le vaccin BCG (vaccin bilié de Calmette et Guérin), reste encore aujourd'hui le seul vaccin validé et est majoritairement efficace pour prévenir la tuberculose chez l'enfant [18]. De plus, l'avènement de nombreuses souches multirésistantes au traitement antibiotique curatif recommandé en première intention (**Figure 3**) explique pourquoi la tuberculose reste encore aujourd'hui un problème de santé publique majeur et l'une des maladies infectieuses les plus meurtrières au monde. L'Organisation Mondiale de la Santé (OMS) estime, en 2021, à 10,6 millions le nombre de personnes ayant contracté la tuberculose, et à 1,6 millions le nombre de décès dus à cette maladie à travers le monde [19].

Tout cela souligne le recours à de nouvelles stratégies de traitements et notamment de nouveaux antibiotiques ou combinaisons thérapeutiques plus efficaces.

## 2.2. Mycobactéries à croissance rapide : *Mycobacterium fortuitum* et *Mycobacterium abscessus*

Les mycobactéries à croissance rapide comprennent de nombreuses espèces ubiquitaires de l'environnement et sont généralement non-pathogènes à l'instar de *M. smegmatis*. Ce sous-groupe des MCR contient néanmoins certains pathogènes opportunistes tels que le complexe *M. fortuitum* ou le complexe *M. abscessus-chelonae* [20]. Ces espèces sont considérées comme non-pathogènes dans l'environnement, mais peuvent le devenir en fonction de facteurs environnementaux ainsi que du statut immunitaire et infectieux de l'hôte [21]. De plus, les modifications de l'environnement par l'Homme ainsi que l'interaction avec celui-ci, tels que l'installation de dispositifs mécaniques pouvant altérer la température ou l'humidité du milieu, peuvent expliquer l'émergence de maladies infectieuses humaines causées par ces agents pathogènes [22].

**Figure 4 : Différents régimes d'antibiothérapie recommandés contre une infection à *M. fortuitum* selon le type d'infection**

Le régime thérapeutique contre *M. fortuitum* diffère selon le type d'infection et se doit d'être adapté à l'isolat clinique rencontré.

La prescription pendant 12 mois de deux antibiotiques est recommandée en cas d'infections pulmonaires, seulement après un prélèvement exempt de pathogène.

Dans le cas d'infections de la peau, des os ou des tissus mous, il est recommandé d'utiliser au moins deux antibiotiques sur une période pouvant aller de 4 à 6 mois.

Puis dans le cas d'infections disséminées, une première phase de 2 à 6 semaines comprend 2 agents parentéraux (AMK et une  $\beta$ -lactamine -CFX ou IMP-) suivie d'une seconde phase plus longue allant de 2 à 6 mois et incluant des antibiotiques oraux.

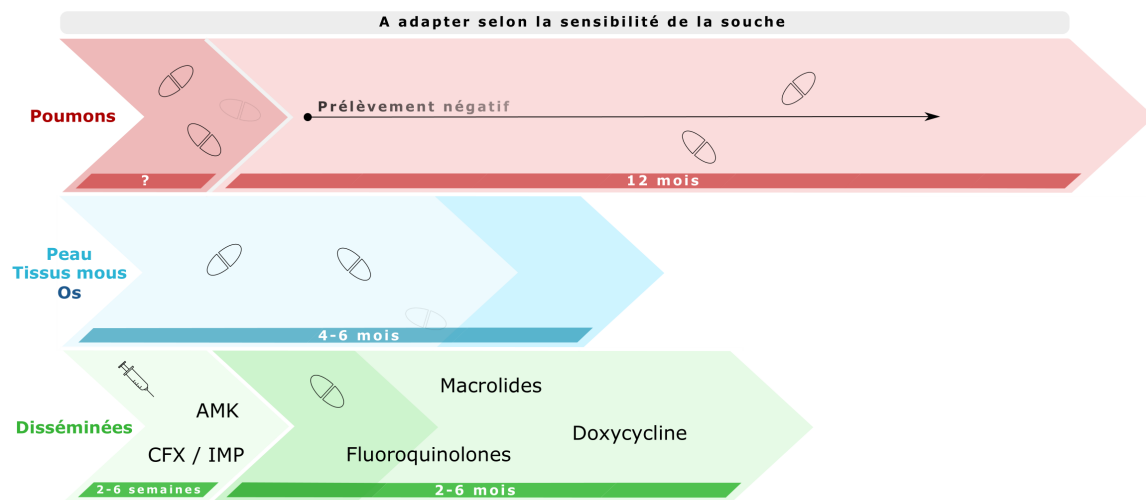
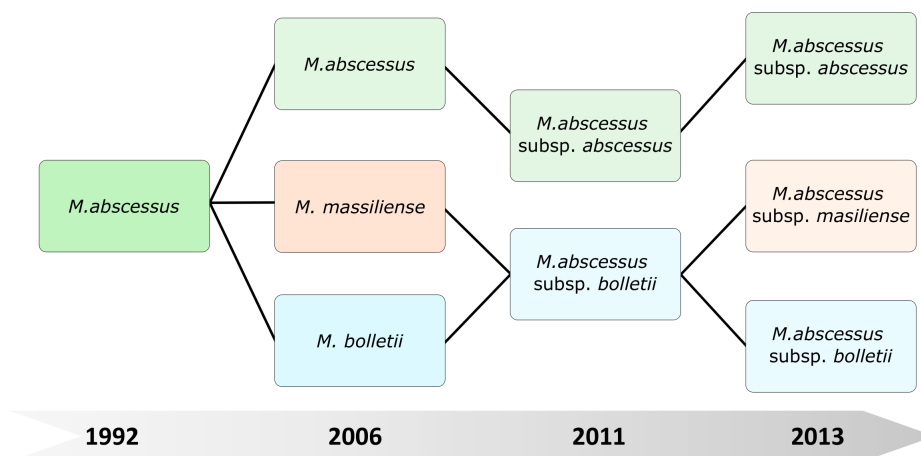


**Figure 5 : Modification de la classification taxonomique et de la nomenclature du complexe *M. abscessus* depuis sa distinction en tant qu'espèce en 1992 jusqu'en 2013**

adapté de Lee M-R, et al. 2015 [23]





### 2.2.1. *Mycobacterium fortuitum*

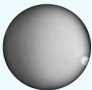
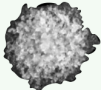


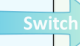
*M. fortuitum* a été nommée pour la première fois par da Costa Cruz en 1938 et identifiée comme étant la cause d'une infection cutanée chez l'Homme [24,25]. Actuellement, le complexe *M. fortuitum* contient différentes espèces (*M. fortuitum*, *Mycobacterium peregrinum*, *Mycobacterium senegalense*, *Mycobacterium porcinum*, *Mycobacterium neworleansense*, *Mycobacterium boenickei*, *Mycobacterium houstonense*, *Mycobacterium brisbanense*, *Mycobacterium septicum*, *Mycobacterium conceptionense*, *Mycobacterium farcinogenes* et *Mycobacterium setense*) [20]. *M. fortuitum*, tout comme l'ensemble des MNT, est une bactérie environnementale que l'on retrouve notamment dans les réseaux de distribution d'eau, les sources d'eau naturelles, mais aussi dans le sol et la poussière [26]. Cette mycobactérie fait partie des MNT les plus communément isolées avec *M. avium* et *M. abscessus* [21] et se trouve être la seconde MCR la plus fréquemment retrouvée chez les patients atteints de mucoviscidose, après *M. abscessus* [27]. Généralement, on retrouve des infections pulmonaires à *M. fortuitum* chez des patients ayant des pathologies pulmonaires sous-jacentes telles que la mucoviscidose, un cancer pulmonaire, une bronchiectasie, une fibrose pulmonaire idiopathique, une tuberculose antérieure, ou encore une surinfection mycobactérienne [28]. Les infections à *M. fortuitum* ne sont pas uniquement pulmonaires mais peuvent également être localisées au niveau cutané [29], affecter des tissus mous, des os, ou encore être disséminées à tout l'organisme [30] et sont responsables de la majorité des infections post-chirurgicales liées aux MCR [31]. *M. fortuitum* est un pathogène difficile à traiter en clinique avec des isolats hautement résistants à de nombreux antibiotiques, notamment aux anti-tuberculeux tels que l'INH, l'EMB, l'éthionamide (ETH) et la clofazimine (CFZ) [32,33]. On retrouve également une résistance inductible aux macrolides et notamment à la clarithromycine (CLR), s'expliquant par la présence de la méthylase Erm39 [34,35]. Il n'en reste pas moins que *M. fortuitum* est sensible à différents antibiotiques oraux ou parentéraux comprenant les fluoroquinolones tels que la ciprofloxacine (CIP) ou la moxifloxacine (MOX) ; les  $\beta$ -lactamines tels que l'imipénème (IMP) ou la céfoxitine (CFX) ; ou bien les aminoglycosides comme l'amikacine (AMK). C'est pourquoi des directives sont tout de même établies pour le traitement de ces infections, même si celles-ci sont plutôt empiriques et dépendent de la sensibilité de chaque isolat clinique (**Figure 4**). Il n'existe donc pas de choix optimal d'antibiotiques à prescrire, comme pour la plupart des autres infections mycobactériennes [36]. En général pour des infections pulmonaires à *M. fortuitum*, il est recommandé d'utiliser a minima deux antibiotiques pendant au moins 12 mois à la suite d'un prélèvement négatif.

Au moins deux agents antibactériens sont également préconisés pour des infections de la peau, des tissus mous ou des os, sur une période plus courte de 4 à 6 mois, avec la possibilité de procéder à des résections chirurgicales en cas de difficulté thérapeutique. Enfin, pour des infections disséminées, un



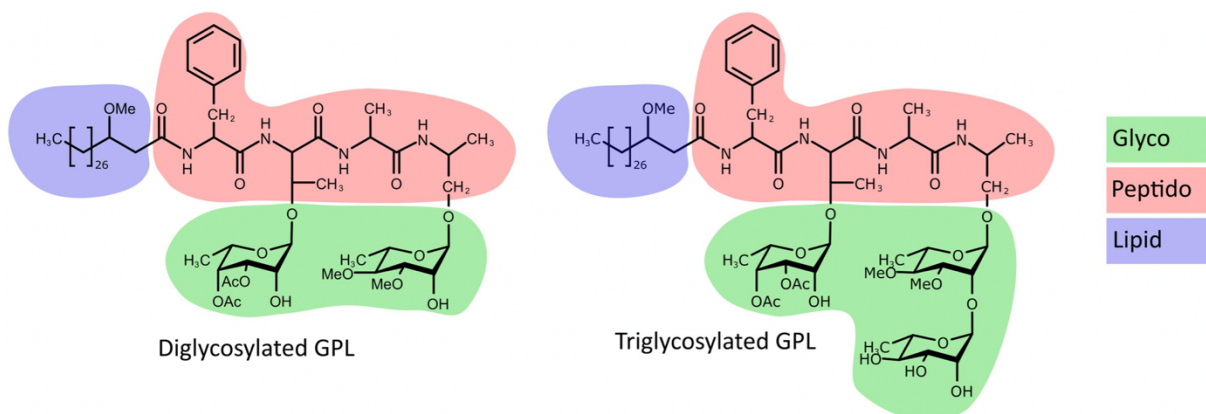
**Figure 6 : Différentes caractéristiques différenciant le morphotype lisse de morphotype rugueux de *M. abscessus***

Images de colonies sur milieu solide issues de Medjahed H, *et al.* 2010 [37]

Morphotype lisse	Morphotype rugueux
	
GPL +	GPL -
Sliding	Cording
<b>Biofilms</b>	
 <p>Apoptose Inflammation TNF</p>	 <p>Apoptose Inflammation TNF</p>
Forme colonisante	 <p>Forme virulente</p>

**Figure 7 : Structure des glycopeptidolipides synthétisés par *M. abscessus***

Gutiérrez AV, *et al.* 2018, [38]



traitement de 2 à 6 semaines comprenant deux agents parentéraux (AMK et une  $\beta$ -lactamine -CFX ou IMP-) est recommandé, suivi de 2 à 6 mois de traitement incluant des antibiotiques oraux (macrolides, fluoroquinolones, doxycycline (DOX), etc.) devant être adaptés aussi selon la susceptibilité de la souche infectieuse [31,36] (**Figure 4**). L'ensemble de ces difficultés thérapeutiques, associées à la prévalence assez élevée de ces infections soulignent l'urgence de pouvoir proposer de nouvelles stratégies antibiotiques aux patients.

### 2.2.2. *Mycobacterium abscessus*

#### 2.2.2.1. Présentation générale du complexe et différents morphotypes

*M. abscessus* a été isolée pour la toute première fois en 1953 chez une patiente ayant un abcès du genou [39]. Cette MNT à croissance rapide ubiquitaire de l'environnement a d'abord été assimilée à *M. chelonae* en 1972 [40], mais sa phylogénie et sa place dans la classification a été modifiée de nombreuses fois [23] (**Figure 5**). Ce n'est qu'en 1992 que *M. abscessus* fût classée comme espèce à part entière. À ce jour, le complexe *M. abscessus* comprend trois sous-espèces : *M. abscessus subsp. abscessus*, *M. abscessus subsp. bolletii* et *M. abscessus subsp. massiliense* [41,42]. Ces trois sous-espèces diffèrent par leur profil génétique mais aussi par leur susceptibilité respective aux antibiotiques et notamment aux macrolides [43], d'où l'importance de pouvoir les discriminer en thérapeutique [44]. Une caractéristique supplémentaire non négligeable est que *M. abscessus* existe sous la forme de deux morphotypes distincts que l'on peut distinguer en milieu solide ou liquide. On différencie le morphotype lisse, ou « smooth » (S) du morphotype rugueux, ou « rough » (R) (**Figure 6**). Phénotypiquement, le variant S présente des colonies rondes, lisses et crémeuses, et est relativement homogène en suspension liquide ; à l'inverse les colonies du variant R sont très rugueuses et organisées en structures serpentine et seront capables de former des agrégats en milieu liquide. Au niveau de la membrane mycobactérienne, le morphotype S se distingue du morphotype R par la présence abondante de glycopeptidolipides (GPLs) [38,45]. Ces molécules comprennent une partie lipidique reliée au noyau peptidique qui peut être soit di- ou tri-glycosylé chez *M. abscessus* [46] (**Figure 7**). La présence de GPLs à la surface de *M. abscessus* influence grandement ses propriétés physiopathologiques (**Figure 6**). En effet, ces GPLs seraient responsable en grande partie des capacités de mobilité (« sliding motility ») du variant S et d'agrégation du variant R [45]. Ce phénomène d'agrégation exacerbé, nommé « cording », permet au morphotype R de former de larges structures organisées de bacilles tête-bêches appelées « cordes » [47] (**Figure 8**). Ces cordes représentent un phénomène physiopathologique de virulence dans les infections à *M. abscessus*. De plus, contrairement à ce que l'on pouvait penser, le morphotype S n'est pas le seul à pouvoir former des

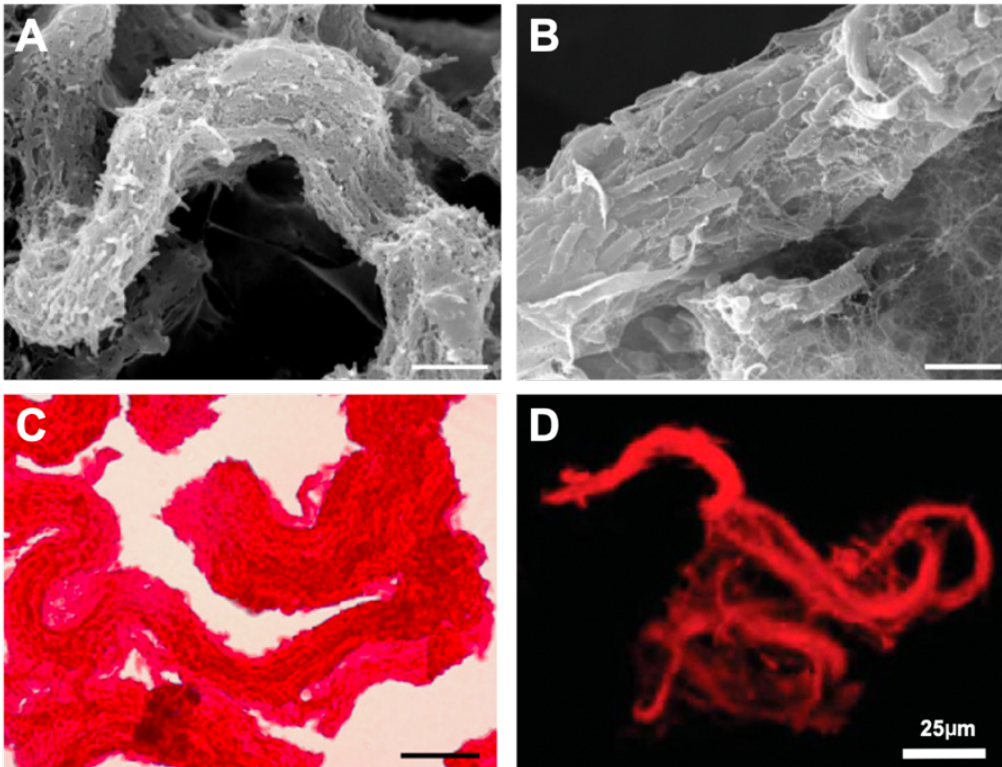
**Figure 8 : Représentation de cordes formées par le morphotype rugueux de *M. abscessus***

adapté de Bernut, *et al.* 2014 et Sánchez-Chardi A, *et al.* 2011, [47,48]

**A, B** : Images de microscopie électronique à balayage à différents grossissements présentant l'organisation étroite des bacilles au sein d'une corde. Échelles : **(A)** 7,5  $\mu\text{m}$  et **(B)** 1,9  $\mu\text{m}$ .

**C** : Coloration Ziehl-Neelsen montrant une corde. Échelle : 20  $\mu\text{m}$ .

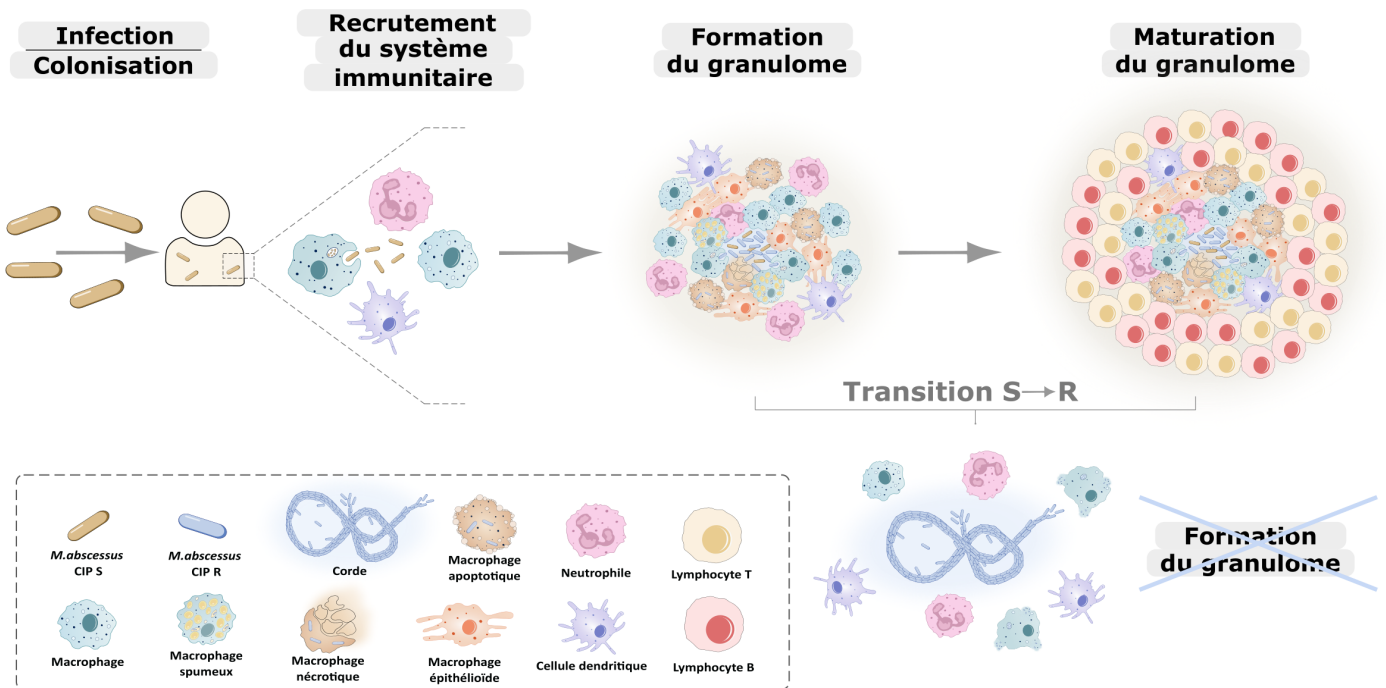
**D** : Image de microscopie confocale présentant une corde extracellulaire dans le zebrafish infecté. Échelle : 25  $\mu\text{m}$ .



biofilms puisque l'absence de GPL n'empêche pas au morphotype R d'en produire [49]. Ces structures sont définies comme étant une communauté de bactéries agrégées au sein d'une matrice extracellulaire permettant l'agrégation, l'adhésion, la rétention d'eau et l'apport de nutriments sur une surface solide. Cette matrice, ajoutée à l'agrégation mycobactérienne, permet aux biofilms d'être plus résistants aux agressions environnementales, aux désinfectants, à la pénétration d'antimicrobiens mais aussi au système immunitaire au sein d'un hôte infecté [50–52]. Les biofilms sont donc un phénomène physiopathologique contribuant largement à la persistance des infections à *M. abscessus*. En outre, lors de l'infection à *M. abscessus*, les deux morphotypes de *M. abscessus* interagissent différemment avec les cellules immunitaires. Par exemple, le variant S, contrairement au type R, est plutôt phagocyté de manière individuelle au sein de macrophages et est capable de limiter l'acidification du phagosome [53]. Ce morphotype lisse inhibe l'apoptose *via* l'action des GPLs polaires, contrairement au morphotype R qui entraîne une apoptose caspase-dépendante plus importante [54]. Les GPLs à la surface de la mycomembrane permettent également de masquer les agonistes des Toll-Like Receptor 2 (TLR-2) tels que les phosphatidyl-*myo*-isonitol dimmannosides (PIM<sub>2</sub>) [55] ce qui limite la mise en place de la réponse inflammatoire. En effet, le variant R, délesté de ces GPLs, va pouvoir interagir avec les TLR entraînant une forte production de TNF- $\alpha$  et ainsi une réaction hyperinflammatoire [55]. De plus, le variant R forme naturellement plus d'agrégats que le variant S et notamment les cordes qui empêchent la phagocytose de *M. abscessus* par les cellules immunitaires innées tels que les macrophages et neutrophiles [48]. De manière générale, suite à la colonisation et la détection des bacilles par les premières lignes de défenses immunitaires (macrophages, neutrophiles), l'inflammation générée va engendrer un recrutement massif de cellules immunitaires environnantes au site d'infection menant à la formation d'un granulome [56] (**Figure 9**). Le granulome est caractéristique des infections mycobactériennes et représente une interface dynamique entre hôte et pathogène qui a pour rôle de contenir l'infection. Celui-ci est formé de cellules immunitaires innées infectées ou non, telles que des macrophages, des neutrophiles ou des cellules dendritiques [5]. Certaines de ces cellules dans un état apoptotique, ou nécrotique, peuvent favoriser la prolifération mycobactérienne et vont engendrer une activation de l'immunité [57]. La maturation du granulome est associée au recrutement de cellules de l'immunité adaptative telles que des lymphocytes T et B en périphérie de cette structure. Néanmoins, lors de l'infection, une transition irréversible du variant S vers le variant R peut survenir [58]. Cette transition est associée à la perte des GPLs à la surface de la bactérie qui engendre une virulence accrue associée à une hyperinflammation et à la formation massive de cordes entraînant des lésions tissulaires. Ces cordes peuvent perturber la formation et l'intégrité des granulomes, occasionnant un moins bon contrôle de l'infection à long terme et participant ainsi à l'expansion et à la dissémination du processus infectieux [5,57] (**Figure 9**). Des

**Figure 9 : Colonisation de *M. abscessus*, recrutement du système immunitaire et échappement du granulome**

Après infection et colonisation, *M. abscessus* est reconnu par les cellules immunitaires environnantes créant une certaine inflammation qui va entraîner un recrutement massif du système immunitaire inné et adaptatif jusqu'à la formation du granulome. Cette structure permet de contenir l'infection mycobactérienne, mais dans certains cas, notamment une présence trop importante de cordes formées par le variant rugueux de *M. abscessus*, ce granulome peut ne se former générant un contrôle défaillant de l'infection



études de transcriptomique et génomique comparative ont révélé l'existence d'insertions, de délétions et de polymorphisme nucléotidique au niveau des gènes impliqués dans la synthèse (*mps1* et *mps2*) ainsi que dans le transport (*mmpS4* - *mmpL4a* et *mmpL4b*) des GPLs [59,60] expliquant la survenue de cette transition vers le morphotype R. Cependant, les éléments déclencheurs de cette transition phénotypique demeurent inconnus. L'ensemble de ces caractéristiques explique toutefois pourquoi le morphotype R est considéré comme la forme la plus virulente et retrouvée dans les infections aiguës et sévères à *M. abscessus* à la fois dans de nombreux modèles cellulaires, animaux et chez l'Homme [48,61,62], tandis que le variant S est considéré comme la forme environnementale colonisante et persistante de la bactérie (**Figure 6**) [63].

#### 2.2.2.2. Physiopathologie de l'infection chez l'Homme

*M. abscessus* entraîne des manifestations cliniques diverses, comprenant des infections pulmonaires ainsi que des infections extra-pulmonaires et dans de plus rares cas, disséminées à tout l'organisme. De nombreuses études suggèrent que la prévalence des infections aux MNT, et notamment à *M. abscessus*, a fortement augmenté ces dernières décennies [64,65], jusqu'à dépasser celle de la tuberculose dans les pays industrialisés [66] où la majorité de ces infections sont décrites. De manière générale, la prévalence mondiale des infections à MNT est largement sous-estimée. Cela est dû à l'absence de déclaration obligatoire dans certains pays mais aussi car elles sont considérées à tort *via* la similarité des symptômes, comme des infections à *M. tuberculosis* dans des pays en développement fortement touchés par la tuberculose [67,68].

##### a. Épidémiologie et symptômes des infections extra-pulmonaires à *M. abscessus*

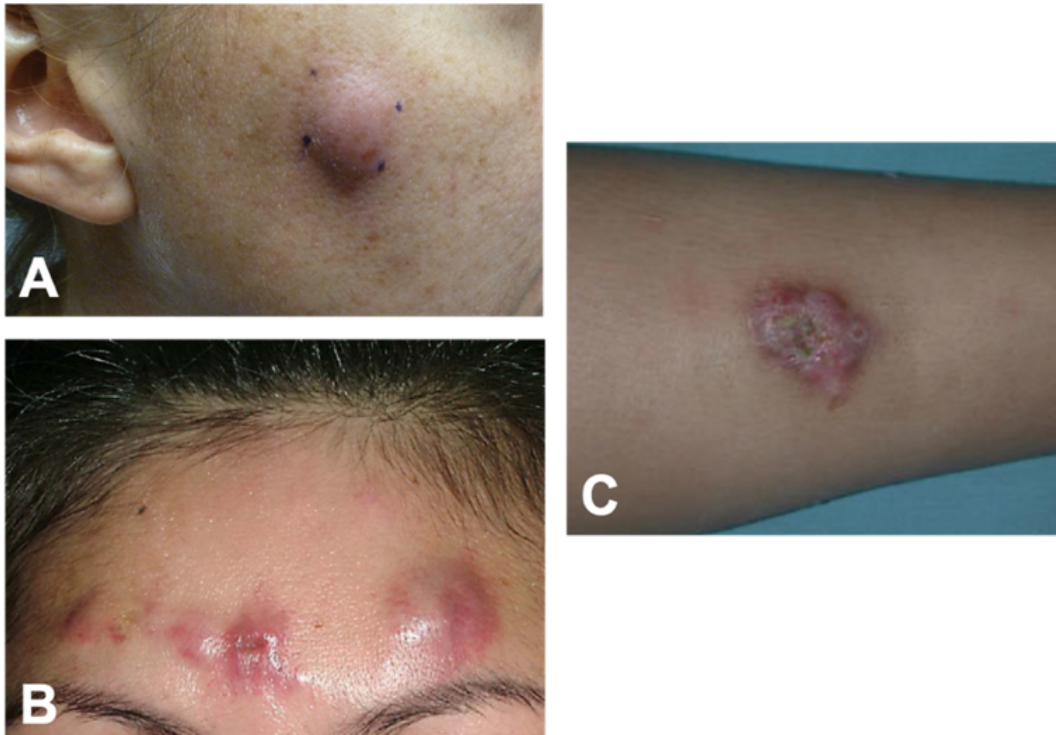
*M. abscessus* est l'une des MNT les plus couramment retrouvées dans des infections extra-pulmonaires. Celle-ci se retrouve au niveau de la peau, des tissus mous, des os, ou encore dans de plus rares cas disséminées à tout l'organisme [23]. Au niveau cutané, *M. abscessus* peut causer des lésions multiples telles que des abcès, des nodules érythémateux pourpres ou des lésions ulcéraives [29,69] (**Figure 10**). Deux mécanismes majeurs d'acquisition d'une infection extra-pulmonaire à *M. abscessus* sont connus : un passage de l'agent infectieux à travers la barrière cutanée ou bien une atteinte secondaire après une infection disséminée. Dans le premier cas, le passage transcutané peut survenir après des actes chirurgicaux [70,71], des tatouages [72,73], de l'acupuncture [74] ou encore de la mésothérapie [69]. Ces infections peuvent être causées suite à l'utilisation de matériel contaminé ou bien *via* les réseaux d'eaux potables [75] et leur localisation dépend de la nature de l'intervention.



**Figure 10 : Symptômes extra-pulmonaires visibles suite à une infection à *M. abscessus***

adapté de Lee M-R, *et al.* 2015 ; Grubbs J, *et al.* 2019 et Wongkitisophon P, *et al.* 2011, [23,69,76]

**A** : abcès cutané sur la joue droite, **B** : nodules érythémateux et plaques sur le front, **C** : nodule sous-cutané sur le bras



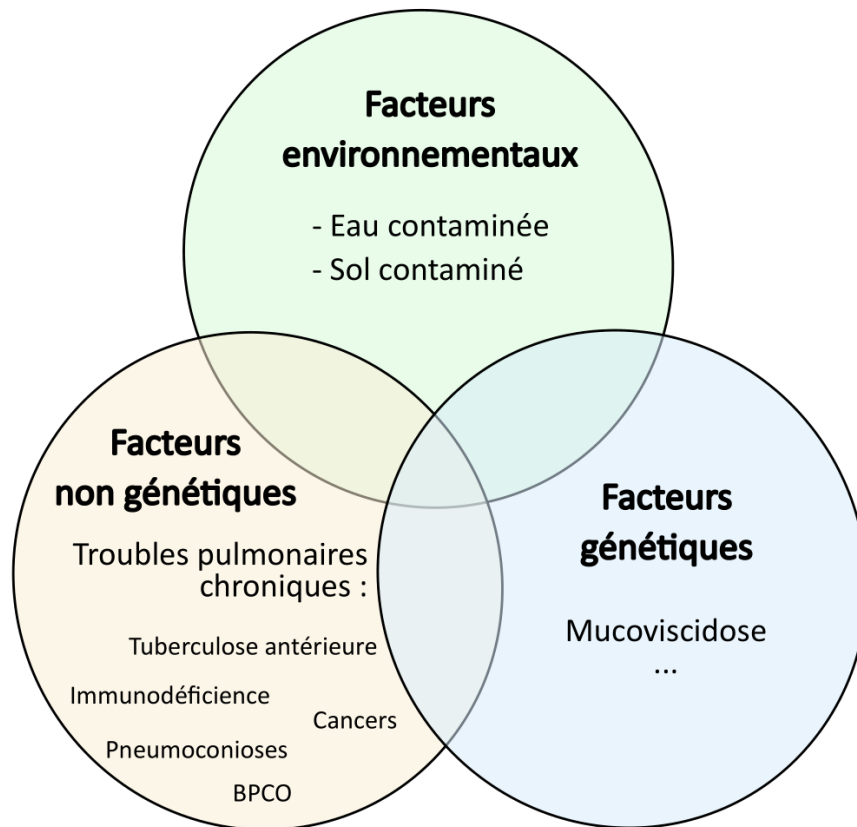
Ces infections extra-pulmonaires peuvent, dans certains cas, engendrer une infection disséminée chez des personnes immunodéprimées ou sous traitement immunosuppresseur. Enfin, des bactériémies peuvent être observées lors d'une infection du système circulatoire, notamment lors d'utilisation de cathéters [77–79].

b. Épidémiologie et symptômes des infections pulmonaires à *M. abscessus*

Les infections pulmonaires aux MNT ne cessent d'augmenter à travers le monde depuis plusieurs décennies mais la quantification de la prévalence de ces maladies reste difficile et complexe. Ceci s'explique du fait de la déclaration non obligatoire des infections dans certains pays, puisqu'un prélèvement positif n'est pas forcément corrélé à un syndrome afférent au micro-organisme [64]. *M. abscessus* est la MCR la plus fréquemment retrouvée dans les infections pulmonaires causées par les MNT. Néanmoins sa répartition géographique est très hétérogène et diffère selon les continents et les pays [22,80,81]. Globalement la proportion d'infections pulmonaires à *M. abscessus* est plus élevée dans les pays occidentaux tels que la France, le Royaume-Uni ou les États-Unis que dans les pays orientaux comme la Chine [82]. Les infections pulmonaires à *M. abscessus* sont généralement chroniques et évoluent progressivement avec une altération de la qualité de vie, comprenant des symptômes persistants et parfois irréversibles tels que le déclin de la fonction pulmonaire. Néanmoins, ce pathogène peut entraîner une maladie fulgurante avec une insuffisance respiratoire aiguë [23,36]. Les symptômes des infections pulmonaires à *M. abscessus* sont caractérisés par de la fièvre, des douleurs musculaires, une toux persistante, une fatigue générale, une perte de poids, une dyspnée, une hémoptysie ainsi qu'une production excessive de mucus pouvant favoriser des infections pulmonaires diverses. Ces symptômes ainsi que la sévérité du syndrome varient grandement d'une personne à l'autre, néanmoins ils peuvent évoluer si l'infection n'est pas prise en charge correctement. Dans ce cas, on retrouve des cas de bronchiectasie nodulaire où les voies respiratoires sont endommagées, des simples nodules pulmonaires, une inflammation des poumons, ou encore des formes plus graves de fibroses cavitaires, où des cicatrices irréversibles peuvent entraîner *in fine* une insuffisance respiratoire (<https://rarediseases.org/rare-diseases/nontuberculous-mycobacterial-lung-disease/>). Ces affections pulmonaires surviennent majoritairement chez des personnes ayant des problèmes pulmonaires sous-jacents ou des prédispositions médicales génétiques ou environnementales.



Figure 11 : Différentes catégories de facteurs de risques aux infections aux MNT et notamment à *M. abscessus*



c. Facteurs de risques environnementaux et humains aux infections à *M. abscessus*

Parmi les facteurs de risques favorisant les infections aux MNT et notamment à *M. abscessus*, on compte trois différentes catégories : les facteurs de risques environnementaux, les facteurs humains non génétiques, et les facteurs de risques génétiques (**Figure 11**).

*M. abscessus* étant un micro-organisme de l'environnement, des niches écologiques comme l'eau ou le sol peuvent être considérées comme une source d'infection humaine [21]. Différentes études montrent que ces niches peuvent être la source d'infection des patients, que ce soit l'eau des canalisations ménagères [83,84], de l'hôpital [75], ou encore la terre des jardins domestiques [85].

Les facteurs de risques non génétiques sont divers et variés, et provoquent généralement une inflammation accrue du système respiratoire exacerbant le risque d'infection à *M. abscessus*. Ils comprennent notamment des maladies structurelles des poumons telles que les Broncho-Pneumopathies Chroniques Obstructives (BPCO), appelées aussi emphysème lors de la dégradation des alvéoles pulmonaires ou bronchite chronique lorsque la toux chronique s'accompagne d'expectorations. Les BPCO réduisent le flux d'air, entraînent une difficulté à respirer et augmentent donc le risque d'infections pulmonaires [86]. Les pneumoconioses sont également un facteur aggravant des infections aux MNT, et représentent l'ensemble des inflammations pulmonaires résultant de l'inhalation de particules solides, majoritairement minérales telles que la silice, le charbon ou l'amiante et pouvant mener à des fibroses pulmonaires [87]. Les séquelles pulmonaires irréversibles causées par une tuberculose antérieure peuvent également exacerber le risque d'infections à *M. abscessus* [88]. Parmi les autres facteurs de risques, on retrouve également certains cancers, tels que des leucémies ou cancers du poumon [89–91], pouvant s'expliquer par les agents thérapeutiques utilisés pour lutter contre ces maladies et qui entraînent une immunosuppression et donc favorisent les infections microbiennes [92]. Dans cette même lignée, l'ensemble des traitements immunosuppresseurs tels que les corticostéroïdes [93,94] ou les agents anti-TNF- $\alpha$  [95] entraînent une augmentation du risque d'infection aux MNT. Enfin, l'immunodéficience qu'engendre le Virus de l'Immunodéficience Humaine (VIH) augmente le risque des maladies associées aux MNT [96], suite à la déplétion de l'immunité à médiation cellulaire liée à la chute des lymphocytes CD4<sup>+</sup> T-helper (Th1), qui ont un rôle majeur dans la défense et le contrôle des infections mycobactériennes [92]. Ces défauts immunitaires sont retrouvés majoritairement dans les infections disséminées à *M. avium*, ou encore *M. kansasii* mais quelques cas rapportent aussi des infections pulmonaires à *M. abscessus* chez des patients atteints de VIH [97,98].

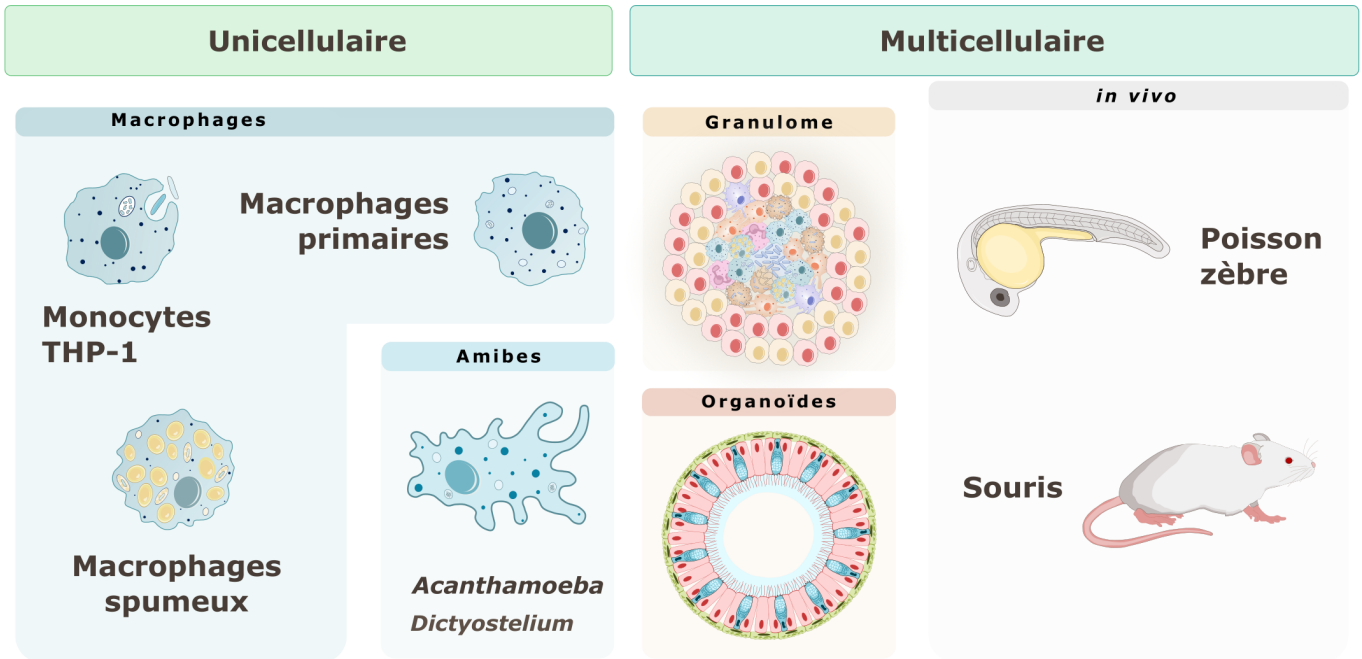
Enfin, parmi les facteurs de risques d'origine génétique, la maladie qui prédispose le plus aux infections aux MNT est la mucoviscidose. La prévalence globale de ces infections chez les patients atteints de



mucoviscidose est en moyenne de 8% à travers le monde [99], avec une dominance des complexes *M. avium* et *M. abscessus* [100]. La colonisation mycobactérienne représente dans la plupart des cas une contre-indication pour la greffe pulmonaire, d'où la nécessité de surveiller activement ces patients [82,101]. Cette maladie autosomale récessive est causée par des mutations au sein du gène *cftr* codant le canal chlorure transmembranaire CFTR (Cystic Fibrosis Transmembrane conductance Regulator). Cette protéine a pour rôle de réguler les niveaux d'ions entre le compartiment extracellulaire et intracellulaire des cellules épithéliales de plusieurs organes tels que le foie, le pancréas, l'appareil génital ou encore les poumons [102]. L'altération de la fonction du canal CFTR au niveau pulmonaire va modifier la composition et la densité-viscosité du mucus qui empêchera la fonction mucociliaire ainsi que le renouvellement du mucus [103]. Cette accumulation de mucus pathologique augmente la colonisation polymicrobienne et limite l'accès des cellules immunitaires ce qui va faciliter les infections bactériennes. À cela s'ajoute l'inflammation chronique des bronches et les potentiels dommages tissulaires au niveau des poumons qui favoriseront l'établissement d'infections chroniques. De plus, la protéine CFTR régule de nombreux processus tels que la défense des voies respiratoires. La proximité de ce canal avec d'autres transporteurs d'ions permet une régulation directe ou indirecte du pH des voies respiratoires, et un pH acide est retrouvé dans les voies aériennes des patients atteints de mucoviscidose, ce qui complique l'élimination des bactéries par les défensines qui sont très sensibles aux variations de pH [104]. Enfin, les infections mycobactériennes sont exacerbées chez ces patients ; en effet, il a été montré chez le modèle zebrafish que CFTR joue un rôle important dans l'élimination intramacrophagique de *M. abscessus* [105]. En effet, ces canaux CFTR vont permettre une production de dérivés réactifs de l'oxygène (« Reactive Oxygen Species », ROS) par la NADPH oxydase Nox2 qui donnera lieu à l'élimination des bacilles phagocytés. Dans ce modèle de mucoviscidose, le défaut de l'activité de CFTR engendre une baisse de l'activité Nox2, et donc une chute de la production des ROS qui représentent les principaux effecteurs antimycobactériens produits par le macrophage. Il s'en suit une augmentation de la multiplication intra- et extracellulaire de *M. abscessus*, ainsi qu'une baisse du chimiotactisme des neutrophiles aboutissant à un stade aigu de l'infection.

L'ensemble de ces facteurs de risques explique l'augmentation de la prévalence des infections à *M. abscessus*. Néanmoins, de nombreuses recherches se doivent d'être menées afin de mieux comprendre la pathogenèse de ces infections et pour contrecarrer plus activement ces infections. Pour ce faire, différents modèles cellulaires ou animaux ont été mis en place ces dernières années pour contribuer à ces avancées.

Figure 12 : Différents modèles d'études expérimentaux précliniques (*in vitro*, *ex vivo* et *in vivo*) pour l'étude de la pathogénèse de *M. abscessus* et l'activité de molécules candidats



### 2.2.2.3. Modèles d'étude expérimentaux

Le développement de traitements efficaces contre *M. abscessus* a été retardé par le manque de modèles appropriés pour étudier les phases chroniques et aiguës de l'infection. Néanmoins, les récents progrès sur les modèles cellulaires et animaux permettent à présent de mieux appréhender les interactions hôte-pathogène, ainsi que l'action de nouvelles molécules actives contre *M. abscessus* [106] (**Figure 12**).

Dans un premier temps, les cellules naturellement infectées par *M. abscessus* chez l'Homme sont les macrophages. Ainsi, ce type cellulaire a permis des avancées majeures dans la description des premières étapes d'invasion des morphotypes S et R (voir **Chapitre I : Le genre *Mycobacterium*, 2.2.2.1. Présentation générale du complexe et différents morphotypes**). Pour cela, la lignée de cellules monocytaires THP-1 différenciées en macrophages grâce à l'action de Phorbol 12-myristate 13-acetate (PMA) est largement utilisée. Des macrophages humains primaires peuvent être également adoptés, et sont d'un point de vue physiologique plus pertinents que les monocytes différenciés de type THP-1. Néanmoins, certains biais peuvent survenir aux vues de l'origine différente des cellules contrairement à l'utilisation d'une lignée immortalisée. De plus, les cellules THP-1 représentent un modèle bien établi et validé dans de nombreuses études impliquant les mycobactéries et sont comparables aux macrophages humains primaires concernant différents aspects cruciaux de l'infection [107]. Les « foamy macrophages » ou macrophages spumeux jouent un rôle important dans la persistance des mycobactéries, et notamment *M. tuberculosis* [108]. Ces macrophages très riches en gouttelettes lipidiques sont retrouvés dans les granulomes et contiennent des bacilles gorgés d'Inclusions Lipidiques Intracellulaires (ILI) riches en triacylglycérol (TAG) [109] servant de source de carbone et d'énergie sur le long terme. Des modèles expérimentaux de macrophages spumeux ont été mis en place pour la compréhension de l'accumulation, de la consommation et de l'utilité de ces lipides chez les mycobactéries [109–111].

Le modèle macrophagique présente des analogies avec certaines amibes considérées comme des niches environnementales pour certaines MNT [112] et pouvant également représenter une source potentielle d'infections humaines. Cette niche unicellulaire permet une protection des mycobactéries dans la nature ainsi que des échanges génétiques favorables entre bactéries, ou entre mycobactéries et amibes [113]. Ainsi, en laboratoire, ce modèle a permis la mise en évidence de certains facteurs déterminants dans la survie et la virulence intracellulaire de *M. abscessus* [114–116]. De plus, il devient un outil remarquable permettant un criblage de composés anti-mycobactérien vis-à-vis de leur activité intracellulaire ainsi qu'une identification des meilleurs candidats [117,118].

Des modèles multicellulaires plus complexes peuvent être également exploités dans l'étude des infections à *M. abscessus* préalablement à l'utilisation de modèles animaux. Un modèle *in vitro* de



granulomes a été mis en place pour mimer la formation de granulomes naturels ainsi que l'ensemble du recrutement cellulaire mis en place autour des bacilles [119]. Nous savons que ces structures sont caractéristiques des infections mycobactériennes de par le recrutement de cellules immunitaires innées et adaptatives dans le but de contenir l'infection [120] (voir **Chapitre I : Le genre *Mycobacterium***, 2.2.2.1. Présentation générale du complexe et différents morphotypes). Ainsi ce modèle mis en place permet de mieux appréhender la physiopathologie des infections mycobactériennes, la réponse immunitaire précoce [121] et éventuellement, d'identifier des traitements thérapeutiques plus adaptés.

Les organoïdes représentent un autre modèle multicellulaire récemment développé dans le but de mieux appréhender les interactions entre hôte et mycobactéries, notamment au niveau des cellules pulmonaires. Ce modèle permet de mimer et reproduire *in vitro* la structure et les propriétés biologiques de l'environnement pulmonaire humain *in vivo*. En effet, des organoïdes des voies respiratoires humaines ont permis d'étudier les étapes précoces de l'infection au niveau pulmonaire [122] et montrent que *M. abscessus* est capable de se développer au sein de cet environnement. Les organoïdes sont formés de cellules basales, de cellules ciliées et de cellules caliciformes permettant d'élucider la façon dont *M. abscessus* peut interférer avec la fonction mucociliaire ou encore l'expression de cytokines proinflammatoires lors de l'infection. À partir de cela, un modèle d'organoïdes pulmonaires alvéolaires dérivés de cellules de patients atteints de mucoviscidose a été mis au point [123]. Ces organoïdes présentent des caractères représentatifs des poumons de patients atteints de mucoviscidose tels qu'un dysfonctionnement du transporteur CFTR, une accumulation accrue de mucus, un stress oxydatif accentué, une mort cellulaire augmentée ainsi qu'une infection accrue à *M. abscessus*. Ce modèle représente un outil supplémentaire permettant de décrypter les infections mycobactériennes dans un contexte de mucoviscidose, mais aussi de tester l'action de composés antibactériens dans un environnement mucoviscidosique.

Enfin, des modèles animaux sont utilisés pour étudier la physiopathologie de *M. abscessus*. Le poisson zèbre (*Danio rerio*) représente un modèle de choix pour suivre en temps réel la chronologie de l'infection et comparer la pathogenèse des variant S et R de *M. abscessus* ainsi que d'étudier l'importance de l'immunité innée dans le contrôle des infections à *M. abscessus* [48,57]. En effet, cet organisme possède une immunité innée proche de celle de l'Homme et donne accès à l'étude des phases précoces d'interaction entre pathogène et cellules immunitaires innées [124], permettant d'étudier notamment la formation des granulomes qui sont difficiles à observer dans les modèles mammifères classiques [125,126]. De par la transparence de ses embryons, ce modèle permet un suivi spatiotemporel aisé de l'infection et de l'interaction hôte-pathogène à travers des techniques de microscopie non-invasives [127]. Cette caractéristique est exacerbée par la modification génétique





simple du poisson zèbre qui permet la génération de cellules immunitaires fluorescentes. Grâce à son développement rapide et ses bonnes capacités reproductives, le poisson zèbre présente également un intérêt croissant dans le criblage de composés chimiques présentant une activité antimycobactérienne [128,129]. De plus, la transparence des embryons vient accentuer les intérêts du poisson zèbre en pharmacologie de par la possibilité de quantifier et suivre l'efficacité antibactérienne du composé ainsi que la toxicité potentielle des molécules *via* la visualisation de modification morphologiques, phénotypiques ou fonctionnelles [128].

Enfin, l'emploi du modèle murin reste encore aujourd'hui le plus pertinent pour l'étude des infections et de l'efficacité de nouveaux agents antimicrobiens [130]. Néanmoins, il ne permet pas une observation directe des interactions entre cellules de l'hôte et pathogènes, ni d'une réelle infection. En effet, l'infection de souris immunocompétentes telles que les BALB/c ou C57BL/6 par *M. abscessus* ne permet pas d'observer la persistance de l'infection mais plutôt une clairance de celle-ci en 1 mois [128,131]. Ainsi, de nombreux modèles murins immunodéprimés ont été développés permettant un haut niveau d'infection à *M. abscessus*, tels que les souris SCID (Severe Combined ImmunoDeficiency), GMSCF-KO (Granulocyte-Macrophage Colony-Stimulating Factor Knock-Out) ou les nude qui permettent une infection pulmonaire visible et stable jusqu'à 40 jours accompagnée de symptômes pulmonaires [132]. Plus récemment, un modèle de souris immunocompétentes (C57BL/6NCrI) infectées de manière intratrachéale par des billes d'agar incorporant *M. abscessus* a été mis au point. Celui-ci va générer une infection pulmonaire chronique capable de persister sur plus de 2 mois permettant de pouvoir étudier la pathologie et les lésions pulmonaires ainsi que les marqueurs de l'inflammation sur une période plus longue [133]. Un modèle d'infection par aérosols, se rapprochant plus de la porte d'entrée naturelle des mycobactéries, a été mis en place pour l'étude des infections à *M. abscessus* chez des souris immunocompétentes C3HeB/FeJ préalablement utilisées pour l'étude de *M. tuberculosis* [134,135]. Associé à des corticostéroïdes, tels que la dexaméthasone, ce modèle permet une infection pulmonaire durable et constante par *M. abscessus* avec des symptômes pulmonaires favorisant ainsi l'évaluation d'antibiotiques administrés par voie intranasale. De manière générale, les modèles murins sont primordiaux dans l'étude préclinique de l'efficacité et de l'innocuité de nouveaux anti-bactériens, mais aussi dans l'optimisation de la posologie et de la voie d'administration de ces molécules [130]. Ces propriétés sont indispensables lorsque la thérapie souffre, à ce jour, d'un manque alarmant de traitements efficaces.



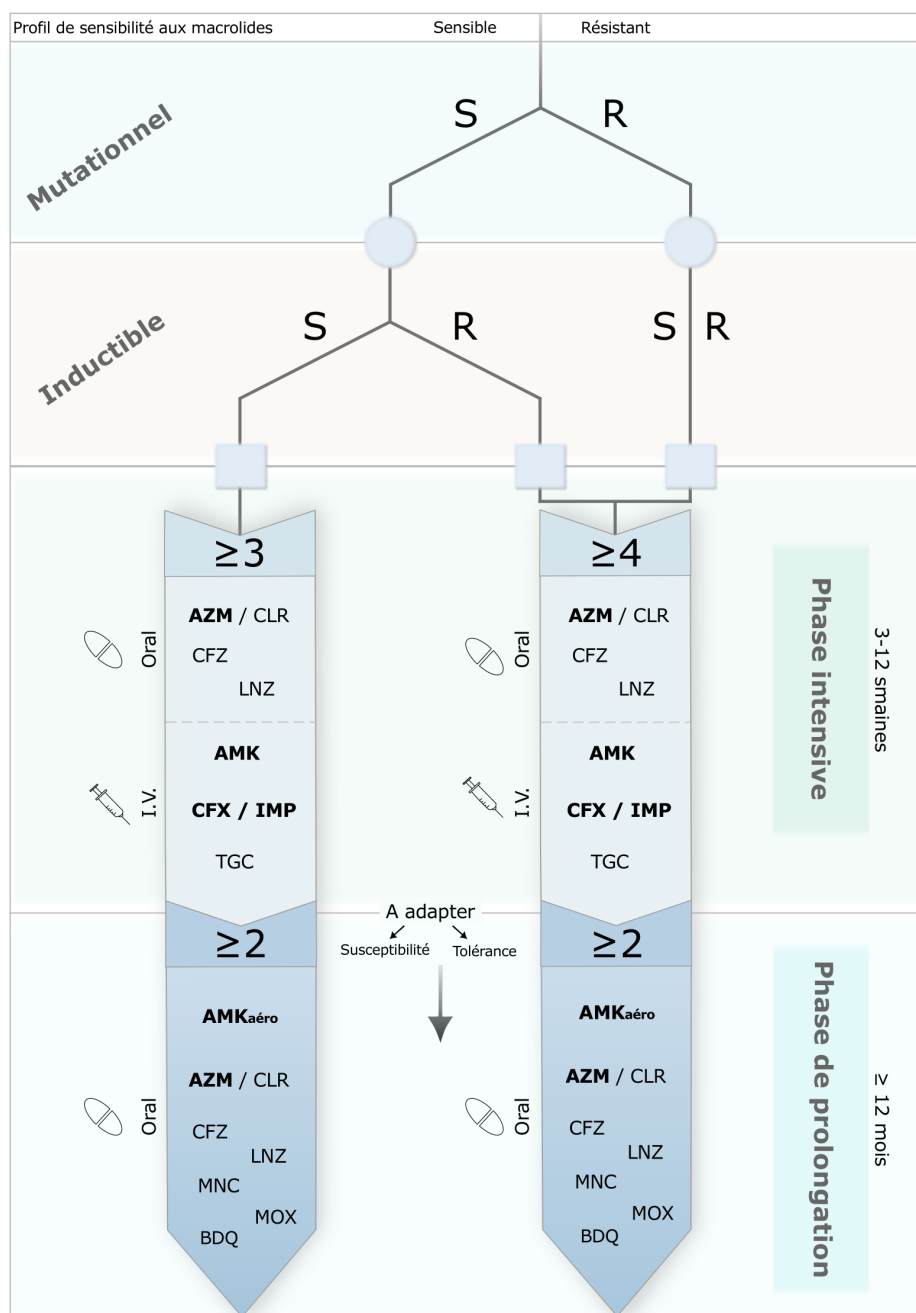
# Chapitre II :

## Antibiothérapie et mécanismes de résistances chez *M. abscessus*

**Figure 13 : Régime thérapeutique recommandé dans le cadre d'une infection à *M. abscessus***

Le régime antibiotique contre les infections à *M. abscessus* est divisé en deux phases et son contenu, notamment le nombre de molécules associées, va dépendre du profil de sensibilité de la souche aux macrolides (S : sensible, R : résistant).

La première phase, ou « phase intensive » dure de 3 à 12 semaines et comprend une dose quotidienne d'un macrolide oral (CLR ou AZM), d'AMK parentérale ainsi que d'une β-lactamine injectée (CFX ou IMP). La seconde phase, ou « phase de prolongation » peut durer jusqu'à plus d'un an où un macrolide et de l'AMK en aérosol seront prescrits. A ces cocktails d'antibiotiques peuvent s'ajouter de nombreux autres antibiotiques à adapter selon la susceptibilité de la souche pathogène impliquée.



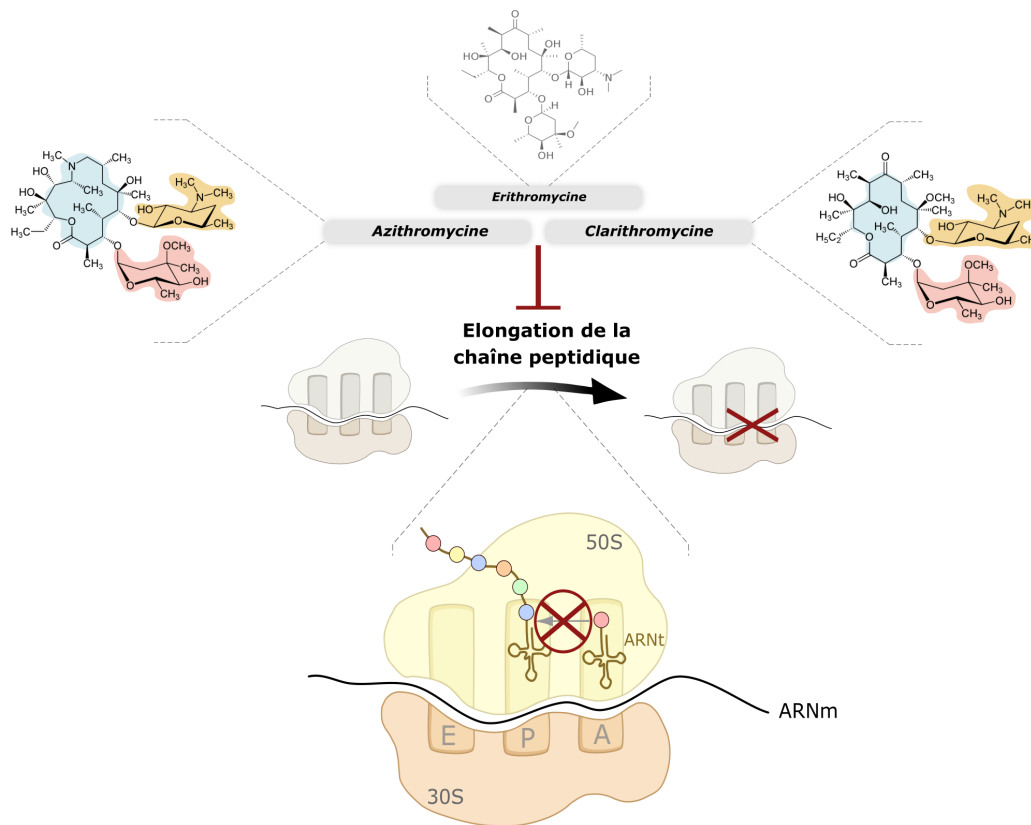
## 1. L'antibiothérapie conventionnelle contre *M. abscessus*

Les infections causées par *M. abscessus* représentent un réel défi en clinique pour les patients et les professionnels de santé car elles restent très difficiles à traiter du fait de la résistance naturelle de cette bactérie à la plupart des classes d'antibiotiques disponibles. Les raisons expliquant cette résistance sont multiples. D'une part, la paroi de *M. abscessus* est très riche en lipides complexes et constitue un véritable bouclier pour l'entrée de nombreux agents antimicrobiens. D'autre part, cette bactérie met en place de nombreux mécanismes (innés ou acquis) lui permettant de résister à l'action des antibiotiques [136]. Ainsi, de nombreux comités d'experts se réunissent régulièrement pour définir des stratégies thérapeutiques optimales et recommandations à suivre pour traiter ces infections. Le consortium de 2016 a permis de réunir la fondation américaine de la mucoviscidose (US Cystic Fibrosis Foundation) ainsi que la société européenne de la mucoviscidose (European Cystic Fibrosis Society) pour essayer d'harmoniser la gestion et la thérapie des infections aux MNT dans le cadre de la mucoviscidose [100]. En 2020, des recommandations ont été énoncées à l'encontre des infections pulmonaires aux MNT *via* le regroupement d'un panel d'experts sélectionnés par les quatre principales sociétés internationales de médecine respiratoire et de maladies infectieuses que sont l'ATS (American Thoracic Society), l'ERS (European Respiratory Society), l'ESCMID (European Society of Clinical Microbiology and Infectious Diseases) et l'IDSA (Infectious Diseases Society of America) [137]. Ces recommandations ont été reprises et ajustées en 2022 par le Centre de Contrôle des Maladies de Colombie Britannique (BC Centre for Disease Control) dans la section 12 de leur manuel du médecin pour la tuberculose abordant les MNT pulmonaires et leur traitement [138]. Ces comités mettent en évidence la difficulté d'attribuer un traitement optimal et universel contre les MNT, notamment vis-à-vis de *M. abscessus*. En effet, le traitement est largement dépendant de chaque patient et de chaque souche infectieuse, et il existe très peu de corrélation entre la susceptibilité d'une souche *in vitro* (concentration minimale inhibitrice -CMI-) et l'efficacité thérapeutique d'un composé *in vivo*, ce qui accentue la complexité et la prédictibilité du traitement en clinique [137]. Néanmoins, de ces différentes recommandations émerge une stratégie thérapeutique divisée en deux étapes, incluant une phase initiale dite « intensive » suivie d'une phase de « prolongation » (**Figure 13**). Ces phases contiennent des combinaisons d'antibiotiques différentes, et celles-ci varient selon la sensibilité de l'isolat clinique aux macrolides, une classe d'antibiotiques cruciale dans le traitement des infections à *M. abscessus* [139]. De manière générale, la phase intensive a pour objectif de faire baisser rapidement la charge bactérienne globale. Elle comprend l'administration quotidienne d'au moins 3 molécules en cas de sensibilité aux macrolides, ou 4 dans le cas contraire (**Figure 13**). On y retrouve principalement un macrolide oral tel que l'azithromycine (AZM) ou la CLR, une  $\beta$ -lactamine (CFX ou IMP) parentérale ainsi que l'injection quotidienne d'AMK. Ce régime thérapeutique peut également être complété par

**Figure 14 : Structure des macrolides, dont ceux utilisés dans le traitement contre *M. abscessus* et leur mode d'action sur la synthèse des protéines procaryotes**

Les macrolides (AZM et CLR utilisées contre *M. abscessus*) ciblent la boucle de l'ARNr 23S de la grande sous-unité 50S du ribosome mycobactérien à travers des liaisons hydrogènes, ainsi que des liaisons électrostatiques et hydrophobes qui empêcheront la liaison peptidique entre le néo-peptide et l'acide aminé de l'ARNt. Cela aura pour conséquence d'inhiber l'élongation de la chaîne peptidique en cours de synthèse et donc être délétère pour *M. abscessus*.

Les cycles lactones sont représentés en bleu, les sucres désosamines et cladinoses sont respectivement représentés en orange et en rouge.



d'autres classes d'antibiotiques. La phase de prolongation s'étend sur au moins 12 mois et le choix de son contenu dépendra du profil de sensibilité/résistance de chaque isolat clinique mais aussi de la tolérance du patient aux antibiotiques prescrits. Néanmoins, elle comporte en général au moins l'administration d'AMK en aérosol et d'un macrolide administré par voie orale.

En définitive, ces régimes thérapeutiques diffèrent énormément entre chaque patient et sont en constante évolution. Une certaine adaptabilité est ainsi demandée aux praticiens afin de choisir un cocktail d'antibiotiques approprié et optimal tenant compte de l'ensemble des informations à leur disposition. Enfin, ces associations d'antibiotiques ciblant des enzymes ou voies métaboliques différentes doivent se compléter afin de pouvoir contrecarrer les potentielles résistances qui pourraient émerger au cours du traitement.

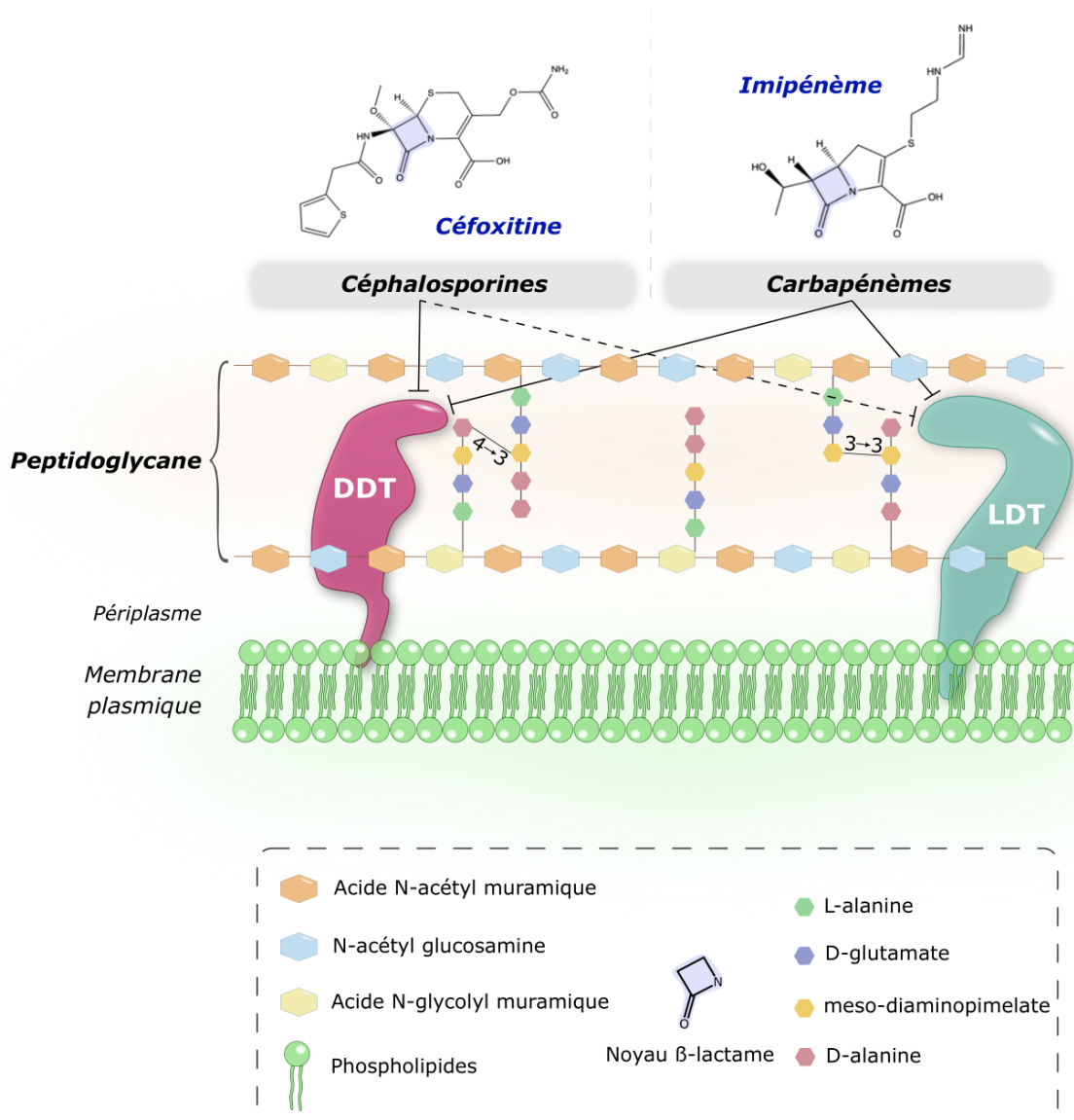
### 1.1. Les macrolides

Les macrolides sont la pierre angulaire du traitement des infections à *M. abscessus* avec notamment l'utilisation recommandée de l'AZM ou de la CLR [137]. Cette classe d'antibiotiques a vu le jour avec la découverte de l'érythromycine en 1952, produite par l'actinomycète *Saccharopolyspora erythraea* (autrefois nommée *Streptomyces erythraeus*) [140]. Depuis sept décennies, de nombreux dérivés de l'érythromycine ont été synthétisés afin de contrecarrer l'instabilité acide de l'érythromycine ainsi que les résistances à cet antibiotique, tout en améliorant ses propriétés pharmacocinétiques. Les années 1980 ont vu la découverte de certains macrolides de seconde génération dérivés de l'érythromycine tels que la CLR et l'AZM [141], encore aujourd'hui largement utilisés en clinique et particulièrement dans le traitement des infections mycobactériennes. Cette classe d'antibiotiques est formée de molécules ayant un cycle lactone de 14 (CLR) ou 15 carbones (AZM), ainsi que des sucres désosamines et cladinoses (**Figure 14**) et inhibe la synthèse protéique [142]. En effet, en se fixant sur la boucle de l'ARNr 23S de la grande sous-unité 50S du ribosome *via* des liaisons hydrogènes réversibles entre le désosamine et les résidus adénine A2058 et A2059, la CLR et l'AZM vont pouvoir inhiber l'élongation du néo-peptide [143]. De plus, ils vont former des interactions électrostatiques et hydrophobes bloquant le tunnel de sortie par lequel le peptide en cours de synthèse s'éloigne du centre peptidyltransférase en empêchant la liaison peptidique entre le néo-peptide et l'acide aminé provenant de l'ARNt [143,144] (**Figure 14**). Puisque les macrolides représentent la base du traitement contre *M. abscessus*, ce pathogène a pu sélectionner de nombreux mécanismes de résistance afin de contrecarrer son action [145]. Ainsi dans certains cas, les macrolides peuvent être prescrits pour leurs propriétés immunomodulatrices, ce qui vient accentuer la sélection de résistances causée par l'administration de doses sub-inhibitrices. En outre, différents travaux ont mis en garde contre



**Figure 15 : Structure des  $\beta$ -lactamines (céfoxitine et imipénème) et leur mode d'action sur les transpeptidases du peptidoglycane de *M. abscessus***

Les  $\beta$ -lactamines, en mimant le dipeptide D-alanyl-D-alanine, vont venir inhiber les D,D-transpeptidases (DDTs) et principalement chez *M. abscessus* les L,D-transpeptidases (LDTs) et ainsi bloquer la synthèse finale du peptidoglycane, qui aura pour conséquence un effet bactéricide sur la mycobactérie.



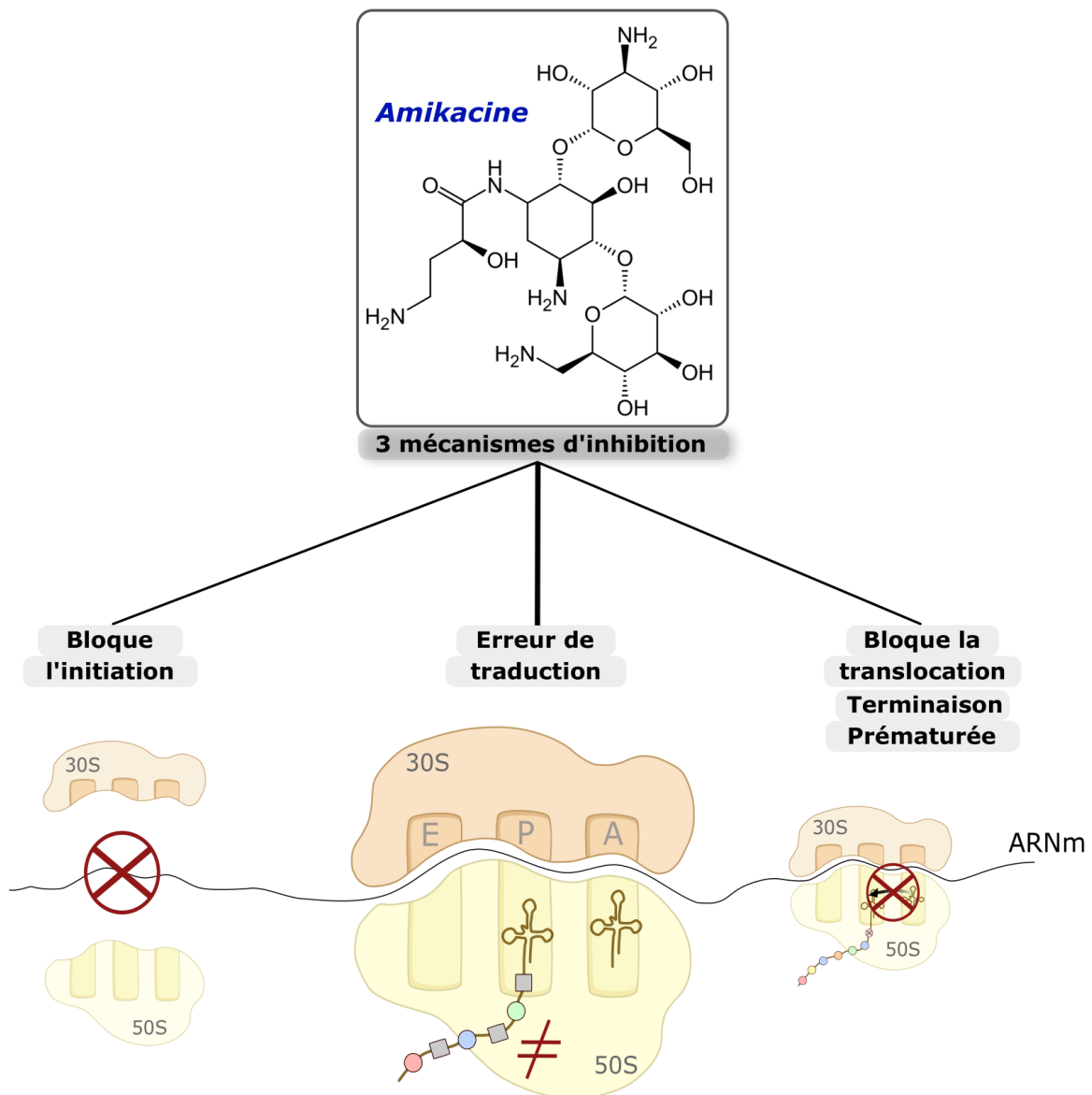
l'utilisation prolongée d'AZM, principalement à cause de ces propriétés immunodulatrices qui vont empêcher l'acidification lysosomale, la dégradation phagosomale et l'autophagie et perturber les voies IFN- $\gamma$  et TNF- $\alpha$  requises pour le contrôle des infections mycobactériennes [146]. Cela pourrait entraîner, notamment chez des patients atteints de mucoviscidose, une élimination insuffisante des bacilles et engendrer l'établissement d'une infection chronique à *M. abscessus*. Néanmoins, une étude de cas française n'a montré aucun lien entre la hausse des maladies pulmonaires causées par *M. abscessus* et l'utilisation de thérapies inhalées ou de faibles doses d'AZM [147]. Malgré tout, l'utilisation prolongée d'antibiotiques, dont les macrolides, n'est pas recommandée afin de limiter l'apparition de souches cliniques multirésistantes aux antibiotiques.

### 1.2. Les $\beta$ -lactamines

Les  $\beta$ -lactamines représentent la classe d'antibiotiques la plus utilisée contre les bactéries pathogènes, et celle-ci existe depuis près d'un siècle avec la découverte de la pénicilline dans la fin des années 1920 par Alexander Fleming [148]. Ce n'est que dans le début des années 1940 que cette molécule fut purifiée et développée dans un but thérapeutique et médical par Howard Florey, Ernst Chain et leurs collaborateurs [149,150]. Aujourd'hui, les  $\beta$ -lactamines regroupent différentes familles d'antibiotiques telles que les analogues de pénicilline, les monobactames, les carbapénèmes et les céphalosporines [151]. Ces molécules, contenant toutes un noyau  $\beta$ -lactame (**Figure 15**), inhibent la synthèse finale du peptidoglycane (PG), composé essentiel de la paroi mycobactérienne [152]. Cette dernière étape consiste en la réticulation du PG par la formation de liaisons covalentes entre les chaînes peptidiques latérales (L-Alaninyl-D-isoGlutaminyL-meso-diaminopimelyl-D-alanyl-D-Alanine) du disaccharide composé de N-acétylglucosamine (NAG) et d'acide N-acétylmuramique (NAM) ou d'acide N-glycolylmuramique (NGM) (**Figure 15**) [153]. Cette inhibition résulte du blocage de l'activité des transpeptidases mycobactériennes de la famille des protéines liant la pénicilline (« Penicillin-Binding Proteins » -PBP-), notamment les D,D-transpeptidases (DDTs) et majoritairement chez *M. abscessus* les L,D-transpeptidases (LDTs) qui catalysent respectivement les réactions de transpeptidation de type 4 $\rightarrow$ 3 et 3 $\rightarrow$ 3 [153]. Les DDTs et les LDTs sont donc la cible des deux seules  $\beta$ -lactamines utilisées dans le traitement contre *M. abscessus*, à savoir la CFX, une céphalosporine semi-synthétique de seconde génération et l'IMP, un carbapénème [137]. Ces deux molécules (**Figure 15**) vont inhiber de la même manière l'étape finale de synthèse du PG, en mimant le dipeptide D-alanyl-D-alanine, substrat des LDTs et DDTs, elles se lient au site actif de ces enzymes et ainsi avoir un effet antibactérien [154]. Cependant, les deux  $\beta$ -lactamines utilisées possèdent des efficacités différentes. En effet, l'IMP exerce une meilleure activité sur *M. abscessus* que ce soit *in vitro* [155] ou au sein de macrophages infectés [156],

**Figure 16 : Structure de l'amikacine et mécanismes d'inhibition de la synthèse protéique bactérienne associés**

Les aminoglycosides et l'AMK inhibent la synthèse protéique de trois manières différentes. En venant se lier au site A de l'ARNr 16S de la petite sous-unité (30S) du ribosome mycobactérien, l'AMK inhibe l'initiation en bloquant l'association des deux sous-unités du ribosome, mais aussi la translocation en entraînant une terminaison prématurée et donc des protéines synthétisées non fonctionnelles. Enfin le mécanisme majeur retrouvé chez cette classe d'antibiotiques est la perturbation de l'arrivée de l'aminocyl-ARNt correct au site de décodage qui aura pour conséquence des erreurs de traduction et donc des protéines non fonctionnelles.



ce qui s'explique notamment par le fait que les DDTs sont activement inhibées par l'ensemble des  $\beta$ -lactamines tandis que les LDTs, majoritaires chez *M. abscessus*, sont préférentiellement inhibées par les carbapénèmes [157].

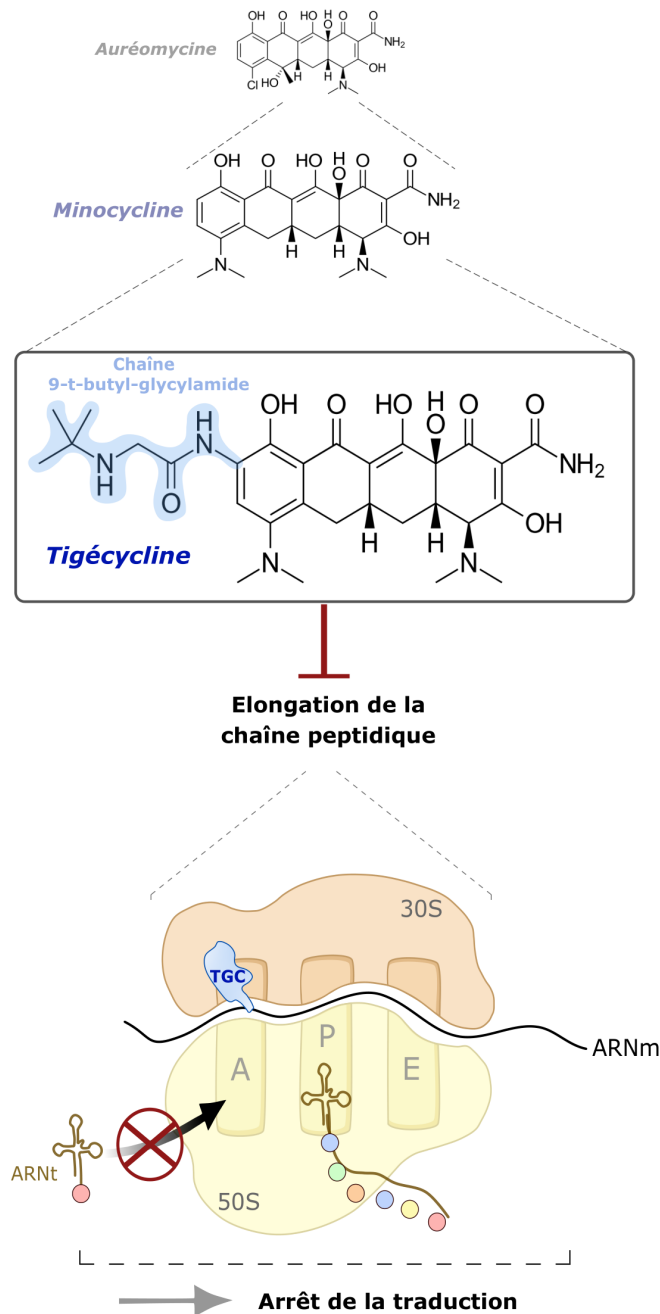
Dans l'ensemble, les  $\beta$ -lactamines représentent une classe d'antibiotiques indispensable dans le traitement des infections à *M. abscessus*, bien que seulement deux molécules soient recommandées en thérapeutique. Récemment, plusieurs études ont montré que l'utilisation simultanée de plusieurs  $\beta$ -lactamines présente une synergie *in vitro* [158,159] contre des isolats cliniques [160] et *in vivo* dans un modèle murin [161] ouvrant la voie à l'optimisation des traitements .

### 1.3. Les aminoglycosides

L'AMK est le troisième antibiotique recommandé en première intention dans le traitement de *M. abscessus* avec les macrolides et les  $\beta$ -lactamines. Elle fait partie de la famille des aminoglycosides, une classe d'antibiotiques découverte au début des années 1940 avec l'isolation, à partir de l'actinobactérie *Streptomyces griseus*, de la streptomycine par Albert Schatz [162,163]. La streptomycine s'est avérée comme étant le premier traitement efficace contre *M. tuberculosis* [164] et reste utilisée aujourd'hui en seconde intention [165]. A partir de cette molécule, de nombreux dérivés ont été isolés ou synthétisés, telle que la kanamycine (KAN) isolée à partir de *Streptomyces kanamyceticus* en 1957 [166]. C'est à partir de cette dernière qu'a été synthétisée l'AMK [167], rapidement approuvée par la Food and Drug Administration (FDA) en 1981 et fréquemment utilisée dans la thérapie contre *M. abscessus* [137]. L'AMK est formée d'une structure centrale de sucres aminés reliés par des liaisons glycosidiques, et dérive de la KAN par l'ajout d'une chaîne S-4-amino-2-hydroxybutyryl en position 1 du cycle désoxystreptamine (**Figure 16**). Ses caractéristiques cationiques l'aident à traverser les membranes bactériennes et atteindre sa cible [168,169]. Les aminoglycosides, dont l'AMK, inhibent la synthèse protéique en se liant au site A de l'ARNr 16S de la petite sous-unité (30S) du ribosome bactérien (**Figure 16**) [170]. Cette liaison inhibe l'initiation et l'élongation de la traduction et engendre des erreurs de traduction [171]. Plus précisément, l'AMK va élaborer des liaisons électrostatiques avec les adénines A1408, A1492 et A1493 du site de décodage au niveau de l'ARNr 16S qui auront pour conséquence de perturber l'arrivée de l'aminoacyl-ARNt portant l'acide aminé correspondant à l'ARNm en cours de traduction [172]. En outre, ces erreurs de traduction peuvent conduire à une accumulation de protéines mal repliées au sein de la membrane engendrant des dommages qui faciliteront l'entrée et l'action d'antibiotiques qui vont ainsi exacerber les phénomènes bactéricides [169,173]. En effet, les aminoglycosides se démarquent des autres inhibiteurs de synthèse de par leur effet bactéricide, notamment dû à cette altération des membranes

**Figure 17 : Structure des tétracyclines, et notamment de la tigécycline utilisée contre les infections à *M. abscessus* et son mode d'inhibition de l'élongation de la traduction mycobactérienne**

La TGC se lie à l'ARNr 16S de la petite sous-unité 30S du ribosome mycobactérien, particulièrement avec sa chaîne 9-t-butyl-glycylamide qui va lier le site de décodage, ce qui empêche l'entrée de l'ARNt au niveau du site A. La liaison de cet antibiotique entraîne donc un arrêt de la traduction en empêchant l'incorporation d'un nouvel acide aminé au néo-peptide en formation.



bactériennes [169,174].

Différentes études ont montré la synergie de l'AMK avec d'autres antibiotiques tel que la CFZ [175,176] ou encore le linézolide (LNZ) [177], qui peuvent être utilisés lors du traitement contre *M. abscessus*. De plus, l'association avec certains antibiotiques, tel que la CFZ, permet de prévenir l'émergence de résistances à l'AMK [178]. Cependant, une étude récente n'a pas retrouvé la synergie entre AMK et LNZ et a montré un antagonisme fort entre AMK et AZM [179]. Ces travaux démontrent que de nombreux efforts doivent encore être réalisés pour mieux appréhender les interactions entre antibiotiques dans un but d'optimisation des traitements.

#### 1.4. Les tétracyclines

D'autres classes d'antibiotiques sont recommandées dans le traitement des infections à *M. abscessus*, notamment en cas de difficulté d'éradication. Celles-ci incluent, entre autres, les tétracyclines, telles que la tigécycline (TGC) ou la minocycline (MNC). La famille des tétracyclines a vu le jour dans les années 1940 avec l'auréomycine (ou chlortétracycline) isolée à partir de l'actinomycète *Streptomyces aureofaciens* par le professeur Benjamin Duggar au sein des laboratoires Lederle [180]. L'utilisation à grande échelle de cet antibiotique après la seconde guerre mondiale, en agronomie et en thérapie humaine, a favorisé l'émergence et la sélection d'organismes résistants. Par la suite, d'autres tétracyclines naturelles ou semi-synthétiques ont été décrites, telles que la DOX ou la MNC, utilisée parfois dans la phase de prolongation du traitement (**Figure 13**) [100]. Cette dernière fait partie plus particulièrement de la famille des glycylyclines et sert de molécule parent à la TGC. En effet, la MNC est modifiée sur sa partie hydrophobe désignée par le cycle D afin de donner lieu à la TGC, aussi nommée 9-(*t*-butyl-glycylamido)-minocycline, ou anciennement GAR-936 [181,182] (**Figure 17**). La synthèse de ces nouveaux dérivés glycylyclines a permis de contrecarrer les mécanismes de résistance existant contre les tétracyclines classiques que sont l'efflux, la protection du ribosome ou encore la modification chimique [182–184]. De manière générale, l'ajout de la chaîne 9-*t*-butyl-glycylamide augmente l'affinité de la TGC au ribosome [185] améliorant ainsi son activité *in vitro* sur les MCR, et principalement *M. abscessus* [186]. Cet antibiotique a également montré son efficacité en clinique dans un usage compassionnel où le traitement standard présentait ses limites [187]. Cette étude rapporte une amélioration de l'état infectieux de plus de 60% des patients traités grâce à l'administration parentérale de TGC pendant plus d'un mois. Toutefois, si son utilisation reste limitée au vue de sa forte toxicité, une formulation de TGC inhalée a permis d'améliorer la posologie et présente une efficacité notoire dans un modèle murin d'infection pulmonaire [188].

D'un point de vue mécanistique, les tétracyclines inhibent la synthèse protéique. La TGC se lie de

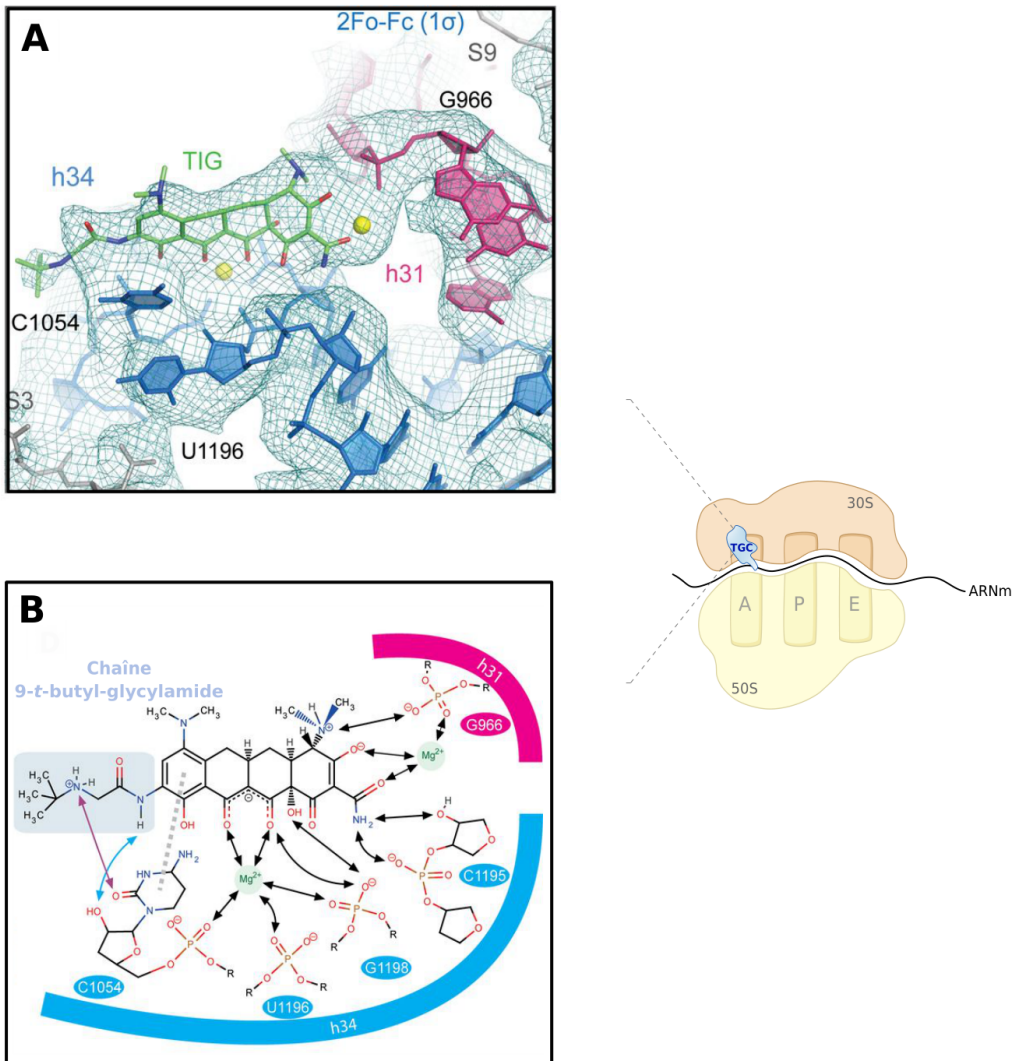
**Figure 18 : Liaison de la tigécycline à l'ARNr 16S du ribosome bactérien**

La TGC se lie au niveau de la sous-unité 30S du ribosome bactérien dans un poche formée par la boucle h34 et la boucle h31.

**A** : Modèle de la carte de densité électronique du site de liaison de la TGC (vert). L'hélice h34 et h31 sont respectivement représentées en bleu et en rose, les ions  $Mg^{2+}$  sont en jaune.

**B** : Structure de la TGC et vue schématique d'ensemble des liaisons de cette molécule avec la poche de liaison de l'ARNr 16S. La chaîne 9-*t*-butyl-glycylamide est encadrée en bleu et ses interactions avec le résidu C1054 sont indiquées *via* les flèches cyan et violette.

**A et B** provenant de Schedlbauer A, *et al.* 2015, [189]





manière réversible à différents résidus des régions hélicoïdales H31 et H34 de l'ARNr 16S de la petite sous-unité 30S du ribosome bactérien [189,190] (**Figure 18**). En particulier le substituant 9-*t*-butylglycylamide va se lier au nucléotide C1054 de l'ARNr 16S au niveau du site de décodage, ce qui empêche l'entrée de l'ARNt au niveau du site A [185,189]. La liaison de la TGC entraînera donc un arrêt de la traduction en bloquant l'incorporation de nouveaux acides aminés au sein de la chaîne peptidique en cours de synthèse [190] (**Figure 17**).

Bien que la TGC contourne les mécanismes de résistance classiquement déployés par *M. abscessus* vis-à-vis des tétracyclines, des améliorations de ces molécules peuvent être entreprises. Ainsi, de nouveaux dérivés de tétracycline ont récemment vu le jour, notamment l'omadacycline qui, en dépit d'une activité *in vitro* similaire à la TGC, présente l'avantage de pouvoir être administrée oralement, ce qui augmente sa tolérabilité [191,192]. L'éravacycline est une tétracycline validée par la FDA au même titre que l'omadacycline ou la TGC qui présente une certaine efficacité *in vitro* sur *M. abscessus* [193] et qui pourrait s'ajouter au traitement actuel contre ce pathogène [194]. Enfin, différentes études ont montré une synergie entre la TGC et différents antibiotiques, tels que la rifabutine (RFB) [195,196]. Ces travaux soulignent l'intérêt que peut représenter cette classe de molécules, même si un développement reste nécessaire dans l'espoir de pouvoir les inclure définitivement dans les traitements contre *M. abscessus*.

### 1.5. Les fluoroquinolones

Parmi les autres antibiotiques utilisés, la MOX peut être prescrite oralement durant la longue phase de prolongation (**Figure 13**) [100]. Cet antibiotique fait partie de la classe des quinolones qui a vu le jour avec le développement de l'acide nalidixique en 1962 par George Y. Leshner et ses collaborateurs [197]. Cette molécule a rapidement été utilisée chez l'Homme pour ses propriétés antibactériennes, notamment dans les infections du tractus urinaire, puis a été modifiée dans un but d'amélioration thérapeutique. Ainsi dans les années 1970, l'ajout d'un groupement fluor a permis d'améliorer son efficacité antibactérienne, donnant naissance aux fluoroquinolones [198]. Depuis, de nombreux autres analogues ont été synthétisés, grâce à l'attrait que représente cette classe d'antibiotiques de par son efficacité élevée, son large spectre d'activité, ses bons paramètres pharmacocinétiques, ses formulations orales ou intraveineuses et ses faibles effets secondaires [198].

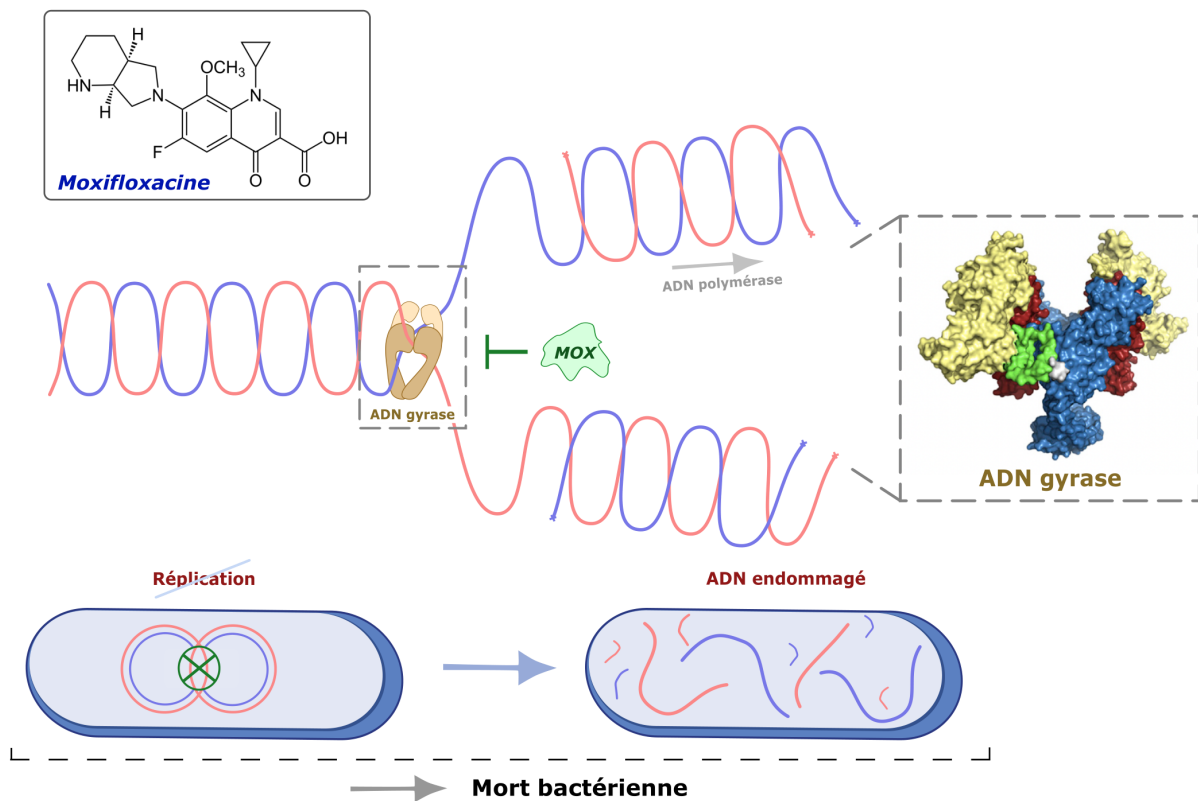
Parmi ces analogues, nous pouvons citer la CIP, datant de 1983 qui reste largement prescrite aujourd'hui, ou la MOX, qui a vu le jour plus récemment avec un premier brevet datant de 1991. La MOX a été approuvée en 1999 par la FDA et reste très largement utilisée dans le cadre d'infections bactériennes pulmonaires. Cette fluoroquinolone de 4<sup>ème</sup> génération a montré une efficacité accrue et



**Figure 19 : Structure et mode d'action de la moxifloxacin**

La MOX interagit et se lie à l'ADN gyrase, une enzyme impliquée dans le désenroulement de la double hélice d'ADN bactérien. Cette topoisomérase de type II crée des brèches simple- ou double-brins dans l'ADN pour permettre à l'ADN polymérase de répliquer le chromosome bactérien. En interagissant avec cette enzyme, la MOX vient inhiber la réplication de l'ADN et laisse des brèches au sein du chromosome, engendrant un effet bactéricide sur *M. abscessus*.

Structure de l'ADN gyrase de *M. tuberculosis* dans sa forme apo provenant de Petrella S, et al. 2019, [199]



meilleure que d'autres fluoroquinolones contre *M. tuberculosis*, mutée ou non au sein de sa cible [200–203]. Cependant, des travaux montrent une action de cette molécule sur une faible proportion d'isolats cliniques de *M. abscessus in vitro* [204,205], même si des études montrent une large efficacité dans des cas ophtalmiques de kératite [206,207]. De plus, un modèle d'infection à *M. abscessus* chez le poisson zèbre révèle une très faible activité de la MOX [208]. Toujours est-il que la MOX est entrée dans le traitement des infections à *M. abscessus* grâce à sa capacité à inhiber la réplication de l'ADN mycobactérien, permettant ainsi de la combiner aux autres classes d'antibiotiques. En effet, cet antibiotique interagit avec les topoisomérases de type II, telles que l'ADN gyrase, une enzyme impliquée dans la résolution de la topologie nucléaire. L'ADN gyrase a pour rôle de dénouer et séparer les brins de la double hélice d'ADN bactérien pour permettre à l'ADN polymérase de répliquer l'ADN en créant des brèches simple- ou double-brins [209]. Cette étape est donc indispensable à la réplication du chromosome bactérien, et donc à la multiplication bactérienne. En interagissant principalement avec les sous-unités  $\alpha$  de l'ADN gyrase, la MOX vient former un complexe ternaire avec l'ADN et la topoisomérase qui aura pour conséquence d'inhiber la réplication du chromosome mycobactérien [210] (**Figure 19**). De plus, l'inhibition de l'action des topoisomérases va maintenir la présence de brèches dans l'ADN qui engendrera l'effet bactéricide des fluoroquinolones [211]. Malheureusement, l'utilisation accrue des fluoroquinolones chez l'Homme et l'animal a engendré un relargage massif de ces molécules dans l'environnement qui a exacerbé la pression de sélection sur les micro-organismes et a contribué à l'émergence de résistances [210]. De plus, une étude a montré un antagonisme dans plus de 60% des cas lorsque la MOX est associée à la CLR, ou dans plus de 40% des cas avec l'AZM *in vitro*, *ex vivo* et dans un modèle murin contre des isolats cliniques de *M. abscessus* subsp. *abscessus* [212]. Cependant, cette même étude ne montre que très peu d'antagonisme entre la MOX et les macrolides contre des isolats cliniques de *M. abscessus* subsp. *massiliense*. Puis, une observation prospective a montré une résolution de lésions cutanées causées par *M. abscessus* plus rapide avec un traitement combinant CLR et MOX, en comparaison à un traitement conjuguant AMK et MOX [213]. Cela met à nouveau en évidence l'importance d'adapter correctement le traitement antibiotique à l'isolat clinique impliqué.

## 1.6. Nouvelles classes d'antibiotiques et alternatives

### 1.6.1. Les phénazines

La classe des phénazines, incluant particulièrement la CFZ, une riminophénazine, figure parmi les nouvelles classes d'antibiotiques récemment incluses dans le traitement des infections mycobactériennes. Cette molécule a vu le jour en Irlande dans les années 1950 grâce à l'équipe de

**Figure 20 : Structure et mode d'action de la clofazimine**

La CFZ fonctionnerait comme une pro-drogue chez les mycobactéries en étant réduite par la protéine NADH:quinone oxydoréductase NDH-2 de la chaîne respiratoire. Cette molécule rentre en compétition avec le substrat de cette enzyme, la ménaquinone (MQ) et est ensuite oxydée par l'O<sub>2</sub> permettant une production de ROS délétères pour la mycobactérie.

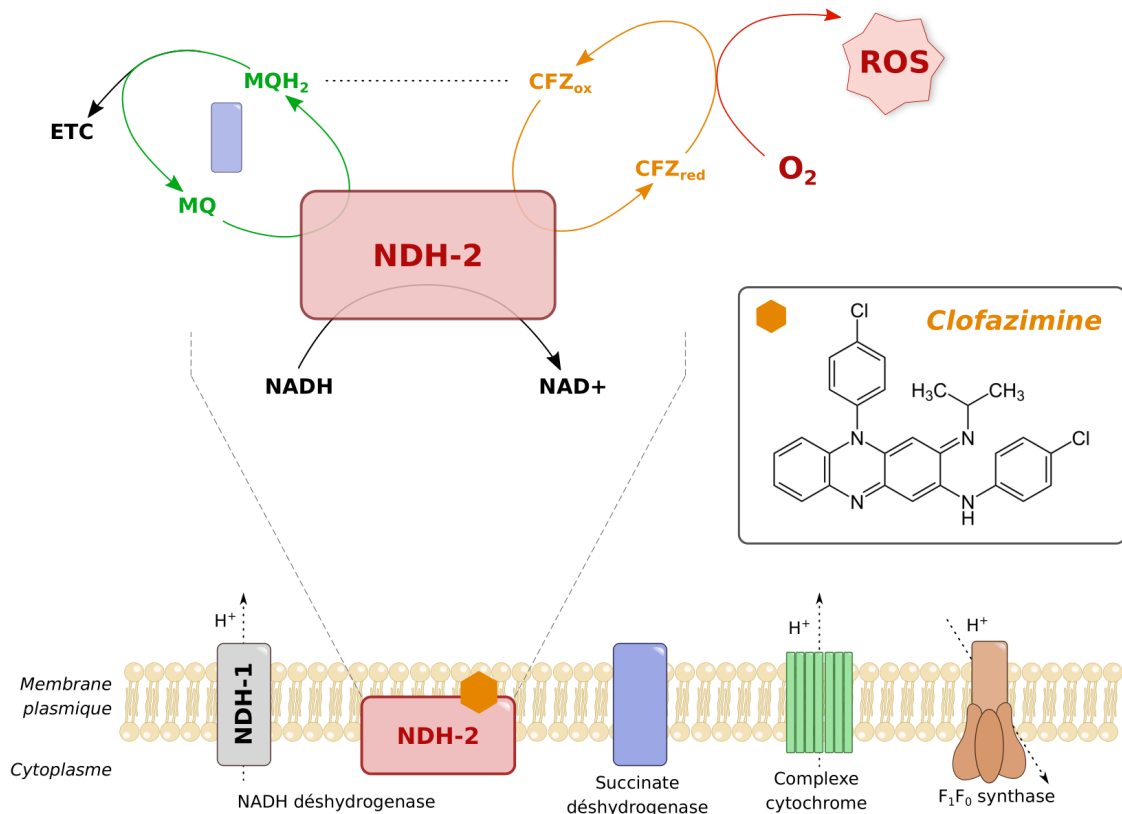
La chaîne respiratoire contient la NADH déshydrogenase NDH-1 qui permet la translocation de protons, tandis que NDH-2 ne transfère pas de protons, mais permet, tout comme la NDH-1, de déshydrogéner le NADH en NAD<sup>+</sup>. La succinate déshydrogenase permet l'oxydation du succinate en fumarate, ainsi que la réduction de la MQ en ménaquinol (MQH<sub>2</sub>).

Le complexe cytochrome, pompant des protons, contient les cytochromes bcc, aa3 et bd, et permet la réoxydation de la MQ.

La F<sub>1</sub>F<sub>0</sub> synthase est une ATP synthase permettant la synthèse d'ATP de par la rotation de l'anneau membranaire du domaine F<sub>0</sub>. Cette rotation est due au flux de protons, qui va *in fine* permettre de piéger l'ADP dans le domaine F1 qui sera ensuite phosphorylé en ATP.

MQ, ménaquinone ; MQH<sub>2</sub>, ménaquinol ; ETC, « electron transport chain » ; ROS, « reactive oxygen species », CFZ, clofazimine

Adapté de Foo CS-Y, *et al.* 2020, et Yano T, *et al.* 2011, [214,215].



Vincent Barry, initialement pour son activité antituberculeuse [216]. Ce n'est qu'en 1986 que Novartis reçoit l'approbation de la FDA pour sa production et son utilisation contre les infections à *M. leprae*, après qu'une étude ait prouvé son efficacité en combinaison avec la RIF et la dapsonne [217]. Toutefois, cette molécule, démontrant son activité sur *M. tuberculosis* est aujourd'hui utilisée dans le traitement des infections causées par des isolats multirésistants de ce pathogène [165,218,219] et peut entrer également dans la phase de prolongation des infections à *M. abscessus* [100,137] (**Figure 13**). Bien qu'il n'y ait pas d'évaluation franche et validée de l'activité de la CFZ en comparaison à d'autres antibiotiques du régime thérapeutique, cette molécule présente une très bonne activité *in vitro* sur différents isolats cliniques de *M. abscessus* [220]. De plus, la CFZ s'est montrée efficace dans différents cas cliniques, notamment des cas d'ostéomyélites de la mâchoire dues à *M. abscessus* [221] ou de péritonites infectieuses [222]. Puis l'ajout de la CFZ à un traitement antibiotique existant a permis une large amélioration des résultats thérapeutiques d'infections pulmonaires à *M. abscessus* [223]. Ces études illustrent la tolérance et la sûreté de cet antibactérien au sein du traitement actuellement utilisé, tout en apportant une valeur ajoutée dans un but d'éradication des infections persistantes. Cela démontre également les certaines synergies retrouvées au préalable *in vitro* avec d'autres antibiotiques tels que l'AMK, la CLR, la TGC ou encore plus récemment avec l'omadacycline [175,176,178,224,225].

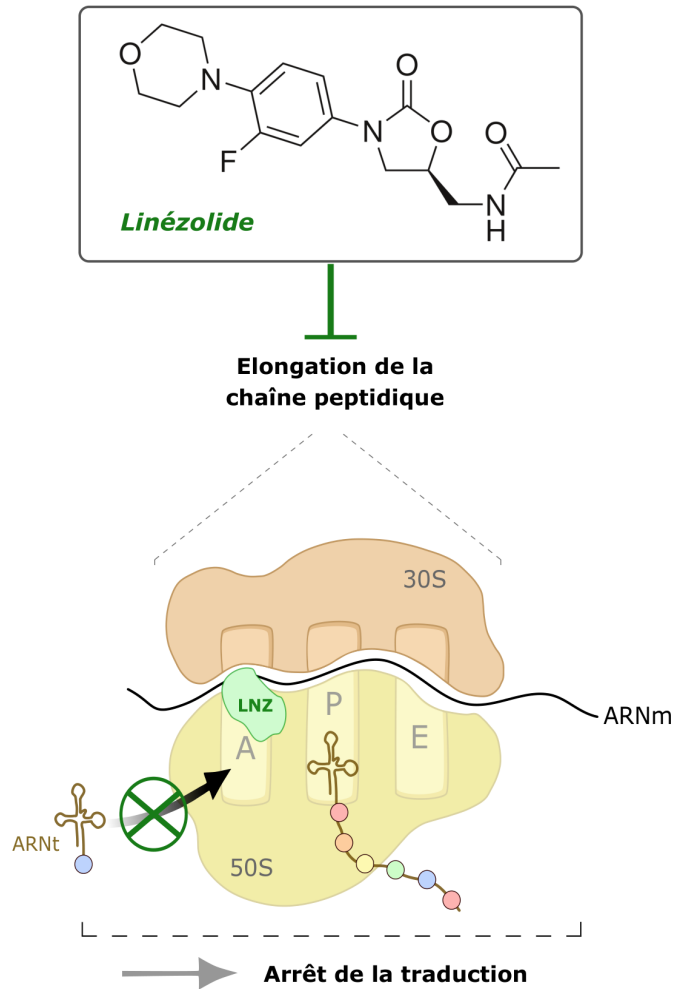
Le mode d'action de la CFZ n'est pas encore entièrement élucidé, et n'a pas encore été décrit chez *M. abscessus*. Néanmoins, des études suggèrent que la CFZ fonctionne principalement comme un pro-drogue chez *M. smegmatis* en étant réduite par la NADH:quinone oxydoréductase NDH-2, enzyme de la chaîne respiratoire bactérienne [215]. La CFZ rentre en compétition avec la ménaquinone (MQ), substrat de la NDH-2 chez *M. tuberculosis*, suggérant le même mécanisme d'action chez cette espèce [226]. Une oxydation spontanée par l'O<sub>2</sub> de la CFZ réduite permet ensuite la production de ROS, compromettant la survie de la bactérie [215,227] (**Figure 20**). Ce mode d'action basé sur la production de ROS peut expliquer pourquoi on ne retrouve que très peu d'isolats cliniques présentant des résistances à la CFZ, ce qui en fait une molécule très intéressante à développer dans les traitements antimycobactériens. Néanmoins, des études approfondies sur son mode d'action chez *M. abscessus* demeurent nécessaires dans un objectif de compréhension et d'approbation totale de ce composé.

### 1.6.2. Les oxazolidinones

Connue depuis la fin des années 1970, la classe des oxazolidinones, comprend notamment le LNZ. Ce dernier a été synthétisé au milieu des années 1990 sous le nom de U-100766 [228] et représente le premier membre de la famille des oxazolidinones rapidement approuvée en 2000 [229]. Cette

**Figure 21 : Structure et mode d'action du linézolide**

Le LNZ inhibe l'élongation de la synthèse protéique en se liant au site A de l'ARNr 23S au sein du site catalytique de la sous-unité ribosomale 50S, proche de la petite sous-unité 30S. La présence du LNZ perturbe l'arrivée de l'aminoacyl-ARNt, ce qui s'accompagne d'un arrêt de la synthèse protéique.



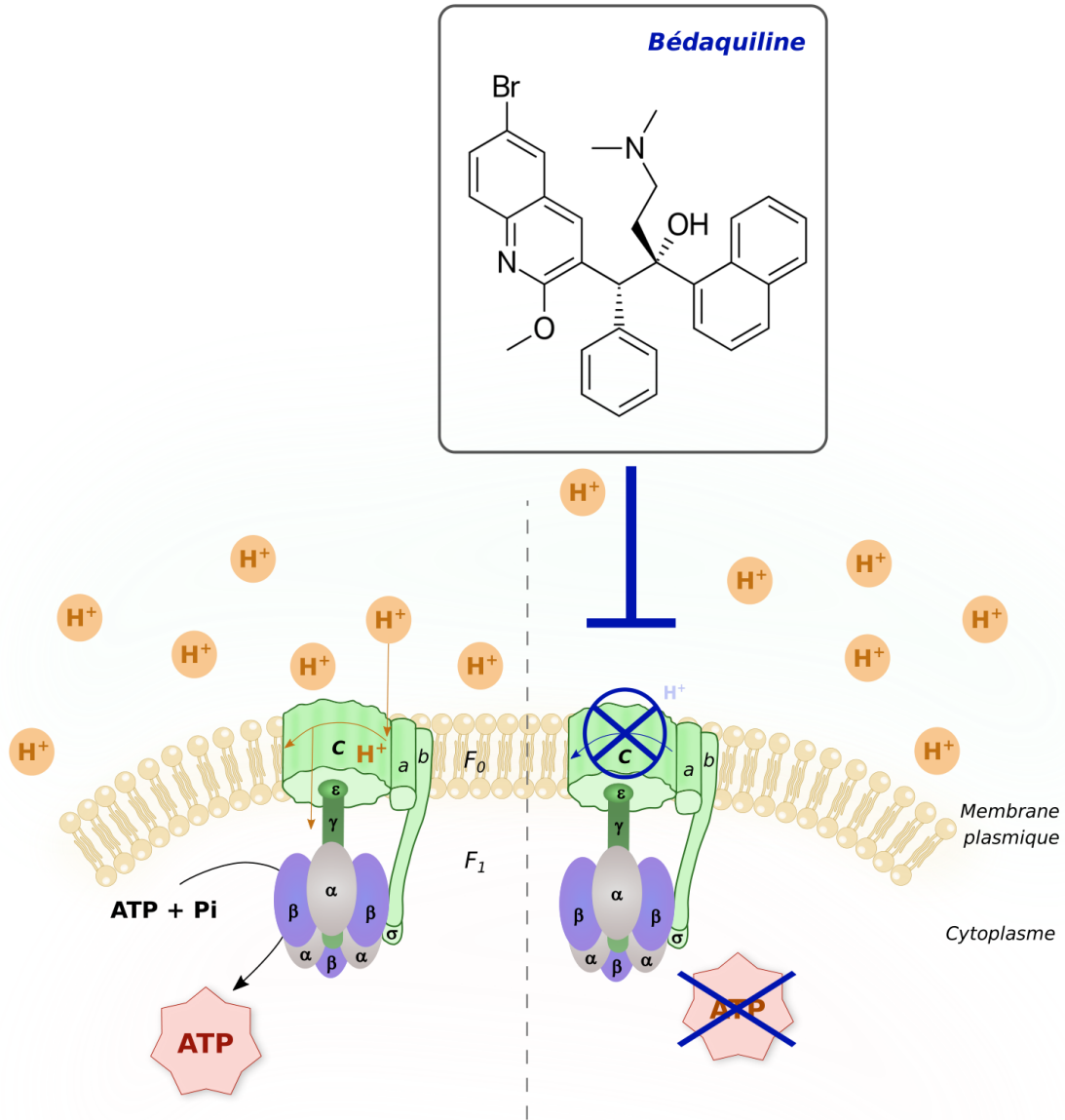
molécule présente un large spectre d'activité, avec notamment un effet sur des bactéries à Gram positive telles que *Enterococcus faecium*, *Staphylococcus aureus* ou encore *Streptococcus pyogenes* et *Streptococcus pneumoniae* [230]. L'étude originale de 1996 montre une très bonne activité *in vitro* contre *M. tuberculosis* avec des CMI inférieures à celles de l'INH [228]. Cette activité s'explique de par la présence du groupement N-aryl au centre et du groupement 5-acylaminométhyl [231] (**Figure 21**). Le LNZ présente de très bonnes propriétés pharmacocinétiques avec une bonne absorption après administration orale. Cet antibiotique synthétique inhibe la synthèse protéique comme de nombreuses autres classes d'antibiotiques. Plus particulièrement, cette inhibition est permise grâce à la liaison au niveau du site A proche du site catalytique de la sous-unité 50S du ribosome bactérien, à proximité de la petite sous-unité 30S, perturbant ainsi l'arrivée de l'aminocyl-ARNt [232–235] (**Figure 21**). La majorité des études sur le LNZ conduites envers ce genre bactérien montrent son activité *in vitro*, et sont principalement réalisées contre *M. tuberculosis*. Celles-ci présentent une bonne activité sur des isolats cliniques [236,237] ainsi qu'un bon effet chez les patients contre des infections multirésistantes à *M. tuberculosis* malgré les effets secondaires qu'engendre ce traitement [238]. Néanmoins, cette molécule peut être incluse dans les traitements contre *M. abscessus* (**Figure 13**) due à la très bonne activité du LNZ *in vitro* contre des souches cliniques de *M. abscessus* [204] et à son efficacité dans différents cas cliniques [239,240]. Cela peut s'expliquer *via* les synergies existantes entre le LNZ et d'autres antibiotiques tels que l'AMK, la TGC [177] ou la CLR [241]. Malheureusement le LNZ ne fait pas exception en termes d'effets indésirables dans le traitement des infections mycobactériennes [240]. Ainsi, des analogues structuraux du LNZ, tels que le tédizolide (TDZ) et la pro-drogue phosphate ester associée (TDZ phosphate) ont été conçus de façon à limiter ces effets délétères [242–244]. Le TDZ présente une meilleure activité *in vitro* que le LNZ contre *M. abscessus* [245,246], avec un effet bactériostatique sur les trois sous-espèces du complexe [247]. En outre, une synergie est retrouvée avec des antibiotiques classiquement inclus dans le régime thérapeutique comme l'AMK, la CLR ou l'IMP *in vitro* et dans un modèle macrophagique [248,249]. Ainsi, ces études suggèrent que le LNZ et particulièrement le TDZ pourraient représenter des molécules avantageuses à inclure dans le traitement des infections particulièrement difficiles à éradiquer.

### 1.6.3. Les diarylquinolines

Les diarylquinolines, notamment la bédaquiline (BDQ) sont également positionnées dans les recommandations au traitement des infections à *M. abscessus*. La BDQ a vu le jour dans les années 2000 sous le nom de R207910, ou encore TMC207, dans le cadre du traitement de la tuberculose [250]. La première mention de cette molécule de synthèse date de 2004 par des chercheurs de la compagnie

**Figure 22 : Structure et mode d'action de la bédaquiline**

La diarylquinoline de synthèse (BDQ) inhibe la synthèse métabolique d'ATP chez *M. abscessus*. La BDQ vient cibler les sous-unités *c* de la  $F_0F_1$  ATP synthase mycobactérienne qui va ainsi empêcher la rotation de l'anneau transmembranaire indispensable à la force motrice et donc au transfert de protons nécessaire à la synthèse d'ATP.



Johnson & Johnson, et un fort engouement est rapidement apparu avec les premières descriptions de ce composé [251–253]. La molécule s'est avérée être très efficace sur des souches multirésistantes de *M. tuberculosis in vitro* tout en présentant de bons paramètres pharmacocinétiques et pharmacodynamiques chez la souris mais aussi chez l'Homme avec une bonne absorption [251]. Ces données expliquent pourquoi la BDQ a été le premier antibiotique validé par la FDA depuis plus de 40 ans dans le traitement de la tuberculose multirésistante aux antibiotiques [254]. Par la suite, sa très bonne activité *in vitro* contre de nombreux isolats cliniques du complexe *M. abscessus* a été montrée [220,255], et le repositionnement de molécules antituberculeuses représente une option intéressante et rapide dans le développement de molécules efficaces contre *M. abscessus* [256]. Ainsi, la BDQ a un effet bactériostatique sur *M. abscessus* et présente une haute efficacité dans un modèle d'infection de macrophages [257] ainsi que dans un modèle d'infection chez le poisson-zèbre [258]. Par ailleurs, une étude de cas présente l'efficacité de la BDQ dans le traitement d'une ostéomyélite causée par *M. abscessus* en association avec d'autres antimycobactériens, notamment la CFZ [259]. La BDQ présente un mécanisme d'action unique et différent de celui des autres antimycobactériens en bloquant la production d'ATP, molécule vitale et source d'énergie nécessaire à toute cellule, en ciblant la F<sub>0</sub>F<sub>1</sub> ATP synthase mycobactérienne. Plus particulièrement, elle se fixe sur les sous-unités c de l'ATP synthase, codées par le gène *atpE*, qui forment l'anneau transmembranaire nécessaire au transfert de protons permettant la synthèse métabolique d'ATP pour la mycobactérie [253,258] (**Figure 22**). Enfin, l'ajout de la BDQ dans le régime thérapeutique contre les infections à *M. abscessus* est également attrayant de par les synergies retrouvées. Une activité synergique a été mise en évidence lorsqu'elle est combinée à la RFB aussi bien sur des populations bactériennes en croissance qu'en dormance [260]. On retrouve également une combinaison favorable *in vitro* entre la BDQ, les oxazolidinones tels que le LNZ ou le TDZ [261] ou encore avec la CFZ [262]. Enfin, des résultats contradictoires concernent l'IMP où certains groupes présentent une certaine synergie *in vitro* ou dans un modèle d'infection murin [263] alors que d'autres montrent un effet antagoniste [264].

L'ensemble de ces données démontrent que la BDQ est un antibiotique intéressant à prendre en considération dans les traitements difficiles à *M. abscessus*, néanmoins des études poussées sur les interactions médicamenteuses et le développement d'analogues doivent être entreprises.

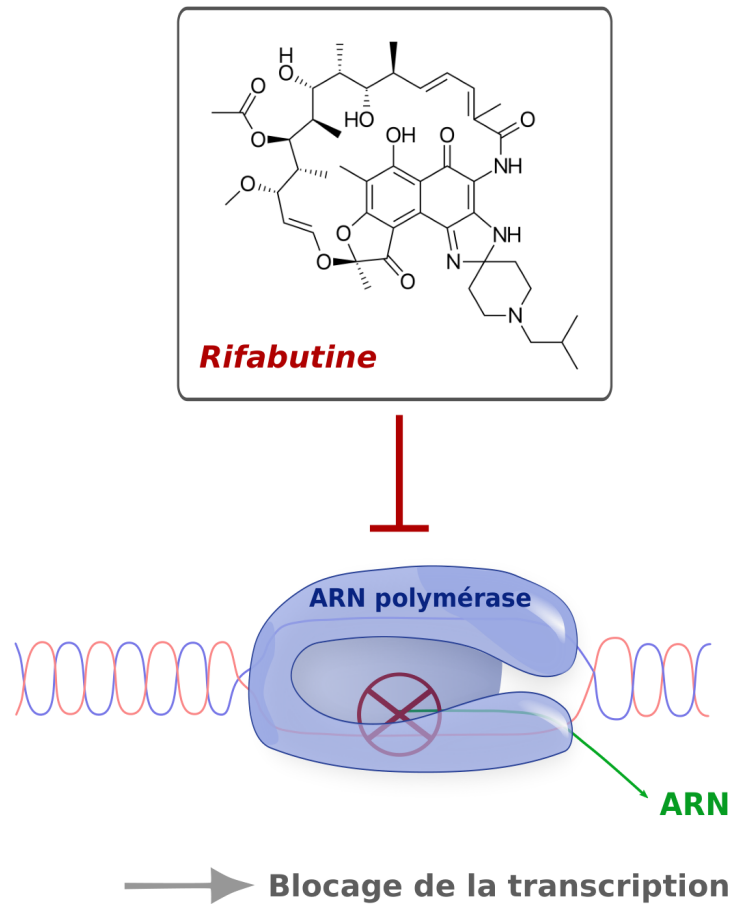
### 1.6.1. Les autres classes d'antibiotiques

Il existe d'autres classes d'antibiotiques qui apparaissent ou sont repositionnées contre *M. abscessus* et qui présentent un fort intérêt dans le traitement de ses infections persistantes. Ces antibiotiques ne sont pas conventionnellement inclus dans le régime thérapeutique mais pourraient se positionner



**Figure 23 : Structure et mode d'action de la rifabutine**

La RFB, en ciblant les sous-unités  $\beta$  de l'ARN polymérase, inhibe la synthèse d'ARN par cette enzyme à partir de l'ADN. Ainsi, la transcription de l'ADN mycobactérien est bloquée engendrant des effets dommageables irréversibles chez *M. abscessus*.



comme alternatives possibles lors d'un échec thérapeutique [265].

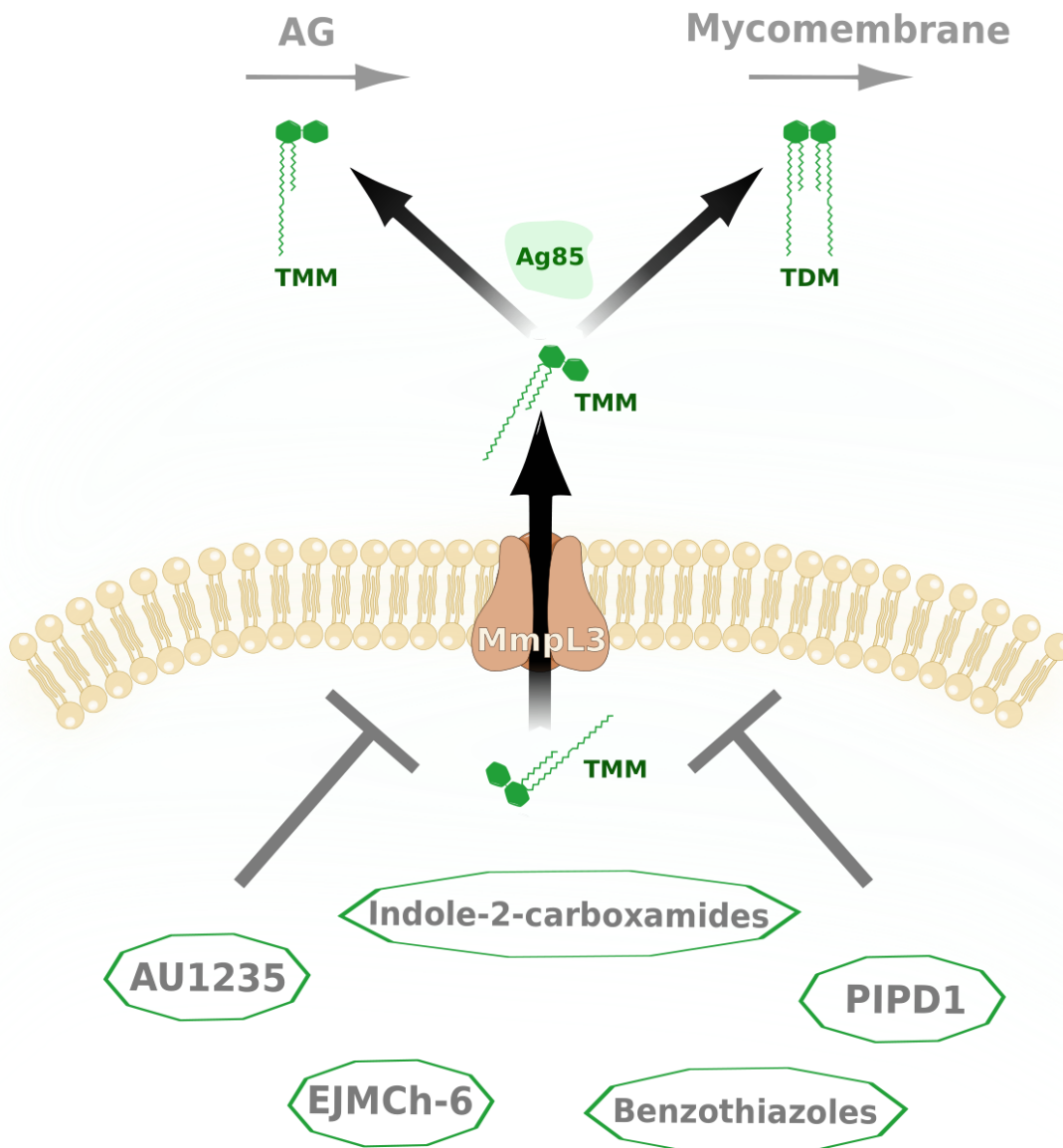
La RIF et ses dérivés, notamment la RFB qui, contrairement à la RIF utilisée contre *M. tuberculosis*, présente une activité sur le complexe *M. abscessus* [266]. Cette molécule est active *in vitro* sur de nombreux isolats cliniques [267], aussi bien dans des modèles d'infections de macrophages que dans des modèles murins [248,268]. De plus, la RFB exerce une activité synergique avec d'autres antibiotiques du régime thérapeutique classique, tels que l'IMP [159,248], la TGC ou la CLR [195]. En outre, la RFB est déjà approuvée par la FDA dans le traitement de la tuberculose, et peut donc facilement être repositionnée dans le traitement des infections à *M. abscessus* [269]. S'ajoutant aux synergies retrouvées, la RFB présente l'avantage d'un mécanisme d'action distinct de celui des autres classes d'antibiotiques. En effet, elle inhibe l'ARN polymérase, et plus particulièrement la sous-unité  $\beta$  codée par le gène *rpoB*, engendrant un arrêt de la transcription (**Figure 23**). Enfin, des dérivés de RIF et de RFB ont été synthétisés afin de contrecarrer les mécanismes de résistance qu'a *M. abscessus* contre cette classe d'antibiotiques, notamment par la modification des groupements en C25 et présentent un intérêt tout particulier dans le traitement de ce pathogène opportuniste [270,271].

Une autre classe de molécules plus récente et de plus en plus étudiée est basée sur les inhibiteurs de MmpL3. Cette protéine mycobactérienne est un transporteur transmembranaire de la famille des RND (Resistance-Nodulation-Cell Division) et permet le transport à travers la membrane des tréhalose monomycolates (TMM) [272,273] (**Figure 24**). Ces TMM serviront de substrats à l'antigène 85 (Ag85) pour estérifier l'arabinogalactane (AG) ou pour la synthèse de tréhalose dimycolates (TDM) ancrés dans le feuillet externe de la mycomembrane (voir **Chapitre III : Paroi et acides mycoliques. 2.3. Transport et transfert à la paroi**). Le caractère essentiel de MmpL3 chez les mycobactéries, dont *M. abscessus*, en fait une très bonne cible à inhiber [274]. La première mention de cette classe d'antimycobactériens date de 2012 avec la mise en évidence de l'urée adamantyle AU1235 [275] qui présente une très bonne activité *in vitro* contre *M. abscessus* [276]. De nombreuses études s'en sont suivies décrivant d'autres inhibiteurs de MmpL3, qu'ils soient basés sur des criblages de molécules actives contre *M. tuberculosis* tels que le composé PIPD1, premier inhibiteur de MmpL3 décrit chez *M. abscessus*, [277,278] ou originalement synthétisés. Des familles chimiques distinctes peuvent inhiber ce transporteur, parmi celles-ci on retrouve de manière non exhaustive les dérivés de pipéridinol (PIP1), les indoles-2-carboxamides (Composé 6 et 12, IC5 et IC25) [279,280], les benzimidazoles (EJMCh-6) [281] ou encore les benzothiazoles (CRS400393) (voir **Discussion générale et Perspectives**) [282,283] (**Figure 25**).

Dans l'ensemble, le défi quotidien que représente le traitement antibiotique a dynamisé les études visant à proposer de nouvelles stratégies thérapeutiques, notamment *via* des alternatives aux antibiotiques qui suscitent de plus en plus d'intérêt dans la communauté scientifique.

**Figure 24 : Mode d'action et inhibition du transporteur MmpL3**

La protéine transmembranaire MmpL3 (Mycobacterial membrane protein Large 3) est un transporteur essentiel mycobactérien de la famille des RND (Resistance-Nodulation-Cell Division). Il permet le transport à travers la membrane plasmique des tréhalose monomycolates (TMM) qui serviront de substrat à l'antigène 85 (Ag85) pour estérifier l'arabinogalactane (AG), composé essentiel de la paroi mycobactérienne ou pour synthétiser le tréhalose dimycolate (TDM) qui sera ancré dans le feuillet externe de la mycomembrane. L'inhibition du transporteur MmpL3 *via* différentes classes de molécules engendre une accumulation de TMM dans le cytoplasme de la mycobactérie et l'absence d'acides mycoliques au niveau de l'AG étant délétère pour la bactérie.

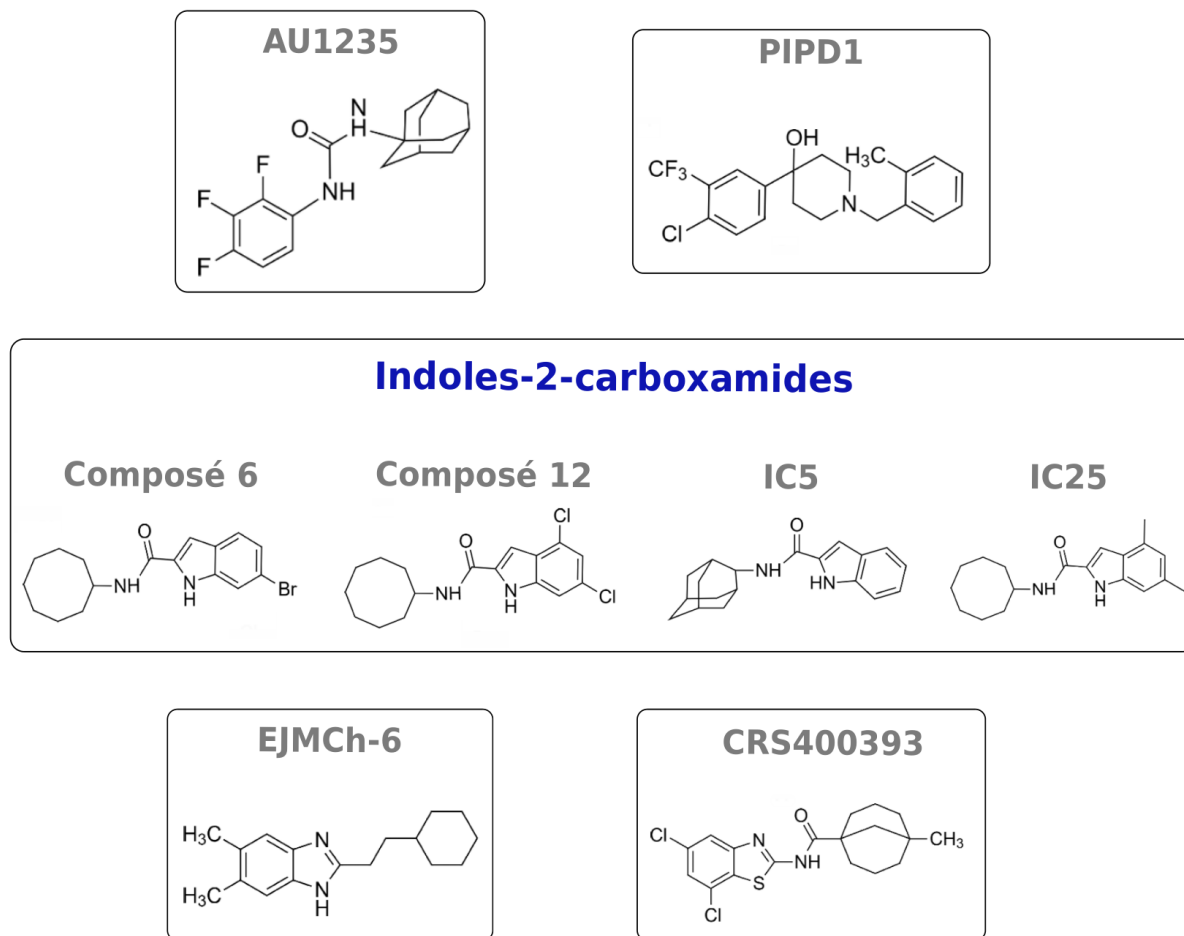


## 1.6.2. Les bactériophages : une alternative aux antibiotiques

Différentes alternatives aux antibiotiques peuvent être envisagées pour contrecarrer et éradiquer les infections à *M. abscessus* en contournant les mécanismes de résistance existant. Ainsi, cet objectif provoque un intérêt croissant notamment autour des mycobactériophages dans le traitement d'infections mycobactériennes [284]. Les bactériophages sont connus sous ce nom depuis plus d'un siècle avec leur première dénomination par Félix d'Hérelle [285] bien que d'autres avant lui aient décrit ces agents comme pouvant infecter et lyser les bactéries [286]. Les bactériophages sont des virus ubiquitaires de l'environnement infectant spécifiquement les bactéries. On peut les classer en deux types : les phages lysogéniques et les phages lytiques qui se différencient selon leur cycle d'infection [287,288] (**Figure 26**). Brièvement, ce cycle consiste en une phase d'adsorption à la bactérie, suivie de l'injection de l'ADN phagique qui peut mener à deux voies différentes. Les phages lysogéniques, ou tempérés, vont venir insérer leur ADN au sein du chromosome bactérien, ou en formant un plasmide, ce prophage est ainsi maintenu de manière stable au sein de la bactérie jusqu'au passage en phase lytique qui peut être induite par un stress. A l'inverse, les phages lytiques, présentant un intérêt dans un usage thérapeutique, vont eux se répliquer au sein de la bactérie, engendrer la lyse bactérienne et ainsi libérer de nombreux virions dans l'environnement extérieur pouvant à leur tour réinfecter d'autres bactéries du même type [289].

Les bactériophages rencontrèrent un succès notoire pendant l'entre-deux-guerres, mais sont rapidement tombés en désuétude avec l'arrivée en force des antibiotiques au cours du 20ème siècle et notamment de la pénicilline [148], bien qu'ils soient encore largement utilisés dans certains pays de l'Est, tels que la Géorgie [290]. Néanmoins, avec l'usage massif des antibiotiques, de nombreuses espèces multirésistantes ont vu le jour et ont engendré des infections persistantes difficiles à traiter. Ainsi, l'engouement autour des bactériophages s'est intensifié récemment, pour parer au besoin urgent de nouvelles thérapies et contourner le développement très long et coûteux de nouvelles classes d'antibiotiques [66]. Les succès observés dans différents cas cliniques utilisant des phages à titre compassionnel pour traiter des infections à *M. abscessus* rendent compte de ces efforts en matière de phagothérapie. Une première étude datant de 2019 décrit l'utilisation d'un cocktail de trois mycobactériophages modifiés génétiquement en association avec des antibiotiques pour traiter une infection disséminée à *M. abscessus* subsp. *massiliense* chez une patiente atteinte de mucoviscidose [291]. Ce traitement intraveineux a permis, de résoudre l'infection sans effets secondaires notoires et de permettre une amélioration du tableau clinique de la patiente sans pour autant éradiquer *M. abscessus*. Cette étude princeps a ouvert la voie à d'autres traitements personnalisés et compassionnels de patients infectés par *M. abscessus* ou *M. avium* avec une augmentation de l'état de santé chez environ 50% des patients traités par phagothérapie [292]. Néanmoins, le succès du

Figure 25 : Structures de différents inhibiteurs de MmpL3 décrits chez *M. abscessus*



traitement phagique peut être entravé par la production d'anticorps neutralisants chez certains patients [293,294]. Ainsi de nombreuses études doivent encore être menées sur l'action des bactériophages et leur association avec d'autres antibactériens afin de mieux comprendre leur rôle et leur place dans la médecine personnalisée du futur. Il est néanmoins peu probable que l'utilisation généralisée des bactériophages puisse remplacer les antibiotiques. Cependant, son utilisation pourrait tout de même constituer une aide précieuse contre des infections mycobactérienne multirésistantes [295].

## 2. Mécanismes de résistance aux antibiotiques chez *M. abscessus*

Le traitement des infections à *M. abscessus* est connu pour être très difficile et fréquemment associé à des impasses thérapeutiques, ce qui s'explique, entre autres, par la résistance accrue de cette bactérie à la plupart des antibiotiques. Ces mécanismes de résistance mis en jeu sont soit des mécanismes innés naturellement présents, soit acquis *via* des mutations au sein des gènes codant les cibles des antibiotiques [136].

### 2.1. Polymorphisme génétique et mutations acquises

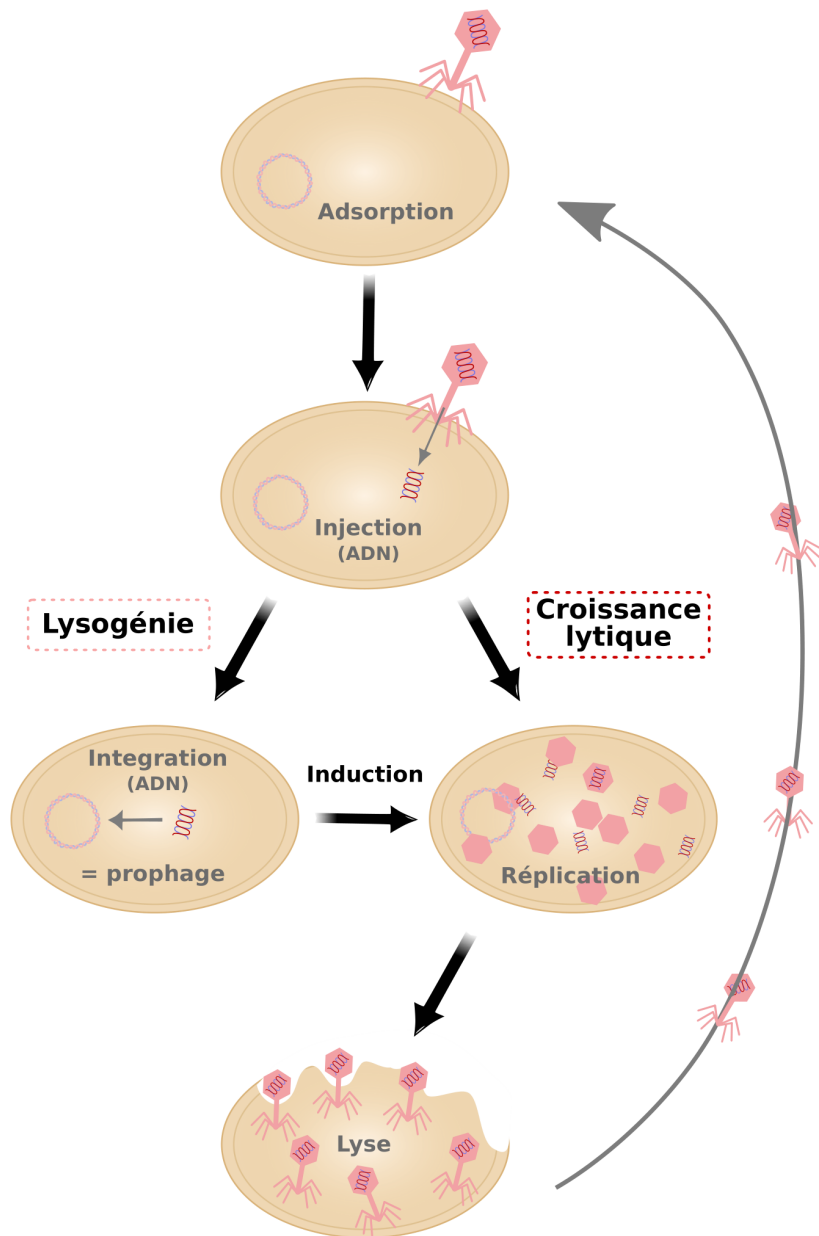
Le polymorphisme génétique retrouvé chez *M. abscessus* peut notamment expliquer la résistance intrinsèque aux antituberculeux de première intention.

Nous pouvons citer l'exemple de l'INH, antibiotique de première ligne dans le traitement de la tuberculose. Cette molécule inhibe l'énoyl-ACP-réductase *InhA* du complexe FAS-II de *M. tuberculosis*, impliquée dans la synthèse des acides mycoliques retrouvés à la paroi, grâce à sa bioactivation par la protéine *KatG* [296,297] (voir **Chapitre III : Paroi et acides mycoliques**, 3.2.1. Inhibiteurs indirects d'*InhA*). Or, chez *M. abscessus*, le gène *katG* diffère de celui de *M. tuberculosis* (74% d'identité), ce qui peut expliquer en quoi l'INH est totalement inopérant contre cette MNT [298]. Les enjeux causés par cette résistance et les limites de traitement engendrées feront notamment l'objet d'une partie des travaux de cette thèse.

Un second antituberculeux de première intention, l'EMB, présente une faible activité sur *M. abscessus* contrairement à *M. tuberculosis*. Cet antibiotique cible les trois arabinosyltransférases *EmbA*, *EmbB* et *EmbC* impliquées dans la synthèse de l'AG et du lipoarabinomannane (LAM), tous deux des composants majeurs de la paroi [299–301]. La résistance intrinsèque de *M. abscessus* à l'EMB s'explique notamment par des différences ponctuelles dans la séquence d'acides aminés de la région ERDR (*embB* resistance-determining region) de la protéine *EmbB* entre les deux espèces. *M. abscessus*

**Figure 26 : Cycle d'infection des bactériophages lytiques et lysogéniques**

Le cycle d'infection débute par l'adsorption du bactériophage à la membrane bactérienne suivie de l'injection de son matériel génétique. Deux voies différentes sont possibles selon la nature du phage : les phages lysogéniques ou tempérés, vont intégrer leur ADN au sein du génome bactérien (prophage) qui pourra être répliqué à chaque division bactérienne. Sous l'induction d'un stress, le génome phagique peut reprendre un cours lytique et grâce à l'utilisation des machineries transcriptionnelles et traductionnelles de la bactérie, le phage va pouvoir se multiplier activement, engendrant la lyse bactérienne et la libération de nombreux virions dans l'environnement extérieur, lesquels pourront alors infecter d'autres bactéries environnantes pour perpétuer le cycle lytique.



présente un résidu glutamine en position 303 à la place de l'isoleucine (I303Q) et une méthionine en position 304 au lieu d'une leucine (L304M), ce qui pourrait expliquer la résistance à l'EMB chez *M. abscessus* [136,302].

Un autre exemple de polymorphisme génétique est observé vis-à-vis de certaines fluoroquinolones. Des acteurs de cette classe d'antibiotiques ciblant les sous unités A et B de l'ADN gyrase (GyrA et GyrB) présentent une assez faible activité contre *M. abscessus* contrairement à d'autres pathogènes. Cela se traduit par les différences nucléotidiques et protéiques présentes chez *M. abscessus*, principalement au niveau de l'acide aminé 83 de GyrA, un résidu critique pour la résistance aux fluoroquinolones, où la sérine est remplacée par une alanine chez les espèces résistantes [303]. Au sein de GyrB, les résidus lysine 447 et sérine 464, sont respectivement remplacés chez les mycobactéries par une arginine et une asparagine. Ces éléments expliquent, du moins en partie, le niveau de résistance de *M. abscessus* aux fluoroquinolones en comparaison à *Escherichia coli* ou d'autres bactéries sensibles à ces composés [303,304].

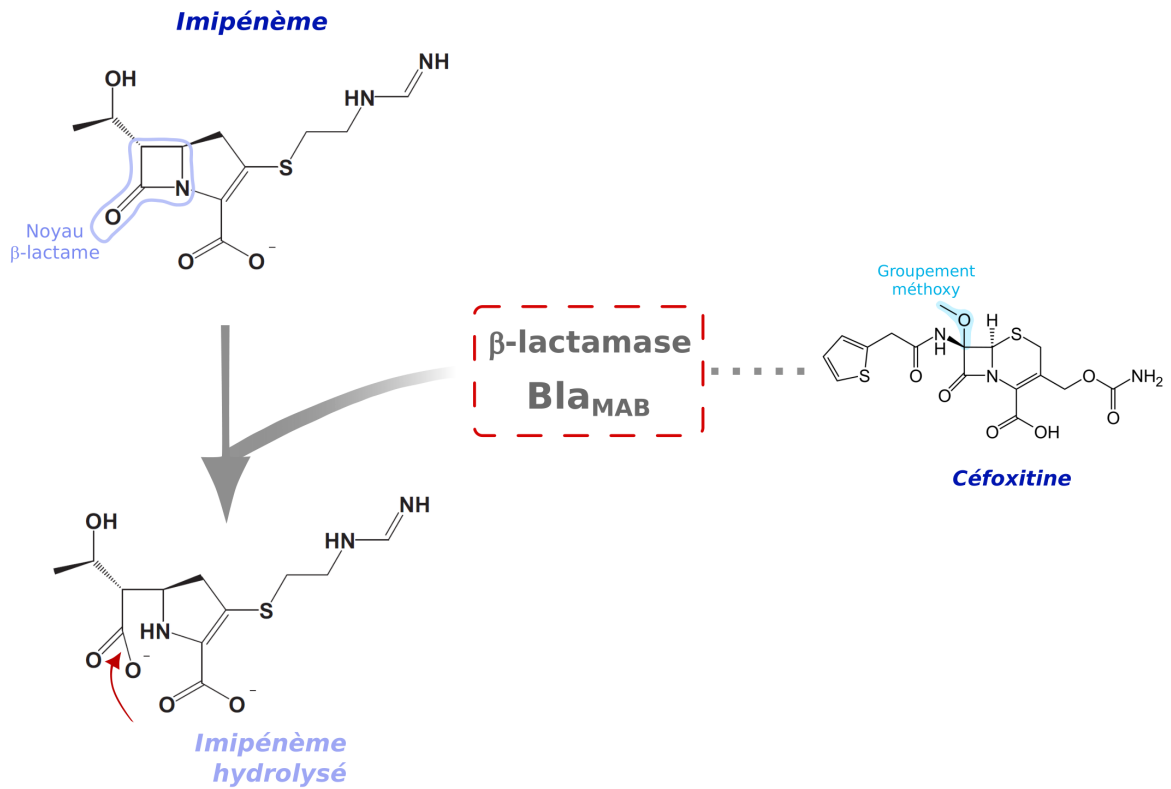
Des mutations chromosomiques spontanément acquises peuvent également être observées après une exposition à des concentrations trop faibles en antibiotiques. Par ailleurs, l'émergence de résistances peut également résulter d'une mauvaise observance du traitement et de la pression de sélection exercée par le traitement antibiotique chez certains patients. Les populations bactériennes sensibles vont être les premières à être éliminées tandis que les quelques bacilles résistants vont perdurer, se multiplier et prendre le dessus si le traitement n'est pas correctement poursuivi jusqu'à son terme. Cette domination de souches résistantes peut conduire à l'échec thérapeutique que l'on connaît chez *M. abscessus*.

Concernant les macrolides (AZM et CLR), certaines mutations apparaissent au sein du gène *rrl* codant l'ARNr 23S et plus particulièrement au niveau des adénines A2058 et A2059 de la région peptidyltransférase du gène de l'ARNr 23S [305,306] conférant un niveau élevé de résistance aux macrolides [307]. Des mutations au niveau de la guanine G2659 de *rrl* peuvent également être retrouvées chez des souches résistantes au LNZ [235]. Néanmoins, dans le cas des macrolides, ces événements restent assez rares, car sont souvent masqués par la présence d'un autre mécanisme de résistance inductible aux macrolides impliquant Erm41 une « erythromycin ribosome methyltransferase » [43] (voir **Chapitre II : Antibiothérapie et mécanismes de résistance aux antibiotiques chez *M. abscessus***, 2.3. Enzymes protégeant la cible des antibiotiques : Erm41). La pression de sélection va être supérieure si cette protéine n'est pas fonctionnelle pouvant entraîner davantage de mutations au sein de *rrl*, ce qui est notamment le cas chez la sous-espèce *M. massiliense* qui présente une protéine Erm41 tronquée [308].



**Figure 27 : Mécanisme d'hydrolyse de l'imipénème par la  $\beta$ -lactamase Bla<sub>MAB</sub>**

La  $\beta$ -lactamase Bla<sub>MAB</sub> de *M. abscessus* hydrolyse l'IMP au niveau de son noyau  $\beta$ -lactame (flèche rouge). Le groupement méthoxy de la CFX protège cet antibiotique de l'hydrolyse par Bla<sub>MAB</sub>. Adapté de Zhai L, *et al.* 2012, [309].



De nombreux experts recommandent d'utiliser l'AMK comme alternative lors d'une résistance aux macrolides. Néanmoins, des mutations spontanées sont également retrouvées au niveau du gène *rrs*, codant la sous-unité 16S du ribosome, cible des aminoglycosides dont l'AMK. On peut noter majoritairement la substitution du résidu alanine en position 1374 (A1408 selon la numérotation faite chez *E. coli*) qui engendre une importante résistance à l'AMK ainsi qu'à d'autres aminoglycosides [310,311]. D'autres mutations au sein du gène *rrs* ont également été mises en évidence, telles que les substitutions T1406A, A1408G, C1409T ou encore G1491T (numérotation *E. coli*) [136,312,313]. Ces résidus sont nécessaires pour la bonne liaison de l'antibiotique à l'ARNr 16S expliquant les forts taux de résistance retrouvés en cas de mutations à ce niveau.

Bien que ces exemples restent les plus relatés, l'ensemble des cibles des antibiotiques peuvent spontanément muter engendrant une inefficacité des antibiotiques du régime thérapeutique.

## 2.1. Enzymes modifiant / inactivant les antibiotiques

Les mécanismes de résistance les plus courants chez *M. abscessus* sont en lien avec une pléthore d'enzymes capables de modifier ou inactiver chimiquement les antibiotiques pour les rendre inopérants [145].

### 2.1.1. $\beta$ -lactamines

Le résistome de *M. abscessus* contient une seule enzyme identifiée permettant de cibler et hydrolyser les  $\beta$ -lactamines. Celle-ci est codée par le gène *MAB\_2875* et représente la  $\beta$ -lactamase de classe A  $Bla_{MAB}$ . Cette enzyme à large spectre peut hydrolyser efficacement plusieurs membres des  $\beta$ -lactamines tels que les carbapénèmes, les pénicillines ou les céphalosporines [314]. La  $\beta$ -lactamase  $Bla_{MAB}$  agit sur le noyau  $\beta$ -lactame de cette classe d'antibiotiques ce qui permet leur dégradation et une certaine résistance de *M. abscessus* à ceux-ci (**Figure 27**). Il est intéressant de noter que la CFX, une des  $\beta$ -lactamines utilisée dans le traitement clinique de *M. abscessus*, n'est quasiment pas hydrolysée par  $Bla_{MAB}$  ce qui justifie son utilisation actuelle [314]. Cela peut s'expliquer par le groupement méthoxy arborée par la CFX et qui altère la fonction d'hydrolyse de  $Bla_{MAB}$  en bloquant l'acylation de l'enzyme [314,315]. De plus, cette  $\beta$ -lactamase n'hydrolyse que très lentement l'IMP, expliquant également son efficacité certaine dans le traitement clinique de *M. abscessus*.

Afin de contrecarrer l'effet des  $\beta$ -lactamases telles que  $Bla_{MAB}$ , de nombreux inhibiteurs de ces enzymes ont vu le jour. L'avibactam, développée par Actavis et AstraZeneca, est un inhibiteur réversible de  $Bla_{MAB}$ . Son ajout *in vitro* permet de faire baisser les CMI de l'IMP, de la CFX et d'autres  $\beta$ -lactamines. De plus, cette molécule permet aussi une activité supérieure de  $\beta$ -lactamines au sein de

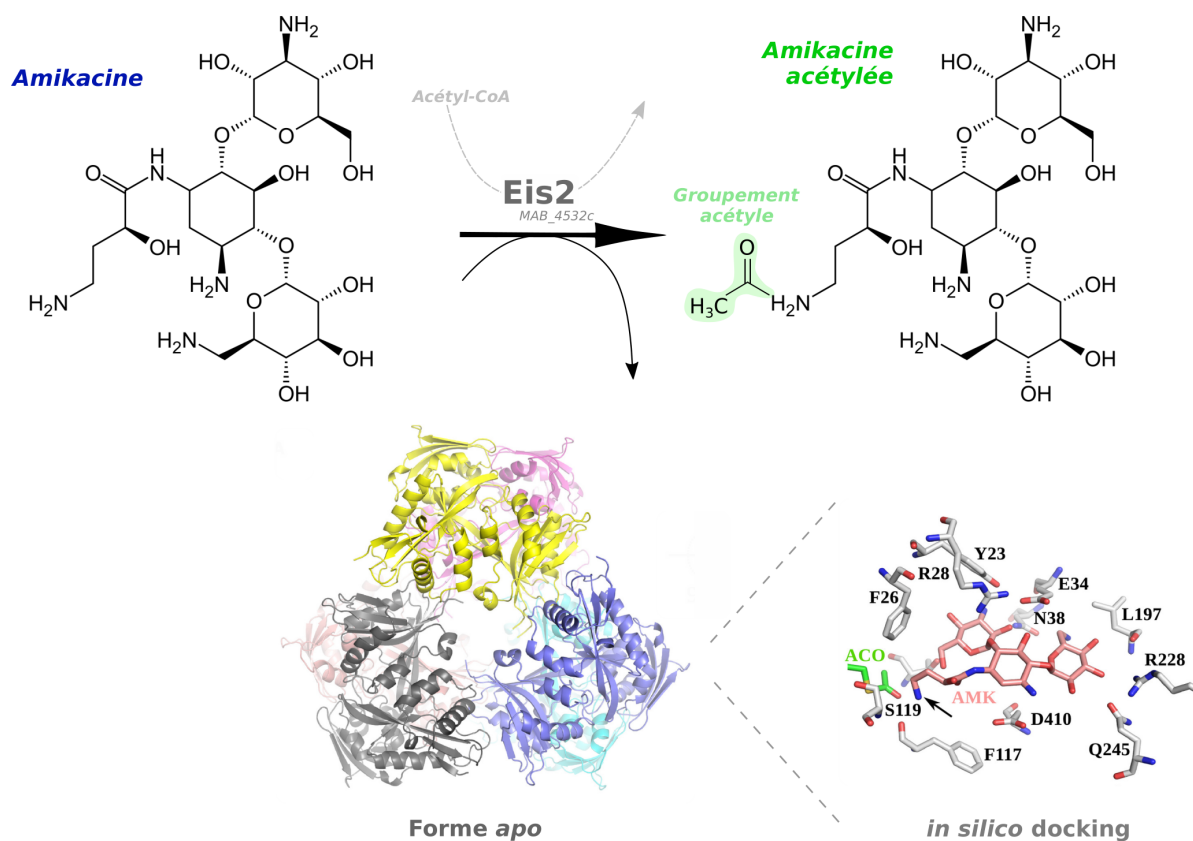
### Figure 28 : Inactivation enzymatique de l'amikacine par l'acétyltransférase Eis2 et sa structure cristallographique

Eis2 modifie directement l'AMK en transférant un groupement acétyle (vert) d'une molécule d'acétyl-CoA sur le premier groupement amine situé en 2' de l'AMK.

Représentation de la forme *apo* de l'enzyme Eis2, sans substrat. La structure est composée de deux trimères superposés, chaque monomère contient 16 feuillets  $\beta$  et 11 hélices  $\alpha$ .

Représentation *in silico* du docking de l'AMK au sein de la poche de liaison d'Eis2 liée à l'acétyl-CoA (ACO). Les résidus majeurs interagissant avec l'AMK *via* des liaisons hydrogènes sont : Y23, F26, R28, E34, N38, F117, S119, L197, R228, Q245 et D410.

Adapté de Ung KL, *et al.* 2019, [316]



macrophages infectés, dans un modèle d'infection *in vivo* de poisson zèbre [317] ou encore dans un modèle murin d'infections pulmonaires à *M. abscessus* [318]. En augmentant l'efficacité des  $\beta$ -lactamines, l'avibactam ouvre la voie vers de nouvelles approches thérapeutiques associant antibiotiques et inhibiteurs enzymatiques, néanmoins la formulation actuelle de l'avibactam associé à la ceftazidime qui n'a pas d'activité contre *M. abscessus* ne permet pas encore son utilisation en clinique [319]. Ainsi, d'autres inhibiteurs des  $\beta$ -lactamases ont émergés, tels que le relebactam [320], le vaborbactam [321], le nacubactam ou encore le zidebactam [322]. Tous montrent un effet lorsqu'ils sont combinés avec différentes  $\beta$ -lactamines, telle que l'IMP. Enfin, il a été suggéré de remplacer l'IMP seul par l'association IMP-relebactam dans le régime thérapeutique actuel des infections à *M. abscessus* [319]. Ainsi, ces études démontrent qu'il est important d'envisager de nouvelles associations thérapeutiques pour contrer les résistances de la bactérie et d'optimiser les traitements.

### 2.1.2. Aminoglycosides

*M. abscessus* produit également des enzymes capables de modifier les aminoglycosides conférant une certaine résistance à l'AMK. Il existe notamment deux acétyltransférases (Eis2 -Enhanced Intracellular Survival 2- et AAC(2') -Aminoglycoside 2'-Acétyltransférase-) et une phosphotransférase (APH(3'')) capables de neutraliser ces molécules [145]. La modification chimique des aminoglycosides va empêcher la liaison à l'ARN ribosomal en diminuant leur affinité et donc entraver leur activité.

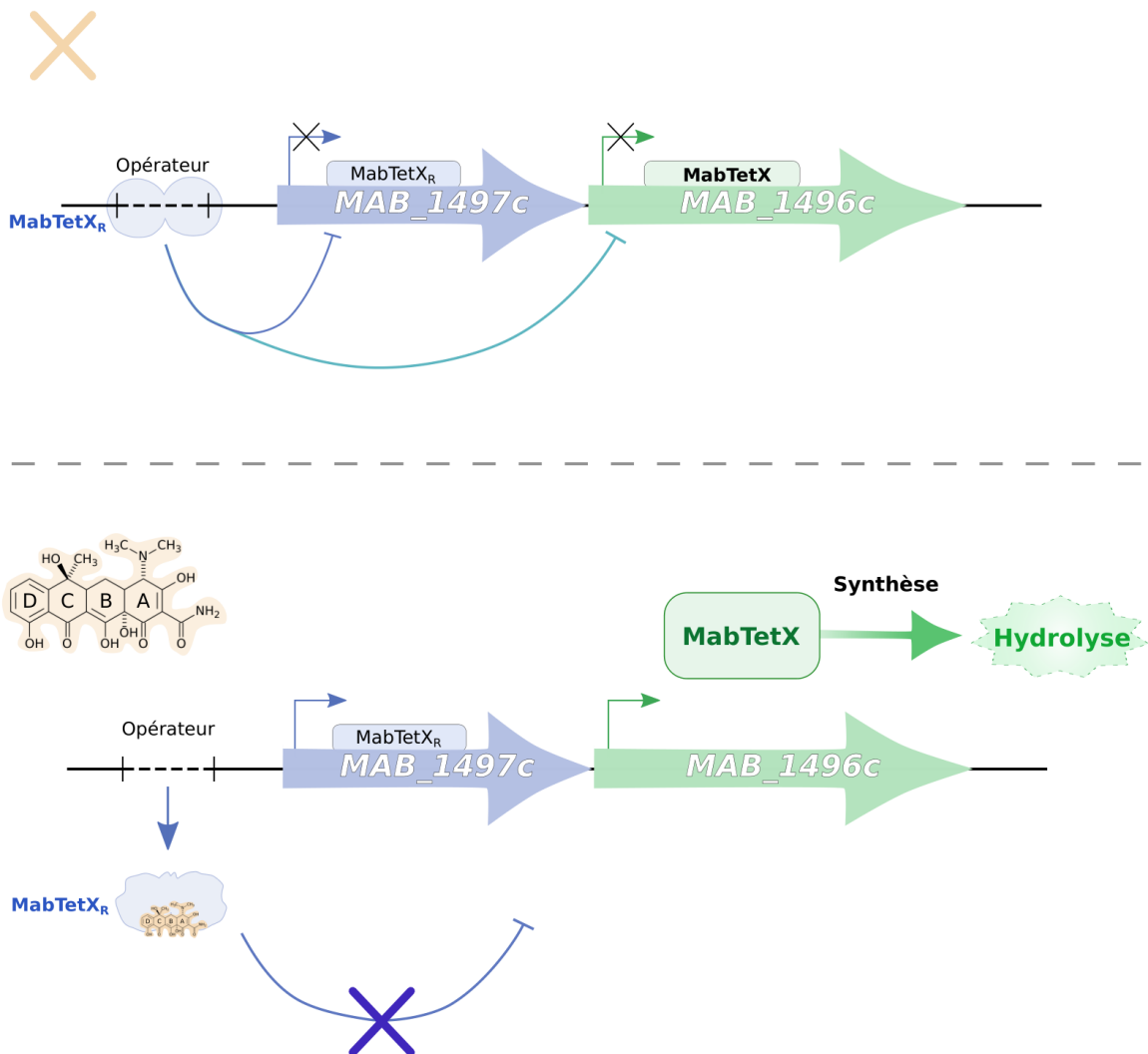
AAC(2') codée par le gène *MAB\_4395* est capable d'acétyler le groupement amine situé en position 2' [323] de certains aminoglycosides, tels que la KAN B, la dibékacine, la tobramycine ou encore la gentamicine C [324]. Similairement, Eis2 codée par le gène *MAB\_4532c* va venir acétyler le premier groupement amine de différents aminoglycosides tels que la KAN B, la capréomycine, l'hygromycine B ou l'AMK ce qui va augmenter la résistance à ces composés (**Figure 28**) [316,324]. Globalement, l'inactivation des gènes *MAB\_4395* ou *MAB\_4532c* codant ces acétyltransférases engendre une sensibilité accrue de *M. abscessus* aux aminoglycosides, démontrant le rôle crucial de ces enzymes dans la résistance à cette classe de molécules [324].

Une autre famille d'enzymes modifiant les aminoglycosides comporte la 3''-O-phosphotransférase codée par le gène *MAB\_2385*. Parmi les douze phosphotransférases d'aminoglycosides codées par *M. abscessus* [325], la 3''-O-phosphotransférase est responsable de la résistance à la streptomycine [326] tout comme son proche homologue APH(3'')-Ic chez *M. fortuitum* [327]. Néanmoins, d'autres phosphotransférases d'aminoglycosides (*MAB\_0163c*, *MAB\_0313c*, *MAB\_0327*, *MAB\_0951*, *MAB\_1020*, *MAB\_3637c*, *MAB\_4910c* ou *MAB\_4395*) et d'autres acétyltransférases d'aminoglycosides (*MAB\_0247c*, *MAB\_0404c*, *MAB\_0745*, *MAB\_4235c*, et *MAB\_4324c*) potentielles n'ont pas encore été

**Figure 29 : Mécanisme de résistance à la tétracycline via la monooxygénase FAD-dépendante MabTetX**

Le gène *MAB\_1496c* code pour la monooxygénase FAD-dépendante MabTetX permettant d'hydrolyser la tétracycline et certains de ses dérivés comme la doxycycline. L'expression de cette enzyme est régulée par le répresseur transcriptionnel MabTetX<sub>R</sub> de la famille des régulateurs TetR. Ce dernier va venir se lier sur la séquence d'ADN en amont de son gène *MAB\_1497c* (opérateur) engendrant l'inhibition de sa propre expression et celle de MabTetX.

La présence de tétracyclines va engendrer un changement conformationnel du répresseur permettant la synthèse de MabTetX qui pourra hydrolyser l'antibiotique.



étudiées mais leur forte homologie de séquence avec les protéines citées précédemment laissent à penser qu'elles peuvent également participer à la résistance contre certains aminoglycosides [136,145,328]. Des études biochimiques et structurales approfondies de ces enzymes modifiant les aminoglycosides pourraient ouvrir la voie sur le développement de nouveaux inhibiteurs spécifiques pouvant contourner ces mécanismes de résistance intrinsèques.

### 2.1.3. Tétracyclines

Bien qu'efficace contre *M. tuberculosis*, la famille des tétracyclines présente assez peu d'efficacité sur *M. abscessus*. En effet, ce pathogène opportuniste exprime une monooxygénase FAD (Flavine Adénine Dinucléotide)-dépendante, la MabTetX, codée par le gène *MAB\_1496c* [184]. Cette enzyme permet d'hydrolyser la tétracycline et la DOX chez *M. abscessus*. De plus, la délétion du gène *MAB\_1496c* rend la bactérie extrêmement sensible à ces antibiotiques, démontrant l'importance de cette protéine sur la résistance intrinsèque de *M. abscessus*. L'expression de MabTetX est régulée par le répresseur transcriptionnel MabTetX<sub>R</sub> codé par le gène *MAB\_1497c*, appartenant à la superfamille des régulateurs TetR [184]. Ce répresseur va réprimer sa propre expression ainsi que celle de MabTetX en absence de son ligand, les tétracyclines, en se liant en dimères à des séquences inversées répétées (opérateurs) en amont de la région promotrice de l'opéron *MAB\_1497c/MAB\_1496c* (**Figure 29**). À l'inverse, en présence de tétracycline, un changement conformationnel du régulateur MabTetX<sub>R</sub> permettra la dissociation du répresseur au niveau de la région opératrice, permettant la levée de la répression et l'expression de MabTetX. La TGC, glycylicycline inclus dans le traitement de *M. abscessus*, est la seule tétracycline qui n'est pas un substrat de MabTetX et qui n'est donc pas impactée par la monooxygénase MabTetX. La modification structurale au niveau de la partie hydrophobe de la TGC désignée par le cycle D via l'ajout d'une chaîne 2-tert butylglycylamido rend incapable l'expression de MabTetX ce qui lui permet de résister à ce mécanisme d'inactivation enzymatique intrinsèque [184].

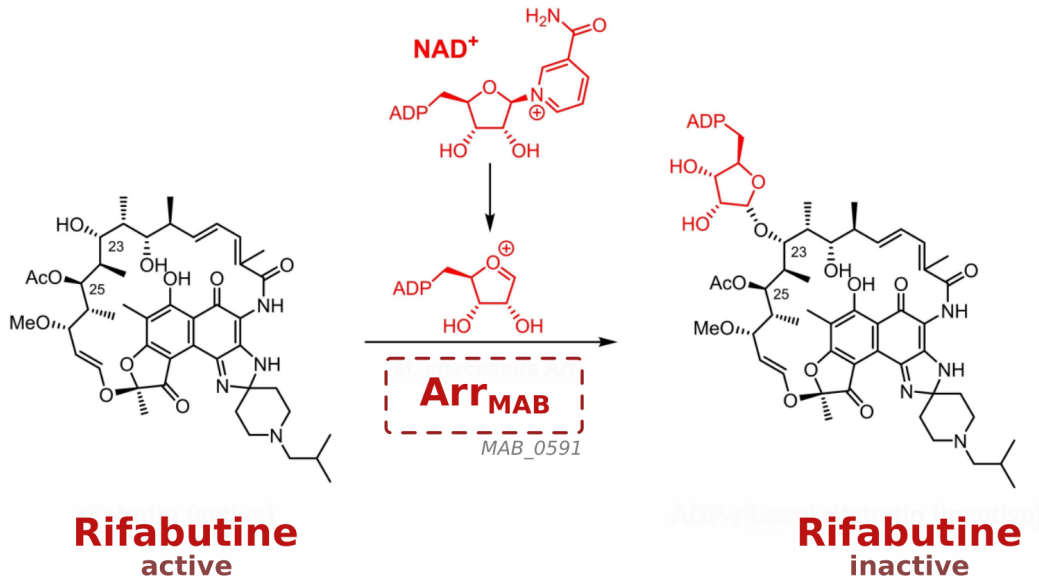
### 2.1.4. Rifamycines

La résistance intrinsèque de *M. abscessus* aux rifamycines telles que la RIF et la rifapentine (RFP) s'explique par différents mécanismes. Ces molécules sont sensibles à l'auto-oxydation intra- ou extracellulaire en présence d'oxygène et de cations métalliques divalents en lien avec leur motif hydroquinone [269,329]. À l'inverse, la RFB n'est pas sujette à l'auto-oxydation, ce qui explique son activité antibactérienne contre *M. abscessus*.

De plus, le mécanisme principal d'inactivation réside dans la présence de l'ADP-ribosyltransférase

**Figure 30 : Inactivation de la rifabutine par Arr<sub>MAB</sub>**

La RFB est inactivée chez *M. abscessus* grâce à la présence de l'ADP-ribosyltransférase Arr<sub>MAB</sub> codée par le gène *MAB\_0591*. Cette enzyme catalyse la formation d'un intermédiaire ADP-ribosyl-oxocarbénium de NAD<sup>+</sup> ainsi que l'ADP-ribosylation sur le groupement OH positionnée en C23 de la RFB.



Arr<sub>MAB</sub> codée par le gène *MAB\_0591* [325,330]. La délétion génétique de ce gène chez *M. abscessus* entraîne une activité *in vitro* plus de 100 fois supérieure de la RIF par rapport à la souche parentale. L'enzyme Arr<sub>MAB</sub> catalyse l'ADP-ribosylation du groupement hydroxyle sur le C23, rendant ainsi inactive la RIF [269,331]. Un autre mécanisme potentiel est basé sur le fait que *M. abscessus* exprime des homologues de monooxygénases FAD-dépendantes, notamment de la famille des Rox qui inactivent les rifamycines chez d'autres bactéries [332]. Néanmoins, il reste à déterminer si *M. abscessus* possède réellement cette activité monooxygénase envers les rifamycines.

Bien que la structure de la RFB permette de contourner l'auto-oxydation, cet antibiotique peut être ADP-ribosylé par Arr<sub>MAB</sub> comme les autres rifamycines de par la présence du même groupement en C23 [271,333] (**Figure 30**). Néanmoins, la RFB est moins efficacement modifiée par cette enzyme, suggérant l'importance d'autres parties de ces molécules dans la résistance. Par ailleurs, des études ont démontré l'intérêt du C25 des rifamycines, où des modifications au niveau de ce carbone peuvent augmenter son activité et protéger contre l'action d'Arr<sub>MAB</sub>, notamment grâce à de gros groupements carbamates [330,334,335]. Ainsi récemment, des dérivés de rifamycines ou de RFB possédant des groupements en C25 liés par un carbamate ont montré une résistance à la modification par Arr<sub>MAB</sub> en empêchant la liaison de l'enzyme à ceux-ci [271] sans pour autant être affectés dans leur liaison à l'ARN polymérase conférant une bonne activité antimycobactérienne [270].

Ces travaux montrent que la connaissance des mécanismes de résistance est primordiale afin de développer de nouveaux traitements capables de les contourner.

## 2.2. Enzymes protégeant la cible des antibiotiques : Erm41

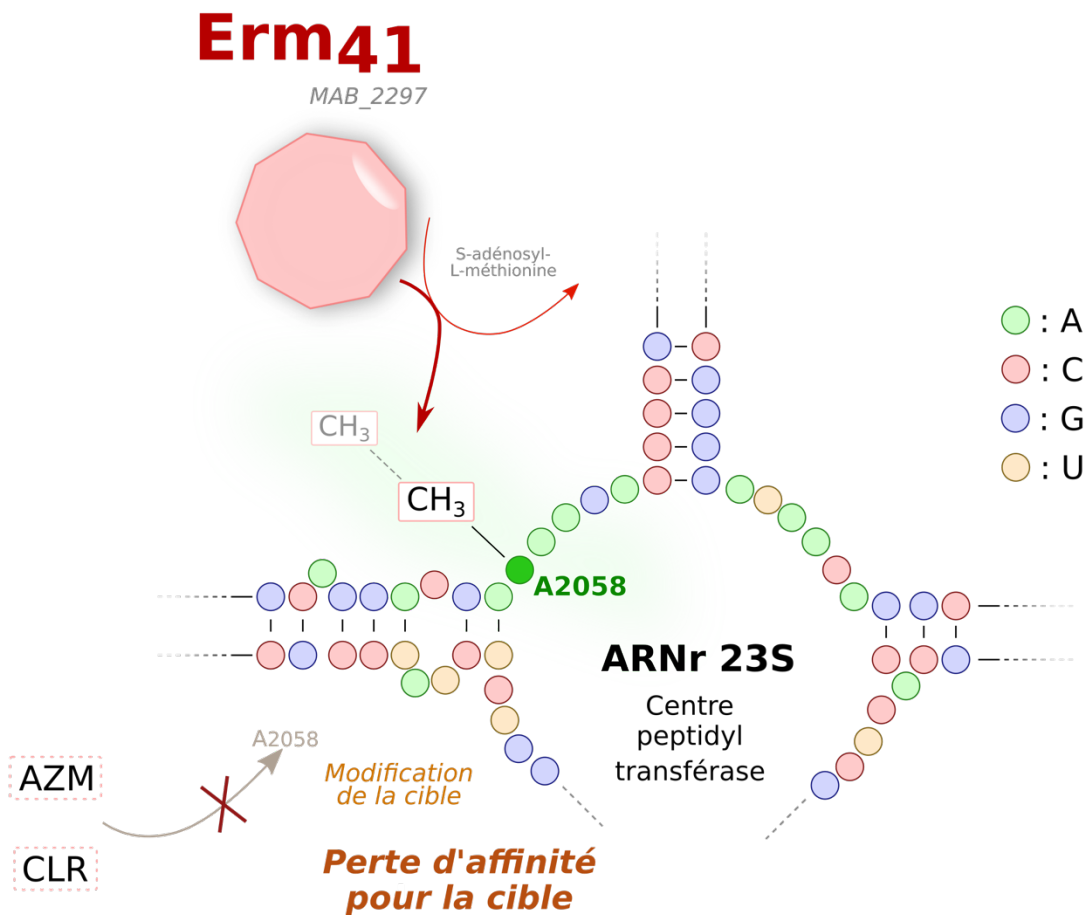
Intrinsèquement, *M. abscessus* est également capable de protéger la cible des antibiotiques et ainsi diminuer l'affinité des composés pour celle-ci. C'est le cas avec la méthyltransférase Erm41, codée par le gène *MAB\_2297*, protégeant la cible des macrolides [43]. Cette enzyme vient transférer des groupements méthyles sur l'ARNr 23S de la boucle du centre peptidyltransférase au niveau de la grande sous-unité du ribosome. Plus particulièrement, le transfert d'un ou deux méthyles provenant de la S-adenosyl-L-méthionine se fait sur l'adénine en position 2058, entraînant une perte d'affinité des macrolides pour leur cible en empêchant la mise en place de la liaison hydrogène entre le sucre désosamine et ce résidu, et non pas seulement chez *M. abscessus* (**Figure 31**) [336,337]. En effet, ce genre d'enzyme est présent chez d'autres bactéries telles que *E. coli* ou *S. aureus* [338] ou chez différentes mycobactéries. On retrouve, par exemple, la protéine Erm37 chez *M. tuberculosis* [339], Erm38 chez *M. smegmatis* [340] ou encore Erm39 chez *M. fortuitum* [35]. Néanmoins, certaines différences au sein même du complexe *M. abscessus* sont à noter. *M. abscessus* subsp. *massiliense*



**Figure 31 : Méthylation de l'ARNr 23S par Erm41**

La méthyltransférase de *M. abscessus* Erm41, codée par le gène *MAB\_2297*, transfère un ou deux groupements méthyles sur l'ARNr 23S de la boucle du centre peptidyltransférase de la grande sous-unité du ribosome. Les groupements méthyles proviennent de la S-adenosyl-L-méthionine, et sont ajoutés à l'adénine A2058, cible des macrolides. Ainsi, l'azithromycine et la clarithromycine perdent leur activité et sont inopérants chez les souches exprimant ce mécanisme de résistance inductible.

Erm, « erythromycin resistance methylase » ; A, adenine ; C, cytosine ; G, guanine ; U, uracile ; AZM, azithromycine ; CLR, clarithromycine.



présente une protéine Erm41 tronquée [308] et est donc sensible à l'action des macrolides si aucun polymorphisme dans le gène *rrl* n'est retrouvé (voir **Chapitre II : Antibiothérapie et mécanismes de résistance aux antibiotiques chez *M. abscessus***, 2.1. Polymorphisme génétique et mutations acquises). Cependant, chez les espèces possédant la protéine fonctionnelle, il peut exister un polymorphisme du gène *erm(41)* étant associé à la perte de l'activité méthylase. La modification la plus courante consiste en la modification en cytosine du nucléotide thymine en position 28 (sequovar T28C), engendrant une substitution du résidu tryptophane en arginine en position 10 de la protéine Erm41. Cette modification entraîne la perte d'activité d'Erm41 et ainsi une sensibilité aux macrolides [307]. Ces enzymes Erm entraînent une résistance inductible à la classe d'antibiotiques fondamentale des macrolides. En effet, la présence de CLR, ou plus favorablement d'AZM, induit l'expression d'Erm41 chez *M. abscessus* permettant la résistance à ces antibiotiques de première ligne [341]. Cette inductibilité est notamment dû, chez *M. abscessus*, à l'activateur de transcription WhiB7, codé par le gène *MAB\_3508c*, fortement induit en présence de macrolides et conservé chez les actinomycètes [342,343]. Ce régulateur transcriptionnel WhiB7 est impliqué dans de nombreux autres mécanismes de résistance aux antibiotiques. Il peut être induit en présence de différents antibiotiques ciblant le ribosome, tels que les tétracyclines, les macrolides ou les aminoglycosides. L'implication de WhiB7 dans la résistance à l'AMK a été rapportée *via* l'induction du gène *eis2* codant une acétyltransférase précédemment citée [342]. Néanmoins, la résistance aux macrolides gouvernée par Erm41 n'est généralement pas détectée en début de traitement clinique, c'est pourquoi il est primordial de déceler une potentielle résistance au plus vite afin de pouvoir adapter la thérapie curative (**Figure 13**).

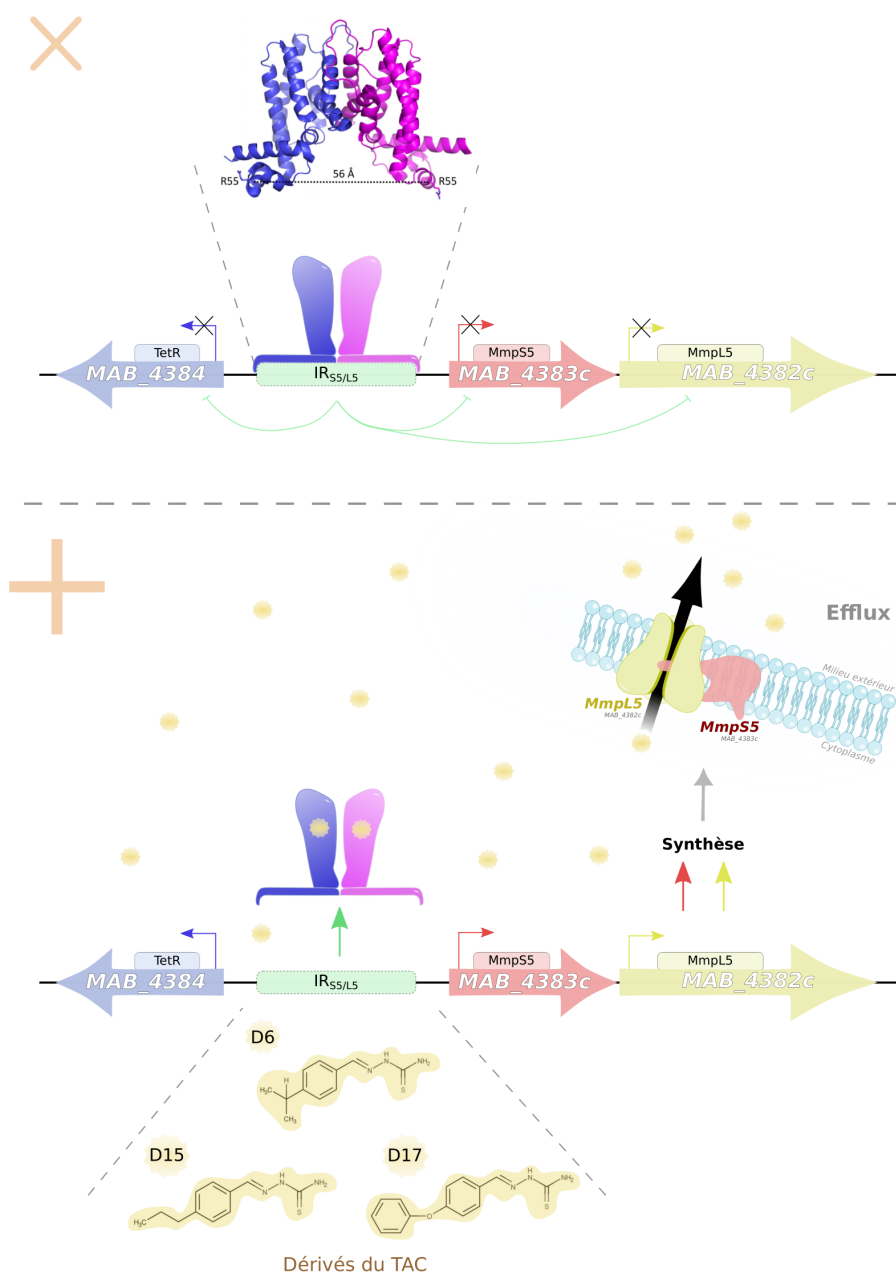
### 2.3. Export actif *via* des pompes à efflux

*M. abscessus* exprime également une vaste panoplie de protéines membranaires jouant le rôle de pompes à efflux. Ces dernières assurent le maintien de l'homéostasie de la cellule bactérienne en transportant une large gamme de substrats tels que des composants nécessaires à l'assemblage de la paroi, des facteurs de virulence ou encore des toxines. Ainsi, ces pompes à efflux peuvent également participer à l'export de substances exogènes tels que les antibiotiques. Parmi celles-ci, il existe chez les mycobactéries les transporteurs de la famille des MmpL (Mycobacterial membrane protein Large) [272], pouvant agir de concert avec les transporteurs MmpS (Mycobacterial membrane protein Small). Dans cette lignée, une certaine résistance naturelle aux dérivés du thiacétazone (TAC) est retrouvée [344,345]. Plus particulièrement, le TAC est une molécule précédemment utilisée contre *M. tuberculosis*, mais retirée du régime thérapeutique à cause de ses effets secondaires, notamment en cas d'infection par le VIH [346,347]. Le repositionnement récent de ce composé a conduit au

**Figure 32 : Mécanisme de résistance aux dérivés du thiacétazone**

*M. abscessus* est capable de résister aux dérivés du thiacétazone (TAC), tels que les composés D6, D15 et D17, à travers l'export de ces molécules dans le milieu extérieur *via* le système MmpS5/MmpL5. Ce couple est codé par les gènes *MAB\_4383c* (*mmps5*) et *MAB\_4382c* (*mmpL5*), tous deux régulés par un régulateur transcriptionnel de la famille TetR codé par le gène *MAB\_4384*. Ce régulateur se lie en dimère sur la séquence nucléotidique palindromique *IR<sub>S5/L5</sub>* en amont du gène *MAB\_4383c* permettant la répression de l'expression des protéines d'efflux. En présence d'analogues du TAC, ces derniers viennent se lier au répresseur qui se détache de l'ADN et permet l'expression de MmpS5 et MmpL5 engendrant l'efflux des molécules.

Adapté de Halloum I, *et al.* 2017 et Richard M, *et al.* 2018, [345,348].

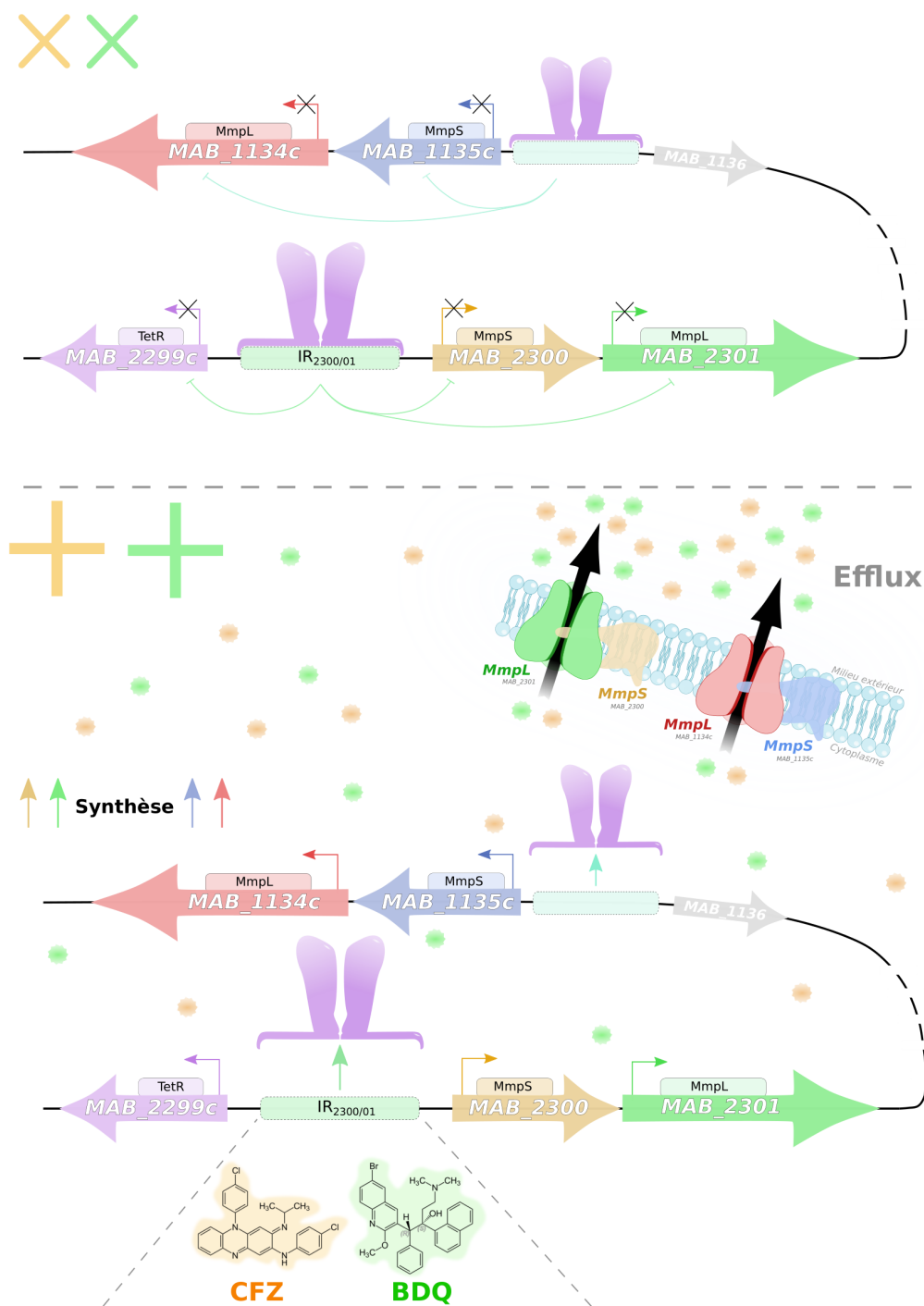


développement de différents analogues, dont les plus performants (D6, D15 et D17) présentent une activité bactériostatique vis-à-vis de *M. abscessus* [345]. Ces molécules sont bioactivées par EthA<sub>MAB</sub> codé par *MAB\_0985*, lui-même régulé par EthR<sub>MAB</sub>, codé par *MAB\_0984c*, qui appartient à la famille des régulateurs transcriptionnels TetR. Néanmoins, la sélection de mutants résistants spontanés aux analogues du TAC ont mis en évidence des mutations au sein du gène *MAB\_4384*. Ce dernier code un répresseur TetR du système de pompes à efflux *MAB\_4383c/MAB\_4382c*, permettant l'export actif des analogues du TAC. Ainsi, des mutations dans *MAB\_4384* (notamment au niveau de l'asparagine N15 ou de la phénylalanine F57) ou sa délétion génétique entraînent une surexpression des protéines d'efflux codées par *MAB\_4383c* et *MAB\_4382c* conduisant à une résistance accrue à ces composés [345,348]. Les deux protéines codées par *MAB\_4383c* et *MAB\_4382c* sont homologues du système MmpS5/MmpL5 de *M. tuberculosis* connues pour permettre l'efflux de la CFZ ou encore de la BDQ [349]. Chez *M. abscessus*, le régulateur codé par *MAB\_4384* se lie en dimère sur la séquence palindromique au sein de la région IR<sub>S5/L5</sub> en amont des gènes *MAB\_4383c* et *MAB\_4382c* ce qui permet la répression des protéines d'efflux associées [348] (**Figure 32**). Les analogues de TAC viennent lier ce répresseur, ce qui résulte, en cas de traitement, au détachement de l'ADN du répresseur et à une induction de l'expression du système MmpS5/MmpL5 générant un efflux important de ces molécules (**Figure 32**).

Un système équivalent à ce dernier est également responsable de la résistance à la CFZ et la BDQ chez *M. abscessus*. En effet, à l'instar de chez *M. tuberculosis*, l'export de ces deux antibiotiques est également régulé par une protéine de la famille TetR, codée par le gène *MAB\_2299c* [350]. Des mutations au sein de ce gène, ou une délétion génétique de *MAB\_2299c* vont entraîner une surexpression des transporteurs membranaires codés par *MAB\_2300* et *MAB\_2301* correspondants à un couple MmpS/MmpL, facilitant l'efflux de la CFZ et la BDQ vers le milieu extérieur. De plus, la délétion supplémentaire des gènes *MAB\_2300* et *MAB\_2301* restaurent la sensibilité à ces deux antimycobactériens prouvant le rôle des protéines d'efflux associées dans la résistance à la CFZ et la BDQ [350]. D'un point de vue mécanistique, le régulateur *MAB\_2299c* se fixe à l'ADN, sur la région promotrice IR<sub>2300/01</sub> en amont des gènes *MAB\_2300/MAB\_2301* et réprime leur expression. Ainsi, en présence de BDQ ou de CFZ, ces derniers se lient à TetR qui va se dissocier du promoteur permettant une transcription plus importante des protéines MmpS/MmpL codées par *MAB\_2300/MAB\_2301* (**Figure 33**). De plus, il a été démontré que *MAB\_2299c* peut également se lier à une séquence nucléotidique en amont d'un autre système MmpS/MmpL analogue au précédent, codé par les gènes *MAB\_1134c/MAB\_1135c* [351]. Ce couple de gènes code pour un système d'efflux pouvant aussi exporter la CFZ et la BDQ à l'extérieur de la bactérie. En effet, la délétion des gènes *MAB\_1134c/MAB\_1135c* augmente la sensibilité aux deux agents antibactériens cités. En outre, cette

**Figure 33 : Mécanisme de résistance à la clofazimine et la bédaquiline**

*M. abscessus* résiste à la clofazimine (CFZ) et la bédaquiline (BDQ) *via* un système d'export impliquant des protéines de la famille MmpL/MmpS. Les protéines impliquées sont codées par les gènes *MAB\_1134c* et *MAB\_1135c* pour le premier système d'efflux, et par les gènes *MAB\_2300* et *MAB\_2301* pour le second système. Ces deux couples protéiques sont régulés par le régulateur transcriptionnel TetR codé par le gène *MAB\_2299c* qui, en se détachant de l'ADN en présence de CFZ ou de BDQ, permet l'expression des protéines d'export.

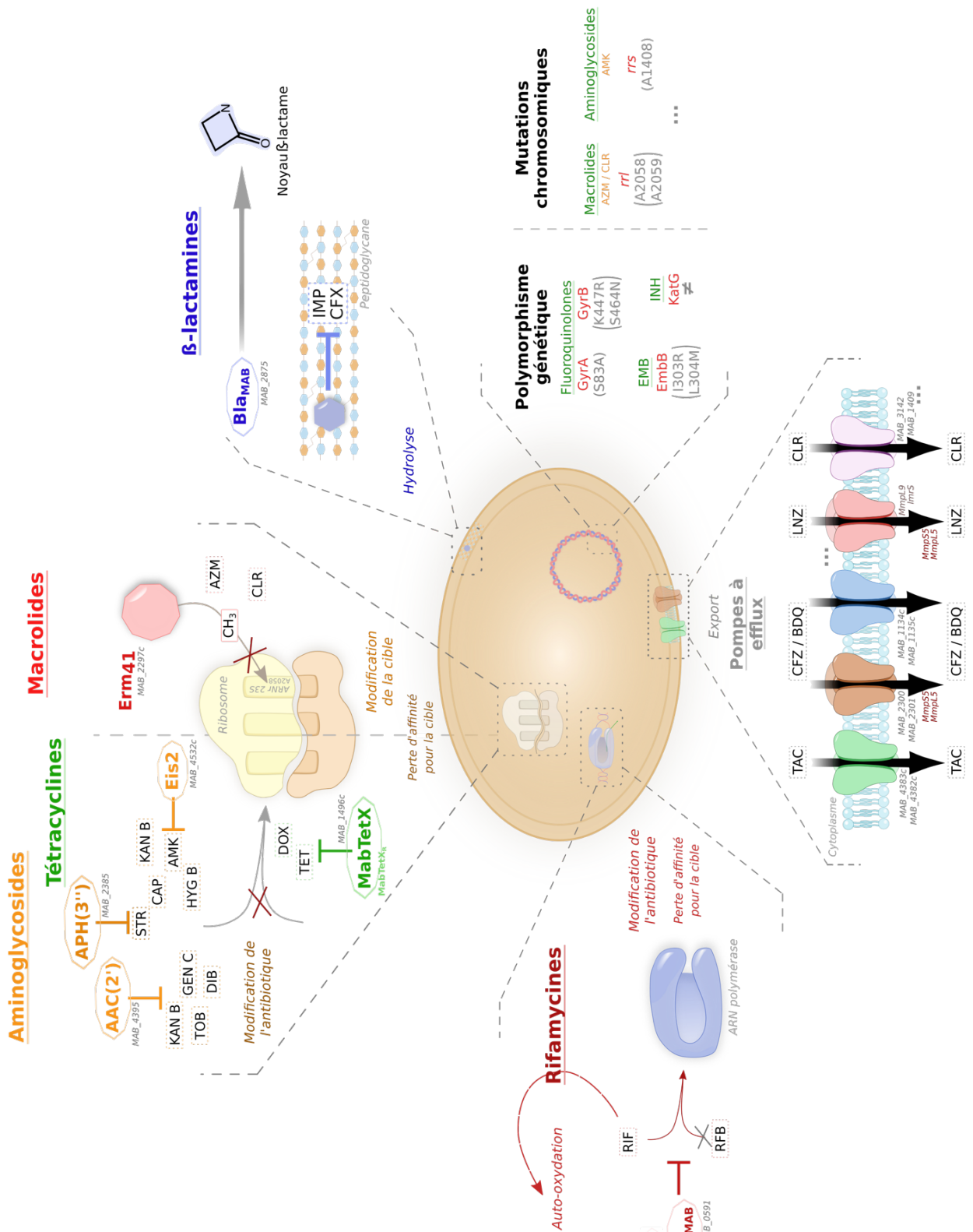


même délétion au sein de la souche sensible délétée de *MAB\_2299c*, *MAB\_2300* et *MAB\_2301* [350] exacerbe la sensibilité de ce mutant à la CFZ et la BDQ [351]. Ainsi, le répresseur *MAB\_2299c* régule l'expression de deux systèmes d'efflux indispensables à la résistance de *M. abscessus* contre la CFZ et la BDQ (**Figure 33**).

Le rôle des pompes à efflux a également été identifié dans la résistance au LNZ. Il a été montré que certains isolats cliniques résistants au LNZ présentent des niveaux transcriptionnels plus importants des gènes *mmpL9* et *ImrS* (lyncomycin resistance protein of *Staphylococcus aureus*) [352]. Cette étude suggère donc une potentielle implication de transporteurs dans la résistance au LNZ, qui sera corroborée par une récente étude montrant un rôle du répresseur codé par *MAB\_4384* [235]. En effet, ici une fréquence élevée de mutants spontanés faiblement résistants au LNZ présentent des mutations au sein du gène *MAB\_4384* impliqué dans la régulation du système d'efflux MmpS5/Mmpl5 cité plus haut et ayant un rôle dans la résistance aux analogues du TAC.

D'autres études récentes ont suggéré un rôle de ces pompes à efflux dans la résistance à la CLR. Celles-ci montrent une transcription supérieure des pompes à efflux codées par les gènes *MAB\_3142* et *MAB\_1409* [353] ou encore *MAB\_2355C*, *MAB\_1409c* ou *MAB\_1846* [354] chez les souches présentant une résistance à la CLR, sans que ces souches présentent une surexpression d'Erm41. Même si ces résultats ne montrent qu'une hausse des transcrits et non pas des protéines, ni de l'activité de celles-ci, l'utilisation d'inhibiteurs de pompes à efflux (verapamil-VP-, phenylalanine-arginine  $\beta$ -naphtylamide-PA $\beta$ N- ou carbonyl cyanide 3-chlorophenylhydrazone-CCCP-) réduit les CMI de la CLR vis-à-vis de souches cliniques [353] suggérant un rôle de l'efflux de ce macrolide dans la résistance que possède *M. abscessus*.

En effet, différents inhibiteurs des pompes à efflux ont vu le jour ces dernières années dans le but de contrecarrer cette résistance intrinsèque de *M. abscessus* [355]. Parmi ceux-ci on compte ceux précédemment cités (VP, PA $\beta$ N, CCCP) mais aussi la thioridazine ou encore la tétrahydropyridine (THP). Le VP va, entre autres, permettre d'améliorer l'activité *in vitro* et *ex vivo* de la BDQ sur différentes souches cliniques du complexe *M. abscessus* [257,356]. La THP, et ses dérivés, régulent les pompes à efflux des ions calcium et peut conférer un effet additif dans le traitement de *M. abscessus* en réduisant les CMI de l'AMK, la CIP et la CLR [357,358]. De plus, la thioridazine va favorablement réduire l'efflux des antibiotiques ciblant le ribosome bactérien tels que l'AMK, la CLR ou encore la TGC *via* la surexpression de gènes codant des systèmes de transport [359]. L'ensemble de ces inhibiteurs permettent de mieux décrypter le rôle des pompes à efflux dans la résistance intrinsèque aux antibiotiques de *M. abscessus* et ouvrent la voie à une nouvelle approches dans le traitement des infections mycobactériennes.





En conclusion, *M. abscessus* présente une large variété de mécanismes de résistance (**Figure 34**) qui expliquent la difficulté à traiter et éradiquer les infections à ce pathogène. L'ensemble de ces travaux soulignent également l'importance de développer de nouveaux antimycobactériens efficaces et ciblant de nouvelles voies métaboliques pour contrecarrer ces mécanismes de résistances, bien qu'une des résistances naturelles aux antibiotiques de ce pathogène opportuniste est conférée par les propriétés particulières de sa paroi.

**Figure 34 : Mécanismes de résistance, innés ou acquis, à diverses classes d'antibiotiques chez *M. abscessus***

*M. abscessus* contient un large panel de mécanismes de résistance aux antibiotiques expliquant la difficulté d'éradication des infections causées par ce pathogène en clinique. Parmi ceux-ci, il existe des mécanismes acquis telles que les mutations chromosomiques au sein des gènes codant les cibles de ces antibiotiques tels que *rrl* ou *rrs* mais aussi des mécanismes innés à la bactérie. Cette dernière catégorie regorge de protéines modifiant les antibiotiques tels que la  $\beta$ -lactamase  $Bla_{MAB}$ , capable d'hydrolyser certaines  $\beta$ -lactamines comme l'IMP, la monooxygénase FAD-dépendante *MabTetX* hydrolysant les tétracyclines, l'ADP-ribosyltransférase *Arr<sub>MAB</sub>* qui neutralise les rifamycines. *M. abscessus* détient également des enzymes cytoplasmiques capables de modifier chimiquement les aminoglycosides, comprenant les acétyltransférases *Eis2* et *AAC(2')* ou encore la phosphotransférase *APH(3'')*. Un autre mécanisme de résistance mis en jeu consiste en la modification de la cible des antibiotiques, comme *Erm41* capable de méthyle l'adénine A2058 de l'ARNr 23S de la grande sous-unité ribosomale, ce qui conduit à une perte d'affinité pour les macrolides (*AZM* et *CLR*). Enfin, la membrane plasmique renferme une grande variété de pompes à efflux pouvant exporter des antibiotiques vers l'extérieur.

STR, streptomycine ; KAN B, kanamycine B ; HYG B, hygromycine B ; AMK, amikacine ; CAP, capréomycine ; TOB, tobramycine ; DIB, dibécacine ; GEN C, gentamycine C ; DOX, doxycycline ; TET, tétracycline ; AZM, azithromycine ; CLR, clarithromycine ; RIF, rifampicine ; RFB, rifabutine ; IMP, imipénème ; CFX, céfoxitine ; EMB, éthambutol ; INH, isoniazide ; TAC, thiacétazone ; CFZ, clofazimine ; BDQ, bédaquiline ; LNZ, linézolide.





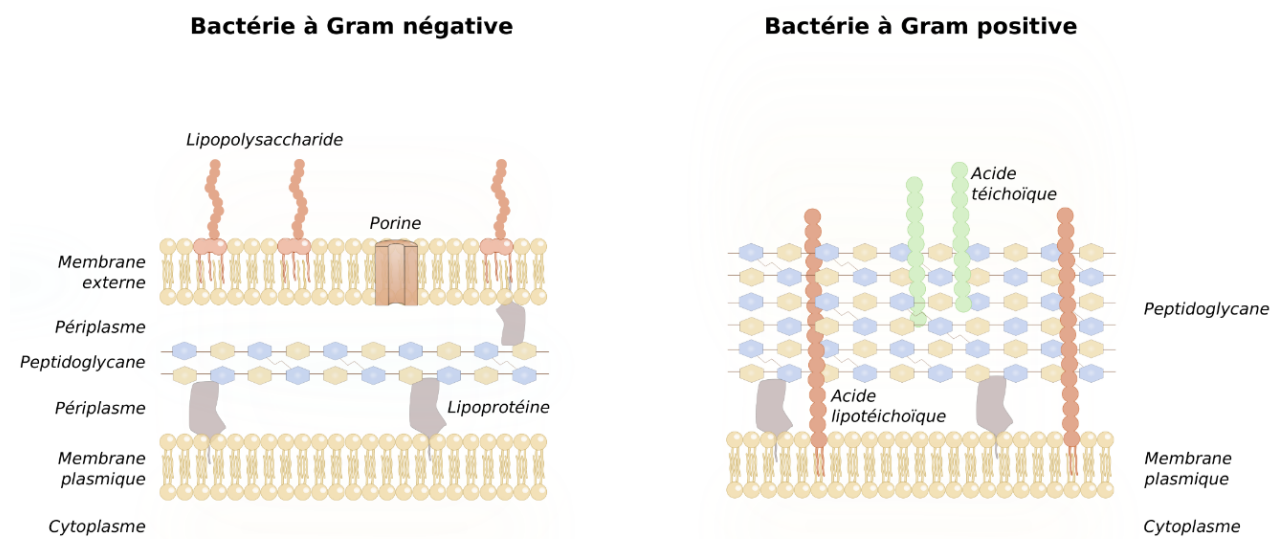
# Chapitre III :

## Paroi et acides mycoliques

**Figure 35 : Structure de la paroi des bactéries à Gram négative et à Gram positive**

Les bactéries à Gram négative présentent un espace périplasmique contenant le peptidoglycane localisé entre la membrane plasmique et la membrane externe. Cette dernière renferme des porines ou d'autres transporteurs spécifiques, ainsi que le lipopolysaccharide fortement immunogène.

Les bactéries à Gram positive présentent une large couche de peptidoglycane qui surplombe la membrane plasmique. Au sein de cette membrane sont ancrés les acides lipotéichoïques tandis que les acides téichoïques sont liés au peptidoglycane.



## 1. La paroi mycobactérienne, une structure atypique

Les mycobactéries possèdent une paroi particulière et complexe qui la distingue des autres bactéries et qui en fait un atout majeur dans les mécanismes de pathogénèse et de résistance aux antibiotiques. Généralement, les bactéries sont classées en deux grands groupes selon la composition de cette paroi grâce à la coloration de Gram.

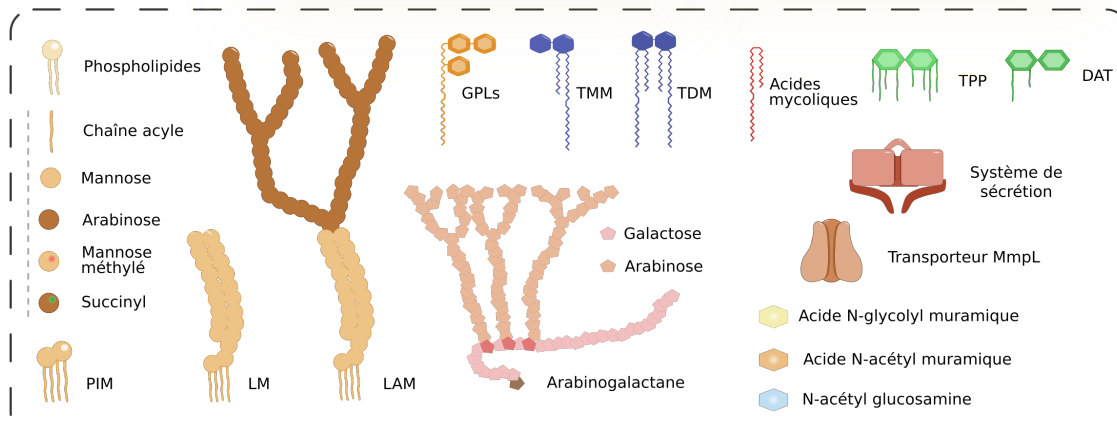
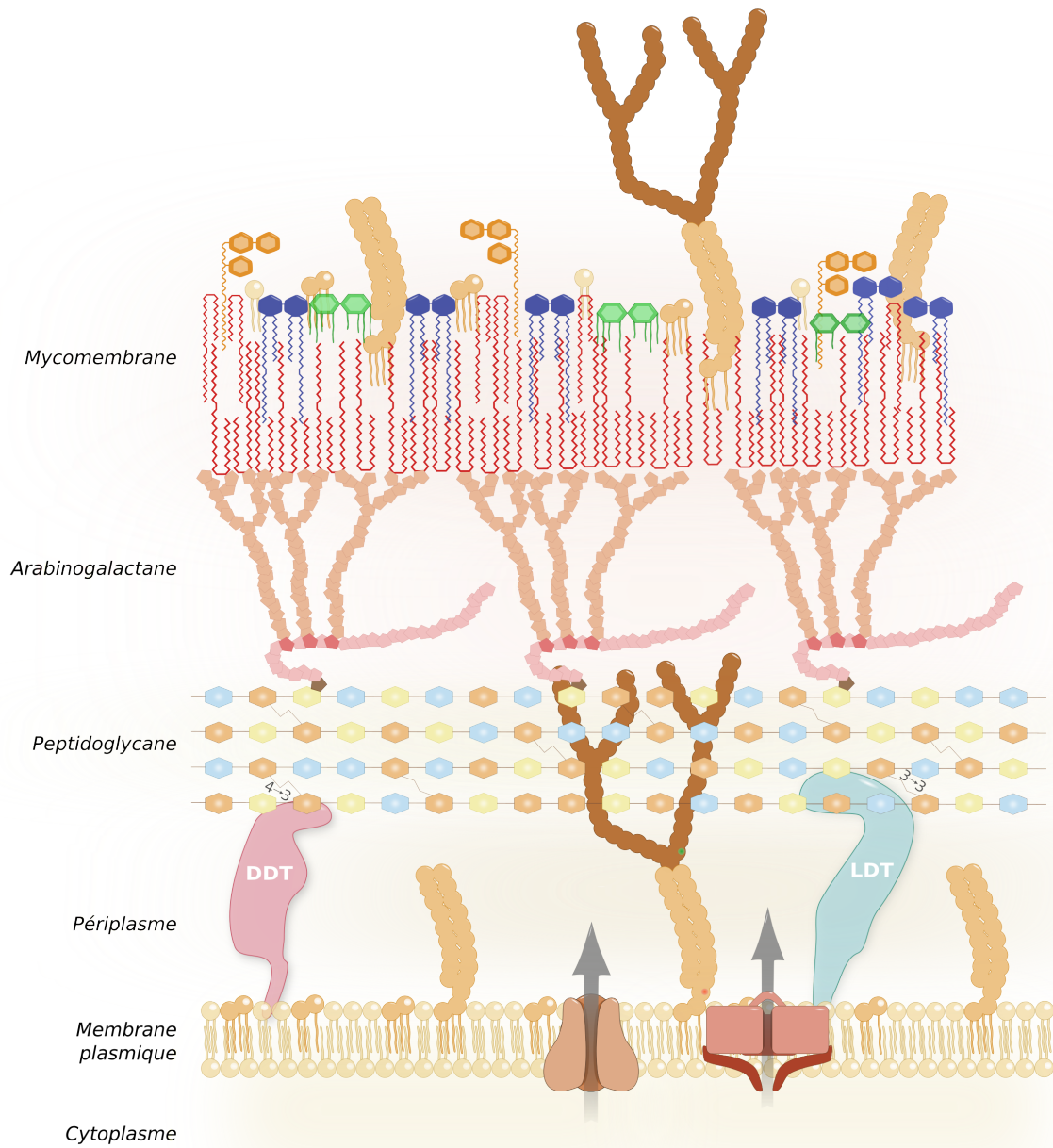
### 1.1. Paroi des Gram positive et Gram négative

Il y a plus d'un siècle, en 1884, le docteur Hans Christian Gram a mis au point la technique de coloration éponyme encore utilisée aujourd'hui pour discriminer les types de bactéries [360,361]. Ainsi, les bactéries à Gram positive, colorées en bleu retenant le complexe cristal violet-iode se distinguent des bactéries à Gram négative qui adoptent une coloration rose sur frottis permise par la décoloration à l'éthanol suivie de la coloration à la fuschine [362,363]. Cela résulte d'une composition différente de leur paroi (**Figure 35**) qui vont, selon leurs propriétés d'hydrophobicité respectives, retenir ou non la coloration de Gram. Brièvement, les bactéries à Gram négative présentent une membrane interne et externe espacées par une fine couche de périplasme [364]. Au sein de cet espace périplasmique se retrouvent de nombreuses protéines ainsi que le PG formé d'unités répétées de NAM et de NAG liées par des liaisons peptidiques  $\beta$ -1 $\rightarrow$ 4 permettant de maintenir la forme et l'intégrité des cellules [365]. La membrane externe est marquée par la présence de porines ou encore de glycolipides, dont le lipopolysaccharide (LPS), connu pour être une endotoxine et un facteur de virulence activant fortement le système immunitaire inné [366,367]. A l'inverse, les bactéries à Gram positive n'ont qu'une membrane interne surplombée par un large périplasme contenant de nombreuses couches de PG [363]. De longs polymères composés de phosphates de glycérol et de phosphates de ribitol se lient de manière covalente au PG (acides téichoïques), tandis que certains sont ancrés à la membrane interne *via* un diacylglycérol et traversent le PG (acides lipotéichoïques). Ces polymères représentent à eux deux les constituants majeurs de la paroi bactérienne à Gram positive [364] (**Figure 35**).

Les membres du genre *Mycobacterium* se distinguent de cette classification binaire car ils présentent une paroi unique non colorée par la coloration de Gram.

### 1.2. La paroi mycobactérienne

Anciennement, les mycobactéries étaient associées aux bactéries à Gram positive de par la structure de leur paroi, néanmoins la distinction avec les deux autres groupes bactériens s'est faite de par



l'architecture de la paroi et sa composition particulière, caractérisée par sa richesse en lipides qui représentent environ 40% de la masse sèche de la cellule [368]. La paroi de *M. abscessus* présente de grandes similarités avec d'autres espèces mycobactériennes à croissance lente ou rapide. Ainsi, de l'intérieur vers l'extérieur, la paroi mycobactérienne est composée d'une membrane plasmique, d'un périplasme contenant le PG lié de manière covalente à l'AG qui est lui-même surplombé par la membrane externe ou mycomembrane.

### 1.2.1. Membrane plasmique

La membrane plasmique mycobactérienne est semblable à celle retrouvée chez les autres bactéries, et joue un réel rôle dans la physiologie cellulaire. Elle permet le transport d'électrons et de métabolites divers, la production d'ATP et participe au maintien de l'intégrité cellulaire. Elle est composée principalement de phospholipides polaires associés à des protéines, assemblés en une bicouche lipidique asymétrique [369]. La membrane interne contient les phospholipides typiques tels que la cardiolipine, le phosphatidylinositol, le phosphatidylglycérol et le phosphatidyléthanolamine [368,370]. Au sein de celle-ci, et principalement dans le feuillet externe plus épais, sont ancrés différents glycoconjugués [371] (**Figure 36**), dont les phosphatidyl-*myo*-inositol-mannosides (PIM) ou les lipoglycanes tels que le lipomannane (LM) et le LAM. Les PIM sont les phospholipides majoritaires de la membrane interne en représentant plus de 40% de la masse lipidique de cette structure [370]. Ils sont formés d'une base phosphatidyl-*myo*-inositol contenant d'un à six résidus mannoses et jusqu'à quatre chaînes acyles ( $Ac_{1-4}PIM_{1-6}$ ) [372]. Ces derniers se retrouvent également à la surface mycobactérienne et servent de base lipidique à la formation du LM et du LAM par l'ajout successif de groupement mannoses et arabinoses [372,373]. L'ensemble de ces glycolipides joue un rôle important dans l'intégrité de la membrane interne et dans la perméabilité de l'enveloppe bactérienne [374–376]. Chez *M. abscessus*, la structure des PIM, LAM et LM diffèrent légèrement des autres espèces mycobactériennes, avec une taille supérieure et un squelette mannane du LM et du LAM présentant une ramification différente leur apportant une certaine plus-value dans la virulence et la survie intracellulaire. Des substitutions au sein du LAM telles que des groupements succinyles ou acétyles, ainsi qu'un groupement méthyle sur l'un des résidus mannosyle des PIM ont également été mis en évidence [377]. De plus, les mycobactéries, y compris *M. abscessus*, sont capables de modifier la structure des PIM en réponse à l'environnement. En effet, il a été montré qu'en présence d'un stress engendrant une fluidification membranaire importante, une chaîne acyle s'ajoute au groupement inositol des PIM, naturellement tri-acylés, afin de maintenir l'intégrité de la membrane plasmique et de faire face aux changements environnementaux [378]. Enfin, la membrane interne des

**Figure 36 : Représentation schématique de la paroi mycobactérienne de *M. abscessus***

La paroi mycobactérienne est une structure multicouche riche et complexe se composant d'une membrane plasmique, d'un périplasma surplombé par le peptidoglycane auquel vient se lier de manière covalente l'arabinogalactane. Ce dernier est estérifié par les acides mycoliques formant le feuillet interne de la mycomembrane qui contient en sa partie externe de nombreux lipides et glycolipides. La membrane plasmique est composée de phospholipides et contient des phosphatidyl-*myo*-inositol-mannosides (PIM), du lipomannane (LM), du lipoarabinomannane (LAM), ou encore des transporteurs de la famille des MmpL (Mycobacterial membrane protein Large) et des complexes protéiques impliqués dans la sécrétion. Le peptidoglycane est composé d'acide N-glycolyl muramiques, d'acide N-acétyl muramiques et de N-acétyl glucosamines. Les chaînes peptidiques latérales du peptidoglycane sont réticulées par les D,D-transpeptidases (DDT) et L,D-transpeptidases (LDT). Associé au PG, l'arabinogalactane est lui-même estérifié par les chaînes d'acides mycoliques qui composent le feuillet interne de la mycomembrane. Le feuillet externe de cette mycomembrane contient une grande diversité de lipides « libres » tels que les glycopeptidolipides (GPLs), les tréhalose monomycolates (TMM), les tréhaloses dimycolates (TDM), les diacyl-tréhaloses (DAT), les tréhaloses polyphléates (TPP), ainsi que des glycolipides ou lipoglycane présents également dans la membrane plasmique, tels que les PIM, le LM et le LAM.

mycobactéries contient de nombreuses protéines jouant le rôle de pompes à efflux, incluant notamment les transporteurs lipidiques de la famille MmpL/MmpS permettant de maintenir l'homéostasie et le bon assemblage de la paroi [272], ainsi que divers systèmes de sécrétion de type VII exportant de nombreuses protéines effectrices [5,379].

### 1.2.2. Périplasma, peptidoglycane et arabinogalactane

L'espace périplasmique ceinturant la membrane plasmique, est défini comme une couche granulaire de faible densité et est délimité en sa périphérie par le PG, lui-même lié de manière covalente à l'AG [371] (**Figure 36**). Ce PG est composé d'une base glycanique d'unités alternées de NAG et de NAM reliées entre elles par des liaisons  $\beta$ -1 $\rightarrow$ 4 et de courtes chaînes latérales peptidiques [380]. Contrairement aux autres bactéries, chez les mycobactéries les acides muramiques peuvent être N-acétylés (NAM) ou bien N-glycosylés lorsque la fonction N-acétyl est oxydée pour former de l'acide N-glycolylmuramique (NGM) [381,382]. Les chaînes peptidiques latérales de L-Alaninyl-D-isoGlutaminyl-*meso*-diaminopimelyl-D-alanyl-D-Alanine sur le NAM sont réticulées entre-elles à plus de 70% [152]. Cette réticulation du PG est catalysée par les DDTs et principalement par les LDTs chez *M. abscessus*, formant respectivement des liaisons 4 $\rightarrow$ 3 et 3 $\rightarrow$ 3 [153] (**Figure 15**). La structure globale du PG permet, *via* une certaine rigidité, de maintenir l'intégrité et la forme de la cellule mycobactérienne et de résister à la pression osmotique [380,383]. De plus, les modifications N-glycolyl sur les acides muramiques pourraient exercer un effet de renforcement de la structure et potentiellement de protection contre la dégradation due au lysozyme et aux  $\beta$ -lactamines [382]. Les résidus NGM du PG sont reliés de manière covalente à l'AG par une liaison phosphodiester entre le domaine galactane de l'AG et environ 10% des NGM [384]. L'AG est un hétéropolysaccharide hautement ramifié composé de D-galactofuranosyl et D-arabinofuranosyl [380]. La partie galactane contient une trentaine de molécules de D-galactofuranosyl alternativement liées par des liaisons  $\beta$ (1 $\rightarrow$ 5) et  $\beta$ (1 $\rightarrow$ 6) [385,386]. A ces unités D-galactofuranosyls  $\beta$ (1 $\rightarrow$ 6) se lient trois tricosamères (23 résidus) de D-arabinofuranosyls, en particulier aux groupement hydroxy en C5 des unités positionnées en 8, 10 et 12 de la chaîne galactane [383]. Cette couche d'AG permet de faire le lien entre le PG et la mycomembrane externe *via* les acides mycoliques, qui sont caractéristiques des mycobactéries (**Figure 36**).

### 1.2.3. La mycomembrane

La structure la plus externe de la paroi, définie sous le terme de mycomembrane, est caractérisée par sa haute teneur en acides mycoliques composant le feuillet interne de celle-ci. Les acides mycoliques,





définis comme de longues chaînes d'acides gras  $\alpha$ -alkyl  $\beta$ -hydroxy de 60 à 90 atomes de carbone (voir **Chapitre III : Paroi et acides mycoliques**, 2. Les acides mycoliques) estérifient les D-arabinofuranosyls terminaux de l'AG [387,388]. Le feuillet externe de la mycomembrane consiste en une riche variété de lipides et de glycolipides libres non liés de manière covalente [368]. Parmi les lipides et lipoglycans de la mycomembrane de *M. abscessus*, on retrouve des PIM, du LAM, du LM, des lipides dérivés du tréhalose (TMM, TDM, des tréhalose-polyphléates -TPP-, et les précurseurs de ces derniers les 2,3 diacyl tréhaloses -DAT-) ou encore des GPLs [389,390]. Certains de ces lipides sont communs au genre *Mycobacterium* tels que les TMM ou les TDM, tandis que d'autres sont restreints à certaines espèces à l'instar des GPLs produits par *M. abscessus*, *M. fortuitum* ou encore *M. avium* et non pas par *M. tuberculosis* [391,392]. Ces lipides de surface ont notamment un rôle dans la modulation de l'immunité de l'hôte [393]. En effet, les PIM interfèrent avec la maturation du phagosome et stimulent la fusion avec les endosomes précoces pour avoir accès aux nutriments nécessaires à la survie intraphagosomale [394]. Nous savons, de surcroît, que les PIM sont des agonistes des TLR-2 [55], entraînant une forte réponse pro-inflammatoire TNF- $\alpha$ . Ces activateurs de l'immunité sont, chez le variant S de *M. abscessus*, masqués par les GPLs ayant un rôle dans sa morphologie mais également dans sa virulence [38]. La modulation des niveaux de GPLs à la surface entraîne la transition du morphotype S vers le morphotype R associé à une hypervirulence, une hydrophobicité accrue et une agrégation des bacilles sous la forme de « cordes », ce qui altère le contrôle de l'infection par les cellules immunitaires [53]. S'ajoutant aux PIM, le LM et le LAM exposés à la surface constituent également des antigènes initiant la réponse immunitaire chez l'Homme. Les différentes structures chimiques de ces glycoconjugués interagissent avec des récepteurs du système immunitaire tels que les TLR ou encore les lectines de type C [395]. Enfin, l'ensemble de ces lipides externes participent à la très faible perméabilité, et à l'hydrophobicité de la paroi mycobactérienne jouant un rôle de barrière naturelle à la pénétration de certains antibiotiques [396]. En outre, ces lipides sont impliqués dans les phénomènes de « cording » et de formation de biofilms qui contribuent à la résistance intrinsèque des mycobactéries à divers agents antimicrobiens.

## 2. Les acides mycoliques

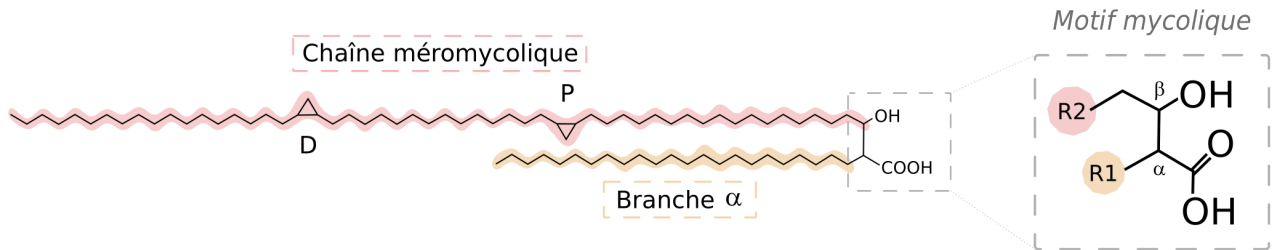
### 2.1. Description, structure et propriétés

Les acides mycoliques sont des composés essentiels et représentent plus de 60% du contenu de la paroi mycobactérienne et 50% de sa masse sèche [396]. Ils se retrouvent sous trois formes chez les mycobactéries : libres, liés au tréhalose (TMM et TDM) ou encore estérifiés sur les unités terminales

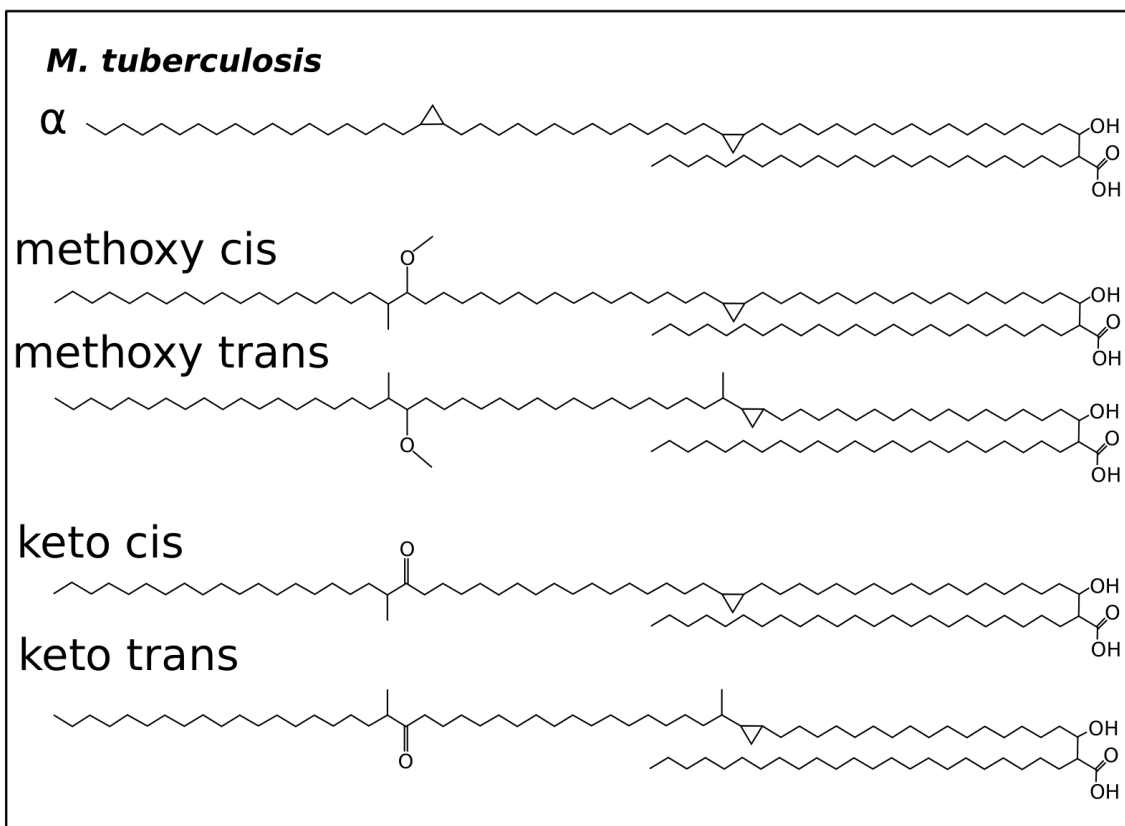
**Figure 37 : Structure générale des acides mycoliques**

Cette représentation est basée sur les acides mycoliques de type  $\alpha$  chez *M. tuberculosis*.

La branche  $\alpha$  (ou R1) est représentée en orange tandis que la longue chaîne d'acide méromycolique (ou R2) est surlignée en rouge. Le motif mycolique est encadré, et met en évidence le caractère  $\alpha$ -ramifié et  $\beta$ -hydroxylé de ces acides gras. P, site proximal ; D, site distal.

**Figure 38 : Acides mycoliques de *M. tuberculosis***

*M. tuberculosis* synthétise trois classes d'acides mycoliques. Les acides mycoliques  $\alpha$  représentent l'espèce majoritaire et présentent deux cycles cyclopropanes situés en position proximale et distale de la chaîne méromycolique. Les mycolates méthoxy portent un groupement oxygéné (en *cis* ou en *trans*), ainsi que des branchements méthyles et un cyclopropane. Enfin, les acides mycoliques keto présentent un groupement cétone (en *cis* ou en *trans*) ainsi qu'un cycle cyclopropane et des méthyles.

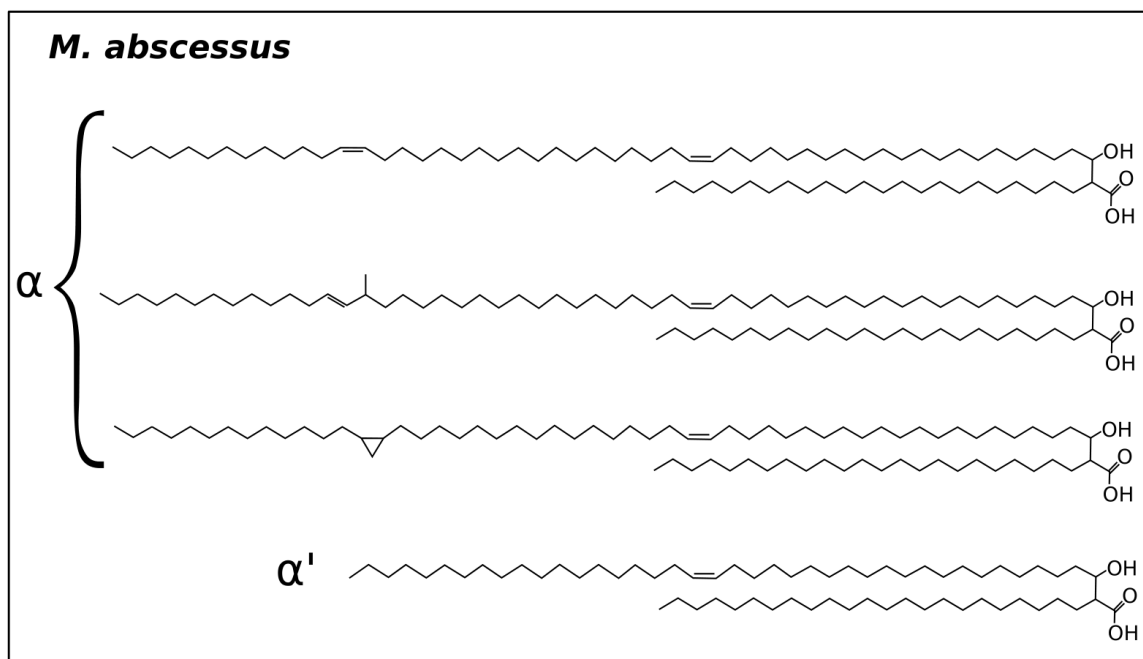


de l'AG [387,388]. Ces acides gras  $\alpha$ -ramifiés et  $\beta$ -hydroxylés à très longues chaînes carbonées ont été désignés sous le nom d'acides mycoliques pour la première fois en 1938 [397] et structurellement décrits en 1950 [398]. Ils affichent une très grande variabilité structurale parmi les espèces mycobactériennes et jouent un rôle majeur dans l'architecture et l'imperméabilité de la paroi, la résistance aux lésions chimiques, la déshydratation, ou encore la virulence [399,400]. Structurellement, ces acides mycoliques se composent d'une courte chaîne alkyl (branche  $\alpha$ ) de 24 à 26 carbones en position  $\alpha$  du groupe acide carboxylique et d'une chaîne méroaldéhyde, en position  $\beta$  (chaîne méromycolique), plus longue et constituée de 42 à 62 atomes de carbone selon l'espèce [387] (**Figure 37**). La variabilité entre les classes d'acides mycoliques est définie par trois caractéristiques, la longueur de la chaîne  $\alpha$  et de la chaîne méromycolique ainsi que de la position des différents groupements chimiques. Ces groupes fonctionnels se positionnent principalement à deux endroits de la chaîne méromycolique, au niveau du site proximal proche de l'acide  $\beta$ -hydroxylé ou au niveau du site distal situé plus à l'extrémité de cette chaîne [399,401] (**Figure 37**).

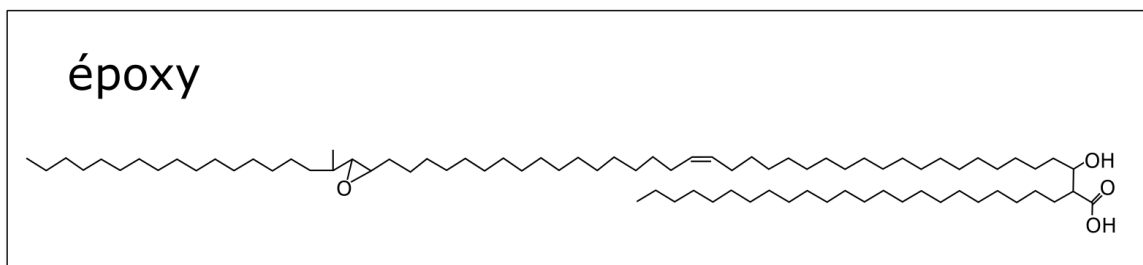
Chez *M. tuberculosis*, trois types d'acides mycoliques sont décrits, en majorité les acides mycoliques  $\alpha$  présentant deux cycles *cis*-cyclopropanes, ainsi que les mycolates méthoxy portant un groupement oxygéné du même nom (*cis* ou *trans*) et les acides mycoliques keto avec un groupement cétone (*cis* ou *trans*), tous deux portant un cycle cyclopropane en position proximale et des branches méthyles (**Figure 38**) [399]. Chaque espèce de mycolates présente des propriétés cruciales pour la physiologie de la bactérie en fonction des groupements associés. De manière générale, les acides mycoliques  $\alpha$  jouent un rôle dans la structure et la stabilité de la paroi. Les fonctions localisées en position proximale sont responsables du maintien de la viscosité de la paroi, par exemple les insaturations *trans* proximales et la cyclopropanation proximale entraînent une baisse de la fluidité, rendant la chaîne méromycolique plus rigide [401,402]. A l'inverse, les insaturations *cis* et les groupements méthyles en position distale perturbent l'empaquetage local des acides mycoliques ce qui permet aux lipides extractibles d'intercaler leurs chaînes acyles [396]. De plus, l'ajout d'un cycle cyclopropane en position distale permet une meilleure résistance au stress oxydatif expliquant, en partie, la persistance intramacrophagique de *M. tuberculosis* [403]. L'ensemble de ces mycolates cyclopropanés présentent un rôle crucial dans la pathogénicité et la virulence dans un modèle murin. En effet, la perte totale d'acides mycoliques cyclopropanés confère une atténuation sévère lors de l'infection *in vivo* [404]. Puis, la délétion du gène *pcaA* chez *M. tuberculosis*, entraînant un défaut de *cis*-cyclopropanation proximale des mycolates  $\alpha$ , cause une défaillance de virulence *in vivo* notamment par l'incapacité à former des cordes, phénomène largement impliqué dans la physiopathologie mycobactérienne [405]. Les acides mycoliques extractibles ont également leur rôle dans la pathogénèse et la virulence mycobactérienne de par leur rôle immunostimulant. En effet, il a été montré que les TDM sont

**Figure 39 : Acides mycoliques de *M. abscessus***

*M. abscessus* synthétise trois types d'acides mycoliques  $\alpha$  avec une insaturation *cis* en position proximale et une insaturation *cis* ou *trans* en position distale ou un groupement cyclopropane au niveau distal de la chaîne méromycolique. Une chaîne d'acide méromycolique plus courte avec une insaturation *cis* caractérise les acides mycoliques de type  $\alpha'$ .

**Figure 40 : Structure des acides mycoliques époxy**

Les acides mycoliques époxy, retrouvés notamment chez *M. fortuitum* ou encore *M. smegmatis* présentent une insaturation proximale, ainsi qu'un groupement époxyde avec un méthyle adjacent en position distale.



reconnus par les lectines de type C Mincle qui engendrent, avec le segment transmembranaire du récepteur Fc $\gamma$ , une large production de cytokines proinflammatoires tels que le TNF, l'IL-1 $\beta$  et l'IL-6, permettant le recrutement de cellules immunitaires *via* une inflammation de type M1 médiée par les macrophages et la formation de granulomes *in vivo* [406,407]. Les acides mycoliques méthoxy activent également l'immunité et notamment les lymphocytes T en se liant à la protéine présentatrice d'antigène CD1b présente sur les cellules immunitaires innées [408,409]. Enfin, les groupements oxygénés vont, de la même manière, être essentiels à la virulence de *M. tuberculosis*. Ces derniers ont un rôle dans la croissance intracellulaire [410] et la virulence *in vivo* dans un modèle murin [411]. En outre, l'oxygénation du groupe distal des mycolates méthoxy et keto intervient dans l'induction de la réponse inflammatoire tandis que les mycolates  $\alpha$  ne provoquent pas d'inflammation [412]. En plus des différences dans les groupements fonctionnels, les acides mycoliques peuvent adopter des conformations variées (huit différentes) selon la courbure de leurs chaînes dépendante de l'arrangement des extrémités ou des différents groupements fonctionnels [413]. Une certaine adaptabilité de conformation est d'ailleurs possible en réponse à la pression, ou la température ambiante. Cet empilement divergent est un des facteurs majeurs qui déterminera l'épaisseur, la densité, la résistance ou encore la perméabilité de la mycomembrane avec des stabilités plus ou moins grande pour chaque conformation. Il a notamment été montré que la présence d'un cycle *trans*-cyclopropane va préférentiellement stabiliser les mycolates keto et méthoxy en comparaison aux groupement *cis*-cyclopropanes [414]. De plus, la présence des composants oxygénés stabilise certaines conformations plus stables des acides mycoliques  $\alpha$ , et pourrait favoriser une mycomembrane nettement plus résistante et imperméable aux molécules externes [413].

*M. abscessus* synthétise des acides mycoliques  $\alpha$  et des espèces comprenant une chaîne méromycolique plus courte, nommés  $\alpha'$  qui présentent une double liaison *cis* au niveau de la chaîne méromycolique [344,399] (**Figure 39**). Les mycolates  $\alpha$ , contenant de 76 à 80 atomes de carbones, sont les espèces les plus abondantes chez *M. abscessus*. Cette espèce présente une gamme de trois types d'acides mycoliques  $\alpha$  comprenant exclusivement des doubles liaisons *cis* en position proximale, tandis que la position distale peut présenter une insaturation *cis*, *trans* ou alors, en plus faible proportion, un cycle *cis*-cyclopropane [344] (**Figure 39**). En outre, la synthèse des acides mycoliques  $\alpha'$  de 62 ou 64 atomes de carbone est permise par le seul gène *MAB\_1915*. En effet, l'introduction du gène orthologue *MSMEG\_4301* dans la souche Pasteur 1173 de *M. bovis* BCG a permis l'expression de mycolates  $\alpha'$  non produits naturellement par cette espèce [415]. Ces données montrent ainsi que le produit de ce gène exerce une action enzymatique qui entre en jeu dans l'étape de condensation entre les courtes chaînes acyles  $\alpha$  et les chaînes méromycoliques chez les espèces mycobactériennes [416].



Enfin, nous savons que *M. abscessus* est capable de former des biofilms *in vitro* et chez les patients infectés, qui viennent renforcer la résistance intrinsèque de ce pathogène. Une étude récente a montré une régulation différentielle de gènes impliqués dans la synthèse des acides mycoliques lorsque *M. abscessus* est dans cette conformation communautaire [51]. On retrouve notamment une surexpression de gènes impliqués dans l'élongation et la modification de la chaîne méromycolique, tels que *MAB\_2030* et *MAB\_2028* codant les protéines KasA/B impliquées dans l'élongation ; le gène *MAB\_2032* codant une réductase ; *MAB\_3354* ayant un potentiel rôle de désaturase et *MAB\_3455c* codant un acyl-CoA thiolase putative. Le contenu des biofilms présente davantage de mycolates libres ainsi que d'acides mycoliques plus longs avec probablement une augmentation de la cyclopropanation en comparaison à ceux retrouvés dans un état planctonique [51].

A l'instar de *M. abscessus*, *M. fortuitum* présente des acides mycoliques  $\alpha$  et des quantités variables d'espèces  $\alpha'$  plus courtes, mais aussi des acides mycoliques oxygénés de type époxy [399,417]. Ces derniers présentent, sur leur chaîne méromycolique, une insaturation au niveau proximal ainsi qu'un groupement époxyde *trans* à la position distale avec une branche méthyle adjacente [418] (**Figure 40**). La composition en acides mycoliques de *M. fortuitum* est comparable à celle retrouvée chez la souche non-pathogène *M. smegmatis* bien que cette dernière contienne plus de mycolates  $\alpha'$  [419].

La biosynthèse des acides mycoliques nécessite de nombreuses étapes impliquant diverses enzymes décrites ci-dessous. Cette synthèse se fait en trois grandes étapes clés : 1) la synthèse et l'élongation des chaînes  $\alpha$  et méromycoliques ; 2) l'insertion des diverses modifications au niveau de la chaîne méromycolique donnant la signature au mycolate ; 3) l'activation et la condensation de ces deux chaînes d'acides gras précédant l'élaboration du motif mycolique. Cette synthèse met en jeu les systèmes FAS (« Fatty Acid Synthase ») qui, à chaque cycle, ajouteront deux atomes de carbone apportés par un malonyl-CoA.

La grande diversité et l'implication des acides mycoliques à différents niveaux en font une cible thérapeutique de choix. Plus particulièrement, le ciblage des multiples enzymes impliquées dans la synthèse des acides mycoliques présente une certaine attractivité du fait de leur spécificité et absence chez les mammifères.

## 2.2. Voie de synthèse des acides mycoliques

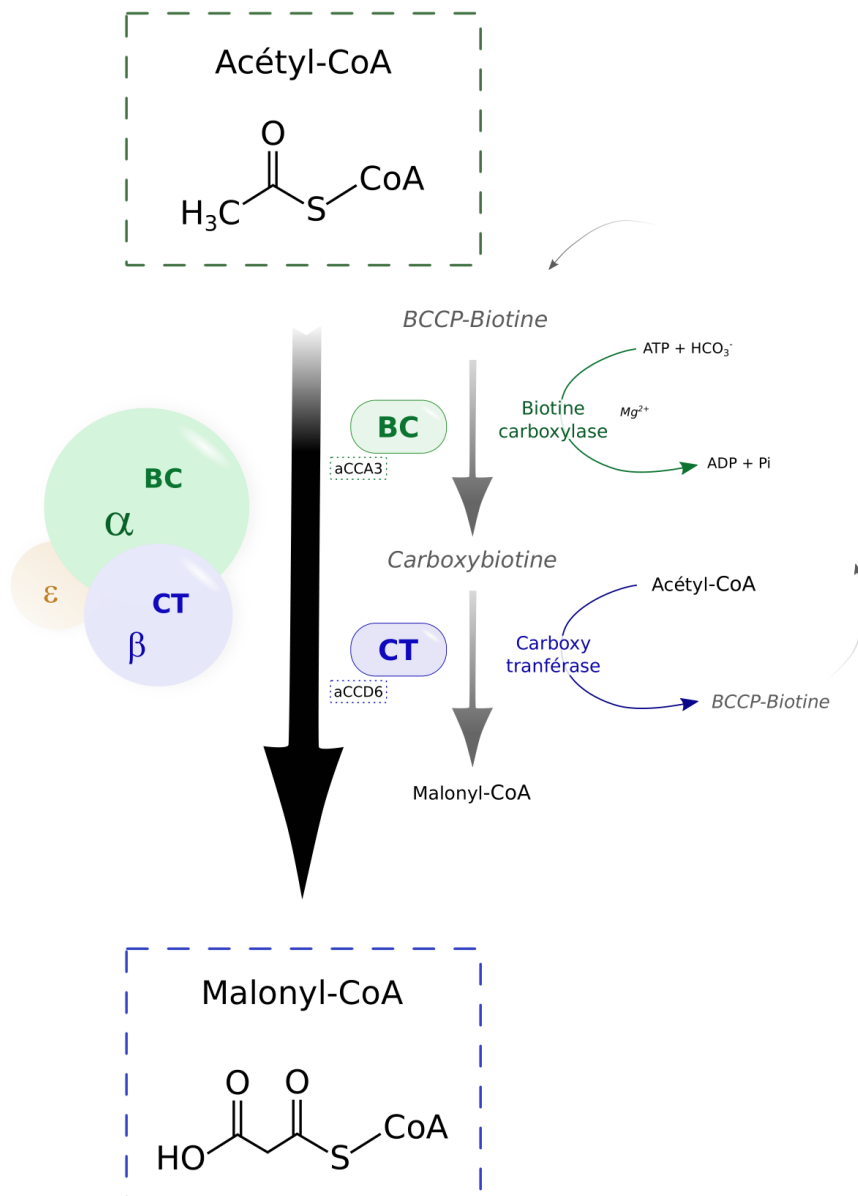
### 2.2.1. Synthèse de malonyl-CoA et carboxyacyl-CoA

Le malonyl-CoA est un substrat universel chez les mycobactéries et essentiel à la synthèse des acides mycoliques et autres acides gras venant s'incorporer à la chaîne acyle en cours de synthèse durant les



**Figure 41 : Synthèse de malonyl-CoA à partir d'acétyl-CoA**

La carboxylation d'une molécule d'acétyl-CoA est catalysée par un complexe acyl-CoA carboxylase subdivisé en trois sous-parties,  $\alpha$ ,  $\beta$  et  $\epsilon$ . La sous-unité  $\alpha$  (vert) est responsable de la carboxylation de la biotine grâce à son activité biotine carboxylase (BC). Cette carboxybiotine est ensuite transférée à une molécule d'acétyl-CoA via l'activité carboxy transférase (CT) de la sous-unité  $\beta$  (bleu) du complexe. La sous-unité  $\epsilon$  (orange) permet de réguler positivement l'activité du complexe acyl-CoA carboxylase.



cycles itératifs impliquant les systèmes FAS. Il est généré à partir de la carboxylation d'une molécule d'acétyl-CoA catalysée par un complexe acétyl-CoA carboxylase [420]. Chez les mycobactéries, ces complexes enzymatiques ayant une large diversité de substrats sont appelés acyl-CoA carboxylases (ACC) et permettent les deux demi-réactions nécessaires à l'étape de carboxylation. Elle consiste, dans un premier temps, à la carboxylation ATP-dépendante de la biotine par le domaine biotine carboxylase (BC) ou sous-unité  $\alpha$ . Cette étape est suivie, dans un second temps, par le transfert du groupement carboxyle (de la carboxybiotine) à la molécule d'acétyl-CoA par la sous-unité  $\beta$  ou carboxyltransférase (CT). De plus, ces ACC contiennent une sous-unité  $\epsilon$  modulant positivement l'activité du complexe [421–424] (**Figure 41**). Chaque sous-unité catalytique est codée par un gène distinct [425]. Chez *M. tuberculosis*, trois gènes codent la sous-unité  $\alpha$  (*accA1*, *accA2* et *accA3*), six gènes codent la sous-unité  $\beta$  (*accD1*, *accD2*, *accD3*, *accD4*, *accD5* et *accD6*) et le gène *accE5* (*Rv3281*) code la sous-unité  $\epsilon$  [387,425]. L'association de trois types de sous-unités va donner la spécificité au complexe, notamment *via* les sous-unités  $\beta$ . Il a été montré chez *M. tuberculosis* que la protéine AccA3 forme des complexes fonctionnels d'ACC avec AccE associée aux trois protéines essentielles pour la synthèse d'acides gras, AccD4, AccD5 ou AccD6 [426]. AccA3 permet de fournir la biotine carboxylée aux trois protéines AccD essentielles [427]. L'enzyme essentielle AccD6 va permettre la biosynthèse des acides mycoliques, et plus particulièrement la néosynthèse de malonyl-CoA (à partir -préférentiellement- d'acétyl-CoA ou encore de propionyl-CoA) qui va constituer la base du fonctionnement du système FAS II [426,428–430]. Le remplacement par l'AccD5 dans le complexe va permettre de générer du méthylmalonyl-CoA nécessaire à l'élongation de substrats lipidiques méthylés préférentiellement à partir de propionyl-CoA [422,423,431,432]. Tandis que l'AccD4 va être responsable de la carboxylation des acyl-CoA  $C_{24-26}$  produit par FAS I, donnant lieu aux carboxyacil-CoAs entrant en jeu dans l'étape de condensation mycolique entre les deux chaînes ( $\alpha$  et méromycolique) des acides mycoliques [426,431,433] (voir **Chapitre III : Paroi et acides mycoliques**, 2.2.4. Modifications, activations et condensation des chaînes d'acides mycoliques).

### 2.2.2. FAS I

La biosynthèse des acides gras, et notamment des acides mycoliques implique des étapes successives et cycliques intégrant les systèmes de types FAS avec en premier lieu le système FAS I. Ce polypeptide multifonctionnel est initialement retrouvé chez les champignons et les eucaryotes supérieurs, mais est également présent chez les actinomycètes tels que les mycobactéries [434,435]. Ce dernier codé par le gène *Rv2524c* chez *M. tuberculosis*, contrairement au complexe FAS II des procaryotes, est capable d'une synthèse *de novo* d'acides gras à partir du malonyl-CoA précédemment synthétisé et a été

**Figure 42 : Organisation du système multifonctionnel FAS I**

L'enzyme FAS I présente sept domaines distincts aboutissant à la synthèse *de novo* d'acyl-CoAs à partir de malonyl-CoA. Les sept domaines de cette enzyme sont organisés ainsi : acyltransférase (AT), 2-*trans*-énoyl réductase (ER), déshydratase (DH), malonyl/palmitoyl transférase (MPT), « acyl carrier protein » (ACP),  $\beta$ -ketoacyl réductase (KR) et  $\beta$ -ketoacyl synthase (KS).

Adapté de Elad N, *et al.* 2018, [436]



montré comme essentiel chez *M. smegmatis* [437] et potentiellement chez *M. tuberculosis* [438]. L'enzyme FAS I a une structure complexe et présente sept domaines distincts [436,439]. Ces derniers, organisés dans un ordre précis, sont les suivants : acyltransférase, 2-*trans*-énoyl réductase, déshydratase, malonyl/palmitoyl transférase, « acyl carrier protein » (ACP) ou protéine porteuse d'acyl,  $\beta$ -ketoacyl réductase et  $\beta$ -ketoacyl synthase [439] (**Figure 42**). Cette enzyme multifonctionnelle va générer des intermédiaires qui resteront liés à l'enzyme et qui subiront une transacylation vers les autres domaines catalytiques de FAS I [401]. Grâce à cela, les mycobactéries sont capables d'une synthèse bimodale d'acyl-CoAs [434,437]. En effet, bien que les acyl-CoAs  $C_{16-18}$  soient synthétisés en majorité, le système FAS I peut également entraîner leur élongation en acyl-CoAs  $C_{24-26}$  constituant la chaîne  $\alpha$  des acides mycoliques suite à la carboxylation par un complexe ACC [440,441]. Enfin, les acyl-CoAs  $C_{16-18}$  sont utilisés pour la synthèse des phospholipides membranaires, mais représentent également les substrats du complexe FAS II nécessaires à la synthèse et l'élongation de la chaîne méromycolique.

### 2.2.3. FAS II

Le système FAS II, incapable de synthèse d'acides gras *de novo*, a pour rôle l'élongation des acyl-CoAs  $C_{16-18}$  résultant de FAS I en acyl-ACPs  $C_{40-60}$ . Il est composé d'enzymes monofonctionnelles distinctes agissant toutes sur un substrat malonyl porté par une protéine ACP, plus particulièrement nommée AcpM et codée par le gène *Rv2244* chez *M. tuberculosis* [442]. La protéine AcpM transfère les intermédiaires de la chaîne acyle à chaque enzyme de FAS II [443] et sa forme active, ou *holo*-ACP, est 4'-phosphopantéthénylée sur le résidu sérine 41 conservé par l'action de la phosphopantéthényl transférase PptT [444,445]. AcpM va être transacylée avec une molécule de malonyl-CoA grâce à l'action catalytique de la transacylase de malonyl-CoA-ACP FabD, codée par le gène *Rv2243* chez *M. tuberculosis*, permettant la synthèse de malonyl-ACP, unité d'élongation et substrat de FAS II [446]. Chaque cycle permet d'introduire 2 atomes de carbone à la chaîne acyl en cours d'élongation et comporte quatre étapes menées par quatre enzymes distinctes et essentielles (**Figure 43**). Dans un premier temps, une première étape de pivot entre FAS I et FAS II consiste en la réaction de condensation de Claisen entre les acyl-CoAs  $C_{16-18}$  et le malonyl-ACP grâce à la  $\beta$ -ketoacyl ACP synthase de type III FabH et permet la formation de  $\beta$ -ketoacyl-ACPs [447]. Ensuite, la première étape du cycle répétitif réside en la réduction du dérivé  $\beta$ -ketoacyl-ACP en  $\beta$ -hydroxyacyl-ACP par la  $\beta$ -ketoacyl-ACP réductase NADPH-dépendante MabA [448]. Cette enzyme codée par le gène *Rv1483* chez *M. tuberculosis* et *MAB\_2723c* chez *M. abscessus* présente une spécificité pour les substrats à longue chaîne  $C_{8-20}$ . MabA s'organise spontanément en tétramère et renferme une poche de liaison largement

### Figure 43 : Voie de biosynthèse des acides mycoliques chez les mycobactéries

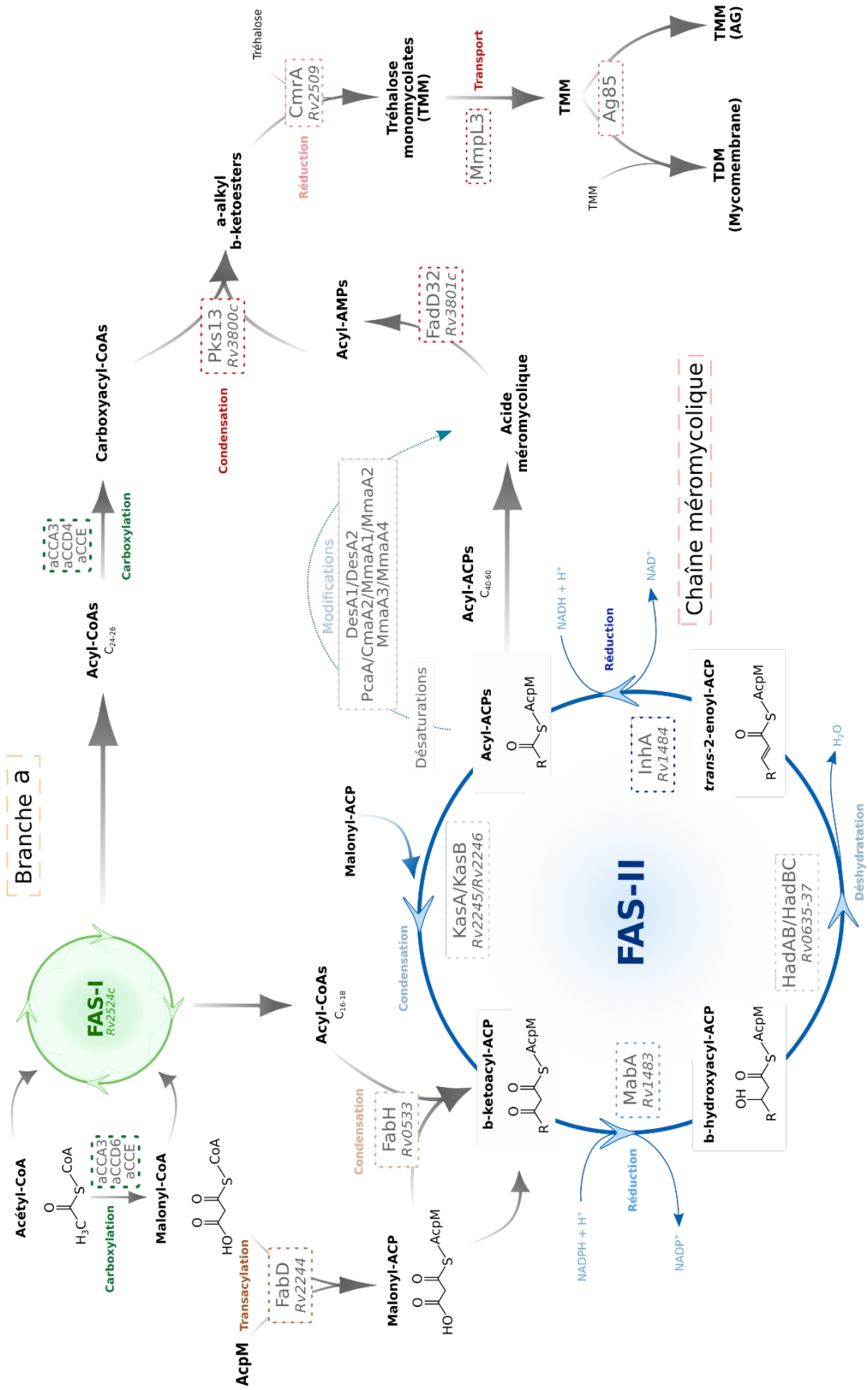
Schéma basé sur la voie de synthèse des acides mycoliques chez *M. tuberculosis*. Celle-ci débute par la synthèse *de novo* d'acides gras par le complexe FAS I, à partir d'acétyl-CoA et de malonyl-CoA, aboutissant à la formation d'acyl-CoAs  $C_{24-26}$  (future branche  $\alpha$ ) et d'acyl-CoAs  $C_{16-18}$ . Ces derniers, après condensation avec le malonyl-ACP par FabH pour donner les  $\beta$ -ketoacyl-ACP, entreront dans le complexe FAS II d'élongation. Cette étape d'élongation comprend de nombreux cycles itératifs comprenant quatre enzymes monofonctionnelles, chacune ayant un rôle particulier. MabA permet de réduire les  $\beta$ -ketoacyl-ACP en  $\beta$ -hydroxyacyl-ACP qui seront ensuite déshydratés en *trans*-2-enoyl-ACP par HadAB et HadBC. Les produits de cette déshydratation seront réduits par la protéine InhA donnant lieu aux acyl-ACPs qui reprendront le cycle d'élongation en étant pris en charge par KasA ou KasB pour être condensés avec une molécule de malonyl-ACP. Lorsque l'élongation arrive à son terme les acyl-ACPs (future chaîne méromycolique) vont subir diverses modifications ou ajout de groupements conférant la signature des acides mycoliques finaux. Après activation de chacune des deux branches, leur condensation par la protéine Pks13 permet la production d' $\alpha$ -alkyl- $\beta$ -ketoesters. Enfin la réductase CmrA permet la production d'acides mycoliques matures liés au tréhalose pour former les tréhalose monomycolates (TMM). Ces produits, transportés par MmpL3, seront ensuite transférés à la mycomembrane par l'Ag85 pour former une molécule de tréhalose dimycolate (TDM) ou être estérifiés à l'arabinogalactane (AG).

hydrophobe [449,450]. De plus, il a été montré que *M. tuberculosis* est capable de réguler la biosynthèse des acides mycoliques à travers des modifications post-traductionnelles de MabA. Plus particulièrement, la phosphorylation de trois thréonines (T21, T114 et préférentiellement T191) par la sérine/thréonine kinase PknB diminue l'activité  $\beta$ -ketoacyl-ACP réductase de MabA, notamment via une altération de la liaison du cofacteur NADPH [451].

Les  $\beta$ -hydroxyacyl-ACP résultant de l'étape précédente vont ensuite être pris en charge par les deux hétérodimères de  $\beta$ -hydroxyacyl-ACP déshydratases HadAB/HadBC codés par le cluster essentiel de gènes *Rv0635-Rv0636-Rv0637*. Ce complexe catalyse la déshydratation aboutissant à la production des 2-*trans*-énoyl ACPs [452]. Ces enzymes sont, de la même manière que MabA ou d'autres enzymes, régulées par la phosphorylation de sérines et de thréonines apparaissant comme un mécanisme de régulation clé chez les mycobactéries [453]. Cette phosphorylation est dépendante de la phase de croissance, agissant principalement pendant la phase stationnaire, elle permet de réguler négativement l'activité des déshydratases HadAB/BC et la synthèse des acides mycoliques via l'inhibition de l'élongation des chaînes méromycoliques [454].

Suite à cela, les intermédiaires énoyl-ACPs vont être réduits par la 2-*trans*-énoyl-ACP réductase InhA. Cette protéine, codée par le gène *Rv1484* chez *M. tuberculosis* ou *MAB\_2722c* chez *M. abscessus*, va catalyser la réduction en acyl-ACP en présence de NADH [455,456] (voir **Chapitre III : Paroi et acides mycoliques**, 3. L'énoyl-ACP réductase InhA).

Enfin, les cycles additionnels d'élongation sont initiés par les  $\beta$ -ketoacyl-ACP synthases KasA et KasB qui catalysent la réaction de condensation entre les acyl-ACPs et le malonyl-ACP. Cette réaction va permettre la production, à partir des acyl-ACPs générés par InhA, de  $\beta$ -ketoacyl ACPs requis pour l'élongation de la chaîne méromycolique jusqu'à sa taille définitive [457,458]. Ces deux enzymes ont un rôle similaire en catalysant la même réaction enzymatique, mais ont des substrats et produits différents. En effet, KasA permet la production d'acides gras monoinsaturés jusqu'à 40 atomes de carbone, tandis que KasB va catalyser la production de chaînes polyinsaturées pouvant atteindre 54 atomes de carbone [457,459]. Il a été ainsi proposé que KasA soit impliquée dans les premiers cycles d'élongation et que KasB prenne le relais pour atteindre la taille définitive de la branche méromycolique. Ce qui est appuyé par une étude où la délétion de *kasB* entraîne une diminution de la taille de cette chaîne [460], tandis que la mutation de KasA supprime totalement l'activité de condensation [457]. Pour finir, l'activité de ces protéines est également régulée par la phosphorylation/déphosphorylation mais de manière opposée. Lorsque la phosphorylation de KasA diminue son activité, celle de KasB permet de l'augmenter, permettant ainsi à *M. tuberculosis* de moduler ce processus d'élongation [461].



L'ensemble de ces étapes répétées (**Figure 43**) vont permettre de synthétiser de longues chaînes d'acyl-ACP de 40 à 60 atomes de carbone. La production d'acides mycoliques matures nécessite désormais une étape de condensation des chaînes produites par FAS I et FAS II, précédée par l'activation de ces chaînes et la modification de la branche méromycolique.

#### 2.2.4. Modification de la chaîne méromycolique et condensation

Les chaînes méromycoliques subissent, dans un premier temps, d'importantes modifications avant d'être associées à la branche  $\alpha$ . Ces modifications vont définir la classe d'acides mycoliques et constituer la signature de chaque espèce mycobactérienne. Elles incluent l'introduction d'insaturations, de groupements oxygénés, de fonctions méthyles ou de fonctions cyclopropanes permises par différentes enzymes [387].

L'introduction de doubles liaisons chez les mycobactéries reste assez peu décrite, avec de nombreuses hypothèses, mais il est proposé que les double liaisons *cis* servant de substrats aux enzymes modificatrices ultérieures sont introduites pendant l'élongation par FAS II *via* des réactions de déshydratation/isomérisation [462]. De plus, le génome de *M. tuberculosis* présente les trois désaturases DesA1, DesA2 et DesA3 codées respectivement par les gènes *Rv0824c*, *Rv1094* et *Rv3229c* [425]. Bien que DesA3 ait un rôle dans la synthèse d'acide oléique [463], la délétion conditionnelle de DesA1 conduit à un niveau élevé de dérivés monoénœmiques de petite taille, d'acides gras tronqués et à une perte de la biosynthèse des acides mycoliques suggérant un rôle de cette protéine dans la désaturation distale de la chaîne méromycolique [464]. De plus, il a récemment été suggéré que la protéine essentielle DesA2 ait un rôle précoce dans la synthèse des acides mycoliques, potentiellement dans l'ajout de la double liaison proximale [465]. Néanmoins l'activité exacte de ces enzymes reste encore à démontrer pour le moment.

L'introduction de fonctions oxygénées nécessaires à la formation des mycolates methoxy et keto est liée à la formation d'un précurseur hydroxylé catalysé par la méthyltransférase S-adénosyl-méthionine (SAM)-dépendante MmaA4, ou Hma [411,466]. En effet, la délétion du gène *hma* entraîne une perte de production de mycolates keto ou methoxy [411]. Le précurseur hydroxylé apparaît comme le substrat de l'enzyme MmaA3 qui va permettre la méthylation de la fonction alcool, et ainsi donner lieu aux mycolates methoxy [467,468].

D'autres méthyltransférases SAM-dépendantes seront responsables de l'introduction des cycles cyclopropanes ou des branches méthyles. On peut notamment citer la protéine PcaA (ou UmaA2), responsable de l'ajout d'un cycle *cis*-cyclopropane proximal sur les acides mycoliques  $\alpha$  [405]. Tandis que la protéine MmaA2 catalyse l'addition de cyclopropane en position distale des mycolates  $\alpha$ , ainsi

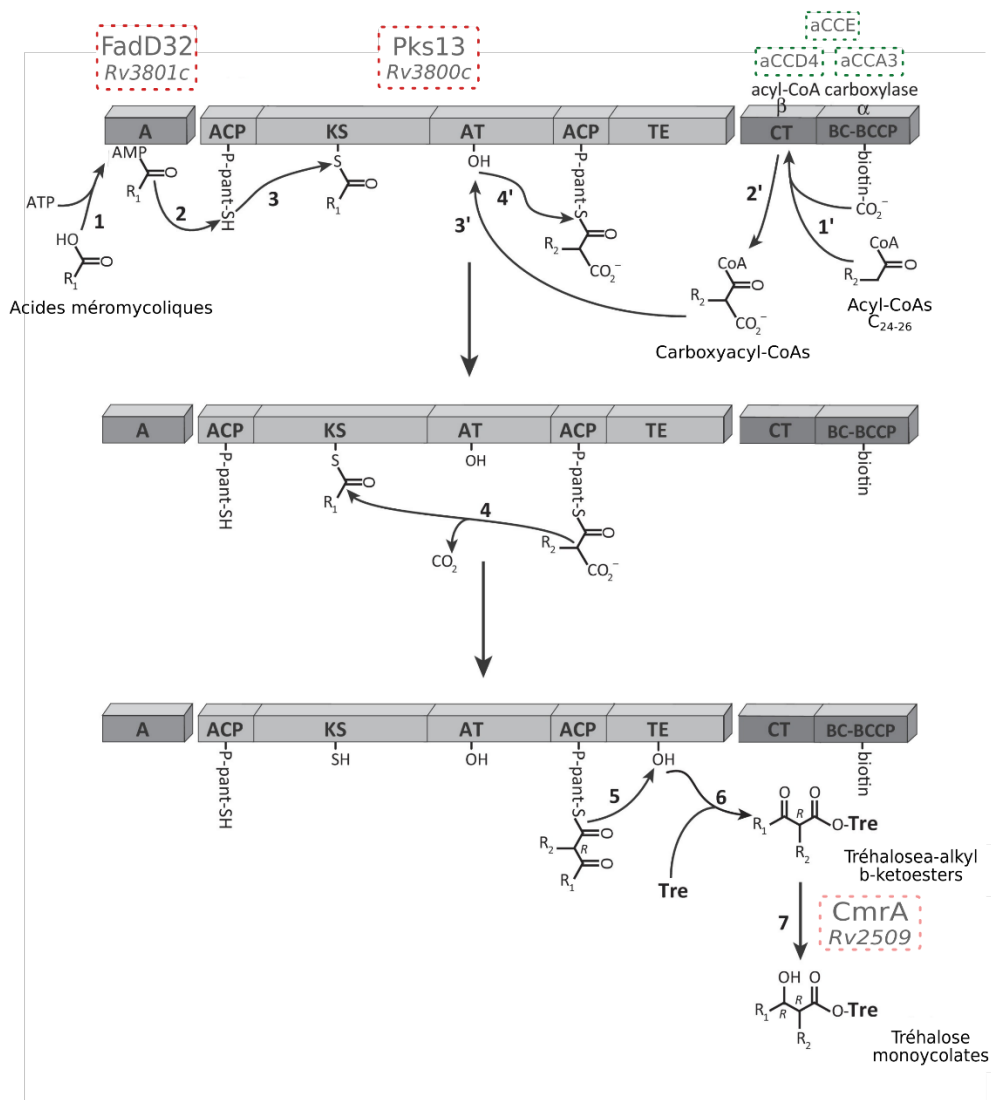


### Figure 44 : Condensation mycolique finale formant les acides mycoliques matures

L'étape de condensation mycolique à proprement dite est précédée par l'activation des deux branches constituant les acides mycoliques. Les acides méromycoliques provenant de FAS II sont activés en acyl-AMPs par FadD32 (1), tandis que les acyl-CoAs  $C_{24-26}$  provenant de FAS I sont carboxylés par le complexe acétyl-CoA carboxylase AccA3-AccE-AccD4 (1' et 2').

Les acyl-AMPs sont chargés sur le domaine ACP N-terminal de la polykétide synthase Pks13 (2) qui les transférera au domaine ketoacylsynthase (KS) (3). Les carboxyacyl-CoAs (2') sont chargés sur le domaine acyltransférase (AT) de Pks13 (3') et transférés au domaine ACP C-terminal (4'). Le domaine KS va ainsi catalyser la condensation entre les deux chaînes produisant les  $\alpha$ -alkyl  $\beta$ -ketoesters (4). Le domaine thioestérase (TE) charge les produits de condensation sur son site actif (5) et catalyse leur transfert au tréhalose (6) donnant lieu aux précurseurs des TMM. Ces derniers seront réduits par CmrA résultant en la formation des TMM (7).

Adapté de Quémard A., *et al.* 2016, [469]



qu'en position proximale des acides mycoliques oxygénés *cis* [470,471]. De plus, l'enzyme CmaA2 accompagnée de MmaA1, vont permettre la cyclopropanation proximale des mycolates oxygénés *trans* [470,472]. Suite à ces modifications, la chaîne méromycolique, mais également la branche  $\alpha$  subissent une activation avant l'étape de condensation à proprement dite (**Figure 44**). Les acyl-CoAs  $C_{24-26}$  produits par FAS I vont être carboxylés par le complexe acétyl-CoA carboxylase AccA3-AccE-AccD4, permettant la synthèse de carboxyacyl-CoAs, futurs substrats de la condensation mycolique [426,433]. En parallèle, l'AMP-ligase d'acides gras FadD32, codée par le gène essentiel *Rv3801c* chez *M. tuberculosis*, catalyse la formation d'acyl-AMPs (ou méromycolyl-AMPs) à partir des acyl-ACPs modifiés provenant de FAS II [416,433,473]. Ces produits activés seront ensuite transférés à la polykétide synthase Pks13 pour l'étape de condensation [474]. Cette enzyme présente cinq domaines essentiels à son activité : ACP N-terminal, ketoacylsynthase, acyltransférase, ACP C-terminal et thioestérase [416,475] (**Figure 44**). De plus, l'activité de Pks13 dépend de l'ajout du groupement phosphopantéthéine par la phosphopantéthényl transférase PptT [444] et va permettre la production d' $\alpha$ -alkyl  $\beta$ -ketoesters précurseurs des acides mycoliques. De plus, le domaine thioestérase catalyse la libération des produits de Pks13, puis le domaine acyltransférase transfère ces produits à une molécule acceptrice de tréhalose, donnant lieu aux précurseurs des TMM [476].

Enfin, suite à cette condensation de Claisen, les précurseurs 3-oxo-mycolates liés au tréhalose sont réduits par la réductase CmrA codée par le gène *Rv2509*. Cette enzyme permet la production d'acides mycoliques matures estérifiés au tréhalose (TMM) et est requise pour la liaison des mycolates à l'AG [477,478].

### 2.3. Transport et transfert à la paroi

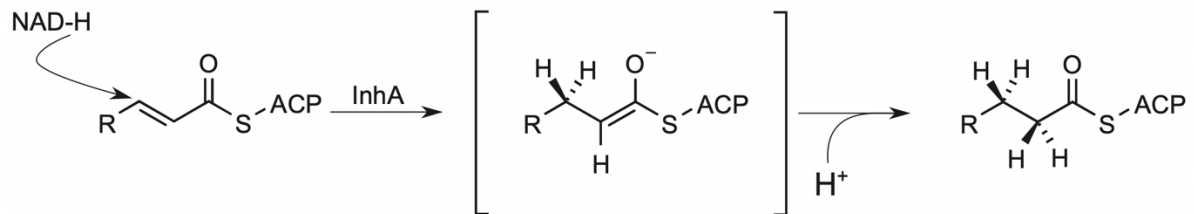
L'étape finale de la biosynthèse des acides mycoliques consiste au transport et au transfert de ces acides gras à la paroi mycobactérienne. Ces étapes sont conduites grâce au transporteur MmpL3 et aux mycolyltransférases du complexe Ag85 (Ag85 ABC) [469,479].

La protéine essentielle MmpL3 transporte les mycolates sous forme de TMM, leur permettant de traverser la membrane plasmique et ainsi pouvant être pris en charge par le complexe Ag85 [273,274,480]. De plus, une étude récente a montré l'existence de deux protéines accessoires s'associant à MmpL3. La protéine codée par *MSMEG\_5308* chez *M. smegmatis*, ou *Rv1057* chez *M. tuberculosis*, permet de stabiliser le complexe en présence d'un stress, tandis que la protéine TtfA codée par le gène *MSMEG\_0736* ou *Rv0383c* est nécessaire au transport des TMM [481,482].

Le complexe Ag85 est formé de protéines sécrétées capables de lier la fibronectine et catalyse le transfert de chaînes mycoloyls sur une molécule de TMM formant le TDM. Un transfert peut également

**Figure 45 : Schéma de la réaction de réduction du substrat énoyl-ACP en acyl-ACP catalysée par la protéine InhA**

Chollet A, *et al.* 2018, [483]



être conduit sur l'AG donnant lieu au complexe mycolates/AG/PG de la mycomembrane [484,485]. Les trois protéines du complexe partagent le même substrat, néanmoins l'activité de l'Ag85C reste supérieure à celle des deux autres [486].

L'ensemble de ces étapes nécessaires à la synthèse et au transport des acides mycoliques à la paroi mycobactérienne implique une majorité d'enzymes essentielles. Ce caractère essentiel fait de chacune de ces enzymes des cibles propices au développement d'inhibiteurs. Ainsi, au cours des années la plupart des étapes ont pu être chimiquement inhibées [387] et un regain d'intérêt récent voit le jour envers la découverte de nouveaux composés ciblant cette voie métabolique [487–489]. L'antibiotique clé de la lutte contre la tuberculose reste depuis plus de 70 ans l'INH, et cette molécule cible la 2-*trans*-énoyl ACP réductase InhA prouvant l'intérêt de cibler cette protéine chez les mycobactéries, bien qu'elle soit principalement exploitée chez *M. tuberculosis*.

### 3. L'énoyl ACP réductase InhA

#### 3.1. Description et fonction d'InhA

La protéine InhA, codée par le gène *Rv1484* chez *M. tuberculosis*, ou *MAB\_2722c* chez *M. abscessus*, est une 2-*trans*-énoyl-ACP réductase impliquée dans l'élongation des acides mycoliques. Elle fait partie de la superfamille des « Short chain Dehydrogenase/Reductase » (SDR), et présente une activité dépendante du cofacteur NADH [490]. En effet, ce dernier apporte un ion hydrure sur le carbone 3 du groupe *trans*-2-acyl permettant la réduction de la double liaison conjuguée au groupe carbonyle énoyl-ACP [456], permettant la formation des acyl-ACPs saturés [455] (**Figure 45**). InhA s'organise généralement en tétramère comprenant 8 hélices  $\alpha$  (H1 à H8) et 7 feuillets  $\beta$  (S1 à S7) et présente le motif hautement conservé des SDR Tyr-X<sub>6</sub>-Lys [483,490]. Le site actif d'InhA pouvant accueillir le cofacteur et le substrat est représenté par une poche délimitée par les feuillets S4 et S5 d'un côté, et par les hélices H6 et H7 de l'autre [483]. Chez *M. tuberculosis*, la lysine 165, présente sur l'hélice H5, a le rôle de stabiliser le cofacteur *via* des liaisons hydrogènes avec les groupes hydroxyles du nicotinamide. En effet, son remplacement par un résidu alanine ou méthionine a empêché la liaison au cofacteur NADH [491]. De plus, la tyrosine 158, présente également sur l'hélice H5, joue un rôle essentiel dans l'activité enzymatique d'InhA. Son remplacement par une phénylalanine ou une alanine fait baisser l'activité catalytique de la protéine, tandis que la mutation Tyr158Ser ne modifie pas son activité [491]. Ces résultats suggèrent que ce résidu tyrosine permet de stabiliser l'état de transition de l'intermédiaire énoilate et non pas d'être un donneur de protons comme chez d'autres énoyl-réductases [490]. En outre, le résidu phénylalanine 149, présent sur le feuillet S5, permet de faciliter

Figure 46 : Mécanisme catalytique de réduction opérée par InhA et représentation des résidus déterminants dans celui-ci

Adapté de Chollet A, *et al.* 2018, [483]

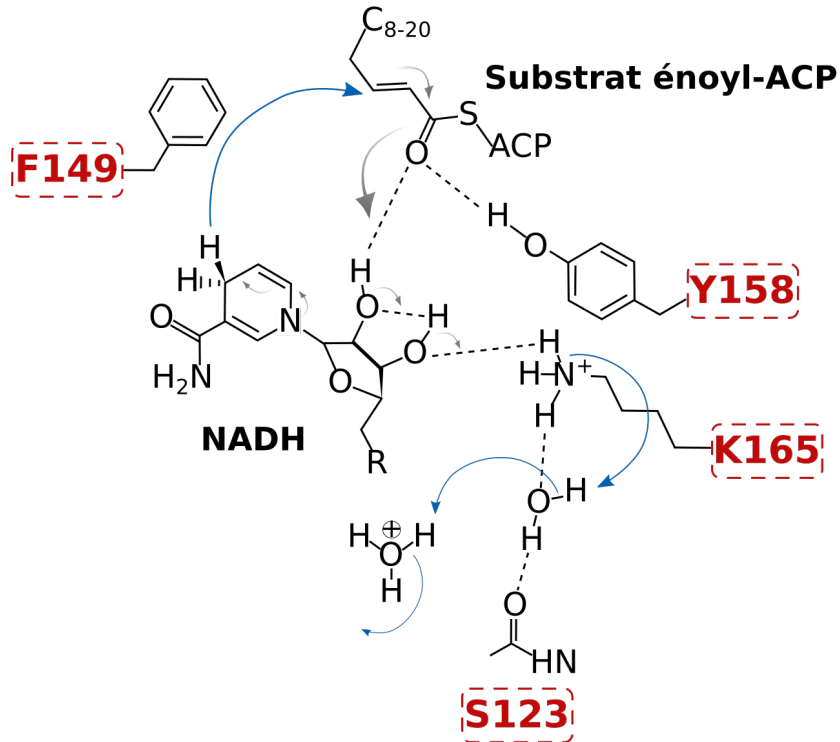
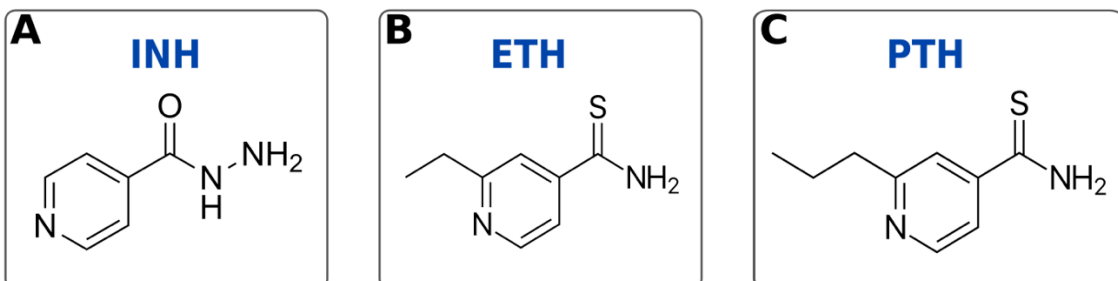


Figure 47 : Structure de différents inhibiteurs indirects d'InhA<sub>MTB</sub>

A : Isoniazide (INH), B : Ethionamide (ETH), C : Prothionamide (PTH)



l'orientation du cycle nicotinamide dans le site actif d'InhA en réduisant l'énergie de l'état de transition et ainsi aider le transfert d'ion  $H^+$  entre NADH et le substrat énoyl [492]. Enfin, le résidu sérine 123 d'InhA permet, *via* des liaisons hydrogènes, le positionnement correct d'une molécule d'eau entre ce résidu et la lysine 165, dans le but de transférer un proton vers le substrat énoilate. L'ensemble des résidus impliqués dans le mécanisme catalytique de réduction du motif énoyl sont représentés en **Figure 46**. Enfin, l'activité de cette énoyl-ACP réductase, à l'instar des autres protéines du complexe FAS II, peut être régulée par la phosphorylation réalisée par différentes sérine/thréonine kinases. L'ajout post-traductionnel d'un groupement phosphate sur le résidu thréonine 266, ou sa mutation en aspartate ou glutamate mimant l'effet de la phosphorylation, conduit à l'inhibition de la synthèse des acides mycoliques à travers une perte d'affinité pour le cofacteur NADH [493].

InhA a été identifiée en 1994 comme étant la cible principale de l'INH, encore aujourd'hui un antituberculeux de première intention très largement utilisé en clinique [296]. L'inactivation de cette protéine chez *M. smegmatis* entraîne une inhibition de la synthèse des acides mycoliques, une accumulation d'acides gras saturés provenant de FAS I et une modification de la morphologie entraînant une lyse des bacilles [494]. Ceci démontre le rôle essentiel de la protéine InhA dans la biosynthèse des acides mycoliques et l'intérêt de cibler cette enzyme chez les mycobactéries.

### 3.2. Inhibiteurs d'InhA

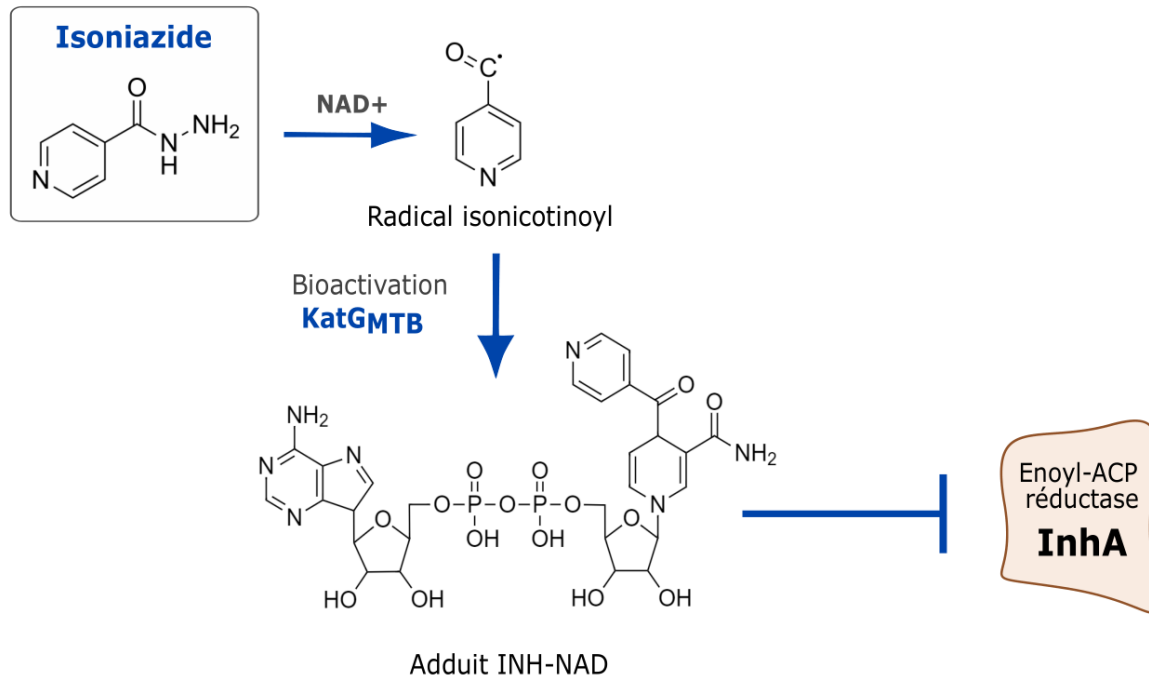
Depuis la découverte de l'activité de l'INH sur cette enzyme, un engouement particulier a vu le jour autour du développement de nouveaux inhibiteurs d'InhA, une cible de choix très largement validée par toute une série d'études combinant génétique, caractérisation biochimique et structurale [487]. Les techniques récentes de criblage à haut débit ont contribué à la découverte de nouvelles familles de composés possédant une activité inhibitrice de la protéine InhA. Ainsi, nous pouvons classer ces familles de molécules selon leur inhibition directe, ou indirecte d'InhA.

#### 3.2.1. Inhibiteurs indirects d'InhA

L'INH et ses analogues structuraux tels que l'ETH ou le prothionamide (PTH) (**Figure 47**) sont les inhibiteurs indirects majoritaires et présentent des similarités d'action. Ces derniers, nécessitant une bioactivation préalable pour pouvoir inhiber l'activité d'InhA sont décrits comme des prodrogues. L'INH requiert une activation par la catalase-péroxydase KatG afin de générer un radical isonicotinoyle qui va réagir avec  $NAD^+$  et ainsi former un adduit INH-NAD pouvant bloquer le site actif d'InhA [495–497] (**Figure 48**). Bien que de nombreuses mutations soient retrouvées au sein du gène *katG* codant

**Figure 48 : Mécanisme d'activation et d'action de l'isoniazide chez *M. tuberculosis***

Chez *M. tuberculosis*, l'isoniazide (INH) est activé par la catalase-péroxydase KatG<sub>MTB</sub> pour former le radical isonicotinoyl réagissant avec NAD<sup>+</sup> pour générer l'adduit INH-NAD capable d'inhiber l'énoyl-ACP-réductase InhA du complexe FAS-II, entraînant l'arrêt de la synthèse d'acides mycoliques et la mort bactérienne.



l'activateur ou *inhA* codant la cible [498], l'INH reste à ce jour l'un des composés les plus efficaces contre la tuberculose expliquant son maintien dans le régime thérapeutique de première ligne, même si des optimisations doivent être entreprises.

En cas de résistance, les analogues thioamides de l'INH sont utilisés en deuxième intention. L'ETH présentant un groupement 2-éthyle pyridine, et la PTH portant un groupement 2-propyl-pyridine (**Figure 47**) sont des prodrogues activées par la monooxygénase EthA, elle-même régulée par le répresseur transcriptionnel EthR [499,500]. De manière similaire au mécanisme impliquant l'INH, l'ETH et le PTH vont former un adduit covalent avec NAD<sup>+</sup> permettant d'inhiber InhA.

Aux vues de l'émergence de nombreuses mutations affectant les activateurs de ces molécules, ces dernières années ont vu le développement en masse de molécules inhibant l'enzyme InhA de manière directe.

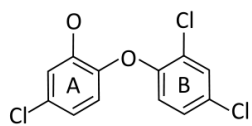
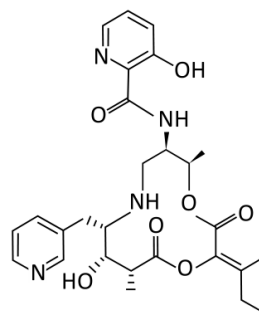
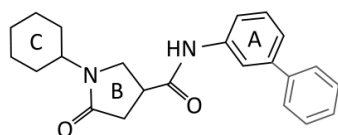
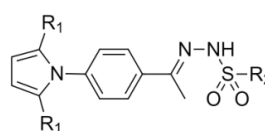
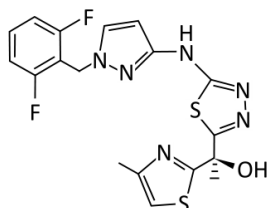
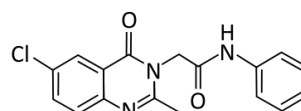
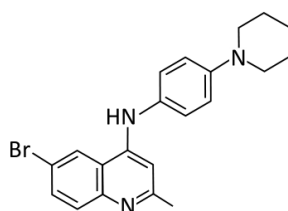
### 3.2.2. Inhibiteurs directs d'InhA

Parmi les nombreux inhibiteurs directs d'InhA décrits, seules les principales classes d'inhibiteurs présentant une activité antimycobactérienne contre *M. tuberculosis* et présentant un intérêt dans le repositionnement pour lutter contre les infections à *M. abscessus* sont décrites ci-dessous.

Le triclosan (TCS), retrouvé dans des produits de soins personnels, est connu pour inhiber la biosynthèse des acides gras chez *E. coli* où il cible l'énoyl-ACP réductase FabI [501]. Ce 5-chloro-2-(2,4-dichlorophénoxy)phénol (**Figure 49**) à large spectre présente une certaine efficacité contre les mycobactéries, et son mode d'action a été mis en évidence par la caractérisation de mutants résistants, et co-résistants à l'INH et l'ETH, chez *M. smegmatis* et *M. tuberculosis* portant des mutations au sein du gène *inhA* [502,503]. Le TCS se lie préférentiellement au complexe InhA-NAD<sup>+</sup> dans le but d'inhiber son activité et être délétère pour les mycobactéries. Cette molécule contenant deux cycles, A et B, est en constante optimisation structurelle afin d'améliorer son activité qui reste relativement modeste. En effet, de nombreux analogues ont vu le jour [504], parmi ceux-ci, certains portent des groupements plus volumineux tels qu'un triazole, des cycles aromatiques azotés, une chaîne carbonée supérieure ou encore une substitution du groupe phényle, et ont montré des interactions améliorées avec InhA et des effets antibactériens accrus [505–507].

Le composé naturel connu sous le nom de pyridomycine (**Figure 49**) est produit par *Streptomyces pyromyces* et *Dactylosporangium fulvum* et présente une activité bactéricide à faible concentration contre *M. tuberculosis* [508]. Ce dernier agit sur la protéine InhA en entrant en compétition avec le cofacteur NADH au niveau du site de liaison de la protéine, entraînant une perte de synthèse des acides mycoliques et un effet bactéricide [509]. Les inhibiteurs directs d'InhA rentrent généralement en



Figure 49 : Structure de divers inhibiteurs directs d'InhA<sub>MTB</sub>**Triclosan****Pyridomycine****Pyrrolidine carboxamide****Pyrroles****Méthyl-thiazoles****Acétamides****4-aminoquinolines (19k)**

compétition avec le substrat et non avec le cofacteur, ce qui fait de la pyridomycine une molécule intéressante de par son mode d'action.

D'autres classes de composés inhibant InhA ont vu le jour à l'instar des pyrrolidines carboxamides (**Figure 49**). Ces derniers possèdent un cycle phényle (A), un cycle 5-oxopyrrolidine (B) et un cycle cyclohexyle (C). Ces composés viennent interagir avec InhA, et une substitution 3-phényle au niveau du cycle A inhibe fortement l'activité de la protéine de *M. tuberculosis* [510].

Des dérivés du pyrrole (**Figure 49**) renfermant des groupements benzamide, pyrazoline, hydrazine, phénylthiourée, phénoxy ou isoaxole sont également retrouvés. Ces composés présentent une activité contre *M. tuberculosis* en interagissant avec InhA *via* des liaisons hydrogène dans la poche de liaison hydrophobe, similairement au TCS [511–513]. Le noyau pyrrole apparaît comme étant le groupement crucial dans l'activité inhibitrice contre InhA, en effet son remplacement par un noyau phényle ou hétéroaryle diminue drastiquement l'activité de cette classe de molécules.

Une liaison réversible d'InhA *via* l'occupation du site de liaison du substrat a été montré pour des analogues de méthyl-thiazoles (**Figure 49**) décrits comme une nouvelle classe de molécules antimycobactériennes [514]. De plus, des nouveaux inhibiteurs à base de thiadiazole ont été décrits et inhibent InhA à des concentrations inférieures avec une efficacité antibactérienne améliorée [515]. Ces analogues sont notamment pourvus de propriétés améliorées en termes d'hydrophobicité, de solubilité, de perméation et de clairance, ce qui représente un atout considérable pour le développement préclinique et clinique de futurs composés.

Des dérivés d'acétamide ont également vu le jour, plus particulièrement des 2-(4-oxoquinazoline-3(4H)-yl)acétamides identifiés comme des inhibiteurs de l'énoyl-ACP réductase InhA. Le candidat inhibiteur principal inhibant la protéine présente un cycle phényle, crucial pour l'inhibition d'InhA et un groupement chlore entraînant une hydrophobicité accrue importante pour la liaison à l'enzyme de *M. tuberculosis* (**Figure 49**) [516].

Enfin, des nouveaux inhibiteurs ont récemment été découverts par criblage, et notamment la famille des 4-aminoquinolines [517]. Plus particulièrement, le composé 19k (**Figure 49**) basé sur le ligand d'InhA préalablement identifié, LABIO-17. Ce composé présente une substitution par un atome de brome à la place du groupe ester éthylique, et exerce une meilleure activité inhibitrice d'InhA ainsi qu'une activité antimicrobienne supérieure sur un panel d'isolats de *M. tuberculosis* [518]. De plus, ce composé présente une bonne solubilité, une bonne stabilité au pH, ainsi qu'un taux d'élimination modéré, ce qui en fait une molécule particulièrement intéressante.

Ces inhibiteurs directs d'InhA offrent de nombreuses possibilités d'amélioration mais surtout valident l'intérêt de InhA en tant que cible thérapeutique dans le développement de nouveaux composés antimycobactériens.



# OBJECTIFS



Les régimes thérapeutiques actuels recommandés contre les infections mycobactériennes ne sont ni adaptés, ni optimaux et ne permettent d'éradiquer l'infection que très rarement, d'autant plus dans des cas de comorbidités. Les cas de tuberculose ne diminuent pas à travers le monde, tandis que l'on assiste à l'émergence des infections causées par des MNT opportunistes telles que *M. abscessus* ou encore *M. fortuitum*. Ce phénomène s'explique notamment par la recrudescence de résistances aux antibiotiques au travers de la sélection naturelle de mutations ou la mauvaise observance des traitements. Nous savons, en outre, que les mycobactéries possèdent naturellement un très grand nombre de mécanismes de résistance incluant de nombreuses protéines capables de neutraliser les antibiotiques ou leur cible. Ces micro-organismes possèdent également une paroi bactérienne complexe et très riche en lipides qui forment un véritable bouclier naturel à la plupart des antimycobactériens.

Les enzymes impliquées dans la synthèse de ces mêmes lipides sont la cible de plusieurs agents antituberculeux majeurs et représentent des cibles particulièrement intéressantes à exploiter dans le cadre de nouveaux développements thérapeutiques, notamment chez les MNT contre qui, paradoxalement aucun antibiotique ne cible cette voie métabolique.

Les enzymes de la biosynthèse des acides mycoliques en sont un exemple frappant, à l'instar de la protéine InhA ciblée par l'INH ou l'ETH dans le traitement de la tuberculose.

C'est dans ce contexte que s'inscrivent mes travaux de thèse, qui ont eu pour objectif d'identifier de nouvelles molécules efficaces vis-à-vis des MNT grâce à la mise en pratique des diverses approches suivantes :

- La modification de molécules efficaces connues afin d'optimiser leurs propriétés intrinsèques et permettre une efficacité antibactérienne accrue,
- La mise en évidence et la validation d'une cible thérapeutique à exploiter chez un pathogène,
- Le repositionnement de molécules précédemment démontrées comme étant efficaces sur une autre espèce mycobactérienne ou un autre pathogène.

La modification de molécules nécessite une collaboration active avec des chimistes synthétisant de nouveaux composés. Un des objectifs de mes travaux a été de cribler une banque de composés dérivés d'INH fournie par l'équipe du Pr Vipin Kumar (Université Guru Navak Dev, Amritsar, Inde) contre l'espèce *M. tuberculosis*. Suite à l'identification des meilleurs candidats, la détermination de leur cible ainsi que des études de type relation structure-activité ont été mises en œuvre afin d'évaluer l'intérêt de ces analogues structuraux d'INH (**Article 1**).



La validation d'une cible thérapeutique et le repositionnement de molécules sont intéressants dans le cas d'impasse thérapeutique rencontrée par exemple dans le cas des infections à *M. abscessus* ou d'autres MNT. Cette problématique a été centrale dans le deuxième axe de mes travaux de thèse dans lequel je me suis focalisé sur l'action du composé NITD-916. Précédemment décrit contre *M. tuberculosis*, l'objectif ici a été de démontrer son mode d'action contre *M. abscessus* à différentes échelles : tout d'abord *via* son action *in vitro* sur les souches de référence ou des isolats cliniques, puis dans un modèle d'infection cellulaire et enfin au sein d'un modèle complexe d'organoïdes pulmonaires dérivés de cellules de patients atteints de mucoviscidose. En parallèle, nous avons apporté des éléments génétiques, biochimiques et structuraux chez *M. abscessus* pour valider InhA comme la cible de ce composé chez ce pathogène (**Article 2**).

La validation de NITD-916 et de sa cible chez *M. abscessus* nous a naturellement conduit à évaluer son efficacité thérapeutique contre *M. fortuitum*, une autre MNT opportuniste émergente. Des méthodes *in vitro* et *in cellulo* similaires à celles réalisées chez *M. abscessus* accompagnées de l'évaluation de l'activité de ce composé dans un modèle d'infection *in vivo* de poisson zèbre, ont permis de démontrer son efficacité contre ce pathogène et de confirmer InhA en tant que cible exploitable (**Article 3**).





# RESULTATS



**Article 1 : “Designing quinoline-isoniazid hybrids as potent anti-tubercular agents inhibiting mycolic acid biosynthesis”**

Matthéo Alcaraz\*, Bharvi Sharma\*, Françoise Roquet-Banères, Cyril Conde, Thierry Cochard, Franck Biet, Vipan Kumar, et Laurent Kremer. *European Journal of Medicinal Chemistry*, 2022, Vol 239, Page 114531. PMID : 357 59907, DOI : 10.1016/j.ejmech.2022.114531.

L'INH est l'antibiotique de première ligne dans la lutte contre la tuberculose, il cible l'énoyl-ACP réductase InhA, une enzyme essentielle et clé de la biosynthèse des acides mycoliques. Cette cible est validée chez *M. tuberculosis* depuis de nombreuses années, néanmoins l'utilisation accrue de l'INH accentue les nombreux échecs thérapeutiques dus à l'émergence de souches résistantes. InhA reste tout de même une cible prometteuse à exploiter dans le développement de nouveaux composés antimycobactériens.

Ces constats nous ont menés à synthétiser divers analogues d'INH, en collaboration avec l'équipe du Pr Vipan Kumar, afin de pouvoir améliorer les propriétés physicochimiques de l'INH et mettre en évidence des structures prometteuses à prendre en compte dans le développement de nouveaux inhibiteurs.

Au sein de ces travaux, nous rapportons la synthèse de nouveaux analogues d'INH et leur activité contre *M. tuberculosis*. Plus particulièrement, les bases de Schiff hybrides d'INH 1H-1,2,3 triazoles liés à la quinoline (16a-16g) ont présenté une certaine activité bactéricide contre la souche de *M. tuberculosis* mc<sup>2</sup> 6230. Ces molécules, tolérées à hautes concentrations par des cellules humaines et présentant de bons paramètres ADMET (Absorption, Distribution, Métabolisme, Excrétion, Toxicité), dépendent de la bioactivation par la catalase peroxydase KatG pour permettre l'inhibition de la synthèse *de novo* des acides mycoliques *via* InhA, à l'instar de l'INH.

Dans l'ensemble, ces résultats présentent des hybrides quinoline-INH prometteurs dans la lutte contre les infections à *M. tuberculosis* qui nécessitent une évaluation préclinique plus poussée.



## Designing quinoline-isoniazid hybrids as potent anti-tubercular agents inhibiting mycolic acid biosynthesis

Matthéo Alcaraz<sup>a,1</sup>, Bharvi Sharma<sup>b,1</sup>, Françoise Roquet-Banères<sup>a</sup>, Cyril Conde<sup>c</sup>,  
Thierry Cochard<sup>c</sup>, Franck Biet<sup>c</sup>, Vipin Kumar<sup>b,\*</sup>, Laurent Kremer<sup>a,d,\*\*</sup>

<sup>a</sup> Centre National de la Recherche Scientifique UMR 9004, Institut de Recherche en Infectiologie de Montpellier (IRIM), Université de Montpellier, 1919 route de Mende, 34293, Montpellier, France

<sup>b</sup> Department of Chemistry, Guru Nanak Dev University, Amritsar, 143005, Punjab, India

<sup>c</sup> INRAE, Université de Tours, ISP, F-37380, Nouzilly, France

<sup>d</sup> INSERM, IRIM, 34293, Montpellier, France

### ARTICLE INFO

#### Keywords:

*Mycobacterium tuberculosis*  
Drug resistance  
Quinoline-isoniazid hybrids  
KatG  
InhA  
Mycolic acids

### ABSTRACT

Isoniazid is a cornerstone of modern tuberculosis (TB) therapy and targets the enoyl ACP reductase InhA, a key enzyme in mycolic acid biosynthesis. InhA is still a promising target for the development of new anti-TB drugs. Herein, we report the design, synthesis, and anti-tubercular activity of new isoniazid hybrids. Among these, 1*H*-1,2,3 triazole-tethered quinoline-isoniazid conjugates **16a** to **16g** exhibited high activity against *Mycobacterium tuberculosis* with minimal inhibitory concentrations in the 0.25–0.50 µg/mL range and were bactericidal *in vitro*. Importantly, these compounds were well tolerated at high doses on mammalian cells, leading to high selectivity indices. The hybrids were dependent on functional KatG production to inhibit mycolic acid biosynthesis. Moreover, overexpression of InhA in *M. tuberculosis* resulted in high resistance levels to **16a–16g** and reduced mycolic acid biosynthesis inhibition, similar to isoniazid. Overall, these findings suggest that the synthesized quinoline-isoniazid hybrids are promising anti-tubercular molecules, which require further pre-clinical evaluation.

### 1. Introduction

*Mycobacterium tuberculosis* (*Mtb*), the pathogen responsible for the centuries-old infectious disease tuberculosis (TB), kills over 1.4 million people worldwide each year [1]. Since the beginning of 2020, the COVID-19 pandemic has had massive health, social, and economic consequences. As a result, the pandemic has threatened to reverse progress toward global TB targets. The WHO reported a 21% decrease in TB care and facilities since 2019, resulting in an estimated half-million additional TB-related deaths, slowing the decade-long progress toward the “End TB Strategy” [2]. The rise in animal-to-human transmission (zoonotic TB) and the increased risk of survival associated with co-infections such as HIV impedes the desired TB control [3,4]. Moreover, the emergence of multi-drug resistant (MDR) and extensive-drug resistant (XDR)-TB strains, prolonged treatment regimens involving a

combination of eight to ten drugs and the possibility of treatment failure highlight the severity of the situation and provide a strong impetus for the search for new anti-TB scaffolds [5,6]. Identifying new functional entities with improved permeability profiles is regarded as an ideal strategy for combating drug resistance [7–9]. Re-engineering of pre-existing anti-TB moieties/drugs, on the other hand, is seen as a more practical and efficient way to generate promising and safe anti-mycobacterial medications in a much shorter time [10].

Quinoline is an intriguing structural core found in a wide range of natural compounds, commercially available pharmaceuticals, and clinically approved anti-TB prospects like ciprofloxacin, levofloxacin, moxifloxacin, and gatifloxacin or bedaquiline (TMC207, Sirturo) (Fig. 1) [11]. This latter has a diarylquinoline core and was approved by the US-FDA in 2012 to treat pulmonary MDR-TB after a 40-year wait. This ATP synthase inhibitor is very effective against both replicating and non-replicating strains [12]. However, side effects such as

\* Corresponding author. Department of Chemistry, Guru Nanak Dev University, Amritsar, 143005, Punjab, India.

\*\* Corresponding author. Centre National de la Recherche Scientifique UMR 9004, Institut de Recherche en Infectiologie de Montpellier (IRIM), Université de Montpellier, 1919 route de Mende, 34293, Montpellier, France.

E-mail addresses: [vipin\\_org@yahoo.com](mailto:vipin_org@yahoo.com) (V. Kumar), [laurent.kremer@irim.cnrs.fr](mailto:laurent.kremer@irim.cnrs.fr) (L. Kremer).

<sup>1</sup> These authors contributed equally to this work.

### Abbreviations

ADMET	absorption, distribution, metabolism, excretion and toxicity
INH	isoniazid
Mab	M. abscessus
MDR	multi-drug resistant
Mma	M. marinum
<i>Mtb</i>	<i>Mycobacterium tuberculosis</i>
RFB	rifabutin
SAR	structure-activity relationship
SI	selectivity index
TB	tuberculosis
TLC	thin-layer chromatography
XDR	extensive-drug resistant

phospholipidosis induction at high concentrations, unexplained deaths, and deadly heart problems owing to QT interval prolongation limit its use [13]. The addition of functionalities such as oxadiazole (I) to the quinoline core has resulted in excellent anti-TB results [14]. Furthermore, the rapid use of hydroxychloroquinoline (HCQ) during the COVID-19 period has boosted the popularity of the quinoline core, which further strengthened the therapeutic potential of this moiety in the pharmaceutical sector.

Type II fatty acid synthase (FAS-II) enoyl-acyl carrier protein (ACP) reductase (InhA) is a validated target in anti-mycobacterial drug discovery. InhA is involved in synthesizing and elongating fatty acids to produce mycolic acids, the primary component of the mycobacterial cell wall [15–17]. The well-known anti-tubercular drug, isoniazid (INH), is an InhA inhibitor [15]. The catalase-peroxidase (KatG) enzyme oxidizes INH to an isonicotinoyl radical that forms a covalent adduct (INH-NAD<sup>+</sup>) with NADH [18–21]. This adduct inhibits InhA by binding to its catalytic domain, forming a ternary complex (InhA-isonicotinoyl-NADH) [22–24]. Consequently, the bacterial surface wrinkles and bulges, resulting in deformed and swollen rods that ultimately burst. It leads to disruption of mycolic acid biosynthesis and bacterial cell death [17,23]. However, the clinical use of INH in drug-resistant TB is limited due to mutations in either *katG* or *inhA* [25,26]. Further, the low permeability of INH (logP = -0.70) in *Mtb* granuloma has indicated its

correlation with the longer duration of treatment [27,28]. In addition, the mycolic acid outer layer is too hydrophobic to allow drugs to pass through efficiently, posing a risk of antibiotic deposition at the cell wall. As a result, chemically modulating INH with a lipophilic core (II) would enhance its diffusion through the cell envelope while preventing the generation of inactive metabolites produced after N-acetylation by the N-acetyl transferase (NAT) prior to KatG activation [29,30]. As a result, the chances of INH resistance are reduced.

We have previously described the 4-aminoquinoline-isoindoline-dione-INH triad's potent anti-mycobacterial activity (III, MIC = 6.0 μM) [31] (Fig. 1). The presence of quinoline and INH was critical for hybrids to inhibit bacterial growth. Furthermore, we reported the synthesis of isatin-bis-INH hybrids as promising bactericidal compounds with improved activity against intracellular *Mtb* compared to INH [32]. Herein, we decided to combine INH and its heterocyclic analogs (nicotinic acid hydrazide/pyrazine-2-carbohydrazide) with quinoline, keeping in mind the synergistic effect of lipophilicity for mycobacterial cell wall permeation (by introducing aryl core) and physicochemical parameters (by introducing triazole) required for effective drug-like properties. To develop a robust structure-activity relationship (SAR), we introduced a variety of linkers and varied the rigidity/flexibility on the synthesized hybrids. The success of the triazole core in anti-TB drug discovery is demonstrated by compound I-A09 (IV), which is currently in clinical studies [33] (Fig. 1). In addition, nicotine- and pyrazine-based scaffolds were added in this investigation to evaluate their anti-mycobacterial potential to that of INH. Moreover, genetic and biochemical studies were also carried out to propose the mode of action of the most active hybrids by targeting InhA and inhibiting mycolic acid biosynthesis.

## 2. Results and discussion

### 2.1. Chemistry

The synthetic methodology involved the initial synthesis of 7-chloroquinoline based precursors 2, 5, and 7. For the synthesis of 4-azido-7-chloroquinoline 2, 4,7-dichloroquinoline 1 was heated with NaN<sub>3</sub> in anhydrous DMF. The reaction of 1 with various alcohol amines (ethanolamine/propanolamine) produced 3, which was then mesylated and azidated to form 4a-b [34]. Propargylation of 4-piperazinyl-7-chloroquinoline 6 (obtained by reacting 1 with piperazine) in the presence of potassium carbonate and propargyl bromide afforded

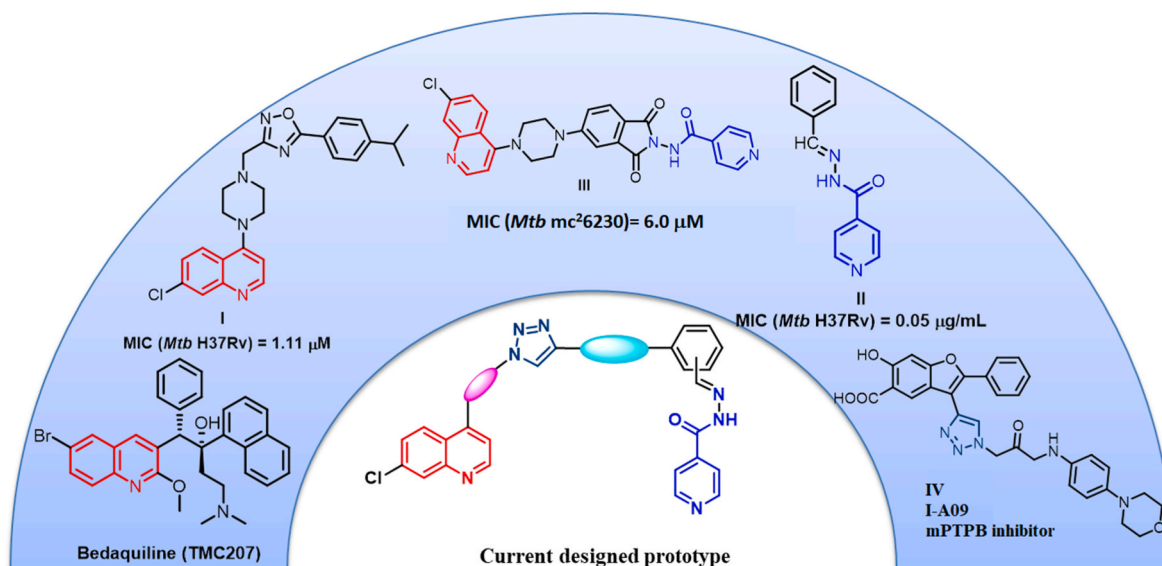


Fig. 1. Design of synthesized hybrids based on anti-mycobacterial drugs/active molecules carrying quinoline core and isoniazid.

N-propargylated-piperazinyl-quinoline **7** [35] (Scheme 1).

The alkyne precursor **9**, was obtained by treating 4-hydroxybenzaldehyde/vanillin **8** with propargyl bromide in dry acetone. Cu-promoted azide-alkyne cycloaddition (CuAAC) between appropriate azides (**2** and **5**) and alkyne **9** yielded **12a-b** and **13a-d** with latent free aldehydic functionality. 2-azido-benzaldehyde **11** was synthesized by reacting 2-nitrobenzaldehyde with NaN<sub>3</sub> and HMPA (hexamethylphosphoramide). Click reaction of **11** with **7** in the presence of CuSO<sub>4</sub>·5H<sub>2</sub>O and sodium ascorbate afforded **14** in excellent yield (Scheme 2).

The target hybrids viz. 7-chloroquinoline-isoniazid Schiff bases **16a-g** were synthesized by the condensation reaction of triazolylquinolines **12-14** with INH **15a** by heating in a microwave synthesizer (Scheme 3). The structures to the synthesized hybrids were assigned based on spectral data and analytical techniques. For instance, hybrid **16g** exhibited a molecular ion peak at *m/z* 552.1923 [M+1]<sup>+</sup> in its HRMS spectrum. In <sup>1</sup>H NMR, the presence of singlet at δ 2.75 and 3.16 corresponding to methylene (-CH<sub>2</sub>) protons of piperazine, singlet at δ 3.79 corresponding to methylene (-CH<sub>2</sub>) proton attached to triazole, singlets at δ 8.19 and 8.51 corresponding to triazole and iminic protons, multiplet ranging between δ 7.43–7.65 along with doublets at δ 8.64 (*J* = 4.8 Hz) and 8.69 (*J* = 3.6 Hz), corresponding to INH (H<sup>b</sup> and H<sup>a</sup>) protons, together with other required numbers of protons favored the formation of **16g**. In addition, the appearance of characteristic absorption peaks at δ 52.2, 52.7, 52.8, corresponding to methylene, and δ 162.3 corresponding to amide carbons of INH in <sup>13</sup>C NMR confirmed the assigned structure.

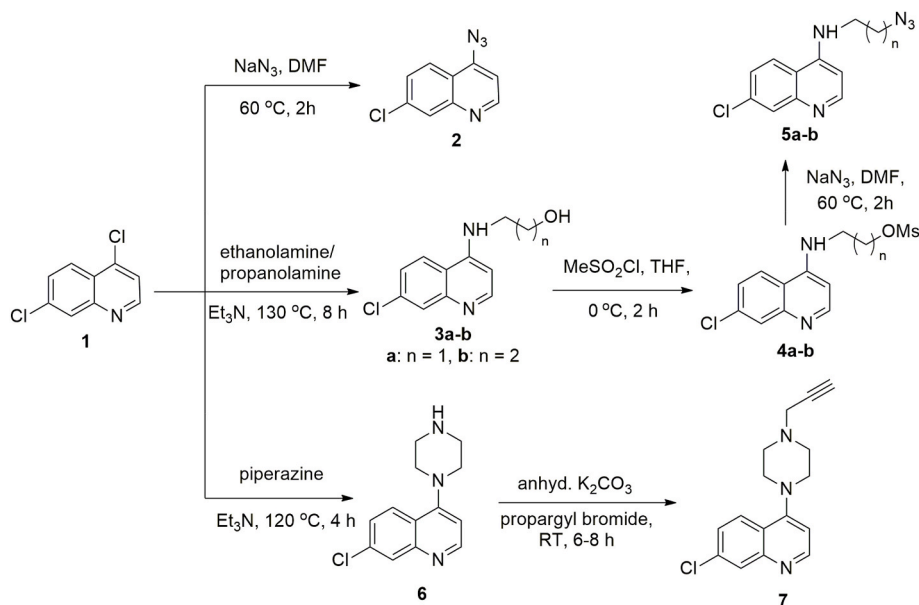
Further, to compare the anti-mycobacterial activities of 7-chloroquinoline-isoniazid, the corresponding INH analogs, namely, nicotinic hydrazide **15b** and pyrazine-2-carbohydrazide **15c**, were incorporated to synthesize their complementary 7-chloroquinoline hybrids. The reaction resulted in the formation of 7-chloroquinoline-nicotinic hydrazones **17a-g** and 7-chloroquinoline-pyrazine hydrazones **18a-g**, as shown in Scheme 4.

## 2.2. Anti-mycobacterial activity and structure-activity relationship

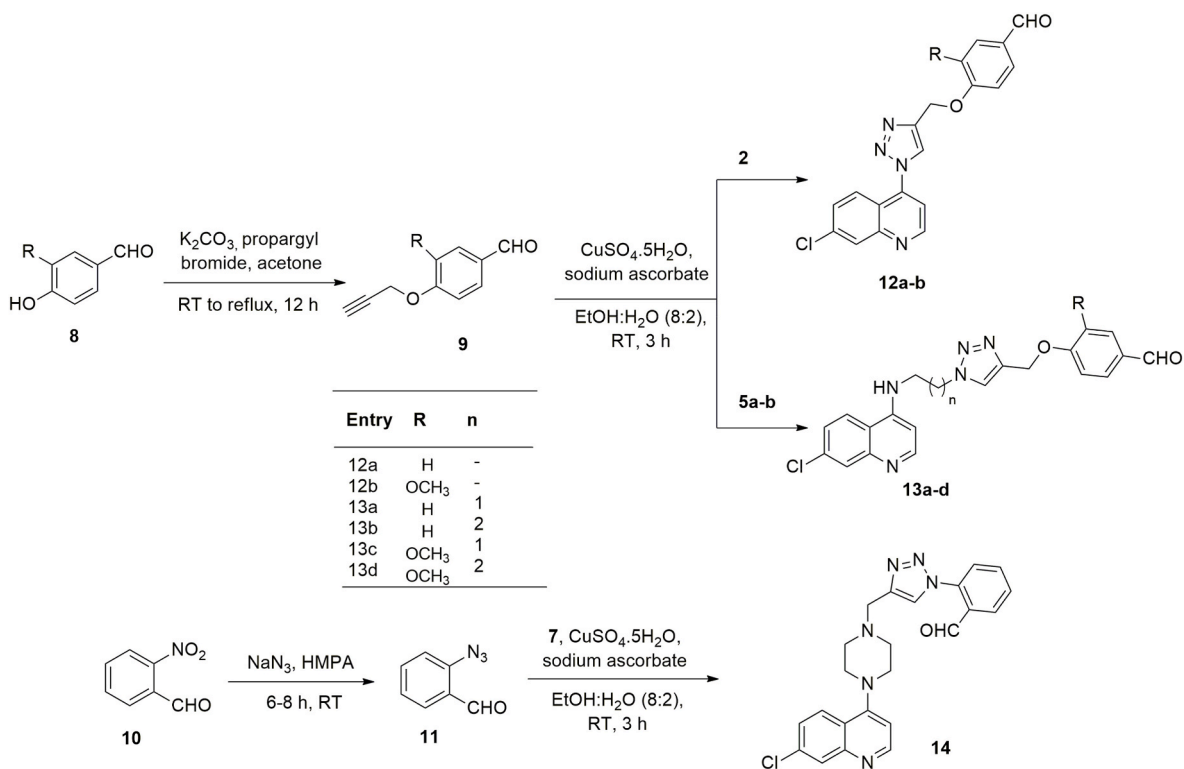
We evaluated the synthesized library of compounds (precursors and the target hybrids) for their anti-mycobacterial activities against *Mtb* mc<sup>2</sup>6230, *M. marinum* (*Mma*) M strain, and *M. abscessus* (*Mab*) CIP104536<sup>T</sup> (S and R variants) using INH as a standard drug. The anti-mycobacterial activities, expressed as minimum inhibitory

concentrations (MIC) are listed in Table 1. As apparent, even at the highest tested concentration of 200 µg/mL, most precursors, 1*H*-1,2,3-triazole tailored quinoline (**12-14**) with a free aldehydic group, were inactive on the tested strains. The inclusion of the INH core in these precursors resulted in hybrids **16a-g** with MIC values ranging from 0.25 to 0.50 µg/mL. The MIC value of the hybrid **16a**, which has a triazole ring at the C-4 position of the quinoline core, was 0.25 µg/mL, which is in the same range as the MIC values reported for isatin-bis-INH conjugates [32]. The inclusion of a methoxy substituent at the *ortho*-position of the phenyl ring in **16b** resulted in decreased anti-mycobacterial activity with a MIC of 0.50 µg/mL. The presence of flexible linkers such as ethyl and propyl on the 4-aminoquinoline ring resulted in hybrids **16c-f** having anti-mycobacterial activities ranging from 0.25 to 0.50 µg/mL. Among these hybrids, **16f** having a propyl chain as a spacer and an *ortho*-anisyl ring proved to be the most potent with a MIC value of 0.25 µg/mL. Compound **16g** with a rigid piperazine ring at the C-4 position of quinoline again showed potent activity (MIC = 0.25 µg/mL). Additionally, two of the most promising compounds, **16d** and **16g**, exhibited MIC values of 50 µg/mL against *Mma*, two-fold lower potency than INH (25 µg/mL). The non-tuberculous *Mma* is closely affiliated to *Mtb* and is responsible for TB-like illness in fish, frogs, and humans (upon exposure of injured skin to aqueous environment infected with the strain) [36]. *Mma*'s genetic similarity and pathology to human TB, as well as its improved safety profile for lab workers, make it an ideal surrogate model for studying *Mtb*. In addition, these hybrids failed to show any activity (MIC >200 µg/mL) against smooth or rough variants of *Mab* strains in the same manner as INH does (MIC >200 µg/mL). Pyrazine-2-carbohydrazide and nicotinic hydrazide were included in the present study to see if the anti-mycobacterial activity is attributable to hydrophilic INH. The lack of activity caused by pyrazine-2-carbohydrazide and nicotinic hydrazide confirmed INH's need to achieve good anti-mycobacterial outcomes. Generalized SAR in the graphical form is sketched in Fig. 2.

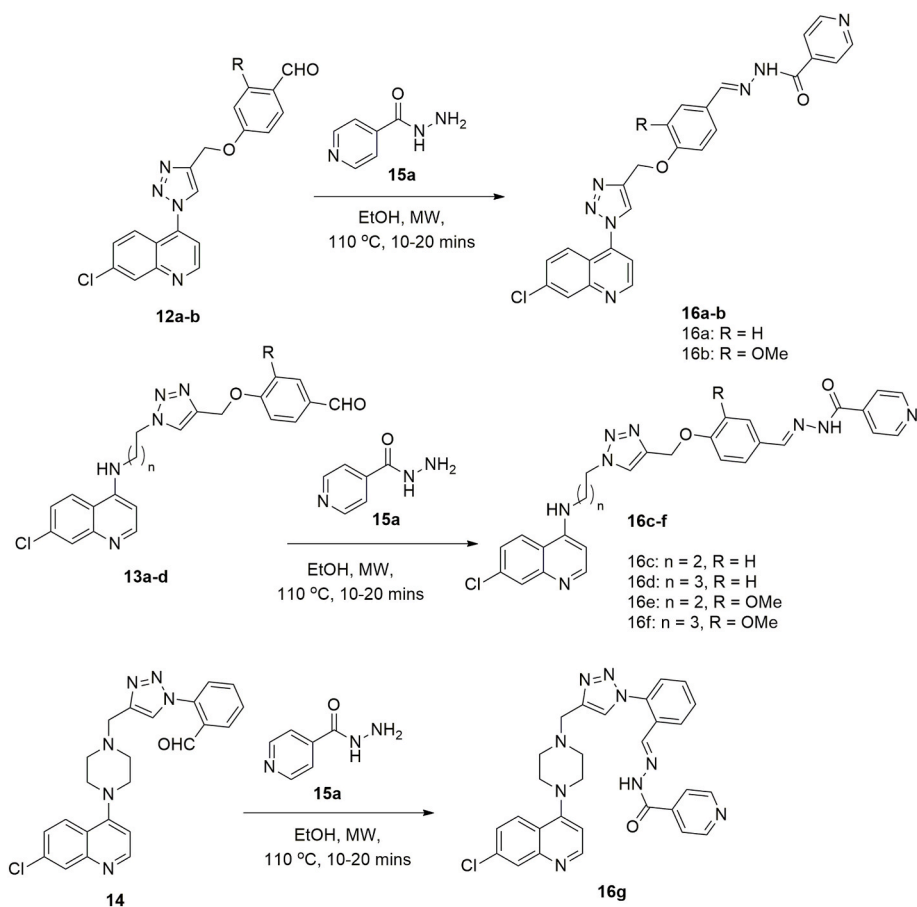
To explore the safety, effectiveness, physicochemical characteristics, and drug-like properties of the most potent hybrids **16a-g**, we theoretically calculated ADMET studies (Table S1). Compound **16a** showed an intestinal absorption value of 100%, indicating its high oral bioavailability. Poor diffusion values (LogBB values ranging between -1.45 and -1.64) for permeating the blood-brain barrier subsides the chances of side effects associated with the central nervous system. In addition, all the most potent compounds possess the potential to act as P-



Scheme 1. Synthesis of quinoline-based precursors 2-7.

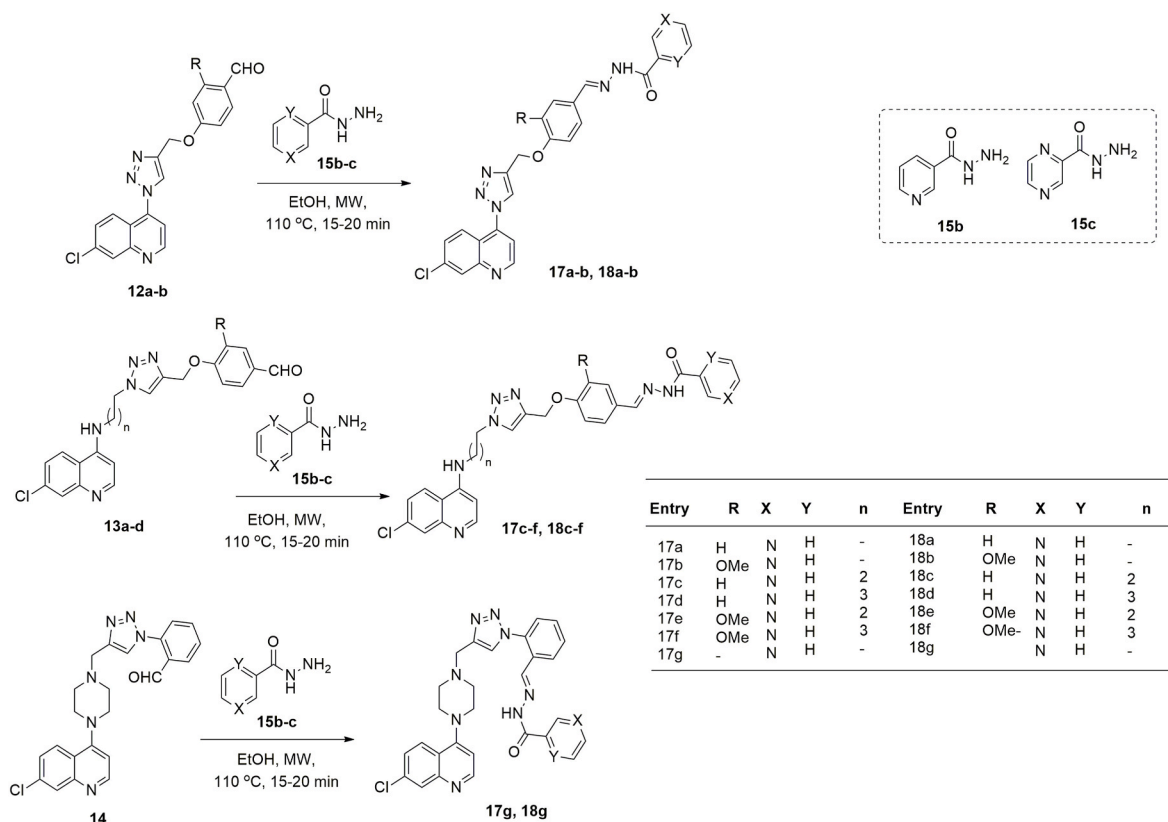


**Scheme 2.** Synthesis of Cu catalyzed 1H-1,2,3 triazolylquinoline derivatives **12–15** possessing a free aldehyde group.



**Scheme 3.** Synthesis of 1H-1,2,3 triazole-tethered quinoline-isoniazid hybrids **16a-g**.





**Scheme 4.** Synthesis of 1H-1,2,3 triazole-tethered quinoline-nicotinoyl **17a-g** and quinoline-pyrazine-2-carbohydrazone **18a-g**.

**Table 1**

MIC<sup>a</sup> (μg/mL) values determined in either 7H9 broth against *M. tuberculosis* (*Mtb*) mc<sup>2</sup>6230 carrying the empty pMV261 and *M. marinum* (*Mma*) M strain or in Cation-adjusted Mueller-Hinton broth (CaMHB) against *M. abscessus* (*Mab*) CIP104536<sup>T</sup> (S and R variants). ND, non-determined.

Entry	clogP <sup>b</sup>	<i>Mtb</i>	<i>Mma</i>	<i>Mab</i> (S)	<i>Mab</i> (R)	Entry	clogP <sup>b</sup>	<i>Mtb</i>	<i>Mma</i>	<i>Mab</i> (S)	<i>Mab</i> (R)
12a	4.12	>200	ND	ND	ND	17a	4.26	>200	ND	ND	ND
12b	3.71	>200	ND	ND	ND	17b	3.85	>200	ND	ND	ND
13a	3.91	>200	ND	ND	ND	17c	4.04	>200	ND	ND	ND
13b	4.18	50	200	>200	>200	17d	4.31	>200	ND	ND	ND
13c	3.50	>200	ND	ND	ND	17e	3.63	>200	ND	ND	ND
13d	3.77	>200	ND	ND	ND	17f	3.90	>200	ND	ND	ND
14	3.60	100	>200	>200	>200	17g	3.74	>200	ND	ND	ND
16a	4.20	0.25	>200	>200	>200	18a	4.03	>200	ND	ND	ND
16b	3.79	0.5	>200	>200	>200	18b	3.62	>200	ND	ND	ND
16c	3.99	0.5	200	>200	>200	18c	3.81	ND	ND	ND	ND
16d	4.26	0.5	50	>200	>200	18d	4.08	>200	ND	ND	ND
16e	3.58	0.5	>200	>200	>200	18e	3.40	>200	ND	ND	ND
16f	3.85	0.25	100	>200	>200	18f	3.67	>200	ND	ND	ND
16g	3.68	0.25	50	>200	>200	18g	3.51	>200	ND	ND	ND
INH <sup>c</sup>		0.05	25	>200	>200	6 <sup>d</sup>	2.23	92			

<sup>a</sup> MIC<sub>99</sub>, Minimum inhibitory concentration that inhibits 99% of bacterial growth (μg/mL).

<sup>b</sup> clogP, lipophilicity parameter calculated from Molinspiration.

<sup>c</sup> INH, isoniazid (reference drug).

<sup>d</sup> from reference [37].

glycoprotein I and II inhibitors. The majority of the hybrids showed resistance to inhibition of most CYP450 isoforms, which increases the possibility of drug clearance and reduces the risk of drug-drug interactions and other negative side effects. These compounds had high lipophilicity values, with LogP >3.95, good drug permeability, and solubilization. There was also an intriguing correlation between lipophilicity (clogP) and anti-mycobacterial activity (MIC). In the case of **14**, for example, the addition of a lipophilic aryl moiety to quinoline-piperazinyl precursor **6** (clogP = 2.23, MIC = 92 μg/mL) resulted in decreased antimycobacterial activity (clogP = 3.60, MIC = 200 μg/mL). Except for quinoline-INH derivatives **16a-g**, converting free aldehyde to

heterocyclic hydrazones had little effect on lipophilicity and anti-mycobacterial activity. Interestingly, conversion of precursor **6** (MIC = 92 μg/mL) to **16g** (MIC = 0.25 μg/mL) substantially increased the antimycobacterial activity by ~370 fold [37]. This could be attributed to the synergism between INH and the lipophilic aryl core, contributing to anti-mycobacterial potential and cell permeability.

It is also worth noting that the current framework **16f** (MIC = 0.25 μg/mL) with INH coupled via a hydrazone motif has 24 times the anti-TB activity than INH condensed to 4-aminoquinoline-isoindoline-dione motif III (Fig. 1, MIC = 6.0 μM). As a result, the improved antimycobacterial effects in the current set of hybrids over the previously

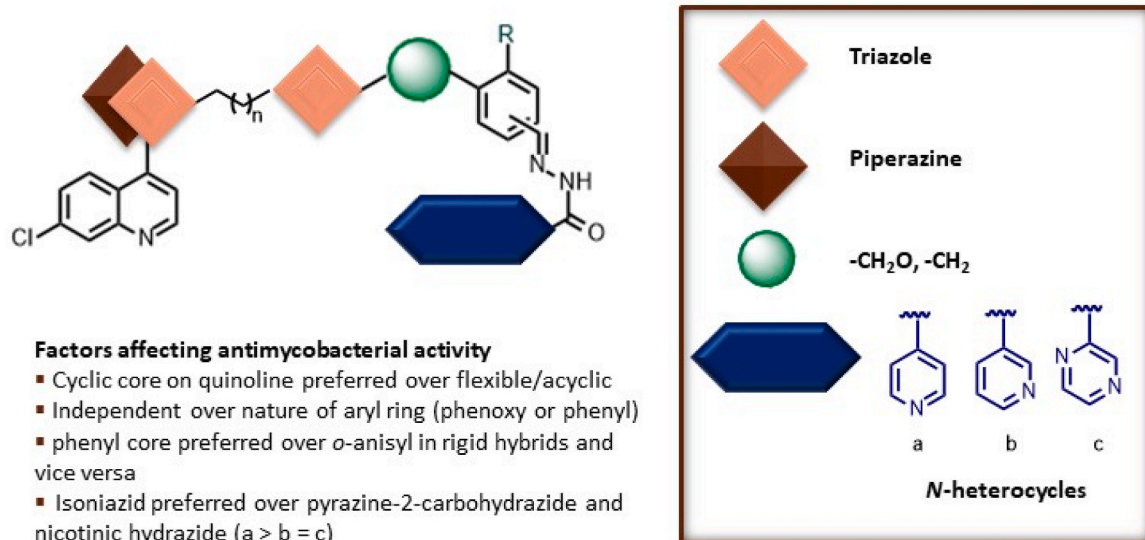


Fig. 2. Graphical representation of anti-mycobacterial SAR.

reported ones [32,37] highlight the importance of the existing structural framework in designing effective anti-mycobacterial agents.

### 2.3. Quinoline-INH conjugates (16a-g) are bactericidal against *M. tuberculosis*

We next investigated the bactericidal potency of the quinoline-INH hybrids (**16a-16g**) exhibiting low MIC values (0.25–0.50  $\mu\text{g/mL}$ ) towards *Mtb*. Bacterial cultures were individually treated with low concentrations of each **16a-16g** for 6 days, analogous to their respective MIC values that resulted in a deduction of kill curves by determining the colony-forming units (CFU). Exposure of the bacterial cultures to 1x MIC of the test compounds resulted in a progressive growth decline over time, likewise INH (Fig. 3A). Increased concentration (5x MIC) of the test compounds caused a more rapid decrease in bacteria's growth during the first 3 days of treatment, whereas an appreciable 2-log reduction in CFU compared to the inoculum was achieved on day 6 (Fig. 3B). An increase in dose to 20x MIC further improved the killing activity of the quinoline-INH hybrids (**16a-16g**) after 6 days of exposure

to the compounds ( $\sim 3$ -log reduction in CFU) but did not show a higher activity as compared to INH (Fig. 3C). Overall, these results suggest that hybrids **16a-g** exert a bactericidal activity comparable to INH against replicating *Mtb*.

### 2.4. In vitro cytotoxicity against macrophages

Many anti-TB drugs display toxicity toward eukaryotic cells. Herein, we evaluated the eventual cytotoxic activity of **16a-16g** in human THP-1 macrophages, incubated for 24 or 72 h with increasing concentrations of each compound. INH and rifabutin (RFB) were used as internal control drugs. As shown in Fig. 4, most compounds had a little effect on cell survival after 24 h of exposure, particularly at concentrations  $\leq 10$   $\mu\text{g/mL}$  ( $\text{CC}_{50} > 100$   $\mu\text{g/mL}$ ), except for **16g** ( $\text{CC}_{50} = 13$   $\mu\text{g/mL}$ ). In general, **16a, 16c, 16d, 16e, 16f** showed reduced cytotoxicity compared to RFB ( $\text{CC}_{50} = 60$   $\mu\text{g/mL}$ ) but higher cytotoxicity than INH, which did not alter cell survival at the highest concentration tested. Similar effects on cell survival were observed when testing cytotoxicity against Vero cells (Fig. S1). Further exposure of THP-1 macrophage to the compounds for

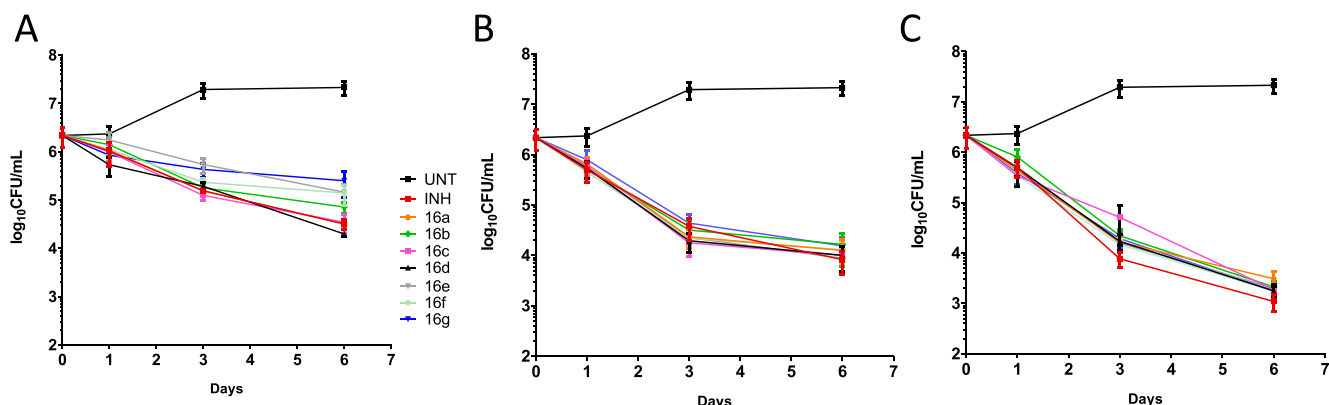
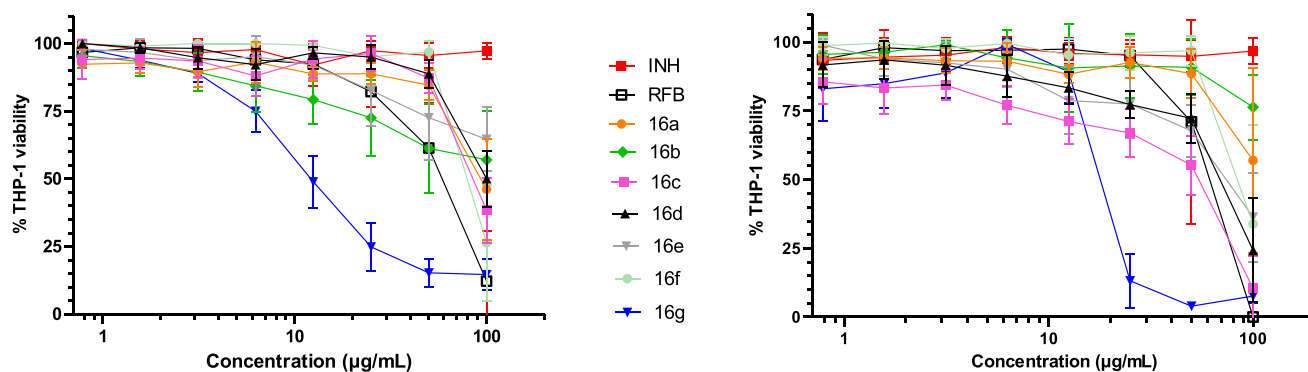


Fig. 3. Growth of *M. tuberculosis* mc<sup>2</sup>6230 treated with the **16a-g** hybrids. Bacteria grown in 7H9 broth supplemented with 10% OADC, 0.025% tyloxapol and 109  $\mu\text{M}$  pantothenic acid were incubated at 37  $^{\circ}\text{C}$  for 6 days with increasing drug concentrations corresponding to 1x MIC (A), 5x MIC (B), and 20x MIC (C) of each compound. At different time points, CFU was determined by plating 10-fold dilutions of each culture onto Middlebrook 7H10 agar plates supplemented with 10% OADC and pantothenic acid. The average of four independent experiments completed in technical triplicates is shown, with error bars representing standard deviations.



**Fig. 4.** Cytotoxicity assay of INH, rifabutin, and **16a-g** in THP-1 cells. Cells were differentiated with PMA for 48 h and exposed to increasing concentrations of each compound (starting at 100 µg/mL) for an additional 24 h (left panel) or 72 h (right panel) at 37 °C with 5% CO<sub>2</sub>. INH and RFB were included as reference drugs. Results are the mean of three independent experiments done in triplicates.

72 h (Figs. 4), **16g** appeared as the most cytotoxic compound (CC<sub>50</sub> = 18 µg/mL), followed by **16c**, **16d** and **16e** (CC<sub>50</sub> = 34 µg/mL, 67 µg/mL and 73 µg/mL, respectively). With CC<sub>50</sub> > 100 µg/mL, **16a**, **16b** and **16f** display selectivity indices (SI = CC<sub>50</sub>/MIC) of >200. Overall, these results indicate that most quinoline-INH hybrids are well tolerated at high doses on Vero kidney cells and macrophages, leading to high selectivity indices. The high SI is of particular interest for subsequent medicinal chemistry improvements to produce related compounds with augmented activity and biophysical properties, although some of the molecules already have shown good ADMET and physicochemical properties predictions.

### 2.5. Overexpression of *InhA* increases resistance to the quinoline-INH hybrids

Increased *InhA* expression or mutations that result in a decreased enzymatic affinity for binding to NADH are critical parameters in INH resistance. The covalent connection between INH and quinoline fragments in structural templates of hybrids **16a-g** causes substantial changes in the parent structure of INH either by imparting lipophilicity or by protecting the free NH<sub>2</sub> of INH. Consequently, it remains to be established whether the new hybrids share the exact mechanism of inhibition as INH by targeting *InhA* or follow a different pathway in the mechanism of action. The *inhA* gene of the FAS-II system was cloned under the control of the strong *hsp60* promoter into pMV261 [39], and the resulting plasmid was introduced into *Mtb* to explore whether **16a-g** inhibits the enoyl ACP reductase *InhA* of the FAS-II pathway [38]. The influence of *InhA* overexpression determined the MIC of **16a-g** on Middlebrook 7H9 broth and on Middlebrook 7H10 supplemented with OADC enrichment. Overexpression of *inhA* mediated high levels of resistance to each compound (25-fold enhanced MIC on pMV261-*inhA*) as compared to the control strain harboring the empty pMV261, similar to INH (20-fold enhanced MIC), and this was confirmed in both liquid medium as well as on agar plates (Table 2 and Fig. S2). Together, these results suggest that both INH and the INH hybrids share a similar mode of action, implicating the enoyl ACP reductase *InhA*.

### 2.6. *16g* inhibits de novo synthesis of mycolic acids

We next assessed the mechanisms of action of the quinoline-INH hybrids by extracting the radioactive lipids from *Mtb* cultures treated for 15 h with increasing concentrations of INH (0.01, 0.05 and 0.25 µg/mL) or **16g** (0.05, 0.25 and 1.25 µg/mL) before labeling with 1 µCi/mL [<sup>14</sup>C]acetate for an additional 7 h [40]. Mycolic acid methyl esters (MAMEs) were then separated and analyzed by thin-layer chromatography (TLC). Similar to INH, the production of the three mycolic acid

**Table 2**

MIC (µg/mL) values were determined in 7H9 broth or 7H10 agar supplemented with 10% OADC and 109 µM pantothenic acid of the most potent analogs against *M. tuberculosis* mc<sup>2</sup>6230 overexpressing *InhA*.

Compound	MIC (µg/mL)			
	7H9 broth		7H10 agar	
	pMV261	pMV261- <i>inhA</i>	pMV261	pMV261- <i>inhA</i>
<b>16a</b>	0.25	>200	0.25	6.25
<b>16b</b>	0.5	50	0.25	12.5
<b>16c</b>	0.5	12.5	0.25	6.25
<b>16d</b>	0.5	12.5	0.25	6.25
<b>16e</b>	0.5	25	0.5	12.5
<b>16f</b>	0.25	25	0.25	6.25
<b>16g</b>	0.25	6.25	0.25	6.25
INH	0.05	1	0.05	1

classes (α, methoxy, keto) was altered in a dose-dependent manner (Fig. 5). Treatment with 1.25 µg/mL **16g** abolished mycolic biosynthesis, whereas the production of fatty acid methyl esters (FAMES) remained unaffected. This indicates that, like INH, **16g** specifically inhibits FAS-II but not FAS-I, as expected for *InhA* inhibition. Notably, the mycolic acid profile of the recombinant strain carrying pMV261-*inhA* remained unaltered in the presence of 1.25 µg/mL **16g** (Fig. 5). This confirms that this strain is refractory to mycolic acid biosynthesis inhibition by **16g**, consistent with its high resistance level to **16g**. Overall, these observations are in line with specific inhibition of *InhA*, similarly to INH or isatin-bis-INH hybrids [32].

### 2.7. Strains resistant to *16d*, *16f*, and *16g* are cross-resistant to INH and mutated in *KatG*

To assess the mechanism of action of the hybrids and investigate their functional relatedness with INH, we selected spontaneously resistant strains of *Mtb* in the presence of 5x MIC or 20x MIC of either **16g** (designated strains Mtb-16g<sup>R</sup>), **16f** (designated Mtb-16f<sup>R</sup>) or **16d** (designated Mtb-16d<sup>R</sup>). The resistance frequency to these inhibitors ranged from 1.16 × 10<sup>-6</sup> to 7.1 × 10<sup>-7</sup> (Table 3). Each resistant mutant was highly cross-resistant to all other inhibitors as well as to INH, as defined by their very high resistance levels (MIC ≥200 µg/mL) (Table S2). That these strains remained susceptible to ethionamide (ETH), a drug that also targets *InhA* [15] (Table S2), suggests that mutations do not occur in *inhA*, which was subsequently confirmed by sequencing the *inhA* gene and its promoter region and whole genome sequencing (data not shown).

Since resistance to INH is mainly driven by mutations in *katG* [41],

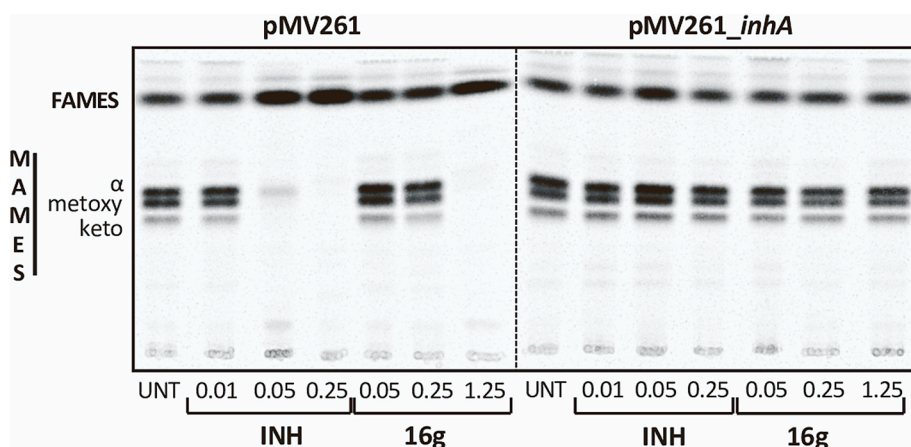


**Fig. 5.** Inhibition of mycolic acid biosynthesis by **16g**. *M. tuberculosis* mc<sup>2</sup>6230 carrying either the empty pMV261 or the pMV261-*inhA* were treated with increasing concentrations of INH or **16g** in 7H9 broth supplemented with 10% OADC, 0.025% tyloxapol and 109 μM pantothenic acid at 37 °C for 15 h with agitation. The cultures were labeled with 1 μCi/ml [<sup>14</sup>C]acetate at 37 °C for 7 h. Following extraction, total mycolic acids and fatty acids were derivatized and equal counts (50,000 cpm) of the corresponding methyl esters were loaded onto a TLC plate. [<sup>14</sup>C]-labeled lipids were separated after 2 runs in hexane/ethyl acetate (19/1, v/v) and exposed overnight.

**Table 3**

Spontaneous mutation frequency conferring resistance to **16g**, **16f** and **16d** in *M. tuberculosis* following exposure to 5x or 20x MIC. One resistant colony from each plate was subjected to whole genome sequence or PCR/sequencing of *katG*.

Strain	Mutation frequency	Gene	SNP	AA change
Mtb-16g <sub>5x</sub> <sup>R</sup>	1.8 × 10 <sup>-6</sup>	<i>katG</i>	A1780C	F594C
Mtb-16g <sub>20x</sub> <sup>R</sup>	7.1 × 10 <sup>-7</sup>	<i>katG</i>	1_557del	186 del
Mtb-16f <sub>5x</sub> <sup>R</sup>	1.16 × 10 <sup>-6</sup>	<i>katG</i>	A480G	W161R
Mtb-16d <sub>5x</sub> <sup>R</sup>	1.52 × 10 <sup>-6</sup>	<i>katG</i>	665_666insC	Stop
Mtb-16d <sub>20x</sub> <sup>R</sup>	5 × 10 <sup>-7</sup>	<i>katG</i>	G1484A	G495D

this gene was sequenced in each clone selected for resistance on plates (Table 3). Results indicate that single nucleotide polymorphisms (SNPs) occurred in *katG*. The resistor selected in the presence of 5 x MIC **16d** harbored a single nucleotide insertion at position 665, resulting in a premature stop codon after residue 274. The mutant chosen in the presence of 20x MIC **16d** harbored a G495D amino acid replacement while those selected with 5x MIC **16f** or **16g** harbored W161R and F594C single point mutations, respectively (Table 3). Whole genome sequencing of mutant Mtb-16g<sub>20x</sub><sup>R</sup> revealed a 3.6 kb deletion ranging from position 2155554 to 2159232, comprising essentially *fadB5*, *lppC*, *Rv1910c*, *furA* and part of the *katG* gene (Fig. S3). In addition, *Mtb* strains Mtb-11c<sup>R</sup>, Mtb-11d<sup>R</sup> and Mtb-INH<sup>R3</sup> carrying the G421D, L430P, and W438Stop mutations in *KatG*, respectively [32], were growing in the presence of 1 μg/mL **16a-g**, while the parental strain failed to grow at these concentrations (Fig. S4). Complementation of Mtb-11c<sup>R</sup>, Mtb-11d<sup>R</sup> and Mtb-INH<sup>R3</sup> by introducing the pSMT3-*katG* [42] restored the susceptibility to INH as well as to **16a-g** (Table S3).

Overall, this confirms that mutations in *KatG* are prominent contributors of resistance to the quinoline-INH conjugates. The point mutations, insertions or large deletions reported here are different from those identified previously with isatin-bis-INH conjugates [32] and are not frequently detected in clinical strains resistant to INH [25,43]. These findings imply that the antimicrobial activity of quinoline-INH hybrids relies on *KatG* biotransformation, similarly to isatin-bis-INH hybrids [32].

We anticipate that further functional and structural studies should confirm the binding of **16a-g** to the *KatG* binding pocket and should help explain how these mutations affect the binding of quinoline-INH hybrids and the activity of *KatG*. However, since these compounds cannot overcome bioactivation by *KatG*, it can be inferred that they are probably less potent against INH-resistant clinical strains carrying mutations in *katG*. Although subsequent studies should investigate this point using a broad panel of clinical isolates resistant to INH, this may represent a limiting step compared to direct *InhA* inhibitors [44–48]. From a mechanistic point of view, these genetic studies indicate that the quinoline-INH hybrids, similarly to isatin-INH hybrids [32] or to INH,

are pro-drugs that undergo biotransformation by *KatG* and, upon activation, are likely to react with NAD to generate the corresponding adducts, which in turn inhibit *InhA* activity, ultimately leading to mycolic acid cessation. That **16a-g** appear completely inactive against *Mab* (Table 1) is caused by the poor capacity of *KatG<sub>MAB</sub>* to activate the compounds, as previously shown for INH [49], further validating the *KatG*-dependent requirements of this family of compounds to be active. Collectively, these results provide strong evidence that quinoline-INH hybrids and isatin-INH hybrids share the same mode of bioactivation and action and that the mycolic acid pathway represents the primary target of these compounds. In addition, despite sharing a quinoline core with fluoroquinolones or bedaquiline (Fig. 1), which are clinically used drugs targeting the DNA gyrase [50] or the ATP synthase [51], respectively, the most active quinoline-INH hybrids display another mode of action. Taken collectively, the comparison of the structures and mode of action of these families of molecules indicates that bioactivation and activity of INH-containing hybrids rely mainly on INH rather than on the other structural elements.

### 3. Conclusion

INH is one of the most effective first-intent anti-TB drugs and is still utilized as a scaffold for generating new compounds to fight TB. In this study, we have synthesized and explored the anti-mycobacterial efficacy of new quinoline-based heterocyclic hydrazones. Among these, quinoline-INH hybrids **16a-g** appeared to be the most promising ones with MIC values ranging from 0.25 to 0.50 μg/mL and 50 to >200 μg/mL against *Mtb* and *Mma*, respectively. In contrast, hybrids of quinoline with nicotinic acid hydrazide and pyrazine-2-carbohydrazide failed to elicit favorable results. The potent anti-TB INH-based chemical entities exert high *in vitro* killing activity against *Mtb* and displayed low toxicity against various mammalian cell types. The compounds are pro-drugs that require *KatG* activation to inhibit *de novo* synthesis of mycolic acids by targeting *InhA*. Substantially improved (370- and 24-fold) anti-mycobacterial activity of the current set of hybrids involving an appropriately arranged quinoline, triazole, and INH exemplifies the success of the present approach compared to previously reported quinoline-based hybrids [32,37]. Future studies are requested for the advancement of these compounds to the next level of *in vivo* studies.

### 4. Materials and methods

#### 4.1. Chemistry

##### 4.1.1. General information

The reactions were performed by employing standard protocols and techniques. Schiff base condensation reactions were carried out on an



Anton Paar Monowave-50 microwave reactor. Melting points were recorded using open capillaries and Stuart digital melting-point apparatus (SMP10) and uncorrected. JEOL (400 MHz) and Bruker Avance II (500 MHz) spectrometers were used to record  $^1\text{H}$  NMR spectra, and JEOL (100 MHz) and Bruker Avance II (125 MHz) spectrometers for  $^{13}\text{C}$  NMR spectra with DMSO- $d_6$  as a solvent. The chemical shifts ( $\delta$ ) were expressed in parts per million (ppm) and coupling constants ( $J$  values) were specified in hertz (Hz). Splitting patterns are designated as s: singlet, d: doublet, t: triplet, m: multiplet, dd: double of the doublet. Using ESI as the source, mass spectral data were assembled on Bruker high-resolution mass spectrometer (micrOTOF QII) equipment.

#### 4.1.2. General procedure for the synthesis of conjugates 12-13

$\text{K}_2\text{CO}_3$  (1.2 mmol) was added to a well-stirred solution of 4-hydroxybenzaldehyde/vanillin **8** (1 mmol) in acetone, and the resulting mixture was stirred for 30 min at room temperature to generate anion. On addition of propargyl bromide (1 mmol), the reaction mixture was refluxed for 12 h. After completion of the reaction as monitored by TLC,  $\text{K}_2\text{CO}_3$  was filtered off, and acetone was evaporated under reduced pressure to yield *O*-propargylated benzaldehyde/*O*-propargylated vanillin **9** in excellent yields. The precursors **9** (1 mmol) and 4-azido-7-chloroquinoline **2** (1 mmol) were dissolved in EtOH:  $\text{H}_2\text{O}$  (8:2) mixture, and  $\text{CuSO}_4 \cdot 5\text{H}_2\text{O}$  (0.055 mmol) and sodium ascorbate (0.143 mmol) were added in a catalytic amount. The reaction mixture was stirred for 3 h at room temperature. After TLC monitoring of the reaction, the crude product was extracted with chloroform and water. The organic layer was dried with  $\text{Na}_2\text{SO}_4$  and concentrated under reduced pressure to yield the desired hybrids **12a-b**. Compounds were purified by recrystallization using ethyl acetate: hexane (8:2) mixture. The same protocol was employed for the synthesis of target compounds **13a-d** with propargylated precursor **9** and azidoquinolines **5a-b**.

4.1.2.1. 4-((1-(7-chloroquinolin-4-yl)-1H-1,2,3-triazol-4-yl)methoxy)benzaldehyde (**12a**). Yield 88%, pale white solid, MP = 194–196 °C,  $^1\text{H}$  NMR (500 MHz, DMSO- $d_6$ )  $\delta$ : 5.45 (s, 2H,  $-\text{OCH}_2$ ), 7.31 (d,  $J = 8.4$  Hz, 2H, Ar-H), 7.79 (d,  $J = 9.0$  Hz, 1H, Ar-H), 7.85 (d,  $J = 4.5$  Hz, 1H, Ar-H), 7.91 (d,  $J = 8.4$  Hz, 2H, Ar-H), 7.99 (d,  $J = 9.1$  Hz, 1H, Ar-H), 8.28 (s, 1H, triazole-H), 8.97 (s, 1H, Ar-H), 9.14 (d,  $J = 4.6$  Hz, 1H, Ar-H), 9.88 (s, 1H,  $-\text{CHO}$ ).  $^{13}\text{C}$  NMR (100 MHz, DMSO- $d_6$ )  $\delta$ : 61.5, 115.7, 117.6, 120.7, 125.7, 127.5, 128.5, 129.5, 130.4, 132.3, 135.9, 140.7, 143.4, 149.7, 152.8, 163.3, 192.0. HRMS (ESI) calcd for  $\text{C}_{19}\text{H}_{13}\text{ClN}_4\text{O}_2$   $[\text{M}+1]^+$  365.0727, found 365.0745.

4.1.2.2. 4-((1-(7-chloroquinolin-4-yl)-1H-1,2,3-triazol-4-yl)methoxy)-3-methoxybenzaldehyde (**12b**). Yield 84%, pale white solid, MP = 193–195 °C,  $^1\text{H}$  NMR (400 MHz, DMSO- $d_6$ )  $\delta$ : 3.74 (s, 3H,  $-\text{OCH}_3$ ), 5.40 (s, 2H,  $-\text{OCH}_2$ ), 6.43 (d,  $J = 5.4$  Hz, 1H, Ar-H), 7.31–7.37 (m, 2H, Ar-H), 7.42 (dd,  $J = 8.9$ , 2.0 Hz, 1H, Ar-H), 7.49 (dd,  $J = 8.5$ , 1.9 Hz, 1H, Ar-H), 7.78 (d,  $J = 1.9$  Hz, 1H, Ar-H), 8.25 (d,  $J = 9.1$  Hz, 1H, Ar-H), 8.29 (s, 1H, triazole-H), 8.37 (d,  $J = 5.2$  Hz, 1H, Ar-H), 9.88 (s, 1H,  $-\text{CHO}$ ).  $^{13}\text{C}$  NMR (125 MHz, DMSO- $d_6$ )  $\delta$ : 55.9, 61.7, 109.3, 114.6, 115.6, 117.4, 120.7, 122.4, 125.4, 128.3, 129.5, 135.8, 140.6, 143.7, 144.5, 149.6, 152.9, 162.9, 192.1. HRMS (ESI) calcd for  $\text{C}_{20}\text{H}_{15}\text{ClN}_4\text{O}_3$   $[\text{M}+1]^+$  395.0833, found 395.0865.

4.1.2.3. 4-((1-(2-((7-chloroquinolin-4-yl)amino)ethyl)-1H-1,2,3-triazol-4-yl)methoxy)benzaldehyde (**13a**). Yield 84%, pale white solid, MP = 103–107 °C,  $^1\text{H}$  NMR (400 MHz, DMSO- $d_6$ )  $\delta$ : 3.84 (s, 3H,  $-\text{CH}_2+\text{NH}$  (exchangeable with  $\text{D}_2\text{O}$ )), 4.69 (s, 2H,  $-\text{CH}_2$ ), 5.17 (s, 2H,  $-\text{OCH}_2$ ), 7.35 (d,  $J = 8.3$  Hz, 2H, Ar-H), 7.81 (d,  $J = 9.1$  Hz, 1H, Ar-H), 7.86 (d,  $J = 4.3$  Hz, 1H, Ar-H), 7.93 (d,  $J = 8.3$  Hz, 2H, Ar-H), 8.01 (d,  $J = 9.1$  Hz, 1H, Ar-H), 8.29 (s, 1H, triazole-H), 8.98 (s, 1H, Ar-H), 9.15 (d,  $J = 4.4$  Hz, 1H, Ar-H), 9.87 (s, 1H,  $-\text{CHO}$ ).  $^{13}\text{C}$  NMR (100 MHz, DMSO- $d_6$ )  $\delta$ : 42.7, 48.1, 61.9, 115.7, 116.2, 124.3, 125.1, 125.3, 125.9, 130.1, 132.3, 132.7, 135.9, 142.2, 152.8, 163.3, 191.8. HRMS (ESI) calcd for

$\text{C}_{21}\text{H}_{18}\text{ClN}_5\text{O}_2$   $[\text{M}+1]^+$  408.1149, found 408.1112.

4.1.2.4. 4-((1-(3-((7-chloroquinolin-4-yl)amino)propyl)-1H-1,2,3-triazol-4-yl)methoxy)benzaldehyde (**13b**). Yield 82%, brown semisolid,  $^1\text{H}$  NMR (400 MHz, DMSO- $d_6$ )  $\delta$ : 2.18–2.25 (m, 2H,  $-\text{CH}_2$ ), 3.33–3.38 (m, 3H,  $-\text{CH}_2+\text{NH}$  (exchangeable with  $\text{D}_2\text{O}$ )), 4.50 (t,  $J = 6.9$  Hz, 2H,  $-\text{CH}_2$ ), 5.20 (s, 2H,  $-\text{OCH}_2$ ), 6.57 (s, 1H, Ar-H), 7.17 (d,  $J = 8.7$  Hz, 2H, Ar-H), 7.51 (d,  $J = 9.0$  Hz, 1H, Ar-H), 8.28 (s, 1H, triazole-H), 8.36 (d,  $J = 8.5$  Hz, 1H, Ar-H), 9.82 (s, 1H,  $-\text{CHO}$ ).  $^{13}\text{C}$  NMR (100 MHz, DMSO- $d_6$ )  $\delta$ : 28.7, 40.5, 47.9, 61.9, 115.6, 116.3, 124.3, 125.3, 125.4, 125.8, 130.3, 132.3, 132.5, 135.9, 142.5, 152.7, 163.4, 191.8. HRMS (ESI) calcd for  $\text{C}_{22}\text{H}_{20}\text{ClN}_5\text{O}_2$   $[\text{M}+1]^+$  422.1306, found 422.1364.

4.1.2.5. 4-((1-(2-((7-chloroquinolin-4-yl)amino)ethyl)-1H-1,2,3-triazol-4-yl)methoxy)-3-methoxybenzaldehyde (**13c**). Yield 84%, pale white solid, MP = 203–205 °C,  $^1\text{H}$  NMR (400 MHz, DMSO- $d_6$ )  $\delta$ : 3.32–3.36 (m, 3H,  $-\text{CH}_2+\text{NH}$  (exchangeable with  $\text{D}_2\text{O}$ )), 3.76 (s, 3H,  $-\text{OCH}_3$ ), 4.54 (t,  $J = 7.1$  Hz, 2H,  $-\text{CH}_2$ ), 5.24 (s, 2H,  $-\text{OCH}_2$ ), 6.45 (d,  $J = 5.4$  Hz, 1H, Ar-H), 7.29–7.35 (m, 2H, Ar-H), 7.41 (dd,  $J = 8.7$ , 2.0 Hz, 1H, Ar-H), 7.51 (dd,  $J = 8.5$ , 1.9 Hz, 1H, Ar-H), 7.79 (d,  $J = 1.9$  Hz, 1H, Ar-H), 8.24 (d,  $J = 9.0$  Hz, 1H, Ar-H), 8.30 (s, 1H, triazole-H), 8.36 (d,  $J = 5.2$  Hz, 1H, Ar-H), 9.86 (s, 1H,  $-\text{CHO}$ ).  $^{13}\text{C}$  NMR (100 MHz, DMSO- $d_6$ )  $\delta$ : 42.8, 48.3, 61.9, 100.1, 110.3, 113.4, 117.5, 124.5, 124.6, 125.7, 126.2, 127.1, 130.5, 134.2, 142.3, 148.6, 149.6, 150.2, 151.7, 153.2, 192.0. HRMS (ESI) calcd for  $\text{C}_{22}\text{H}_{20}\text{ClN}_5\text{O}_3$   $[\text{M}+1]^+$  438.1255, found 438.1205.

4.1.2.6. 4-((1-(3-((7-chloroquinolin-4-yl)amino)propyl)-1H-1,2,3-triazol-4-yl)methoxy)-3-methoxybenzaldehyde (**13d**). Yield 86%, brown semisolid,  $^1\text{H}$  NMR (400 MHz, DMSO- $d_6$ )  $\delta$ : 2.16–2.24 (m, 2H,  $-\text{CH}_2$ ), 3.25–3.30 (m, 3H,  $-\text{CH}_2+\text{NH}$  (exchangeable with  $\text{D}_2\text{O}$ )), 3.76 (s, 3H,  $-\text{OCH}_3$ ), 4.50 (t,  $J = 6.9$  Hz, 2H,  $-\text{CH}_2$ ), 5.21 (s, 2H,  $-\text{OCH}_2$ ), 6.41 (d,  $J = 5.5$  Hz, 1H, Ar-H), 7.33–7.39 (m, 2H, Ar-H), 7.44 (dd,  $J = 9.0$ , 2.0 Hz, 1H, Ar-H), 7.51 (dd,  $J = 8.3$ , 1.7 Hz, 1H, Ar-H), 7.76 (d,  $J = 1.9$  Hz, 1H, Ar-H), 8.23 (d,  $J = 9.0$  Hz, 1H, Ar-H), 8.28 (s, 1H, triazole-H), 8.36 (d,  $J = 5.0$  Hz, 1H, Ar-H), 9.80 (s, 1H,  $-\text{CHO}$ ).  $^{13}\text{C}$  NMR (100 MHz, DMSO- $d_6$ )  $\delta$ : 28.9, 47.9, 55.9, 62.2, 99.2, 110.1, 113.0, 117.8, 124.7, 124.8, 125.6, 126.3, 127.3, 130.4, 134.3, 142.5, 148.7, 149.7, 150.8, 151.8, 153.3, 191.9. HRMS (ESI) calcd for  $\text{C}_{23}\text{H}_{22}\text{ClN}_5\text{O}_3$   $[\text{M}+1]^+$  452.1411, found 452.1473.

#### 4.1.3. General procedure for the synthesis of conjugates 14

To a well-stirred solution of *O*-nitrobenzaldehyde **10** (1 mmol) in HMPA,  $\text{NaN}_3$  (2 mmol) was added, and the resulting mixture was heated at 60 °C for 5–6 h. After completion of the reaction, the reaction mixture was extracted with ether and ice-cold water. The organic layer was dried over  $\text{Na}_2\text{SO}_4$  and concentrated under reduced pressure to afford **11**. *O*-azido-benzaldehyde **11** and *N*-propargylated-piperazinylquinoline **7** were dissolved in ethanol: $\text{H}_2\text{O}$  (8:2) along with subsequent addition of a catalytic amount of  $\text{CuSO}_4 \cdot 5\text{H}_2\text{O}$  (0.055 mmol) and sodium ascorbate (0.143 mmol). The reaction mixture was stirred for 3 h at room temperature. After the reaction as monitored by TLC, the crude product was extracted with chloroform and water. The organic layer was dried with  $\text{Na}_2\text{SO}_4$  and then concentrated under reduced pressure to yield the desired conjugates **14**. Compounds were purified by column chromatography using silica gel (60–120 mesh) and ethyl acetate: hexane (8:3) mixture.

4.1.3.1. 2-(4-((4-(7-chloroquinolin-4-yl)piperazin-1-yl)methyl)-1H-1,2,3-triazol-1-yl)benzaldehyde (**14**). Yield 87%, brown semisolid,  $^1\text{H}$  NMR (400 MHz,  $\text{CDCl}_3$ )  $\delta$ : 2.87 (s, 4H,  $-\text{CH}_2$ ), 3.25 (s, 4H,  $-\text{CH}_2$ ), 3.91 (s, 2H,  $-\text{CH}_2$ ), 6.81 (d,  $J = 3.3$  Hz, 1H, Ar-H), 7.39 (d,  $J = 8.9$  Hz, 1H, Ar-H), 7.53 (d,  $J = 7.9$  Hz, 1H, Ar-H), 7.65 (t,  $J = 7.5$  Hz, 1H, Ar-H), 7.75 (td,  $J = 7.7$ , 1.5 Hz, 1H, Ar-H), 7.90–8.00 (m, 4H, triazole-H + 3Ar-H), 8.08

(dd,  $J = 7.7, 1.3$  Hz, 1H, Ar-H), 9.90 (s, 1H, -CHO).  $^{13}\text{C}$  NMR (100 MHz,  $\text{CDCl}_3$ )  $\delta$ : 52.0, 52.9, 53.1, 109.1, 125.0, 125.3, 125.5, 126.3, 128.8, 129.9, 130.2, 130.3, 134.8, 135.0, 145.0, 151.9, 156.9, 188.6. HRMS (ESI) calcd for  $\text{C}_{23}\text{H}_{21}\text{ClN}_6\text{O}$   $[\text{M}+1]^+$  433.1465, found 433.1412.

#### 4.1.4. General procedure for the synthesis of conjugates 16-18

Conjugates **16a-g** were synthesized by subjecting **12-14** (1 mmol) and INH (1 mmol) to microwave irradiation at 100 °C for 15–20 min in ethanol as a solvent. **16a-g** precipitated out from reaction mixture upon cooling the mixture, which upon filtration and washing with ether afforded pure **16a-g** in excellent yields. The same protocol was applied for the synthesis of hybrids **17, 18**.

**4.1.4.1. (E)-N'-(4-((1-(7-chloroquinolin-4-yl)-1H-1,2,3-triazol-4-yl)methoxy)benzylidene)isonicotinohydrazide (16a)**. Yield 74%, pale white solid, MP = 230–232 °C,  $^1\text{H}$  NMR (500 MHz,  $\text{DMSO}-d_6$ )  $\delta$ : 5.38 (s, 2H, -OCH<sub>2</sub>), 7.20 (d,  $J = 8.4$  Hz, 2H, Ar-H), 7.74–7.81 (m, 5H, 2H<sup>b</sup> + 3Ar-H), 7.83 (d,  $J = 4.5$  Hz, 1H, Ar-H), 7.98 (d,  $J = 9.1$  Hz, 1H, Ar-H), 8.26 (s, 1H, triazole-H), 8.39 (s, 1H, -CH=N), 8.77 (s, 2H, H<sup>a</sup>), 8.95 (s, 1H, Ar-H), 9.13 (d,  $J = 4.5$  Hz, 1H, Ar-H), 12.02 (s, 1H, -NH (exchangeable with D<sub>2</sub>O)).  $^{13}\text{C}$  NMR (125 MHz,  $\text{DMSO}-d_6$ )  $\delta$ : 61.3, 115.6, 117.5, 120.7, 122.0, 125.7, 127.4, 128.4, 129.5, 135.9, 140.7, 140.9, 143.8, 149.5, 149.7, 150.7, 152.8, 160.2, 162.1. HRMS (ESI) calcd for  $\text{C}_{25}\text{H}_{18}\text{ClN}_7\text{O}_2$   $[\text{M}+1]^+$  484.1211, found 484.1256.

**4.1.4.2. (E)-N'-(4-((1-(7-chloroquinolin-4-yl)-1H-1,2,3-triazol-4-yl)methoxy)-3-methoxybenzylidene)isonicotinohydrazide (16b)**. Yield 73%, light brown solid, MP = 188–190 °C,  $^1\text{H}$  NMR (500 MHz,  $\text{DMSO}-d_6$ )  $\delta$ : 3.81 (s, 3H, OCH<sub>3</sub>), 5.19 (s, 2H, -OCH<sub>2</sub>), 6.72 (d,  $J = 5.3$  Hz, 1H Ar-H), 7.20–7.23 (m, 2H, Ar-H), 7.41 (s, 1H, Ar-H), 7.67 (d,  $J = 8.3$  Hz, 1H, Ar-H), 7.79–7.85 (m, 4H, 2H<sup>b</sup> + 3Ar-H), 8.29 (s, 1H, triazole-H), 8.39–8.41 (m, 2H, -CH=N+Ar-H), 8.78 (d,  $J = 5.1$  Hz, 2H, H<sup>a</sup>), 12.01 (s, 1H, -NH (exchangeable with D<sub>2</sub>O)).  $^{13}\text{C}$  NMR (125 MHz,  $\text{DMSO}-d_6$ )  $\delta$ : 55.8, 61.9, 109.3, 113.9, 117.9, 120.4, 121.2, 122.7, 125.9, 127.5, 127.8, 128.5, 129.4, 135.8, 140.7, 143.2, 144.2, 148.1, 149.7, 150.8, 152.7, 160.1, 162.9. HRMS (ESI) calcd for  $\text{C}_{26}\text{H}_{20}\text{ClN}_7\text{O}_3$   $[\text{M}+1]^+$  514.1316, found 514.1372.

**4.1.4.3. (E)-N'-(4-((1-(2-((7-chloroquinolin-4-yl)amino)ethyl)-1H-1,2,3-triazol-4-yl)methoxy)benzylidene)isonicotinohydrazide (16c)**. Yield 72%, pale white solid, MP = 196–198 °C,  $^1\text{H}$  NMR (500 MHz,  $\text{DMSO}-d_6$ )  $\delta$ : 3.84–3.86 (m, 2H, -CH<sub>2</sub>), 4.72 (s, 2H, -CH<sub>2</sub>), 5.29 (s, 2H, -OCH<sub>2</sub>), 6.95 (s, 1H, -NH (exchangeable with D<sub>2</sub>O)), 7.25 (d,  $J = 8.3$  Hz, 2H, Ar-H), 7.71–7.79 (m, 5H, 2H<sup>b</sup> + 3Ar-H), 7.89 (d,  $J = 4.4$  Hz, 1H, Ar-H), 7.98 (d,  $J = 9.1$  Hz, 1H, Ar-H), 8.29 (s, 1H, triazole-H), 8.37 (s, 1H, -CH=N), 8.79 (s, 2H, H<sup>a</sup>), 8.96 (s, 1H, Ar-H), 9.12 (d,  $J = 4.5$  Hz, 1H, Ar-H), 12.01 (s, 1H, -NH (exchangeable with D<sub>2</sub>O)).  $^{13}\text{C}$  NMR (125 MHz,  $\text{DMSO}-d_6$ )  $\delta$ : 42.8, 48.1, 61.7, 115.7, 117.9, 120.8, 121.2, 125.6, 127.3, 128.1, 129.6, 134.9, 140.1, 140.9, 143.7, 149.6, 149.9, 150.3, 152.9, 160.1, 162.4. HRMS (ESI) calcd for  $\text{C}_{27}\text{H}_{23}\text{ClN}_8\text{O}_2$   $[\text{M}+1]^+$  527.1632, found 527.1681.

**4.1.4.4. (E)-N'-(4-((1-(3-((7-chloroquinolin-4-yl)amino)propyl)-1H-1,2,3-triazol-4-yl)methoxy)benzylidene)isonicotinohydrazide (16d)**. Yield 75%, pale white solid, MP = 148–150 °C,  $^1\text{H}$  NMR (400 MHz,  $\text{DMSO}-d_6$ )  $\delta$ : 2.17–2.23 (m, 2H, -CH<sub>2</sub>), 4.49 (t,  $J = 6.9$  Hz, 2H, -CH<sub>2</sub>), 5.16 (s, 2H, -OCH<sub>2</sub>), 6.44 (d,  $J = 5.7$  Hz, 1H, Ar-H), 7.09 (d,  $J = 8.7$  Hz, 2H, Ar-H), 7.46 (dd,  $J = 9.0, 2.1$  Hz, 1H, Ar-H), 7.65–7.68 (m, 3H, Ar-H), 7.76–7.78 (m, 4H, 2H<sup>b</sup> + 2Ar-H), 8.26 (s, 1H, triazole-H), 8.36–8.37 (m, 2H, -CH=N + -NH (exchangeable with D<sub>2</sub>O)), 8.73 (d,  $J = 5.5$  Hz, 2H, INH), 11.94 (s, 1H, -NH (exchangeable with D<sub>2</sub>O)).  $^{13}\text{C}$  NMR (125 MHz,  $\text{DMSO}-d_6$ )  $\delta$ : 28.6, 47.7, 49.3, 61.8, 115.6, 116.4, 119.9, 121.4, 125.3, 126.9, 127.2, 128.9, 130.1, 135.1, 140.1, 140.3, 142.9, 148.9, 149.8, 150.2, 152.7, 158.2, 162.2. HRMS (ESI) calcd for  $\text{C}_{28}\text{H}_{25}\text{ClN}_8\text{O}_2$   $[\text{M}+1]^+$  541.1789, found 541.1724.

**4.1.4.5. (E)-N'-(4-((1-(2-((7-chloroquinolin-4-yl)amino)ethyl)-1H-1,2,3-triazol-4-yl)methoxy)-3-methoxybenzylidene)isonicotinohydrazide (16e)**. Yield 73%, light brown solid, MP = 183–185 °C,  $^1\text{H}$  NMR (400 MHz,  $\text{DMSO}-d_6$ )  $\delta$ : 3.24–2.83 (m, 3H, -CH<sub>2</sub>+NH (exchangeable with D<sub>2</sub>O)), 3.81 (s, 3H, -OCH<sub>3</sub>), 4.71 (s, 2H, -CH<sub>2</sub>), 5.17 (s, 2H, -OCH<sub>2</sub>), 6.78 (d,  $J = 5.1$  Hz, 1H Ar-H), 7.21 (dd,  $J = 18.5$  Hz, 6.2 Hz, 2H, Ar-H), 7.41 (s, 1H, Ar-H), 7.64 (d,  $J = 8.4$  Hz, 1H, Ar-H), 7.78–7.83 (m, 5H, 2H<sup>b</sup> + 3Ar-H), 8.27 (s, 1H, triazole-H), 8.38 (s, 1H, -CH=N), 8.77 (d,  $J = 5.1$  Hz, 2H, H<sup>a</sup>), 12.01 (s, 1H, -NH (exchangeable with D<sub>2</sub>O)).  $^{13}\text{C}$  NMR (100 MHz,  $\text{DMSO}-d_6$ )  $\delta$ : 42.6, 48.3, 55.8, 61.9, 109.3, 113.4, 117.9, 120.9, 121.3, 122.7, 125.9, 127.5, 127.9, 129.5, 135.6, 140.7, 143.1, 144.3, 148.2, 149.6, 150.9, 152.7, 160.2, 162.9. HRMS (ESI) calcd for  $\text{C}_{28}\text{H}_{25}\text{ClN}_8\text{O}_3$   $[\text{M}+1]^+$  557.1738, found 557.1756.

**4.1.4.6. (E)-N'-(4-((1-(3-((7-chloroquinolin-4-yl)amino)propyl)-1H-1,2,3-triazol-4-yl)methoxy)-3-methoxybenzylidene)isonicotinohydrazide (16f)**. Yield 71%, pale white solid, MP = 132–134 °C,  $^1\text{H}$  NMR (400 MHz,  $\text{DMSO}-d_6$ )  $\delta$ : 2.29–2.32 (m, 2H, -CH<sub>2</sub>), 3.81 (s, 3H, -OCH<sub>3</sub>), 4.59 (t,  $J = 6.0$  Hz, 2H, -CH<sub>2</sub>), 5.20 (s, 2H, -OCH<sub>2</sub>), 6.74 (d,  $J = 5.0$  Hz, 1H, Ar-H), 7.20–7.23 (m, 2H, Ar-H), 7.45 (s, 1H, Ar-H), 7.65 (d,  $J = 8.3$  Hz, 1H, Ar-H), 7.76–7.81 (m, 5H, 2H<sup>b</sup> + 3Ar-H), 8.29 (s, 1H, triazole-H), 8.37 (s, 1H, -CH=N), 8.78 (d,  $J = 5.1$  Hz, 2H, H<sup>a</sup>), 12.02 (s, 1H, -NH (exchangeable with D<sub>2</sub>O)).  $^{13}\text{C}$  NMR (100 MHz,  $\text{DMSO}-d_6$ )  $\delta$ : 28.5, 40.9, 47.8, 55.5, 62.3, 109.8, 113.7, 117.7, 120.1, 121.7, 122.4, 125.7, 127.5, 127.9, 128.2, 129.4, 133.2, 140.8, 142.9, 144.1, 148.3, 149.7, 150.8, 152.8, 160.1, 162.4. HRMS (ESI) calcd for  $\text{C}_{29}\text{H}_{27}\text{ClN}_8\text{O}_3$   $[\text{M}+1]^+$  571.1895, found 571.1845.

**4.1.4.7. (E)-N'-(2-((4-((7-chloroquinolin-4-yl)piperazin-1-yl)methyl)-1H-1,2,3-triazol-1-yl)benzylidene)isonicotinohydrazide (16g)**. Yield 76%, brown semisolid,  $^1\text{H}$  NMR (400 MHz,  $\text{DMSO}-d_6$ )  $\delta$ : 2.75 (s, 4H, -CH<sub>2</sub>), 3.16 (s, 4H, -CH<sub>2</sub>), 3.79 (s, 2H, -CH<sub>2</sub>), 6.93 (d,  $J = 4.9$  Hz, 1H, Ar-H), 7.43–7.65 (m, 7H, 5Ar-H + 2H<sup>b</sup>), 7.92 (d,  $J = 1.9$  Hz, 1H, Ar-H), 7.96 (d,  $J = 9.0$  Hz, 1H, Ar-H), 8.19 (s, 1H, triazole-H), 8.51 (s, 1H, -CH=N), 8.64 (d,  $J = 4.8$  Hz, 1H, H<sup>a</sup>), 8.69 (d,  $J = 3.6$  Hz, 1H, H<sup>a</sup>), 8.95 (s, 1H, Ar-H), 12.13 (s, 1H, -NH (exchangeable with D<sub>2</sub>O)).  $^{13}\text{C}$  NMR (100 MHz,  $\text{DMSO}-d_6$ )  $\delta$ : 52.2, 52.7, 52.8, 109.1, 121.8, 124.0, 126.2, 126.5, 126.9, 128.5, 129.3, 129.8, 130.6, 131.5, 134.1, 135.2, 143.8, 144.3, 149.1, 150.1, 152.2, 152.7, 156.7, 162.3. HRMS (ESI) calcd for  $\text{C}_{29}\text{H}_{26}\text{ClN}_9\text{O}$   $[\text{M}+1]^+$  552.1949, found 552.1923.

**4.1.4.8. (E)-N'-(4-((1-(7-chloroquinolin-4-yl)-1H-1,2,3-triazol-4-yl)methoxy)benzylidene)nicotinohydrazide (17a)**. Yield 76%, pale white solid, MP = 238–241 °C,  $^1\text{H}$  NMR (400 MHz,  $\text{DMSO}-d_6$ )  $\delta$ : 5.16 (s, 2H, -OCH<sub>2</sub>), 7.15 (d,  $J = 7.6$  Hz, 2H, Ar-H), 7.48–7.61 (m, 4H, 3Ar-H + H<sup>d</sup>), 8.01–8.06 (m, 2H, Ar-H), 8.26 (s, 1H, triazole-H), 8.31–8.36 (m, 3H, -CH=N+Ar-H), 8.91–9.09 (m, 3H, H<sup>b</sup> + H<sup>c</sup> + H<sup>a</sup>), 11.97 (s, 1H, -NH (exchangeable with D<sub>2</sub>O)).  $^{13}\text{C}$  NMR (100 MHz,  $\text{DMSO}-d_6$ )  $\delta$ : 61.4, 115.6, 117.6, 120.7, 125.9, 127.5, 127.6, 128.6, 129.5, 129.5, 130.5, 132.3, 135.9, 140.8, 143.8, 144.6, 149.9, 150.0, 152.8, 159.8, 160.2, 163.3. HRMS (ESI) calcd for  $\text{C}_{25}\text{H}_{18}\text{ClN}_7\text{O}_2$   $[\text{M}+1]^+$  484.1211, found 484.1171.

**4.1.4.9. (E)-N'-(4-((1-(7-chloroquinolin-4-yl)-1H-1,2,3-triazol-4-yl)methoxy)-3-methoxybenzylidene)nicotinohydrazide (17b)**. Yield 71%, brown solid, MP = 270–272 °C,  $^1\text{H}$  NMR (400 MHz,  $\text{DMSO}-d_6$ )  $\delta$ : 3.79 (s, 3H, -OCH<sub>3</sub>), 5.32 (s, 2H, -OCH<sub>2</sub>), 7.23–7.27 (m, 2H, Ar-H), 7.36 (s, 1H, H<sup>d</sup>), 7.71–7.99 (m, 4H, Ar-H), 8.22–8.35 (m, 4H, triazole-H + CH=N + 2Ar-H), 8.94–9.12 (m, 3H, H<sup>a</sup> + H<sup>b</sup> + H<sup>c</sup>), 11.91 (s, 1H, -NH (exchangeable with D<sub>2</sub>O)).  $^{13}\text{C}$  NMR (100 MHz,  $\text{DMSO}-d_6$ )  $\delta$ : 56.2, 62.4, 109.3, 113.9, 121.0, 122.7, 125.7, 126.3, 127.1, 128.0, 138.0, 143.1, 144.0, 144.7, 144.9, 145.4, 148.5, 150.0, 150.3, 150.6, 155.4, 160.0. HRMS (ESI) calcd for  $\text{C}_{26}\text{H}_{20}\text{ClN}_7\text{O}_3$   $[\text{M}+1]^+$  514.1316, found 514.1367.

4.1.4.10. (*E*)-*N'*-(4-((1-(2-((7-chloroquinolin-4-yl)amino)ethyl)-1*H*-1,2,3-triazol-4-yl)methoxy)benzylidene)nicotinohydrazide (**17c**). Yield 72%, light brown solid, MP = 226–228 °C, <sup>1</sup>H NMR (400 MHz, DMSO-*d*<sub>6</sub>): 3.82 (s, 3H, -CH<sub>2</sub>+NH (exchangeable with D<sub>2</sub>O)), 4.66 (s, 2H, -CH<sub>2</sub>), 5.13 (s, 2H, -OCH<sub>2</sub>), 7.05 (d, *J* = 7.6 Hz, 2H, Ar-H), 7.50–7.64 (m, 4H, 3Ar-H + H<sup>d</sup>), 8.01–8.06 (m, 2H, Ar-H), 8.25–8.36 (m, 5H, triazole-H + -CH=N + H<sup>c</sup> + Ar-H), 8.92–9.01 (m, 2H, H<sup>a</sup> + H<sup>b</sup>), 11.97 (s, 1H, -NH (exchangeable with D<sub>2</sub>O)). <sup>13</sup>C NMR (100 MHz, DMSO-*d*<sub>6</sub>): 42.7, 48.2, 61.6, 115.3, 116.2, 123.1, 124.3, 125.2, 125.4, 125.6, 128.6, 129.8, 130.2, 132.4, 132.9, 135.1, 135.4, 135.8, 142.1, 148.9, 151.6, 152.9, 159.8, 160.2. HRMS (ESI) calcd for C<sub>27</sub>H<sub>23</sub>ClN<sub>8</sub>O<sub>2</sub> [M+1]<sup>+</sup> 527.1632, found 527.1676.

4.1.4.11. (*E*)-*N'*-(4-((1-(3-((7-chloroquinolin-4-yl)amino)propyl)-1*H*-1,2,3-triazol-4-yl)methoxy)benzylidene)nicotinohydrazide (**17d**). Yield 70%, pale white solid, MP = 136–138 °C, <sup>1</sup>H NMR (400 MHz, DMSO-*d*<sub>6</sub>): 2.16–2.21 (m, 2H, -CH<sub>2</sub>), 4.21 (t, *J* = 6.8 Hz, 2H, -CH<sub>2</sub>), 5.17 (s, 2H, -OCH<sub>2</sub>), 7.10 (d, *J* = 7.8 Hz, 2H, Ar-H), 7.52–7.68 (m, 4H, 3Ar-H + H<sup>d</sup>), 8.04–8.08 (m, 2H, Ar-H), 8.29–8.38 (m, 5H, triazole-H + -CH=N + H<sup>c</sup> + Ar-H), 8.93–9.01 (m, 2H, H<sup>a</sup> + H<sup>b</sup>), 12.01 (s, 1H, -NH (exchangeable with D<sub>2</sub>O)). <sup>13</sup>C NMR (100 MHz, DMSO-*d*<sub>6</sub>): 28.9, 47.9, 49.2, 62.2, 115.8, 116.4, 120.1, 123.4, 124.4, 124.9, 125.1, 125.3, 125.6, 129.8, 132.4, 132.6, 135.1, 135.9, 140.1, 141.9, 142.7, 148.9, 151.9, 152.8, 162.1. HRMS (ESI) calcd for C<sub>28</sub>H<sub>25</sub>ClN<sub>8</sub>O<sub>2</sub> [M+1]<sup>+</sup> 541.1789, found 541.1721.

4.1.4.12. (*E*)-*N'*-(4-((1-(2-((7-chloroquinolin-4-yl)amino)ethyl)-1*H*-1,2,3-triazol-4-yl)methoxy)-3-methoxybenzylidene)nicotinohydrazide (**17e**). Yield 72%, light brown solid, MP = 194–196 °C, <sup>1</sup>H NMR (400 MHz, DMSO-*d*<sub>6</sub>): 3.23–2.84 (m, 3H, -CH<sub>2</sub> + NH (exchangeable with D<sub>2</sub>O)), 3.82 (s, 3H, -OCH<sub>3</sub>), 4.74 (s, 2H, -CH<sub>2</sub>), 5.19 (s, 2H, -OCH<sub>2</sub>), 7.21–7.26 (m, 2H, Ar-H), 7.41 (s, 1H, H<sup>d</sup>), 7.72–8.10 (m, 4H, Ar-H), 8.27 (s, 1H, triazole-H), 8.32 (m, 3H, triazole-H + CH=N + 2Ar-H), 8.94–9.12 (m, 3H, H<sup>a</sup> + H<sup>b</sup> + H<sup>c</sup>), 11.91 (s, 1H, -NH (exchangeable with D<sub>2</sub>O)). <sup>13</sup>C NMR (100 MHz, DMSO-*d*<sub>6</sub>): 42.6, 47.9, 55.7, 61.9, 100.2, 113.7, 117.8, 123.1, 124.6, 124.8, 125.9, 126.3, 126.4, 127.2, 129.8, 130.4, 134.1, 135.1, 142.6, 148.6, 151.2, 151.7, 152.8, 159.8, 162.1. HRMS (ESI) calcd for C<sub>28</sub>H<sub>25</sub>ClN<sub>8</sub>O<sub>3</sub> [M+1]<sup>+</sup> 557.1738, found 557.1778.

4.1.4.13. (*E*)-*N'*-(4-((1-(3-((7-chloroquinolin-4-yl)amino)propyl)-1*H*-1,2,3-triazol-4-yl)methoxy)-3-methoxybenzylidene)nicotinohydrazide (**17f**). Yield 78%, brown semisolid, <sup>1</sup>H NMR (400 MHz, DMSO-*d*<sub>6</sub>): 2.27–2.31 (m, 2H, -CH<sub>2</sub>), 3.83 (s, 3H, -OCH<sub>3</sub>), 4.57 (t, *J* = 6.0 Hz, 2H, -CH<sub>2</sub>), 5.21 (s, 2H, -OCH<sub>2</sub>), 7.23–7.29 (m, 2H, Ar-H), 7.47 (s, 1H, H<sup>d</sup>), 7.73–8.11 (m, 4H, Ar-H), 8.29 (s, 1H, triazole-H), 8.31 (m, 3H, CH=N + 2Ar-H), 8.94–9.10 (m, 3H, H<sup>a</sup> + H<sup>b</sup> + H<sup>c</sup>), 11.97 (s, 1H, -NH (exchangeable with D<sub>2</sub>O)). <sup>13</sup>C NMR (100 MHz, DMSO-*d*<sub>6</sub>): 28.7, 40.9, 47.8, 56.0, 62.3, 109.8, 113.2, 117.9, 123.4, 124.3, 124.9, 125.8, 126.0, 127.1, 127.3, 129.8, 135.1, 135.6, 142.8, 148.7, 148.9, 149.7, 150.7, 151.8, 152.3, 155.2, 160.2. HRMS (ESI) calcd for C<sub>29</sub>H<sub>27</sub>ClN<sub>8</sub>O<sub>3</sub> [M+1]<sup>+</sup> 571.1895, found 571.1834.

4.1.4.14. (*E*)-*N'*-(2-(4-((7-chloroquinolin-4-yl)piperazin-1-yl)methyl)-1*H*-1,2,3-triazol-1-yl)benzylidene)nicotinohydrazide (**17g**). Yield 78%, brown semisolid, <sup>1</sup>H NMR (400 MHz, DMSO-*d*<sub>6</sub>): 2.76 (s, 4H, -CH<sub>2</sub>), 3.14 (s, 4H, -CH<sub>2</sub>), 3.81 (s, 2H, -CH<sub>2</sub>), 6.97 (d, *J* = 5.1 Hz, 1H, Ar-H), 7.39–7.60 (m, 6H, 5Ar-H + H<sup>d</sup>), 7.78 (m, 1H, Ar-H), 8.30 (s, 1H, triazole-H), 8.31–8.35 (m, 2H, Ar-H), 8.38 (s, 1H, -CH=N), 8.91–9.09 (m, 3H, H<sup>a</sup> + H<sup>b</sup> + H<sup>c</sup>), 11.98 (s, 1H, -NH (exchangeable with D<sub>2</sub>O)). <sup>13</sup>C NMR (100 MHz, DMSO-*d*<sub>6</sub>): 52.1, 52.6, 52.9, 109.1, 123.4, 124.9, 125.2, 125.7, 126.9, 128.7, 129.1, 129.8, 130.4, 131.2, 134.4, 135.0, 135.2, 138.1, 139.4, 145.2, 148.9, 151.8, 152.4, 156.8, 162.4. HRMS (ESI) calcd for C<sub>29</sub>H<sub>26</sub>ClN<sub>9</sub>O [M+1]<sup>+</sup> 552.1949, found 552.1921.

4.1.4.15. (*E*)-*N'*-(4-((1-(7-chloroquinolin-4-yl)-1*H*-1,2,3-triazol-4-yl)methoxy)benzylidene)pyrazine-2-carbohydrazide (**18a**). Yield 75%, pale white solid, MP = 235–237 °C, <sup>1</sup>H NMR (500 MHz, DMSO-*d*<sub>6</sub>): 5.41 (s, 2H, -OCH<sub>2</sub>), 7.23 (d, *J* = 8.3 Hz, 2H, Ar-H), 7.73 (d, *J* = 8.2 Hz, 2H, Ar-H), 7.81 (d, *J* = 9.0 Hz, 1H, Ar-H), 7.89 (d, *J* = 4.0 Hz, 1H, Ar-H), 8.02 (d, *J* = 9.0 Hz, 1H, Ar-H), 8.30 (s, 1H, triazole-H), 8.61 (s, 1H, -CH=N), 8.79 (s, 1H, Ar-H), 8.93 (s, 1H, Ar-H), 9.01 (s, 1H, H<sup>c</sup>), 9.17 (d, *J* = 4.0 Hz, 1H, H<sup>b</sup>), 9.27 (s, 1H, H<sup>a</sup>), 12.19 (s, 1H, -NH (exchangeable with D<sub>2</sub>O)). <sup>13</sup>C NMR (125 MHz, DMSO-*d*<sub>6</sub>): 61.4, 115.7, 117.6, 120.7, 125.8, 127.5, 127.6, 128.6, 129.4, 129.5, 135.8, 143.7, 143.8, 144.5, 145.2, 148.2, 149.8, 150.0, 152.8, 159.8, 160.2. HRMS (ESI) calcd for C<sub>24</sub>H<sub>17</sub>ClN<sub>8</sub>O<sub>2</sub> [M+1]<sup>+</sup> 485.1163, found 485.1121.

4.1.4.16. (*E*)-*N'*-(4-((1-(7-chloroquinolin-4-yl)-1*H*-1,2,3-triazol-4-yl)methoxy)-3-methoxybenzylidene)pyrazine-2-carbohydrazide (**18b**). Yield 72%, brown solid, MP = 249–251 °C, <sup>1</sup>H NMR (500 MHz, DMSO-*d*<sub>6</sub>): 3.82 (s, 3H, -OCH<sub>3</sub>), 5.36 (s, 2H, -OCH<sub>2</sub>), 7.27–7.32 (m, 2H, Ar-H), 7.47 (s, 1H, Ar-H), 7.77–7.84 (m, 2H, Ar-H), 7.98 (d, *J* = 8.6 Hz, 1H, Ar-H), 8.26 (s, 1H, triazole-H), 8.53 (s, 1H, -CH=N), 8.78–8.94 (m, 3H, H<sup>b</sup> + H<sup>c</sup> + Ar-H), 9.14 (s, 1H, Ar-H), 9.27 (s, 1H, H<sup>a</sup>), 12.22 (s, 1H, -NH (exchangeable with D<sub>2</sub>O)). <sup>13</sup>C NMR (125 MHz, DMSO-*d*<sub>6</sub>): 55.9, 61.7, 109.2, 113.8, 117.5, 120.7, 122.6, 125.7, 127.6, 127.9, 128.4, 129.5, 135.9, 140.7, 143.7, 144.3, 148.2, 149.7, 149.8, 149.9, 150.5, 152.8, 160.0. HRMS (ESI) calcd for C<sub>25</sub>H<sub>19</sub>ClN<sub>8</sub>O<sub>3</sub> [M+1]<sup>+</sup> 515.1269, found 515.1213.

4.1.4.17. (*E*)-*N'*-(4-((1-(2-((7-chloroquinolin-4-yl)amino)ethyl)-1*H*-1,2,3-triazol-4-yl)methoxy)benzylidene)pyrazine-2-carbohydrazide (**18c**). Yield 74%, pale white solid, MP = 231–23 °C, <sup>1</sup>H NMR (500 MHz, DMSO-*d*<sub>6</sub>): 3.85 (d, *J* = 4.3 Hz, 2H, -CH<sub>2</sub>), 4.70 (s, 2H, -CH<sub>2</sub>), 5.19 (s, 2H, -OCH<sub>2</sub>), 6.95 (s, 1H, -NH (exchangeable with D<sub>2</sub>O)), 7.11 (d, *J* = 8.2 Hz, 2H, Ar-H), 7.51 (d, *J* = 8.8 Hz, 1H, Ar-H), 7.66–7.79 (m, 4H, Ar-H), 8.26–8.29 (m, 2H, triazole-H, Ar-H), 8.58 (s, 1H, -CH=N), 8.79–8.93 (m, 3H, H<sup>b</sup> + H<sup>c</sup> + Ar-H), 9.27 (s, 1H, H<sup>a</sup>), 12.17 (s, 1H, -NH (exchangeable with D<sub>2</sub>O)). <sup>13</sup>C NMR (125 MHz, DMSO-*d*<sub>6</sub>): 42.9, 48.3, 61.6, 115.5, 124.7, 125.3, 125.6, 127.4, 129.3, 132.2, 132.7, 134.6, 142.8, 143.0, 143.7, 144.5, 145.2, 148.2, 150.1, 159.7, 160.2. HRMS (ESI) calcd for C<sub>26</sub>H<sub>22</sub>ClN<sub>9</sub>O<sub>2</sub> [M+1]<sup>+</sup> 528.1585, found 528.1543.

4.1.4.18. (*E*)-*N'*-(4-((1-(3-((7-chloroquinolin-4-yl)amino)propyl)-1*H*-1,2,3-triazol-4-yl)methoxy)benzylidene)pyrazine-2-carbohydrazide (**18d**). Yield 74%, pale white solid, MP = 144–147 °C, <sup>1</sup>H NMR (400 MHz, DMSO-*d*<sub>6</sub>): 2.22 (t, *J* = 5.5 Hz, 2H, -CH<sub>2</sub>), 3.36–3.37 (m, 2H, -CH<sub>2</sub>), 4.50 (t, *J* = 6.7 Hz, 2H, -CH<sub>2</sub>), 5.15 (s, 2H, -OCH<sub>2</sub>), 7.08 (d, *J* = 8.6 Hz, 2H, Ar-H), 7.55 (d, *J* = 8.9 Hz, 1H, Ar-H), 7.64 (d, *J* = 8.5 Hz, 3H, Ar-H), 8.27 (s, 1H, triazole-H), 8.29–8.39 (m, 2H, Ar-H), 8.51–8.73 (m, 3H, H<sup>c</sup> + Ar-H), 8.87 (s, 1H, H<sup>b</sup>), 9.21 (s, 1H, H<sup>a</sup>), 12.13 (s, 1H, -NH (exchangeable with D<sub>2</sub>O)). <sup>13</sup>C NMR (125 MHz, DMSO-*d*<sub>6</sub>): 28.7, 40.5, 47.8, 61.6, 115.5, 125.3, 125.5, 125.9, 127.4, 129.4, 129.6, 132.2, 136.0, 142.8, 143.8, 144.4, 145.1, 148.2, 150.1, 152.9, 159.8, 160.2. HRMS (ESI) calcd for C<sub>27</sub>H<sub>24</sub>ClN<sub>9</sub>O<sub>2</sub> [M+1]<sup>+</sup> 542.1741, found 542.1782.

4.1.4.19. (*E*)-*N'*-(4-((1-(2-((7-chloroquinolin-4-yl)amino)ethyl)-1*H*-1,2,3-triazol-4-yl)methoxy)-3-methoxybenzylidene)pyrazine-2-carbohydrazide (**18e**). Yield 75%, pale white solid, MP = 234–237 °C, <sup>1</sup>H NMR (500 MHz, DMSO-*d*<sub>6</sub>): 3.23–3.29 (m, 3H, -CH<sub>2</sub> + NH (exchangeable with D<sub>2</sub>O)), 3.81 (s, 3H, -OCH<sub>3</sub>), 4.73 (s, 2H, -CH<sub>2</sub>), 5.18 (s, 2H, -OCH<sub>2</sub>), 6.81 (d, *J* = 5.1 Hz, 1H, Ar-H), 7.24 (dd, *J* = 18.4, 6.5 Hz, 2H, Ar-H), 7.39 (s, 1H, Ar-H), 7.71 (d, *J* = 8.5 Hz, 1H, Ar-H), 8.21 (s, 1H, Ar-H), 8.35 (s, 1H, triazole-H), 8.51 (s, 1H, -CH=N), 8.54 (d, *J* = 8.6 Hz, 1H, Ar-H), 8.79–8.86 (m, 3H, H<sup>b</sup> + H<sup>c</sup> + Ar-H), 9.27 (s, 1H, H<sup>a</sup>), 12.19 (s, 1H, NH (exchangeable with D<sub>2</sub>O)). <sup>13</sup>C NMR (125 MHz, DMSO-*d*<sub>6</sub>): 42.9, 48.3, 55.8, 61.6, 109.2, 113.8, 122.3, 125.3, 126.0,

126.9, 127.4, 137.8, 142.9, 143.7, 144.3, 145.1, 148.5, 149.8, 150.1, 150.3, 155.9, 160.1. HRMS (ESI) calcd for  $C_{27}H_{24}ClN_9O_3$   $[M+1]^+$  558.1691, found 558.1635.

4.1.4.20. (*E*)-*N'*-(4-((1-(3-((7-chloroquinolin-4-yl)amino)propyl)-1*H*-1,2,3-triazol-4-yl)methoxy)-3-methoxybenzylidene)pyrazine-2-carbohydrazide (**18f**). Yield 76%, pale white solid, MP = 146–148 °C,  $^1H$  NMR (500 MHz, DMSO- $d_6$ )  $\delta$ : 2.28–2.30 (m, 2H,  $-CH_2$ ), 3.52–3.54 (m, 3H,  $-CH_2$ +NH (exchangeable with  $D_2O$ )), 3.82 (s, 3H,  $-OCH_3$ ), 4.57 (t,  $J$  = 5.9 Hz, 2H,  $-CH_2$ ), 5.18 (s, 2H,  $-OCH_2$ ), 6.78 (d,  $J$  = 5.2 Hz, 1H, Ar-H), 7.22 (dd,  $J$  = 18.0, 8.0 Hz, 2H, Ar-H), 7.37 (s, 1H, Ar-H), 7.73 (d,  $J$  = 8.6 Hz, 1H, Ar-H), 8.00 (s, 1H, Ar-H), 8.34 (s, 1H, triazole-H), 8.55 (s, 1H,  $-CH=N$ ), 8.59 (d,  $J$  = 8.8 Hz, 1H, Ar-H), 8.79–8.93 (m, 3H,  $H^b$ + $H^c$ +Ar-H), 9.26 (s, 1H,  $H^a$ ), 12.18 (s, 1H,  $-NH$  (exchangeable with  $D_2O$ )).  $^{13}C$  NMR (125 MHz, DMSO- $d_6$ ) $\delta$ : 28.6, 40.8, 47.7, 55.9, 62.1, 109.1, 113.6, 122.4, 125.5, 126.0, 126.9, 127.7, 137.7, 142.8, 143.8, 144.5, 145.2, 148.2, 149.7, 150.0, 150.3, 155.1, 159.8. HRMS (ESI) calcd for  $C_{28}H_{26}ClN_9O_3$   $[M+1]^+$  572.1847, found 572.1872.

4.1.4.21. (*E*)-*N'*-(2-(4-((1-(7-chloroquinolin-4-yl)piperazin-1-yl)methyl)-1*H*-1,2,3-triazol-1-yl)benzylidene)pyrazine-2-carbohydrazide (**18g**). Yield 73%, brown semisolid,  $^1H$  NMR (400 MHz, DMSO- $d_6$ )  $\delta$ : 2.76 (s, 4H,  $-CH_2$ ), 3.16 (s, 4H,  $-CH_2$ ), 3.80 (s, 2H,  $-CH_2$ ), 6.93 (d,  $J$  = 5.0 Hz, 1H, Ar-H), 7.47 (dd,  $J$  = 9.0 Hz, 2.0 Hz, 1H, Ar-H), 7.55–7.64 (m, 3H, Ar-H), 7.91 (d,  $J$  = 1.7 Hz, 1H, Ar-H), 7.96 (d,  $J$  = 9.0 Hz, 1H, Ar-H), 8.16–8.18 (m, 1H, Ar-H), 8.41 (s, 1H, triazole-H), 8.49 (s, 1H,  $-CH=N$ ), 8.64 (s, 2H,  $H^c$ +Ar-H), 8.82 (d,  $J$  = 2.2 Hz, 1H,  $H^b$ ), 9.19 (s, 1H,  $H^a$ ), 12.47 (s, 1H,  $-NH$  (exchangeable with  $D_2O$ )).  $^{13}C$  NMR (100 MHz, DMSO- $d_6$ ) $\delta$ : 52.1, 52.7, 52.9, 109.2, 121.9, 124.3, 126.1, 126.6, 126.8, 128.6, 129.8, 130.7, 131.6, 134.2, 135.3, 137.7, 143.9, 144.2, 149.4, 150.2, 152.3, 152.8, 156.9, 162.1. HRMS (ESI) calcd for  $C_{28}H_{25}ClN_{10}O$   $[M+1]^+$  553.1901, found 553.1934.

#### 4.2. Strains, plasmids, and culture conditions

The pantothenate-auxotrophic *Mtb* mc<sup>2</sup>6230 strain [52] was grown in Middlebrook 7H9 broth supplemented with 10% oleic-albumin-dextrose-catalase enrichment (OADC), 0.025% tyloxapol and 109  $\mu$ M pantothenic acid or Middlebrook 7H10 agar supplemented with OADC and with 109  $\mu$ M pantothenic acid at 37 °C without agitation. Recombinant strains carrying pMV261-*inhA* [39] were grown in a 7H9 broth medium containing 25  $\mu$ g/mL kanamycin or on Middlebrook 7H10 agar supplemented with 10% OADC containing 25  $\mu$ g/mL kanamycin at 37 °C for either 2 weeks. *M ma* M strain [53] and *Mab* CIP104536<sup>T</sup> [54] were grown in 7H9 broth supplemented with OADC enrichment and 0.025% tyloxapol.

#### 4.3. Drug susceptibility testing

MIC was defined as the lowest concentration of compound inhibiting 99% of bacterial growth, at which no change in turbidity was observed and performed in 7H9 broth supplemented with 10% OADC, 0.025% tyloxapol at 37 °C (for *Mtb*) and 30 °C (for *Mma*) without agitation and in CaMHB for *Mab*, according to the CLSI guidelines [55]. For *Mtb* mc<sup>2</sup>6230, 109  $\mu$ M pantothenic acid was added to all experiments. MIC determination was done using the broth dilution method. Briefly, a log-phase ( $OD_{600} \sim 1$ ) culture was diluted to an  $OD_{600} = 0.05$  (*Mtb*) in 7H9 medium or with an inoculum containing  $5.10^6$  CFU/mL (*Mma* and *Mab*) and deposited in 96-well plates. Compounds were then directly added (in general 4  $\mu$ L/well of a 10 mg/mL stock solution) to the first-row wells. Serial 2-fold dilutions were then completed starting from the first row. Plates were wrapped in parafilm and were then placed in a 37 °C incubator and observed after 7 days for *Mtb* or at 30 °C and observed after 6 days for *Mma* and 4 days for *Mab*. Control wells included DMSO as vehicle control, in which bacterial growth was not

inhibited (as for untreated wells). INH was included as a reference drug.

#### 4.4. Kill kinetics

Kill kinetic experiments were completed as previously described [56, 57]. Briefly, *Mtb* mc<sup>2</sup>6230 was grown to log-phase ( $OD_{600} \sim 1$ ), diluted to an  $OD_{600} = 0.05$  and deposited into all wells of a 96-well microtiter plate. Increasing concentrations of compounds **16a-g** and INH (positive control) were added to each well corresponding to 1x, 5x, and 20x the respective MIC values. DMSO was included as a negative control and was added to the respective wells at the highest volume used in the experiment. Plates were sealed with parafilm and left to incubate at 37 °C until required. At the designated time points, 20  $\mu$ L of each required well was serially diluted in sterile PBS and plated on 7H10 agar medium supplemented with 10% OADC and 109  $\mu$ M pantothenic acid. Plates were incubated at 37 °C for 3 weeks until visible colonies formed and were enumerated by visual inspection.

#### 4.5. Cell culture and cytotoxicity assay

Vero kidney epithelial cells (ATCC® CCL-81) and human THP-1 monocytes were cultured in RPMI 1640 (Life Technologies) supplemented with 10% foetal calf serum (Sigma-Aldrich) and incubated at 37 °C with 5% CO<sub>2</sub>. Once the desired confluency was achieved, cells were detached from the flask surface using trypsin (ThermoFisher) before adding 4 mL of culture medium and enumerated in a Malassez counting chamber. Cell density was adjusted to  $2 \times 10^4$  cells/well in a 96-well microtiter plate and left to adhere overnight at 37 °C with 5% CO<sub>2</sub>. Monocytes were differentiated into macrophages in the presence of 20 ng/mL Phorbol Myristate Acetate (PMA) in a 96-well flat-bottom tissue culture plate ( $1 \times 10^5$  cells/well) and incubated for 48 h at 37 °C with 5% CO<sub>2</sub>. Serial dilutions of the test compounds (ranging from 100  $\mu$ g/mL to 0.78  $\mu$ g/mL) were added to the cells, which were further incubated at 37 °C with 5% CO<sub>2</sub> for 24 h or 72 h after which 10% (vol/vol) resazurin dye was added to each well and left to incubate for 4 h at 37 °C with 5% CO<sub>2</sub>. INH and RFB were included as reference drugs. Data were acquired using a fluorescent plate reader (excitation 540 nm, emission 590 nm).

#### 4.6. Generation of spontaneous mutants and genotyping

Spontaneous *Mtb* mutants resistant to compounds **16d**, **16g**, and **16f** were selected by diluting and plating mid-log phase cultures at  $\sim 1 \times 10^8$  CFU/mL on 7H10 agar medium supplemented with OADC, pantothenic acid, and 5x or 20x the respective MIC of the compounds. The frequency of spontaneous resistant mutants was enumerated by visual inspection of the colonies. One individual colony growing on each compound was picked and subsequently grown in 7H9 medium supplemented with OADC, tyloxapol and pantothenic acid. The degree of resistance (and cross-resistance) to compounds **16d**, **16g**, and **16f** and INH was evaluated by MIC determination. The *katG* gene in the various resistant mutants was PCR amplified using Q5 high fidelity polymerase (NEB), and the resulting products were purified using a PCR clean-up system (Macherey-Nagel) prior to sequencing using the specific oligonucleotides: 5'-cggcttgcggggttatcgc-3'; 5'-gaagctctcatggcgacc-3'; 5'-cctctcgtcggggtgatc-3' and 5'-aactactcggaaaggcaacc-3'.

#### 4.7. Whole-genome sequencing

DNA was extracted using NucleoBond AXG 100 DNA kit (Macherey-Nagel, Germany) according to the manufacturer's instructions. DNA was quantified using Qubit™ dsDNA BR Assay Kit and Qubit™ 4 fluorometer (Invitrogen, Thermo Fischer Scientific). Library preparation and Illumina sequencing was performed by Novogene (Cambridge, UK) on IlluminaNovaSeq platform (2x150bp). The short-read data were first trimmed using fastp v0.23.2 [58], based on a Phred scale base quality



threshold of Q30 and removing reads of less than 21 bp. Kraken2 v2.0.9-beta [59] with the bacteria database was used to perform taxonomic identification at the read level in order to check for potential contamination. All reads assigned to the Mycobacteriaceae family were extracted and then assembled using SPAdes v3.15.3 [60] with the “-careful” option. Reads were mapped to H37Rv reference genome using Burrow-Wheeler Aligner (BWA) mem (v0.7.17-r1188) (<http://arxiv.org/abs/1303.3997>).

#### 4.8. Fatty acid and mycolic acid analysis

To appreciate the drug-induced changes in the lipid profile, *Mtb* mc<sup>2</sup>6230 cultures were exposed to increasing drug concentrations of INH or **16g** for 15 h prior to metabolic labeling in the presence of 1  $\mu$ Ci/mL of [<sup>14</sup>C]acetate (59 mCi/mmol, PerkinElmer) for an additional 7 h at 37 °C. Extraction of total mycolic acids was carried out as previously reported [61]. Briefly, cell pellets were washed and treated with 15% tetrabutylammonium hydroxide (TBAH) at 100 °C overnight. Fatty acids and mycolic acids were methyl-esterified and extracted in diethyl ether. Extracts were dried and resuspended in dichloromethane for application to a silica-coated plate. Fatty acid methyl esters (FAMES) and mycolic acid methyl esters (MAMES) were developed twice on normal phase TLC in hexane/ethyl acetate (19/1, v/v). The [<sup>14</sup>C]-labeled FAME and MAME contents were analyzed using an Amersham Typhoon imaging system.

#### 4.9. Statistical analyses

Statistical analyses were performed on Prism 5.0 (Graphpad) and detailed for each figure legend. \*p < 0.05; \*\*p < 0.01; \*\*\*p < 0.001.

#### Author contributions

MA, BS, FRB, CC, TC conducted experiments and analyzed the data. FB, VK and LK analyzed the data. MA, BS, VK, and LK wrote the manuscript. VK and LK conceived, supervised the project, and acquired funding.

#### Declaration of competing interest

The authors declare that they have no known competing financial interests or personal relationships that could have appeared to influence the work reported in this paper.

#### Acknowledgments

The authors wish to thank A. Speer for the generous gift of pSMT3-*katG*, the Ministère de l'Enseignement Supérieur, de la Recherche et de l'Innovation for funding MA. VK thanks Council of Scientific and Industrial Research (CSIR) for providing financial support (grant no. 02 (0400)/21/EMR-II). B.S. acknowledges the Council of Scientific and Industrial Research, New Delhi, India, for providing CSIR-SRF fellowship (CSIR Ref No. 09/254(0257)/2016-EMR-I).

#### Appendix A. Supplementary data

Supplementary data to this article can be found online at <https://doi.org/10.1016/j.ejmech.2022.114531>.

#### References

- [1] WHO, Global tuberculosis report 2020, Geneva, World Health Organization, [http://www.who.int/tb/publications/global\\_report/en/](http://www.who.int/tb/publications/global_report/en/), 2020. n.d..
- [2] WHO, Impact of the covid-19 pandemic on TB detection and mortality in 2020. <https://www.who.int/publications/m/item/impact-of-the-covid-19-pandemic-on-tb-detection-and-mortality-in-2020>, 2020. (Accessed 18 February 2015). <http://arxiv.org/abs/1303.3997>.
- [3] S.C. Duffy, S. Srinivasan, M.A. Schilling, T. Stuber, S.N. Danchuk, J.S. Michael, M. Venkatesan, N. Bansal, S. Maan, N. Jindal, D. Chaudhary, P. Dandapat, R. Katani, S. Chothe, M. Veerasami, S. Robbe-Austerman, N. Juleff, V. Kapur, M. A. Behr, Reconsidering *Mycobacterium bovis* as a proxy for zoonotic tuberculosis: a molecular epidemiological surveillance study, *Lancet Microbe* 1 (2020), [https://doi.org/10.1016/S2666-5247\(20\)30038-0](https://doi.org/10.1016/S2666-5247(20)30038-0) e66–e73.
- [4] GBD 2019 Tuberculosis Collaborators, Global, regional, and national sex differences in the global burden of tuberculosis by HIV status, 1990–2019: results from the Global Burden of Disease Study 2019, *Lancet Infect. Dis.* (21) (2021) S1473–S3099, [https://doi.org/10.1016/S1473-3099\(21\)00449-7](https://doi.org/10.1016/S1473-3099(21)00449-7), 00449–7.
- [5] K. Dheda, T. Gumbo, G. Maartens, K.E. Dooley, R. McNerney, M. Murray, J. Furin, E.A. Nardell, L. London, E. Lessem, G. Theron, P. van Helden, S. Niemann, M. Merker, D. Dowdy, A. Van Rie, G.K.H. Siu, J.G. Pasipanodya, C. Rodrigues, T. G. Clark, F.A. Sirgel, A. Esmail, H.-H. Lin, S.R. Atre, H.S. Schaaf, K.C. Chang, C. Lange, P. Nahid, Z.F. Udawadia, C.R. Horsburgh, G.J. Churchyard, D. Menzies, A. C. Hesselning, E. Nuermberger, H. McIlleron, K.P. Fennelly, E. Goemaere, E. Jaramillo, M. Low, C.M. Jara, N. Padayatchi, R.M. Warren, The epidemiology, pathogenesis, transmission, diagnosis, and management of multidrug-resistant, extensively drug-resistant, and incurable tuberculosis, *Lancet Respir. Med.* 15 (2017), [https://doi.org/10.1016/S2213-2600\(17\)30079-6](https://doi.org/10.1016/S2213-2600(17)30079-6). S2213-2600(17) 30079–6.
- [6] S. Huszár, K. Chibale, V. Singh, The quest for the holy grail: new antitubercular chemical entities, targets and strategies, *Drug Discov. Today* 25 (2020) 772–780, <https://doi.org/10.1016/j.drudis.2020.02.003>.
- [7] A. Koul, E. Arnoult, N. Lounis, J. Guillemont, K. Andries, The challenge of new drug discovery for tuberculosis, *Nature* 469 (2011) 483–490, <https://doi.org/10.1038/nature09657>.
- [8] J. Harrison, J.A.G. Cox, Changing the rules of TB-drug discovery, *J. Med. Chem.* 62 (2019) 10583–10585, <https://doi.org/10.1021/acs.jmedchem.9b01716>.
- [9] S. Wellington, D.T. Hung, The expanding diversity of *Mycobacterium tuberculosis* drug targets, *ACS Infect. Dis.* 4 (2018) 696–714, <https://doi.org/10.1021/acsinfectdis.7b00255>.
- [10] Q. An, C. Li, Y. Chen, Y. Deng, T. Yang, Y. Luo, Repurposed drug candidates for antituberculosis therapy, *Eur. J. Med. Chem.* 192 (2020), 112175, <https://doi.org/10.1016/j.ejmech.2020.112175>.
- [11] B.S. Matada, R. Pattanashettar, N.G. Yernale, A comprehensive review on the biological interest of quinoline and its derivatives, *Bioorg. Med. Chem.* 32 (2021), 115973, <https://doi.org/10.1016/j.bmc.2020.115973>.
- [12] A. Koul, N. Dendouga, K. Vergauwen, B. Molenberghs, L. Vranckx, R. Willebrords, Z. Ristic, H. Lill, I. Dorange, J. Guillemont, D. Bald, K. Andries, Diarylquinolines target subunit c of mycobacterial ATP synthase, *Nat. Chem. Biol.* 3 (2007) 323–324, <https://doi.org/10.1038/nchembio884>.
- [13] A.K. Kakkar, N. Dahiya, Bedaquiline for the treatment of resistant tuberculosis: promises and pitfalls, *Tuberculosis* 94 (2014) 357–362, <https://doi.org/10.1016/j.tube.2014.04.001>.
- [14] T.G. Shruthi, S. Eswaran, P. Shivarudraiah, S. Narayanan, S. Subramanian, Synthesis, antituberculosis studies and biological evaluation of new quinoline derivatives carrying 1,2,4-oxadiazole moiety, *Bioorg. Med. Chem. Lett.* 29 (2019) 97–102, <https://doi.org/10.1016/j.bmlc.2018.11.002>.
- [15] A. Banerjee, E. Dubnau, A. Quemard, V. Balasubramanian, K.S. Um, T. Wilson, D. Collins, G. de Lisle, W.R. Jacobs, *inhA*, a gene encoding a target for isoniazid and ethionamide in *Mycobacterium tuberculosis*, *Science* 263 (1994) 227–230, <https://doi.org/10.1126/science.8284673>.
- [16] A. Bhatt, V. Molle, G.S. Besra, W.R. Jacobs, L. Kremer, The *Mycobacterium tuberculosis* FAS-II condensing enzymes: their role in mycolic acid biosynthesis, acid-fastness, pathogenesis and in future drug development, *Mol. Microbiol.* 64 (2007) 1442–1454, <https://doi.org/10.1111/j.1365-2958.2007.05761.x>.
- [17] C. Vilchèze, H.R. Morbidoni, T.R. Weisbrod, H. Iwamoto, M. Kuo, J.C. Sacchettini, W.R. Jacobs, Inactivation of the *inhA*-encoded fatty acid synthase II (FASII) enoyl-acyl carrier protein reductase induces accumulation of the FASI end products and cell lysis of *Mycobacterium smegmatis*, *J. Bacteriol.* 182 (2000) 4059–4067, <https://doi.org/10.1128/jb.182.14.4059-4067.2000>.
- [18] K. Johnsson, W.A. Froland, P.G. Schultz, Overexpression, purification, and characterization of the catalase-peroxidase KatG from *Mycobacterium tuberculosis*, *J. Biol. Chem.* 272 (1997) 2834–2840, <https://doi.org/10.1074/jbc.272.5.2834>.
- [19] Y. Zhang, B. Heym, B. Allen, D. Young, S. Cole, The catalase-peroxidase gene and isoniazid resistance of *Mycobacterium tuberculosis*, *Nature* 358 (1992) 591–593, <https://doi.org/10.1038/358591a0>.
- [20] D.A. Rozwarski, Modification of the NADH of the isoniazid target (InhA) from, *Mycobacterium tuberculosis*, *Science* 279 (1998) 98–102, <https://doi.org/10.1126/science.279.5347.98>.
- [21] M. Wilming, K. Johnsson, Spontaneous formation of the bioactive form of the tuberculosis drug isoniazid, *Angew. Chem., Int. Ed. Engl.* 38 (1999) 2588–2590, [https://doi.org/10.1002/\(sici\)1521-3773\(19990903\)38:17<2588::aid-anie2588>3.0.co;2-8](https://doi.org/10.1002/(sici)1521-3773(19990903)38:17<2588::aid-anie2588>3.0.co;2-8).
- [22] R. Rawat, A. Whitty, P.J. Tonge, The isoniazid-NAD adduct is a slow, tight-binding inhibitor of InhA, the *Mycobacterium tuberculosis* enoyl reductase: adduct affinity and drug resistance, *Proc. Natl. Acad. Sci. USA* 100 (2003) 13881–13886, <https://doi.org/10.1073/pnas.2235848100>.
- [23] C. Vilchèze, F. Wang, M. Arai, M.H. Hazbón, R. Colangeli, L. Kremer, T. R. Weisbrod, D. Alland, J.C. Sacchettini, W.R. Jacobs, Transfer of a point mutation in *Mycobacterium tuberculosis inhA* resolves the target of isoniazid, *Nat. Med.* 12 (2006) 1027–1029, <https://doi.org/10.1038/nm1466>.

- [24] M. Nguyen, A. Quémard, S. Broussy, J. Bernadou, B. Meunier, Mn(III) pyrophosphate as an efficient tool for studying the mode of action of isoniazid on the InhA protein of *Mycobacterium tuberculosis*, *Antimicrob. Agents Chemother.* 46 (2002) 2137–2144, <https://doi.org/10.1128/aac.46.7.2137-2144.2002>.
- [25] A.N. Unissa, S. Subbian, L.E. Hanna, N. Selvakumar, Overview on mechanisms of isoniazid action and resistance in *Mycobacterium tuberculosis*, *Infect. Genet. Evol.* 45 (2016) 474–492, <https://doi.org/10.1016/j.meegid.2016.09.004>.
- [26] M. Seifert, D. Catanzaro, A. Catanzaro, T.C. Rodwell, Genetic mutations associated with isoniazid resistance in *Mycobacterium tuberculosis*: a systematic review, *PLoS One* 10 (2015), e0119628, <https://doi.org/10.1371/journal.pone.0119628>.
- [27] S.R. Khan, Y. Manialawy, A.G. Siraki, Isoniazid and host immune system interactions: a proposal for a novel comprehensive mode of action, *Br. J. Pharmacol.* 176 (2019) 4599–4608, <https://doi.org/10.1111/bph.14867>.
- [28] M.C. Kjellsson, L.E. Via, A. Goh, D. Weiner, K.M. Low, S. Kern, G. Pillai, C.E. Barry, V. Dartois, Pharmacokinetic evaluation of the penetration of antituberculosis agents in rabbit pulmonary lesions, *Antimicrob. Agents Chemother.* 56 (2012) 446–457, <https://doi.org/10.1128/AAC.05208-11>.
- [29] C.F. de Faria, T. Moreira, P. Lopes, H. Costa, J.R. Krewall, C.M. Barton, S. Santos, D. Goodwin, D. Machado, M. Viveiros, M. Machuqueiro, F. Martins, Designing new antitubercular isoniazid derivatives with improved reactivity and membrane trafficking abilities, *Biomed. Pharmacother.* 144 (2021), 112362, <https://doi.org/10.1016/j.biopha.2021.112362>.
- [30] M.J. Hearn, M.H. Cynamon, M.F. Chen, R. Coppins, J. Davis, H. Joo-On Kang, A. Noble, B. Tu-Sekine, M.S. Terrot, D. Trombino, M. Thai, E.R. Webster, R. Wilson, Preparation and antitubercular activities *in vitro* and *in vivo* of novel Schiff bases of isoniazid, *Eur. J. Med. Chem.* 44 (2009) 4169–4178, <https://doi.org/10.1016/j.ejmech.2009.05.009>.
- [31] A. Rani, M.D. Johansen, F. Roquet-Banères, L. Kremer, P. Awolade, O. Ebenezer, P. Singh Sumanjit, V. Kumar, Design and synthesis of 4-Aminoquinoline-isoindoline-dione-isoniazid triads as potential anti-mycobacterials, *Bioorg. Med. Chem. Lett.* 30 (2020), 127576, <https://doi.org/10.1016/j.bmcl.2020.127576>.
- [32] M.D. Johansen Shalini, S. Kumar, C. Raynaud, D.H. Quan, W.J. Britton, P. M. Hansbro, V. Kumar, Kremer L, Biological and biochemical evaluation of isatin-isoniazid hybrids as bactericidal candidates against *Mycobacterium tuberculosis*, *Antimicrob. Agents Chemother.* 65 (2021), e0001121, <https://doi.org/10.1128/AAC.00011-21>.
- [33] B. Zhou, Y. He, X. Zhang, J. Xu, Y. Luo, Y. Wang, S.G. Franzblau, Z. Yang, R. J. Chan, Y. Liu, J. Zheng, Z.-Y. Zhang, Targeting mycobacterium protein tyrosine phosphatase B for antituberculosis agents, *Proc. Natl. Acad. Sci. U.S.A.* 107 (2010) 4573–4578, <https://doi.org/10.1073/pnas.0909133107>.
- [34] B. Sharma, S. Kaur, J. Legac, P.J. Rosenthal, V. Kumar, Synthesis, anti-plasmodial and cytotoxic evaluation of 1H-1,2,3-triazole/acyl hydrazide integrated tetrahydro- $\beta$ -carboline-4-aminoquinoline conjugates, *Bioorg. Med. Chem. Lett.* 30 (2020), 126810, <https://doi.org/10.1016/j.bmcl.2019.126810>.
- [35] A. Singh, J. Gut, P.J. Rosenthal, V. Kumar, 4-Aminoquinoline-ferrocenyl-chalcone conjugates: synthesis and anti-plasmodial evaluation, *Eur. J. Med. Chem.* 125 (2017) 269–277, <https://doi.org/10.1016/j.ejmech.2016.09.044>.
- [36] P. Tenbrick, M. Beer, K. Beer, Treatment of biopsy and culture negative *Mycobacterium marinum*: diagnostic and therapeutic considerations, *J. Drugs Dermatol.* 13 (2014) 204–206.
- [37] S. Shalini, A. Viljoen, L. Kremer, V. Kumar, Alkylated/aminated nitroimidazoles and nitroimidazole-7-chloroquinoline conjugates: synthesis and anti-mycobacterial evaluation, *Bioorg. Med. Chem. Lett.* 28 (2018) 1309–1312, <https://doi.org/10.1016/j.bmcl.2018.03.021>.
- [38] C.K. Stover, V.F. de la Cruz, T.R. Fuerst, J.E. Burlein, L.A. Benson, L.T. Bennett, G. P. Bansal, J.F. Young, M.H. Lee, G.F. Hatfull, New use of BCG for recombinant vaccines, *Nature* 351 (1991) 456–460, <https://doi.org/10.1038/351456a0>.
- [39] M.H. Larsen, C. Vilchèze, L. Kremer, G.S. Besra, L. Parsons, M. Salfinger, L. Heifets, M.H. Hazbon, D. Alland, J.C. Sacchettini, W.R. Jacobs, Overexpression of *inhA*, but not *kasA*, confers resistance to isoniazid and ethionamide in *Mycobacterium smegmatis*, *M. bovis* BCG and *M. tuberculosis*, *Mol. Microbiol.* 46 (2002) 453–466, <https://doi.org/10.1046/j.1365-2958.2002.03162.x>.
- [40] L. Kremer, J.D. Douglas, A.R. Baulard, C. Morehouse, M.R. Guy, D. Alland, L. G. Dover, J.H. Lakey, W.R. Jacobs, P.J. Brennan, D.E. Minnikin, G.S. Besra, Thioloactomycin and related analogues as novel anti-mycobacterial agents targeting *KasA* and *KasB* condensing enzymes in *Mycobacterium tuberculosis*, *J. Biol. Chem.* 275 (2000) 16857–16864, <https://doi.org/10.1074/jbc.M000569200>.
- [41] S. Ramaswamy, J.M. Musser, Molecular genetic basis of antimicrobial agent resistance in *Mycobacterium tuberculosis*: 1998 update, *Tuber. Lung Dis.* 79 (1998) 3–29, <https://doi.org/10.1054/tuld.1998.0002>.
- [42] V.Q.T. Ho, T. Verboom, M.K. Rong, E. Habjan, W. Bitter, A. Speer, Heterologous expression of *ethA* and *katG* in *Mycobacterium marinum* enables the rapid identification of new prodrugs active against, *Mycobacterium tuberculosis*, *Antimicrob. Agents Chemother.* 65 (2021), <https://doi.org/10.1128/AAC.01445-20>.
- [43] C. Vilchèze, W.R. Jacobs, The mechanism of isoniazid killing: clarity through the scope of genetics, *Annu. Rev. Microbiol.* 61 (2007) 35–50, <https://doi.org/10.1146/annurev.micro.61.111606.122346>.
- [44] K. Rožman, I. Sosić, R. Fernandez, R.J. Young, A. Mendoza, S. Gobec, L. Encinas, A new 'golden age' for the antitubercular target InhA, *Drug Discov. Today* 22 (2017) 492–502, <https://doi.org/10.1016/j.drudis.2016.09.009>.
- [45] C. Vilchèze, A.D. Baughn, J. Tufariello, L.W. Leung, M. Kuo, C.F. Basler, D. Alland, J.C. Sacchettini, J.S. Freundlich, W.R. Jacobs, Novel inhibitors of InhA efficiently kill *Mycobacterium tuberculosis* under aerobic and anaerobic conditions, *Antimicrob. Agents Chemother.* 55 (2011) 3889–3898, <https://doi.org/10.1128/AAC.00266-11>.
- [46] B. Inturi, G.V. Pujar, M.N. Purohit, Recent advances and structural features of enoyl-ACP reductase inhibitors of *Mycobacterium tuberculosis*, *Arch. Pharm. (Weinheim)* 349 (2016) 817–826, <https://doi.org/10.1002/ardp.201600186>.
- [47] L. Flint, A. Korkegian, T. Parish, InhA inhibitors have activity against non-replicating *Mycobacterium tuberculosis*, *PLoS One* 15 (2020), e0239354, <https://doi.org/10.1371/journal.pone.0239354>.
- [48] T. Armstrong, M. Lamont, A. Lanne, L.J. Alderwick, N.R. Thomas, Inhibition of *Mycobacterium tuberculosis* InhA: design, synthesis and evaluation of new di-triclosan derivatives, *Bioorg. Med. Chem.* 28 (2020), 115744, <https://doi.org/10.1016/j.bmc.2020.115744>.
- [49] A. Gagliardi, P. Selchow, S. Luthra, D. Schäfle, B. Schulthess, P. Sander, KatG as counterselection marker for nontuberculous mycobacteria, *Antimicrob. Agents Chemother.* 64 (2020) e02508–e02519, <https://doi.org/10.1128/AAC.02508-19>.
- [50] F. Maruri, T.R. Sterling, A.W. Kaiga, A. Blackman, Y.F. van der Heijden, C. Mayer, E. Cambau, A. Aubry, A systematic review of gyrase mutations associated with fluoroquinolone-resistant *Mycobacterium tuberculosis* and a proposed gyrase numbering system, *J. Antimicrob. Chemother.* 67 (2012) 819–831, <https://doi.org/10.1093/jac/ckr566>.
- [51] K. Andries, P. Verhasselt, J. Guillemont, H.W.H. Göhlmann, J.-M. Neefs, H. Winkler, J. Van Gestel, P. Timmerman, M. Zhu, E. Lee, P. Williams, D. de Chaffoy, E. Huitric, S. Hoffner, E. Cambau, C. Truffot-Pernot, N. Lounis, V. Jarlier, A diarylquinoline drug active on the ATP synthase of *Mycobacterium tuberculosis*, *Science* 307 (2005) 223–227, <https://doi.org/10.1126/science.1106753>.
- [52] V.K. Sambandamurthy, S.C. Derrick, T. Hsu, B. Chen, M.H. Larsen, K.V. Jalapathy, M. Chen, J. Kim, S.A. Porcelli, J. Chan, S.L. Morris, W.R. Jacobs, *Mycobacterium tuberculosis* DeltarD1 DeltapanCD: a safe and limited replicating mutant strain that protects immunocompetent and immunocompromised mice against experimental tuberculosis, *Vaccine* 24 (2006) 6309–6320, <https://doi.org/10.1016/j.vaccine.2006.05.097>.
- [53] T.P. Stinear, T. Seemann, P.F. Harrison, G.A. Jenkin, J.K. Davies, P.D.R. Johnson, Z. Abdellah, C. Arrowsmith, T. Chillingworth, C. Churcher, K. Clarke, A. Cronin, P. Davis, I. Goodhead, N. Holroyd, K. Jagels, A. Lord, S. Moule, K. Mungall, H. Norbertczak, M.A. Quail, E. Rabinowitz, D. Walker, B. White, S. Whitehead, P.L.C. Small, R. Brosch, L. Ramakrishnan, M.A. Fischbach, J. Parkhill, S.T. Cole, Insights from the complete genome sequence of *Mycobacterium marinum* on the evolution of *Mycobacterium tuberculosis*, *Genome Res.* 18 (2008) 729–741, <https://doi.org/10.1101/gr.075069.107>.
- [54] F. Ripoll, S. Pasek, C. Schenowitz, C. Dossat, V. Barbe, M. Rottman, E. Macheras, B. Heym, J.-L. Herrmann, M. Daffé, R. Brosch, J.-L. Risler, J.-L. Gaillard, Non mycobacterial virulence genes in the genome of the emerging pathogen *Mycobacterium abscessus*, *PLoS One* 4 (2009), e5660, <https://doi.org/10.1371/journal.pone.0005660>.
- [55] G.L. Woods, B.A. Brown-Elliott, P.S. Conville, E.P. Desmond, G.S. Hall, G. Lin, G. E. Pfyffer, J.C. Ridderhof, S.H. Siddiqi, R.J. Wallace, N.G. Warren, F.G. Witebsky, Susceptibility Testing of Mycobacteria, Nocardiae, and Other Aerobic Actinomycetes, second ed., Clinical and Laboratory Standards Institute, Wayne (PA), 2011. <http://www.ncbi.nlm.nih.gov/books/NBK544374/>. (Accessed 12 April 2021).
- [56] U.H. Manjunatha, S.P.S. Rao, R.R. Kondreddi, C.G. Noble, L.R. Camacho, B.H. Tan, S.H. Ng, P.S. Ng, N.L. Ma, S.B. Lakshminarayana, M. Herve, S.W. Barnes, W. Yu, K. Kuhn, F. Blasco, D. Beer, J.R. Walker, P.J. Tonge, R. Glynn, P.W. Smith, T. T. Diagana, Direct inhibitors of InhA are active against, *Mycobacterium tuberculosis*, *Sci. Transl. Med.* 7 (2015), <https://doi.org/10.1126/scitranslmed.3010597>, 269ra3.
- [57] C. Dupont, Y. Chen, Z. Xu, F. Roquet-Banères, M. Blaise, A.-K. Witt, F. Dubar, C. Biot, Y. Guéardel, F.P. Maurer, S.-S. Chng, L. Kremer, A piperidinol-containing molecule is active against *Mycobacterium tuberculosis* by inhibiting the mycolic acid flippase activity of MmpL3, *J. Biol. Chem.* 294 (2019) 17512–17523, <https://doi.org/10.1074/jbc.RA119.010135>.
- [58] S. Chen, Y. Zhou, Y. Chen, J. Gu, fastp: an ultra-fast all-in-one FASTQ preprocessor, *Bioinformatics* 34 (2018), <https://doi.org/10.1093/bioinformatics/bty560> i884–i890.
- [59] D.E. Wood, J. Lu, B. Langmead, Improved metagenomic analysis with Kraken 2, *Genome Biol.* 20 (2019) 257, <https://doi.org/10.1186/s13059-019-1891-0>.
- [60] A. Bankevich, S. Nurk, D. Antipov, A.A. Gurevich, M. Dvorkin, A.S. Kulikov, V. M. Lesin, S.I. Nikolenko, S. Pham, A.D. Prjibelski, A.V. Pyshkin, A.V. Sirokin, N. Vyahhi, G. Tesler, M.A. Alekseyev, P.A. Pevzner, SPAdes: a new genome assembly algorithm and its applications to single-cell sequencing, *J. Comput. Biol.* 19 (2012) 455–477, <https://doi.org/10.1089/cmb.2012.0021>.
- [61] L.G. Dover, A. Alahari, P. Gratraud, J.M. Gomes, V. Bhowruth, R.C. Reynolds, G. S. Besra, L. Kremer, EthA, a common activator of thiocarbamide-containing drugs acting on different mycobacterial targets, *Antimicrob. Agents Chemother.* 51 (2007) 1055–1063, <https://doi.org/10.1128/AAC.01063-06>.

## Supporting information

# Designing Quinoline-Isoniazid hybrids as potent antitubercular agents inhibiting mycolic acid biosynthesis

Matthéo Alcaraz<sup>1\*</sup>, Bharvi Sharma<sup>2\*</sup>, Françoise Roquet-Banères<sup>1</sup>, Cyril Conde<sup>3</sup>,  
Thierry Cochard<sup>3</sup>, Franck Biet<sup>3</sup>, Vipin Kumar<sup>2,#</sup>, and Laurent Kremer<sup>1,4,#</sup>

<sup>1</sup>Centre National de la Recherche Scientifique UMR 9004, Institut de Recherche en Infectiologie de Montpellier (IRIM), Université de Montpellier, 1919 route de Mende, 34293, Montpellier, France.

<sup>2</sup>Department of Chemistry, Guru Nanak Dev University, Amritsar-143005, Punjab, India

<sup>3</sup>INRAE, Université de Tours, ISP, F-37380, Nouzilly, France

<sup>4</sup>INSERM, IRIM, 34293 Montpellier, France.

**\*These authors contributed equally to this work.**

#To whom correspondence should be addressed:

Tel: (+91) 183-258802 extn 3286; E-Mail: [vipan\\_org@yahoo.com](mailto:vipan_org@yahoo.com)

Tel: (+33) 4 34 35 94 47; E-mail: [laurent.kremer@irim.cnrs.fr](mailto:laurent.kremer@irim.cnrs.fr)

## Contents

- 1) Table S1. ADMET properties of the most active molecules.
- 2) Table S2. MIC ( $\mu\text{g/mL}$ ) values of quinoline-INH compounds
- 3) Table S3. Drug susceptibility profiles of *M. tuberculosis* katG mutants and complemented strains.
- 4) Figure S1. Cytotoxicity assay of INH and **16a-16g** in Vero cells.
- 5) Figure S2. Drug susceptibility profiles of *M. tuberculosis* mc<sup>2</sup>6230 carrying either pMV261 or pMV261-*inhA* towards compounds **16a-16g**.
- 6) Figure S3. Deletion within the *katG* locus in the *M. tuberculosis* mc<sup>2</sup>6230 16g<sup>R</sup><sub>20X</sub> mutant.
- 7) Figure S4. Drug susceptibility phenotypes of *M. tuberculosis* mc<sup>2</sup>6230 mutants carrying the G421D (Mtb-11c<sup>R</sup>), L430P (Mtb-11d<sup>R</sup>) and W438Stop (Mtb-INH<sup>R3</sup>) mutations in KatG.
- 8) Figure S5-S30. Scanned copies of <sup>1</sup>H and <sup>13</sup>C-NMR spectra of representative compounds *viz.* **12a, 13b, 13d, 14, 16a, 16g, 17b, 18a, 18b, 18c, 18d, and 18f.**

**Table S1.** ADMET properties of the most active molecules.

<b>Properties Predicted values</b>							
<b>Compound</b>	<b>16a</b>	<b>16b</b>	<b>16c</b>	<b>16d</b>	<b>16e</b>	<b>16f</b>	<b>16g</b>
<b>Absorption</b>							
Water solubility (log mol/L)	-3.604	-3.179	-3.565	-3.798	-3.624	-3.844	-3.662
Caco2 permeability log Papp in 10 <sup>-6</sup> cm/s	0.637	0.952	1.386	1.431	1.163	1.135	0.599
Intestinal absorption (human) (%)	100	95.172	93.496	94.35	88.027	88.932	89.692
Skin Permeability log Kp	-2.735	-2.735	-2.737	-2.737	-2.736	-2.736	-2.734
P-glycoprotein substrate	Yes	No	Yes	Yes	Yes	Yes	Yes
P-glycoprotein I inhibitor	Yes	Yes	Yes	Yes	Yes	Yes	Yes
P-glycoprotein II inhibitor	Yes	Yes	Yes	Yes	Yes	Yes	Yes
<b>Distribution</b>							
VDss (Log L/Kg)	0.517	0.174	0.339	0.377	0.356	0.391	0.699
Fraction unbound Human	0.132	0.197	0	0	0.003	0	0.115
BBB permeability	-1.494	-1.679	-1.54	-1.555	-1.648	-1.656	-1.457
CNS permeability	-3.085	-3.776	-3.316	-3.259	-3.492	-3.442	-2.393
<b>Metabolism</b>							
CYP2D6 substrate	No	No	No	No	No	No	No
CYP3A4 substrate	Yes	Yes	Yes	Yes	Yes	Yes	Yes
CYP1A2 inhibitor	No	No	No	No	No	No	No
CYP2C19 inhibitor	Yes	No	Yes	Yes	Yes	Yes	No
CYP2C9 inhibitor	Yes	Yes	Yes	Yes	Yes	Yes	Yes
CYP2D6 inhibitor	No	No	No	No	No	No	No
CYP3A4 inhibitor	Yes	Yes	Yes	Yes	Yes	Yes	Yes
<b>Excretion</b>							
Total Clearance (log ml/min/kg)	-0.141	0.049	-0.098	-0.218	0.099	-0.019	0.35
Renal OCT2 substrate	No	No	No	No	No	No	Yes
<b>Toxicity</b>							
Oral Rat Acute Toxicity (LD <sub>50</sub> ) (mol/kg)	2.826	0.546	2.893	2.898	2.918	2.89	3.239
Hepatotoxicity	Yes	Yes	Yes	Yes	Yes	Yes	Yes
Skin Sensitisation	No	No	No	No	No	No	No
<i>T. pyriformis</i> toxicity (Log µg/L)	0.285	0.285	0.286	0.286	0.285	0.285	0.286
Minnow toxicity (log mM)	-1.104	-1.827	1.979	0.793	1.132	-0.381	1.01
<b>LogP</b>	4.2068	4.2154	4.3297	4.7198	4.3383	4.7284	3.95
<b>TPSA (in °A<sup>2</sup>)</b>	107.18	116.41	116.41	119.21	128.44	128.44	104.43
<b>Num of HBA/HBD</b>	7	8	8	4.5	4	4	9
<b>Molar refractivity</b>	131.61	138.10	138.10	149.98	151.66	156.47	161.38

**Table S2.** MIC ( $\mu\text{g/mL}$ ) values of quinoline-INH compounds determined in 7H9 broth supplemented with OADC against *M. tuberculosis* mc<sup>2</sup>6230 *katG* mutants. INH and ETH were included as control drugs.

<b>Cpd</b>	<b>WT</b>	<b>Mtb-16g<sup>R</sup><sub>20x</sub></b>	<b>Mtb-16g<sup>R</sup><sub>5x</sub></b>	<b>Mtb-16f<sup>R</sup><sub>5x</sub></b>	<b>Mtb-16d<sup>R</sup><sub>5x</sub></b>	<b>Mtb-16d<sup>R</sup><sub>20x</sub></b>
<b>16a</b>	0.25	>200	200	>200	>200	>200
<b>16b</b>	0.5	>200	200	200	200	>200
<b>16c</b>	0.5	>200	100	200	100	200
<b>16d</b>	0.5	200	50	50	50	200
<b>16e</b>	0.5	>200	200	200	200	>200
<b>16f</b>	0.25	>200	100	200	100	200
<b>16g</b>	0.25	>200	10	50	200	200
<b>INH</b>	0.05	>2	>2	>2	>2	>2
<b>ETH</b>	1.56	1.56	1.56	1.56	1.56	1.56

**Table S3.** Drug susceptibility profiles of *M. tuberculosis* mc<sup>2</sup>6230 mutants carrying the G421D (Mtb-11c<sup>R</sup>), L430P (Mtb-11d<sup>R</sup>) and W438Stop (Mtb-INH<sup>R3</sup>) mutations in KatG and the corresponding strains complemented with pSMT3-*katG* towards compounds **16a-16g**. INH was included as a positive control. MIC (μg/mL) values were determined in 7H9 broth supplemented with OADC.

Cpd	Mtb mc <sup>2</sup> 6230	Mtb-INH <sup>R3</sup>	Mtb-11c <sup>R</sup>	Mtb-11d <sup>R</sup>	Mtb-INH <sup>R3</sup> (pSMT3- <i>katG</i> )	Mtb-11c <sup>R</sup> (pSMT3- <i>katG</i> )	Mtb-11d <sup>R</sup> (pSMT3- <i>katG</i> )
<b>16a</b>	0.25	200	200	>200	0.5	1	1
<b>16b</b>	0.5	>200	>200	>200	0.5	1	1
<b>16c</b>	0.5	200	200	200	0.5	0.5	0.5
<b>16d</b>	0.5	200	200	100	0.5	1	1
<b>16e</b>	0.5	>200	>200	200	0.5	1	1
<b>16f</b>	0.25	>200	>200	200	0.5	1	1
<b>16g</b>	0.25	200	>200	100	0.5	1	0.5
<b>INH</b>	0.05	>2	>2	>2	0.05	0.1	0.05

**Figure S1. Cytotoxicity assay of INH and 16a-16g in Vero cells.** Cells were exposed to increasing concentration of each compound for 24 hrs at 37°C with 5% CO<sub>2</sub>. Results are representative of three independent experiments done in duplicate.

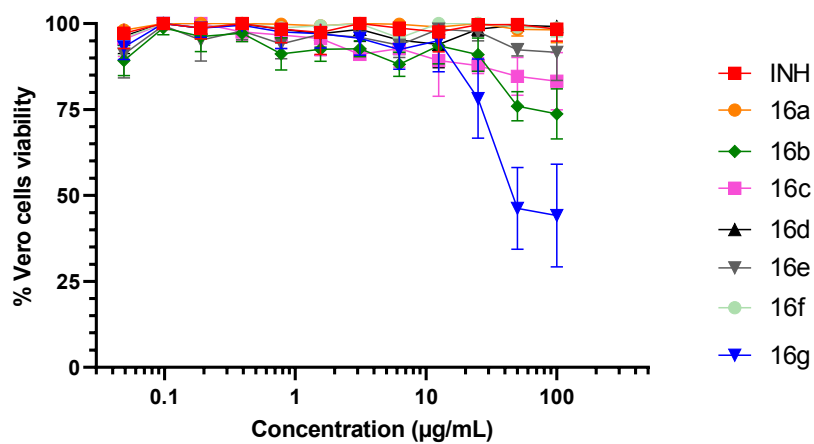




**Figure S2.** Drug susceptibility profiles of *M. tuberculosis* mc<sup>2</sup>6230 carrying either pMV261 or pMV261-*inhA* towards compounds **16a-16g**. INH was included as a positive control. Two microliters of 10-fold serially diluted bacterial suspensions of exponentially growing cultures were spotted on Middlebrook 7H10 plates supplemented with OADC enrichment and pantothenate in the presence of increasing concentrations of compounds ( $\mu\text{g/mL}$ ). Plates were incubated at 37 °C for 20 days.

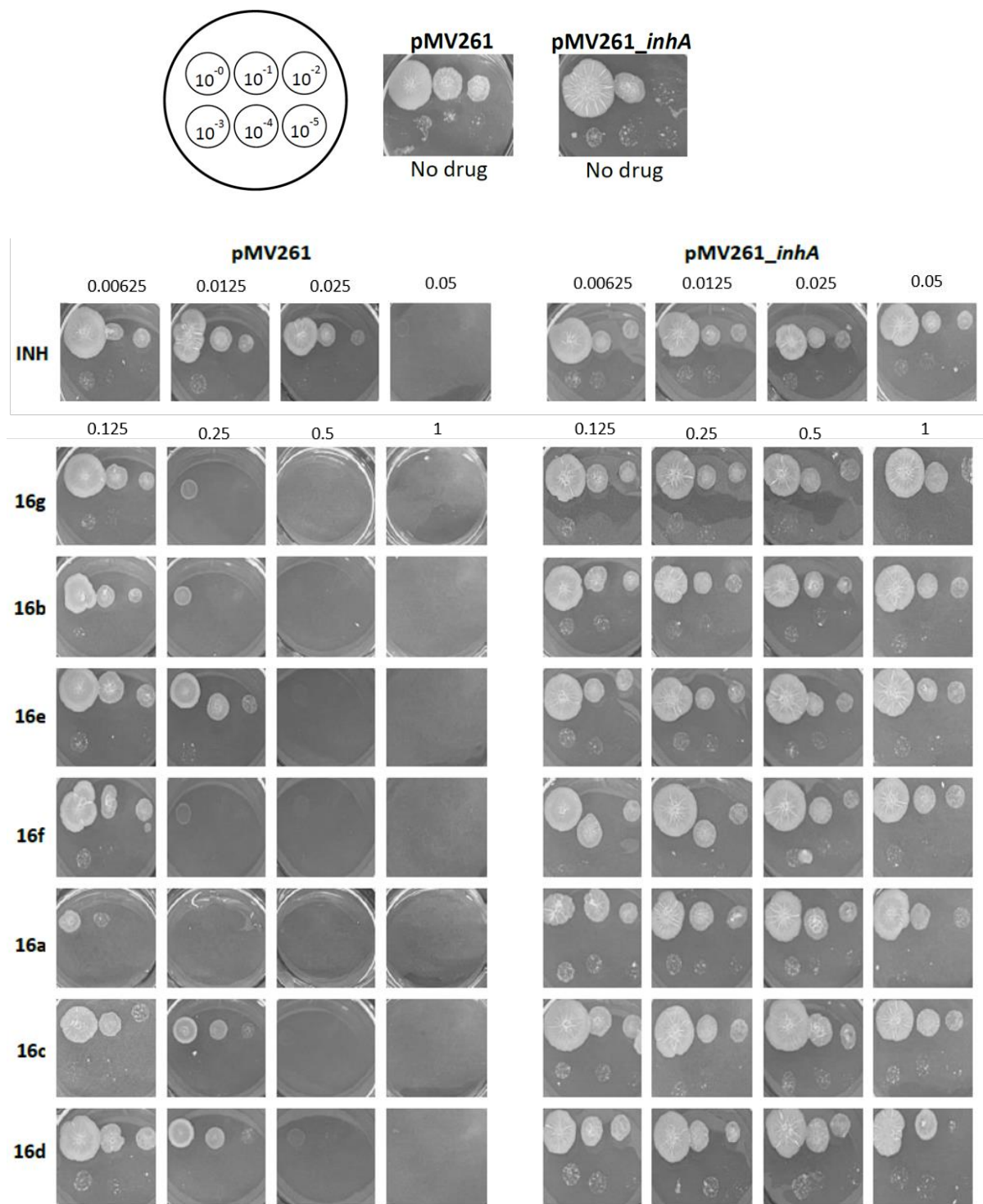




**Figure S3. Deletion within the *katG* locus in the *M. tuberculosis* mc<sup>2</sup>6230 16g<sup>R</sup><sub>20X</sub> mutant strain.** Schematic representation of deleted genes in the 3679 bp region detected by WGS. The top line shows the gene organization in the parental strain mc<sup>2</sup>6230. The bottom line shows the gene organization in 16g<sup>R</sup><sub>20X</sub> and the consequence of the gene deletion affecting multiple genes including *katG* and *Rv1913* reduced as pseudogene (black hatched box). Red cross-links indicate regions with shared homologies. Coordinates were extracted from the H37Rv reference genome (RefSeq accession: NC\_000962.3). The deletion spans the first 558 bp of *katG*, *furA*, *Rv1910c*, *lppC*, *fadB5* as well as the first 42 bp of *Rv1913*.

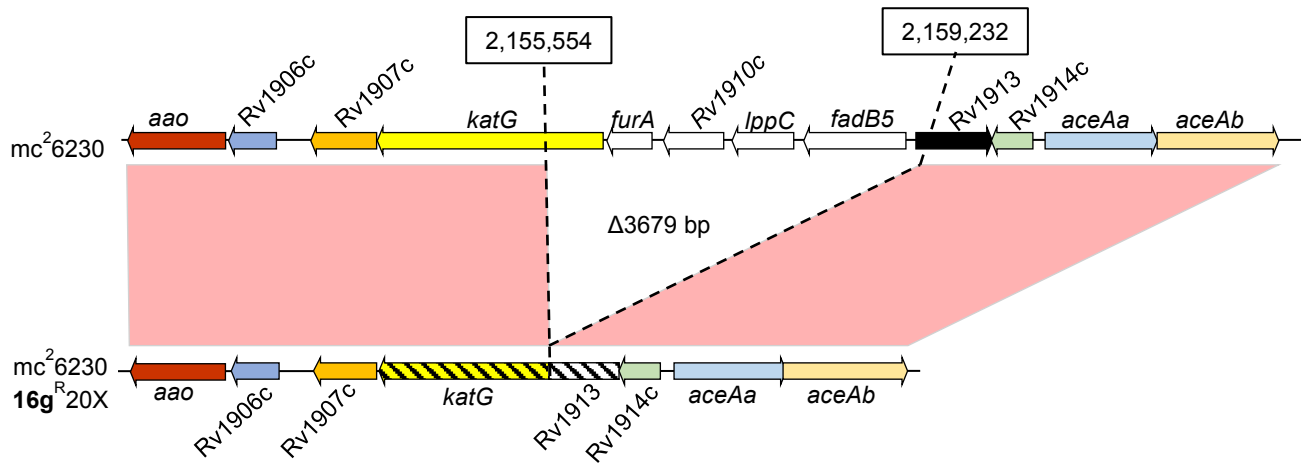


**Figure S4.** Drug susceptibility phenotypes of *M. tuberculosis* mc<sup>2</sup>6230 mutants carrying the G421D (Mtb-11c<sup>R</sup>), L430P (Mtb-11d<sup>R</sup>) and W438Stop (Mtb-INH<sup>R3</sup>) mutations in KatG. Strains of exponentially growing cultures were streaked on Middlebrook 7H10 supplemented with OADC enrichment and pantothenate and containing 0.05 µg/mL INH or 1 µg/mL of compounds **16a** to **16g**. Plates were incubated at 37°C for two weeks.

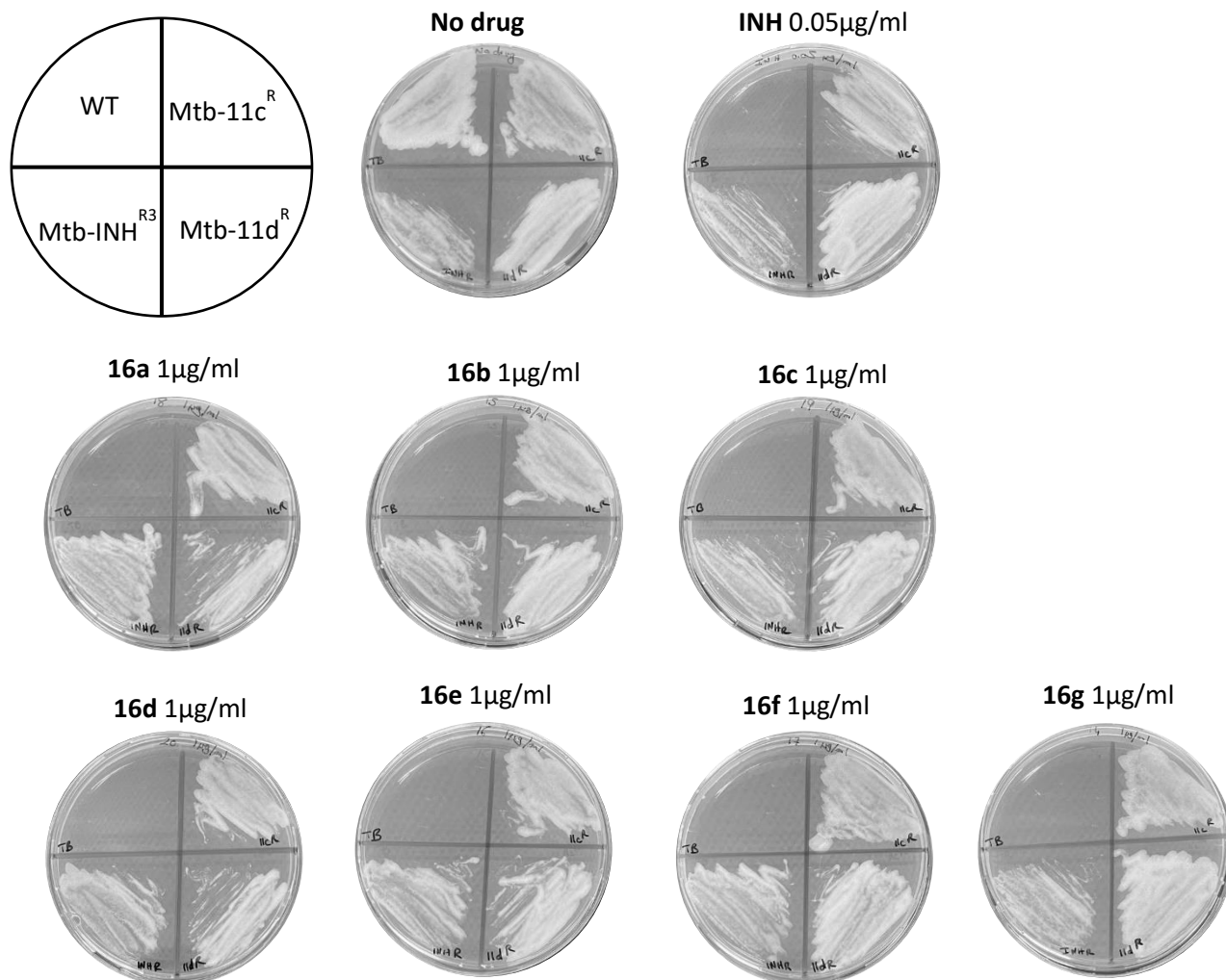


**Figure S5.**  $^1\text{H}$  NMR of 4-((1-(7-chloroquinolin-4-yl)-1*H*-1,2,3-triazol-4-yl)methoxy)benzaldehyde (**12a**)

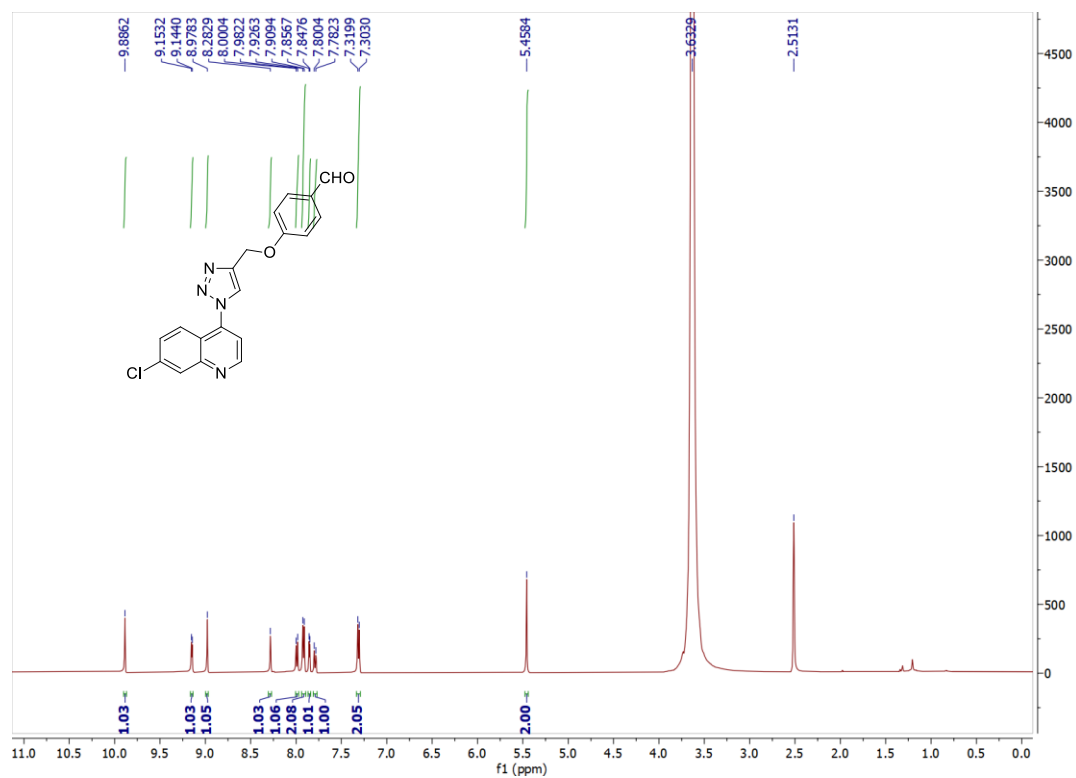


**Figure S6.**  $^{13}\text{C}$  NMR of 4-((1-(7-chloroquinolin-4-yl)-1H-1,2,3-triazol-4-yl)methoxy)benzaldehyde (**12a**)

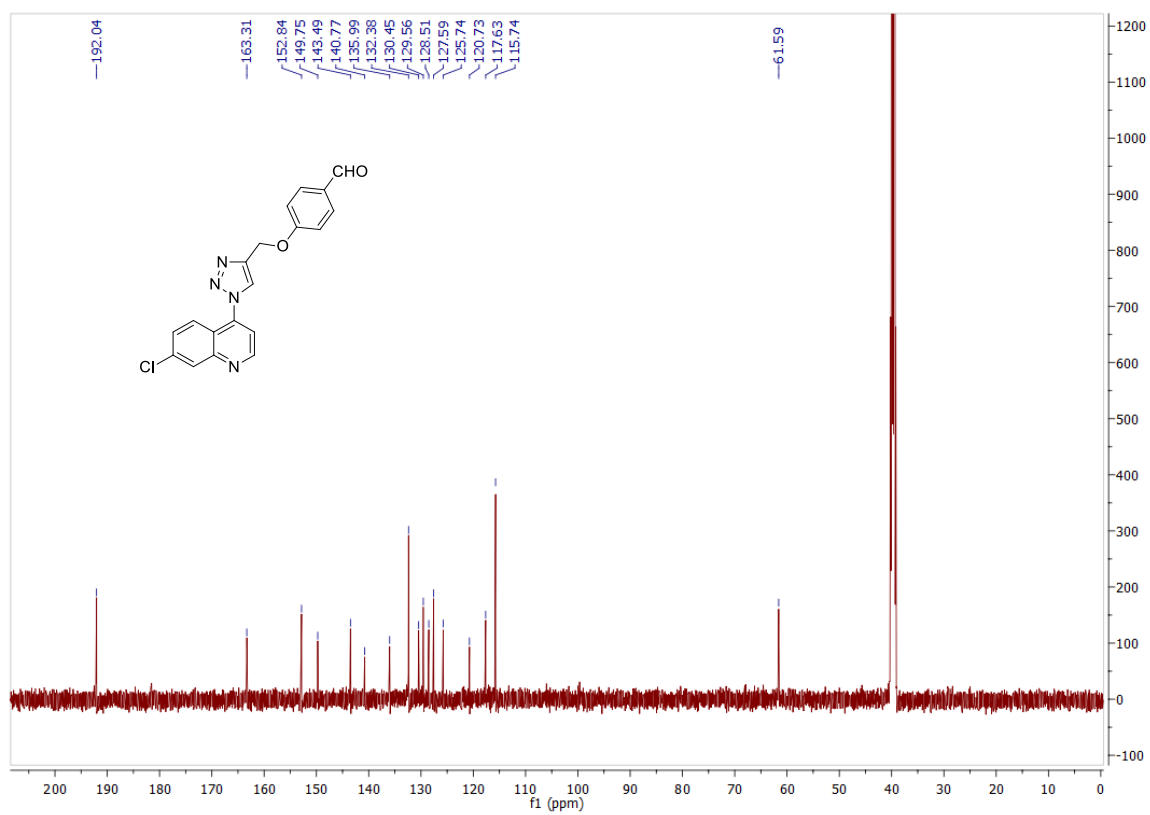


**Figure S7.**  $^1\text{H}$  NMR of 4-((1-(3-((7-chloroquinolin-4-yl)amino)propyl)-1*H*-1,2,3-triazol-4-yl)methoxy)benzaldehyde (**13b**)

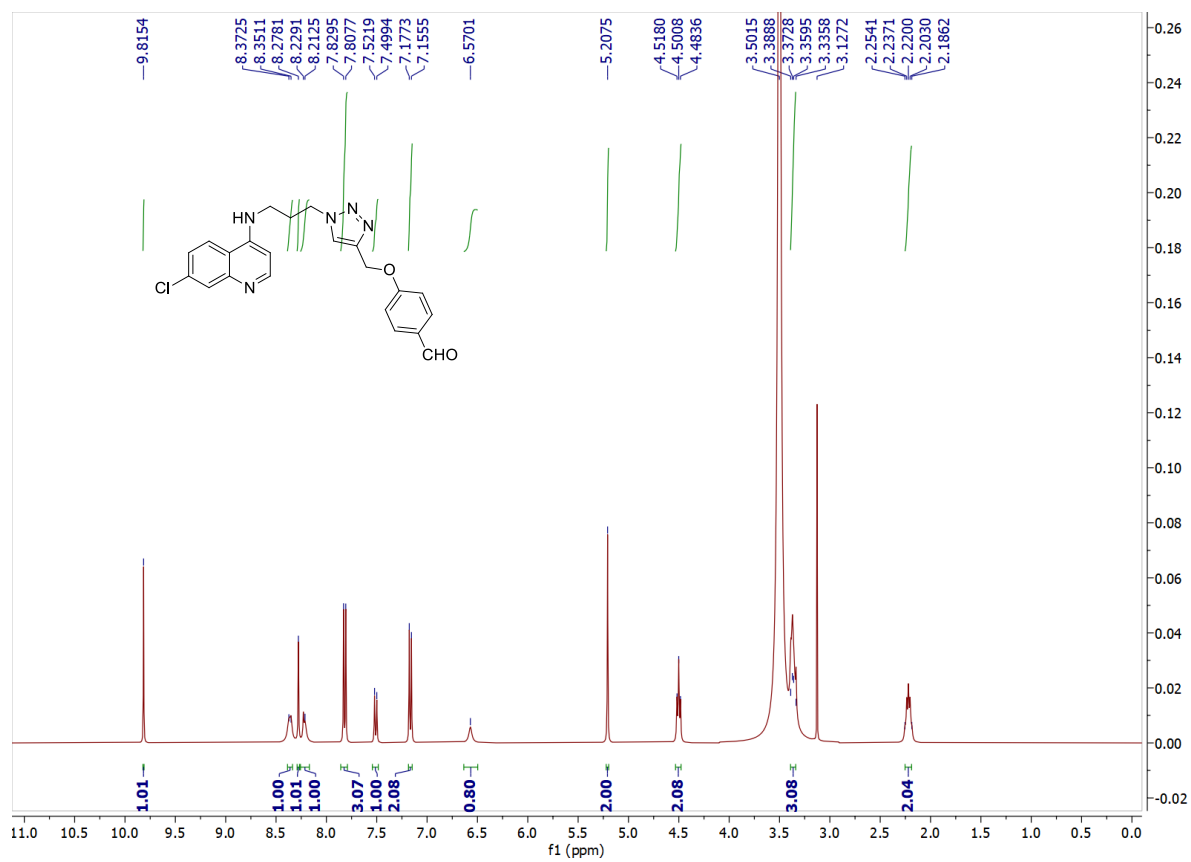


**Figure S8.**  $^{13}\text{C}$  NMR of 4-((1-(3-((7-chloroquinolin-4-yl)amino)propyl)-1*H*-1,2,3-triazol-4-yl)methoxy)benzaldehyde (**13b**)

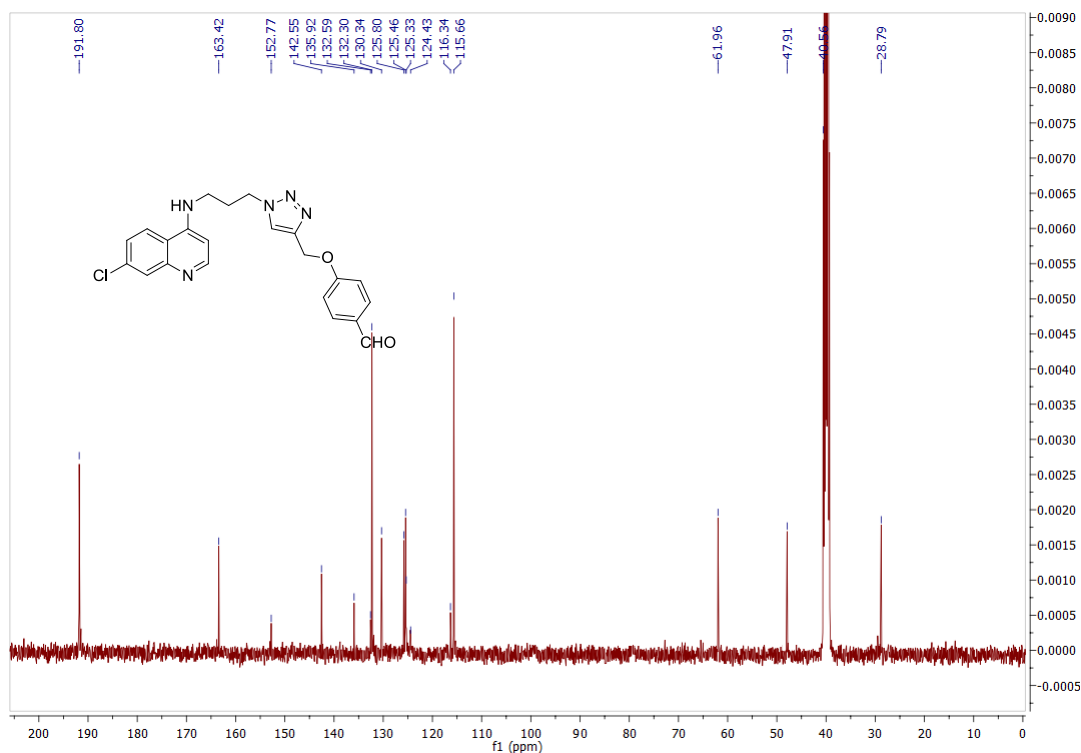


**Figure S9.** DEPT-135 of 4-((1-(3-((7-chloroquinolin-4-yl)amino)propyl)-1*H*-1,2,3-triazol-4-yl)methoxy)benzaldehyde (**13b**)

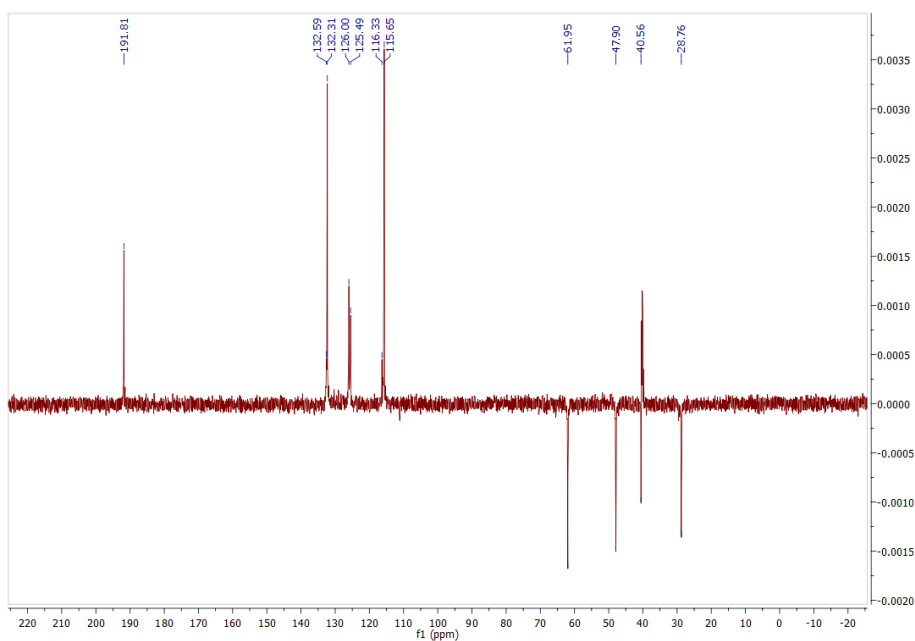


**Figure S10.**  $^1\text{H}$  NMR of 4-((1-(3-((7-chloroquinolin-4-yl)amino)propyl)-1H-1,2,3-triazol-4-yl)methoxy)-3-methoxybenzaldehyde (**13d**)

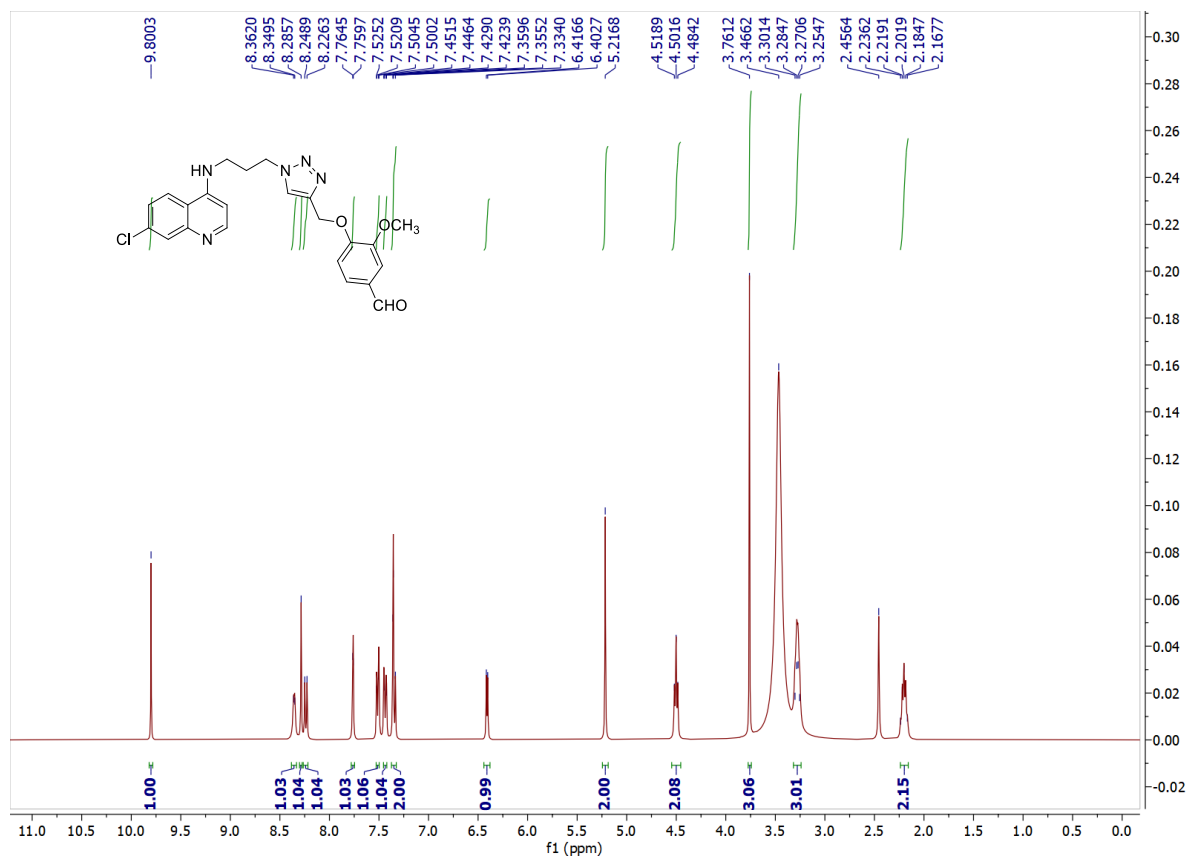


**Figure S11.**  $^{13}\text{C}$  NMR of 4-((1-(3-((7-chloroquinolin-4-yl)amino)propyl)-1H-1,2,3-triazol-4-yl)methoxy)-3-methoxybenzaldehyde (**13d**)

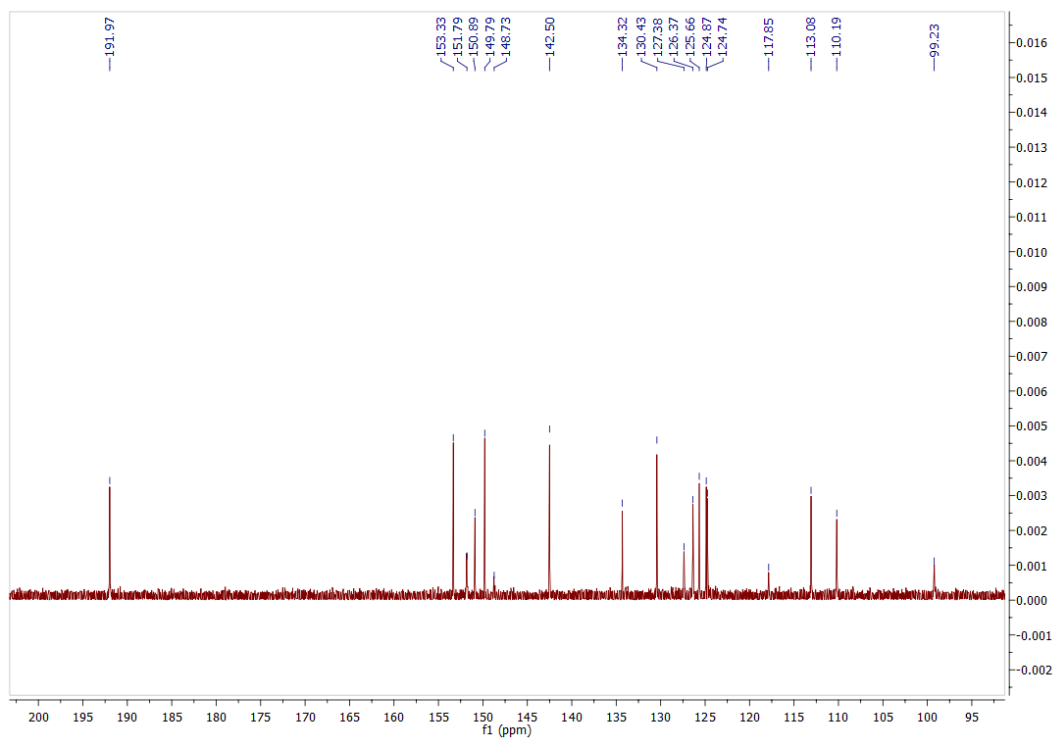
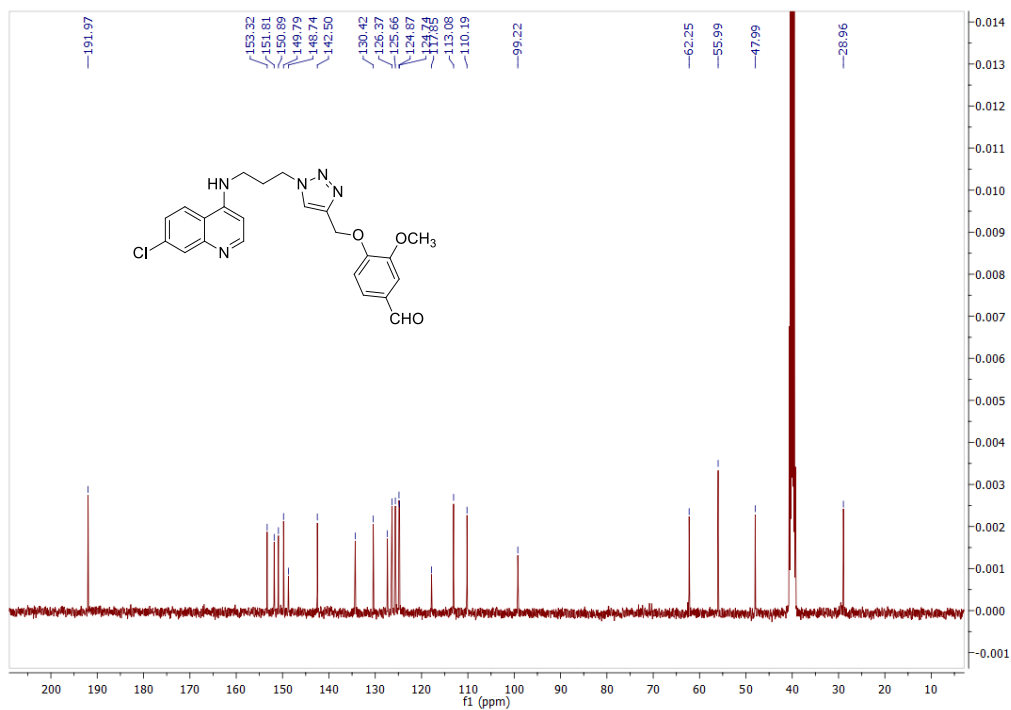




**Figure S12.** <sup>1</sup>H NMR of 2-(4-((4-(7-chloroquinolin-4-yl)piperazin-1-yl)methyl)-1H-1,2,3-triazol-1-yl)benzaldehyde (**14**)

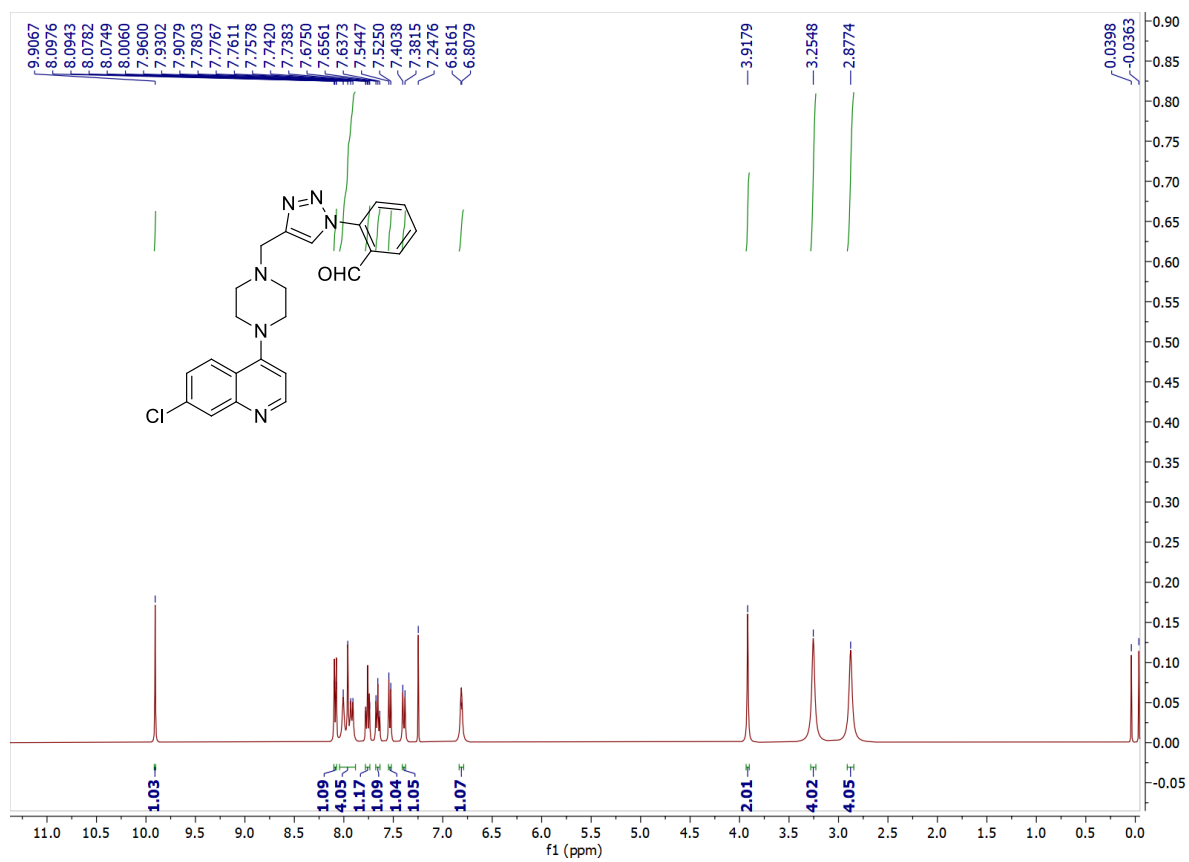


**Figure S13.**  $^{13}\text{C}$  NMR of 2-(4-((4-(7-chloroquinolin-4-yl)piperazin-1-yl)methyl)-1H-1,2,3-triazol-1-yl)benzaldehyde (**14**)

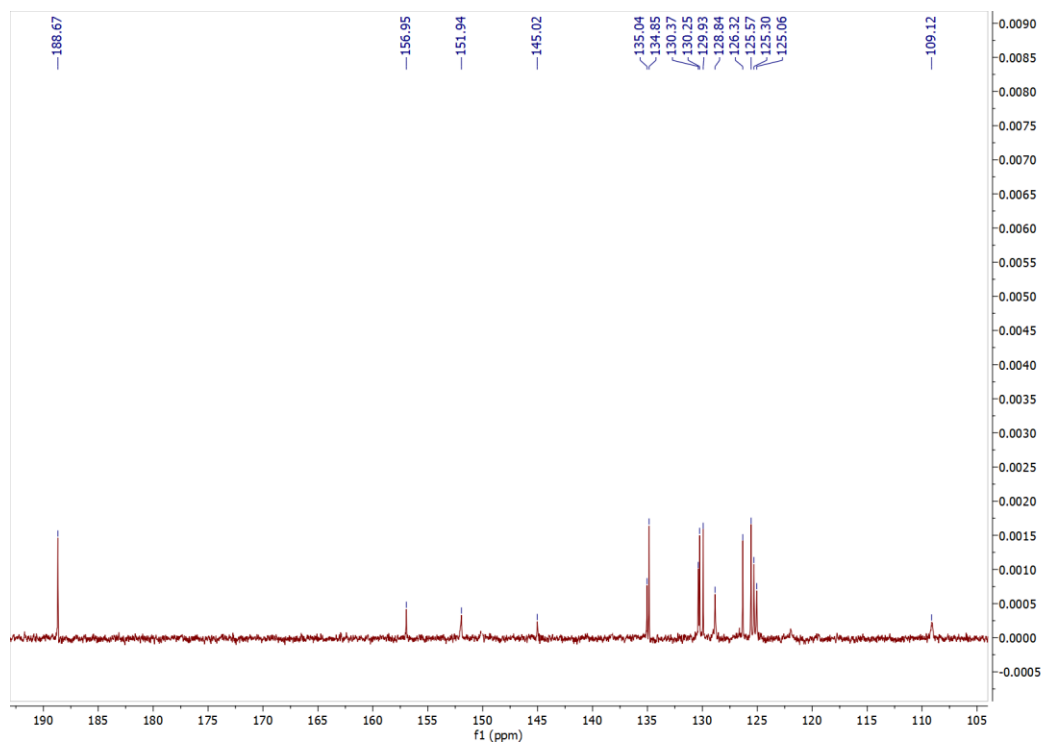
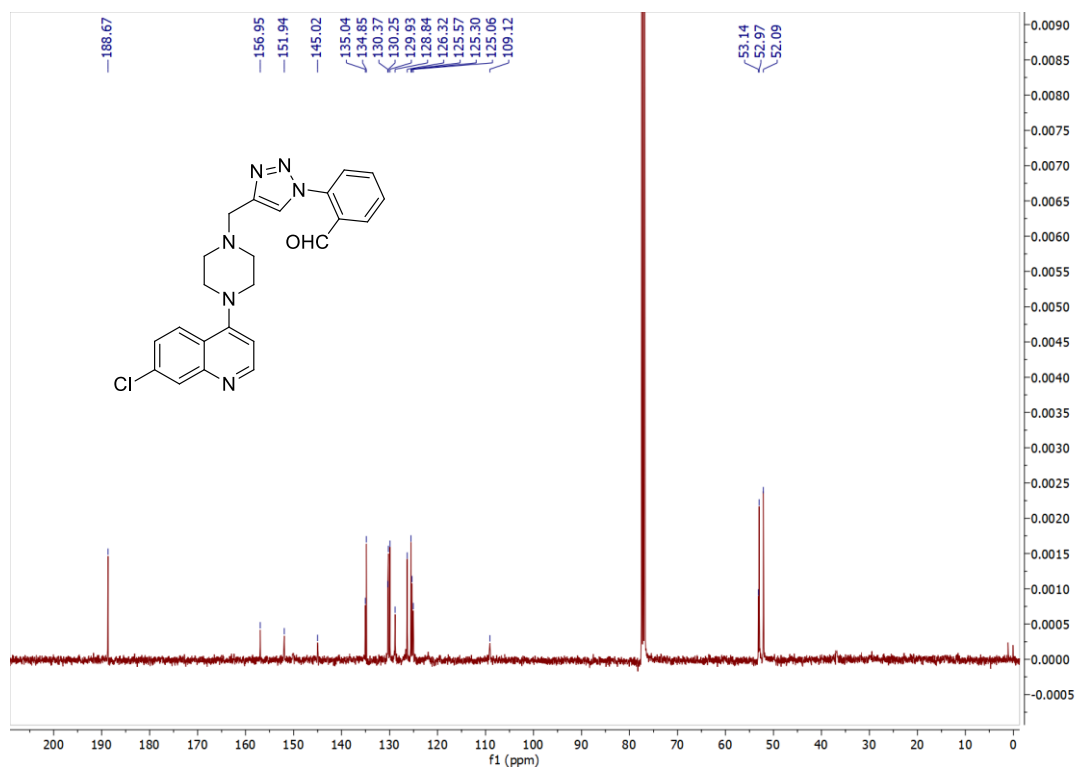


**Figure S14.**  $^1\text{H}$  NMR of (*E*)-*N'*-(4-((1-(7-chloroquinolin-4-yl)-1*H*-1,2,3-triazol-4-yl)methoxy)benzylidene)isonicotinohydrazide (**16a**)

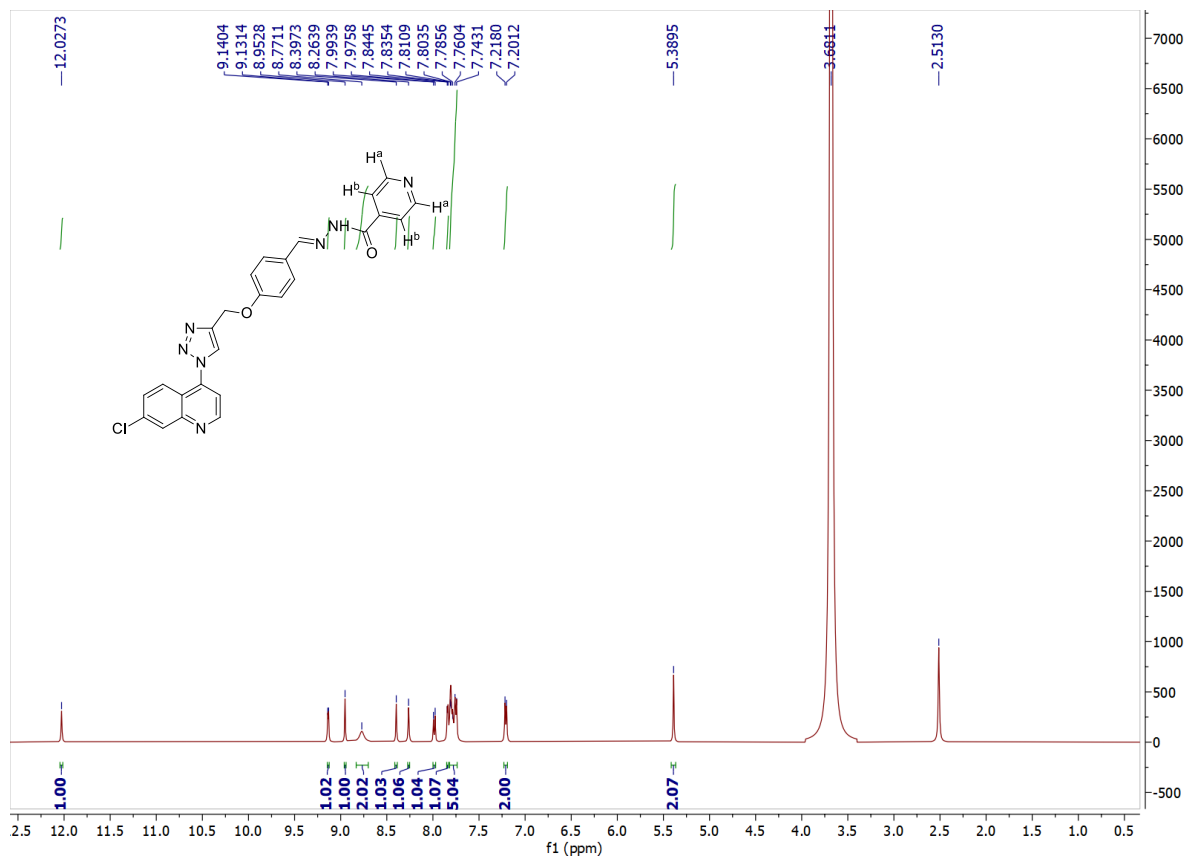


**Figure S15.**  $^{13}\text{C}$  NMR of (*E*)-*N'*-(4-((1-(7-chloroquinolin-4-yl)-1*H*-1,2,3-triazol-4-yl)methoxy)benzylidene)isonicotinohydrazide (**16a**)

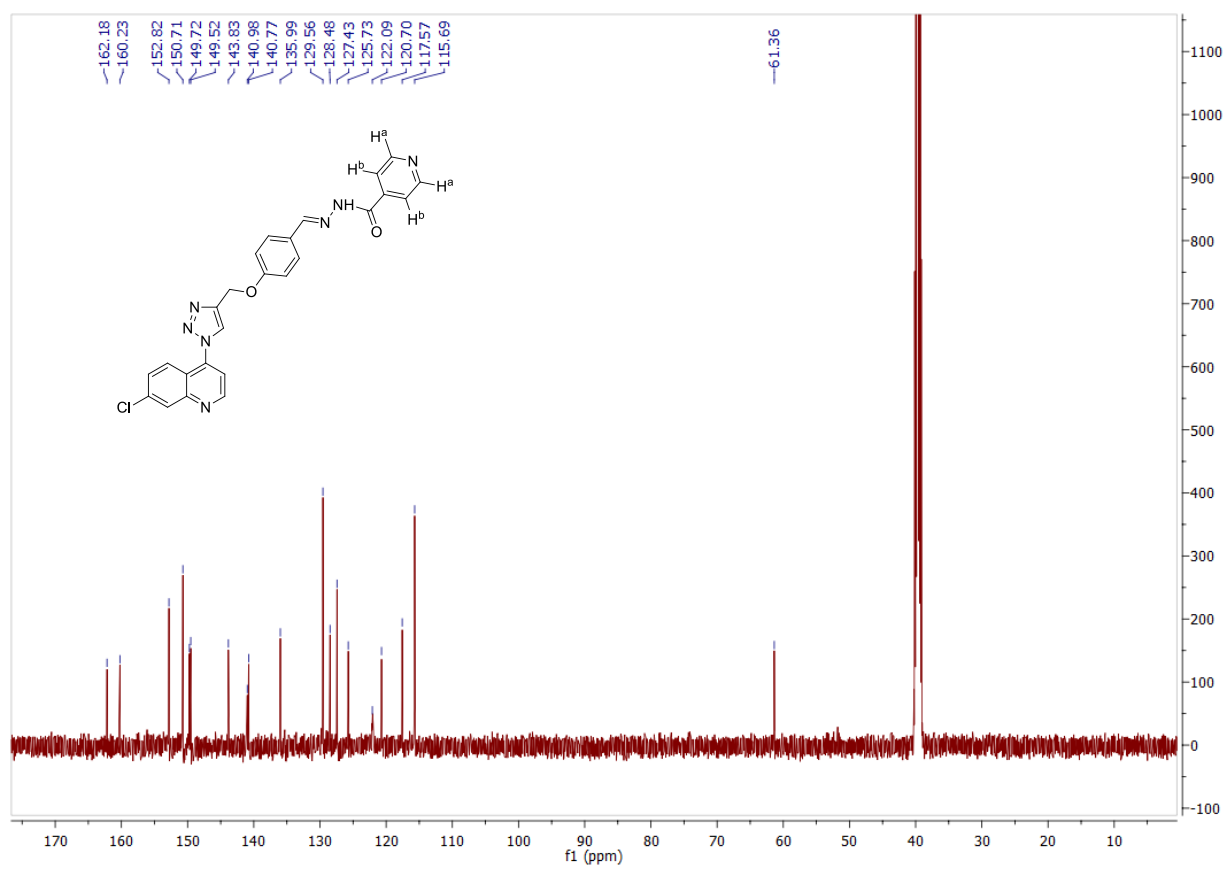


**Figure S16.**  $^1\text{H}$  NMR of (*E*)-*N'*-(2-(4-((4-(7-chloroquinolin-4-yl)piperazin-1-yl)methyl)-1*H*-1,2,3-triazol-1-yl)benzylidene)isonicotinohydrazide (**16g**)

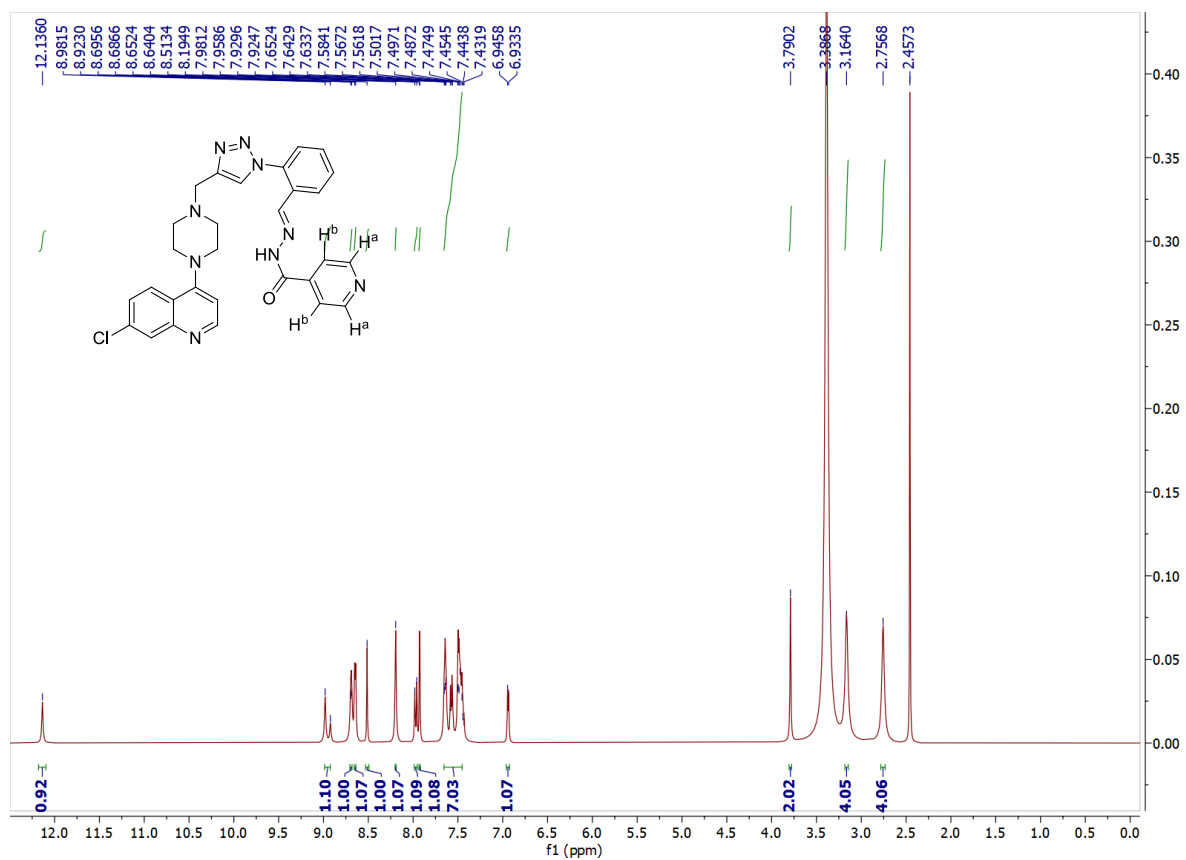


**Figure S17.**  $^{13}\text{C}$  NMR of (*E*)-*N'*-(2-(4-((7-chloroquinolin-4-yl)piperazin-1-yl)methyl)-1*H*-1,2,3-triazol-1-yl)benzylidene)isonicotinohydrazide (**16g**)

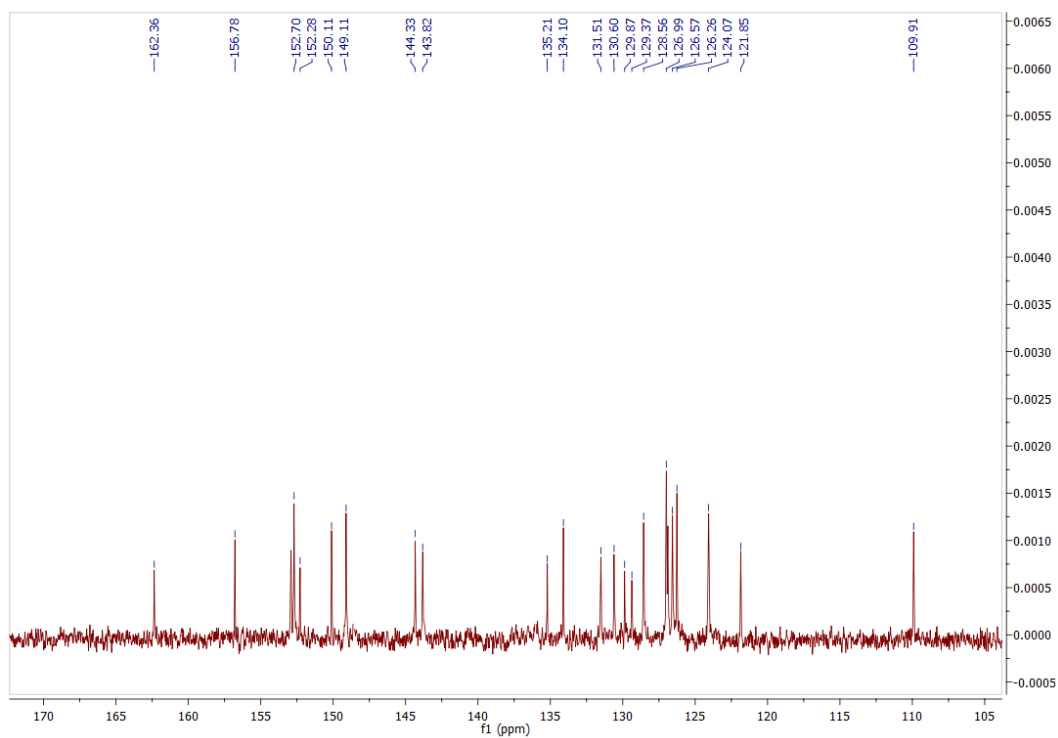
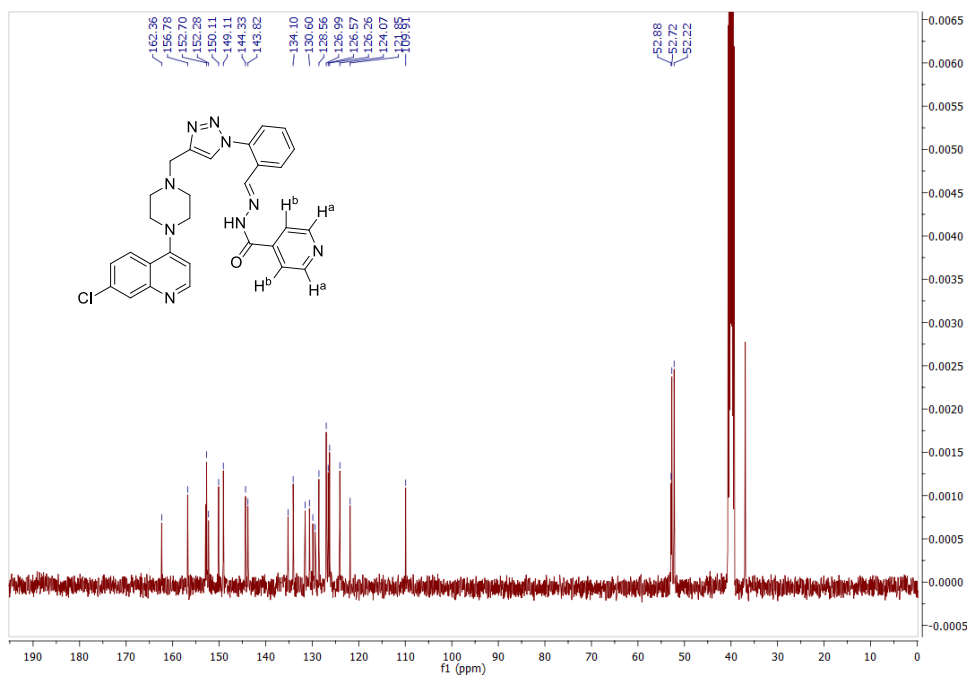


**Figure S18.**  $^1\text{H}$  NMR of (*E*)-*N'*-(4-((1-(7-chloroquinolin-4-yl)-1*H*-1,2,3-triazol-4-yl)methoxy)-3-methoxybenzylidene)nicotinohydrazide (**17b**)

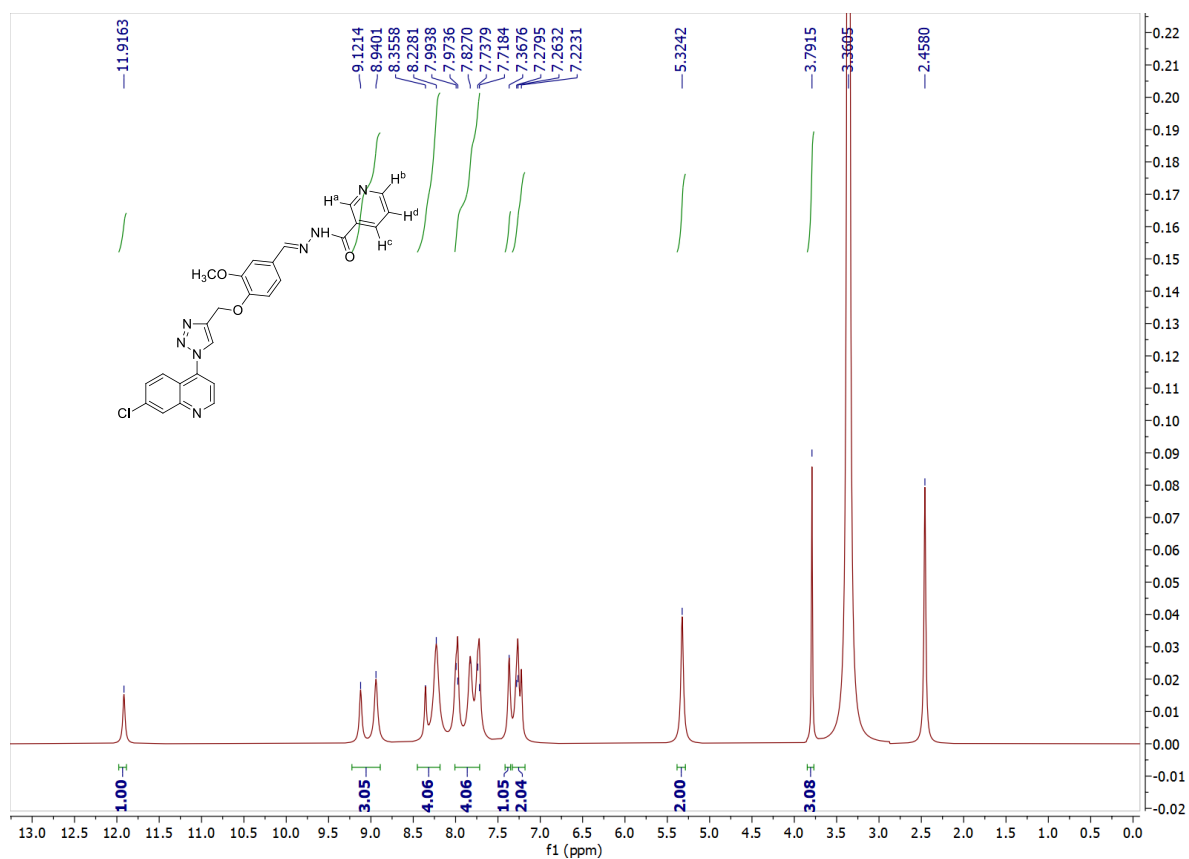


**Figure S19.**  $^{13}\text{C}$  NMR of (*E*)-*N'*-(4-((1-(7-chloroquinolin-4-yl)-1*H*-1,2,3-triazol-4-yl)methoxy)-3-methoxybenzylidene)nicotinohydrazide (**17b**)

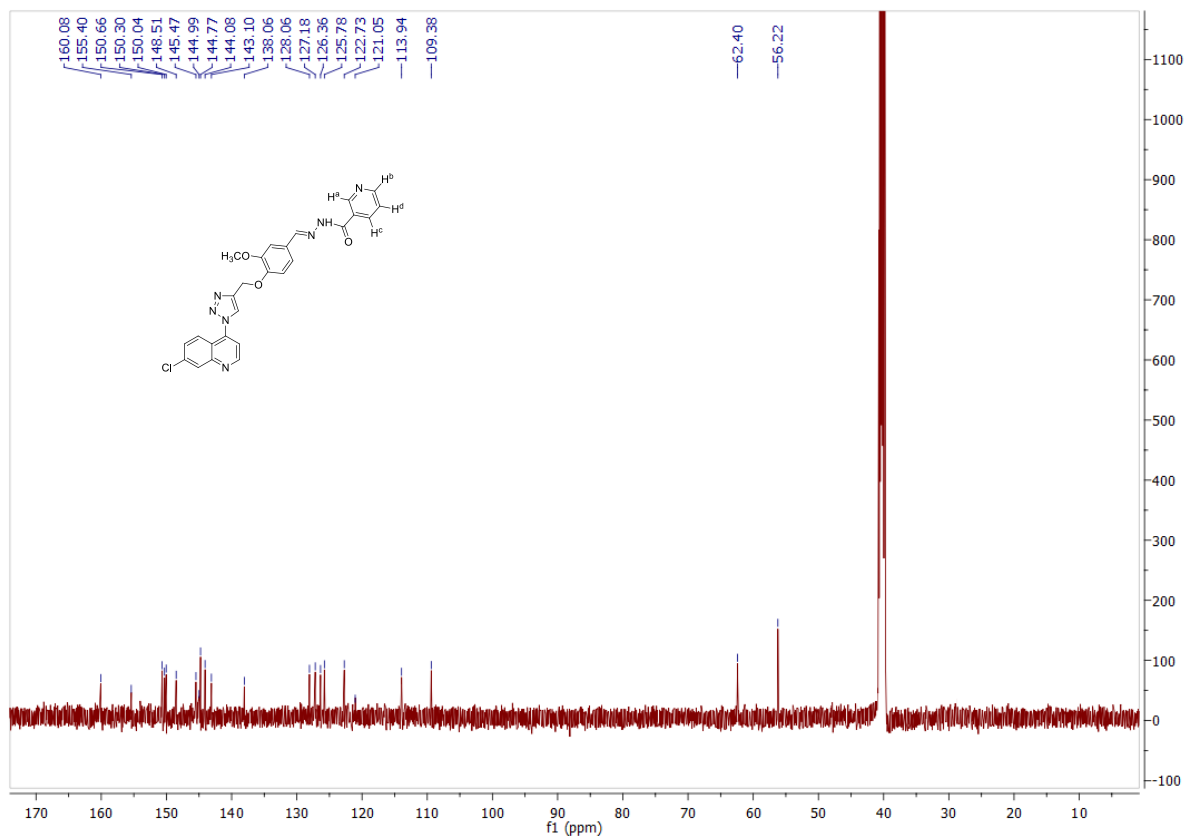




**Figure S20.**  $^1\text{H}$  NMR of (*E*)-*N'*-(4-((1-(7-chloroquinolin-4-yl)-1*H*-1,2,3-triazol-4-yl)methoxy)benzylidene)pyrazine-2-carbohydrazide (**18a**)

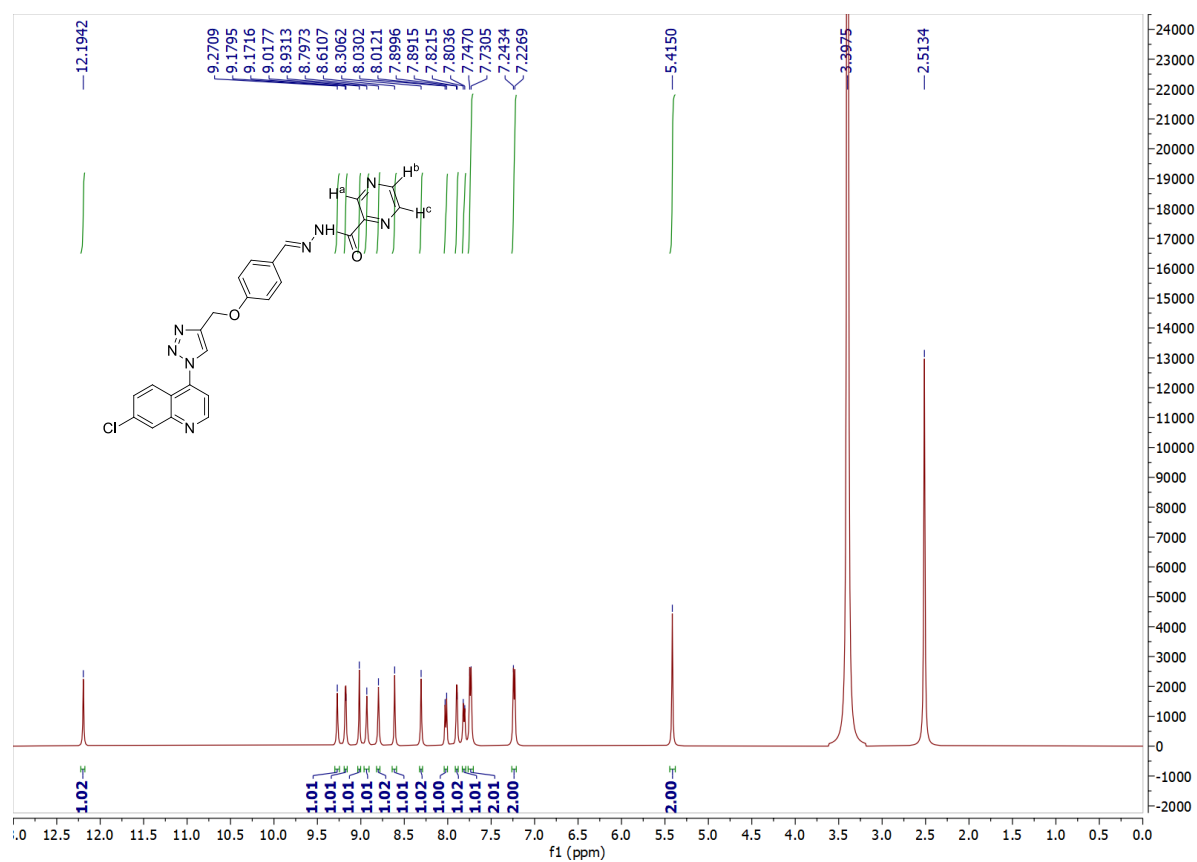


**Figure S21.**  $^{13}\text{C}$  NMR of (*E*)-*N'*-(4-((1-(7-chloroquinolin-4-yl)-1*H*-1,2,3-triazol-4-yl)methoxy)benzylidene)pyrazine-2-carbohydrazide (**18a**)

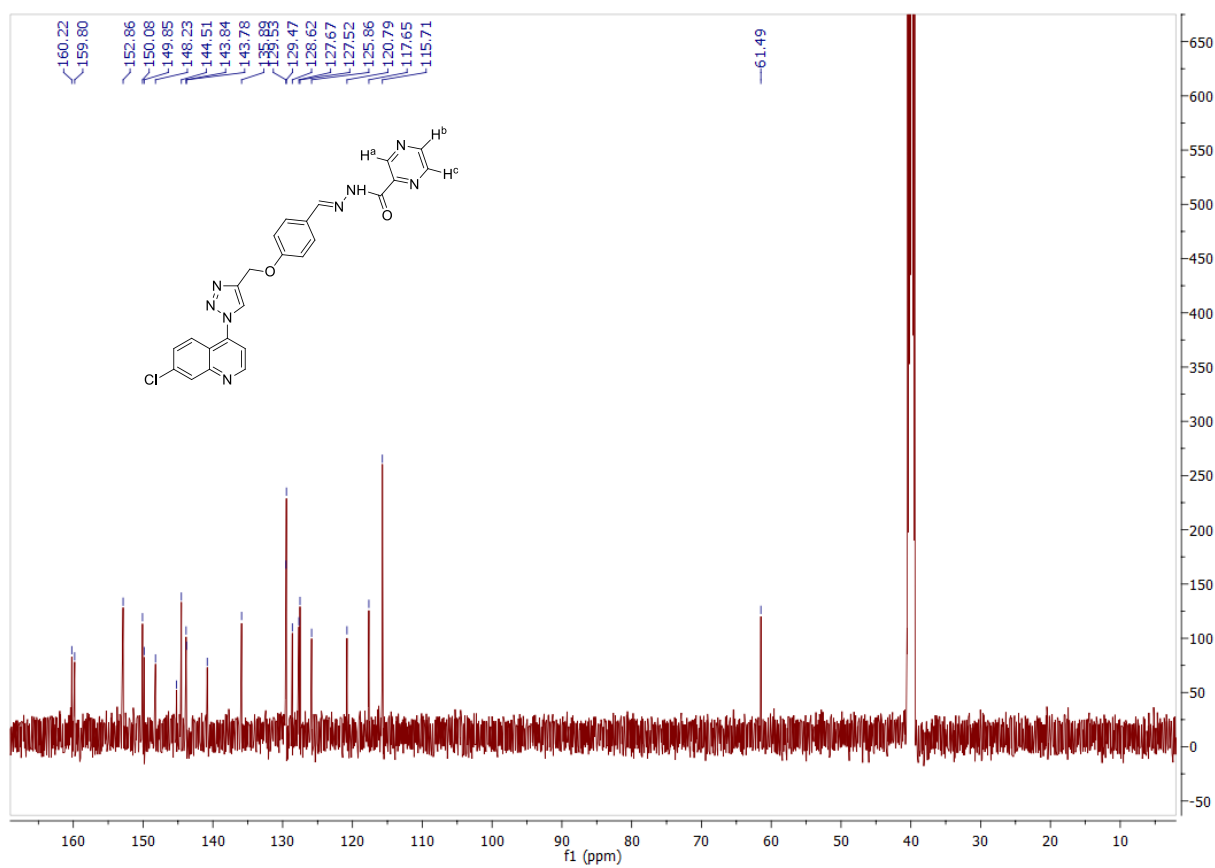


**Figure S22.**  $^1\text{H}$  NMR of (*E*)-*N'*-(4-((1-(7-chloroquinolin-4-yl)-1*H*-1,2,3-triazol-4-yl)methoxy)-3-methoxybenzylidene)pyrazine-2-carbohydrazide (**18b**)

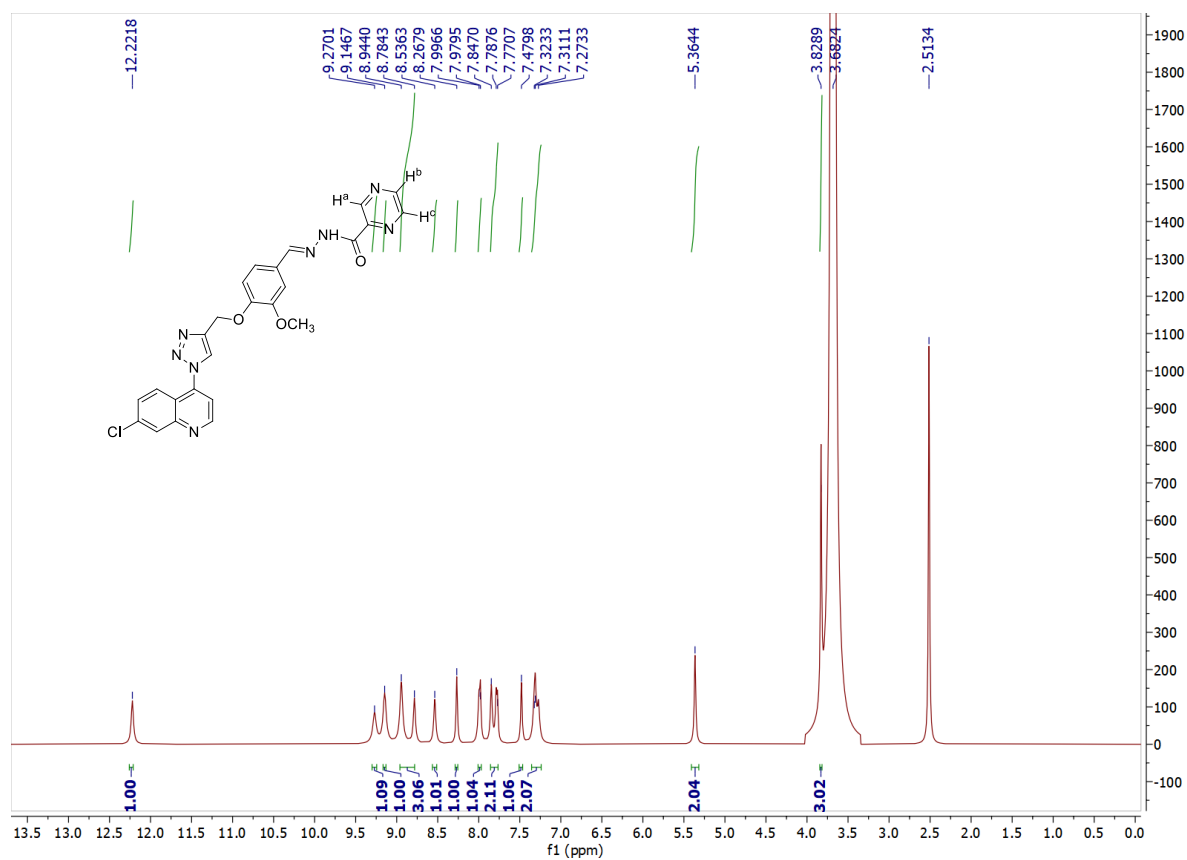


**Figure S23.**  $^{13}\text{C}$  NMR of (*E*)-*N'*-(4-((1-(7-chloroquinolin-4-yl)-1*H*-1,2,3-triazol-4-yl)methoxy)-3-methoxybenzylidene)pyrazine-2-carbohydrazide (**18b**)

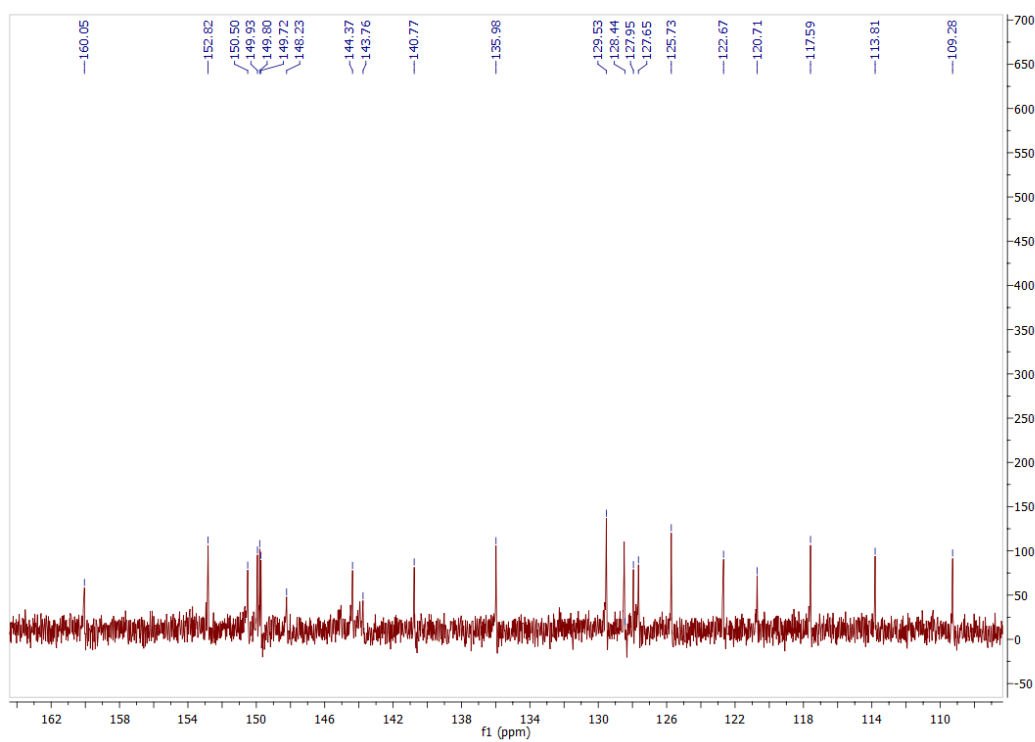
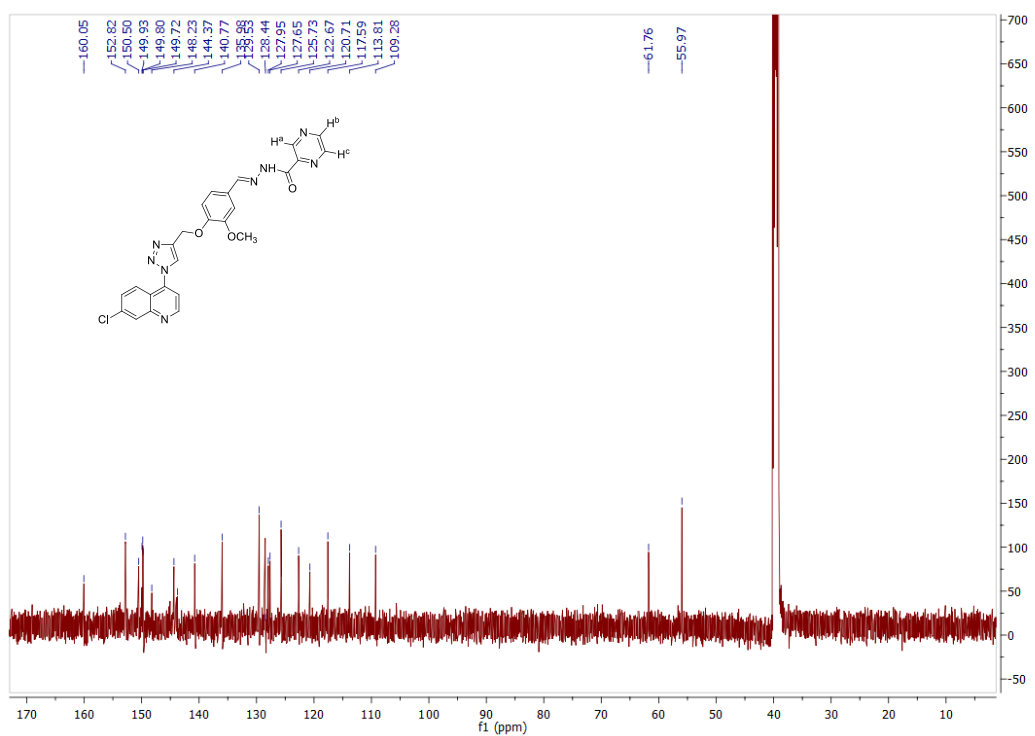


**Figure S24.**  $^1\text{H}$  NMR of (*E*)-*N'*-(4-((1-(2-((7-chloroquinolin-4-yl)amino)ethyl)-1*H*-1,2,3-triazol-4-yl)methoxy)benzylidene)pyrazine-2-carbohydrazide (**18c**)

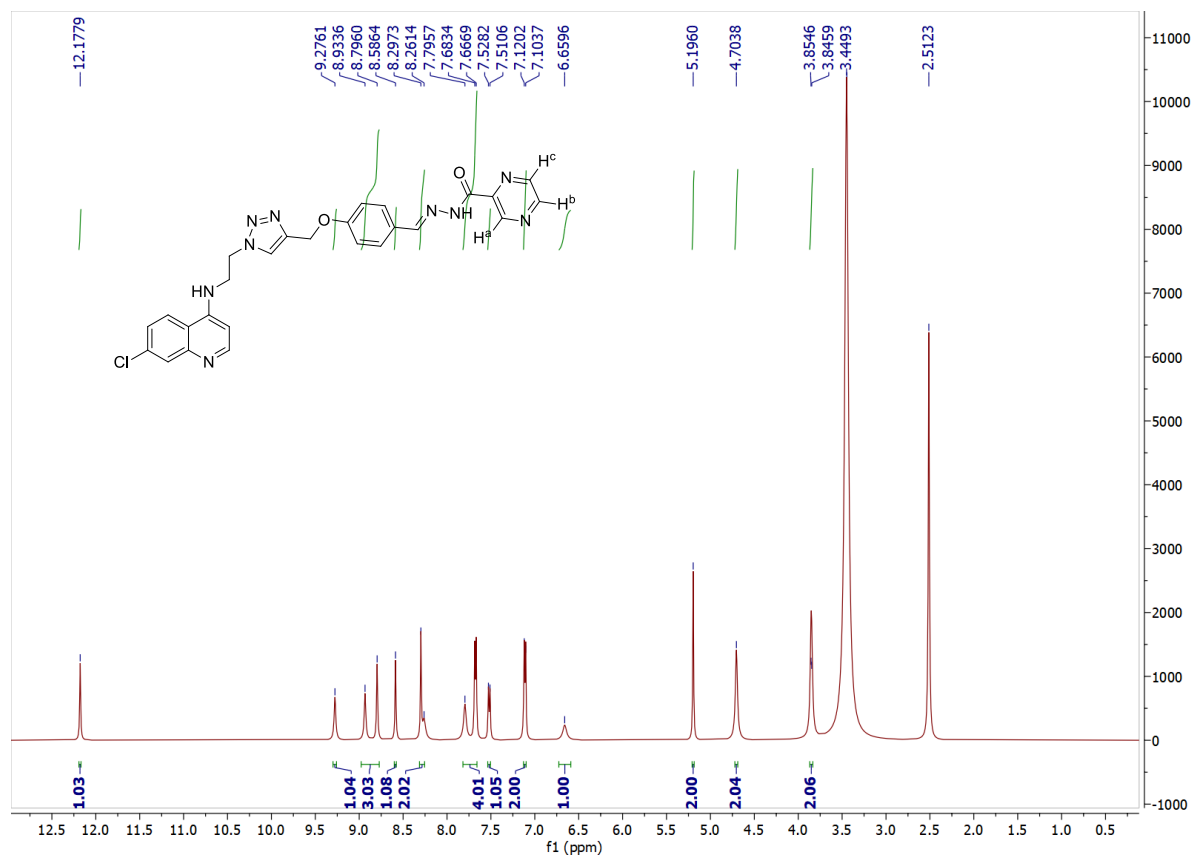


**Figure S25.**  $^{13}\text{C}$  NMR of (*E*)-*N'*-(4-((1-(2-((7-chloroquinolin-4-yl)amino)ethyl)-1*H*-1,2,3-triazol-4-yl)methoxy)benzylidene)pyrazine-2-carbohydrazide (**18c**)

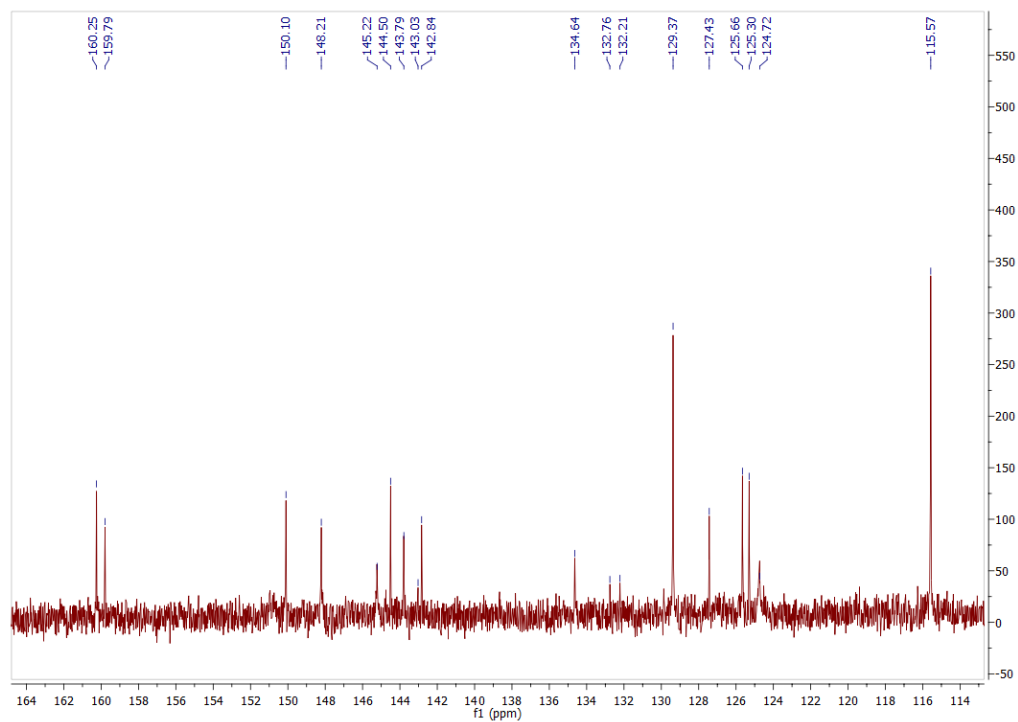
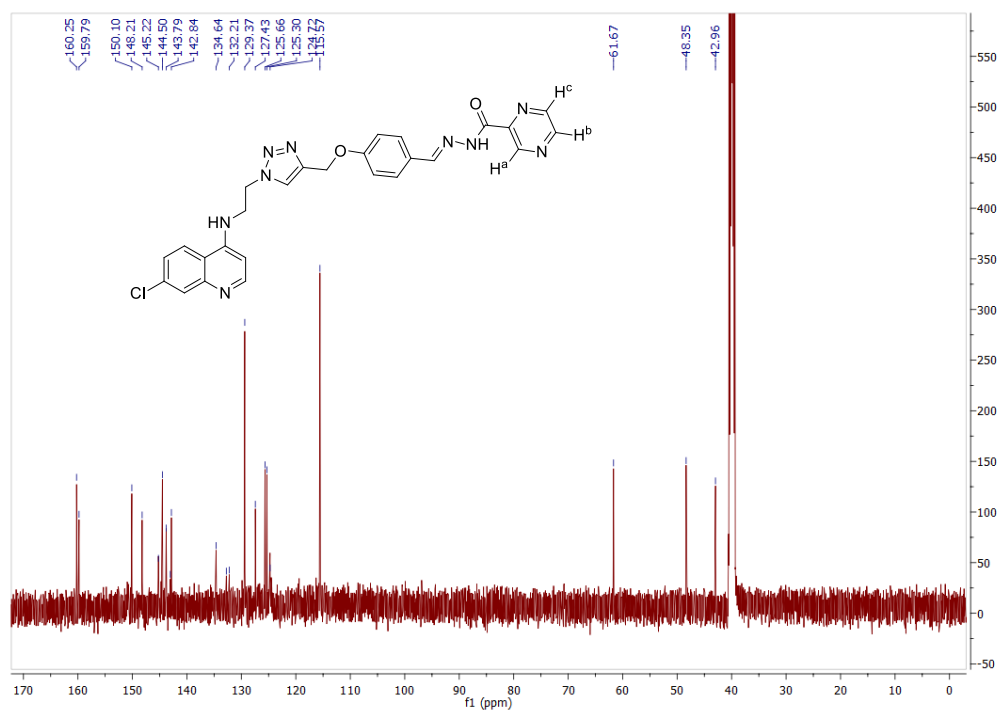


**Figure S26.**  $^1\text{H}$  NMR of (*E*)-*N*'-(4-((1-(3-((7-chloroquinolin-4-yl)amino)propyl)-1*H*-1,2,3-triazol-4-yl)methoxy)benzylidene)pyrazine-2-carbohydrazide (**18d**)

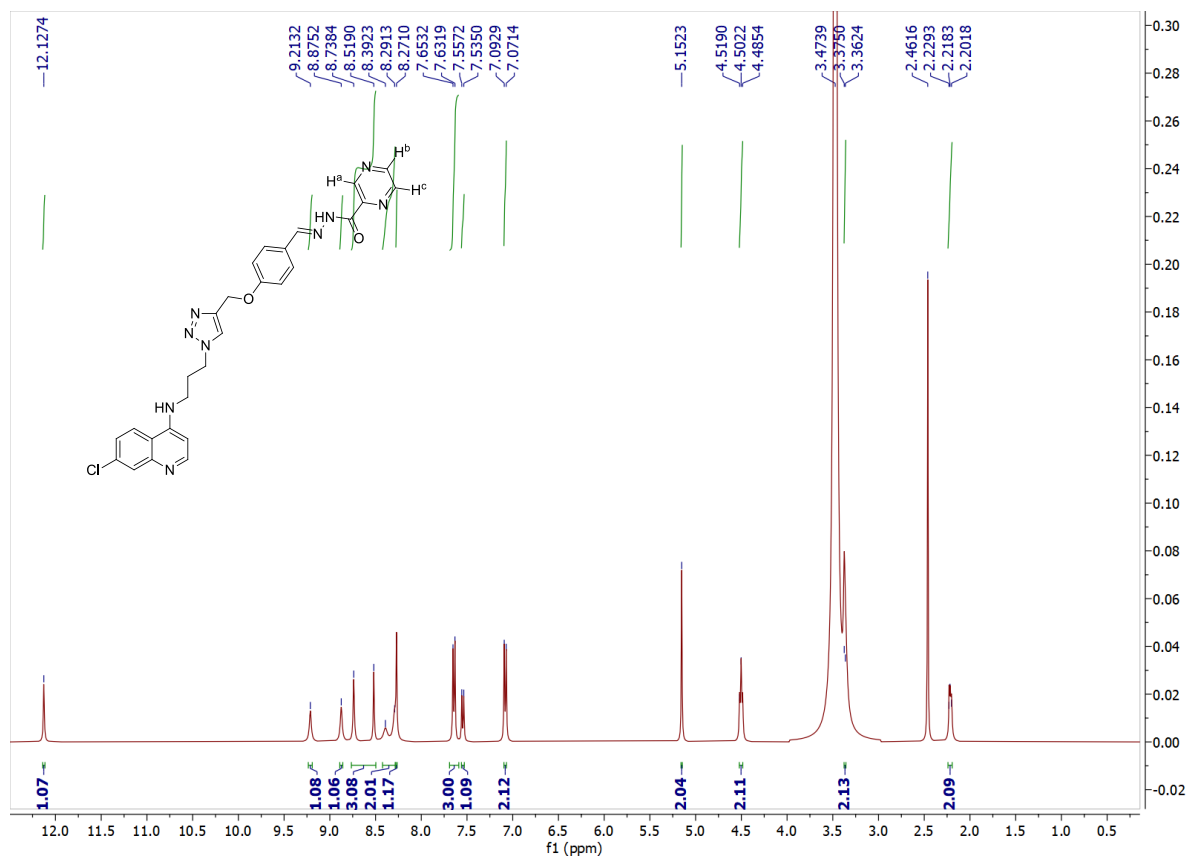


**Figure S27.**  $^{13}\text{C}$  NMR of (*E*)-*N'*-(4-((1-(3-((7-chloroquinolin-4-yl)amino)propyl)-1*H*-1,2,3-triazol-4-yl)methoxy)benzylidene)pyrazine-2-carbohydrazide (**18d**)

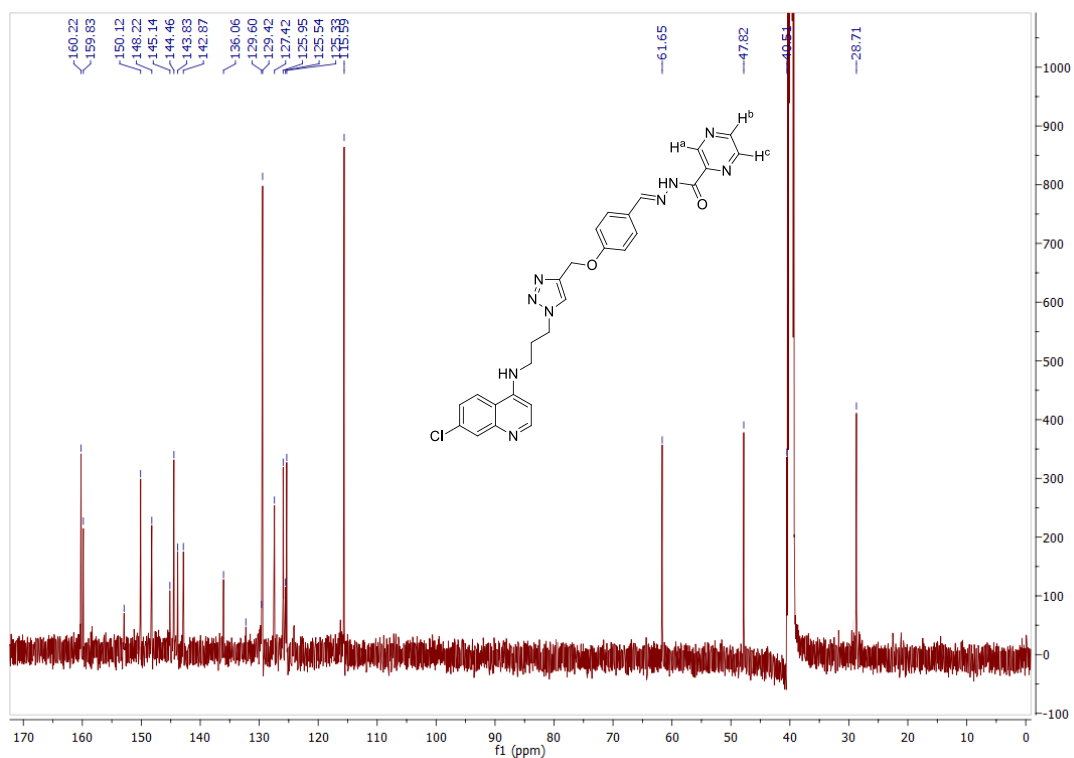


**Figure S28.** DEPT-135 spectrum of (*E*)-*N'*-(4-((1-(3-((7-chloroquinolin-4-yl)amino)propyl)-1*H*-1,2,3-triazol-4-yl)methoxy)benzylidene)pyrazine-2-carbohydrazide (**18d**)

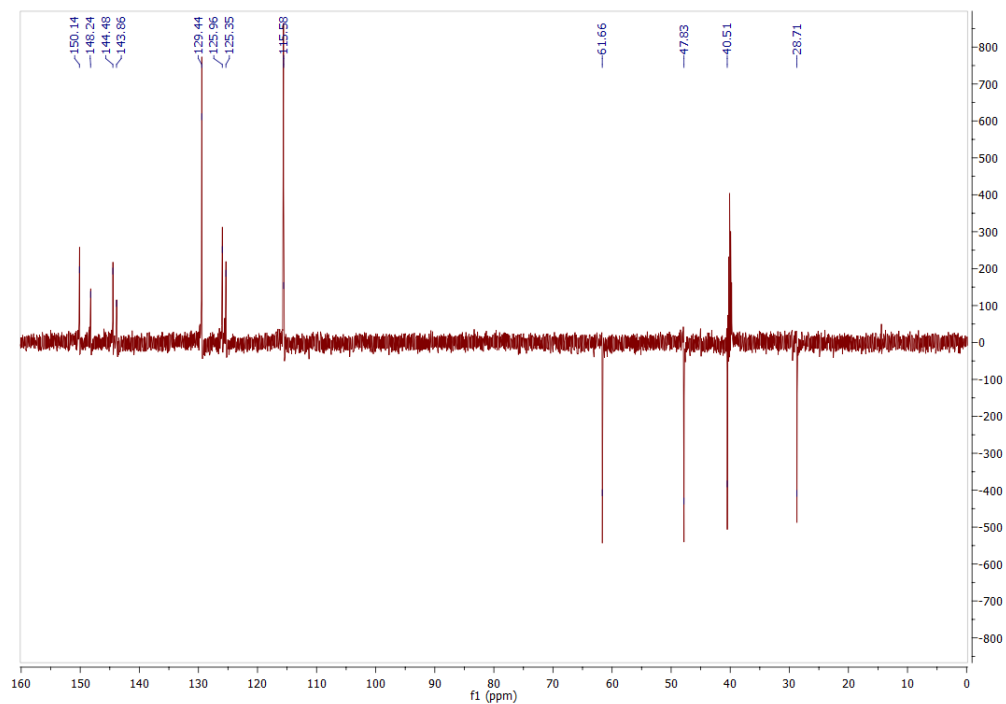




**Figure S29.**  $^1\text{H}$  NMR of (*E*)-*N'*-(4-((1-(3-((7-chloroquinolin-4-yl)amino)propyl)-1*H*-1,2,3-triazol-4-yl)methoxy)-3-methoxybenzylidene)pyrazine-2-carbohydrazide (**18f**)

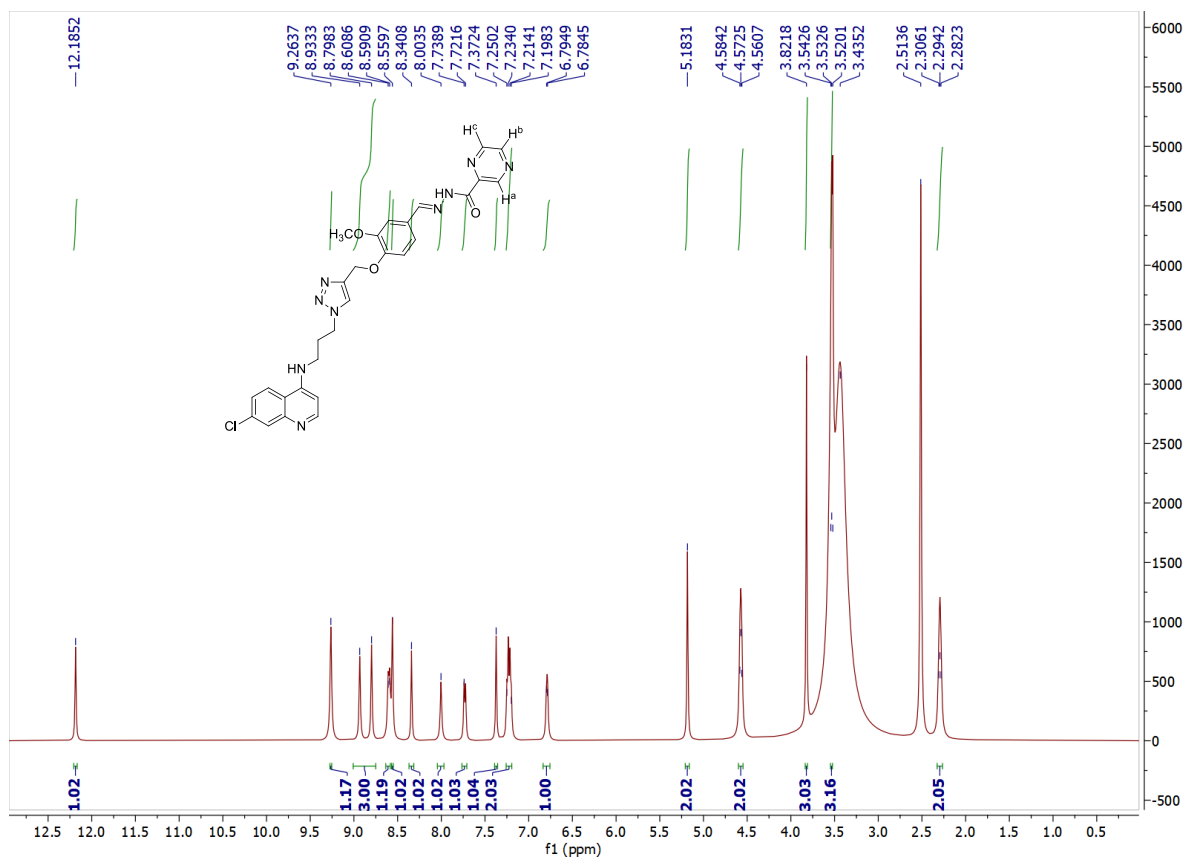
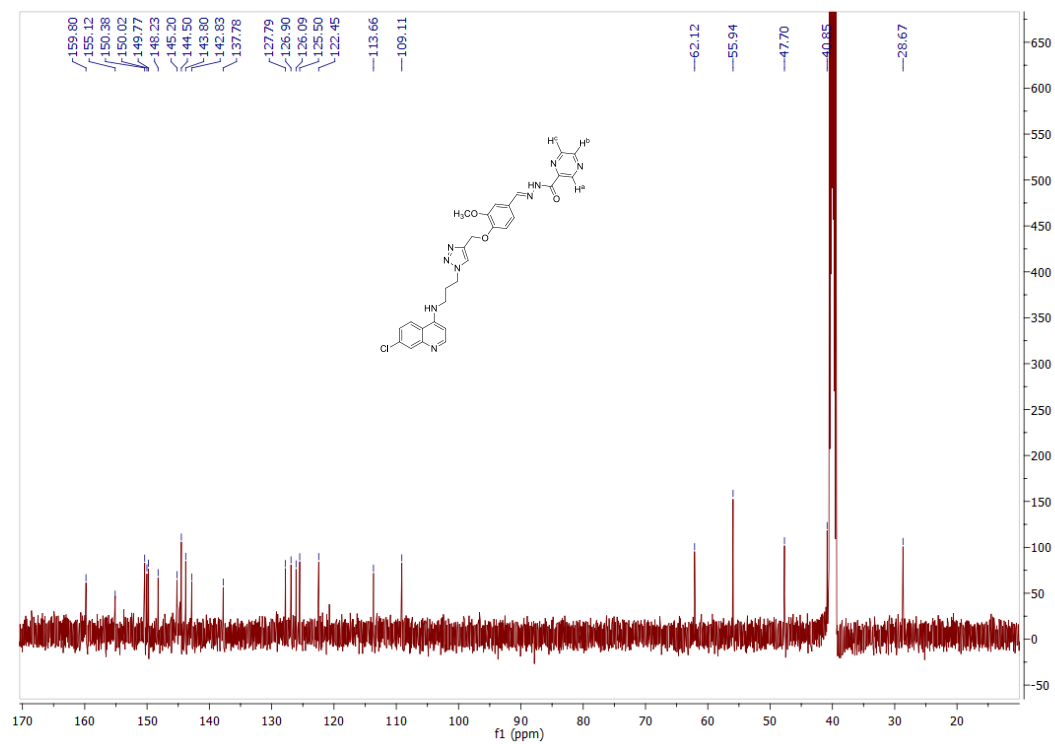


**Figure S30.**  $^{13}\text{C}$  NMR of (*E*)-*N'*-(4-((1-(3-((7-chloroquinolin-4-yl)amino)propyl)-1*H*-1,2,3-triazol-4-yl)methoxy)-3-methoxybenzylidene)pyrazine-2-carbohydrazide (**18f**)





**Article 2 : “Efficacy and mode of action of a direct inhibitor of *Mycobacterium abscessus* InhA”**

Matthéo Alcaraz, Françoise Roquet-Banères, Stephen Adonai Leon-Icaza, Jan Abendroth, Yves-Marie Boudehen, Céline Cougoule, Thomas E. Edwards, et Laurent Kremer. *ACS Infectious Diseases*, 2022, Vol 8, N° 10, Page 2171-2186, PMID : 36107992, DOI : 10.1021/acsinfecdis.2c00314

Le traitement actuel contre les infections à *M. abscessus* souffre d'une inefficacité alarmante, notamment chez les patients atteints de mucoviscidose, ce qui met en exergue le besoin urgent de proposer de nouvelles molécules. Nous supposons que la protéine InhA est une cible intéressante à explorer, néanmoins l'INH, et ses dérivés, sont inactifs contre *M. abscessus* en raison de l'incapacité de la catalase-péroxydase KatG<sub>MAB</sub> à convertir cette pro-drogue en un métabolite actif. Ainsi, l'objectif ici a été de valider InhA<sub>MAB</sub> en tant que cible médicamenteuse chez *M. abscessus* à travers l'étude de l'activité du composé NITD-916, une 4-hydroxy-2-pyridone contournant l'activation par KatG précédemment décrite chez *M. tuberculosis*.

Ces travaux ont démontré l'activité à faible concentration de NITD-916 sur les souches de référence ainsi qu'un large panel d'isolats cliniques des trois sous-espèces du complexe *M. abscessus*. De plus, cette molécule permet d'inhiber la croissance et l'infection macrophagique de *M. abscessus*, mais aussi de réduire la formation et la croissance de cordes intracellulaires, fondamentales dans la physiopathologie de ce pathogène. Notre collaboration avec l'équipe de Céline Cougoule (IPBS, Toulouse) a permis de montrer que NITD-916 réduit également la charge bactérienne (S ou R) au sein d'organoïdes des voies respiratoires pulmonaires dérivés de cellules de patients atteints de mucoviscidose.

D'un point de vue mécanistique, NITD-916 inhibe la synthèse *de novo* des acides mycoliques de manière InhA dépendante, lorsque des mutants résistants spontanés étaient mutés au sein du gène *inhA*. La structure cristallographique résolue grâce à l'équipe de Thomas Edwards (UCB, Washington, Etats-Unis) du complexe ternaire InhA:NADH:NITD-916 a permis de confirmer l'inhibition directe de l'énoyl-ACP réductase par ce composé.

Dans l'ensemble, ces résultats indiquent que le ciblage direct d'InhA<sub>MAB</sub> est intéressant à exploiter dans le développement de futurs antibactériens efficaces contre *M. abscessus*.

Efficacy and Mode of Action of a Direct Inhibitor of *Mycobacterium abscessus* InhA

Matthéo Alcaraz, Françoise Roquet-Banères, Stephen Adonai Leon-Icaza, Jan Abendroth, Yves-Marie Boudehen, Céline Cougoule, Thomas E. Edwards, and Laurent Kremer\*

Cite This: *ACS Infect. Dis.* 2022, 8, 2171–2186

Read Online

ACCESS |



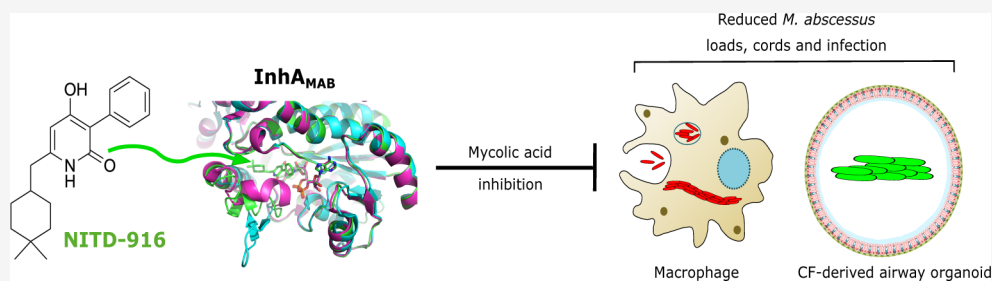
Metrics &amp; More



Article Recommendations



Supporting Information



**ABSTRACT:** There is an unmet medical need for effective treatments against *Mycobacterium abscessus* pulmonary infections, to which cystic fibrosis (CF) patients are particularly vulnerable. Recent studies showed that the antitubercular drug isoniazid is inactive against *M. abscessus* due to the incapacity of the catalase-peroxidase to convert the pro-drug into a reactive metabolite that inhibits the enoyl-ACP reductase InhA. To validate InhA<sub>MAB</sub> as a druggable target in *M. abscessus*, we assayed the activity of NITD-916, a 4-hydroxy-2-pyridone lead candidate initially described as a direct inhibitor of InhA that bypasses KatG bioactivation in *Mycobacterium tuberculosis*. The compound displayed low MIC values against rough and smooth clinical isolates in vitro and significantly reduced the bacterial burden inside human macrophages. Moreover, treatment with NITD-916 reduced the number and size of intracellular mycobacterial cords, regarded as markers of the severity of the infection. Importantly, NITD-916 significantly lowered the *M. abscessus* burden in CF-derived lung airway organoids. From a mechanistic perspective, NITD-916 abrogated de novo synthesis of mycolic acids and NITD-916-resistant spontaneous mutants harbored point mutations in InhA<sub>MAB</sub> at residue 96. That NITD-916 targets InhA<sub>MAB</sub> directly without activation requirements was confirmed genetically and by resolving the crystal structure of the protein in complex with NADH and NITD-916. These findings collectively indicate that InhA<sub>MAB</sub> is an attractive target to be exploited for future chemotherapeutic developments against this difficult-to-treat mycobacterium and highlight the potential of NITD-916 derivatives for further evaluation in preclinical settings.

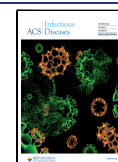
**KEYWORDS:** *Mycobacterium abscessus*, NITD-916, macrophage, organoid, InhA, mycolic acid

*M. abscessus* is a rapidly growing nontuberculous mycobacterium (NTM) of rising clinical significance and the cause of difficult-to-cure pulmonary diseases, particularly in patients with cystic fibrosis (CF).<sup>1</sup> In these patients, infection with *M. abscessus* is often associated with a more rapid decline in lung function, and the presence of *M. abscessus* can be deleterious for subsequent lung transplantation.<sup>2–4</sup> The *M. abscessus* complex comprises three subspecies exhibiting different clinical outcomes and drug susceptible profiles to antibiotics:<sup>5</sup> *M. abscessus* subsp. *abscessus* (designated hereafter *M. abscessus*), *M. abscessus* subsp. *bolletii* (designated hereafter *M. bolletii*), and *M. abscessus* subsp. *massiliense* (designated hereafter *M. massiliense*).<sup>6</sup> All three subspecies can display either a smooth (S) or a rough (R) morphotype as a consequence of the presence or absence, respectively, of surface-associated glycopeptidolipids (GPL).<sup>7–10</sup> These morphological changes are linked to major phenotypic differences, including sliding motility, biofilm formation,<sup>8,9,11</sup> or produc-

tion of large bacterial cords.<sup>11,12</sup> S and R variants can be viewed as two representative forms of the same isolate, which can coexist in the patient and evolve differently in response to the host immune pressure. They can also display specific pathophysiological characteristics;<sup>10</sup> S variants are generally less virulent than their corresponding R variants,<sup>11,13,14</sup> the latter being more frequently associated with severe pulmonary diseases in CF patients.<sup>2,4</sup> In addition, different susceptibility profiles to drugs have been reported between S and R

Received: June 14, 2022

Published: September 15, 2022



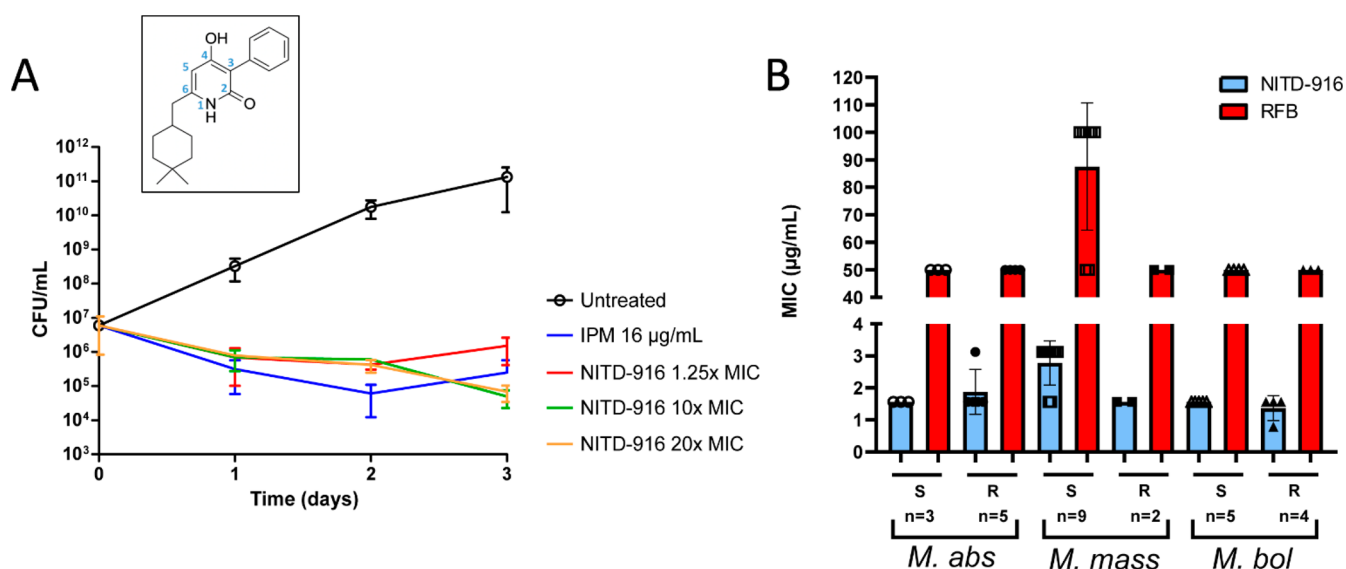


**Figure 1.** In vitro activity of NITD-916 against *M. abscessus*. (A) Cultures of *M. abscessus* CIP104536<sup>T</sup> (S) were exposed to either 1.95, 15.6, 31.2  $\mu\text{g/mL}$  NITD-916 (corresponding to 1.25 $\times$ , 10 $\times$ , and 20 $\times$  MIC) or 16  $\mu\text{g/mL}$  imipenem (IPM) in CaMHB at 30  $^{\circ}\text{C}$ . At various time points, bacteria were plated on LB agar and incubated at 37  $^{\circ}\text{C}$  for 4 days prior to CFU counting. Results are expressed as the mean of 2 independent experiments in triplicates  $\pm$  SD. Inset: structure of NITD-916. (B) MIC (in  $\mu\text{g/mL}$ ) of NITD-916 and RFB against *M. abscessus* complex clinical isolates. MIC values were determined in CaMBH for *M. abscessus* subsp. *abscessus* ( $n = 8$ ), *M. abscessus* subsp. *massiliense* ( $n = 11$ ), and *M. abscessus* subsp. *bolletii* ( $n = 9$ ). Data are plotted as mean values  $\pm$  SD. S refers to smooth strains; R refers to rough strains.

variants,<sup>15,16</sup> thus warranting the need for evaluating compounds/drug regimens against both variants.

Due to intrinsic resistance to a wide panel of antimicrobials, including most antitubercular drugs, treatment of *M. abscessus* lung disease remains extremely challenging.<sup>17–20</sup> Multidrug regimens are administered for months to years, generally comprising an oral macrolide (clarithromycin or azithromycin) and intravenously administered aminoglycosides (amikacin) and  $\beta$ -lactams (imipenem or ceftazidime).<sup>21–23</sup> Other drugs, such as tigecycline or clofazimine, can be added to strengthen the regimen, mostly in response to toxic side effects or poor clinical response.<sup>24</sup> However, despite intensive chemotherapy, treatment success rates typically remain very low in the case of macrolide resistance (25–40%), which occurs in at least 40–60% of clinical isolates.<sup>25</sup> Thus, given the unsatisfactory performances of the current regimens, more effective drugs are required. Unfortunately, de novo drug discovery efforts to identify new chemical scaffolds are impeded by low hit rates,<sup>26,27</sup> explaining why the *M. abscessus* drug pipeline focuses mainly on repurposing and reformulation of approved drugs.

In addition to mutations in genes encoding the drug targets conducting to acquired drug resistance,<sup>7,26</sup> the widespread resistome of *M. abscessus* results also from the low permeability properties of the cell envelope, the expression of a wide range of drug-modifying enzymes, the induction of efflux pumps and the absence or dysfunctional drug-activating enzymes.<sup>17,20,28</sup> The latter, for instance, explains why isoniazid (INH) is totally inactive against *M. abscessus*. Indeed, it has been recently shown that the catalase-peroxidase KatG<sub>MAB</sub> is unable to transform INH into an active metabolite.<sup>29</sup> INH, the most efficient first-line anti-TB drug against actively replicating *M. tuberculosis*, remains the first choice for prophylaxis and treatment. Its biotransformation requires the catalase-peroxidase KatG<sup>30,31</sup> to generate an isonicotinoyl radical that reacts with NAD<sup>+</sup> to produce an INH-NAD adduct.<sup>32,33</sup> This adduct blocks the enoyl-ACP reductase (InhA) of the type II fatty acid synthase (FAS-II),<sup>34–37</sup> leading to the arrest of mycolic acid

biosynthesis. Mycolic acids are essential and unique long-chain (C<sub>70</sub>–C<sub>90</sub>)  $\alpha$ -alkyl,  $\beta$ -hydroxy fatty acids,<sup>35,38</sup> and their inhibition ultimately results in mycobacterial cell death.<sup>39</sup> However, while being a validated drug target in *M. tuberculosis*, it remains to be established whether InhA represents an attractive target for future drug developments against *M. abscessus*.

To fill this gap, this study was undertaken to test the hypothesis whether NITD-916, a direct inhibitor of InhA that bypasses the KatG bioactivation process,<sup>40</sup> offers potential for future chemotherapeutic developments against *M. abscessus*. NITD-916 is a 4-hydroxy-2-pyridone lead candidate previously identified in a phenotypic screen against *M. tuberculosis* that exerts bactericidal activity against common INH-resistant TB clinical isolates. Herein, we aimed at assessing the activity of NITD-916 against *M. abscessus* S and R strains in vitro, in macrophages as well as in CF lung airway organoids and report the mechanism of action of the inhibitor in *M. abscessus*.

## RESULTS

***M. abscessus* Strains Are Susceptible to NITD-916 Treatment in Vitro.** To address whether InhA inhibitors bypassing KatG bioactivation can offer potential chemotherapeutic options against *M. abscessus*, we first screened the literature for commercially available direct InhA inhibitors, previously validated against *M. tuberculosis* and for which in vitro data and efficacy in mice have been reported. This led to the 4-hydroxy-2-pyridone lead compound NITD-916.<sup>40</sup> Initial experiments revealed that the *M. abscessus* CIP104536<sup>T</sup> S reference strain was particularly susceptible to NITD-916 in CaMHB (MIC = 1.56  $\mu\text{g/mL}$  which is 5  $\mu\text{M}$ ). However, as shown previously for other compounds,<sup>41</sup> the MIC was greatly dependent on the medium, with values of 0.195  $\mu\text{g/mL}$  and 6.25  $\mu\text{g/mL}$  in Sauton's medium and Middlebrook 7H9, respectively (Table S1). MICs in an artificial sputum medium

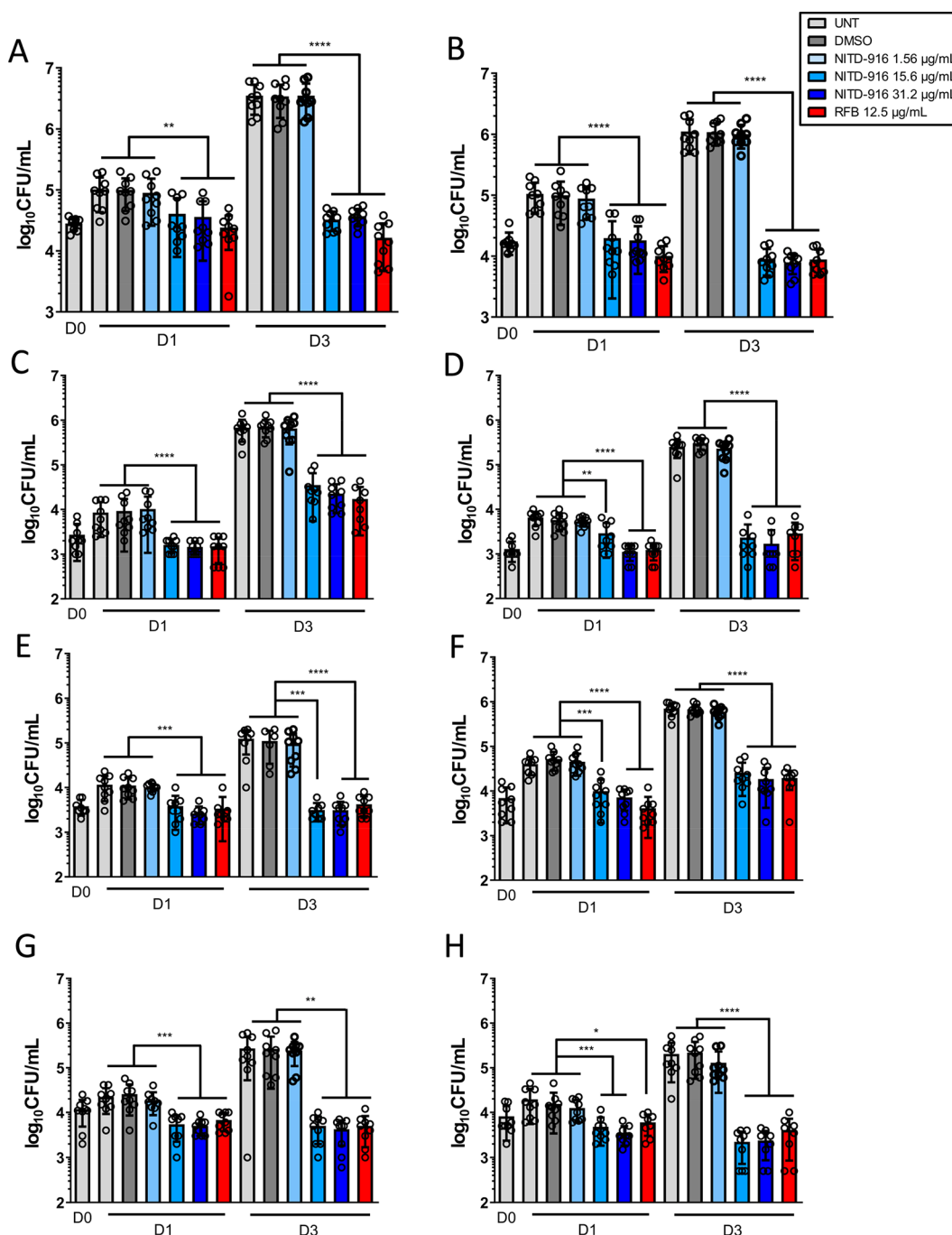


**Figure 2.** Intracellular activity of NITD-916 on *M. abscessus* complex-infected THP-1 cells. Macrophages were infected with *M. abscessus* reference strains and clinical isolates (MOI of 2:1) for 4 h prior to treatment with 250  $\mu$ g/mL AMK for 2 h to kill extracellular bacteria. Cells were then exposed to either NITD-916 or to RFB at the indicated concentrations. Untreated (UNT) or DMSO-exposed cells were included as controls. CFU were determined at 0, 1, and 3 days postinfection. The various strains tested and morphotypes are as follows: (A) *M. abscessus* CIP104536<sup>T</sup> (S); (B) *M. abscessus* CIP104536<sup>T</sup> (R); (C) *M. abscessus* 2069 (S); (D) *M. abscessus* 2524 (R); (E) *M. massiliense* 179 (R); (F) *M. massiliense* 120 (S); (G) *M. bolletii* 112 (R); (H) *M. bolletii* 108 (R). Data of 3 independent experiments in triplicates were analyzed with a Mann–Whitney *t* test. \* $P \leq 0.05$ ; \*\* $P \leq 0.01$ ; \*\*\* $P \leq 0.001$ ; \*\*\*\* $P \leq 0.0001$ .

(ASM) containing components of the CF sputum<sup>42</sup> were comparable to those obtained in CaMHB.

To determine the effect of the compound in broth culture, exponentially growing *M. abscessus* was exposed to increasing concentrations of NITD-916, corresponding to 1.25 $\times$ , 10 $\times$ , and 20 $\times$  MIC. This resulted in a noticeable growth inhibition (Figure 1A). However, the number of colony-forming units (CFU) remained relatively stable at the lowest concentration

tested during the 3 days of treatment and comparable to those in the inoculum, suggesting a bacteriostatic effect. In addition, the killing effect was not concentration-dependent, at least during the first 2 days of treatment. An additional 1-Log drop was observed after 3 days with 10 $\times$  or 20 $\times$  MIC. At these concentrations, NITD-916 resulted in a growth inhibitory effect comparable to the one of imipenem (IPM) used at the MIC (16  $\mu$ g/mL), a known  $\beta$ -lactam antibiotic active against



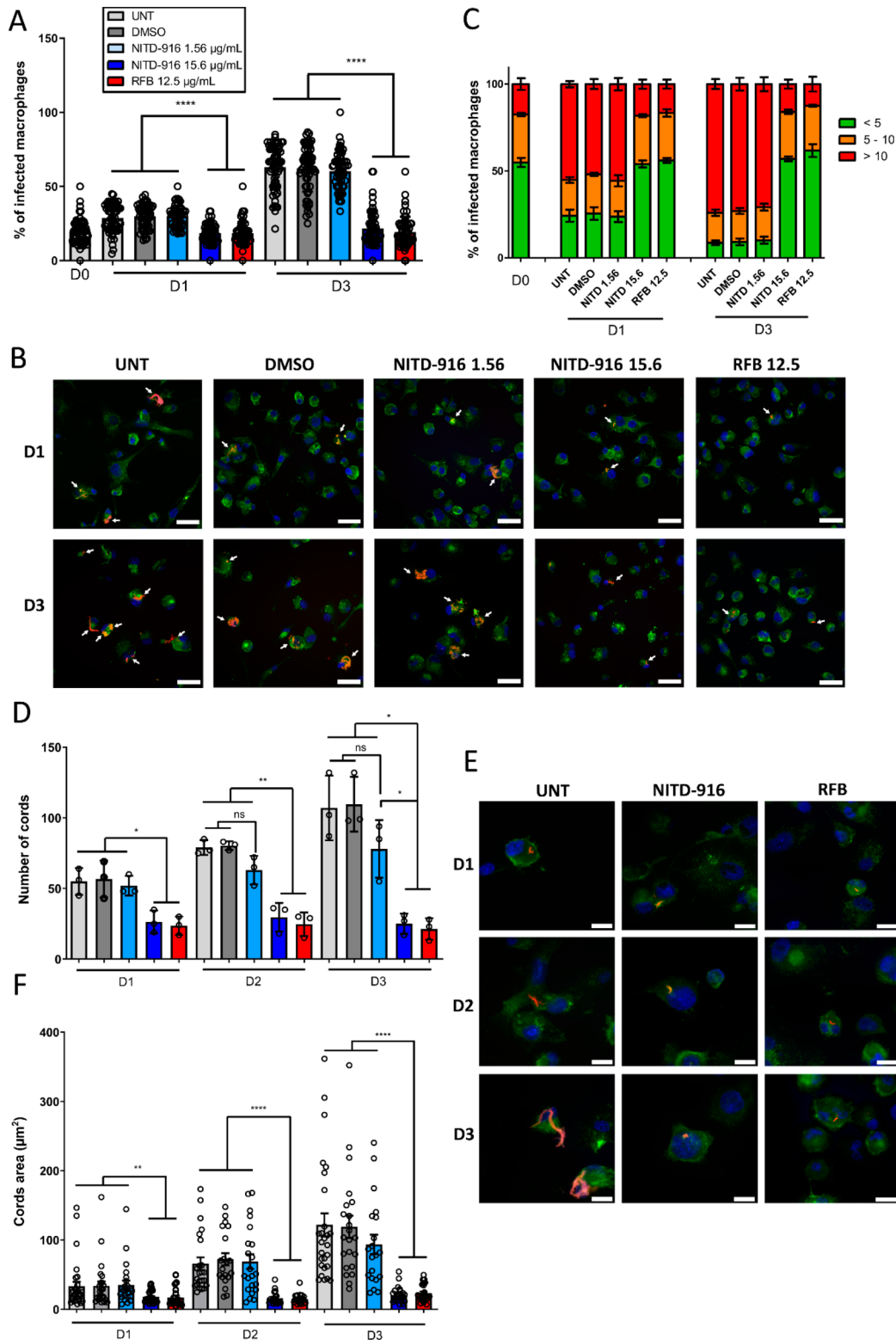


**Figure 3.** Effect of NITD-916 treatment on intracellular *M. abscessus* loads and cording. (A) Percentage of infected THP-1 macrophages at 0, 1, and 3 days postinfection with *M. abscessus* CIP104536<sup>T</sup> (R) (MOI of 2:1) in the absence (UNT) of antibiotics or presence of NITD-916 (1.56  $\mu\text{g}/\text{mL}$  and 15.6  $\mu\text{g}/\text{mL}$ ) or RFB (12.5  $\mu\text{g}/\text{mL}$ ). DMSO-exposed cells were included as controls. Results are expressed as mean values  $\pm$  SD for three independent experiments with 30 fields per condition. Data were analyzed using the *t* test. \*\*\*\* $P \leq 0.0001$ . (B) Representative immunofluorescent fields were taken at 1 and 3 days postinfection showing macrophages infected with *M. abscessus* CIP104536<sup>T</sup> (R) expressing TdTomato (red) in the absence of antibiotics (UNT) or in the presence of NITD-916 (1.56  $\mu\text{g}/\text{mL}$  and 15.6  $\mu\text{g}/\text{mL}$ ) or RFB (12.5  $\mu\text{g}/\text{mL}$ ). DMSO-exposed cells were included as controls. The surface and the endolysosomal system of the macrophages were detected using anti-CD63 antibodies (green). The nuclei were stained with DAPI (blue). White arrows indicate individual or mycobacterial aggregates. Scale bar, 50  $\mu\text{m}$ . (C) Percentage of macrophages categories infected with different number of bacilli (<5 bacilli/cell, 5–10 bacilli/cell, >10 bacilli/cell). The categories were counted at 0, 1, and 3 days postinfection in the absence of antibiotics or in the presence of NITD-916 (1.56  $\mu\text{g}/\text{mL}$  and 15.6  $\mu\text{g}/\text{mL}$ ) or RFB (12.5  $\mu\text{g}/\text{mL}$ ). Untreated



Figure 3. continued

(UNT) or DMSO-exposed cells were included as controls. Data are mean values  $\pm$  SD for three independent experiments performed in triplicates. (D) Total number of intracellular cords displayed in 30 fields at 1, 2, and 3 days postinfection. Results are expressed as mean values  $\pm$  SD for three independent experiments. Data were analyzed using the two-tailed nonpaired *t* test.  $*P \leq 0.05$ ;  $**P \leq 0.01$ . (E) Representative images of intracellular cords at macrophage 1, 2, and 3 days postinfection. Cords are in red, the macrophage surface is green, and the nucleus in blue as in (B). Scale bar, 20  $\mu$ m. (F) Size of the intracellular cords (expressed by the area in  $\mu$ m<sup>2</sup>) displayed in 10 fields. Results are expressed as mean values  $\pm$  SD for three independent experiments, and each symbol represents the size of a cord ( $n = 30$ ). Data were analyzed using the Mann–Whitney *t* test.  $**P \leq 0.01$ ;  $****P \leq 0.0001$ .

*M. abscessus*.<sup>43</sup> In addition, while overexpression of KatG from *M. tuberculosis* restored susceptibility to INH in *M. abscessus* carrying pSMT3-*katG*<sub>MTB</sub>-*tdTomato* as previously reported,<sup>29</sup> the MIC of NITD-916 remained unchanged in this strain as compared to its parental progenitor (Table S2). This implies that, in contrast to INH, the activity of NITD-916 is KatG-independent in *M. abscessus*.

The potency of NITD-916 was next assayed using a representative panel of clinical isolates from CF patients or non-CF patients, comprising 8 *M. abscessus*, 11 *M. abscessus*, and 9 *M. abscessus* strains. All these strains were susceptible to NITD-916, similarly to the CIP104536<sup>T</sup> reference strains (Figure 1B) and, in general, the MIC of R and S strains were similar, although slight variations were observed between the *M. massiliense* strains. The MIC values of NITD-916 were found to be much lower than those of rifabutin (RFB), included as a control drug.<sup>41</sup> Overall, these results demonstrate that NITD-916 exerts potent activity on the *M. abscessus* complex and is equally active against strains isolated from CF and non-CF patients.

**NITD-916 Inhibits Intramacrophage Growth of *M. abscessus*.** To assess whether NITD-916 is active against *M. abscessus* in a macrophage infection model, we next compared the intracellular efficacy of the compound in human THP-1 macrophages infected with either CIP104536<sup>T</sup> S or R variants after 1 and 3 days of exposure to the compound (Figure 2A and 2B). First, the cytotoxicity of NITD-916 against THP-1 cells was investigated after 1 and 3 days of exposure to the compound. Figure S1 clearly shows that NITD-916 exerts cytotoxicity only at very high concentrations (>100  $\mu$ g/mL) at both time points. NITD-916-induced cytotoxicity was intermediate between INH (no cytotoxicity at 100  $\mu$ g/mL) and RFB (100% macrophage killing at 100  $\mu$ g/mL) after 3 days of exposure to each drug. These results indicate that NITD-916 exhibits very little toxicity at concentrations below 100  $\mu$ g/mL and, based on these results, all subsequent macrophage studies were conducted with 1.56, 15.6, and 31.2  $\mu$ g/mL NITD-916, corresponding to 1 $\times$ , 10 $\times$ , and 20 $\times$  MIC. RFB was included as a positive control at 12.5  $\mu$ g/mL, a concentration at which it significantly reduces the intracellular burden.<sup>41</sup> DMSO-treated macrophages were added as a negative control for intracellular bacterial replication. At 0, 1, and 3 days postinfection (dpi), macrophages were lysed and plated to determine the intracellular bacterial burden after drug treatment. Similarly to the DMSO condition, exposure of macrophages to NITD-916 at 1 $\times$  MIC failed to inhibit intramacrophage growth of *M. abscessus* CIP104536<sup>T</sup> S (Figure 2A) and CIP104536<sup>T</sup> R (Figure 2B) at 1 and 3 dpi. In contrast, exposure to 10 $\times$  MIC strongly decreased the intracellular bacterial loads at 1 dpi and this effect was further amplified at 3 dpi in both strains. Interestingly, there was no difference between 10 $\times$  and 20 $\times$  MIC of NITD-916, and the CFU counts were comparable to

those in the inoculum (Day 0), similarly to what was observed in liquid cultures (Figure 1A). In addition, the NITD-916 susceptibility profile for the S variant at 1 and 3 dpi was comparable to that of the R variant, with a  $\sim$ 2 log reduction in the CFU counts at day 3, reaching the same level of inhibition as RFB (Figure 2A and 2B).

We further explored the activity of NITD-916 against S and R clinical isolates of the *M. abscessus* complex within THP-1 macrophages. Supporting our previous observations with the CIP104536<sup>T</sup> reference strains, we found that NITD-916 was very active against all *M. abscessus* subspecies tested within macrophages at 1 and 3 dpi when compared to day 0 and DMSO treatment, irrespective of S and R morphotype: *M. abscessus* 2069 (S) (Figure 2C), *M. abscessus* 2524 (R) (Figure 2D), *M. massiliense* 179 (R) (Figure 2E), *M. massiliense* 120 (S) (Figure 2F), *M. bolletii* 112 (R) (Figure 2G), and *M. bolletii* 108 (R) (Figure 2H). In all cases, the optimal activity was reached in the presence of 10 $\times$  MIC of NITD-916. Overall, these results indicate that NITD-916 is a potent intracellular growth inhibitor of *M. abscessus*.

**Intracellular *M. abscessus* Loads and Cording Are Reduced by NITD-916.** THP-1 macrophages were infected with red fluorescent *M. abscessus* strains expressing TdTomato and exposed to either DMSO, NITD-916, or RFB, stained with anti-CD63 and DAPI, and observed under the microscope. A quantitative analysis highlighted a marked reduction in the percentage of *M. abscessus* R-infected cells treated with NITD-916 at 10 $\times$  MIC (while no effect was observed at 1 $\times$  MIC), which was comparable to the effect observed with 12.5  $\mu$ g/mL RFB at 1 dpi (Figure 3A). This trend was even more pronounced at 3 dpi. Since the proportion of NITD-916-treated infected cells remained similar to the one at day 0, this suggests that the compound is very likely to be bacteriostatic inside the macrophage. Similar results were found when macrophages were infected with *M. abscessus* S (Figure S2A). Representative immunofluorescent fields illustrate the reduced number of macrophages infected with the R (Figure 3B) or S (Figure S2B) variants treated with NITD-916 at 1 and 3 dpi, as compared to the untreated or DMSO-treated control cells.

Macrophages infected with the R variant were then classified into three classes as judged by their bacterial load content: poorly infected (<5 bacilli/cell), moderately infected (5–10 bacilli/cell), and heavily infected (>10 bacilli/cell). Bacteria-containing macrophages were then individually observed under the microscope and scored for their belonging to one of the three categories. The quantitative analysis indicates that treatment with NITD-916 at 10 $\times$  MIC or RFB significantly reduces the percentage of heavily infected THP-1 cells and increases the proportion of the poorly infected category, as compared to the untreated or DMSO-treated cells at 1 and 3 dpi (Figure 3C), with  $\approx$ 20% of the infected bacilli belonging to the heavily infected category and  $\approx$ 50% associated with the poorly infected category at 3 dpi. Analysis performed on

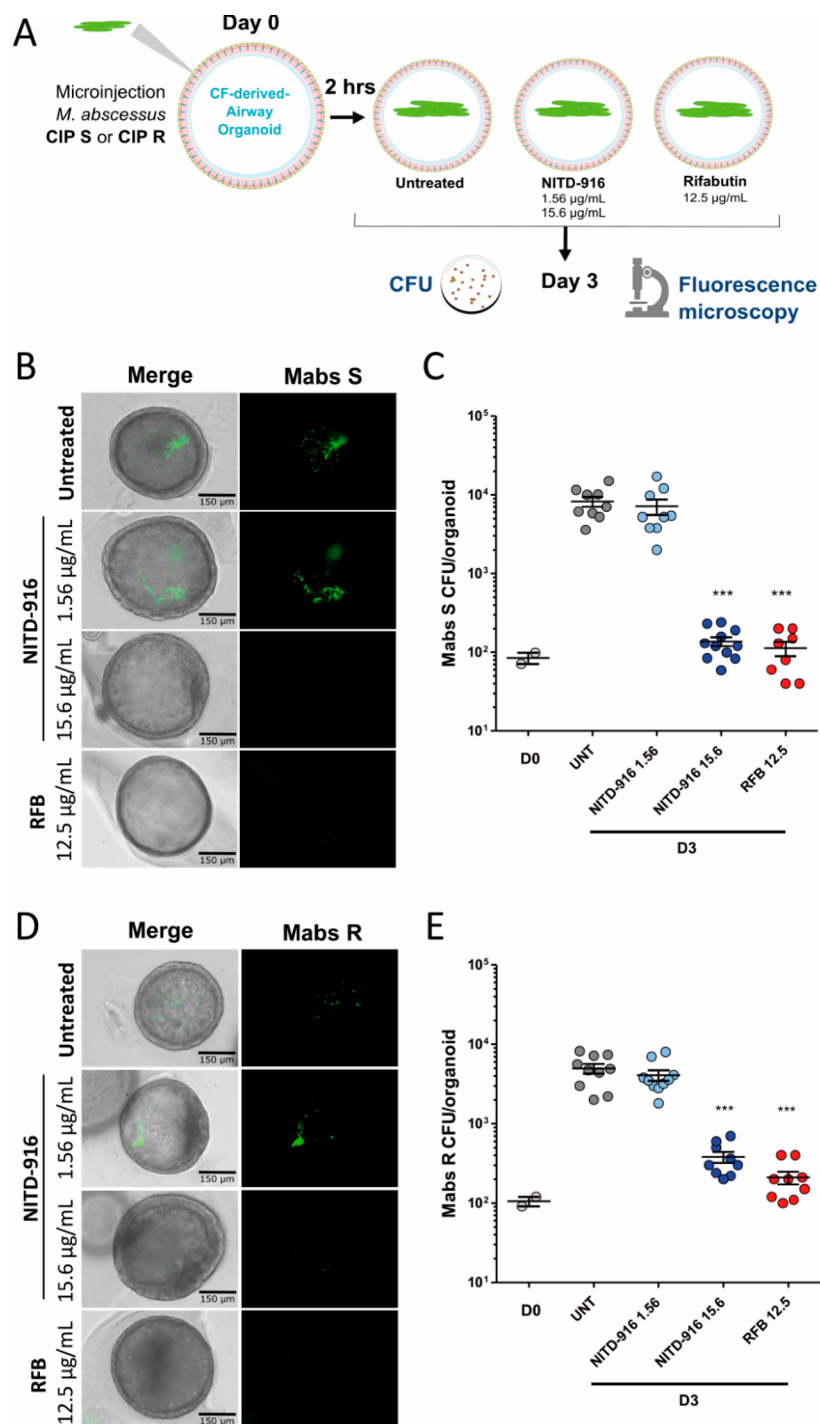


**Figure 4.** Activity of NITD-916 in *M. abscessus*-infected CF-derived airway organoids. (A) A generalized schematic showing the experimental design. Representative images (B, D) and corresponding bacterial loads determined by CFU counting (C, E) of CF-derived airway organoids at 3 days postinfection with *M. abscessus* S (B, C) or R (D, E) expressing Wasabi in the presence or absence of treatment: untreated groups ( $S n = 9$ ;  $R n = 10$ ), treated with NITD-916 at  $1.56 \mu\text{g/mL}$  ( $S n = 9$ ;  $R n = 10$ ), NITD-916 at  $15.6 \mu\text{g/mL}$  ( $S n = 11$ ;  $R n = 9$ ), or RFB at  $12.5 \mu\text{g/mL}$  ( $S n = 8$ ;  $R n = 9$ ). Graphs show means  $\pm$  SD of two independent experiments. Each dot represents one organoid. Data were analyzed using the Mann–Whitney  $t$  test. \*\*\* $P \leq 0.001$ .

macrophages infected with the S variant generated a similar category pattern (Figure S2C). Collectively, these data indicate that NITD-916 enters THP-1 macrophages and impedes bacterial replication of both *M. abscessus* S and R variants.

In contrast to the S variant, strains exhibiting a R morphotype are typified by increased bacterial clumping and R bacilli remain aggregated to generate compact colonies

comprising corded structures on agar, in broth medium, and inside macrophages.<sup>8,12,14,41</sup> Figure 3D clearly illustrates that, upon infection with TdTomato-expressing *M. abscessus* R, the total number of intracellular cords displayed in 30 fields was significantly reduced in the presence of NITD-916 at 10 $\times$  MIC or  $12.5 \mu\text{g/mL}$  RFB when compared to untreated or DMSO-treated cells, and this effect was maintained at 1, 2, and 3 dpi.

Table 1. Characteristics of NITD-916 Spontaneous Resistant Mutants of *M. abscessus*<sup>a</sup>

strain	MIC ( $\mu\text{g/mL}$ )			mutation in <i>inhA<sub>MAB</sub></i>		
	NITD-916	RFB	ETH	AA change	frequency of mutation	
CIP104536 <sup>T</sup> (S)	1.56	100	25			
NITD916 <sup>R1</sup>	>100	50	12.5	G287T	G96V	$2.3 \times 10^{-7}$
NITD916 <sup>R2</sup>	>100	100	25	G286A	G96S	$2.3 \times 10^{-7}$
NITD916 <sup>R3</sup>	>100	50	50	G286A	G96S	$2.3 \times 10^{-7}$
NITDR916 <sup>R4</sup>	>100	50	25	G287T	G96V	$2.3 \times 10^{-7}$
CIP104536 <sup>T</sup> (R)	1.56	12.5	25			
NITD916 <sup>R5</sup>	>100	12.5	12.5	G287T	G96V	$2.4 \times 10^{-6}$
NITD916 <sup>R6</sup>	>100	12.5	25	G287T	G96V	$2.4 \times 10^{-6}$
NITD916 <sup>R7</sup>	>100	25	25	G287T	G96V	$2.4 \times 10^{-6}$
NITD916 <sup>R8</sup>	>100	12.5	25	G287T	G96V	$2.4 \times 10^{-6}$

<sup>a</sup>MIC ( $\mu\text{g/mL}$ ) were determined in CaMHB. Resistant strains were derived from either the smooth (S) or rough (R) *M. abscessus* CIP104536<sup>T</sup> parental strains on LB agar supplemented with 15.6  $\mu\text{g/mL}$  NITD-916 (10 $\times$  MIC). Single-nucleotide polymorphism (SNP) in *inhA<sub>MAB</sub>* (*MAB\_2722c*) and corresponding amino acid (AA) changes as well as frequency of mutation are indicated.

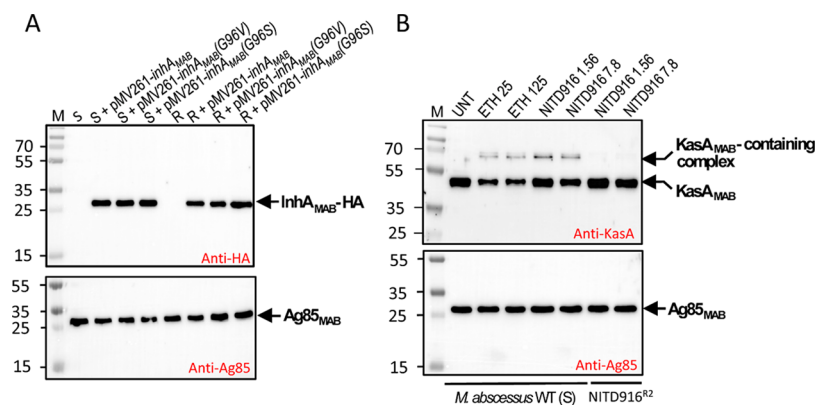


**Figure 5.** Overexpression of *InhA<sub>MAB</sub>* variants in *M. abscessus* S and R strains. (A) Western blots using antibodies against the HA-epitope (upper panel) and the Ag85 complex (lower panel) as loading control were done to assess the expression levels of the *InhA<sub>MAB</sub>* variants in various strains overproducing either *InhA<sub>MAB</sub>*(WT), *InhA<sub>MAB</sub>*(G96V), or *InhA<sub>MAB</sub>*(G96S). Equal amounts of total lysates (10  $\mu\text{g}$ ) of each strain were separated on a 12% SDS-PAGE. (B) Wild-type *M. abscessus* CIP104536<sup>T</sup> (S) and NITD916<sup>R2</sup> strains were grown in CaMHB and exposed for 9 h with increasing concentrations of ethionamide (ETH) or NITD-916 at concentrations corresponding to 1 $\times$  and 5 $\times$  MIC. Equal amounts of total lysates (10  $\mu\text{g}$ ) of each strain were separated on a 12% SDS-PAGE and probed with anti-KasA (upper panel) anti-Ag85 complex (lower panel) antibodies (used as loading control).

The effect was not significant at 1 $\times$  MIC. Representative images of intracellular cords show the kinetics of cord formation at 1, 2, and 3 dpi (Figure 3E). While very small in size at 1 dpi, cords continue to elongate at 2 dpi and 3 dpi, often leading to a structure capable of extruding out of the cells at 3 dpi, presumably participating in macrophage killing. In the presence of drugs (NITD-916 or RFB), there was a clear reduction in size of the cords as compared to the untreated cells. This effect is supported by a quantitative analysis of the cord surface area (expressed in  $\mu\text{m}^2$ ). While control cords continue to increase in size over time (reaching a surface area >100  $\mu\text{m}^2$ ), their size remained constant ( $\approx 20 \mu\text{m}^2$ ) upon exposure to NITD-916 or RFB (Figure 3F). Together, these results indicate that NITD-916 is highly effective in reducing the number and size of *M. abscessus* cords, which is thought to affect the outcome of the infection.

**NITD-916 Reduces *M. abscessus* Loads in Human Airway Organoids.** Lung airway organoids (AO) from healthy individuals have recently been developed to study the early steps of interaction between *M. abscessus* and the airway.<sup>44</sup> In this biological model where mycobacteria are injected in AO, *M. abscessus* was found to actively replicate over 7 days in the lumen, and this was accompanied by

reduced expression of mucin genes, usually participating in the clearance of pulmonary pathogens.<sup>44</sup> Moreover, AO derived from CF patients were characterized by low CFTR activity and enhanced mucus accumulation, and the subsequent injection of *M. abscessus* in these 3D structures revealed the production of biofilms formed by the S variant and serpentine cords formed by the R variant.<sup>45</sup> Importantly, both variants replicated more efficiently in CF AO than in AO derived from healthy lungs, thus highlighting the relevance of this model to study the pathogenesis of *M. abscessus* and to test the therapeutic potential of compounds in a system that recapitulates a CF environment.<sup>45</sup> As illustrated in Figure 4A, CF-derived AO were injected with the *M. abscessus* S and R variants expressing Wasabi, and drug treatment was commenced 2 h later with NITD-916 at 1.56  $\mu\text{g/mL}$  or 15.6  $\mu\text{g/mL}$  and with RFB at 12.5  $\mu\text{g/mL}$ , included as a control drug. After 3 days of treatment, fluorescence microscopy showed high bacterial loads in AO left untreated or exposed to 1.56  $\mu\text{g/mL}$  NITD-916, while exposing the AO to the 15.6  $\mu\text{g/mL}$  dose significantly reduced the green fluorescence signal, similarly to the RFB treatment (Figure 4B). AO were then lysed at 3 dpi, and plating the lysates on agar indicated a 2 log increase in the CFU of *M. abscessus* S in the untreated control



or in the presence of 1.56  $\mu\text{g/mL}$  NITD-916 (Figure 4C). In contrast, treatment with either 15.6  $\mu\text{g/mL}$  NITD-916 or 12.5  $\mu\text{g/mL}$  RFB was associated with a striking decrease in the CFU counts, at levels similar to those found in the inoculum (Day 0) (Figure 4C). Very similar results were observed for *M. abscessus* R-containing AO (Figure 4D and 4E). Overall, these results clearly indicate that NITD-916 is active in CF patient-derived AO characterized with severe CF airway dysfunction and susceptibility to *M. abscessus* infection.

**Mutations in *inhA<sub>MAB</sub>* Confer High Resistance Levels to NITD-916.** Mutations in *inhA* coding for the enoyl-ACP reductase of the type II fatty acid synthase have been reported previously in *M. tuberculosis* mutants resistant to NITD-916.<sup>40</sup> To get insights into the mode of action of NITD-916 in *M. abscessus*, a genetic approach was conducted involving the selection of spontaneous NITD-916-resistant mutants derived from either the smooth (S) or rough (R) *M. abscessus* parental strains on agar supplemented with 15.6  $\mu\text{g/mL}$  NITD-916 (10 $\times$  MIC) at frequencies estimated to  $2.3 \times 10^{-7}$  (S resistant strains) and  $2.4 \times 10^{-6}$  (R resistant strains). MIC determination of four individual colonies for each morphotype confirmed their high resistance levels (MIC > 100  $\mu\text{g/mL}$ ) against NITD-916 while remaining susceptible to RFB and ETH (Table 1). Sequencing the *inhA<sub>MAB</sub>* (*MAB\_2722c*) locus identified single nucleotide polymorphisms (SNPs) across the different resistors, leading to amino acid replacements at position 96. In the S resistors, NITD916<sup>R1</sup> and NITD916<sup>R4</sup>, Gly96 was replaced by a Val residue, while in NITD916<sup>R2</sup> and NITD916<sup>R3</sup>, Gly96 was replaced by a Ser residue. All four mutants derived from the R variant (NITD916<sup>R5</sup> to NITD916<sup>R8</sup>) harbored a G96V amino acid exchange (Table 1). As shown for NITD916<sup>R2</sup>, resistance to NITD-916 was independent of the medium (Table S1).

To validate *inhA<sub>MAB</sub>* as a specific target of NITD-916, wild-type and mutated *inhA<sub>MAB</sub>* alleles were cloned in frame with a HA-tag under the control of the constitutive *hsp60* promoter to allow overexpression of the wild-type and mutated versions of the protein. The resulting constructs, pMV261-*inhA<sub>MAB</sub>*, pMV261-*inhA<sub>MAB</sub>*(G96V), and pMV261-*inhA<sub>MAB</sub>*(G96S), were introduced in both S and R variants and expression of the different *InhA<sub>MAB</sub>* variants was confirmed by Western blotting using anti-HA antibodies, while levels of the Ag85 complex remain constant (Figure 5A). Whereas overproduction of the wild-type proteins did not significantly alter the MIC values as compared to the parental progenitors (2-fold effect), overproduction of *InhA<sub>MAB</sub>*(G96V) or *InhA<sub>MAB</sub>*(G96S) resulted in 8- to 32-fold upshift in the MIC level (Table 2). These effects were specific to NITD-916 as the MIC of RFB against the

same recombinant strains were comparable to those of the parental progenitors (Table 2). This indicates that transferring the single point mutations identified in the NITD-916 spontaneous resistant mutants into a susceptible strain is sufficient to confer high resistance levels to NITD-916.

It was previously reported that isoniazid, diazaborine, or ethionamide (ETH) induced the production of a KasA-containing complex in *M. smegmatis* and that formation of this complex is a consequence of *InhA* inhibition while other FAS-II inhibitors such as thiolactomycin or isoxyl, inhibiting KasA and the HadABC dehydratase, respectively, fail to induce this complex.<sup>46</sup> Thus, we inquired whether NITD-916 induces this complex in *M. abscessus* by probing crude lysates from cultures exposed to 1 $\times$  and 5 $\times$  MIC NITD-916 with anti-KasA antibodies. Figure 5B reveals, in addition to free KasA<sub>MAB</sub>, the presence of an additional immunoreactive band at both concentrations. This protein comigrated with a protein also present in the ETH-treated lysates (used as a positive control of *InhA<sub>MAB</sub>* inhibition) while absent in the untreated sample. Importantly, this KasA-containing complex was not induced in strain NITD916<sup>R2</sup> resistant to NITD-916, presumably because the G96S mutation in *InhA<sub>MAB</sub>* renders the enzyme insensitive to NITD-916. Overall, these results suggest that *InhA<sub>MAB</sub>* is the primary target of NITD-916 in *M. abscessus* and that its inhibition leads to the induction of a KasA-containing complex.

**NITD-916 Inhibits De Novo Mycolic Acid Biosynthesis in *M. abscessus*.** In contrast to *M. tuberculosis*, *M. abscessus* does not synthesize oxygenated mycolic acids but produces exclusively  $\alpha$  and  $\alpha'$  mycolates, corresponding to long-chain (C<sub>77-79</sub>) and short chain (C<sub>62-64</sub>) mycolic acid subspecies, respectively.<sup>47</sup> To interrogate whether NITD-916 inhibits de novo synthesis of mycolic acids, [<sup>14</sup>C]-labeled lipids were extracted from wild-type *M. abscessus* cultures treated with increasing concentrations of NITD-916 prior to labeling with 1  $\mu\text{Ci/mL}$  [2-<sup>14</sup>C]acetate. Mycolic acid methyl esters (MAMEs) and fatty acid methyl esters (FAMEs) were then separated by thin-layer chromatography (TLC). Synthesis of both  $\alpha$  and  $\alpha'$  mycolates was dramatically affected in a dose-dependent manner (Figure 6A). De novo synthesis was almost completely abrogated in the presence of 1.56  $\mu\text{g/mL}$  (1 $\times$  MIC). ETH, a drug known to target *InhA* and whose biotransformation is dependent on *EthA* instead of *KatG*,<sup>48</sup> was included as a positive control. However, due to the elevated MIC of ETH against *M. abscessus* (25  $\mu\text{g/mL}$ ), only partial inhibition was achieved at the concentrations tested. Importantly, no inhibition was noticed in the production of fatty acid methyl esters (FAMEs) during treatment with NITD-916, which indicates that, like ETH or INH, NITD-916 specifically inhibits FAS-II rather than FAS-I, as expected for *InhA*-dependent inhibition.

We next addressed whether resistance to NITD-916 can be linked to an unaltered mycolic acid profile in strains carrying mutations in *InhA<sub>MAB</sub>*. Supporting this hypothesis, mycolic acid biosynthesis in strain NITD916<sup>R2</sup> (carrying G96S point mutation) was much more refractory to inhibition by NITD-916 as compared to the wild-type progenitor (Figure 6B). Collectively, these biochemical data underline a mode of action that results in the abolishment of mycolic acid biosynthesis by targeting *InhA<sub>MAB</sub>*.

**Structural Basis for *InhA<sub>MAB</sub>* Inhibition by NITD-916.** To demonstrate direct target engagement, we obtained a 1.45 Å resolution crystal structure of *InhA<sub>MAB</sub>* bound to NITD-916 and NAD (Figure 7A and Table S3). As described above,

**Table 2. MIC ( $\mu\text{g/mL}$ ) of NITD-916 and RFB Determined in CaMHB at 30 °C against *M. abscessus* Overexpressing Wild-Type and Mutated *inhA<sub>MAB</sub>* (*MAB\_2722c*) Alleles**

strain	NITD-916	RFB
CIP104536 <sup>T</sup> (S)	1.56	50
S + pMV261- <i>inhA<sub>MAB</sub></i>	3.12	50
S + pMV261- <i>inhA<sub>MAB</sub></i> (G96V)	25	50
S + pMV261- <i>inhA<sub>MAB</sub></i> (G96S)	50	50
CIP104536 <sup>T</sup> (R)	1.56	12.5
R + pMV261- <i>inhA<sub>MAB</sub></i>	3.12	12.5
R + pMV261- <i>inhA<sub>MAB</sub></i> (G96V)	12.5	12.5
R + pMV261- <i>inhA<sub>MAB</sub></i> (G96S)	50	12.5

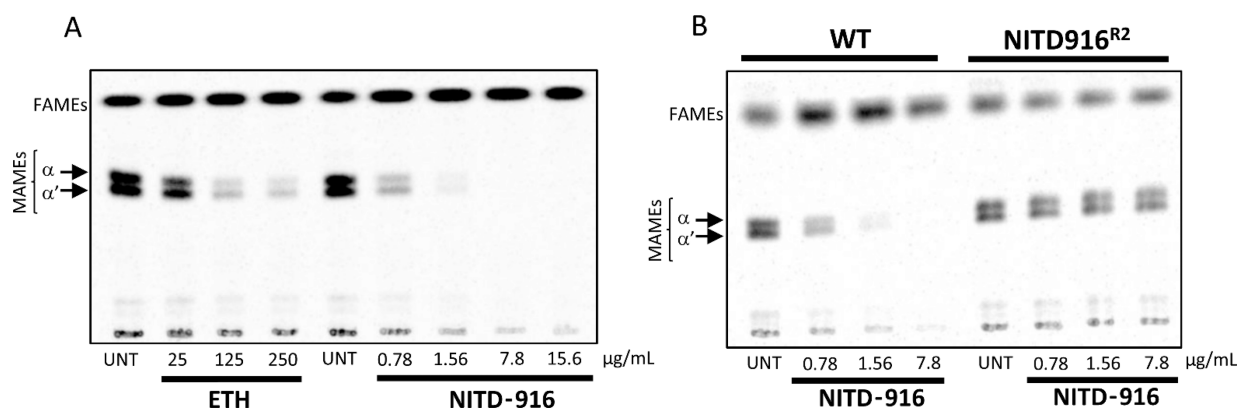


**Figure 6.** Inhibition of mycolic acid biosynthesis by NITD-916 in *M. abscessus*. (A) Dose–response effects of ETH and NITD-916 in *M. abscessus* CIP104536<sup>T</sup> (S). The inhibitory effect on the incorporation of [2-<sup>14</sup>C]acetate was assayed by exposing cultures to increasing concentrations of ETH or NITD-916 for 1 h prior to labeling for another 2 h at 37 °C under shaking. The corresponding radiolabeled FAMES and MAMES were extracted. Equal counts (50 000 cpm) were loaded onto a TLC plate and lipids were developed in petroleum ether/acetone (95/5, v/v). (B) Mutant NITD916<sup>R2</sup> is refractory to mycolic acid inhibition by NITD-916. *M. abscessus* CIP104536<sup>T</sup> (S) and its derivative NITD916<sup>R2</sup> were exposed to concentrations corresponding to 0.5×, 1×, and 5× MIC of NITD-916, labeled and subjected to lipid extraction and analysis as in (A).

resistance mutants arose at residue Gly96. In our structure, the C<sub>α</sub> of Gly96 residues is in proximity to the 2'-hydroxyl of the NMN portion of NAD as well as the phenyl moiety of NITD-916 (Figure 7A). Mutation of this residue would cause a steric clash with the phenyl ring of NITD-916, potentially explaining the G96S and G96V resistance mutations. Modifying the phenyl ring of NITD-916 could potentially result in molecules which overcome resistance at G96. However, given the proximity to the 2'-hydroxyl of the NMN portion of NAD, mutation of G96 could also cause loss of InhA specific activity and these resistance mutations may not arise in a clinical setting. Residues interacting with NITD-916 are indicated in Figure 7A.

Overall, our structure is similar to a previously obtained 3.2 Å resolution structure of InhA<sub>MTB</sub> bound to NITD-916 and NAD<sup>40</sup> (Figure 7B). The 4-hydroxy-2-pyridin-2-one moiety stacks on top of the nicotinamide ring, presumably where the unsaturated portion of the substrate binds, whereas the 4,4-dimethylcyclohexyl moiety projects into the hydrophobic cavity presumably where the lipid portion of the substrate binds. Thus, NITD-916 appears to be a direct substrate competitor. In addition, there appears to be some induced fit upon NITD-916 binding when compared to our structures of the InhA<sub>MAB</sub> apoenzyme (1.75 Å resolution) or the holoenzyme (1.85 Å resolution) (Figure 7C). Our structures of InhA<sub>MAB</sub> in the apoenzyme, holoenzyme, and NITD-916 inhibited state show that the residues spanning Thr196 through Gly212 move considerably in response to the ligand-bound state. In the InhA<sub>MAB</sub> apoenzyme state these residues form a β-hairpin turn and generate an open catalytic cavity. In the holoenzyme state, these residues change to an α-helix which packs tightly against the cofactor and generate a narrow substrate binding cleft. In the inhibited form, this new α-helix moves away from the cofactor to accommodate the binding of NITD-916. These residues and to a lesser extent α6 (numbering using the apoenzyme state) are the only major conformational changes that occur between the different states. Similar conformational changes have been observed previously for InhA<sub>MTB</sub> substrates (e.g., PDB ID 1BVR<sup>49</sup>) and other inhibitor-bound structures (e.g., PDB ID 1P44<sup>50</sup>).

To complement the crystallography work and gain some understanding of the effects of the inhibitor NITD-916 on the

thermal stability of InhA<sub>MAB</sub>, we performed differential scanning fluorimetry (DSF). Apoenzyme InhA<sub>MAB</sub> had a melting temperature of 39.3 °C (Table S4 and Figure S3). Incubation with the cofactor NAD to generate the holoenzyme resulted in a modest increase in melting temperature to 39.8 °C (ΔT<sub>m</sub> = 0.5 °C). Generation of the inhibited complex of InhA<sub>MAB</sub> with NAD and NITD-916 resulted in a large increase in the melting temperature to 54.0 °C (ΔT<sub>m</sub> = 14.7 °C relative to apo or 14.2 °C relative to NAD alone). Although such stability measurements are not directly correlated with affinity, significant stabilization can be indicative of potency in biochemical experiments.

## DISCUSSION

The success rate of *M. abscessus* pulmonary disease treatment remains very poor despite prolonged, multidrug antibiotherapy with an important risk of severe secondary effects, emphasizing the rapid need for more effective treatments.<sup>26</sup> While mycolic acids represent essential cell wall components in mycobacteria and are the primary target of INH and ETH in *M. tuberculosis*, none of the current drugs used in clinical settings against *M. abscessus* infections are hitting mycolic acid biosynthesis. However, recent studies have emphasized that this metabolic pathway represents an attractive niche for druggable targets in *M. abscessus*. First, thiacetazone has proven to bind to the HadA component of the FAS-II HadABC dehydratase complex, leading to mycolic acid inhibition in *M. tuberculosis*,<sup>51</sup> and thiacetazone derivatives exhibited potent activity against the *M. abscessus* complex.<sup>52</sup> Second, a large number of hits against *M. abscessus* have recently been shown to inhibit the transport of mycolic acids across the membrane by targeting the MmpL3 transporter.<sup>27,53,54</sup> In this context, the present study was undertaken to evaluate the potential of inhibiting the FAS-II enoyl-ACP reductase in *M. abscessus*. In agreement with a previous study,<sup>29</sup> our results indicate that the lack of activity of INH in *M. abscessus* presumably relies on the incapacity of KatG<sub>MAB</sub> to convert INH into an active metabolite, while partial susceptibility levels to INH were recovered when overexpressing the *katG* gene from *M. tuberculosis*. This indicates that while KatG-dependent inhibition of InhA is compromised in *M. abscessus*, it opens, however, the possibility of inhibiting mycolic acid biosynthesis via KatG-independent



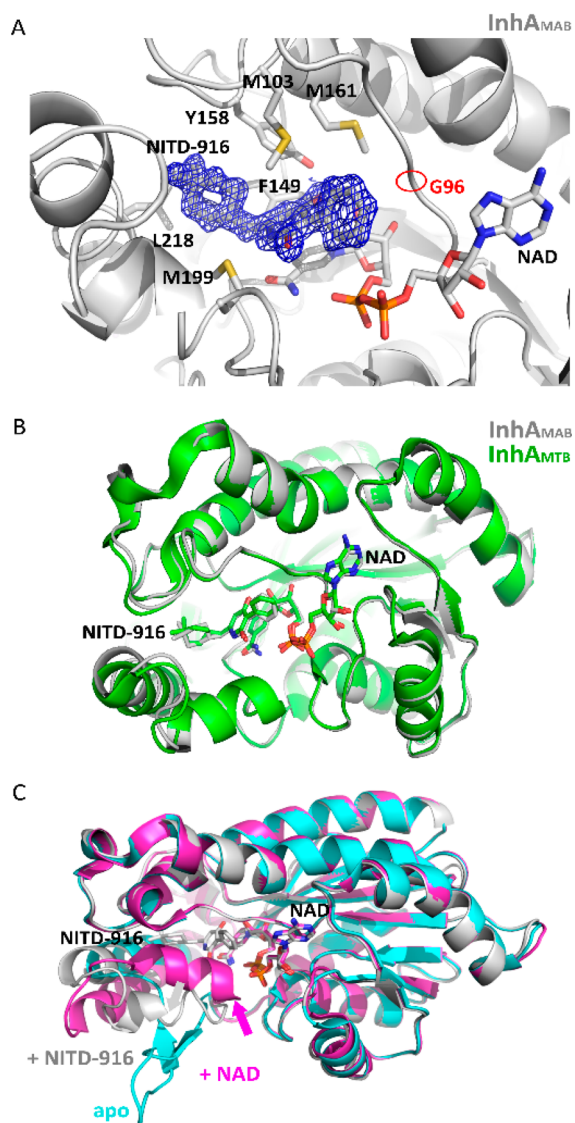


**Figure 7.** Structural basis of inhibition of *M. abscessus* InhA by NITD-916. (A) Crystal structure of *M. abscessus* InhA bound to NITD-916 and NAD solved at 1.45 Å resolution. For simplicity only one protomer of the tetrameric structure is shown. The protein is depicted as gray ribbons and the inhibitor NITD-916 and cofactor NAD are shown rendered in sticks. The final  $2|F_o| - |F_c|$  map for NITD-916 is shown in blue mesh contoured at 1.0 sigma. The site of resistance mutations G96 is circled in red and other residues which interact with NITD-916 are labeled and shown with their side chains rendered in sticks. (B) Overlay of the crystal structures of InhA<sub>MAB</sub> bound to NITD-916 and NAD depicted as above, and InhA<sub>MTB</sub> bound to NITD-916 and NAD shown in green ribbons for the protein and green carbon sticks for the inhibitor and cofactor. (C) Overlay of the crystal structure of InhA<sub>MAB</sub> in the apo state shown in cyan ribbons, the holoenzyme state bound to NAD in magenta with NAD in magenta sticks, and the inhibited state bound to NAD and NITD-916 in gray as in the upper panels. The loop spanning residues Thr196 through Gly212 moves significantly upon cofactor and inhibitor binding.

inhibitors of InhA. This proof-of-concept was verified here through the use and characterization of the mode of action of the 4-hydroxy-2-pyridone lead candidate NITD-916, originally identified in a phenotypic screen against *M. tuberculosis*.<sup>40</sup>

NITD-916 displayed low MIC values against a wide panel of clinical isolates and exerted an in vitro static activity against

*M. abscessus* at 1× MIC. This higher MIC value of NITD-916 against *M. abscessus* as compared to *M. tuberculosis*<sup>40</sup> is currently not known but may rely on differences in the composition and/or architecture of the cell wall between the two species, potentially affecting cell wall permeability to this inhibitor. In addition, *M. abscessus* possesses a large number of efflux pumps, which may also contribute to the lower susceptibility of this species to NITD-916. However, at 1× MIC concentration, the compound did not show any activity in *M. abscessus*-infected macrophages. In contrast, at 10× MIC there was a significant reduction in the intracellular bacterial loads at 1 dpi, which remained comparable at 3 dpi, with similar results obtained against various clinical isolates, with no distinctions between S and R morphotypes. In general, at 3 dpi, the CFU levels remained equivalent to those in the inoculum (Day 0), indicating that NITD-916 behaves as a bacteriostatic drug in the macrophage under the conditions tested. NITD-916 not only reduced the intracellular bacterial burden but also the proportion of infected macrophages, similarly to RFB, a drug recently proposed to be included in drug regimens to reduce treatment duration of *M. abscessus* pulmonary diseases.<sup>55</sup> Furthermore, exposure of macrophages infected with the R variant to NITD-916 was associated with a reduction in the number and size of cords, presumably resulting from bacterial growth inhibition. Therefore, compounds, such as NITD-916 or RFB, inhibiting intracellular cord formation participate also in the prevention of macrophage death caused by the disruptive activity of cords on macrophage integrity. Consistently, we found that NITD-916 was as active as RFB in CF patient-derived AO recapitulating the CF airway dysfunctions, such as thick mucus, and with increased susceptibility to *M. abscessus* infection.<sup>45</sup> Thus, our data emphasize an unexploited chemical structure class active against *M. abscessus* infections with promising translational development possibilities for the treatment of CF patients.

From a mechanistic perspective, our genetic and biochemical studies unambiguously indicate that NITD-916 does not undergo bioactivation by KatG prior to binding to InhA<sub>MAB</sub>, but rather inhibits biosynthesis of mycolic acids by directly binding to InhA<sub>MAB</sub>. These assumptions can be inferred from the following results: (i) A panel of spontaneous mutants resistant to NITD-916 harbored point mutations in InhA<sub>MAB</sub> at residue 96, and the mycolic acid pattern of these mutants remained unchanged upon exposure to NITD-916. Replacement of Gly96 by a more bulky residue is associated with NITD-916 resistance, suggesting that conservation of Gly96 is requested for susceptibility to this compound. Multiple sequence alignments of InhA proteins from different mycobacterial species indicate that Gly96 is very well conserved (Figure S4), thus suggesting that other NTM may be susceptible to NITD-916 inhibition, although this remains to be investigated in future studies. Interestingly, while replacements occurred only at Gly96 in all *M. abscessus* resistant mutants selected, many more mutations were identified in residues within or near the active site of InhA in *M. tuberculosis* resistant mutants.<sup>40,56</sup> In addition, strains harboring the InhA<sub>MAB</sub> G96S or G96V point mutations remained fully sensitive to ETH, as shown previously in *M. tuberculosis*.<sup>40</sup> (ii) Overexpression of the mutated *inhA* alleles in a susceptible strain conferred resistance to the inhibitor. (iii) NITD-916 treatment induced the formation of a KasA-containing complex, reported previously as a marker of InhA inhibition.<sup>46</sup> (iv) NITD-916 could be identified in a

ternary NITD-916:NAD:InhA<sub>MAB</sub> costructure. Collectively, these results indicate that NITD-916 shares the same mode of action in *M. abscessus* and *M. tuberculosis* and confirms that the biosynthetic steps of mycolic acids represent an excellent pathway to be further exploited in drug discovery programs against *M. abscessus*. Previous work indicated that NITD-916 has no mutagenic or cardiotoxicity potential and showed no in vitro safety pharmacological liabilities and did not inhibit the major CYP450 isoenzyme 3A4,<sup>40</sup> thus stimulating new medicinal chemistry programs for the rational optimization of NITD-916-related analogues targeting InhA<sub>MAB</sub> with improved efficacy. Changes in the 4-hydroxy 2-pyridone may include substitutions of the R6 lipophilic group and replacement of the R3 phenyl group with other aromatic substituents. In addition, to increase solubility and lipophilicity, phosphate ester prodrugs are typically designed, favoring oral administration and are rapidly hydrolyzed by intestinal alkaline phosphatases. This has been emphasized by synthesizing a 4-hydroxy methyl phosphate ester prodrug of NITD-916, designated NITD-113, displaying improved aqueous solubility by two log orders and with good bioconversion to NITD-916 in mice.<sup>40</sup> The availability of the InhA<sub>MAB</sub> crystal structure in complex with NAD and NITD-916 will greatly facilitate and guide the chemistry to generate these analogues. In addition, the very high structural conservation between InhA<sub>MAB</sub> and InhA<sub>MTB</sub> is a key factor prompting the future testing of a large panel of validated direct InhA<sub>MTB</sub> inhibitors against *M. abscessus*. Indeed, such direct InhA<sub>MTB</sub> inhibitory scaffolds have been identified in high throughout screenings, encoded library technology, or fragment-based screenings and have received considerable attention during these past few years.<sup>57</sup> Another important feature to consider in future studies relies on the possibility to increase the activity of NITD-916 when given in combination with other drugs. Since any *M. abscessus* antibiotic has to be clinically administered in combination with other drugs,<sup>22</sup> the absence of drug–drug interactions is critical for clinical development and needs to be checked. Using the checkerboard assay, we found that the Fractional Inhibitory Concentration Index (FICI) values between NITD-916 and most drugs used in clinics were in the 0.5–1.5 range (Table S5), suggestive of an indifferent interaction between the compounds, and thus highlighting the suitability of including NITD-916 in combination therapy.

## CONCLUSIONS

This work reports the potent in vitro and intracellular anti-*M. abscessus* activity of NITD-916 and underscores the strong activity of this unexploited chemical scaffold in CF-derived AO, opening future possibilities for the treatment of CF patients. Subsequent studies should now advance this compound as well as its derivatives into preclinical animal models. Our findings also support the view that targeting mycolic acid biosynthesis has serious translational potential for development into a real tool for treatment and control of *M. abscessus* pulmonary diseases.

## METHODS

**Mycobacterium abscessus Strains and Culture Conditions.** *M. abscessus* subspecies *abscessus* CIP104536<sup>T</sup>, *M. abscessus* subspecies *bolletii* CIP108541<sup>T</sup>, and *M. abscessus* subspecies *massiliense* CIP108297<sup>T</sup> reference strains as well as

clinical strains from CF and non-CF patients were reported earlier.<sup>52,58</sup> Bacteria were routinely grown and maintained at 37 °C in Middlebrook 7H9 broth (BD Difco) containing 0.025% Tyloxapol (Sigma-Aldrich) and 10% oleic acid, albumin, dextrose, catalase (OADC enrichment; BD Difco) (7H9<sup>T/OADC</sup>) or on Middlebrook 7H10 agar (BD Difco) containing 10% OADC enrichment (7H10<sup>OADC</sup>). *M. abscessus* carrying pTEC27 and expressing TdTomato was reported earlier and grown in the presence of 1000 µg/mL hygromycin.<sup>14</sup> *M. abscessus* smooth and rough strains were transformed with pSMT3-*katG*<sub>MTB</sub>-*tdTomato*<sup>59</sup> and grown in the presence of 1000 µg/mL hygromycin.

For drug susceptibility testing, bacteria were grown in Cation-Adjusted Mueller–Hinton Broth (CaMHB; Sigma-Aldrich). Rifabutin and NITD-916 were purchased from Selleckchem and Merck, respectively, and dissolved in DMSO.

**Drug Susceptibility Testing.** The minimal inhibitory concentrations (MIC) were determined according to the CLSI guidelines.<sup>60</sup> The broth microdilution method was used in CaMHB with an inoculum of 5 × 10<sup>6</sup> CFU/mL in exponential growth phase. The bacterial suspension was seeded in 100 µL volumes in all of the wells of a 96-well plate, except for the first column, to which 198 µL of the bacterial suspension was added. In the first column, 2 µL of drug at its highest concentration was added to the first well containing 198 µL of bacterial suspension. Two-fold serial dilutions were then carried out, and the plates were incubated for 3–5 days at 30 °C. MICs were recorded by visual inspection. MIC were also determined using Middlebrook 7H9 supplemented with OADC, Sauton's medium, or an artificial sputum medium (ASM) containing components of the CF sputum.<sup>42</sup>

**Growth Kinetics.** To monitor growth inhibition of *M. abscessus* CIP104536<sup>T</sup> (S), 96-well plates were setup as for MIC determination, and serial dilutions of the bacterial suspensions exposed to increasing concentrations of NITD-916 were plated on LB agar plates after 0, 1, 2, and 3 days. Colony-forming units (CFUs) were counted after 4 days of incubation at 37 °C. Results from each drug concentration are representative of 2 independent experiments in triplicates.

**Cytotoxicity Assay.** Human THP-1 monocytes were grown in RPMI medium supplemented with 10% Fetal bovine serum (Sigma-Aldrich) (RPMI<sup>FBS</sup>) and incubated at 37 °C in the presence of 5% CO<sub>2</sub>. Cells were differentiated with 20 ng/mL Phorbol Myristate Acetate (PMA) in 96-well flat-bottom tissue culture microplates (2 × 10<sup>4</sup> cells/well) for 48 h at 37 °C with 5% CO<sub>2</sub> and exposed to decreasing concentrations of NITD-916, RFB, or INH (starting at 100 µg/mL) for 24 or 72 h at 37 °C with 5% CO<sub>2</sub>. Following incubation, 10% (v/v) resazurin dye was added to each well and left to incubate for another few hours at 37 °C and 5% CO<sub>2</sub>. Data were acquired using a fluorescent plate reader (excitation 540 nm, emission 590 nm).

**Intracellular Killing Assay.** THP-1 were grown and differentiated into macrophages as reported above but wells were seeded with 10<sup>5</sup> cells. Infection with *M. abscessus* strains was carried out at 37 °C in the presence of 5% CO<sub>2</sub> for 4 h at a MOI 2:1. After extensive washing with 1× phosphate buffered saline (PBS), macrophages were incubated with RPMI<sup>FBS</sup> containing 250 µg/mL amikacin for 2 h and washed again with PBS prior to the addition of 500 µL RPMI<sup>FBS</sup> containing DMSO (negative control) or 500 µL RPMI<sup>FBS</sup> containing either RFB or NITD-916. Drugs were renewed on a daily basis. Cells were washed with PBS and lysed with 100 µL of 1%



Triton X-100 after 1 day or 3 days postinfection. Serial dilutions of macrophage lysates were plated onto LB agar plates, and colonies were counted to determine intracellular CFU.

**Microscopy-Based Infectivity Assays.** Differentiated THP-1 macrophages were grown on coverslips in 24-well plates at a density of  $10^5$  cells/mL for 48 h at 37 °C with 5% CO<sub>2</sub> prior to infection with *M. abscessus* expressing TdTomato for 4 h at a MOI of 2:1. After washing and AMK treatment to remove the extracellular bacilli, cells were exposed to DMSO (negative control), RFB, or NITD-916 and fixed at 0, 1, and 3 days postinfection with 4% paraformaldehyde in 1× PBS for 20 min. Cells were then permeabilized using 0.2% Triton X-100 for 20 min, blocked with 2% BSA in PBS supplemented with 0.2% Triton X-100 for 20 min, incubated with anti-CD63 antibodies (Becton Dickinson; dilution 1:1000) for 1 h and with an Alexa Fluor 488-conjugated antimouse secondary antibody (Molecular Probes, Invitrogen; dilution 1:1000) for 45 min. After 5 min of incubation with DAPI (dilution 1:1000), cells were mounted onto microscope slides using Immu-mount (Calbiochem) and examined with an epifluorescence microscope using a 40× objective. Images were acquired by focusing on combined signals (CD63 in green and *M. abscessus* in red) and captured on a Zeiss Axioimager upright microscope equipped with a 40× and 100× oil objective and processed using ImageJ software. Equal parameters for the capture and scoring of images were consistently applied to all samples. For each condition, approximately 1000 infected macrophages were analyzed. The presence of the intra- or extracellular cords within or among the macrophages infected exclusively with the *M. abscessus* (R) variant were treated in the presence of DMSO, RFB, or NITD-916, counted, and imaged using full-field upright microscopy. Areas of intracellular cords were quantified using ImageJ.

**Selection of Resistant *M. abscessus* Mutants and Target Identification.** Exponentially growing *M. abscessus* CIP104536<sup>T</sup> S and R cultures were plated on LB agar containing 15.6 μg/mL NITD-916, corresponding to 10× MIC. After 1 week of incubation at 37 °C, four individual colonies deriving from the S and R strains were selected, grown in CaMHB and individually assessed for MIC determination and scored for resistance to NITD-916. Identification of SNPs in the NITD-916-resistant strains was completed by PCR amplification using the primers *MAB\_2722c s1 (F)* 5'-GTG GCA GGA CTA CTT GAG GGC-3' and *MAB\_2722c s2 (R)* 5'-TCA GAG CAG CTG AGT GTG AGC G-3' to produce a 810 bp amplicon for full coverage sequencing of the *inhA<sub>MAB</sub>* gene.

**Cloning and Overexpression of the *inhA<sub>MAB</sub>* Alleles in *M. abscessus*.** Wild-type *inhA<sub>MAB</sub>* and the corresponding mutated genes harboring the G287T or G286A polymorphisms were amplified by PCR (Q5 polymerase) using genomic DNA prepared from the WT or spontaneous resistant mutants as well the forward 5'-GGG GCA GGA TCC GAG TGG CAG GAC TAC TTG AGG GCA A-3' and reverse 5'-GGG CTA CGA ATT CTG CTA AGC GTA ATC TGG AAC ATC GTA TGG GTA GAG CAG CTG AGT GTG AGC GC-3' primers (restriction sites are underlined and HA tag coding sequence is in bold). PCR-amplified fragments were cloned into the *Bam*HI and *Eco*RI sites of pMV261,<sup>61</sup> and the resulting plasmids were introduced into *M. abscessus* following selection in the presence of 250 μg/mL kanamycin.

**Immunoblotting.** Bacteria cultures were collected by centrifugation and lysed using 1 mm diameter glass beads and a Mixer Mill MM 301 (Retsch, Germany) at a frequency of 30 Hz for 10 min. Equal amount of total proteins (10 μg) were separated by 12% SDS-PAGE and transferred to a nitrocellulose membrane prior to Western blot analysis. Primary antibodies used were rat anti-HA (1:5000 dilution), rat anti-KasA (1:2000 dilution), or mouse monoclonal antibody 32/15 (1:10 dilution) recognizing the Ag85 complex.<sup>62</sup> After washing, membranes were incubated for 45 min with an anti-rat or anti-mouse antibody conjugated to HRP (dilution 1:5000), incubated with SuperSignal West Femto (ThermoFisher Scientific) and revealed using a ChemiDoc MP system (Bio-Rad).

**Mycolic Acid Analysis.** To investigate the drug-induced changes in the mycolic acid profile, *M. abscessus* cultures were exposed to increasing drug concentrations of either ETH included as a positive control or NITD-916 for 1 h prior to metabolic labeling in the presence of 1 μCi/mL of [<sup>14</sup>C]-acetate (59 mCi/mmol, PerkinElmer) for an additional 2 h under shaking at 37 °C. Extraction of total mycolic acids was carried out as previously reported.<sup>48</sup> Briefly, cell pellets were washed and treated with 15% tetrabutylammonium hydroxide (TBAH) at 100 °C overnight. Fatty acids and mycolic acids were methyl-esterified and extracted in diethyl ether. Lipid extracts were dried and resuspended in dichloromethane and separated by thin-layer chromatography (TLC). Fatty acid methyl esters (FAMES) and mycolic acid methyl esters (MAMES) were developed in petroleum ether/acetone (95:5, v/v). The [<sup>14</sup>C]-labeled FAME and MAME content was analyzed using an Amersham Typhoon imaging system.

**Human Bronchial Organoid Culture.** The CHU of Toulouse (CHU 19 244 C) and the CNRS (CNRS 205782) approved the use of materials for this study. Organoids were derived from a lung biopsy of a cystic fibrosis heterozygous patient (G542X/1811 + 1.6kba → G), as previously reported.<sup>45</sup>

**Organoid Infections.** On the infection day, organoids were infected with *M. abscessus* S and R variants adjusted to OD<sub>600</sub> = 0.2. Organoids in 25 μL drops of Matrigel (Fisher Scientific) were seeded on Nunclon Delta surface 35 × 10 mm Dish (Thermo Scientific). After Matrigel polymerization, 2 mL of airway organoid complete media<sup>45</sup> without *N*-acetylcysteine and without antibiotics were added to each plate. Organoids were microinjected using a Femtojet microinjector (Eppendorf), as previously described.<sup>44</sup> Two hours after infection, organoids were collected, washed in 1× PBS, embedded into a fresh matrix and treated or not for 3 days with 1.56 μg/mL or 15.6 μg/mL NITD-916 or 12.5 μg/mL RFB.

**Live Imaging and Colony-Forming Unit Assay.** At day 3 post infection, images of the organoids were acquired under an EVOS M7000 Imaging System (20×, at 37 °C with 5% CO<sub>2</sub>) (Thermo Scientific). Following image acquisition, infected organoids were individually collected and lysed in 100 μL of 10% Triton X100 in PBS.<sup>44</sup> Serial dilutions of the lysates were plated on LB agar plates and incubated for 4 days at 37 °C prior to CFU counting.

**Crystal Structure Determination.** *M. abscessus* *InhA* (*InhA<sub>MAB</sub>*) was expressed and purified using our standard structural genomics expression and purification protocols reported previously.<sup>63,64</sup> Briefly, the *MAB\_2722c* gene encoding *InhA<sub>MAB</sub>* was cloned from genomic DNA into the bacterial expression vector BG1861, which encodes a non-



cleavable N-terminal His<sub>6</sub> tag. The protein was expressed in BL21(DE3) cells with autoinduction media followed by cell lysis and purification via nickel affinity then size exclusion chromatography. InhA<sub>MAB</sub> crystallized at 23.06 mg/mL in the *apo* state in the MCSG1 crystallization screen condition E1 (2 M (NH<sub>4</sub>)<sub>2</sub>SO<sub>4</sub>, 0.1 M Hepes pH 7.5); the crystal was cryoprotected with reservoir supplemented with 20% v/v ethylene glycol. InhA<sub>MAB</sub> crystallized at 23.06 mg/mL with 4 mM NADH in the JCSG+ crystallization screen condition E1 (0.1 M sodium cacodylate pH 6.27, 1.09 M sodium citrate tribasic); the crystal was cryoprotected with reservoir supplemented with 4 mM NADH and 20% v/v ethylene glycol. InhA<sub>MAB</sub> crystallized at 23.06 mg/mL with 3.5 mM NADH and 3.5 mM NITD-916 in the Index crystallization screen condition H10 (0.2 M sodium citrate tribasic, 20% PEG 3350); the crystal was cryoprotected with reservoir supplemented with 3.5 mM NADH, 3.5 mM NITD-916, and 20% v/v ethylene glycol. The *apo* and the NADH/NITD-916 bound data sets were collected at the Advanced Photon Source beamLine 21 ID-F with a Rayonix MX-300 CCD detector at 0.97872 Å wavelength. The NADH bound data set was collected in house on a Rigaku FR-E+ SuperBright X-ray generator with a Saturn 944+ detector at 1.5406 Å wavelength. The *apo* structure was solved by molecular replacement using MORDA and the *M. tuberculosis* InhA structure (PDB ID 2H71 superseded by 4U0J) as a search model. The structure was refined with iterative rounds of refinement between Phenix<sup>65</sup> and Coot.<sup>66</sup> X-ray diffraction images have been uploaded to the Integrated Resource for Reproducibility in Macromolecular Crystallography (IRRM) database ([www.proteindiffraction.org](http://www.proteindiffraction.org)).<sup>67</sup>

**Ligand Binding via Differential Scanning Fluorimetry (DSF).** Sypro dye based DSF experiments were performed on a Bio-Rad CFX-96 thermal cycler at 0.1 mg/mL InhA<sub>MAB</sub> in a background buffer of 25 mM Tris pH 8.0, 200 mM NaCl, 1 mM TCEP, and 1% v/v glycerol. DMSO was kept constant at 2% v/v for all measurements. NAD alone or NAD and NITD-916 were added to a final concentration of 1 mM.

**Statistical Analyses.** Statistical analyses were performed on Prism 9.0 (Graphpad) and detailed for each figure legend. \**P* ≤ 0.05, \*\* *P* ≤ 0.01, \*\*\* *P* ≤ 0.001, \*\*\*\* *P* ≤ 0.0001.

## ■ ASSOCIATED CONTENT

### SI Supporting Information

The Supporting Information is available free of charge at <https://pubs.acs.org/doi/10.1021/acsinfecdis.2c00314>.

Table S1: MIC of ethionamide and NITD-916 against *M. abscessus* in different media; Table S2: Activity of INH, NITD-916, and the quinoline-INH hybrid 16g against *M. abscessus* strains overexpressing KatG<sub>MTB</sub>; Table S3: Crystallographic data collection and refinement statistics; Table S4: Differential scanning fluorimetry (DSF) measurements on InhA<sub>MAB</sub>; Table S5: Interactions between NITD-916 and other antibiotics using the checkerboard assay; Figure S1: Cytotoxicity assay of NITD-916, isoniazid (INH) and rifabutin (RFB) on THP-1 cells; Figure S2: Percentage of THP-1 macrophages at 0, 1, and 3 days postinfection with *M. abscessus* S in the presence of absence of NITD-916; Figure S3: Differential scanning fluorimetry (DSF) thermal shift analysis of InhA<sub>MAB</sub>; Figure S4: Multiple sequence alignments of the InhA proteins (PDF)

## ■ AUTHOR INFORMATION

### Corresponding Author

Laurent Kremer – Centre National de la Recherche Scientifique UMR 9004, Institut de Recherche en Infectiologie de Montpellier (IRIM), Université de Montpellier, 34293 Montpellier, France; INSERM, IRIM, 34293 Montpellier, France; [orcid.org/0000-0002-6604-4458](https://orcid.org/0000-0002-6604-4458); Phone: (+33) 4 34 35 94 47; Email: [laurent.kremer@irim.cnrs.fr](mailto:laurent.kremer@irim.cnrs.fr)

### Authors

Matthéo Alcaraz – Centre National de la Recherche Scientifique UMR 9004, Institut de Recherche en Infectiologie de Montpellier (IRIM), Université de Montpellier, 34293 Montpellier, France

Françoise Roquet-Banères – Centre National de la Recherche Scientifique UMR 9004, Institut de Recherche en Infectiologie de Montpellier (IRIM), Université de Montpellier, 34293 Montpellier, France

Stephen Adonai Leon-Icaza – Institut de Pharmacologie et de Biologie Structurale (IPBS), Université de Toulouse, CNRS, 31400 Toulouse, France; [orcid.org/0000-0002-7546-8228](https://orcid.org/0000-0002-7546-8228)

Jan Abendroth – UCB BioSciences, Bainbridge Island, Washington 98109, United States; Seattle Structural Genomics Center for Infectious Disease (SSGICID), Seattle, Washington 98109, United States

Yves-Marie Boudehen – Centre National de la Recherche Scientifique UMR 9004, Institut de Recherche en Infectiologie de Montpellier (IRIM), Université de Montpellier, 34293 Montpellier, France

Céline Cougoule – Institut de Pharmacologie et de Biologie Structurale (IPBS), Université de Toulouse, CNRS, 31400 Toulouse, France

Thomas E. Edwards – UCB BioSciences, Bainbridge Island, Washington 98109, United States; Seattle Structural Genomics Center for Infectious Disease (SSGICID), Seattle, Washington 98109, United States; [orcid.org/0000-0002-0474-8003](https://orcid.org/0000-0002-0474-8003)

Complete contact information is available at: <https://pubs.acs.org/doi/10.1021/acsinfecdis.2c00314>

### Notes

The authors declare no competing financial interest.

## ■ ACKNOWLEDGMENTS

This study was supported by the French National Research Agency ANR-19-CE15-0012-01 (SUNLIVE). We acknowledge the Ministère de l'Enseignement Supérieur, de la Recherche et de l'Innovation for funding the PhD of MA. This work was supported by the National Institutes of Health/National Institute of Allergy and Infectious Diseases (Contract No. HHSN272201700059C) to Peter J. Myler (PI for SSGICID). CC and SALI were funded by grants from "Vaincre La Mucoviscidose" and "Grégory Lemarchal" foundations (No. RF20210502852/1/1/48). We would like to thank A. Speer for the generous gift of pSMT3-*katG*<sub>MTB</sub>-*tdTomato*.

## ■ REFERENCES

- (1) Cowman, S.; van Ingen, J.; Griffith, D. E.; Loebinger, M. R. Non-Tuberculous Mycobacterial Pulmonary Disease. *Eur. Respir. J.* **2019**, *54* (1), 1900250.
- (2) Jönsson, B. E.; Gilljam, M.; Lindblad, A.; Ridell, M.; Wold, A. E.; Welinder-Olsson, C. Molecular Epidemiology of *Mycobacterium*

- abscessus*, with Focus on Cystic Fibrosis. *J. Clin. Microbiol.* **2007**, *45* (5), 1497–1504.
- (3) Esther, C. R.; Esserman, D. A.; Gilligan, P.; Kerr, A.; Noone, P. G. Chronic *Mycobacterium abscessus* Infection and Lung Function Decline in Cystic Fibrosis. *J. Cyst. Fibros.* **2010**, *9* (2), 117–123.
- (4) Catherinot, E.; Roux, A.-L.; Macheras, E.; Hubert, D.; Matmar, M.; Dannhoffer, L.; Chinet, T.; Morand, P.; Poyart, C.; Heym, B.; Rottman, M.; Gaillard, J.-L.; Herrmann, J.-L. Acute Respiratory Failure Involving an R Variant of *Mycobacterium abscessus*. *J. Clin. Microbiol.* **2009**, *47* (1), 271–274.
- (5) Koh, W.-J.; Jeon, K.; Lee, N. Y.; Kim, B.-J.; Kook, Y.-H.; Lee, S.-H.; Park, Y. K.; Kim, C. K.; Shin, S. J.; Huitt, G. A.; Daley, C. L.; Kwon, O. J. Clinical Significance of Differentiation of *Mycobacterium massiliense* from *Mycobacterium abscessus*. *Am. J. Respir. Crit. Care Med.* **2011**, *183* (3), 405–410.
- (6) Adekambi, T.; Sassi, M.; van Ingen, J.; Drancourt, M. Reinstating *Mycobacterium massiliense* and *Mycobacterium bolletii* as Species of the *Mycobacterium abscessus* Complex. *Int. J. Syst. Evol. Microbiol.* **2017**, *67* (8), 2726–2730.
- (7) Johansen, M. D.; Herrmann, J.-L.; Kremer, L. Non-Tuberculous Mycobacteria and the Rise of *Mycobacterium abscessus*. *Nat. Rev. Microbiol.* **2020**, *18* (7), 392–407.
- (8) Howard, S. T.; Rhoades, E.; Recht, J.; Pang, X.; Alsop, A.; Kolter, R.; Lyons, C. R.; Byrd, T. F. Spontaneous Reversion of *Mycobacterium abscessus* from a Smooth to a Rough Morphotype Is Associated with Reduced Expression of Glycopeptidolipid and Reacquisition of an Invasive Phenotype. *Microbiology (Reading, Engl.)* **2006**, *152* (6), 1581–1590.
- (9) Gutiérrez, A. V.; Viljoen, A.; Ghigo, E.; Herrmann, J.-L.; Kremer, L. Glycopeptidolipids, a Double-Edged Sword of the *Mycobacterium abscessus* Complex. *Front. Microbiol.* **2018**, *9*, 1145.
- (10) Roux, A.-L.; Viljoen, A.; Bah, A.; Simeone, R.; Bernut, A.; Laencina, L.; Deramaut, T.; Rottman, M.; Gaillard, J.-L.; Majlessi, L.; Brosch, R.; Girard-Misguich, F.; Vergne, I.; de Chastellier, C.; Kremer, L.; Herrmann, J.-L. The Distinct Fate of Smooth and Rough *Mycobacterium abscessus* Variants inside Macrophages. *Open Biol.* **2016**, *6* (11), 160185.
- (11) Bernut, A.; Viljoen, A.; Dupont, C.; Sapriel, G.; Blaise, M.; Bouchier, C.; Brosch, R.; de Chastellier, C.; Herrmann, J.-L.; Kremer, L. Insights into the Smooth-to-Rough Transitioning in *Mycobacterium bolletii* Unravels a Functional Tyr Residue Conserved in All Mycobacterial MmpL Family Members. *Mol. Microbiol.* **2016**, *99* (5), 866–883.
- (12) Sánchez-Chardi, A.; Olivares, F.; Byrd, T. F.; Julián, E.; Brambilla, C.; Luquin, M. Demonstration of Cord Formation by Rough *Mycobacterium abscessus* Variants: Implications for the Clinical Microbiology Laboratory. *J. Clin. Microbiol.* **2011**, *49* (6), 2293–2295.
- (13) Nessar, R.; Reyrat, J.-M.; Davidson, L. B.; Byrd, T. F. Deletion of the *MmpL4b* Gene in the *Mycobacterium abscessus* Glycopeptidolipid Biosynthetic Pathway Results in Loss of Surface Colonization Capability, but Enhanced Ability to Replicate in Human Macrophages and Stimulate Their Innate Immune Response. *Microbiology (Reading, Engl.)* **2011**, *157* (4), 1187–1195.
- (14) Bernut, A.; Herrmann, J.-L.; Kissa, K.; Dubremetz, J.-F.; Gaillard, J.-L.; Lutfalla, G.; Kremer, L. *Mycobacterium abscessus* Cording Prevents Phagocytosis and Promotes Abscess Formation. *Proc. Natl. Acad. Sci. U.S.A.* **2014**, *111* (10), E943–952.
- (15) Madani, A.; Ridenour, J. N.; Martin, B. P.; Paudel, R. R.; Abdul Basir, A.; Le Moigne, V.; Herrmann, J.-L.; Audebert, S.; Camoin, L.; Kremer, L.; Spilling, C. D.; Cnaan, S.; Cavalier, J.-F. Cyclosporins and Cyclophostin Analogues as Multitarget Inhibitors That Impair Growth of *Mycobacterium abscessus*. *ACS Infect. Dis.* **2019**, *5* (9), 1597–1608.
- (16) Lavollay, M.; Dubée, V.; Heym, B.; Herrmann, J.-L.; Gaillard, J.-L.; Gutmann, L.; Arthur, M.; Mainardi, J.-L. *In Vitro* Activity of Cefoxitin and Imipenem against *Mycobacterium abscessus* Complex. *Clin. Microbiol. Infect.* **2014**, *20* (5), O297–O300.
- (17) Nessar, R.; Cambau, E.; Reyrat, J. M.; Murray, A.; Gicquel, B. *Mycobacterium abscessus*: A New Antibiotic Nightmare. *J. Antimicrob. Chemother.* **2012**, *67* (4), 810–818.
- (18) van Ingen, J.; Boeree, M. J.; van Soolingen, D.; Mouton, J. W. Resistance Mechanisms and Drug Susceptibility Testing of Nontuberculous Mycobacteria. *Drug Resist. Updat.* **2012**, *15* (3), 149–161.
- (19) Brown-Elliott, B. A.; Nash, K. A.; Wallace, R. J. Antimicrobial Susceptibility Testing, Drug Resistance Mechanisms, and Therapy of Infections with Nontuberculous Mycobacteria. *Clin. Microbiol. Rev.* **2012**, *25* (3), 545–582.
- (20) Lopeman, R.; Harrison, J.; Desai, M.; Cox, J. *Mycobacterium abscessus*: Environmental Bacterium Turned Clinical Nightmare. *Microorganisms* **2019**, *7* (3), 90.
- (21) Griffith, D. E.; Aksamit, T.; Brown-Elliott, B. A.; Catanzaro, A.; Daley, C.; Gordin, F.; Holland, S. M.; Horsburgh, R.; Huitt, G.; Iademarco, M. F.; Iseman, M.; Olivier, K.; Ruoss, S.; von Reyn, C. F.; Wallace, R. J.; Winthrop, K. ATS Mycobacterial Diseases Subcommittee; American Thoracic Society; Infectious Disease Society of America. An Official ATS/IDSA Statement: Diagnosis, Treatment, and Prevention of Nontuberculous Mycobacterial Diseases. *Am. J. Respir. Crit. Care Med.* **2007**, *175* (4), 367–416.
- (22) Floto, R. A.; Olivier, K. N.; Saiman, L.; Daley, C. L.; Herrmann, J.-L.; Nick, J. A.; Noone, P. G.; Bilton, D.; Corris, P.; Gibson, R. L.; Hempstead, S. E.; Koetz, K.; Sadoski, K. A.; Sermet-Gaudelus, I.; Smyth, A. R.; van Ingen, J.; Wallace, R. J.; Winthrop, K. L.; Marshall, B. C.; Haworth, C. S. US Cystic Fibrosis Foundation and European Cystic Fibrosis Society Consensus Recommendations for the Management of Non-Tuberculous Mycobacteria in Individuals with Cystic Fibrosis: Executive Summary. *Thorax* **2016**, *71* (1), 88–90.
- (23) Daley, C. L.; Iaccarino, J. M.; Lange, C.; Cambau, E.; Wallace, R. J.; Andrejak, C.; Böttger, E. C.; Brozek, J.; Griffith, D. E.; Guglielmetti, L.; Huitt, G. A.; Knight, S. L.; Leitman, P.; Marras, T. K.; Olivier, K. N.; Santin, M.; Stout, J. E.; Tortoli, E.; van Ingen, J.; Wagner, D.; Winthrop, K. L. Treatment of Nontuberculous Mycobacterial Pulmonary Disease: An Official ATS/ERS/ESCMID/IDSA Clinical Practice Guideline. *Eur. Respir. J.* **2020**, *56* (1), 2000535.
- (24) Wallace, R. J.; Dukart, G.; Brown-Elliott, B. A.; Griffith, D. E.; Scerpella, E. G.; Marshall, B. Clinical Experience in 52 Patients with Tigecycline-Containing Regimens for Salvage Treatment of *Mycobacterium abscessus* and *Mycobacterium chelonae* Infections. *J. Antimicrob. Chemother.* **2014**, *69* (7), 1945–1953.
- (25) Roux, A.-L.; Catherinot, E.; Soismier, N.; Heym, B.; Bellis, G.; Lemonnier, L.; Chiron, R.; Fauroux, B.; Le Bourgeois, M.; Munck, A.; Pin, I.; Sermet, I.; Gutierrez, C.; Véziris, N.; Jarlier, V.; Cambau, E.; Herrmann, J.-L.; Guillemot, D.; Gaillard, J.-L. OMA group. Comparing *Mycobacterium massiliense* and *Mycobacterium abscessus* Lung Infections in Cystic Fibrosis Patients. *J. Cyst. Fibros.* **2015**, *14* (1), 63–69.
- (26) Wu, M.-L.; Aziz, D. B.; Dartois, V.; Dick, T. NTM Drug Discovery: Status, Gaps and the Way Forward. *Drug Discovery Today* **2018**, *23* (8), 1502–1519.
- (27) Dupont, C.; Viljoen, A.; Dubar, F.; Blaise, M.; Bernut, A.; Pawlik, A.; Bouchier, C.; Brosch, R.; Guérardel, Y.; Lelièvre, J.; Ballél, L.; Herrmann, J.-L.; Biot, C.; Kremer, L. A New Piperidinol Derivative Targeting Mycolic Acid Transport in *Mycobacterium abscessus*. *Mol. Microbiol.* **2016**, *101* (3), 515–529.
- (28) Luthra, S.; Rominski, A.; Sander, P. The Role of Antibiotic-Target-Modifying and Antibiotic-Modifying Enzymes in *Mycobacterium abscessus* Drug Resistance. *Front. Microbiol.* **2018**, DOI: 10.3389/fmicb.2018.02179.
- (29) Gagliardi, A.; Selchow, P.; Luthra, S.; Schäfle, D.; Schulthess, B.; Sander, P. KatG as Counterselection Marker for Nontuberculous Mycobacteria. *Antimicrob. Agents Chemother.* **2020**, *64* (5), No. e02508-19.
- (30) Johnsson, K.; Froland, W. A.; Schultz, P. G. Overexpression, Purification, and Characterization of the Catalase-Peroxidase KatG



- from *Mycobacterium tuberculosis*. *J. Biol. Chem.* **1997**, *272* (5), 2834–2840.
- (31) Zhang, Y.; Heym, B.; Allen, B.; Young, D.; Cole, S. The Catalase-Peroxidase Gene and Isoniazid Resistance of *Mycobacterium tuberculosis*. *Nature* **1992**, *358* (6387), 591–593.
- (32) Rozwarski, D. A.; Grant, G. A.; Barton, D. H.; Jacobs, W. R.; Sacchettini, J. C. Modification of the NADH of the Isoniazid Target (InhA) from *Mycobacterium tuberculosis*. *Science* **1998**, *279* (5347), 98–102.
- (33) Wilming, M.; Johnsson, K. Spontaneous Formation of the Bioactive Form of the Tuberculosis Drug Isoniazid. *Angew. Chem., Int. Ed. Engl.* **1999**, *38* (17), 2588–2590.
- (34) Rawat, R.; Whitty, A.; Tonge, P. J. The Isoniazid-NAD Adduct Is a Slow, Tight-Binding Inhibitor of InhA, the *Mycobacterium tuberculosis* Enoyl Reductase: Adduct Affinity and Drug Resistance. *Proc. Natl. Acad. Sci. U.S.A.* **2003**, *100* (24), 13881–13886.
- (35) Banerjee, A.; Dubnau, E.; Quemard, A.; Balasubramanian, V.; Um, K. S.; Wilson, T.; Collins, D.; de Lisle, G.; Jacobs, W. R. *InhA*, a Gene Encoding a Target for Isoniazid and Ethionamide in *Mycobacterium tuberculosis*. *Science* **1994**, *263* (5144), 227–230.
- (36) Vilchèze, C.; Wang, F.; Arai, M.; Hazbón, M. H.; Colangeli, R.; Kremer, L.; Weisbrod, T. R.; Alland, D.; Sacchettini, J. C.; Jacobs, W. R. Transfer of a Point Mutation in *Mycobacterium tuberculosis inhA* Resolves the Target of Isoniazid. *Nat. Med.* **2006**, *12* (9), 1027–1029.
- (37) Nguyen, M.; Quémard, A.; Broussy, S.; Bernadou, J.; Meunier, B. Mn(III) Pyrophosphate as an Efficient Tool for Studying the Mode of Action of Isoniazid on the InhA Protein of *Mycobacterium tuberculosis*. *Antimicrob. Agents Chemother.* **2002**, *46* (7), 2137–2144.
- (38) Bhatt, A.; Molle, V.; Besra, G. S.; Jacobs, W. R.; Kremer, L. The *Mycobacterium tuberculosis* FAS-II Condensing Enzymes: Their Role in Mycolic Acid Biosynthesis, Acid-Fastness, Pathogenesis and in Future Drug Development. *Mol. Microbiol.* **2007**, *64* (6), 1442–1454.
- (39) Vilchèze, C.; Morbidoni, H. R.; Weisbrod, T. R.; Iwamoto, H.; Kuo, M.; Sacchettini, J. C.; Jacobs, W. R. Inactivation of the *inhA*-Encoded Fatty Acid Synthase II (FASII) Enoyl-Acyl Carrier Protein Reductase Induces Accumulation of the FASI End Products and Cell Lysis of *Mycobacterium smegmatis*. *J. Bacteriol.* **2000**, *182* (14), 4059–4067.
- (40) Manjunatha, U. H. S.; Rao, S. P.; Kondreddi, R. R.; Noble, C. G.; Camacho, L. R.; Tan, B. H.; Ng, S. H.; Ng, P. S.; Ma, N. L.; Lakshminarayana, S. B.; Herve, M.; Barnes, S. W.; Yu, W.; Kuhlen, K.; Blasco, F.; Beer, D.; Walker, J. R.; Tonge, P. J.; Glynn, R.; Smith, P. W.; Diagan, T. T. Direct Inhibitors of InhA Are Active against *Mycobacterium tuberculosis*. *Sci. Transl. Med.* **2015**, *7* (269), 269ra3–269ra3.
- (41) Johansen, M. D.; Daher, W.; Roquet-Banères, F.; Raynaud, C.; Alcaraz, M.; Maurer, F. P.; Kremer, L. Rifabutin Is Bactericidal against Intracellular and Extracellular Forms of *Mycobacterium abscessus*. *Antimicrob. Agents Chemother.* **2020**, *64* (11), No. e00363-20.
- (42) Kirchner, S.; Fothergill, J. L.; Wright, E. A.; James, C. E.; Mowat, E.; Winstanley, C. Use of Artificial Sputum Medium to Test Antibiotic Efficacy Against *Pseudomonas aeruginosa* in Conditions More Relevant to the Cystic Fibrosis Lung. *J. Visualized Exp.* **2012**, No. 64, 3857.
- (43) Lefebvre, A.-L.; Dubée, V.; Cortes, M.; Dorchène, D.; Arthur, M.; Mainardi, J.-L. Bactericidal and Intracellular Activity of  $\beta$ -Lactams against *Mycobacterium abscessus*. *J. Antimicrob. Chemother.* **2016**, *71* (6), 1556–1563.
- (44) Iakobachvili, N.; Leon-Icaza, S. A.; Knoops, K.; Sachs, N.; Mazères, S.; Simeone, R.; Peixoto, A.; Bernard, C.; Murriss-Espin, M.; Mazières, J.; Cam, K.; Chalut, C.; Guilhot, C.; López-Iglesias, C.; Ravelli, R. B. G.; Neyrolles, O.; Meunier, E.; Lugo-Villarino, G.; Clevers, H.; Cougoule, C.; Peters, P. J. Mycobacteria-Host Interactions in Human Bronchiolar Airway Organoids. *Mol. Microbiol.* **2022**, *117* (3), 682–692.
- (45) Leon-Icaza, S. A.; Bagayoko, S.; Iakobachvili, N.; Ferrand, C.; Aydogan, T.; Bernard, C.; Dafun, A. S.; Murriss-Espin, M.; Mazières, J.; Bordignon, P. J.; Mazères, S.; Bernes-Lasserre, P.; Ramé, V.; Lagarde, J.-M.; Marcoux, J.; Bousquet, M. P.; Chalut, C.; Guilhot, C.; Clevers, H.; Peters, P. J.; Molle, V.; Lugo-Villarino, G.; Cam, K.; Berry, L.; Meunier, E.; Cougoule, C. Cystic Fibrosis Patient-Derived Bronchial Organoids Unveil Druggable Pathways against *Mycobacterium abscessus* Infection. *bioRxiv*, January 3, 2022. DOI: 10.1101/2022.01.03.474765.
- (46) Kremer, L.; Dover, L. G.; Morbidoni, H. R.; Vilchèze, C.; Maughan, W. N.; Baulard, A.; Tu, S.-C.; Honoré, N.; Deretic, V.; Sacchettini, J. C.; Loch, C.; Jacobs, W. R.; Besra, G. S. Inhibition of InhA Activity, but Not KasA Activity, Induces Formation of a KasA-Containing Complex in Mycobacteria. *J. Biol. Chem.* **2003**, *278* (23), 20547–20554.
- (47) Halloum, I.; Carrère-Kremer, S.; Blaise, M.; Viljoen, A.; Bernut, A.; Le Moigne, V.; Vilchèze, C.; Guérardel, Y.; Lutfalla, G.; Herrmann, J.-L.; Jacobs, W. R.; Kremer, L. Deletion of a Dehydratase Important for Intracellular Growth and Cording Renders Rough *Mycobacterium abscessus* Avirulent. *Proc. Natl. Acad. Sci. U.S.A.* **2016**, *113* (29), E4228–4237.
- (48) Dover, L. G.; Alahari, A.; Grattraud, P.; Gomes, J. M.; Bhowruth, V.; Reynolds, R. C.; Besra, G. S.; Kremer, L. EthA, a Common Activator of Thiocarbamide-Containing Drugs Acting on Different Mycobacterial Targets. *Antimicrob. Agents Chemother.* **2007**, *51* (3), 1055–1063.
- (49) Rozwarski, D. A.; Vilchèze, C.; Sugantino, M.; Bittman, R.; Sacchettini, J. C. Crystal Structure of the *Mycobacterium tuberculosis* Enoyl-ACP Reductase, InhA, in Complex with NAD<sup>+</sup> and a C16 Fatty Acyl Substrate. *J. Biol. Chem.* **1999**, *274* (22), 15582–15589.
- (50) Kuo, M. R.; Morbidoni, H. R.; Alland, D.; Sneddon, S. F.; Gourlie, B. B.; Staveski, M. M.; Leonard, M.; Gregory, J. S.; Janjigian, A. D.; Yee, C.; Musser, J. M.; Kreiswirth, B.; Iwamoto, H.; Perozzo, R.; Jacobs, W. R.; Sacchettini, J. C.; Fidock, D. A. Targeting Tuberculosis and Malaria through Inhibition of Enoyl Reductase: Compound Activity and Structural Data. *J. Biol. Chem.* **2003**, *278* (23), 20851–20859.
- (51) Grzegorzewicz, A. E.; Eynard, N.; Quémard, A.; North, E. J.; Margolis, A.; Lindenberger, J. J.; Jones, V.; Korduláková, J.; Brennan, P. J.; Lee, R. E.; Ronning, D. R.; McNeil, M. R.; Jackson, M. Covalent Modification of the *Mycobacterium tuberculosis* FAS-II Dehydratase by Isoxyl and Thiacetazone. *ACS Infect. Dis.* **2015**, *1* (2), 91–97.
- (52) Halloum, I.; Viljoen, A.; Khanna, V.; Craig, D.; Bouchier, C.; Brosch, R.; Coxon, G.; Kremer, L. Resistance to Thiacetazone Derivatives Active against *Mycobacterium abscessus* Involves Mutations in the MmpL5 Transcriptional Repressor MAB\_4384. *Antimicrob. Agents Chemother.* **2017**, *61* (4), No. e02509-16.
- (53) Kozikowski, A. P.; Onajole, O. K.; Stec, J.; Dupont, C.; Viljoen, A.; Richard, M.; Chaira, T.; Lun, S.; Bishai, W.; Raj, V. S.; Ordway, D.; Kremer, L. Targeting Mycolic Acid Transport by Indole-2-Carboxamides for the Treatment of *Mycobacterium abscessus* Infections. *J. Med. Chem.* **2017**, *60* (13), 5876–5888.
- (54) Raynaud, C.; Daher, W.; Johansen, M. D.; Roquet-Banères, F.; Blaise, M.; Onajole, O. K.; Kozikowski, A. P.; Herrmann, J.-L.; Dziadek, J.; Gobis, K.; Kremer, L. Active Benzimidazole Derivatives Targeting the MmpL3 Transporter in *Mycobacterium abscessus*. *ACS Infect. Dis.* **2020**, *6* (2), 324–337.
- (55) Dick, T. Rifabutin: A Repurposing Candidate for *Mycobacterium abscessus* Lung Disease. *Front. Microbiol.* **2020**, *11*, 371.
- (56) McNeil, M. B.; Dennison, D.; Shelton, C.; Flint, L.; Korkegian, A.; Parish, T. Mechanisms of Resistance against NITD-916, a Direct Inhibitor of *Mycobacterium tuberculosis* InhA. *Tuberculosis (Edinb)* **2017**, *107*, 133–136.
- (57) Prasad, M. S.; Bhole, R. P.; Khedekar, P. B.; Chikhale, R. V. *Mycobacterium* Enoyl Acyl Carrier Protein Reductase (InhA): A Key Target for Antitubercular Drug Discovery. *Bioorg. Chem.* **2021**, *115*, 105242.
- (58) Singh, S.; Bouzinbi, N.; Chaturvedi, V.; Godreuil, S.; Kremer, L. *In Vitro* Evaluation of a New Drug Combination against Clinical Isolates Belonging to the *Mycobacterium abscessus* Complex. *Clin. Microbiol. Infect.* **2014**, *20* (12), O1124–1127.
- (59) Ho, V. Q. T.; Verboom, T.; Rong, M. K.; Habjan, E.; Bitter, W.; Speer, A. Heterologous Expression of EthA and KatG in

*Mycobacterium marinum* Enables the Rapid Identification of New Prodrugs Active against *Mycobacterium tuberculosis*. *Antimicrob. Agents Chemother.* **2021**, *65* (4), No. e01445-20.

(60) Woods, G. L.; Brown-Elliott, B. A.; Conville, P. S.; Desmond, E. P.; Hall, G. S.; Lin, G.; Pfyffer, G. E.; Ridderhof, J. C.; Siddiqi, S. H.; Wallace, R. J. *Susceptibility Testing of Mycobacteria, Nocardiae and Other Aerobic Actinomycetes: Approved Standard*, 2nd ed. (M24-A2); Clinical and Laboratory Standards Institute: Wayne, PA, 2011.

(61) Stover, C. K.; de la Cruz, V. F.; Fuerst, T. R.; Burlein, J. E.; Benson, L. A.; Bennett, L. T.; Bansal, G. P.; Young, J. F.; Lee, M. H.; Hatfull, G. F.; et al. New Use of BCG for Recombinant Vaccines. *Nature* **1991**, *351* (6326), 456–460.

(62) Viljoen, A.; Richard, M.; Nguyen, P. C.; Fourquet, P.; Camoin, L.; Paudal, R. R.; Gnawali, G. R.; Spilling, C. D.; Cavalier, J.-F.; Canaan, S.; Blaise, M.; Kremer, L. Cyclosporins and Cyclophostin Analogs Inhibit the Antigen 85C from *Mycobacterium tuberculosis* Both *in Vitro* and *in Vivo*. *J. Biol. Chem.* **2018**, *293* (8), 2755–2769.

(63) Bryan, C. M.; Bhandari, J.; Napuli, A. J.; Leibly, D. J.; Choi, R.; Kelley, A.; Van Voorhis, W. C.; Edwards, T. E.; Stewart, L. J. High-Throughput Protein Production and Purification at the Seattle Structural Genomics Center for Infectious Disease. *Acta Crystallogr. Sect. F Struct. Biol. Cryst. Commun.* **2011**, *67* (9), 1010–1014.

(64) Choi, R.; Kelley, A.; Leibly, D.; Hewitt, S. N.; Napuli, A.; Van Voorhis, W. Immobilized Metal-Affinity Chromatography Protein-Recovery Screening Is Predictive of Crystallographic Structure Success. *Acta Crystallogr. Sect. F Struct. Biol. Cryst. Commun.* **2011**, *67* (9), 998–1005.

(65) Adams, P. D.; Afonine, P. V.; Bunkóczi, G.; Chen, V. B.; Davis, I. W.; Echols, N.; Headd, J. J.; Hung, L.-W.; Kapral, G. J.; Grosse-Kunstleve, R. W.; McCoy, A. J.; Moriarty, N. W.; Oeffner, R.; Read, R. J.; Richardson, D. C.; Richardson, J. S.; Terwilliger, T. C.; Zwart, P. H. PHENIX: A Comprehensive Python-Based System for Macromolecular Structure Solution. *Acta Crystallogr. D Biol. Crystallogr.* **2010**, *66* (2), 213–221.

(66) Emsley, P.; Cowtan, K. Coot: Model-Building Tools for Molecular Graphics. *Acta Crystallogr. D Biol. Crystallogr.* **2004**, *60* (12), 2126–2132.

(67) Grabowski, M.; Cymborowski, M.; Porebski, P. J.; Osinski, T.; Shabalin, I. G.; Cooper, D. R.; Minor, W. The Integrated Resource for Reproducibility in Macromolecular Crystallography: Experiences of the First Four Years. *Struct. Dyn.* **2019**, *6* (6), 064301.

## Recommended by ACS

### Design and Synthesis of Covalent Inhibitors of FabA

James S. Martin, Ian H. Gilbert, *et al.*

MARCH 27, 2023  
ACS OMEGA

READ 

### Structure of the d-Cycloserine-Resistant Variant D322N of Alanine Racemase from *Mycobacterium tuberculosis*

Cesira de Chiara, Luiz P. S. de Carvalho, *et al.*

MARCH 27, 2023  
ACS BIO & MED CHEM AU

READ 

### Screen for New Antimicrobial Natural Products from the NCI Program for Natural Product Discovery Prefractionated Extract Library

Lucero Martínez-Fructuoso, Barry R. O'Keefe, *et al.*

MAY 10, 2023  
ACS INFECTIOUS DISEASES

READ 

### 1,3-Diarylpyrazolyl-acylsulfonamides Target HadAB/BC Complex in *Mycobacterium tuberculosis*

Vinayak Singh, Sandeep R. Ghorpade, *et al.*

NOVEMBER 03, 2022  
ACS INFECTIOUS DISEASES

READ 

Get More Suggestions >

## SUPPORTING INFORMATION

### Efficacy and mode of action of a direct inhibitor of *Mycobacterium abscessus* InhA

Matthéo Alcaraz<sup>1</sup>, Françoise Roquet-Banères<sup>1</sup>, Stephen Adonai Leon-Icaza<sup>3</sup>, Jan Abendroth<sup>4,5</sup>, Yves-Marie Boudehen<sup>1</sup>, Céline Cougoule<sup>3</sup>, Thomas E. Edwards<sup>4,5</sup>,  
and Laurent Kremer<sup>1,2,#</sup>

<sup>1</sup>Centre National de la Recherche Scientifique UMR 9004, Institut de Recherche en Infectiologie de Montpellier (IRIM), Université de Montpellier, 1919 route de Mende, 34293, Montpellier, France.

<sup>2</sup>INSERM, IRIM, Montpellier, France.

<sup>3</sup>Institut de Pharmacologie et de Biologie Structurale (IPBS), Université de Toulouse, CNRS, Toulouse, France.

<sup>4</sup>UCB BioSciences, Bainbridge Island, WA 98109 USA

<sup>5</sup>Seattle Structural Genomics Center for Infectious Disease (SSGCID), Seattle, WA 98109 USA

#To whom correspondence should be addressed:

Tel: (+33) 4 34 35 94 47; E-mail: [laurent.kremer@irim.cnrs.fr](mailto:laurent.kremer@irim.cnrs.fr)

**Running title:** Efficacy of NITD-916 against *M. abscessus*

**Table S1.** MIC of ethionamide and NID-916 against *M. abscessus* in different media.

**Table S2.** Activity of INH, NITD-916 and the quinoline-INH hybrid **16g** against *M. abscessus* strains overexpressing KatG<sub>MTB</sub>.

**Table S3.** Crystallographic data collection and refinement statistics.

**Table S4.** Differential scanning fluorimetry (DSF) measurements on InhA<sub>MAB</sub>.

**Table S5.** Interactions between NITD-916 and other antibiotics using the checkerboard assay.

**Figure S1.** Cytotoxicity assay of NITD-916, isoniazid (INH) and rifabutin (RFB) on THP-1 cells.

**Figure S2.** Percentage of THP-1 macrophages at 0, 1 and 3 days post-infection with *M. abscessus* S in the presence or absence of NITD-916.

**Figure S3.** Differential scanning fluorimetry (DSF) thermal shift analysis of InhA<sub>MAB</sub>.

**Figure S4.** Multiple sequence alignments of the InhA proteins.

**Table S1.** MIC (in  $\mu\text{g/mL}$ ) of ethionamide (ETH) and NID-916 determined in CaMHB, Middlebrook 7H9, Sauton's medium and ASM against wild-type *M. abscessus* CIP104536<sup>T</sup> and against strain NITD916<sup>R2</sup>. Results were completed in triplicate in at least two independent experiments.

Strain	CaMHB		7H9 + OADC		Sauton		ASM	
	ETH	NITD-916	ETH	NITD-916	ETH	NITD-916	ETH	NITD-916
CIP104536 <sup>T</sup> (S)	25	1.56	12.5	6.25	6.25	0.195	25	0.78
NITD916 <sup>R2</sup> (S)	25	>200	12.5	>200	6.25	>200	25	>100

**Table S2.** Activity of INH, NITD-916 and the quinoline-INH hybrid **16g**<sup>1</sup> against *M. abscessus* strains overexpressing KatG<sub>MTB</sub>. MIC (µg/mL) were determined in CaMHB at 30 °C. Results were confirmed in two separate experiments.

Strain	MIC (µg/mL)		
	INH	NITD-916	16g
CIP104536 <sup>T</sup> (S)	> 1000	1.56	> 200
CIP104536 <sup>T</sup> (S) + pSMT3- <i>katG</i> <sub>MTB</sub> - <i>tdTomato</i>	62.5	1.56	100
CIP104536 <sup>T</sup> (R)	> 1000	1.56	> 200
CIP104536 <sup>T</sup> (R) + pSMT3- <i>katG</i> <sub>MTB</sub> - <i>tdTomato</i>	62.5	1.56	100

- (1) Alcaraz, M.; Sharma, B.; Roquet-Banères, F.; Conde, C.; Cochard, T.; Biet, F.; Kumar, V.; Kremer, L. Designing Quinoline-Isoniazid Hybrids as Potent Anti-Tubercular Agents Inhibiting Mycolic Acid Biosynthesis. *Eur J Med Chem* **2022**, *239*, 114531. <https://doi.org/10.1016/j.ejmech.2022.114531>.

**Table S3.** Crystallographic data collection and refinement statistics.

<b>Data collection and processing</b>	<b>InhA<sub>MAB</sub> with NITD-916 and NAD</b>
Wavelength (Å)	0.97872
Resolution range (Å)	50 – 1.45
Space group	C2
Unit Cell	78.31, 102.31, 76.82 / 90, 114.65, 90
Total reflections	95,830 (6037)
Multiplicity	3.87 (2.26)
Completeness (%)	98.2 (84.4)
Mean I/sigma(I)	18.13 (4.29)
Wilson B-factor (Å <sup>2</sup> )	11.58
R-merge (%)	4.6 (22.8)
<b>Refinement</b>	<b>InhA<sub>MAB</sub> with NITD-916 and NAD</b>
Number of reflections	93,841
Number of R-free reflections	1989
R-work %	15.05
R-free %	17.87
RMS(bonds)	0.005
RMS(angles)	0.840
Ramachandran plot	
Favored (%)	96.4
Allowed (%)	3.6
Outliers (%)	0
PDB ID	7U0M



**Table S4.** Differential scanning fluorimetry (DSF) measurements on InhA<sub>MAB</sub>.

Sample	Melting Temperature T <sub>m</sub> (°C)					
	Rep1	Rep2	Rep3	Avg	SD	(ΔT <sub>m</sub> )
<b>Apoenzyme</b>	39.5	39.5	39.0	39.3	0.2	--
<b>NAD</b>	40.0	40.0	39.5	39.8	0.2	+0.5
<b>NAD &amp; NITD-916</b>	54.0	54.0	54.0	54.0	0.0	+14.7

**Table S5.** Interactions between NITD-916 and other antibiotics against *M. abscessus* CIP104536<sup>T</sup> (S) and CIP104536<sup>T</sup> (R) were determined using the checkerboard assay in CaMHB and MICs evaluated by REMA (resazurin microtiter assay). Plates were incubated for 4 days at 30 °C, after which 10 µL (10%, vol/vol) of resazurin 0.025% was added to the wells and incubated overnight at 30 °C.

CIP 104536 <sup>T</sup> (S)		Interaction with NITD-916	
Compound	MIC (µg/mL)	FICI score (mean ± SD)	Outcome
IPM	16	0.75 ± 0.21	Indifferent
AMK	50	1.25	Indifferent
RFB	50	1.21 ± 0.07	Indifferent
CFX	64	1.17 ± 0.07	Indifferent
BDQ	0.0625	1.125	Indifferent
CFZ	1	0.917 ± 0.26	Indifferent
EJMCh6	0.125	1.052 ± 0.07	Indifferent
CIP 104536 <sup>T</sup> (R)		Interaction with NITD-916	
Compound	MIC (µg/mL)	FICI score (mean ± SD)	Outcome
IPM	16	0.625	Indifferent
AMK	50	1.25	Indifferent
RFB	12.5	1.17 ± 0.07	Indifferent
CFX	64	0.83 ± 0.07	Indifferent
BDQ	0.0625	1.125	Indifferent
CFZ	1	0.833 ± 0.26	Indifferent
EJMCh6	0.125	1.542 ± 0.44	Indifferent

The Fractional Inhibitory Concentration Index (FICI) was calculated as follows:  $FICI = (MIC \text{ drug A in combination} / MIC \text{ drug A alone}) + (MIC \text{ drug B in combination} / MIC \text{ drug B alone})$ , where drug A was NITD-916 and drug B was imipenem (IPM), amikacin (AMK), rifabutin (RFB), cefoxitin (CFX), bedaquiline (BDQ), clofazimine (CFZ) or EJMCh6 (benzimidazole inhibiting MmpL3). Interaction between the two compounds was defined as synergistic when FICI was  $\leq 0.5$ , indifferent when  $0.5 < FICI \leq 4$ , and antagonistic when FICI was  $> 4$ .

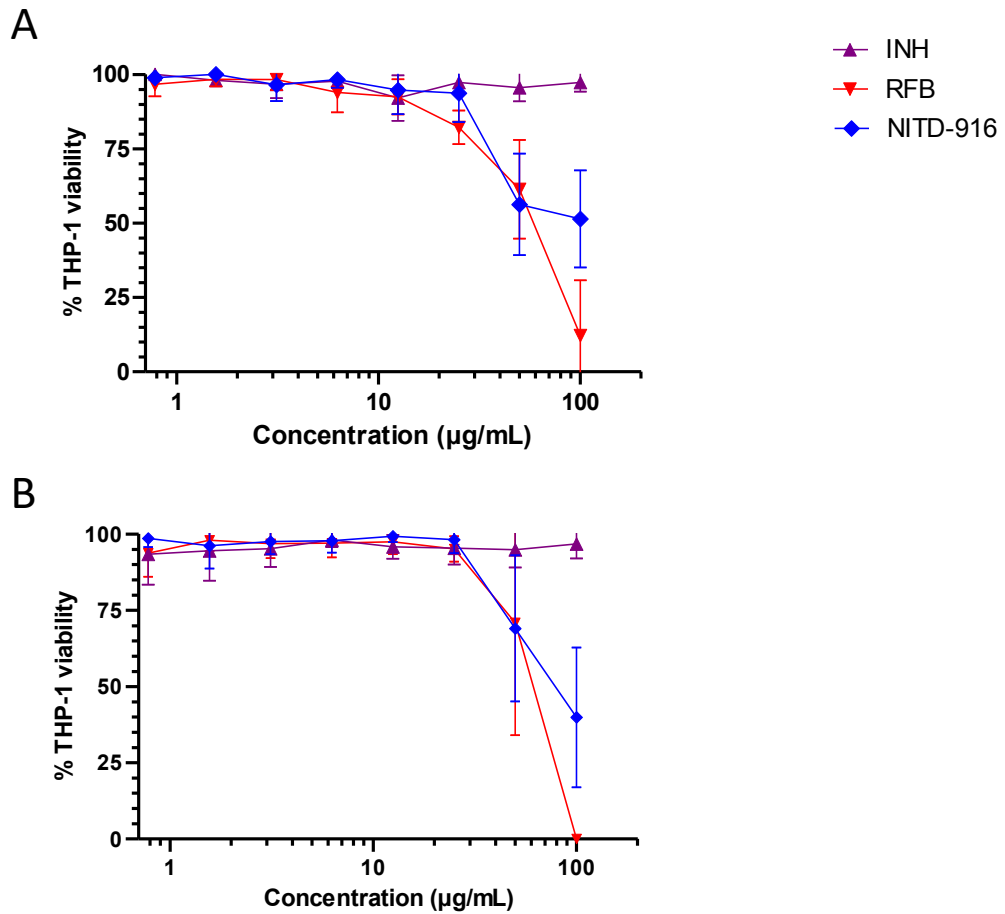


**Figure S1.** Cytotoxicity assay of NITD-916, isoniazid (INH) and rifabutin (RFB) on THP-1 differentiated macrophages. Cells were differentiated with PMA for 48 hrs and exposed to increasing concentration of either NITD-916, INH or RFB (starting at 100 µg/mL) for an additional 24 hrs (**A**) or 72 hrs (**B**) at 37 °C in the presence of 5% CO<sub>2</sub>. Results are the mean of three independent experiments done in duplicates.

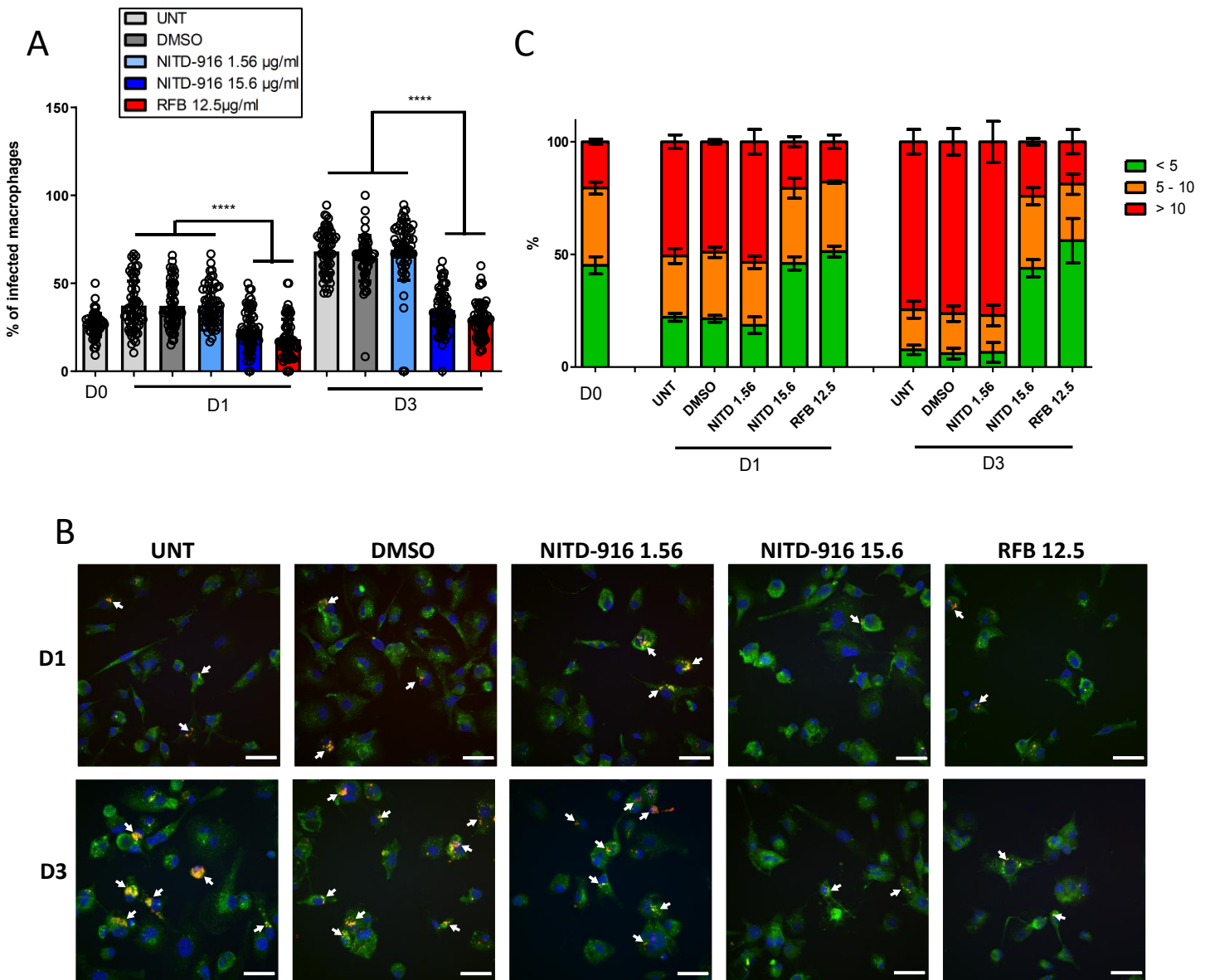


**Figure S2. (A)** Percentage of THP-1 macrophages at 0, 1 and 3 days post-infection with *M. abscessus* CIP104536<sup>T</sup> (S) (MOI of 2:1) in the absence (UNT) of antibiotics or presence of NITD-916 (1.56  $\mu\text{g/ml}$  and 15.6  $\mu\text{g/ml}$ ) or RFB (12.5  $\mu\text{g/ml}$ ). DMSO-exposed cells were included as controls. Results are expressed as mean values  $\pm$  SD for three independent experiments with 30 fields per condition. Data were analyzed using the Mann-Whitney *t* test. \*\*\*\*,  $P \leq 0.0001$ . **(B)** Representative immunofluorescent fields were taken at 1 and 3 days post-infection showing macrophages infected with *M. abscessus* expressing TdTomato (red) in the absence of antibiotics (UNT) or in the presence of NITD-916 (1.56  $\mu\text{g/ml}$  and 15.6  $\mu\text{g/ml}$ ) or RFB (12.5  $\mu\text{g/ml}$ ). DMSO-exposed cells were included as controls. The surface and the endolysosomal system of the macrophages were detected using anti-CD63 antibodies (green). The nuclei were stained with DAPI (blue). White arrows indicate individual or mycobacterial aggregates. Scale bar, 50  $\mu\text{m}$ . **(C)** Percentage of macrophages categories infected with different number of bacilli (<5 bacilli/cell, 5 to 10 bacilli/cell, >10 bacilli/cell). The categories were counted at 0, 1 and 3 days post-infection in the absence of antibiotics or in the presence of NITD-916 (1.56  $\mu\text{g/ml}$  and 15.6  $\mu\text{g/ml}$ ) or RFB (12.5  $\mu\text{g/ml}$ ). Untreated (UNT) or DMSO-exposed cells were included as controls. Data are mean values  $\pm$  SD for three independent experiments.

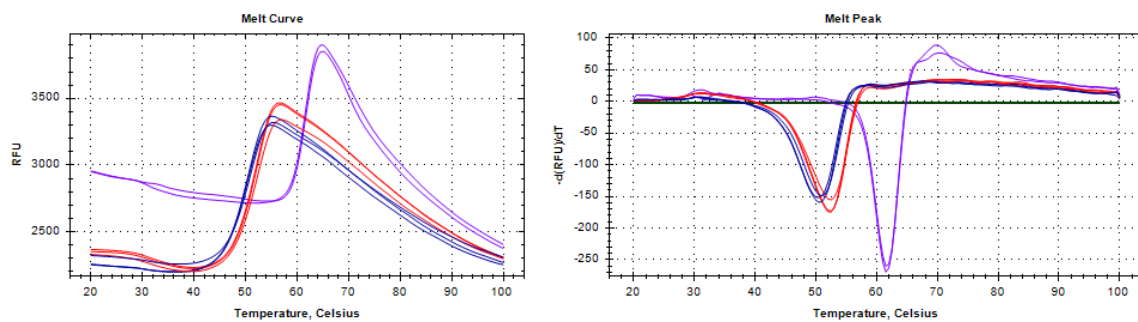


**Figure S3. (A)** Differential scanning fluorimetry (DSF) thermal shift analysis of InhA<sub>MAB</sub> in the apo-enzyme state (blue curves in triplicate), in the presence of NAD (red curves) and NAD & NITD-916 (purple curves). **(B)** First derivative profiles of melting curves.

% ID to InhA_MTB		10	20	30	40	50	60	70	80	90		
InhA_MTB	100%	MTGLLDGKRILVSG	IITDSSIAFH	IARVAQE	QGAQLVLTG	FDRRLIQR	ITDRLPAKAP	LLELDVQNEE	HLASLAGRVTEA	IGAGNKLDG	VVHSGFMPQ	100
InhA_MAB	87.7%	VAGLLEGKRILVSG	IITDSSIAFH	IAKVAQE	GAELVLTG	FDRRLIER	ITQRLPKAP	LLELDVQNEE	HLGSLAGRISEV	IGEGNKLDG	VVHSGFMPQ	100
InhA_MLP	90.3%	MAGLLEGKRILVSG	IITDSSIAFH	IAKVAQE	GAQLVLTG	FDRRLIQR	IADRLPKAP	LLELDVQNEE	HLATLAERVTAE	IGEGNKLDG	VVHSGFMPQ	100
InhA_MBOV	100%	MTGLLDGKRILVSG	IITDSSIAFH	IARVAQE	QGAQLVLTG	FDRRLIQR	ITDRLPAKAP	LLELDVQNEE	HLASLAGRVTEA	IGAGNKLDG	VVHSGFMPQ	100
InhA_MMAR	92.9%	MAGLLEGKRILVSG	IITDSSIAFH	IARVAQE	GAQLVLTG	FDRMLIQR	IVDRLPKAP	LLELDVQNEE	HLASLAGRVTEV	IGEGNKLDG	VVHSGFMPQ	100
InhA_MAC	89.6%	MAGLLEGKRILVSG	IITDSSIAFH	IAKVAQE	GAQLVLTG	FDRRLIQR	IVDRLPEKAP	LLELDVQNEE	HLNTLAQRVTAE	IGEGNKLDG	VVHSGFMPQ	100
InhA_MKAN	95.2%	MAGLLEGKRILVSG	IITDSSIAFH	IARVAQE	GAQLVLTG	FDRRLIQR	ITDRLPKAP	LLELDVQNEE	HLATLADRVEA	IGAGNKLDG	VVHSGFMPQ	100

	110	120	130	140	150	160	170	180	190					
InhA_MTB	TGMGINPFFDAPY	ADVSKG	IHSAYS	ASMAKALLP	IMNPGGS	IVGMDFDPS	SRAMPAYN	WMTVAKS	ALLESVNR	FVAREAGKY	GVRSNL	VAAAGPI	RTLAMS	200
InhA_MAB	SGMGVNPFFDAPF	ADVSKGF	HISAFS	YSLSLAKAVL	PVMNRGGS	IVGMDFDPT	TRAMPAYN	WMTVAKS	ALLESVNR	FVAREAGKY	GVRSNL	VAAAGPI	RTLAMS	200
InhA_MLP	TGMGTNQFFDAPY	EDVSKGI	HISTYS	ASLAKALLL	IMNSGGS	IVGMDFDPT	TRAMPAYN	WMTVAKS	ALLESVNR	FVAREAGKY	GVRSNL	VAAAGPI	RTLAMS	200
InhA_MBOV	TGMGINPFFDAPY	ADVSKGI	HISAYS	ASMAKALLP	IMNPGGS	IVGMDFDPS	SRAMPAYN	WMTVAKS	ALLESVNR	FVAREAGKY	GVRSNL	VAAAGPI	RTLAMS	200
InhA_MMAR	SGMGINPFFDAPY	EDVSKGI	HISAYS	ASLAKALLP	IMNPGGS	IVGMDFDPT	TRAMPAYN	WMTVAKS	ALLESVNR	FVAREAGKY	GVRSNL	VAAAGPI	RTLAMS	200
InhA_MMAR	TGMGINPFFDAPY	EDVSKGI	HISAYS	ASLAKALLP	IMNPGGS	IVGMDFDPS	SRAMPAYN	WMTVAKS	ALLESVNR	FVAREAGPH	GVRSNL	VAAAGPI	RTLAMA	200
InhA_MKAN	TGMGINPFFDAPY	EDVSKGI	HISAYS	ASMAKALLP	IMNPGGS	IVGMDFDPS	SRAMPAYN	WMTVAKS	ALLESVNR	FVAREAGKY	GVRSNL	VAAAGPI	RTLAMA	200

	210	220	230	240	250	260	269	
InhA_MTB	AVGGALGEE	AGAQLQLLE	EGWDRAP	IGWNMKD	ATPVAKT	VCALLSDWLP	PATTGDI	IYADGGAHTQLL
InhA_MAB	AVGGALGDE	AGQMQLL	EEGWDQ	RAPIGWDM	KDPTPVAKT	VCALLSDWLP	PATTGDI	IFADGGAHTQLL
InhA_MLP	AVGGAFGEE	AGAQMLL	EEGWDQ	RAPIGWNM	KDPTPVAKT	VCALLSEWLP	PATTGSI	IYADGGASTQLL
InhA_MBOV	AVGGALGEE	AGAQLQLL	EEGWDQ	RAPIGWNM	KDPTPVAKT	VCALLSDWLP	PATTGDI	IYADGGAHTQLL
InhA_MMAR	AVGGALGEE	AGAQLQLL	EDGWDQ	RAPVGNM	KDPTPVAKT	VCAVLEWLP	PATTGDI	IFADGGAHTQLL
InhA_MAC	GIVGGVLGDQ	AAEQIRLL	EEGWDQ	RAPIGWNM	KDPTPVAKT	VCALLSDWLP	PATTGTI	IYADGGASTQLL
InhA_MKAN	AVGGALGEE	AGAQLQLL	EEGWDQ	RAPIGWNM	KDPTPVAKT	VCALLSEWLP	PATTGDI	IFADGGAHTQLL

**Figure S4.** Multiple sequence alignments using Clustal Omega and the Jalview software of the InhA proteins from *M. tuberculosis* (MTB), *M. abscessus* (MAB), *M. leprae* (MLP), *M. bovis* (MBOV), *M. marinum* (MMAR), *M. avium* (MAC) and *M. kansasii* (MKAN). The percentage of protein identity relative to InhA<sub>MTB</sub> is indicated in the left margin. The red rectangle indicates the position of the highly conserved Gly96 residue.



**Article 3 : “*In vitro* and *in vivo* efficacy of NITD-916 against *Mycobacterium fortuitum*”,**

Françoise Roquet-Banères\*, [Matthéo Alcaraz\\*](#), Claire Hamela\*, Jan Abendroth, Thomas E. Edwards, et Laurent Kremer. *Antimicrobial Agents and Chemotherapy*, 2023, Vol 67, N° 4, Page 1607-1622, PMID : 36920188, DOI : 10.1128/aac.01607-22.

*M. fortuitum* est l'une des espèces mycobactériennes à croissance rapide les plus retrouvées dans les infections avec *M. abscessus*, notamment chez des patients atteints de mucoviscidose ou avec des pathologies sous-jacentes. Le traitement de ce pathogène reste difficile en clinique en raison de sa résistance accrue aux antibiotiques, à l'instar des autres mycobactéries, ce qui souligne un besoin de développer de nouvelles thérapeutiques.

De par la haute identité entre les protéines InhA de *M. abscessus* et *M. fortuitum* (près de 90%), nous avons ainsi évalué l'activité de l'inhibiteur NITD-916 également sur ce pathogène opportuniste émergent. Ce composé a une très bonne activité *in vitro* contre un panel de souches cliniques à faible concentration, ainsi que dans un modèle macrophagique. De plus, nous avons pu étudier l'efficacité de ce composé dans un modèle d'infection de poisson zèbre. Un traitement de courte durée au NITD-916 permet une protection significative des embryons infectés, corrélée à une baisse de la charge bactérienne et des symptômes associés.


D'un point de vue mécanistique, identiquement à ce que l'on retrouve chez *M. tuberculosis* ou *M. abscessus*, NITD-916 inhibe la synthèse des acides mycoliques chez *M. fortuitum* de manière InhA dépendante. La résolution de la structure cristallographique du complexe InhA:NADH:NITD-916 a permis de confirmer l'inhibition directe de cette enzyme.

Dans l'ensemble, ces travaux valident InhA comme une cible à développer également chez *M. fortuitum* et indiquent que NITD-916 est actif contre ce pathogène ce qui renforce l'idée de devoir le prendre en compte dans de futures évaluations précliniques ainsi que de développer des molécules partageant son mécanisme d'action.





# *In Vitro* and *In Vivo* Efficacy of NITD-916 against *Mycobacterium fortuitum*

Françoise Roquet-Banères,<sup>a</sup> Matthéo Alcaraz,<sup>a</sup> Claire Hamela,<sup>a</sup> Jan Abendroth,<sup>c,d</sup> Thomas E. Edwards,<sup>c,d</sup>  Laurent Kremer<sup>a,b</sup>

<sup>a</sup>Centre National de la Recherche Scientifique UMR 9004, Institut de Recherche en Infectiologie de Montpellier (IRIM), Université de Montpellier, Montpellier, France

<sup>b</sup>INSERM, IRIM, Montpellier, France

<sup>c</sup>UCB BioSciences, Bainbridge Island, Washington, USA

<sup>d</sup>Seattle Structural Genomics Center for Infectious Disease (SSGCID), Seattle, Washington, USA

Françoise Roquet-Banères, Matthéo Alcaraz, and Claire Hamela contributed equally to this work. Author order was determined by doing experiments, analyzing the data and participating in writing the manuscript.

**ABSTRACT** *Mycobacterium fortuitum* represents one of the most clinically relevant rapid-growing mycobacterial species. Treatments are complex due to antibiotic resistance and to severe side effects of effective drugs, prolonged time of treatment, and co-infection with other pathogens. Herein, we explored the activity of NITD-916, a direct inhibitor of the enoyl-ACP reductase InhA of the type II fatty acid synthase in *Mycobacterium tuberculosis*. We found that this compound displayed very low MIC values against a panel of *M. fortuitum* clinical strains and exerted potent antimicrobial activity against *M. fortuitum* in macrophages. Remarkably, the compound was also highly efficacious in a zebrafish model of infection. Short duration treatments were sufficient to significantly protect the infected larvae from *M. fortuitum*-induced killing, which correlated with reduced bacterial burdens and abscesses. Biochemical analyses demonstrated an inhibition of *de novo* synthesis of mycolic acids. Resolving the crystal structure of the InhA<sub>MFO</sub> in complex with NAD and NITD-916 confirmed that NITD-916 is a direct inhibitor of InhA<sub>MFO</sub>. Importantly, single nucleotide polymorphism leading to a G96S substitution in InhA<sub>MFO</sub> conferred high resistance levels to NITD-916, thus resolving its target in *M. fortuitum*. Overall, these findings indicate that NITD-916 is highly active against *M. fortuitum* both *in vitro* and *in vivo* and should be considered in future preclinical evaluations for the treatment of *M. fortuitum* pulmonary diseases.

**KEYWORDS** *Mycobacterium fortuitum*, NITD-916, InhA, mycolic acid, macrophage, zebrafish, infection

Infections caused by nontuberculous mycobacteria (NTM) are increasing globally, particularly in countries where the incidence of tuberculosis is declining (1). NTM are environmental microorganisms, capable to induce persistent infections in individuals with an impaired local or systemic immunity. NTM pulmonary diseases represent the most frequently encountered clinical manifestations and can involve slow-growing and rapid-growing mycobacteria (RGM), and has become a public health concern around the world as well as in China (2). *Mycobacterium fortuitum* represents the second most frequent RGM after *M. abscessus* and can sometimes be isolated in cystic fibrosis (CF) patients (3). Several clinical cases have also reported catheter infections, postsurgical infections, peritonitis, eye infections, and pulmonary infections (4, 5). In addition to the lungs (6), *M. fortuitum* can also affect many areas of the body (7), including the skin (8), bones (9), or lymph nodes (10). *M. fortuitum* pulmonary disease occurs predominantly in patients with underlying conditions, such as posttuberculosis changes (11), severe chronic obstructive pulmonary disease (COPD), and cancer (12). It

**Copyright** © 2023 American Society for Microbiology. All Rights Reserved.

Address correspondence to Laurent Kremer, laurent.kremer@irim.cnrs.fr.

The authors declare no conflict of interest.

**Received** 1 December 2022

**Returned for modification** 11 January 2023

**Accepted** 16 February 2023

**Published** 15 March 2023

is generally associated with a poor prognosis and about a third of the affected patients reported in the literature die, despite chemotherapy. The recent established guidelines for *M. fortuitum* pulmonary diseases recommend a combination of two or three drugs (13). Treatment often includes one or two intravenous drugs to be continued for an initial period (4 to 16 weeks)—amikacin and/or imipenem—and at least two oral drugs—a fluoroquinolone (moxifloxacin or levofloxacin), co-trimoxazole, linezolid, clofazimine, doxycycline—should be continued until at least 12 months after conversion to culture negative to complete the treatment regimen. However, there is limited clinical evidence to support these treatment regimens. In addition, *M. fortuitum* infections have been reported with a high prevalence of resistance to several drugs, including macrolides,  $\beta$ -lactams, aminoglycosides and tetracyclines, and also antituberculosis (TB) drugs such as isoniazid (INH), rifampin, ethambutol, clofazimine, ethionamide, and rifabutin (14, 15). *M. fortuitum* is considered resistant to INH because it expresses two unrelated catalase-peroxidases (KatGI and KatGII) that are unlikely able to activate INH efficiently (16), thus highlighting the potential of testing direct inhibitors of InhA to counteract KatG-mediated resistance. The intrinsic resistome potentially responsible for the broad resistance levels to many antibiotic classes has recently been emphasized through analysis of a large set of available *M. fortuitum* genomes (17). *M. fortuitum* strains have also been reported to express inducible clarithromycin resistance due to the presence of *erm*(39) (18), highlighting the need for alternative antibiotics to treat these infections. Thus, in order to increase the performances of the current drug regimens against *M. fortuitum* diseases, new effective compounds targeting so far untapped target/pathways are needed.

The unique cell wall lipids, including mycolic acids, produced in mycobacteria play essential roles in the physiology and virulence of these bacteria (19). In addition, the mycolic acid biosynthetic pathway represents a validated site of action for the first-intent drug INH and the second-intent drug ethionamide (ETH) (20). Therefore, this pathway has also significant potential as a target for the development of novel antimycobacterial drugs, not only in *M. tuberculosis* (21, 22) but also in NTM. In support of this view, we recently demonstrated that inhibition of the mycolic acid pathway has translational potential for treatment and control of *M. abscessus* pulmonary diseases (23). This proof-of-concept was verified through the use and mode of action of the 4-hydroxy-2-pyridone lead candidate NITD-916, initially discovered in a phenotypic screen against *M. tuberculosis* (24). We reported the potent *in vitro* activity of NITD-916 against *M. abscessus*, through direct inhibition of the enoyl-ACP reductase InhA, leading to the arrest of mycolic acid biosynthesis. Importantly, NITD-916 reduced the intracellular bacterial loads in *M. abscessus*-infected macrophages and diminished both the number and size of cords. This compound was also very active in CF patient-derived alveolar organoids recapitulating the CF airway dysfunctions and characterized by the presence of a thick mucus and increased susceptibility to *M. abscessus* infection (25).

These results prompted us to investigate whether NITD-916 may also exert activity in *M. fortuitum* through InhA inhibition, thus offering potential for future chemotherapeutic developments against *M. fortuitum* infections. In this study, we describe the mechanism of action of the NITD-916 in *M. fortuitum* and assess its activity of *in vitro*, in macrophages as well as in a zebrafish model of infection.

## RESULTS

**NITD-916 displays potent *in vitro* activity against *M. fortuitum* strains.** The activity of NITD-916 was first tested against the reference strain ATCC 6841 in three different broth media (Table 1). Following the CLSI guidelines (26), the MIC was found to be extremely low in CaMHB (MIC = 0.04  $\mu$ g/mL). The MIC was higher in 7H9<sup>OADC</sup> (0.31  $\mu$ g/mL) or in Sauton's medium supplemented with OADC (0.16  $\mu$ g/mL). Conversely, the MIC of INH was much lower in 7H9<sup>OADC</sup> or Sauton's media than in CaMHB (50  $\mu$ g/mL). This indicates that the MIC of NITD-916 and INH vary considerably depending on the medium used and that NITD-916 exerts a much more pronounced activity than INH

**TABLE 1** Characteristics MIC (in  $\mu\text{g}/\text{mL}$ ) of INH and NITD-916 determined in CaMHB, Middlebrook 7H9 supplemented with OADC or Sauton's medium supplemented with OADC at 30°C against *M. fortuitum* ATCC 6841<sup>a</sup>

Strain	CaMHB		7H9 + OADC		Sauton + OADC	
	INH	NITD-916	INH	NITD-916	INH	NITD-916
ATCC 6841	50	0.04	6.25	0.31	1.56	0.16

<sup>a</sup>The values shown are representative of three independent experiments.

against *M. fortuitum*. We next determined the potency of NITD-916 using a panel of nine clinical isolates. All strains were highly susceptible to NITD-916 (MIC = 0.16 to 0.31  $\mu\text{g}/\text{mL}$ ) (Table 2) while remaining poorly responsive to INH (50 to 100  $\mu\text{g}/\text{mL}$ ). These isolates remained susceptible to amikacin (AMK) although MIC values (5 to 10  $\mu\text{g}/\text{mL}$ ) were slightly higher than those reported by others (MIC = 1  $\mu\text{g}/\text{mL}$ ) (27). Altogether, these results demonstrate that NITD-916 exerts strong activity on *M. fortuitum* strains *in vitro*.

To assess the influence of NITD-916 in liquid culture, exponentially growing *M. fortuitum* was exposed to 0.02, 0.04, 0.16, and 0.31  $\mu\text{g}/\text{mL}$  NITD-916 (corresponding to 0.5 $\times$ , 1 $\times$ , 4 $\times$ , and 8 $\times$  MIC), followed by CFU counting at various time points. This resulted in noticeable growth inhibition (Fig. 1). At 0.04  $\mu\text{g}/\text{mL}$ , NITD-916 exerted a bacteriostatic effect during the 4 days of treatment. At 0.16  $\mu\text{g}/\text{mL}$ , a 2-Log drop in the CFU was observed during the first 72 h of exposure to the compound, after which the CFU counts remained stable. No further decrease in the CFU counts occurred at higher concentrations. This suggests that NITD-916 displays a moderate bactericidal activity at concentrations above the MIC. This pattern of growth and kill was very similar to the one of AMK, included an internal control drug. However, while AMK showed only limited bactericidal activity at 1 $\times$  MIC (5  $\mu\text{g}/\text{mL}$ ) (Fig. 1), previous studies reported a concentration-dependent activity of AMK with the main fall in CFU observed at 4 $\times$  MIC or higher (27).

**G96S mutations in *inhA*<sub>MFO</sub> confer high resistance levels to NITD-916.** Single nucleotide polymorphisms in *inhA*, encoding the enoyl-ACP reductase InhA involved mycolic acid biosynthesis, have been identified previously in *M. tuberculosis* (InhA<sub>MTB</sub>) (24) and in *M. abscessus* (InhA<sub>MAB</sub>) mutants resistant to NITD-916 (23). Multiple sequence alignments indicate that InhA<sub>MFO</sub> is highly conserved, sharing 89.6% identity with InhA<sub>MAB</sub> and 88.5% with InhA<sub>MTB</sub> (Fig. 2A). To address whether mutations in *inhA* confer high resistance levels to NITD-916 in *M. fortuitum*, we selected independent clones growing on agar supplemented with 3.1  $\mu\text{g}/\text{mL}$  NITD-916 at frequencies estimated to  $1.3 \times 10^{-7}$  (Table 3). Subsequent MIC determination of the two selected colonies confirmed their high resistant levels to NITD-916 (MIC = 5 to 10  $\mu\text{g}/\text{mL}$ ), corresponding to an  $\sim 128$ -fold increased resistance level compared to the parental strain. Both resistors remained susceptible to AMK and INH (Table 3). PCR/sequencing of the *inhA*<sub>MFO</sub> locus identified amino acid replacements at position 96, similarly to mutations identified previously in *M. abscessus*

**TABLE 2** Activity of NITD-916 against *M. fortuitum*<sup>a</sup>

Strain	AMK <sup>b</sup>	INH	NITD-916
ATCC 6841	5	50	0.04
#2	5	100	0.16
#3	5	50	0.16
#4	5	50	0.16
#5	10	50	0.31
#6	10	100	0.31
#7	10	50	0.16
#8	10	100	0.16
#9	10	100	0.31
#10	5	100	0.31

<sup>a</sup>The MIC ( $\mu\text{g}/\text{mL}$ ) was determined in CaMHB at 30°C against the reference ATCC 6841 strain and 9 clinical isolates. The values shown are representative of three independent experiments.

<sup>b</sup>AMK, amikacin; INH, isoniazid.

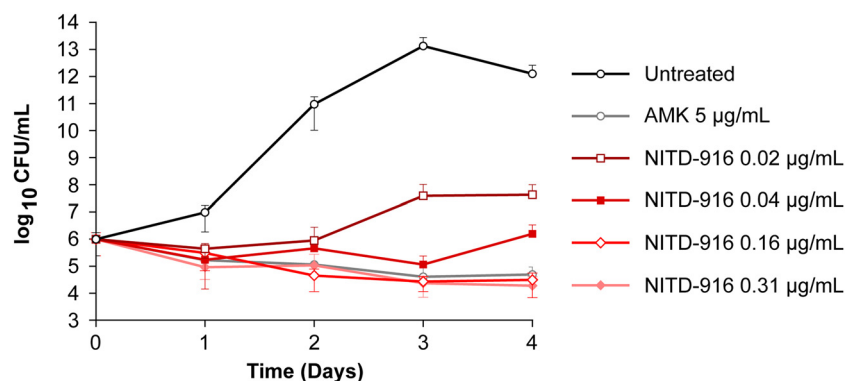


**FIG 1** *In vitro* activity of NITD-916 against *M. fortuitum*. *M. fortuitum* ATCC 6841 was exposed either to 0.02, 0.04, 0.16, 0.31 µg/mL NITD-916 or 5 µg/mL AMK in CaMHB at 30°C. At various time points, bacteria were plated on LB agar and further incubated at 37°C for 3 days prior to CFU counting. Results from each drug concentration are representative of three independent experiments.

and *M. tuberculosis* resistant mutants (23). Both *M. fortuitum*<sup>R18</sup> and *M. fortuitum*<sup>R20</sup> resistors harbored a G96S point mutation. Introduction of the pMV261\_*inhA*<sub>MAB</sub> construct (23) in *M. fortuitum*<sup>R18</sup> resulted in a 2- to 4-fold decrease in the MIC value of NITD-916 (data not shown), thus indicating that complementing the defective *inhA* gene with a wild-type copy of the gene was associated with a slight increase in susceptibility to NITD-916.

**Crystal structures of InhA<sub>MFO</sub> with NAD and NITD-916.** We obtained a crystal structure of the InhA<sub>MFO</sub> holoenzyme complex with NAD at 1.8 Å resolution (Table S1). As with other InhA<sub>MTB</sub> and InhA<sub>MAB</sub> holoenzyme complexes the α-helix spanning residues T196-G204 (α5) resides close to the nicotinamide ring of NAD, generating a closed, small substrate pocket. In the inhibited InhA<sub>MFO</sub> ternary complex crystal structure obtained at 2.05 Å resolution this α-helix moves away from NAD to accommodate the inhibitor NITD-916 (Fig. 2B). Concomitantly, the α-helix spanning residues E210-A226 (α6) moves toward the substrate binding pocket to interact with the inhibitor. The InhA<sub>MFO</sub> ternary complex with NAD and NITD-916 is overall nearly identical to that obtained for InhA<sub>MTB</sub> and InhA<sub>MAB</sub> (Fig. 2C). This result is expected based on similar overall sequence identity between the mycobacterial species and similar overall efficacy of NITD-916. The site of resistance G96S forms packing interactions with the phenyl ring of NITD-916 in a manner similar to that observed in the other mycobacterial species. Mutation of this residue to a serine would be expected to sterically clash with the ligand, thereby decreasing its potency; this is also close to the 3' hydroxyl on the nicotinamide portion of the substrate and the G96S mutation could also cause loss of fitness of mycobacterial InhA.

**NITD-916 inhibits mycolic acid biosynthesis by targeting InhA<sub>MFO</sub>.** The above-mentioned results strongly suggest that NITD-916 targets the enoyl ACP reductase InhA in *M. fortuitum* and is likely to inhibit *de novo* synthesis of mycolic acids. *M. fortuitum* produces essentially α- and epoxy-mycolic acids as well as variable amounts of α' and/or ω1-methoxy mycolic acids, depending on the strain (28, 29). To confirm that NITD-916 affects the mycolic acid profile, *M. fortuitum* cultures were pretreated with increasing concentrations of NITD-916 prior to labeling with 1 µCi/mL [<sup>14</sup>C]acetate. Radioactive lipids were extracted, methyl-esterified and separated by TLC. The *de novo* synthesis of α-, α'-, and epoxy-mycolates was drastically altered in a dose-dependent fashion and production was abrogated in the presence of 1.25 µg/mL NITD-916 (Fig. 2D). Ethionamide (ETH), a drug known to inhibit InhA and whose biotransformation is dependent on EthA (30), was included as a positive control. ETH abrogated mycolic acid biosynthesis at very high concentrations (500 µg/mL), in agreement with its high MIC value (32 to 64 µg/mL; data not shown). However, the synthesis FAMES remained unaffected by NITD-916. This indicates that NITD-916 specifically inhibits the type II but not the type I fatty acid synthase, consistent with inhibition of InhA<sub>MFO</sub>. In contrast, the mycolic acid profile in *M. fortuitum*<sup>R18</sup> carrying a G96S mutation in InhA<sub>MFO</sub> was characterized by a lack of mycolate inhibition compared to the parental strain (Fig. 2E).



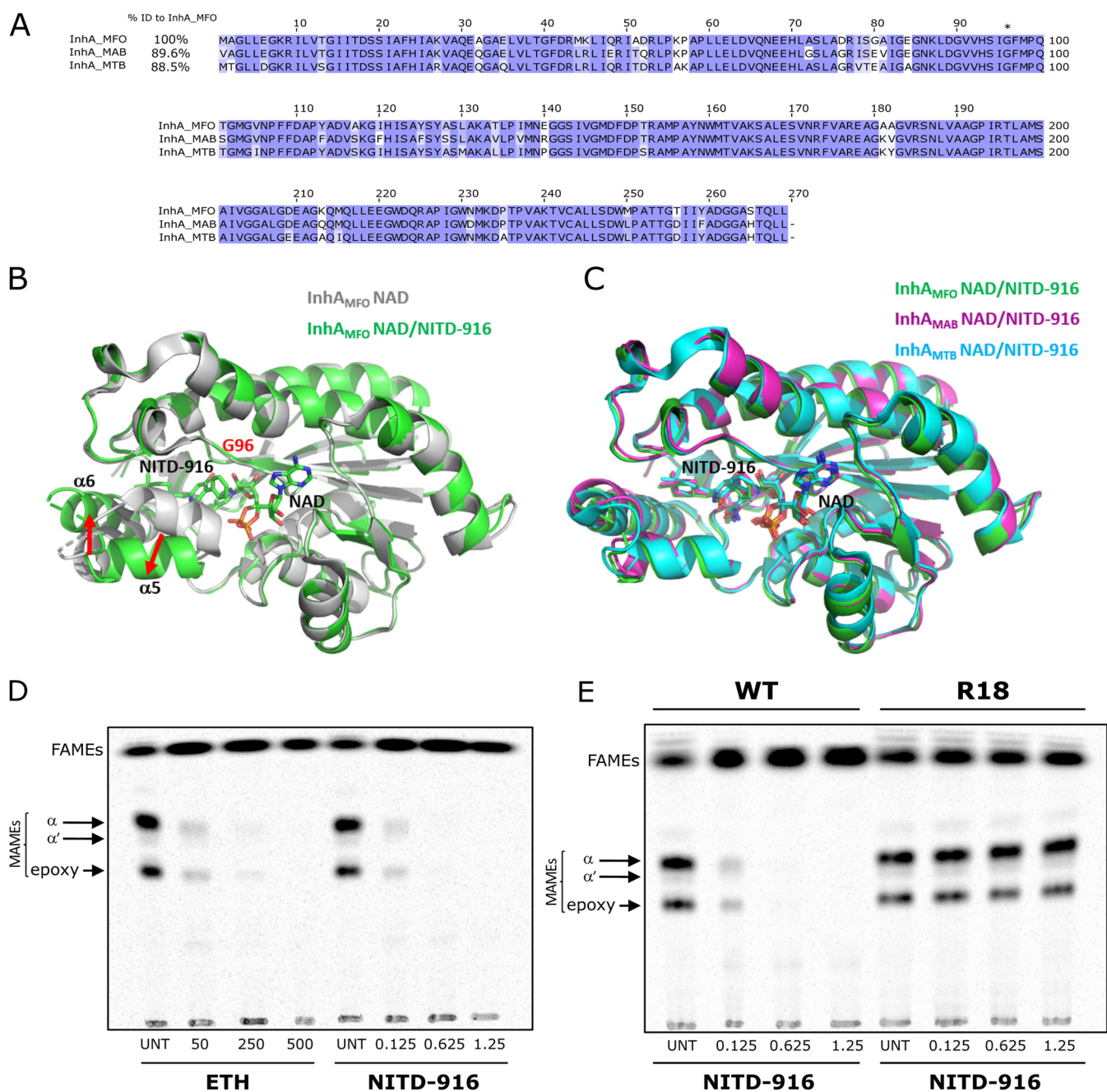


**FIG 2** Structural basis of inhibition of *M. fortuitum* InhA by NITD-916 and effect on mycolic acid biosynthesis. (A) Multiple sequence alignments using Clustal Omega and the Jalview software of the InhA protein from *M. fortuitum* (MFO) along with InhA from *M. abscessus* (MAB) and *M. tuberculosis* (MTB). The percentage of protein identity is indicated in the left margin. The star highlights the position of the highly conserved Gly96 residue. (B) Crystal structures of *M. fortuitum* InhA bound to NAD alone (gray ribbons) or NAD and NITD-916 (green ribbons and sticks). The  $\alpha$ -helix spanning residues Thr196-Gly204 moves away from the active site pocket (red arrow) to accommodate the inhibitor NITD-916 in a manner similar to how it would accommodate its substrate. Resistance mutants arise at Gly96, labeled in red. (C) Overlay of the crystal structures of *M. fortuitum* InhA (green), *M. abscessus* InhA (magenta), and *M. tuberculosis* InhA (cyan) bound to NAD and NITD-916. (D) *M. fortuitum* cultures were grown in 7H9<sup>AD</sup>C Tyloxapal 0.025% at 37°C with agitation for 1 h in the presence of increasing concentrations of either ethionamide (ETH) or NITD-916. Bacteria were then labeled with [<sup>14</sup>C]acetate for 2 h at 37°C with agitation prior to mycolic acid extraction. Equal counts (50, 000 cpm) of radiolabeled lipids were loaded onto a TLC plate and resolved using the solvent system petroleum ether/acetone (95/5, vol/vol). (E) *M. fortuitum* WT and *M. fortuitum*<sup>R18</sup> carrying a G96S mutation in InhA<sub>MFO</sub> were grown in the presence of increasing concentrations of NITD-916. Mycolic acid labeling, extraction and separation were processed as in (D).

Mycolates were still produced at 1.25  $\mu$ g/mL NITD-916, a concentration which abrogated mycolic acid biosynthesis in the parental strain. This supports the idea that the G96S replacement alters the activity of the inhibitor, most probably by preventing the binding of the drug into InhA<sub>MFO</sub>. Overall, biochemical and genetic data underscore

**TABLE 3** Characteristics of two NITD-916 spontaneous resistant mutants of *M. fortuitum*<sup>a</sup>

Strain	MIC ( $\mu\text{g}/\text{mL}$ )			Mutation in <i>inhA</i> <sub>MFO</sub>		
	AMK	INH	NITD-916	SNP	AA change	Frequency of mutation
ATCC 6841	5	50	0.04			
<i>M. fortuitum</i> <sup>R18</sup>	5	50	10	G286A	G96S	$1.3 \times 10^{-7}$
<i>M. fortuitum</i> <sup>R20</sup>	5	50 to 100	5 to 10	G286A	G96S	$1.3 \times 10^{-7}$

<sup>a</sup>MIC ( $\mu\text{g}/\text{mL}$ ) were determined in CaMHB at 30°C. Resistant strains were derived from the ATCC 6841 reference strain in 7H10<sup>ODC</sup> supplemented with 3.1  $\mu\text{g}/\text{mL}$  NITD-916. Single-nucleotide polymorphism (SNP) in *inhA*<sub>MFO</sub> and corresponding amino acid (AA) changes as well as the frequency of mutation are indicated. The MIC values shown are representative of three independent experiments.

the mode of action of NITD-916, which abolishes mycolic acid biosynthesis by targeting *InhA*<sub>MFO</sub>.

#### Reduced intramacrophage *M. fortuitum* loads upon treatment with NITD-916.

Because there is little information available regarding the kinetic of *M. fortuitum* growth in macrophages, we first monitored intramacrophage growth at 1 and 3 days postinfection (dpi) after infection of THP-1 cells using an MOI 5:1. While no increase was noticed at 1 dpi, a  $\approx 2$  Log increase in the CFU was observed at 3 dpi, compared to the inoculum (Fig. 3A). To exclude the possibility of extracellular bacterial growth, macrophages were treated with 25  $\mu\text{g}/\text{mL}$  AMK for 2 h and were extensively washed every day and replenished with fresh medium. However, despite AMK treatment and washing, plating the washes on LB agar revealed the presence of extracellular bacilli, corresponding approximately to  $\approx 3.5\%$  of the intracellular bacterial loads (not shown). It appears also reasonable to propose that the AMK pulse interfered with the intracellular growth of *M. fortuitum* during the first 24 h postinfection, thereby limiting the intracellular replication of *M. fortuitum* observed at 1 dpi. This is supported by the fact that 5  $\mu\text{g}/\text{mL}$  AMK is sufficient to inhibit *in vitro* growth of *M. fortuitum* (Fig. 1). That *M. fortuitum* has the capacity to survive and grow intracellularly prompted us to assess the efficacy of NITD-916 in infected THP-1 macrophages. Previous studies have shown that NITD-916 exerts very little cytotoxicity after exposure of THP-1 to the drug for 1 or 3 days (23). Results in Fig. 3A indicate that NITD-916 did not affect the intracellular loads at 1 dpi as the CFU counts were comparable to those in the inoculum. However, there was a marked and dose-dependent decrease in the intracellular loads at 3 dpi. At 0.62  $\mu\text{g}/\text{mL}$  (the highest concentration tested), there was a  $\approx 3$  Log decrease in the CFU counts compared to the untreated cells at 3 dpi. At this dose, the efficacy of NITD-916 was slightly lower than following treatment with 16  $\mu\text{g}/\text{mL}$  IPM, for which a growth inhibitory effect was already noticed at 1 dpi.

To further investigate the effect of the drug treatment on infected cells, macrophages were infected with eGFP-expressing *M. fortuitum*, exposed to either DMSO, NITD-916, or IPM and stained with anti-CD63 antibodies and DAPI. Quantification of the percentage of infected macrophages indicated that concentrations of NITD-916  $\geq 0.16$   $\mu\text{g}/\text{mL}$  significantly reduced the proportion of macrophages infected with *M. fortuitum* (Fig. 3B). This was further emphasized by examining the cells by at 3 dpi (Fig. 3C). At this time point, very few infected cells were observed in the presence of 0.62  $\mu\text{g}/\text{mL}$  NITD-916.

Collectively, these results indicate that NITD-916 can permeate both the host cell membrane and the cell envelope of intracellular *M. fortuitum*, showing potent activity against the bacteria within infected macrophages.

**NITD-916 increases survival of *M. fortuitum*-infected zebrafish embryos.** We took advantage of the zebrafish embryo as an amenable model to study the chronology of systemic *M. fortuitum* infections and found that intravenous injection of *M. fortuitum* leads to aggressive and lethal infections in wild-type embryos, with worsening effects in the absence of either functional innate immunity or CFTR (31). However, while this model appears particularly conducive to spatiotemporal imaging of *M. fortuitum* infections, it has not been exploited yet to assess the *in vivo* efficacy of antibacterial agents against *M. fortuitum*. We, thus, reasoned that it may represent an interesting biological system allowing noninvasive observations to evaluate, in real time, the efficacy of NITD-916 in a living vertebrate, as shown previously for other NTMs, such as *M. marinum* (32,

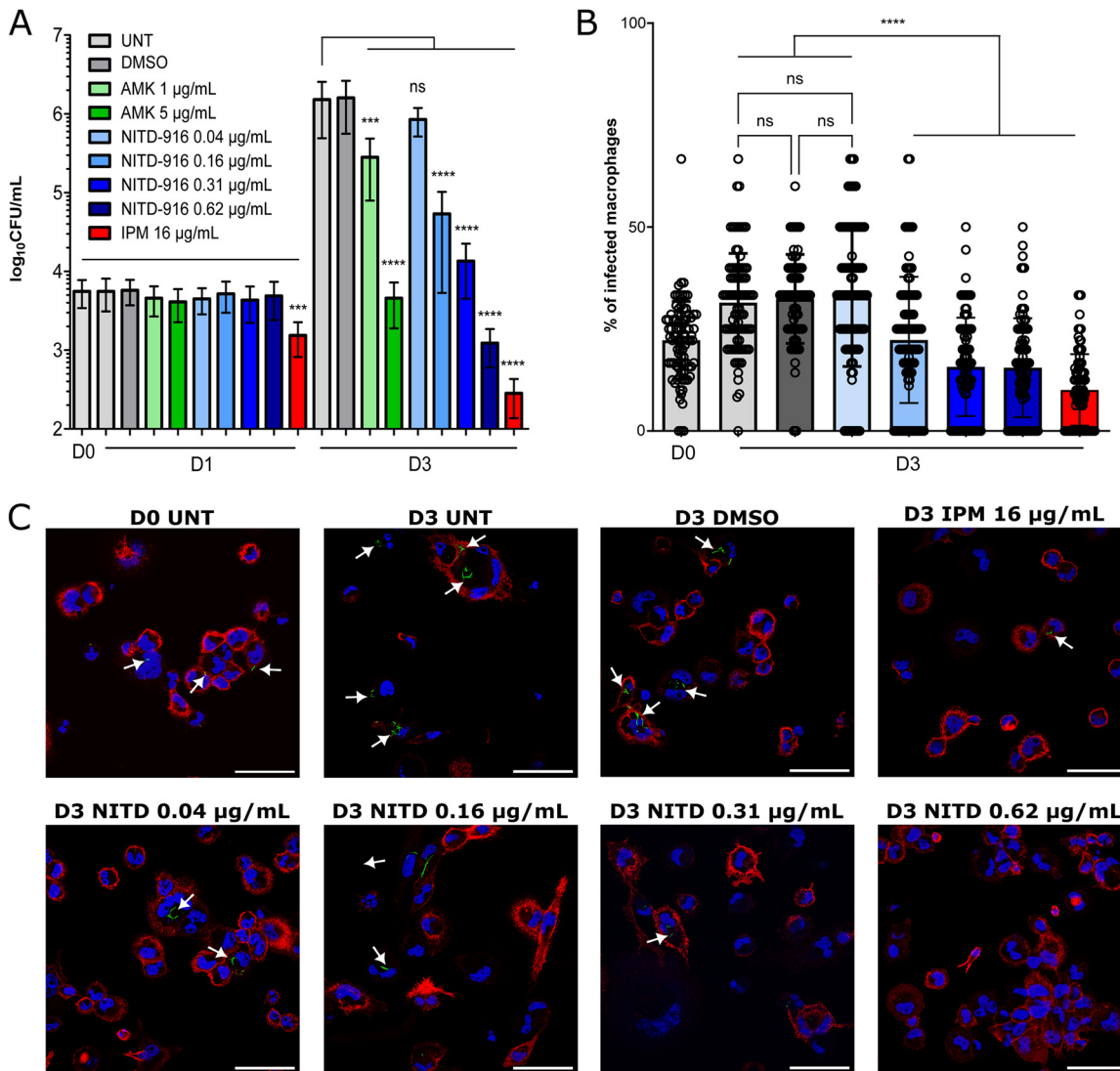


**FIG 3** Intracellular activity of NITD-916 on *M. fortuitum*-infected THP-1 cells. (A) Macrophages were infected with *M. fortuitum* ATCC 6841 at an MOI of 5:1 for 4 h, washed and treated with 25  $\mu\text{g/mL}$  AMK for 2 h to kill the remaining extracellular bacteria. Infected cells were then exposed to either NITD-916 at the indicated concentrations, AMK or IPM. Untreated (UNT) or DMSO-exposed cells were included as controls. Cells were washed three times on a daily basis. CFU were determined at 0, 1, and 3 days postinfection. Data of four independent experiments in triplicates were analyzed with a Mann-Whitney *t* test. \*\*\*,  $P \leq 0.001$ ; \*\*\*\*,  $P \leq 0.0001$ ; ns, nonsignificant. (B) Percentage of infected THP-1 macrophages at 0 and 3 days postinfection with *M. fortuitum* ATCC 6841 (MOI of 5:1) in the absence (UNT) or presence of increasing concentrations of NITD-916 or IPM. DMSO-exposed cells were included as controls. Results are expressed as mean values  $\pm$  SD for three independent experiments with 30 fields per condition. Data were analyzed using the Kruskal-Wallis test. \*\*\*\*,  $P \leq 0.0001$ ; ns, nonsignificant. (C) Representative immunofluorescent fields were taken at 0 and 3 days postinfection showing macrophages infected with *M. fortuitum* expressing eGFP in the absence of antibiotics (UNT) or in the presence of either NITD-916 (1 $\times$ , 0.04  $\mu\text{g/mL}$ ; 4 $\times$ , 0.16  $\mu\text{g/mL}$ ; 8 $\times$ , 0.31  $\mu\text{g/mL}$ ; 16 $\times$ , 0.62  $\mu\text{g/mL}$ ) or IPM (1 $\times$ , 16  $\mu\text{g/mL}$ ). The surface and the endolysosomal system of the macrophages were detected using anti-CD63 antibodies (red). The nuclei were stained with DAPI (blue). White arrows indicate individual or small mycobacterial aggregates. Scale bar, 50  $\mu\text{m}$ .

33) or *M. abscessus* (34–38). In a first set of experiments, noninfected embryos at 2 days postfertilization (dpf) were exposed to increasing concentrations of NITD-916, ranging from 0.4 to 6  $\mu\text{g/mL}$ . The compound was changed on a daily basis for 4 days. No signs of toxicity-induced killing or developmental abnormalities were observed, even at the highest concentration tested (6  $\mu\text{g/mL}$ ). Complete embryo survival was recorded, even at 6  $\mu\text{g/mL}$ , indicating that, at the concentrations tested, NITD-916 was totally safe (Fig. S1). Next, eGFP-expressing *M. fortuitum* was injected in the caudal vein of embryos at 30 h postfertilization (hpf) and subsequently exposed at 1 dpi for 4 days to 2, 4, or 6  $\mu\text{g/mL}$  NITD-916 and the fate of the treated embryos was monitored as illustrated in Fig. 4A. A

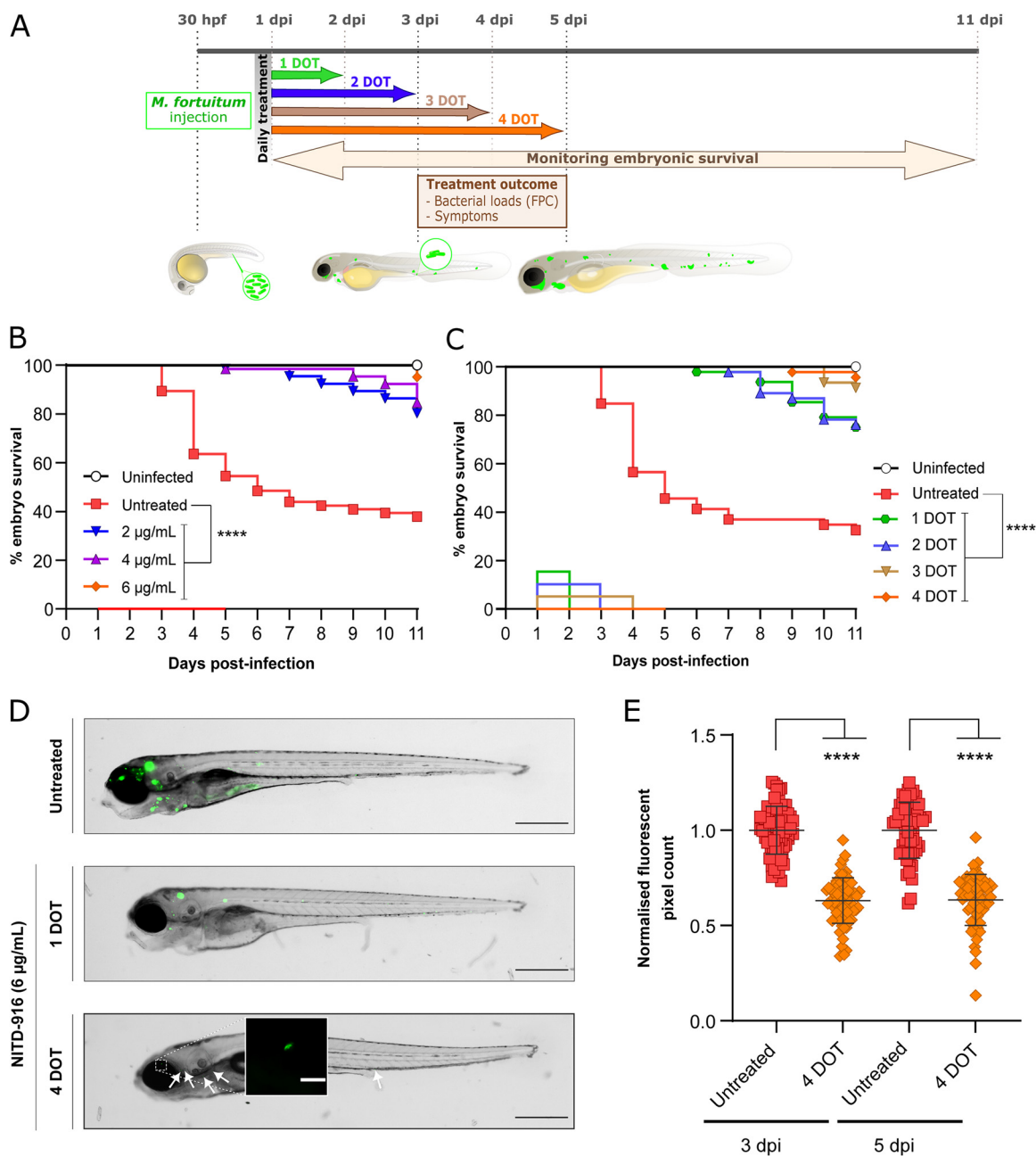


**FIG 4** *In vivo* efficacy of NITD-916 against *M. fortuitum* infected embryonic zebrafish. (A) Schematic of the *in vivo* efficacy protocol showing the timeline of zebrafish embryo infection (*M. fortuitum* expressing eGFP) with various exposure periods or with different concentrations of NITD-916 (daily changes), and compound washout after treatment. dpi, days postinfection. FPC, Fluorescence pixel count; DOT, days of treatment. (B, C, D, E) At 30 hpf, embryos were infected with approximately 2,800 CFU (B, C) and 900 CFU (D, E) of *M. fortuitum* expressing eGFP via caudal vein injection. A standard uninfected controlled was included for each experiment. At 1 day postinfection, embryos were randomly split into equal groups of approximately 24 embryos per group and (B) varying concentrations of NITD-916 (2, 4, and 6 µg/mL) or 6 µg/mL (C) were added to the water. Drugs were changed daily, after treatment, which embryos were washed twice in fresh embryo water and maintained in embryo water. The duration of the treatment is indicated with a colored line along the x axis (1 day in green, 2 days in blue, 3 days in brown, and 4 days in orange or red). Embryo survival was monitored daily over an 11-days period. Each treatment group was compared against the untreated control group with significant differences calculated using the log rank (Mantel-Cox) statistical test for survival curves. (B) Three replicates and (C) two replicates. \*\*\*\*,  $P \leq 0.0001$ . (D) Representative embryos from the untreated group (upper panel) or treated group (6 µg/mL NITD-916) during 1 day (middle panel) or 4 days (lower panel) imaged at 4 dpi. Scale bar, 500 µm. At 4 DOT, the white arrows and white square indicate small infection foci. Enlargement scale bar, 30 µm. (E) The *M. fortuitum* burden was quantified after 2 (3 dpi) or 4 (5 dpi) days of exposure to 6 µg/mL NITD-916 by determination of the FPC using the ImageJ software. The data are from two experiments (containing approximately 36 embryos per group), with each data point representing one infected embryo. The error bar represents the mean and standard deviation of the data set. Statistical comparison was done using a Welch's *t* test, \*\*\*\*,  $P \leq 0.0001$ .



significant increased survival was observed in all treated groups compared to the untreated embryos (Fig. 4B). Remarkably, the 6  $\mu\text{g}/\text{mL}$  NITD-916 treatment extended the life span of infected zebrafish, reaching  $\approx 100\%$  protection at 11 dpi, compared to 40% for the untreated fish. To investigate whether reducing duration of treatment affects the protective efficacy of NITD-916, infected embryos were exposed to 6  $\mu\text{g}/\text{mL}$  NITD-916 for 1, 2, 3, or 4 days of treatment (DOT) and the efficacy of the treatment was judged by monitoring the larval killing. Fig. 4C clearly shows that short treatments (1 or 2 DOT) resulted in very high survival rates against *M. fortuitum* ( $\approx 75\%$  of survival at 11 dpi compared to  $\approx 30\%$  to 40% for the untreated group) while the percentage of survival was greater than 90% for longer periods of treatment (3 or 4 DOT). This dose-dependent effect of NITD-916 was also supported by embryo imaging (Fig. S2). Together, these results highlight a dose- and time-dependent effect of NITD-916 and indicate that this compound is very efficient in this zebrafish test system against *M. fortuitum* infection.

We next monitored the kinetic of the bacterial burden upon intravenous infection of embryos by fluorescence microscopy (Fig. 4D) and determination of the fluorescent pixel counts (FPC) (Fig. 4E) at 3 and 5 dpi in the presence or absence of NITD-916. The addition of 6  $\mu\text{g}/\text{mL}$  NITD-916 for 4 days in fish water was accompanied by an important reduction in the number of FPC at both time points (Fig. 4E). In addition, whole embryo imaging at 5 dpi clearly highlighted the massive effect of the compound after 1 DOT, which was further exacerbated after 4 DOT (Fig. 4D), consistent with bacterial burden quantification (Fig. 4E). At 4 DOT, infection foci were generally not detected and, eventually, only individual bacilli could be observed. This pronounced effect of NITD-916 in reducing the bacterial burden is likely to explain the high protective efficacy of the compound on embryo survival.

**Reduced pathophysiological symptoms in infected larvae treated with NITD-916.** We previously showed that the zebrafish/*M. fortuitum* model recapitulates major mycobacterial pathophysiological features, such as cording and abscess formation (31). Extracellular cord formation within the embryo is often representative of acute infection and can be indicative of mycobacterial escape from the phagosome and macrophage destruction (Fig. 5A, left panel) (39–41). Abscess formation can be linked to loss of infection control, typically occurring following cord formation and expansion (39–41) and representing a marker of disease severity, associated with cell debris, tissue destruction, and acute infection (Fig. 5B, left panel) (39). We, thus, inquired whether treatment of NITD-916 would be associated with limited physiopathological signs, as a consequence of the reduced bacterial burden. Our results indicate that at both 3 and 5 dpi, treatment with NITD-916 coincided with a significant reduction in the proportion of embryos with cords, which was particularly evident after 4 DOT (Fig. 5A, right panel). We observed a significant increase in the number of embryos with abscesses, from  $\approx 30\%$  to  $\approx 50\%$  between 3 and 5 dpi, in line with previous studies (31). Strikingly, we noticed a marked decrease in the proportion of embryos with abscesses in the presence of NITD-916 at both time points and this effect was dependent on the duration of the treatment (Fig. 5B, right panel). After 4 DOT, we failed to detect abscesses in the treated fish. Collectively, these results show that NITD-916 strongly reduces the physiopathological signs characterizing acute and lethal *M. fortuitum* infections in the zebrafish model.

## DISCUSSION

Infections caused by *M. fortuitum* isolates required long-term drug treatments due to their inherent resistance levels to a large variety of antibiotics and standard disinfectants (14, 42) and their capacity to assemble biofilms on surfaces that may contribute to bacterial persistence (43). This emphasizes the urgent medical need to improve the performances of the current drug treatments against *M. fortuitum* diseases and the implementation of new active molecules targeting untapped pathways. Guidelines for *M. fortuitum* treatments recommend multidrug therapy (13) but none of the currently used drugs relies on inhibition of the mycolic acid pathway, despite the fact that mycolic acids are essential cell wall components in mycobacteria and represent the primary target of INH and ETH in *M. tuberculosis* (20, 44). We have previously shown that this metabolic pathway represents

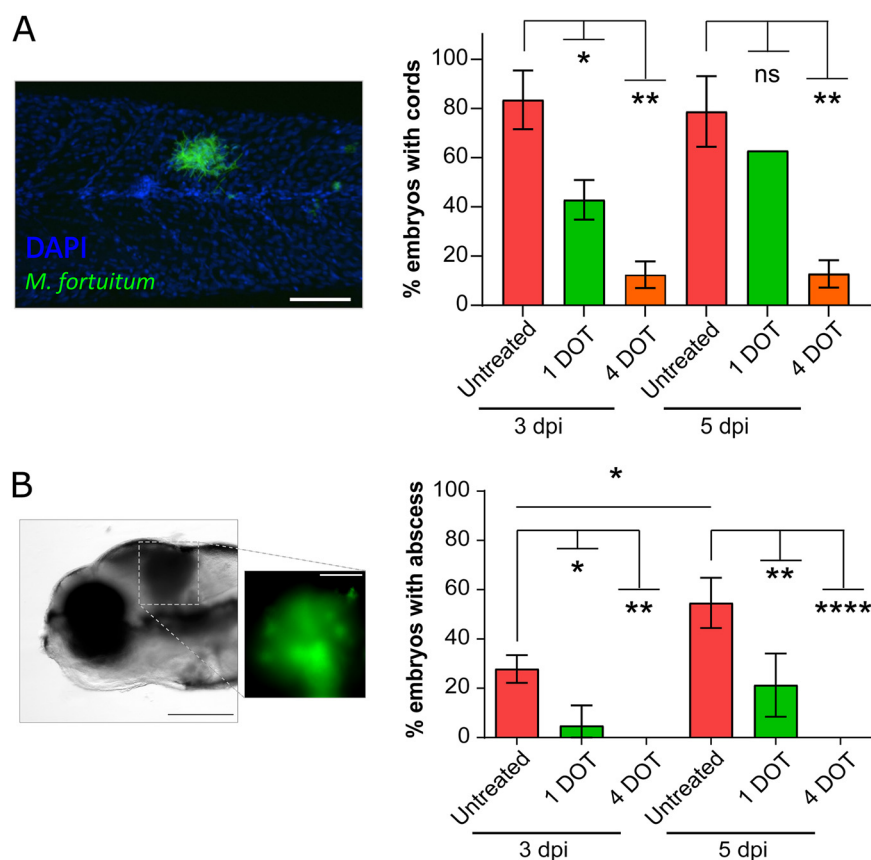


**FIG 5** Impact of NITD-916 on the evolution of *M. fortuitum*-induced symptoms in zebrafish. (A) Confocal microscopy image representing a *M. fortuitum* cord (eGFP-green) in the zebrafish tail (left panel). Nuclei of cells are stained in blue (DAPI). Scale bar, 100  $\mu$ m. Proportion of zebrafish embryos with mycobacterial cords detected with fluorescence microscopy at 3 and 5 days postinfection after 1 or 4 DOT (right panel). Results are from two separate experiments containing 35 to 40 embryos per group. Error bars represent standard deviations. Statistical analysis was performed using Ordinary one-way ANOVA (data passed normality test). \*,  $P \leq 0.05$ ; \*\*,  $P \leq 0.01$ ; ns, nonsignificant. (B) Representative image of a *M. fortuitum* abscess (eGFP-green) at 5 dpi (left panel). Scale bar, 300  $\mu$ m and enlargement scale bar, 100  $\mu$ m. Proportions of embryos with abscess detected by fluorescence microscopy at 3 and 5 days after infection after 1 or 4 DOT (right panel). Results are from three separate experiments containing 34 to 40 embryos per group. Error bars represent standard deviations. Statistical analysis was performed using Ordinary one-way ANOVA (data passed normality test). \*,  $P \leq 0.05$ ; \*\*,  $P \leq 0.01$ ; \*\*\*\*,  $P \leq 0.0001$ .

an attractive target in *M. abscessus* and that the 4-hydroxy-2-pyridone lead candidate NITD-916, originally identified in a phenotypic screen against *M. tuberculosis* (24) inhibits InhA in *M. abscessus* (23). Importantly, NITD-916 significantly diminished the *M. abscessus* burden in infected macrophages and reduced cording of the rough variant. Moreover, NITD-916 reduced the bacterial loads in alveolar organoids derived from CF patients, which are particularly susceptible to *M. abscessus* infection (25). These results prompted us to explore the efficacy of the compound against *M. fortuitum* *in vitro*, *in cellulo*, and in an animal model of infection.

In this study, we found that NITD-916 displays very low MIC values against a wide panel of *M. fortuitum* clinical isolates characterized by a bacteriostatic activity *in vitro* at 1 $\times$  MIC. Importantly, the compound showed very significant activity in reducing the *M. fortuitum* burden in THP-1 macrophage after 3 days at concentrations corresponding to 4 $\times$  MIC and this effect was found to be dose-dependent, thus corroborating previous results observed in *M. abscessus*-infected macrophages (23). We also report here a robust and sustained activity of NITD-916 in infected zebrafish. Our results highlight the *in vivo* efficacy of NITD-916 in this animal model, allowing to report the dose- and time-dependent dynamics of infection foci formation/resorption. NITD-916 exerted

an excellent protective effect at concentrations that had no impact on embryo survival or development. Importantly, we provide evidence that this compound drastically restricted the bacterial burden, even during short exposure times to NITD-916. In addition, we found that NITD-916 treatment was correlated with a significant reduction in cording as well as in abscess formation, both assigned as typical signs of mycobacterial infections and considered as marker of disease severity. Because cords and abscesses are dependent on uncontrolled mycobacterial replication and expansion (39), it is very likely that limited cords and abscesses are a direct consequence of bacterial growth inhibition by NITD-916. That most effects (embryo survival, cording, abscesses) are enlightened after only 1 DOT, this suggests that NITD-916 is acting very rapidly *in vivo*, which is of particular interest to reduce the duration of drug treatment, thereby limiting potential side effects often occurring during prolonged therapy. In addition of representing an increasing public health problem, the *M. fortuitum* group is recognized as a major causative agent of both fresh and saltwater fish mycobacteriosis, associated with ulcerative dermatitis as well as organomegaly and granulomatous lesions in the internal organs (45, 46). Because control of these infections in fish react poorly to antibiotherapy, we propose NITD-916 to be further evaluated as a potent drug candidate for the treatment and control of fish mycobacteriosis.

Overall, the present study reports the usefulness of zebrafish as a preclinical model to evaluate in real time the efficacy of a drug against *M. fortuitum* in the sole context of innate immunity. This biological system may also be further exploited for medium-throughput screenings to rapidly identify new chemical scaffolds with *in vivo* activity against *M. fortuitum*, as reported previously for *M. marinum* (33). Our genetic and biochemical studies unambiguously indicated that NITD-916 inhibits *de novo* biosynthesis of mycolic acids by directly binding to InhA<sub>MFO</sub>, thus sharing the same mode of action than in *M. tuberculosis* or *M. abscessus* (23, 24). This is supported by the following reasons: First, the high resistance levels to NITD-916 of two spontaneous mutants was linked to the presence of G96S point mutations in InhA<sub>MFO</sub>, similarly to those reported previously in *M. abscessus* (23). Second, the mycolic acid profile of *M. fortuitum*<sup>R18</sup> carrying the G96S mutation remained unchanged upon exposure to NITD-916, suggesting that replacement of the conserved Gly96 residue by a bulkier amino acid is likely to affect the binding of the inhibitor into InhA<sub>MFO</sub>. In contrast, *M. fortuitum*<sup>R18</sup> remained sensitive to INH, suggesting that Gly96 is probably not involved in the binding of the INH-NAD adduct; Third, NITD-916 could be modeled in a NITD-916:NAD:InhA<sub>MFO</sub> ternary complex. Together, these results clearly establish a proof of concept that NITD-916 inhibits the enoyl reductase activity of InhA<sub>MFO</sub> and that targeting the fatty acid elongation step leading to mycolic acid production represents an excellent pathway to be exploited in future drug discovery programs against *M. fortuitum*. Previous work indicated that NITD-916 has no mutagenic or cardiotoxicity potential and displays good pharmacological properties (24). This is of particular interest to encourage coming medicinal chemistry programs for the rational optimization of NITD-916-related analogs with improved efficacy. In this context, the availability of the InhA<sub>MAB</sub> crystal structure in complex with NAD and NITD-916 will drive the design and chemical synthesis of such derivatives.

Another important feature to consider in future studies relies on the possibility to increase the activity of NITD-916 when associated with other drugs used in clinical settings. The absence of drug-drug interactions is critical for clinical development and remains to be verified experimentally.

In summary, this study adds a new lead compound to the preclinical *M. fortuitum* drug pipeline and provides an interesting chemical starting point for subsequent optimization programs. It supports the view that targeting mycolic acid biosynthesis has an important translational potential for the development of new treatments against *M. fortuitum* infections. The *in vitro* and *in vivo* activity of NITD-916 underlines the interest of this unexploited chemical entity and additional experimentation is now required to test NITD-916 in mouse infection models developed for *M. fortuitum* (47, 48). It is also

expected that the results arising from this study will be useful in guiding the development of improved 4-hydroxy-2-pyridones and other direct InhA inhibitors currently being evaluated as antitubercular drug candidates (49, 50) against *M. fortuitum* as well as against other NTM.

## MATERIALS AND METHODS

**Mycobacterium fortuitum strains and culture conditions.** *M. fortuitum* subsp. *fortuitum* (ATCC 6841) and *M. fortuitum* clinical isolates were routinely grown and maintained at 37°C in Middlebrook 7H9 broth (BD Difco) supplemented with 10% oleic acid, albumin, dextrose, catalase (OADC enrichment) and 0.025% Tyloxapol (Sigma-Aldrich) (7H9<sup>OADC/T</sup>) or on Middlebrook 7H10 supplemented with 10% OADC enrichment (7H10<sup>OADC</sup>). *M. fortuitum* carrying pVV16-eGFP (31) was maintained in 7H9<sup>OADC/T</sup> supplemented with 100 µg/mL kanamycin (Euromedex).

**Drug susceptibility testing.** The MICs were determined according to the CLSI guidelines (26). All cultures were first incubated at 30°C for 1 week in either Cation-adjusted Mueller-Hinton Broth (CaMHB), 7H9<sup>OADC</sup> or Sauton's medium supplemented with OADC. The broth micro-dilution method was used with an inoculum of 5x10<sup>6</sup> CFU/mL in exponential growth phase in each medium. The bacterial suspension was seeded in 96-well plates (100 µL), except for the first column, to which 198 µL of the bacterial suspension was added. In the first column, 2 µL of drug at its highest concentration was added to the 198 µL of bacterial suspension. Two-fold serial dilutions were carried out and the plates were incubated for 4 days at 30°C. MICs were recorded by visual inspection. Assays were completed in duplicate in three independent experiments.

**Growth kinetics.** To monitor growth inhibition of *M. fortuitum* ATCC 6841, 96-well plates were set-up as for MIC determination (CaMHB, 30°C) and serial dilutions of the bacterial suspensions exposed to increasing concentrations of NITD-916 or amikacin (AMK) were plated on LB agar plates after 0, 1, 2, 3, and 4 days. CFU were counted after 3 days of incubation at 37°C. Results from each drug concentration are representative of three independent experiments in triplicates.

**Monitoring intramacrophage growth inhibition.** Human THP-1 monocytes were grown in RPMI medium supplemented with 10% fetal bovine serum (Sigma-Aldrich) (RPMI<sup>FBS</sup>) and incubated at 37°C in the presence of 5% CO<sub>2</sub>. Cells were differentiated with 20 ng/mL Phorbol Myristate Acetate (PMA) in 24-well flat-bottom tissue culture microplates for 48 h at 37°C with 5% CO<sub>2</sub>. Wells were seeded with 10<sup>5</sup> cells and infection with *M. fortuitum* (MOI 5:1) was carried out at 37°C in the presence of 5% CO<sub>2</sub> for 4 h. After extensive washing with 1 × phosphate-buffered saline (PBS), macrophages were incubated with RPMI<sup>FBS</sup> containing 25 µg/mL AMK for 2 h and washed again with PBS prior to the addition of 500 µL RPMI<sup>FBS</sup> containing either DMSO (negative control), AMK, imipenem (IPM) or NITD-916. Drugs were renewed on a daily basis. Cells were washed 3 times with PBS every day and lysed with 100 µL of 1% Triton X-100 after 0, 1, or 3 dpi. Serial dilutions of macrophage lysates were plated onto LB agar plates and colonies were counted to determine intracellular CFU.

**Microscopy-based infectivity assay.** Differentiated THP-1 cells were grown on coverslips in 24-well plates and infected with *M. fortuitum* carrying pVV16-eGFP (MOI 5:1) for 4 h. After treatment with 25 µg/mL AMK, cells were exposed to DMSO, IPM or different concentrations of NITD-916 and fixed at 0 and 3 dpi with 4% paraformaldehyde in 1 × PBS for 15 min. Cells were permeabilized using 0.2% Triton X-100 before blocking with 2% BSA in PBS supplemented with 0.2% Triton X-100 for 20 min. The surface and the endolysosomal system of macrophages were detected using anti-CD63 antibodies (Becton, Dickinson; dilution 1:1,000 for 1 h) and Alexa Fluor 488-conjugated anti-mouse secondary antibody (Molecular Probes, Invitrogen; dilution 1:100 for 45 min). After staining of nuclei with DAPI (dilution 1:1,000), cells were mounted onto microscope slides using Immuno-mount (Calbiochem). The percentage of infected macrophages were quantified using an Evos M7000 Imaging System (40×, Thermo Fisher Scientific) while images were acquired using a confocal microscope (63×, Zeiss LSM880). For each condition, approximately 1000 infected macrophages were analyzed and quantification of the percentage of infection were performed using ImageJ software.

**Ethics.** Zebrafish experiments were completed under European Union guidelines for the handling of laboratory animals ([http://ec.europa.eu/environment/chemicals/lab\\_animals/home\\_en.htm](http://ec.europa.eu/environment/chemicals/lab_animals/home_en.htm)). Housing and husbandry were approved by the Direction Sanitaire et Vétérinaire de l'Hérault for the ZEFIX-CRBM zebrafish facility (Montpellier) (registration number C-34-172-39). Handling and experiments were approved by "le ministère de l'enseignement supérieur, de la recherche et de l'innovation" under the reference APAFIS#24406-2020022815234677 V3.

**Zebrafish microinjection and infection.** Single cell preparations of fluorescent *M. fortuitum* were generated as previously described (31). At 24 hpf, embryos were dechorionated using Pronase (10 mg/mL; Sigma-Aldrich) for up to 5 min at room temperature, followed by extensive washing in fish water. At 30 hpf, embryos were anaesthetized in 0.02% tricaine and infected with fluorescent *M. fortuitum* via caudal vein injection (5 nL containing ≈560 bacteria/nL for survival experiments and 2 nL containing ≈450 bacteria/nL for FPC and symptom analyses). Bacterial inoculum was checked *a posteriori* by injection of 2 or 5 nL into sterile PBS and plating onto 7H10<sup>OADC</sup>. Following infection, embryos were transferred to 6-well plates (12 embryos/well) and incubated at 28.5°C for the duration of the experiment. Embryo age is expressed as days postinfection.

**Zebrafish monitoring and live imaging.** Embryo survival was monitored daily based on the presence or absence of a heartbeat. Survival curves were determined by counting dead larvae for up to 12 days, or until uninfected embryos begin to die. At designated time points postinfection, embryos were anaesthetized in 0.02% tricaine solution and mounted on 3% (wt/vol) methylcellulose solution for

live imaging. Images were taken using a Zeiss Axio ZoomV16 coupled with an Axiocam 503 monochrome camera (Zeiss). Fluorescent Pixel Count (FPC) measurements were determined using the 'Analyze particles' function in ImageJ. All experiments were completed at least two times independently.

**Selection of NITD-916 resistant *M. fortuitum* mutants.** Exponentially growing *M. fortuitum* were plated on LB agar containing 3.1  $\mu\text{g}/\text{mL}$  NITD-916. After 1 week of incubation at 37°C, two individual colonies selected, grown in CaMHB and individually assessed for MIC determination and scored for resistance to NITD-916. SNP identification was completed by PCR amplification using primers *inhA*<sub>MFO</sub> (F) 5'-CCGGTCAGCTGCCCC-3' and *inhA*<sub>MFO</sub> (R) 5'-GCACCCCTGCCGGAACG-3' to produce a 906-bp amplicon for full coverage sequencing of the *inhA*<sub>MFO</sub> gene.

**Mycolic acid analysis.** *M. fortuitum* cultures were exposed to increasing drug concentrations of either ethionamide (ETH) or NITD-916 for 1 h prior to metabolic labeling in the presence of 1  $\mu\text{Ci}/\text{mL}$  of [<sup>14</sup>C]acetate (59 mCi/mmol, Perkin Elmer) for an additional 2 h at 37°C under shaking. Extraction of total mycolic acids was carried out as previously reported (30). Bacterial pellets were washed and treated with 15% tetrabutylammonium hydroxide (TBAH) at 100°C overnight. Fatty acids and mycolic acids were methyl-esterified and extracted in diethyl ether. Lipid extracts were dried and resuspended in dichloromethane and separated by thin-layer chromatography (TLC). Fatty acid methyl esters (FAMES) and mycolic acid methyl esters (MAMES) were developed in petroleum ether/acetone (95:5, vol/vol). The [<sup>14</sup>C]-labeled FAMES and MAMES were analyzed using an Amersham Typhoon imaging system.

**Crystal structure determination.** *M. fortuitum* InhA (InhA<sub>MFO</sub>) was expressed and purified using standardized structural genomics protocols (51, 52). Briefly, the *fabI* gene encoding InhA<sub>MFO</sub> was cloned from genomic DNA into the bacterial expression vector BG1861, which encodes a N-terminal His<sub>6</sub> tag. The protein was expressed in BL21(DE3) cells with autoinduction media. Following centrifugation, the cell pellet was stored at -80°C until purification. The cells were resuspended and lysed and purification was performed via nickel affinity and size exclusion chromatography which showed a single main peak with a slight shoulder. Fractions from the main peak (without the shoulder) were pooled and concentrated to 28.49 mg/mL with a final yield of 113 mg from 2 L of culture. InhA<sub>MFO</sub> was stored at -80°C until used in crystallography experiments. Apo InhA<sub>MFO</sub> crystallized under several conditions as large plates, but these crystals yielded low angle diffraction unsuitable for X-ray data collection. In contrast, InhA<sub>MFO</sub> crystallized as a large plate at 19 mg/mL with 5 mM NADH in the MCSG-1 crystallization screen condition H3 (0.2 M lithium sulfate, 20% wt/vol PEG 3350); the crystal was cryoprotected with reservoir supplemented with 5 mM NADH and 20% vol/vol ethylene glycol. InhA<sub>MAB</sub> crystallized as a large plate at 19 mg/mL with 3.5 mM NADH and 3.5 mM NITD-916 in the JCSG+ crystallization screen condition A11 (0.2 M ammonium dihydrogen phosphate, 0.1 M Tris pH 8.5, 50% MPD); the crystal was harvested directly without supplemental cryoprotection. The NADH and NADH/NITD-916 bound data sets were collected at the Advanced Photon Source beamline 21 ID-F with a Rayonix MX-300 CCD detector at 0.97872 Å wavelength. The NADH-bound structure was solved by molecular replacement using MORDA and the *M. abscessus* InhA structure (PDB ID 7L6C) as a search model (23). The structures were refined with iterative rounds of refinement between Phenix (53) and Coot (54). X-ray diffraction images have been uploaded to the Integrated Resource for Reproducibility in Macromolecular Crystallography (IRRM) database ([www.proteindiffraction.org](http://www.proteindiffraction.org)) (55). The InhA<sub>MFO</sub> crystal structures were deposited to the PDB with accession codes 7K73 (NADH) and 7U00 (NADH & NITD-916).

**Statistical analyses.** Statistical analyses were performed on Prism 9.0 (GraphPad) and detailed for each figure legend. \*,  $P \leq 0.05$ ; \*\*,  $P \leq 0.01$ ; \*\*\*,  $P \leq 0.001$ ; \*\*\*\*,  $P \leq 0.0001$ ; ns, nonsignificant.

## SUPPLEMENTAL MATERIAL

Supplemental material is available online only.

**SUPPLEMENTAL FILE 1**, PDF file, 0.6 MB.

## ACKNOWLEDGMENTS

We acknowledge the Ministère de l'Enseignement Supérieur, de la Recherche et de l'Innovation for funding the PhD of M.A. This project has been funded by the French National Research Agency ANR-19-CE15-0012-01 (SUNLIVE) and in whole or in part with Federal funds from the National Institute of Allergy and Infectious Diseases, National Institutes of Health, Department of Health and Human Services, under Contract No. HHSN272201700059C. We are grateful to the Montpellier RIO Imaging facilities, M. Plays, and P. Richard for zebrafish husbandry. We thank Jean-Louis Herrmann and Anne-Laure Roux for the *M. fortuitum* clinical strains and Wassim Daher for the help with macrophages infections and fluorescence microscopy.

The authors report there are no competing interests to declare.

## REFERENCES

- Johansen MD, Herrmann J-L, Kremer L. 2020. Non-tuberculous mycobacteria and the rise of *Mycobacterium abscessus*. *Nat Rev Microbiol* 18: 392–407. <https://doi.org/10.1038/s41579-020-0331-1>.
- Sun Q, Yan J, Liao X, Wang C, Wang C, Jiang G, Dong L, Wang F, Huang H, Wang G, Pan J. 2022. Trends and species diversity of non-tuberculous mycobacteria isolated from respiratory samples in Northern China,



- 2014–2021. *Front Public Health* 10:923968. <https://doi.org/10.3389/fpubh.2022.923968>.
3. Richards CJ, Olivier KN. 2019. Nontuberculous mycobacteria in cystic fibrosis. *Semin Respir Crit Care Med* 40:737–750. <https://doi.org/10.1055/s-0039-1693706>.
  4. Brown-Elliott BA, Mann LB, Hail D, Whitney C, Wallace RJ. 2012. Antimicrobial susceptibility of nontuberculous mycobacteria from eye infections. *Cornea* 31:900–906. <https://doi.org/10.1097/ICO.0b013e31823f8bb9>.
  5. Brown-Elliott BA, Philley JV. 2017. Rapidly growing mycobacteria. *Microbiol Spectr* 5. <https://doi.org/10.1128/microbiolspec.TNM17-0027-2016>.
  6. Prevots DR, Marras TK. 2015. Epidemiology of human pulmonary infection with nontuberculous mycobacteria: a review. *Clin Chest Med* 36:13–34. <https://doi.org/10.1016/j.ccm.2014.10.002>.
  7. Wallace RJ, Swenson JM, Silcox VA, Good RC, Tschen JA, Stone MS. 1983. Spectrum of disease due to rapidly growing mycobacteria. *Rev Infect Dis* 5:657–679. <https://doi.org/10.1093/clinids/5.4.657>.
  8. Franco-Paredes C, Marcos LA, Henao-Martínez AF, Rodríguez-Morales AJ, Villamil-Gómez WE, Gotuzzo E, Bonifaz A. 2018. Cutaneous mycobacterial infections. *Clin Microbiol Rev* 32:e00069-18. <https://doi.org/10.1128/CMR.00069-18>.
  9. Tejan-Sie SA, Avery RK, Mossad SB. 2000. Mycobacterium fortuitum osteomyelitis in a peripheral blood stem cell transplant recipient. *Scand J Infect Dis* 32:94–96. <https://doi.org/10.1080/00365540050164317>.
  10. Nguyen D-Q, Righini C, Darouassi Y, Schmerber S. 2011. Nasal infection due to Mycobacterium fortuitum. *Eur Ann Otorhinolaryngol Head Neck Dis* 128:197–199. <https://doi.org/10.1016/j.anorl.2011.01.005>.
  11. Park S, Suh GY, Chung MP, Kim H, Kwon OJ, Lee KS, Lee NY, Koh W-J. 2008. Clinical significance of Mycobacterium fortuitum isolated from respiratory specimens. *Respir Med* 102:437–442. <https://doi.org/10.1016/j.rmed.2007.10.005>.
  12. Lessing MP, Walker MM. 1993. Fatal pulmonary infection due to Mycobacterium fortuitum. *J Clin Pathol* 46:271–272. <https://doi.org/10.1136/jcp.46.3.271>.
  13. Lange C, Böttger EC, Cambau E, Griffith DE, Guglielmetti L, van Ingen J, Knight SL, Marras TK, Olivier KN, Santin M, Stout JE, Tortoli E, Wagner D, Winthrop K, Daley CL, Expert Panel Group for Management Recommendations in Non-Tuberculous Mycobacterial Pulmonary Diseases. 2022. Consensus management recommendations for less common non-tuberculous mycobacterial pulmonary diseases. *Lancet Infect Dis* S1473-3099: e00586–7. [https://doi.org/10.1016/S1473-3099\(21\)00586-7](https://doi.org/10.1016/S1473-3099(21)00586-7).
  14. de Santos DRS, Lourenço MCS, Coelho FS, Mello FCQ, Duarte RS. 2016. Resistance profile of strains of Mycobacterium fortuitum isolated from clinical specimens. *J Bras Pneumol* 42:299–301. <https://doi.org/10.1590/S1806-37562016000000073>.
  15. Shen Y, Wang X, Jin J, Wu J, Zhang X, Chen J, Zhang W. 2018. In vitro susceptibility of Mycobacterium abscessus and Mycobacterium fortuitum isolates to 30 antibiotics. *Biomed Res Int* 2018:4902941. <https://doi.org/10.1155/2018/4902941>.
  16. Menéndez MC, Ainsa JA, Martín C, García MJ. 1997. *katG* and *katGII* encode two different catalases-peroxidases in Mycobacterium fortuitum. *J Bacteriol* 179:6880–6886. <https://doi.org/10.1128/jb.179.22.6880-6886.1997>.
  17. Morgado S, Ramos N de V, Freitas F, da Fonseca ÉL, Vicente AC. 2022. Mycolicibacterium fortuitum genomic epidemiology, resistome and virulome. *Mem Inst Oswaldo Cruz* 116:e210247. <https://doi.org/10.1590/0074-02760210247>.
  18. Kim S-Y, Moon SM, Jhun BW, Kwon OJ, Huh HJ, Lee NY, Lee SH, Shin SJ, Kasperbauer SH, Huitt GA, Daley CL, Koh W-J. 2019. Species distribution and macrolide susceptibility of Mycobacterium fortuitum complex clinical isolates. *Antimicrob Agents Chemother* 63:e02331-18. <https://doi.org/10.1128/AAC.02331-18>.
  19. Daffé M, Draper P. 1998. The envelope layers of mycobacteria with reference to their pathogenicity. *Adv Microb Physiol* 39:131–203. [https://doi.org/10.1016/s0065-2911\(08\)60016-8](https://doi.org/10.1016/s0065-2911(08)60016-8).
  20. Banerjee A, Dubnau E, Quemard A, Balasubramanian V, Um KS, Wilson T, Collins D, de Lisle G, Jacobs WR. 1994. *inhA*, a gene encoding a target for isoniazid and ethionamide in Mycobacterium tuberculosis. *Science* 263:227–230. <https://doi.org/10.1126/science.8284673>.
  21. Bhatt A, Molle V, Besra GS, Jacobs WR, Kremer L. 2007. The Mycobacterium tuberculosis FAS-II condensing enzymes: their role in mycolic acid biosynthesis, acid-fastness, pathogenesis and in future drug development. *Mol Microbiol* 64:1442–1454. <https://doi.org/10.1111/j.1365-2958.2007.05761.x>.
  22. Marrakchi H, Lanéelle M-A, Daffé M. 2014. Mycolic acids: structures, biosynthesis, and beyond. *Chem Biol* 21:67–85. <https://doi.org/10.1016/j.chembiol.2013.11.011>.
  23. Alcaraz M, Roquet-Banères F, Leon-Icaza SA, Abendroth J, Boudehen Y-M, Cougoule C, Edwards TE, Kremer L. 2022. Efficacy and mode of action of a direct inhibitor of Mycobacterium abscessus InhA. *ACS Infect Dis* 8:2171–2186. <https://doi.org/10.1021/acinfecdis.2c00314>.
  24. Manjunatha UH, S Rao SP, Kondreddi RR, Noble CG, Camacho LR, Tan BH, Ng SH, Ng PS, Ma NL, Lakshminarayana SB, Herve M, Barnes SW, Yu W, Kuhen K, Blasco F, Beer D, Walker JR, Tonge PJ, Glynn R, Smith PW, Diagana TT. 2015. Direct inhibitors of InhA are active against Mycobacterium tuberculosis. *Sci Transl Med* 7:269ra3. <https://doi.org/10.1126/scitranslmed.3010597>.
  25. Leon-Icaza SA, Bagayoko S, Iakobachvili N, Ferrand C, Aydogan T, Bernard C, Dafun AS, Murrís-Espin M, Mazières J, Bordignon PJ, Mazères S, Bernes-Lasserre P, Ramé V, Lagarde J-M, Marcoux J, Bousquet MP, Chalut C, Guilhot C, Clevers H, Peters PJ, Molle V, Lugo-Villarino G, Cam K, Berry L, Meunier E, Cougoule C. 2022. Cystic fibrosis patient-derived bronchial organoids unveil druggable pathways against Mycobacterium abscessus infection. *bioRxiv*. <https://doi.org/10.1101/2022.01.03.474765>.
  26. Woods GL, Brown-Elliott BA, Conville PS, Desmond EP, Hall GS, Lin G, Pfyffer GE, Ridderhof JC, Siddiqi SH, Wallace RJ. 2011. Susceptibility testing of mycobacteria, nocardiae and other aerobic actinomycetes, second edition. *Clinical and Laboratory Standards Institute*, Wayne, PA.
  27. Ferro BE, van Ingen J, Wattenberg M, van Soolingen D, Mouton JW. 2015. Time-kill kinetics of antibiotics active against rapidly growing mycobacteria. *J Antimicrob Chemother* 70:811–817. <https://doi.org/10.1093/jac/dku431>.
  28. Minnikin DE, Minnikin SM, Hutchinson IG, Goodfellow M, Grange JM. 1984. Mycolic acid patterns of representative strains of Mycobacterium fortuitum, “Mycobacterium peregrinum” and Mycobacterium smegmatis. *J Gen Microbiol* 130:363–367. <https://doi.org/10.1099/00221287-130-2-363>.
  29. Barry CE, Lee RE, Mdluli K, Sampson AE, Schroeder BG, Slayden RA, Yuan Y. 1998. Mycolic acids: structure, biosynthesis and physiological functions. *Prog Lipid Res* 37:143–179. [https://doi.org/10.1016/S0163-7827\(98\)00008-3](https://doi.org/10.1016/S0163-7827(98)00008-3).
  30. Dover LG, Alahari A, Gratraud P, Gomes JM, Bhowruth V, Reynolds RC, Besra GS, Kremer L. 2007. EthA, a common activator of thiocarbamide-containing drugs acting on different mycobacterial targets. *Antimicrob Agents Chemother* 51:1055–1063. <https://doi.org/10.1128/AAC.01063-06>.
  31. Johansen MD, Kremer L. 2020. CFTR depletion confers hypersusceptibility to Mycobacterium fortuitum in a zebrafish model. *Front Cell Infect Microbiol* 10:357. <https://doi.org/10.3389/fcimb.2020.00357>.
  32. Takaki K, Cosma CL, Troll MA, Ramakrishnan L. 2012. An in vivo platform for rapid high-throughput antitubercular drug discovery. *Cell Rep* 2:175–184. <https://doi.org/10.1016/j.celrep.2012.06.008>.
  33. Habjan E, Ho VQT, Gallant J, van Stempvoort G, Jim KK, Kuijl C, Geerke DP, Bitter W, Speer A. 2021. An anti-tuberculosis compound screen using a zebrafish infection model identifies an aspartyl-tRNA synthetase inhibitor. *Dis Model Mech* 14:dmm049145. <https://doi.org/10.1242/dmm.049145>.
  34. Bernut A, Le Moigne V, Lesne T, Lutfalla G, Herrmann J-L, Kremer L. 2014. In vivo assessment of drug efficacy against Mycobacterium abscessus using the embryonic zebrafish test system. *Antimicrob Agents Chemother* 58:4054–4063. <https://doi.org/10.1128/AAC.00142-14>.
  35. Dubée V, Bernut A, Cortes M, Lesne T, Dorchene D, Lefebvre A-L, Hugonnet J-E, Gutmann L, Mainardi J-L, Herrmann J-L, Gaillard J-L, Kremer L, Arthur M. 2015.  $\beta$ -Lactamase inhibition by avibactam in Mycobacterium abscessus. *J Antimicrob Chemother* 70:1051–1058. <https://doi.org/10.1093/jac/dku510>.
  36. Dupont C, Viljoen A, Thomas S, Roquet-Banères F, Herrmann J-L, Pethe K, Kremer L. 2017. Bedaquiline inhibits the ATP synthase in Mycobacterium abscessus and is effective in infected zebrafish. *Antimicrob Agents Chemother* 61:e01225-17. <https://doi.org/10.1128/AAC.01225-17>.
  37. Raynaud C, Daher W, Johansen M, Roquet-Banères F, Blaise M, Onajole OK, Kozikowski A, Herrmann J-L, Dziadek J, Gobis K, Kremer L. 2020. Active benzimidazole derivatives targeting the MmpL3 transporter in Mycobacterium abscessus. *ACS Infect Dis* 6:324–337. <https://doi.org/10.1021/acinfecdis.9b00389>.
  38. Johansen MD, Daher W, Roquet-Banères F, Raynaud C, Alcaraz M, Maurer FP, Kremer L. 2020. Rifabutin is bactericidal against intracellular and extracellular forms of Mycobacterium abscessus. *Antimicrob Agents Chemother* 64:e00363-20. <https://doi.org/10.1128/AAC.00363-20>.
  39. Bernut A, Herrmann J-L, Kissa K, Dubremetz J-F, Gaillard J-L, Lutfalla G, Kremer L. 2014. Mycobacterium abscessus cording prevents phagocytosis and promotes abscess formation. *Proc Natl Acad Sci U S A* 111:E943–E952. <https://doi.org/10.1073/pnas.1321390111>.

40. Bernut A, Nguyen-Chi M, Halloum I, Herrmann J-L, Lutfalla G, Kremer L. 2016. Mycobacterium abscessus-induced granuloma formation is strictly dependent on TNF signaling and neutrophil trafficking. *PLoS Pathog* 12: e1005986. <https://doi.org/10.1371/journal.ppat.1005986>.
41. Bernut A, Dupont C, Sahuquet A, Herrmann J-L, Lutfalla G, Kremer L. 2015. Deciphering and imaging pathogenesis and cording of Mycobacterium abscessus in zebrafish embryos. *J Vis Exp* 103:e53130. <https://doi.org/10.3791/53130>.
42. Tu H-Z, Lee H-S, Chen Y-S, Lee SS-J. 2022. High rates of antimicrobial resistance in rapidly growing mycobacterial infections in Taiwan. *Pathogens* 11:969. <https://doi.org/10.3390/pathogens11090969>.
43. Sousa S, Bandeira M, Carvalho PA, Duarte A, Jordao L. 2015. Nontuberculous mycobacteria pathogenesis and biofilm assembly. *Int J Mycobacteriol* 4:36–43. <https://doi.org/10.1016/j.ijmyco.2014.11.065>.
44. Pawelczyk J, Kremer L. 2014. The molecular genetics of mycolic acid biosynthesis. *Microbiol Spectr* 2:MGM2. <https://doi.org/10.1128/microbiolspec.MGM2-0003-2013>.
45. Delghandi MR, El-Matbouli M, Menanteau-Ledouble S. 2020. Mycobacteriosis and infections with non-tuberculous mycobacteria in aquatic organisms: a review. *Microorganisms* 8:E1368. <https://doi.org/10.3390/microorganisms8091368>.
46. Mugetti D, Tomasoni M, Pastorino P, Esposito G, Menconi V, Dondo A, Prearo M. 2021. Gene sequencing and phylogenetic analysis: powerful tools for an improved diagnosis of fish mycobacteriosis caused by Mycobacterium fortuitum group members. *Microorganisms* 9:797. <https://doi.org/10.3390/microorganisms9040797>.
47. Parti RPS, Srivastava S, Gachhui R, Srivastava KK, Srivastava R. 2005. Murine infection model for Mycobacterium fortuitum. *Microbes Infect* 7: 349–355. <https://doi.org/10.1016/j.micinf.2004.11.006>.
48. Kashyap VK, Gupta RK, Shrivastava R, Srivastava BS, Srivastava R, Parai MK, Singh P, Bera S, Panda G. 2012. In vivo activity of thiophene-containing trisubstituted methanes against acute and persistent infection of non-tubercular Mycobacterium fortuitum in a murine infection model. *J Antimicrob Chemother* 67:1188–1197. <https://doi.org/10.1093/jac/dkr592>.
49. Prasad MS, Bhole RP, Khedekar PB, Chikhale RV. 2021. Mycobacterium enoyl acyl carrier protein reductase (InhA): a key target for antitubercular drug discovery. *Bioorg Chem* 115:105242. <https://doi.org/10.1016/j.bioorg.2021.105242>.
50. Doğan ŞD, Gündüz MG, Doğan H, Krishna VS, Lherbet C, Sriram D. 2020. Design and synthesis of thiourea-based derivatives as Mycobacterium tuberculosis growth and enoyl acyl carrier protein reductase (InhA) inhibitors. *Eur J Med Chem* 199:112402. <https://doi.org/10.1016/j.ejmech.2020.112402>.
51. Bryan CM, Bhandari J, Napuli AJ, Leibly DJ, Choi R, Kelley A, Van Voorhis WC, Edwards TE, Stewart LJ. 2011. High-throughput protein production and purification at the Seattle Structural Genomics Center for Infectious Disease. *Acta Crystallogr Sect F Struct Biol Cryst Commun* 67:1010–1014. <https://doi.org/10.1107/S1744309111018367>.
52. Choi R, Kelley A, Leibly D, Hewitt SN, Napuli A, Van Voorhis W. 2011. Immobilized metal-affinity chromatography protein-recovery screening is predictive of crystallographic structure success. *Acta Crystallogr Sect F Struct Biol Cryst Commun* 67:998–1005. <https://doi.org/10.1107/S1744309111017374>.
53. Adams PD, Afonine PV, Bunkóczi G, Chen VB, Davis IW, Echols N, Headd JJ, Hung L-W, Kapral GJ, Grosse-Kunstleve RW, McCoy AJ, Moriarty NW, Oeffner R, Read RJ, Richardson DC, Richardson JS, Terwilliger TC, Zwart PH. 2010. PHENIX: a comprehensive Python-based system for macromolecular structure solution. *Acta Crystallogr D Biol Crystallogr* 66:213–221. <https://doi.org/10.1107/S0907444909052925>.
54. Emsley P, Cowtan K. 2004. Coot: model-building tools for molecular graphics. *Acta Crystallogr D Biol Crystallogr* 60:2126–2132. <https://doi.org/10.1107/S0907444904019158>.
55. Grabowski M, Cymborowski M, Porebski PJ, Osinski T, Shabalin IG, Cooper DR, Minor W. 2019. The integrated resource for reproducibility in macromolecular crystallography: experiences of the first four years. *Struct Dyn* 6:e064301. <https://doi.org/10.1063/1.5128672>.

## ONLINE SUPPLEMENTAL INFORMATION

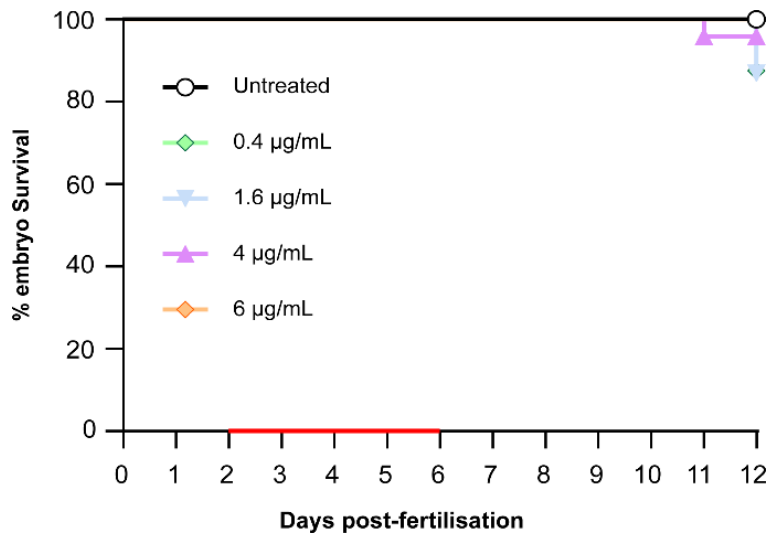
**Table S1. Crystallographic data collection and refinement statistics.**

Data collection and processing	InhA <sub>MFO</sub> with NAD	InhA <sub>MFO</sub> with NITD-916 and NAD
Wavelength (Å)	0.97872	0.97872
Resolution range (Å)	50 – 1.80 (1.84 – 1.80)	50 – 2.05 (2.10 – 2.05)
Space group	<i>P</i> 2 <sub>1</sub>	<i>C</i> 2
Unit Cell	94.94 90.98 91.91 / 90 90.96 90	79.30 101.54 76.48 / 90 114.36 90
Unique reflections	112,564 (8,118)	34,582
Multiplicity	3.8 (3.4)	3.6 (3.6)
Completeness (%)	98.7 (96.2)	99.6 (99.8)
Mean I/sigma(I)	18.2 (4.34)	13.32 (3.30)
R-merge (%)	0.05 (0.268)	0.063 (0.391)

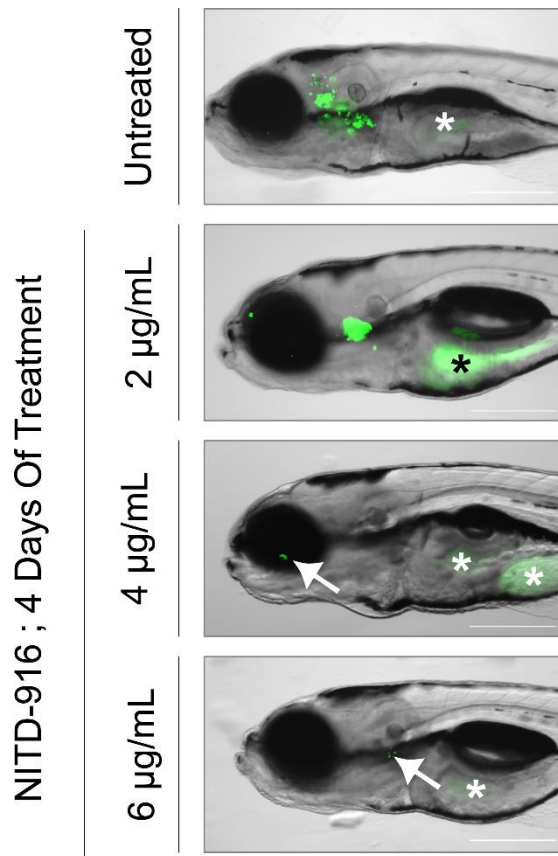
  

Refinement	InhA <sub>MFO</sub> with NAD	InhA <sub>MFO</sub> with NITD-916 and NAD
Number of reflections	112,536	34,555
Number of R-free reflections	1925	2,035
R-work %	0.146	0.205
R-free %	0.177	0.247
RMS(bonds)	0.010	0.007
RMS(angles)	1.197	0.837
Wilson B-factor (Å <sup>2</sup> )	24.64	26.94
Ramachandran plot		
Favored (%)	95.58	95.30
Allowed (%)	4.27	4.32
Outliers (%)	0.15	0.38
PDB ID	7K73	7U00





**Figure S1.** Uninfected embryos were immersed in water containing increasing concentrations of NITD-916 (ranging from 0.4 to 6 µg/mL) for 4 days. The red bar indicates duration of the treatment. The graph shows the percentage of embryo survival exposed to the compound over a 12-day period. Results are from two separate experiments.



**Figure S2.** Representative embryos from the untreated group and from the treated group with 2, 4 and 6  $\mu\text{g}/\text{mL}$  NITD-916 at 5 days post-infection (4 days of treatment). White arrowheads show eGFP-expressing bacteria. Scale bar, 300 $\mu\text{m}$ . \* indicates autofluorescence of the yolk.



# Discussion Générale et Perspectives



Les infections bactériennes dans leur globalité n'ont cessé d'augmenter ces dernières années tirant la sonnette d'alarme sur les infections bactériennes multirésistantes et l'utilisation exagérée ou inadéquate des antibiotiques. Les autorités sanitaires estiment que si rien n'est fait, à partir de 2050 plus de 10 millions de décès annuels seront causés par ces infections bactériennes multirésistantes [519]. Les mycobactéries sont également concernées avec l'exemple frappant de la tuberculose. Définie comme l'une des infections les plus anciennes touchant l'Homme, elle est à ce jour de plus en plus décrite, avec de nombreuses solutions de traitement mises à disposition. Néanmoins, elle n'en reste pas pour le moins éradiquée à travers le monde et continue d'être préoccupante. De plus, une réelle émergence d'infections aux MNT apparaît, notamment à cause de certains pathogènes opportunistes à l'instar de *M. abscessus*, *M. fortuitum* ou encore *M. avium*. La prévalence mondiale des infections aux MNT, en constante hausse, est probablement sous-estimée en raison de l'absence de déclaration obligatoire dans certains pays, mais aussi de par la similarité avec les symptômes tuberculeux [520]. Cette confusion entraîne globalement une mauvaise prise en charge de l'infection et un traitement inadapté. Ces infections sont d'autant moins contrôlées chez des patients présentant des comorbidités, tels que les patients atteints de mucoviscidose sujets à des symptômes pulmonaires aggravés de la maladie.

L'incidence grandissante et la sévérité des infections sont exacerbées par la limite rencontrée avec les traitements actuels. Les infections mycobactériennes sont très difficiles à traiter en clinique et on considère notamment l'espèce *M. abscessus* comme étant la plus résistante aux antibiotiques. En effet, le traitement recommandé est très long et aboutit souvent à des impasses thérapeutiques, ou bien à une rechute suite à un traitement non adapté ou inefficace. Les mycobactéries affichent de nombreux mécanismes de résistance innés ou acquis permettant de contourner l'efficacité des agents thérapeutiques présents sur le marché, comme nous avons pu le décrire pour *M. abscessus* au sein d'une revue présentée en **Annexe 1**. Il a également été montré que ce pathogène opportuniste présente une certaine plasticité génomique lui permettant de s'adapter rapidement à son environnement et acquérir de nouveaux facteurs de virulence ou gènes de résistance exogènes [521].

Ces constats soulignent la nécessité grandissante de proposer de nouvelles thérapies efficaces pour lutter contre ces infections, particulièrement dans une ère où la recherche de nouveaux antibiotiques reste un processus long, fastidieux et onéreux. C'est dans ce contexte qu'ont été initiés ces travaux de thèse qui ont eu pour objectif de mettre en évidence des molécules efficaces, mais également de décrypter et valider une nouvelle cible exploitable dans le traitement des infections aux MNT.

Pour ce faire, une première approche a consisté à optimiser et modifier la structure de l'INH, afin de mettre en évidence de nouvelles entités chimiques présentant des activités améliorées contre



*M. tuberculosis*. Si l'INH est un antibiotique phare dans le traitement antituberculeux, son utilisation est associée à la recrudescence d'isolats cliniques résistants à cet antibiotique, d'où la nécessité d'apporter de nouveaux composés pour lutter contre la tuberculose. Une stratégie efficace peut consister en la modification de molécules connues et validées en générant des dérivés avec des profils pharmacologiques plus favorables [522]. Un concept attractif en chimie médicinale consiste en la synthèse de molécules hybrides où au moins deux pharmacophores avec des fonctions biologiques différentes sont liés afin de profiter de chacune de leur action ou contrebalancer les effets secondaires de l'un ou de l'autre [523]. Par exemple, l'incorporation de groupements lipophiles dans des molécules contenant l'INH peut augmenter la pénétration du composé au sein du bacille pour agir plus efficacement [524]. Plus particulièrement, nous avons mis en évidence l'activité antituberculeuse de bases de Schiff hybrides d'INH 1H-1,2,3 triazoles liés à la quinoline (16a-16g). Ces résultats entrent dans la lignée de travaux précédents menés par l'équipe, en collaboration avec l'équipe du Pr Vipin Kumar, grâce à la description de l'apport des noyaux quinoline [525], isatine [526] ou triazole [527]. La quinoline s'avère être un groupement intéressant retrouvé dans de nombreux produits naturels ou autres composés efficaces et approuvés tels que la BDQ ou les fluoroquinolones tels que la MOX, et s'est montrée nécessaire à l'activité de ces conjugués, au même titre que la partie INH [524,525]. Des diarylquinolines sont actuellement en cours de développement et d'évaluation clinique tels que TBAJ-587 / TBAJ-876 (TB Alliance) [528,529] ou la sudapyridine (ou WX-081) [530], respectivement en évaluation clinique de phase I (NCT04890535 / NCT05526911) et phase II (NCT04608955) contre *M. tuberculosis* [531–533]. Les groupements azoles, et notamment les 1, 2, 3-triazoles, ont également montré leur importance et entrent dans la composition de plusieurs antituberculeux [534]. De nombreuses études ont montré l'attractivité de ce groupement comme en témoigne, de manière non exhaustive, le composé I-A09 [535], les dérivés imidazo-[1,2-a]-pyridine-1,2,3-triazoles [536] ou encore les hybrides isatine bis(isonicotinylhydrazone) [527]. Les hétérocycles 1,2,3-triazoles offrent de nombreux avantages aux molécules tels qu'une meilleure stabilité, une amélioration de la solubilité, ainsi qu'une meilleure activité antimicrobienne [537]. Bien que ces composés soient de grande taille et que les entreprises pharmaceutiques privilégient les petites molécules moins coûteuses à produire, celles-ci présentent des intérêts non négligeables de par leurs différents groupements apportant tous une plus-value. Globalement, les petites molécules diffusent mieux à travers les membranes mais la paroi riche en lipides des mycobactéries représente un véritable bouclier protecteur, ainsi des molécules lipophiles vont, à ce titre, être avantagées. Par conséquent, l'ajout d'un noyau lipophile à l'INH améliore sa diffusion à travers l'enveloppe et permettrait, dans certains cas, d'empêcher la N-acétylation causée par la N-acétyltransférase, décrite comme un mécanisme de résistance important [538,539]. Ici, l'ensemble des molécules actives présentent une lipophilicité élevée avec un LogP





supérieur à celui de l'INH, ainsi que de bons paramètres ADMET indiquant une bonne biodisponibilité orale et un faible risque d'interaction médicamenteuse ou d'effets secondaires néfastes.

En résumé, ces résultats présentent des hybrides d'INH prometteurs dans la lutte contre les infections à *M. tuberculosis* bien que ces inhibiteurs nécessitent des études précliniques et cliniques approfondies. L'évaluation *in vitro* de leur combinaison avec d'autres antituberculeux pourrait être une première étape lorsque l'on sait que le traitement contre les isolats cliniques requiert l'usage d'un cocktail de plusieurs antibiotiques. Enfin, ces études pourraient être complétées par l'évaluation *in vivo* des analogues au sein d'un modèle animal préclinique murin avant de pouvoir envisager les phases cliniques de développement médicamenteux.

Ces premiers travaux ont mis en évidence l'importance de proposer de nouvelles solutions dans le traitement de la tuberculose qui pourraient également être extrapolées aux infections émergentes aux MNT. Dans cet optique, le second volet de mes travaux a permis de mettre en évidence l'activité d'une nouvelle classe de composés, les 4-hydroxy-2-pyridones et particulièrement la molécule NITD-916 contre les pathogènes opportunistes *M. abscessus* et *M. fortuitum*. En effet, ce composé s'est montré très efficace contre des souches cliniques des deux espèces que ce soit *in vitro*, au sein de macrophages et d'organoïdes alvéolaires, ou bien dans un modèle de poisson zèbre infecté par *M. fortuitum*. Des études précédentes ont montré l'innocuité de ce composé, ainsi que de bons paramètres pharmacologiques de distribution et de clairance ce qui en fait un très bon candidat pour des études précliniques et cliniques approfondies [540]. Ces dernières pourraient inclure l'évaluation de potentielles interactions médicamenteuses avec des antibiotiques du traitement, bien que nous ayons pu mettre en évidence une interaction indifférente avec certains des médicaments utilisés en clinique, suggérant la possibilité d'introduire NITD-916 dans le régime thérapeutique actuel.

Nos résultats représentent également une preuve de concept dans laquelle le ciblage direct de la protéine InhA est approuvé chez ces deux MNT. En effet, le rôle essentiel d'InhA au sein des mycobactéries est conservé, et NITD-916 inhibe la biosynthèse *de novo* des acides mycoliques en se liant de manière directe à l'énoyl-ACP réductase InhA comme ont pu le montrer les études biochimiques et la résolution des structures cristallographiques (PDB : 7U0M et PDB : 7U0O). Ces études valident donc InhA comme étant une cible à développer lors des programmes de recherche de nouveaux composés chez les MNT telles que *M. abscessus* ou encore *M. fortuitum*. La résolution et la disponibilité des structures ternaires contenant l'enzyme, le cofacteur et l'inhibiteur faciliteront grandement l'élaboration d'analogues de NITD-916 dans de futures études de type structure-activité. Elles viennent stimuler de nouveaux programmes de chimie médicinale dans un but d'optimisation de pénétration, de solubilité, de distribution et d'activité du composé actif. En outre, la conservation



structurale entre la protéine InhA de *M. tuberculosis* et celle de *M. abscessus* (87,7% d'identité protéique) ou *M. fortuitum* (88,5% d'identité protéique) est un facteur clé poussant à tester les nombreux inhibiteurs directs validés contre *M. tuberculosis*. En effet, les techniques de criblage à haut débit ont permis d'identifier une large diversité d'inhibiteurs directs contre la protéine InhA de *M. tuberculosis* [487]. Ainsi, nos travaux démontrent l'intérêt de repositionner des composés préalablement décrits chez *M. tuberculosis* chez les MNT évitant par là-même d'initier de nouveaux programmes de criblage « *de novo* » souvent très longs et onéreux. Enfin, dans la plupart des cas les études concernant la tolérance, les propriétés pharmacocinétiques ou l'optimisation étant déjà conduites permettent une accélération de la découverte de nouveaux antibiotiques candidats contre les MNT [541,542]. Le potentiel de cette démarche, basé sur l'inhibition directe d'InhA ainsi que les paramètres pharmacologiques et structuraux vis-à-vis d'autres molécules inhibant la voie de synthèse des acides mycoliques sont discutés dans la revue ci-dessous.



**“New therapeutic strategies for *Mycobacterium abscessus* pulmonary diseases - untapping the mycolic acid pathway.”**

Matthéo Alcaraz, Thomas E. Edwards et Laurent Kremer. *Expert Review of Anti-infective Therapy*, 2023, Vol 21, N° 8, Page 813-829, PMID : 37314394, DOI : 10.1080/14787210.2023.2224563

REVIEW



# New therapeutic strategies for *Mycobacterium abscessus* pulmonary diseases – untapping the mycolic acid pathway

Matthéo Alcaraz<sup>a</sup>, Thomas E. Edwards <sup>b,c</sup> and Laurent Kremer <sup>a,d</sup>

<sup>a</sup>Centre National de la Recherche Scientifique UMR 9004, Institut de Recherche En Infectiologie de Montpellier (IRIM), Université de Montpellier, Montpellier, France; <sup>b</sup>Division of Structural Biology, UCB BioSciences, Bainbridge Island, WA, USA; <sup>c</sup>Seattle Structural Genomics Center for Infectious Disease (SSGICD), Seattle, WA, USA; <sup>d</sup>Inserm, IRIM, Montpellier, France

## ABSTRACT

**Introduction:** Treatment options against *Mycobacterium abscessus* infections are very limited. New compounds are needed to cure *M. abscessus* pulmonary diseases. While the mycolic acid biosynthetic pathway has been largely exploited for the treatment of tuberculosis, this metabolic process has been overlooked in *M. abscessus*, although it offers many potential drug targets for the treatment of this opportunistic pathogen.

**Areas covered:** Herein, the authors review the role of the MmpL3 membrane protein and the enoyl-ACP reductase InhA involved in the transport and synthesis of mycolic acids, respectively. They discuss their importance as two major vulnerable drug targets in *M. abscessus* and report the activity of MmpL3 and InhA inhibitors. In particular, they focus on NITD-916, a direct InhA inhibitor against *M. abscessus*, particularly warranted in the context of multidrug resistance.

**Expert opinion:** There is an increasing body of evidence validating the mycolic acid pathway as an attractive drug target to be further exploited for *M. abscessus* lung disease treatments. The NITD-916 studies provide a proof-of-concept that direct inhibitors of InhA are efficient in vitro, in macrophages and in zebrafish. Future work is now required to improve the activity and pharmacological properties of these inhibitors and their evaluation in pre-clinical models.

## ARTICLE HISTORY

Received 28 February 2023  
Accepted 8 June 2023

## KEYWORDS

Chemotherapy; InhA; Inhibition; MmpL3; *Mycobacterium abscessus*; Mycolic acid

## 1. Introduction

*Mycobacterium abscessus* (*Mabs*) is a rapidly growing non-tuberculous mycobacterium (NTM) of increasing clinical concern [1]. This opportunistic pathogen is also often overshadowed by other well-known mycobacteria such as *Mycobacterium tuberculosis* (*Mtb*), particularly in tuberculosis (TB)-endemic countries [2]. There is a probable underestimation of the number of cases of *Mabs* infection, due to the overlapping of its clinical manifestations with diseases caused by *Mtb*. As a consequence of misdiagnosis and because this pathogen only poorly responds to standard TB drug regimens, this can lead to ineffective management of *Mabs* infection, thus contributing to the increase in the number of cases [3]. *Mabs* is responsible for a wide panel of clinical manifestations, such as skin and soft tissue infections as well as severe pulmonary infections in patients with preexisting lung disorders, such as bronchiectasis or cystic fibrosis (CF) [4]. In CF patients, the presence of *Mabs* often correlates with rapid deterioration of the lung function and can be pernicious for subsequent lung transplantation [5–7]. Treatment of *Mabs* infections is very challenging and complicated by the existence of three subspecies with different drug susceptibilities to antibiotics and clinical outcomes [8]: *M. abscessus* subsp. *abscessus*, *M. abscessus* subsp. *bolletii* and *M. abscessus* subsp. *massiliense*. These complications are partially due to the presence or absence of a functional *erm(41)* gene that encodes an rRNA methylase that confers inducible macrolide resistance [9]. While *erm(41)* is

present in both *M. abscessus* subsp. *abscessus* and *M. abscessus* subsp. *bolletii*, it is absent in *M. abscessus* subsp. *massiliense*, explaining the difference in susceptibility to macrolides between these subspecies [10].

*Mabs* is intrinsically resistant to many antibiotic classes, rendering treatments very complicated and often unpredictable [11–14]. Among the many contributing factors to drug resistance, acquired drug resistance resulting from mutations in the drug targets has been reported [1,15]. Importantly, the *Mabs* resistome encompasses various factors, such as the low permeability of the cell envelope and the extraordinary ability of the bacteria to metabolize most antibiotics, converting them to unproductive metabolites, a mechanism which is driven by the production of numerous drug-modifying enzymes [16]. In addition, the expression of a large set of efflux pumps and the absence or dysfunctional drug-activating enzymes are other determinants of antibiotic resistance in this species [11,14,17].

Standard multi-drug chemotherapy is very lengthy (for months to years) and usually includes an oral macrolide (azithromycin or clarithromycin) coupled with intravenously administered aminoglycosides (amikacin) and  $\beta$ -lactams (imipenem or ceftazidime) [18–20]. In some instances, mostly in response to severe side effects or poor clinical response companion drugs, such as tigecycline or clofazimine, are added to strengthen the regimen [21]. Despite intensive chemotherapy, the success

### Article highlights

- *Mycobacterium abscessus* lung disease is a highly drug-resistant bacterial infection with very limited treatment options.
- The need to accelerate and improve novel antibiotics and regimens for *M. abscessus* pulmonary infections is urgent.
- The *M. abscessus* drug discovery pipeline is currently underpopulated and needs to be filled.
- The mycolic acid biosynthesis pathway, containing potential attractive drug targets, has recently been investigated for the search of new effective compounds against *M. abscessus*.
- Hit compounds against InhA and MmpL3, involved in the synthesis and transport of mycolic acids, are active against *M. abscessus*.
- The set of hit compounds identified encourages further hit-to-lead development to improve efficacy and pharmacokinetic properties.

rate of treatment remains very low, particularly in the case of *erm(41)*-induced resistance to macrolides (25–40%), which appears in 40–60% of the clinical strains [22]. Thus, given the poor performances of the current chemotherapy, new effective drugs are highly desired to treat *Mabs* lung diseases. *De novo* drug discovery developments to identify novel chemical scaffolds are usually hampered by low hit rates [23]. However, the rise of pharmacological development activities for NTM diseases during these last few years led to the discovery of new drug targets as well as new chemotypes with good activities against *Mabs in vitro* and in various animal models [1,15,24].

Mycolic acids (MA) represent crucial elements of the mycobacterial cell wall. They are homologous series of C<sub>60–90</sub>  $\alpha$ -alkyl  $\beta$ -hydroxy fatty acids and are primarily found as esters of the non-reducing arabinan terminus of arabinogalactan [25] and as extractable free lipids within the cell wall, mainly associated with trehalose to form trehalose dimycolates (TDM) [26]. MA are the primary targets of isoniazid (INH) and ethionamide (ETH) in *Mtb*, two drugs largely used for the treatment of TB. However, clinically used drugs against *Mabs* infections hitting the MA pathway are not available yet, though recent studies have emphasized that this metabolic pathway represents an excellent niche for druggable targets in *Mabs*. This is exemplified by the large number of hit compounds inhibiting the MA transporter MmpL3 [23,27,28] or the enoyl-ACP reductase InhA of the type II fatty acid synthase (FAS-II) [29], leading to the arrest of MA biosynthesis and mycobacterial cell death. This has raised strong interest in both MmpL3 and InhA as attractive targets for future drug development against *Mabs* lung diseases. In this review, we present recent research on inhibitors of the MA pathway in *Mabs* and discuss how this may be further exploited as alternative approaches to enhance treatment outcomes and reduce the burden on the patient produced by drug-associated side effects.

## 2. Mycolic acids and the mycobacterial cell envelope

### 2.1. The mycobacterial cell envelope

The cell wall of mycobacteria has been widely studied during the last few decades. It comprises a wide range of

complex lipids rendering this envelope highly hydrophobic. Briefly, from the inside to the outside, the cell wall is composed of a plasma membrane, a periplasmic space surrounded by the peptidoglycan, an arabinogalactan layer, and an outer membrane (Figure 1). The innermost plasma membrane consists of a phospholipid bilayer which anchored different glycolipids, such as phosphatidyl-myoinositol mannosides (PIM) [30] as well as lipoglycans, such as lipomannan (LM) or lipoarabinomannan (LAM) [31]. These latter are synthesized by the successive addition of mannose and arabinose residues to the PIM [32]. PIM, LM, and LAM can also be found in the outermost layer of the cell envelope, where they may interact with host cells [33]. They also contribute to the integrity of the cell wall as well as to antibiotic resistance or virulence [34]. The periplasmic space, a granular layer, and low-density zone [35,36] comprises peptidoglycan (PG) covalently linked to arabinogalactan (AG), which is a highly branched heteropolysaccharide composed of D-galactofuranosyl and D-arabinofuranosyl residues. PG consists of a glycan backbone of alternating units of *N*-acetylglucosamine and modified muramic acid (Mur) in a  $\beta$ -(1,4) linkage, with tetrapeptide side chains attached to Mur, typically consisting of L-alanyl-D-glutamine-meso-diaminopimelyl-D-alanyl that are cross-linked. PG cross-links are catalyzed by D, D-transpeptidases and L,D-transpeptidases forming, respectively, 4–3 and 3–3 linkages in mycobacteria [37,38]. This periplasmic structure allows to maintain the cell shape [39]. Muramic residues of PG are covalently tethered to AG via a disaccharide phosphate linker unit [40,41]. AG is itself esterified by  $\alpha$ -alkyl  $\beta$ -hydroxy long-chain C<sub>60</sub>–C<sub>90</sub> MA [42], forming the inner leaflet of the outer membrane (mycomembrane). Interspersed within the outer leaflet of the mycomembrane are found numerous molecules, including proteins and extractible glycolipids [43]. While some of these extractible lipids are common to all mycobacteria, such as trehalose monomycolates (TMM) and TDM, others can be restricted to certain species. *Mabs* or *Mycobacterium avium*, for instance, produce glycopeptidolipids (GPL) which are absent in *Mtb* [44,45]. These lipids are immunogenic [46], participate in biofilm formation and in masking underlying TLR–2 agonists, thus modulating the host immune response [46,47]. The organization and composition of this asymmetrical outer bilayer confer to mycobacteria a high intrinsic resistance to many antimicrobial agents and host defense mechanisms. In addition to the mycolyl arabinogalactan-peptidoglycan (mAGP) complex that constitutes the cell wall core, a loosely attached capsular-like structure outside the mycomembrane has also been described.

### 2.2. Structures and properties of mycolic acids

MA are essential components of the mycobacterial cell envelope, representing up to 60% of the cell wall content and 50% of its dry weight. These very long fatty acids contain up to 90 carbon atoms [26] and offer a broad structural diversity. MA are constituted of a short alkyl chain ( $\alpha$ -branch) of 24–26 carbon atoms and a longer meromycolic chain containing between 42 and 62

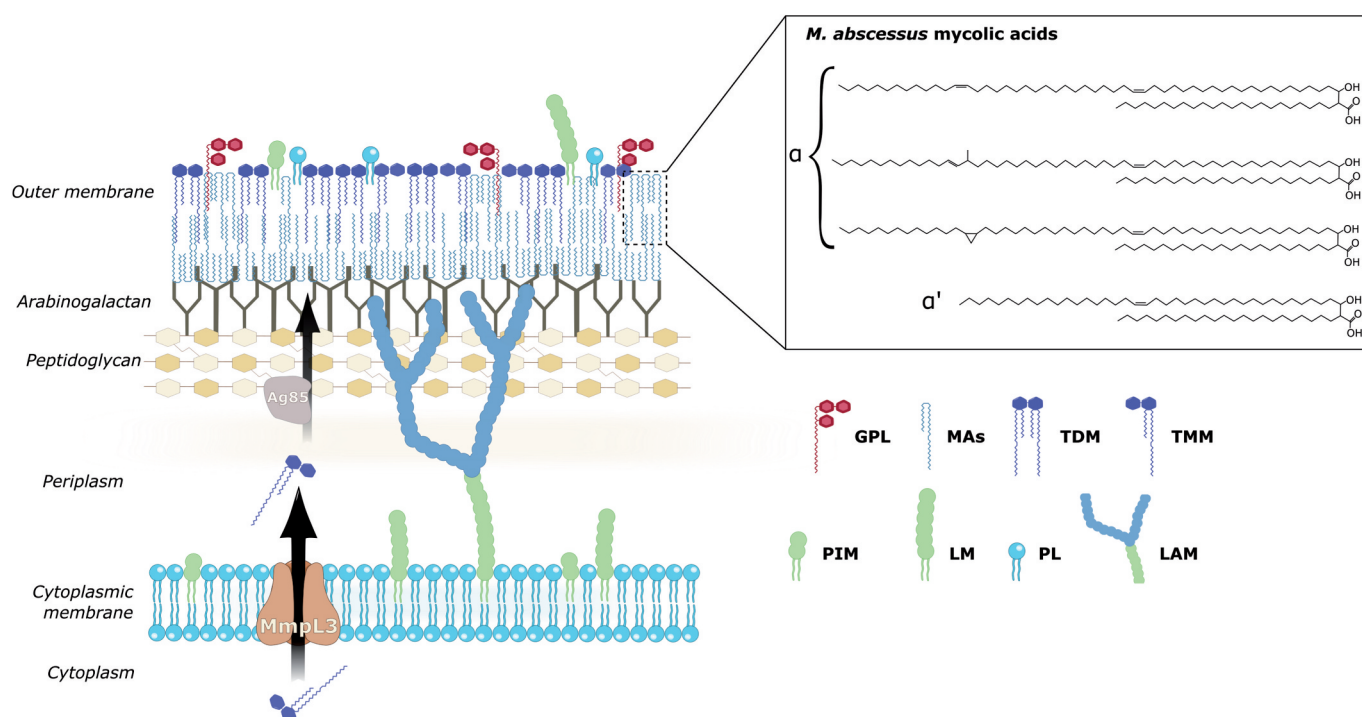


**Figure 1.** Model of the *M. abscessus* cell envelope. This schematic representation shows the multiple concentric layers composing the *M. abscessus* cell envelope, consisting of a cytoplasmic membrane, a periplasmic space surrounded by the peptidoglycan layer, itself covalently attached to the arabinogalactan layer. The latter is esterified by very long chain mycolic acids (MA), forming the inner leaflet of the outer membrane. Various glycolipids, including trehalose dimycolates (TDM), trehalose monomycolates (TMM), glycopeptidolipids (GPL) or phospholipids constitute the outer leaflet of the outer membrane. The MmpL3 membrane protein transports TMM across the cytoplasmic membrane. The Ag85 complex uses TMM as substrate to transfer MA onto arabinogalactan as well as to produce TDM, also known as cord factor. A representation of the main MA subspecies (designated  $\alpha$ -MA and  $\alpha'$ -MA) shows the very long meromycolic acid branch (harboring sites of chemical modification such as desaturation or cyclopropanation) joint to a shorter  $\alpha$ -chain.

carbon atoms, depending on the mycobacterial species. They can be secreted as free lipids, covalently bound to AG to form the inner leaflet of the mycomembrane or esterified to trehalose to generate TMM/TDM associated to the outer leaflet of the mycomembrane [48]. Each mycobacterial species is typified by a specific mycolic acid signature. Differences occur mainly at two positions in the meromycolic acid chain, close to the  $\beta$ -hydroxy acid (proximal site) or close to the -end of the chain (distal site) [49] (Figure 1). *Mabs* synthesizes only  $\alpha$ - and  $\alpha'$ -mycolic acids, the latter comprising a shorter meromycolic chain and one *cis* double bond, synthesized by the enzyme coded by *MAB\_1915* [50].  $\alpha$ -mycolates are the most abundant and the most apolar species, containing 74–80 carbon atoms in *Mabs*. Halloum *et al.* established that *Mabs*  $\alpha$ -MA consist of a mixture of mycolates containing *cis*- or *trans*-double bonds as well as *cis*-cyclopropane rings present in very minor amounts [51]. In general, MA confer important characteristics to mycobacteria, such as low permeability to hydrophilic antibiotics, resistance to chemical injury and to dehydration and persistence in the macrophage phagolysosome [48]. Important structural differences are found between mycobacterial species [49], explaining distinct virulence traits or morphological phenotypes.  $\alpha$ -mycolates play a role in the cell wall structure and stability, cyclopropanated mycolates decrease the fluidity of cell wall [52], while oxygenated MA, found in *Mtb*, are essential for virulence [53]. Cyclopropanated MA also play a crucial role in mycobacterial persistence in macrophages [54] and pathogenicity in

infected mice [55]. Interestingly, a mutant of *Mtb* lacking *pcaA*, with a defect in the proximal *cis*-cyclopropane ring, is affected in cording [56], while cords have been implicated in pathogenesis [57,58]. Due to their essentiality and contribution in multiple aspects of mycobacterial pathogenesis, understanding the various enzymatic steps leading to MA production and transport is of paramount importance for future drug developments.

### 2.3. Mycolic acid biosynthesis and transport

The mycolic acid biosynthetic pathway comprises multiple enzymatic activities that have been widely scrutinized in *M. smegmatis* and *Mtb* [26] and engages the action of the type I and type II fatty acid synthases (FAS), designated FAS-I and FAS-II, respectively (Figure 2). FAS-I is an essential and multifunctional enzyme that has a distinct capacity to elongate acetyl-CoA to fatty acids beyond  $C_{16}$ , up to  $C_{24/26}$  [59,60], providing primers which are further elongated by FAS-II to generate the meromycolic acids ( $C_{56}$ ), ultimately condensed with the  $C_{26}$   $\alpha$ -branch to form mature MA [26].

Unlike FAS-I, FAS-II is not capable of *de novo* synthesis of fatty acids but rather elongates acyl-CoA primers generated by FAS-I. The elongation cycle requires malonyl-ACP, resulting from the transacylation of malonyl-CoA and phosphopantothienylated *holo*-ACP by the malonyl-CoA:ACP transacylase FabD [61]. ACP shuttles the growing acyl chain from one



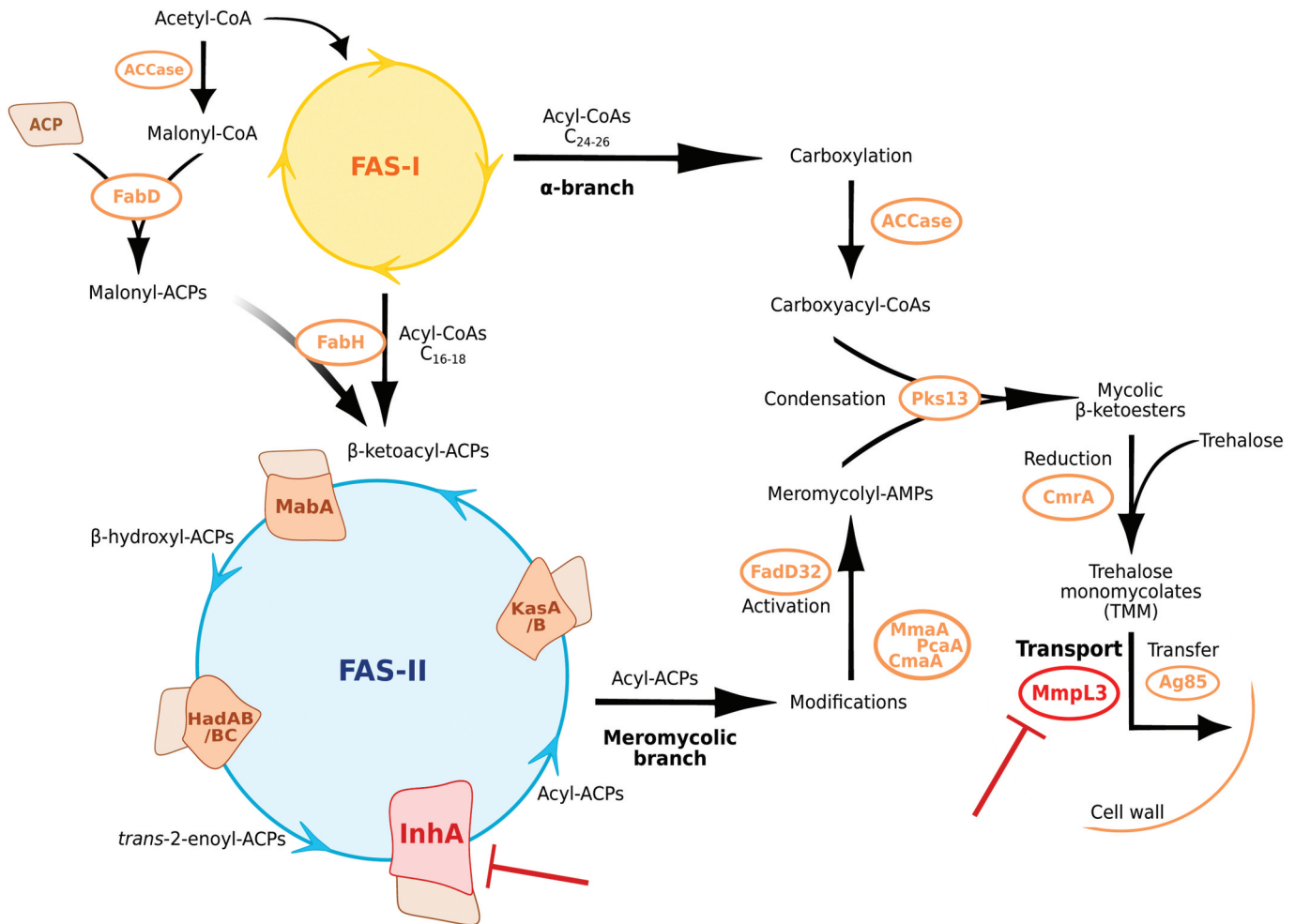


**Figure 2.** Mycolic acid biosynthesis and transport in mycobacteria. The MA biosynthetic pathway starts with de novo synthesis of fatty acids by FAS-I, yielding both the  $C_{24-26}$  acyl-CoA ( $\alpha$ -branch) and the  $C_{16-18}$  acyl-CoA, which will be elongated by FAS-II. The latter substrates undergo a condensation with malonyl-ACP in a reaction catalyzed by FabH and resulting in  $\beta$ -ketoacyl-ACP derivatives. The elongation step is operated by FAS-II through iterative cycles comprising the concerted action of MabA, HadAB/BC, InhA and KasA/B and conducting to the synthesis of the  $C_{56}$  meromycolic acid chain. During synthesis, these products are subjected to chemical modification and the resulting meromycolyl-AMP are then condensed with the  $\alpha$ -branch. The resulting mycolic  $\beta$ -ketoesters are thereafter reduced to yield mature MA, subsequently transported and transferred to the cell wall by MmpL3 and the Ag85 complex, respectively. The red lines indicate the two sites of inhibition which are the focus of this review.

enzyme to the other. The initiation step in elongation relies on the condensation of acetyl-CoA with malonyl-ACP catalyzed by  $\beta$ -ketoacyl-ACP synthase III (FabH), resulting in a  $\beta$ -ketoacyl-ACP [62]. Then, reactions mediated by FAS-II consist of iterative cycles of four enzymatic steps, leading to the  $C_{56}$  meromycolic acid chain. The first elongation step starts with the reduction to the  $\beta$ -keto group of the  $\beta$ -ketoacyl-ACP by MabA to yield a  $\beta$ -hydroxyl-ACP intermediate [63], which is subsequently dehydrated by the action of the dehydratase complexes HadAB and HadBC to generate enoyl-ACP [64]. These intermediates are then reduced by the *trans*-2-enoyl-ACP reductase InhA to produce saturated acyl-ACP [65,66]. Finally, the  $\beta$ -ketoacyl-ACP synthases KasA or KasB initiate the additional cycles of elongation to form  $\beta$ -ketoacyl-ACP of increasing chain length, until the required length for the meromycolic chain is reached [67,68]. Before condensation with the  $\alpha$ -branch, the meromycolic acid undergoes modifications such as desaturation, introduction of oxygenated functions, cyclopropyl or methyl groups, thanks to the action of

multiple S-adenosylmethionine (SAM)-dependent methyltransferases [53,54,55,69,70]. Finally, the polyketide synthase Pks13 catalyzes the condensation of the  $\alpha$ -branch with the activated meromycolic acid chain [71], ultimately leading to a mycolic  $\beta$ -ketoester, further reduced by CmrA to produce mature mycolates esterified to trehalose (TMM) [72]. TMM is then translocated across the membrane *via* the transporter MmpL3 [73], an essential step required for the formation of trehalose dimycolate (TDM) and esterification of arabinogalactan by the antigen Ag85 complex [74,75].

The essentiality of most mycolic acid biosynthetic enzymes makes them particularly suitable for the development of inhibitors, and numerous enzymatic steps can be chemically inhibited in *Mtb*, providing the ground for new anti-TB therapies [76,77]. While this metabolic process is targeted by the first-line (INH) and second-line (ETH) anti-TB drugs, both inhibiting the *trans*-2-enoyl-ACP reductase InhA [78–80], none such clinically used drugs have been developed for the treatment of *Mabs* infections. However, current efforts are



revisiting and/or optimizing existing FAS-II inhibitors and validating InhA and MmpL3 as chemotherapeutic targets for the treatment of *Mabs* diseases (Figure 2).

### 3. Chemical inhibition of MmpL3

MmpL3, encoded by the essential *mmpL3* gene in *Mtb* and *M. smegmatis* [73,81,82], belongs to the Resistance-Nodulation-Cell Division (RND) family of membrane proteins [83] and is a known transporter of TMM across the plasma membrane [84]. Down-regulation of MmpL3 has a rapid bactericidal effect and renders *Mtb* more susceptible to MmpL3 inhibitors [85]. Multiple high-throughput whole cell-based screens identified MmpL3 as the target of several antitubercular compounds, making MmpL3 one of the most promising pharmacological targets in *Mtb* as well as in NTM, thus opening a new field in the inhibition of mycolic acid transport. Blocking this transporter leads to an intracellular accumulation of TMM with

a concomitant reduction in the TDM pool and in MA-bound AG, causing bacterial death [73]. We report below the major MmpL3 inhibitors for which an activity and/or mechanism of action have been reported in *Mabs*. As shown in Table 1, these inhibitors exhibit a wide structural diversity.

The first demonstration of the involvement of MmpL3 in MA transport has been provided by studying the mechanism of action of the adamantyl urea AU1235 in *M. smegmatis* and *Mtb* [73,86]. AU1235 also exhibits low MIC against *Mabs* (1.5  $\mu\text{M}$ ) and other NTM [73,87]. The compound affects the translocation of TMM in *Mtb* and in *M. smegmatis* and whole-genome sequencing of *Mtb* AU1235-resistant mutants unraveled mutations in *mmpL3*.

Following a strategy based on the repositioning of anti-TB molecules, Dupont *et al.* screened a GSK library containing 177 validated compounds against *Mtb* [88] and identified a compound exhibiting very low MIC (0.33  $\mu\text{M}$ ) against *Mabs* [23]. The lead molecule tested (GSK1985270A), also

**Table 1.** Main reported MmpL3 inhibitors against *M. abscessus*.

ID	Name	Structure	MIC	Ref
1	AU1235		<i>M. abscessus</i> = 1.5 $\mu\text{M}$ <i>M. smegmatis</i> = 9.3 $\mu\text{M}$ <i>M. fortuitum</i> = 9.6–19.2 $\mu\text{M}$ <i>M. avium</i> > 96 $\mu\text{M}$ <i>M. tuberculosis</i> = 0.3–0.6 $\mu\text{M}$	[73,87]
2	PIPD1		<i>M. abscessus</i> = 0.33 $\mu\text{M}$ <i>M. tuberculosis</i> = 0.33 $\mu\text{M}$	[23,151]
3	Cpd 6		<i>M. abscessus</i> = 0.36 $\mu\text{M}$ <i>M. tuberculosis</i> = 0.09 $\mu\text{M}$	[27]
4	Cpd 12		<i>M. abscessus</i> = 0.41 $\mu\text{M}$ <i>M. tuberculosis</i> = 0.01 $\mu\text{M}$	[27]
5	IC5		<i>M. abscessus</i> = 0.89 $\mu\text{M}$ <i>M. avium</i> = 28.5 $\mu\text{M}$ <i>M. chelonae</i> = 0.89 $\mu\text{M}$ <i>M. smegmatis</i> = 5.55 $\mu\text{M}$ <i>M. tuberculosis</i> = 0.71 $\mu\text{M}$	[93]
6	IC25		<i>M. abscessus</i> = 0.03 $\mu\text{M}$ <i>M. avium</i> = 0.17–0.84 $\mu\text{M}$ <i>M. chelonae</i> = 0.02 $\mu\text{M}$ <i>M. smegmatis</i> = 1–2 $\mu\text{M}$ <i>M. tuberculosis</i> = 0.07 $\mu\text{M}$	[93]
7	EJMCh-6		<i>M. abscessus</i> = 0.38 $\mu\text{M}$ <i>M. tuberculosis</i> = 0.24 $\mu\text{M}$	[28,96]
8	CRS400393		<i>M. abscessus</i> = 0.04–0.65 $\mu\text{M}$ <i>M. fortuitum</i> = 0.16 $\mu\text{M}$ <i>M. avium</i> = 5.22 $\mu\text{M}$ <i>M. intracellulare</i> = 5.22 $\mu\text{M}$ <i>M. tuberculosis</i> < 0.31 $\mu\text{M}$	[98–100]
9	HC2091		<i>M. abscessus</i> = 20 $\mu\text{M}$ (MIC <sub>95</sub> )	[102]
10	E11		<i>M. abscessus</i> = 12 $\mu\text{M}$	[103]

designated PIPD1, belongs to the piperidinol class of molecules. PIPD1 was not only active *in vitro* but it also reduced the bacterial burden in macrophages as well as in zebrafish embryos infected with *Mabs*. That PIPD1 targets MmpL3 was demonstrated by the fact that it inhibited the transport of TMM and because mutations occurring in *MAB\_4508* (*mmpL3*) in spontaneous resistant strains resulted in high resistance levels to the compound [23]. PIPD1 exhibited a good organ distribution after intraperitoneal administration in mice and was rapidly eliminated with a half-life of about 3 h [89]. Related derivatives were synthesized, some of which exhibiting low MIC, albeit not lower than the parental molecule. Docking simulations further emphasized MmpL3 as the major target for these analogs, paving the way for the design of new generations of anti-MmpL3 inhibitors with improved activity against *Mabs*.

The structurally unrelated compounds, the indole-2-carboxamides (Compounds 6 and 12) originally identified as potent anti-TB molecules targeting MmpL3 [90] showed very high activity against *Mabs in vitro* (MIC of 0.36 and 0.41  $\mu\text{M}$ , respectively) and inhibited MA transport [27]. Analysis of the *mmpL3* sequences in *Mabs* spontaneous resistant mutants unraveled a common A309P replacement in the transmembrane domain 5 of MmpL3. Overproduction of the A309P mutated allele in a wild-type strain of *Mabs* conferred co-resistance to PIPD1 as well as to the indole-2-carboxamides, thus validating their common target. Compound 12 reduced the intramacrophage *Mabs* burden at levels comparable to imipenem when used at 24 $\times$  the MIC concentration. Compounds 6 and 12 were nontoxic to Vero cells and were active at very low concentrations with MIC ranging from 0.18 to 3.28  $\mu\text{M}$  against a wide panel of clinical isolates of the *Mabs* complex (*M. abscessus*, *M. massiliense*, *M. boletii*) from CF and non-CF patients [27]. From a medicinal chemistry view, indole-2-carboxamides are easy to produce and early studies indicated that they show good ADME properties [27,91]. Subsequent studies showed that compounds 6 and 12 act synergistically with imipenem and cefoxitin *in vitro* and increase the bactericidal activity of the  $\beta$ -lactams against *Mabs* [92]. In addition, compound 12 also showed synergism with imipenem and cefoxitin within infected macrophages. These promising results are warranting the further evaluation of this drug combination in preclinical animal models. Other indole-2-carboxamide derivatives, designated IC5 and IC25, showed activity against a large panel of NTM, including *Mabs*, *M. chelonae* and *M. avium* [93]. Importantly, the *in vivo* efficacy of IC5 and IC25 was subsequently proven in a *Mabs* infection mouse model with a significant reduction in the bacterial loads in the lungs and spleens [94]. Pharmacokinetic studies indicate that IC25 has a good oral bioavailability in mice. A dose of 100 mg/kg leads to a maximum concentration of 0.49  $\mu\text{g/ml}$  and 2.47  $\mu\text{g/g}$  in the plasma and lungs, respectively, which is above the MIC against *Mabs* [90]. Recently, some of indole-based compounds were optimized to increase their aqueous solubility and pharmacokinetic profiles by reducing the

number of carbon atoms while maintaining high antimycobacterial activity [95]. The authors showed that acetamide-based compounds with adamantane or isopinocamphe head groups were optimal for antimycobacterial activity compared with the parental molecules. Electron-withdrawing or bulky group substituted in *meta*-position favored the antimycobacterial *in vitro* activity. These compounds display MIC values around 1  $\mu\text{M}$  against *Mabs*. The acetamide-based molecules showed better metabolic stability, the aqueous solubility increased by 30-fold compared to indole-based compounds and showed a 20-fold better permeability. Surface plasma resonance and docking studies further evidenced that MmpL3 is directly inhibited by these acetamide-based compounds.

The benzimidazole lead compound EJMCh-6 (2-(2-cyclohexylethyl)-5,6-dimethyl-1*H*-benzo[*d*]imidazole) showed excellent anti-*Mtb* activity *in vitro* [96] and its mode of action involves the inhibition of MmpL3 in *Mtb* [97]. In a subsequent study, EJMCh-6 was evaluated against *Mabs* and found to show superior *in vitro* activity as compared to imipenem, sutezolid, or linezolid against a large number of clinical strains with MIC values varying from 0.19 to 3  $\mu\text{M}$  [28]. The compound rapidly decreased the bacterial burden in *Mabs*-infected macrophages as well as in a zebrafish model of infection. Strikingly, treatment of the embryos with EJMCh-6 was associated with increased embryo survival as compared to the non-treated embryos. Insights into the mode of action of these compounds were inferred from the generation of spontaneous benzimidazole-resistant strains (generated at a frequency of  $5 \times 10^{-8}$  when plating the bacteria in the presence of 10 $\times$  the MIC concentration of EJMCh-6), followed by the characterization of a large set of missense mutations in MmpL3 [28]. Moreover, overexpression of the mutated *mmpL3* alleles in a susceptible *Mabs* strain induced high resistance levels to EJMCh-6 and to other known MmpL3 inhibitors.

High throughput screening of commercially available chemical libraries resulted in numerous hits active against *Mtb* and NTM [98]. Among them, CRS400393, harboring an amide-linked methylcycloheptyl group and two atoms of chlorine on the amino benzothiazole expressed activity against a broad-spectrum of the clinically-relevant mycobacteria, including *Mabs* (MIC of 0.04–0.65  $\mu\text{M}$ ) with a bactericidal effect against this species and an intracellular activity in *Mabs*-infected THP-1 cells [99,100]. As reported for the benzimidazoles and indole-2-carboxamides, these compounds also inhibit MA transfer to AG and synthesis of TDM in a concentration-dependent manner. Isolation of spontaneous resistant mutants of *Mabs* with mutations in the transmembrane region of MmpL3 forming the binding pocket of known MmpL3 inhibitors confirmed MmpL3 as the target. In addition, the lack of effect of CRS400393 on the membrane potential and electrochemical pH gradient of *Mabs* is in line with a direct inhibition of MmpL3 rather than an inhibition *via* dissipation of the proton motive force from which MmpL3 drives its energy. Determination of pharmacokinetic properties in

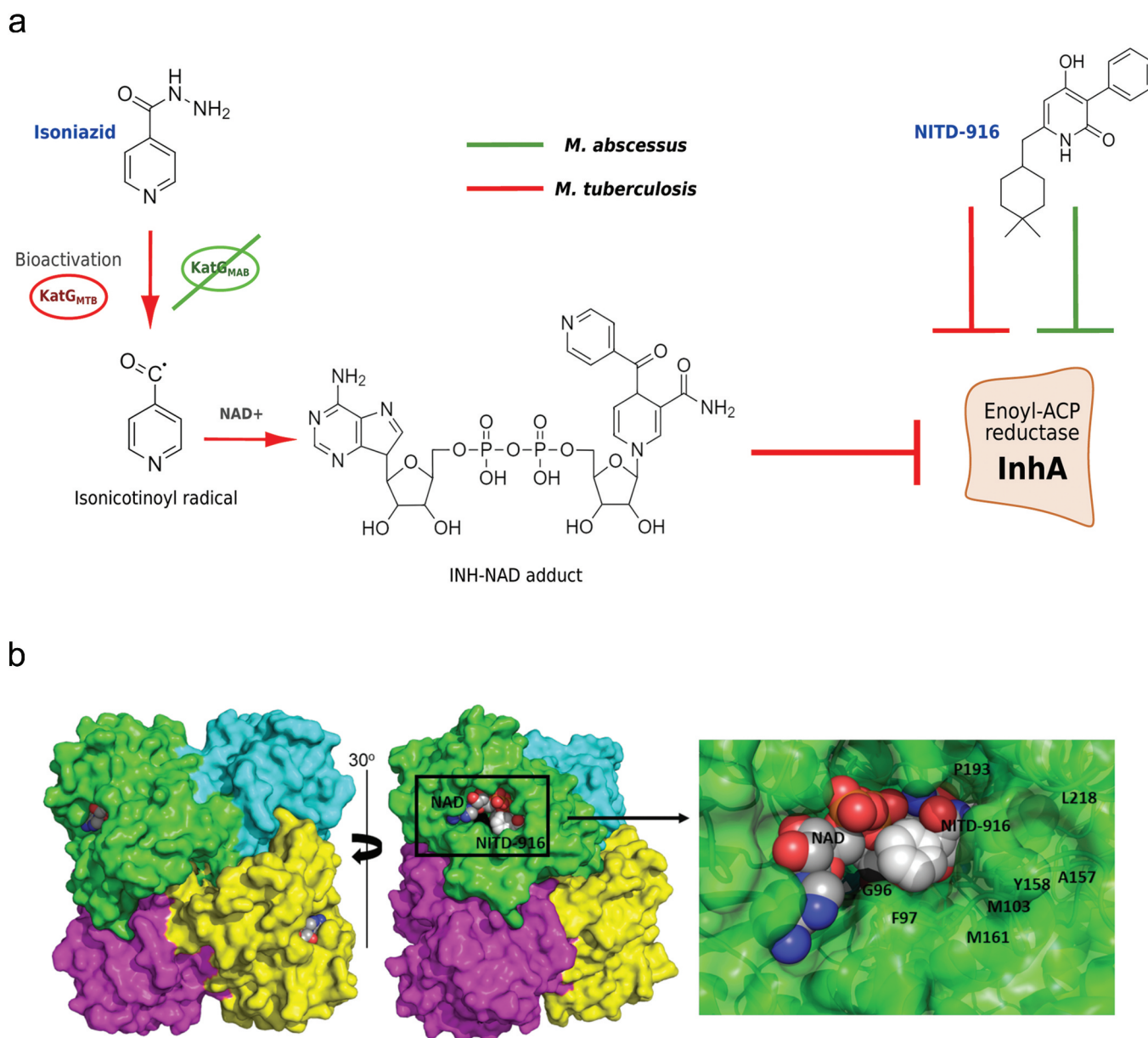


**Figure 3.** Bioactivation of INH and inhibition of InhA by INH and NITD-916 in *M. tuberculosis* and *M. abscessus*. (A) In *M. tuberculosis*, INH is activated by KatG<sub>MTB</sub> to form an isonicotinoyl radical which reacts with NAD<sup>+</sup> to form an INH-NAD adduct that inhibits the catalytic activity of the enoyl-ACP reductase InhA<sub>MTB</sub> of FAS-II. In *M. abscessus*, KatG<sub>MAB</sub> is unable to convert INH into an active metabolite, explaining the intrinsic resistance of this organism to INH. In contrast to INH, NITD-916 is not a prodrug and does not require KatG-mediated activation but has the capacity to inhibit InhA directly, resulting in the arrest of MA synthesis and bacterial death. Red line: activity in *M. tuberculosis*; green line: activity in *M. abscessus*. (B) Crystal structure of InhA<sub>MAB</sub> bound to NAD and NITD-916. InhA<sub>MAB</sub> is a homotetramer with each protomer shown in a different color. The active site cavity is deep yet solvent exposed. NAD is shown in CPK coloring with dark gray carbon atoms, and NITD-916 is shown in CPK coloring with light gray carbon atoms. The surface of G96 is colored in black. The dimethylcyclohexyl ring of NITD-916 is buried in a hydrophobic pocket surrounded by M103, A157, Y158, M161, P193, and L218. T196, M199, and M215 also make up the binding pocket but are obscured by NITD-916 from this perspective.

mouse model showed high concentrations above the MIC of CRS400393 in lung tissues after intratracheal instillation and a good oral bioavailability depending on the formulation. This molecule showed the capacity to decrease lungs CFU in a mouse model of pulmonary *Mabs* disease via the intranasal route [100].

Other MmpL3-targeting inhibitors selected against *Mtb* inhibited *Mabs* growth *in vitro*. For instance, while the benzothiazole derivative HC2184 [101] reduces growth of *Mabs* by 7% at 20  $\mu$ M, the 4-thiophen-2-ylloxane-4-carboxamide

HC2091 reduces this growth by 97% at 20  $\mu$ M. This compound is non-cytotoxic and shows good solubility [102].

Compound E11 is an acetamide inhibitor of MmpL3 in *Mtb*, which is also effective against *Mabs* with a MIC value of 12  $\mu$ M, with no signs of toxicity on HepG2, Vero, and THP-1 cells, thus promoting its further evaluation for the treatment of NTM infections [103].

Overall, these studies illustrate the increasing interest in the development of novel compounds targeting the transporter MmpL3 in mycobacteria and particularly in *Mabs*. Although

most of these compounds require further chemical optimization and need to be tested in preclinical and clinical studies, they support the view that targeting MA transport has strong potential for development into a treatment of *Mabs* pulmonary diseases.

## 4. Chemical inhibition of InhA

### 4.1. NITD-916

As mentioned above, MA biosynthesis inhibition is widely exploited in the treatment of TB, as exemplified with INH and ETH. Both drugs inhibit the enoyl-ACP-reductase InhA of FAS-II, leading to the arrest of MA production and bacterial death [65,78,79]. INH requires to be bioactivated by the catalase-peroxidase KatG [104] to generate an isonicotinoyl radical reacting with NAD<sup>+</sup> to form an INH-NAD adduct, which in turn blocks InhA activity [105,106] (Figure 3A). In contrast, KatG from *Mabs* (KatG<sub>MAB</sub>) is unable to transform INH into an active metabolite in *Mabs* [107], explaining why INH is totally inefficient in this species. However, overexpression of KatG from *Mtb* in *Mabs* increases the susceptibility of the strain to INH [29,107], implying that InhA<sub>MAB</sub> may still be a valuable enzyme to exploit in *Mabs*, provided that the inhibitors do not require KatG-dependent activation. This led to the hypothesis direct inhibitors of InhA<sub>MAB</sub> may be particularly attractive for the development of new therapies targeting the MA pathway. That InhA<sub>MTB</sub> and InhA<sub>MAB</sub> share 88% identity [29], suggests that inhibitors of InhA<sub>MTB</sub> may also be active against InhA<sub>MAB</sub>. This opened the possibility to evaluate the efficacy of KatG-independent InhA<sub>MTB</sub> inhibitors against *Mabs*, such as NITD-916 (Figure 3A), a 4-hydroxy-2-pyridone previously identified in a phenotypic screen against *Mtb* able to inhibit directly InhA<sub>MTB</sub> [29,108]. NITD-916 was very active against the *Mabs* reference strain (MIC of 0.5 μM in Cation-Adjusted Mueller Hinton broth), although the MIC value varied greatly depending on the medium used, and exhibited similar activity against a wide panel of clinical isolates [29]. In addition, this compound diminished the intramacrophage burden of *Mabs* by ~2 Log in the CFU counts at day 3 post-treatment at a concentration corresponding to 10× MIC. This correlated also with a significant reduction in the proportion of infected macrophages. *Mabs* exists in two morphotypes (smooth and rough) with the rough one being able to aggregate in large and compact structures, known as cords, on agar, in broth medium, inside macrophages or *in vivo* [109–111]. This rough morphotype and particularly intracellular cords are responsible of macrophage integrity disruption, lysis and death leading to pro-inflammatory response [46]. NITD-916 treatment correlated with a reduction in the number and size of intracellular cords. Consistently, NITD-916 is active in CF patient-derived airway organoids, used as model to recapitulate CF airway dysfunctions with a low CFTR activity, an accumulation of thick mucus and an increased susceptibility to *Mabs* infection [112,113]. In this CF environment, the efficacy of NITD-916 emphasizes the potential of this class of compounds

for future drug developments and improvements for the treatment of *Mabs*-infected CF patients. As expected, NITD-916 was found to inhibit *de novo* biosynthesis of MA in a dose-response manner, resulting in a bactericidal effect. Spontaneous resistant mutants (obtained at the frequency of  $2.3 \times 10^{-7}$  and  $2.3 \times 10^{-6}$  in the smooth and rough strain, respectively, in the presence of NITD-916 corresponding to 10× the MIC) harbor mutations in InhA<sub>MAB</sub>, particularly at position 96, a glycine which is conserved through different mycobacterial species. These mutants, highly resistant to NITD-916, were unaffected in their mycolates profile upon exposure to NITD-916, unlike the parental strain. Direct binding of NITD-916 to InhA<sub>MAB</sub> was confirmed by solving the ternary complex with InhA<sub>MAB</sub> together the cofactor NAD and NITD-916 at a high resolution. NITD-916 packs tightly against the NAD cofactor in a deep but partially solvent-exposed cavity (Figure 3B). It forms one direct and one water-mediated hydrogen bond with NAD. It forms a single direct hydrogen bond with Tyr158 and one water-mediated hydrogen bond with Thr196. All other interactions are van der Waals-mediated with surrounding hydrophobic residues. Overall, this proof-of-concept study validates the anabolic MA pathway, and particularly the reduction step catalyzed by InhA<sub>MAB</sub>, as an excellent target to be further exploited in drug development programs against *Mabs*.

These encouraging results also prompted to investigate the effect of NITD-916 in other NTM. *Mycobacterium fortuitum* (*Mfor*) represents another rapidly-growing mycobacteria encountered in patients [114]. This opportunistic pathogen is highly resistant to a large variety of antibiotics, including β-lactams, aminoglycosides, macrolides, tetracyclines, or anti-TB drugs [115,116]. As is the case for *Mabs*, none of the currently used drugs relies on the MA pathway in *Mfor*. This difficulty to clinically cure *Mfor* infections emphasizes the need for new molecules to include in the drug regimen. Since InhA from *Mfor* (InhA<sub>MFO</sub>) shares 88.5% identity with InhA<sub>MTB</sub> and 90% identity with InhA<sub>MAB</sub>, it was hypothesized that NITD-916 could also inhibit InhA<sub>MFO</sub>. NITD-916 exhibited very low MICs against several clinical isolates of *Mfor* [117] and strong antimycobacterial activity against *Mfor*-infected macrophages. Remarkably, the molecule was very active in a zebrafish model of *Mfor* infection. Particularly, in this animal model, a short time of treatment (1 day) was sufficient to significantly reduce global bacterial loads, to limit physiopathological symptoms such as cords and abscesses which are often associated with the severity of the disease. This also led to a strong protective effect of the embryos against killing by *Mfor* [117]. As for *Mtb* or *Mabs*, NITD-916 drastically inhibited the *de novo* synthesis of MA in an InhA-dependent manner. Supporting these results, the resolution of the crystal structure of the ternary complex InhA<sub>MFO</sub>-NAD-NITD-916 confirmed the direct binding of NITD-916 with InhA<sub>MFO</sub> [117].

Other 4-hydroxy-2-pyridone analogues, NITD-529 (MIC of 2.5 μM) and NITD-564 (MIC of 0.31 μM), show a weaker activity *in vitro* against *Mtb* as compared to NITD-916 (MIC of 0.08 μM), demonstrating the importance of the pyridone core, the 4-hydroxy-group and a lipophilic group [108]. NITD-916 and other pyridones are neither cytotoxic nor cardiotoxic and

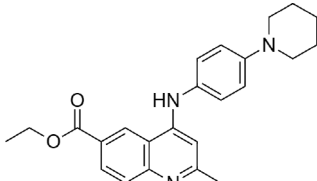
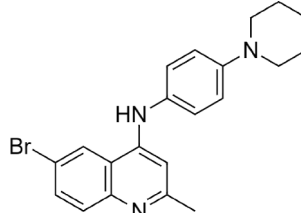


Table 2. Main reported direct InhA inhibitors against *M. tuberculosis*.

ID	Name	Structure	MIC	IC <sub>50</sub>	Ref
1	NITD-916		<i>M. tuberculosis</i> = 0.08 μM <i>M. abscessus</i> = 0.5 μM <i>M. fortuitum</i> = 0.01 μM	InhA <sub>MTB</sub> IC <sub>50</sub> = 0.57 μM	[29,108,117]
2	Triclosan		<i>M. tuberculosis</i> = 43.1 μM <i>M. abscessus</i> = 21.6 μM <i>M. marinum</i> = 21.6 μM <i>M. avium</i> = 64 μM	InhA <sub>MTB</sub> IC <sub>50</sub> = 1 μM	[122, 124, 152]
3	Pyridomycin		<i>M. tuberculosis</i> = 0.72 μM <i>M. abscessus</i> = 11.5 μM <i>M. smegmatis</i> = 1.4 μM <i>M. bovis</i> BCG = 0.72 μM <i>M. marinum</i> = 5.8 μM <i>M. avium</i> = 23 μM	N.D.	[129]
4	Pyrrolidine carboxamides		N.D.		[131]
	p24			p24: InhA <sub>MTB</sub> IC <sub>50</sub> = 0.39 μM 97% of InhA inhibition at 15 μM	
5	Pyrrole derivatives		<i>M. tuberculosis</i> = 0.5–2 μM	N.D.	[134]
6	Methyl-thiazoles		<i>M. tuberculosis</i> = 0.19 μM	InhA <sub>MTB</sub> IC <sub>50</sub> = 3 nM	[135]
7	Triazoles		N.D.	InhA <sub>MTB</sub> IC <sub>50</sub> = 0.074 nM	[137]
8	Acetamides		<i>M. tuberculosis</i> = 4.76 μM	InhA <sub>MTB</sub> IC <sub>50</sub> = 3.12 μM	[138]

(Continued)

Table 2. (Continued).

ID	Name	Structure	MIC	IC <sub>50</sub>	Ref
9	LABIO-17		<i>M. tuberculosis</i> = 12.8 μM	InhA <sub>MTB</sub> IC <sub>50</sub> = 20 μM	[140]
	4-aminoquinoline (19k)		<i>M. tuberculosis</i> = 0.1–0.4 μM	InhA <sub>MTB</sub> IC <sub>50</sub> = 0.23 μM	

present a low metabolic clearance in mouse and human hepatic microsomes. NITD-916 has a good oral bioavailability (66% at 25 mg/kg), and a plasma concentration *in vivo* above the MIC, even if the distribution to mice lungs is weaker, there is a good efficiency in both lungs and spleen of *Mtb*-infected mouse model [108].

Related analogs of NITD-916 could be synthesized to assess the effect of lipophilic or phenyl group replacement by aromatic substituents. One may hypothesize that it remains possible to optimize its structure to increase cell penetration through the thick lipid barrier. Moreover, NITD-916 presents a low aqueous solubility that limits a favorable oral administration of the compound. A phosphate ester prodrug analog (NITD-113) was designed and displaying better aqueous solubility. This prodrug is rapidly hydrolyzed by intestinal alkaline phosphatases and well bio-converted to NITD-916 in mice. Since NITD-916 suffers from poor lung distribution in mice, this prodrug strategy leads to a superior pulmonary distribution and is potentially transposable to other classes of compounds. Importantly, future studies should also assess the eventual harmful drug–drug interactions and a potential profitable synergy with another class of clinically validated drug. Since any *Mabs* antibiotic has to be clinically given in combination with other drugs [19], the lack of drug–drug interaction is critical and needs to be evaluated. Early determination of the Fractional Inhibitory Concentration Index indicates values between NITD-916 and most drugs used in clinics are in the 0.625 to 1.5 range [29], thus highlighting an indifferent interaction between these molecules and the suitability of introducing NITD-916 in combinational therapy. However, this will need to be confirmed in mouse models of infection [118].

Collectively, these results prove that targeting mycolic acid biosynthesis has an important translational potential for the development of new treatments against *Mabs* and *Mfor* infections. These combined *in vitro* and *in vivo* data on NITD-916 underscore the interest of this under-exploited chemical entity. Further experimentations are now required to test NITD-916 and related analogs in mouse infection models. Importantly, these results open the way for the evaluation of other direct InhA inhibitors, currently being tested as antitubercular drug candidates [119,120], against *Mabs* as well as against other NTM.

#### 4.2. Other direct inhibitors of InhA

While *de novo* discovery of InhA<sub>MAB</sub> inhibitors may be time consuming and costly, the vast array of available chemotypes active against InhA<sub>MTB</sub> identified in previous screens against *Mtb* could greatly facilitate the selection of candidates targeting InhA<sub>MAB</sub>, as exemplified with NITD-916. We report below the major InhA<sub>MTB</sub> inhibitors described in the literature, whose antimycobacterial activities are not dependent on KatG and which could be immediately assessed against *Mabs* (Table 2).

Triclosan is a well-known InhA inhibitor, found in personal care products and inhibiting fatty acid biosynthesis as first demonstrated in *Escherichia coli* where it targets the enoyl-ACP reductase FabI [121]. The mode of action of triclosan in mycobacteria came from the characterization of spontaneous resistant mutants in *M. smegmatis* and in *Mtb* carrying mutations in *inhA* and conferring co-resistance to INH [122,123]. This molecule is a reversible inhibitor of InhA binding preferably to the enzyme-NAD<sup>+</sup> complex. Despite its cytotoxicity on eukaryotic cells and its modest antimicrobial activity against *Mtb* (MIC = 43.1 μM), triclosan is still considered as an attractive hit undergoing structural optimization [124]. For instance, a variety of analogs with bulkier groups such as a triazole or a long carbon chain substituted on the A-ring showed increased favorable interactions with InhA and improved antibacterial effects [77,125,126]. Replacement of the phenyl B-ring by aromatic nitrogen heterocycles, addition of heteroaromatics (pyridine, pyrimidine, or pyrazine) or substitution of phenyl group with chloride, acetamide, oxalylic acid, piperazine, or isoxyl has also been performed [77,127]. Despite improvements in *in vitro* activities, these compounds generally suffer from low solubility and low bioavailability, limiting *in vivo* efficiency.

Pyridomycin is a natural product from *Streptomyces pyridomycetes* and *Dactylosporangium fulvum*, exhibiting bactericidal activity against *Mtb* [128] by acting as a direct competitive inhibitor in the NADH-binding site of InhA<sub>MTB</sub> [129], leading to the reduction of α-, methoxy- and keto-MA synthesis. Pyridomycin is efficient at low concentrations against *Mtb* (MIC = 0.72 μM). The absence of toxicity on human cells and its efficacy on other mycobacterial species, including *Mabs*, makes it a promising lead compound for future drug developments against NTM. However, a series of recent

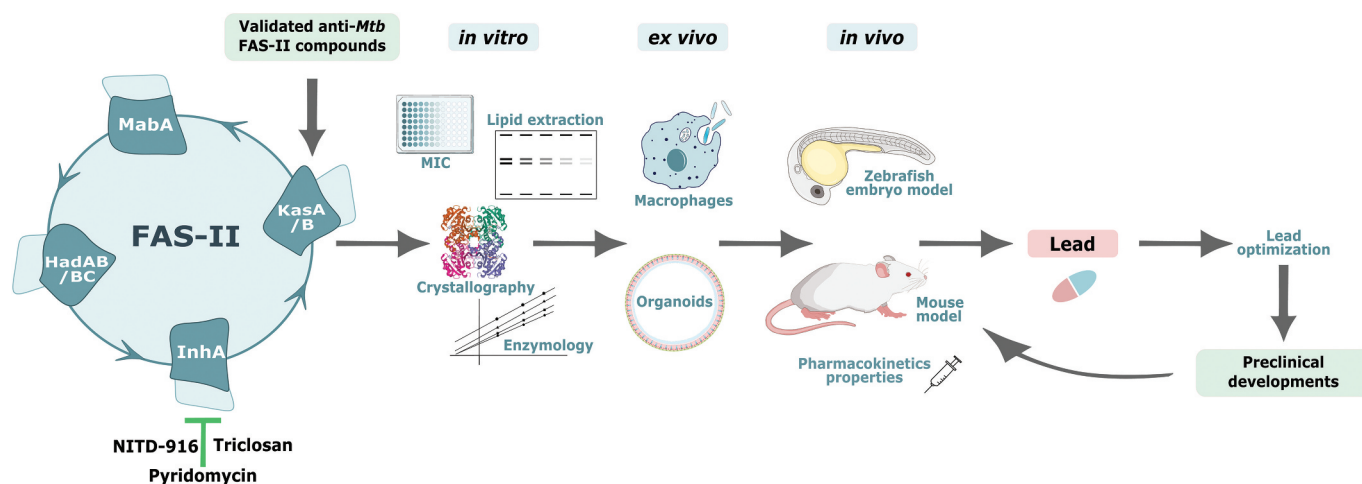


**Figure 4.** Proposed workflow for *M. abscessus* FAS-II drug discovery. Activities against whole *M. abscessus* cells (MIC determination) and assays (inhibition of *de novo* synthesis of MA, crystallography of inhibitors in complex with their target ...) of FAS-II inhibitors, previously validated in *M. tuberculosis* are shown. Specific InhA inhibitors screened against *M. abscessus* are indicated. Compounds are then tested for intracellular activity in macrophages, caseum, mucus and under nutrient/oxygen starvation. The best hits are further evaluated in animal models (zebrafish and mouse) to determine the pharmacokinetics and toxicity parameters. Iterative medicinal chemistry cycles during hit-to-lead optimization will advance compounds to preclinical developments.

pyridomycin derivatives failed to show a better activity than the parental molecule [130], prompting for additional chemical optimization.

Pyrrolidine carboxamides exert a strong antitubercular activity against InhA [131] and possess three rings, a phenyl ring (A), a 5-oxopyrrolidine (B), and a cyclohexyl ring (C). The authors showed that a 3,5-dichloro substitution in ring A or an extension of aromatic rings increase the activity through a better hydrophobic interaction with InhA. The 3-phenyl substituted compound p24 inhibited 97% of InhA<sub>MTB</sub> activity at a concentration of 15  $\mu\text{M}$  with an IC<sub>50</sub> of 0.39  $\mu\text{M}$ .

Pyrrole derivatives harboring hydrazine, phenoxy, benzamide, pyrazoline, isoxazole, or phenyl thiourea moieties were screened and showed an activity against *Mtb* through InhA inhibition [132–134]. Molecular docking studies suggest that these molecules show hydrogen bonding interactions into the hydrophobic-binding pocket of InhA in the same manner as triclosan. Pyrrole hydrazine with naphthoxyring or pyrrol phenyl thioureas present MIC values in the 0.5–2  $\mu\text{M}$  range against *Mtb*. Together with the absence of toxicity against Vero cells, these compounds are fostering further studies on this class of molecules.

Methyl-thiazole analogs are described as a novel class of anti-mycobacterial compounds *via* InhA inhibition by AstraZeneca, based on a former high-throughput screening campaign by GlaxoSmithKline [135], highlighting a reversible inhibition of the enzyme by occupying the substrate-binding site, preferably in the NADH-bound form. The lead compound presents a good inhibition of InhA with an IC<sub>50</sub> of 3 nM and a cellular potency with MIC values of 0.19  $\mu\text{M}$ . Based on this screening, new thiadiazole-based inhibitors were described, with nanomolar InhA IC<sub>50</sub>, antimycobacterial efficiency and improved hydrophobicity, solubility, permeation, and clearance properties that are useful to predict the behavior of the compound, and the ability to have an activity [136].

Recent studies showed new 1,2,3-triazoles tethered to 1,2,4-triazoles structures are strong InhA inhibitors [137]. The most promising compound presents an IC<sub>50</sub> of 0.074 nM against InhA, and docking simulations positioned this molecule in the active site of the enzyme. These compounds await to be tested in biological assays against whole bacteria.

Acetamide derivatives, particularly a series of 2-(4-oxoquinazolin-3(4H)-yl)acetamides was identified as InhA<sub>MTB</sub> inhibitors [138]. The lead compound harbors a phenyl ring and a chloro group and presents 88% InhA inhibition at 10  $\mu\text{M}$ , with an IC<sub>50</sub> of 3.12  $\mu\text{M}$ . This study revealed that the phenyl ring is crucial for good InhA inhibitory activity, favoring a modest antitubercular activity (MIC = 4.76  $\mu\text{M}$ ), while a substitution with chloro group results in increased hydrophobicity that is important for enzyme binding. *In silico* studies revealed binding interactions with InhA and with NAD<sup>+</sup>. The absence of toxicity on cells of this class of compounds and its efficacy are encouraging for future anti-mycobacterial drugs based on this structure.

Several new InhA inhibitors were recently discovered *via* virtual screening and support a recent study describing a series of 4-aminoquinolines [139,140]. The lead compound (19k) was based on LABIO-17, an InhA ligand identified from the initial screen and found to inhibit InhA enzymatic activity. This molecule harbors a substitution of the ethyl ester group of LABIO-17 by a bromine atom and exhibits the best InhA inhibitory activity of the series (IC<sub>50</sub> = 0.23  $\mu\text{M}$ ) and shows activity against a panel of resistant isolates of *Mtb* (MIC = 0.1–0.4  $\mu\text{M}$ ), respectively, 87-fold and 32-fold better than LABIO-17. This molecule displays good pH stability, solubility, or high permeant properties. Metabolic studies showed a moderate elimination rate in rat liver microsome fractions for 19k, with a longer half-life than other halogenated compounds. In addition to these parameters, the lead compound presents a bacteriostatic activity in *Mtb*-infected macrophages and in lungs of mice.

Overall, these studies show that a plethora of direct InhA inhibitors are available and ready to be assessed against NTM.

## 5. Conclusion

There is currently no treatment regimen that offers a reliable cure for *Mabs* pulmonary disease [20], a situation that arises from the intrinsic resistance of this species to a wide range of antimicrobial agents, including most anti-TB drugs [16]. While new drugs are urgently needed to populate the *Mabs* drug discovery pipeline, *de novo* discovery efforts are time-consuming and require important resources [15]. Recent screens of anti-TB active molecules for anti-*Mabs* activity have already generated new scaffolds as advanced lead compounds for *Mabs* pulmonary infections with *in vivo* proof-of-concept in animal models of infection [141]. These selected leads target a wide range of enzymes/pathways such as protein biosynthesis, cell wall biosynthesis, DNA replication, DNA topology, or ATP synthesis. PIPD1 was one of the first compound identified from a screen of anti-TB validated molecules and exerts potent *Mabs* activity via MmpL3 inhibition [23]. Deciphering the mode of action of PIPD1 highlighted the particular vulnerability of the MmpL3 transporter in *Mabs* and stimulated the discovery of other MmpL3 inhibitors reported in this review, validating the MA pathway as a valuable source for potential targets for the development of new anti-*Mabs* drugs. This hypothesis was successfully confirmed with the demonstration that NITD-916, a previously identified anti-TB compound and a direct inhibitor of the enoyl-ACP reductase InhA, that overcomes KatG bioactivation, is very active against *Mabs* and *Mfor* *in vitro*, in macrophages, in pulmonary airway organoids as well as in zebrafish [29,117]. Overall, these data indicate that targeting the MA biosynthesis pathway (transporter and biosynthetic enzymes) has a strong potential for development into novel tools for the development of efficient *Mabs* anti-infective chemotherapy.

## 6. Expert opinion

There are currently no FDA approved antibiotics to treat *Mabs* lung diseases. Antibiotherapy against *Mabs* infection suffers from a weak success rate, despite the long course of multidrug treatment, thus prompting to the rapid discovery of more efficient active compounds targeting *Mabs* *in vitro* and *in vivo*. MA anabolism is currently being exploited for the treatment of tuberculosis and has been deeply explored in recent years to identify new anti-TB actives. This pathway has only recently been the focus of studies aiming at disclosing new inhibitors for future anti-*Mabs* therapy. Because MA is not targeted by any anti-*Mabs* drug used in clinics, hitting the MA pathway would also allow to bypass common acquired resistance mechanisms found in clinical isolates. One way to populate the anti-*Mabs* chemotype pipeline consists of screen, against *Mabs*, chemical libraries generated during previous TB drug discovery campaigns. This relies on the fact that the genomes of *Mabs* shares considerable sequence similarity with that of *Mtb* [142,143]. As predicted from DNA sequence

similarity at a broad level, these two species have in common many biochemical pathways, intimating that drugs in development for TB can serve as starting points to ‘jump start’ *Mabs* drug discovery programs. It offers considerable advantages, obviating the need to initiate the long-lasting and onerous *de novo* chemical screens [141]. Similarly, many different InhA<sub>MTB</sub> inhibitors have been described that await to be tested against whole *Mabs*. These sets of hit compounds identified are fostering further hit-to-lead development to improve efficacy and pharmacokinetic properties.

The validation that inhibitors against MmpL3 and InhA are promising drug candidates opens the avenue to the evaluation of small molecules hitting the other FAS-II components in *Mabs*. Since inhibitors of many enzymatic steps in MA biosynthesis have been reported in *Mtb* [76,77], this multiplies the possibility to rapidly identifying additional active molecules against *Mabs* (Figure 4). Iterative medicinal chemistry cycles coupled to *in vitro* assays should help at optimizing compounds with improved efficacy. The best hits should then be advanced in *ex vivo* as well as in *in vivo* studies to determine toxicity, tolerability, and pharmacokinetic properties. In this context, zebrafish embryos have been validated as a relevant model to study the chronology of *Mabs* infection and used to rapidly test the efficacy of compounds *in vivo* [23,144,145]. It appears particularly suited in drug screening programs and predictive for drugs that might be orally administrated [146]. The use of murine models of *M. abscessus* respiratory infection is also warranted to address the efficacy and safety of new antimicrobial agents and to determine the best dosage and route of drug administration. Many different mouse models have been reported to assay experimental antimicrobial therapies against *Mabs*, such as C3HeB/FeJ, M-CSF KO, GKO, SICD, NOD mice, and be exploited to modulate dosing frequency and determine eventual adverse effects and the efficacy of combinatorial drug regimens [118,147]. Alternatively, administration of corticosteroids in immunocompetent C3HeB/FeJ mice permits higher levels of *Mabs* burden in the lungs and pathology and is shown to be useful for the treatment with antibiotics given intranasally [148].

*M. avium* is another opportunistic pathogen associated with biofilm-related infections of the respiratory tract, which is emerging globally and remains particularly laborious to treat [149]. It causes pulmonary infections in immunocompromised individuals and represents, together with *Mabs*, the major NTM found in CF patients [150]. Since *M. avium* produces MA and possesses highly conserved InhA and MmpL3 proteins with *Mabs* or *Mtb*, this explains why inhibitors of InhA or MmpL3 are also active against *M. avium* (Tables 1 and 2). As a corollary, new drugs targeting the MA pathway in *M. avium*, which is a more common pathogen than *Mabs*, may perhaps foster pharmaceutical companies to invest more efforts for therapeutic strategies involving MA inhibition.

## Funding

We acknowledge the Ministère de l'Enseignement Supérieur, de la Recherche et de l'Innovation for funding the PhD of MA and the “Equipe FRM EQU202103012588” funding to LK. This project has been funded in



whole or in part with federal funds from the National Institute of Allergy and Infectious Diseases, National Institutes of Health, Department of Health and Human Services, under Contract No: HHSN272201700059C.

## Declaration of interest

The authors have no relevant affiliations or financial involvement with any organization or entity with a financial interest in or financial conflict with the subject matter or materials discussed in the manuscript.

## Reviewers disclosure

Peer reviewers on this manuscript have no relevant financial or other relationships to disclose

## Author contribution

All authors substantially contributed to the conception and design of the review article and interpreting the relevant literature and were involved in the writing the review article or revised it for intellectual content.

## ORCID

Thomas E. Edwards  <http://orcid.org/0000-0002-0474-8003>

Laurent Kremer  <http://orcid.org/0000-0002-6604-4458>

## References

**Papers of special note have been highlighted as either of interest (\*) or of considerable interest (\*\*) to readers**

- Johansen MD, Herrmann J-L, Kremer L. Non-tuberculous mycobacteria and the rise of *Mycobacterium abscessus*. *Nat Rev Microbiol*. 2020;18(7):392–407. doi:10.1038/s41579-020-0331-1.
- Gopinath K, Singh S, Phillips RO. Non-tuberculous mycobacteria in TB-endemic countries: are we neglecting the danger? *PLoS Negl Trop Dis*. 2010;4(4):e615. doi:10.1371/journal.pntd.0000615.
- Raju RM, Raju SM, Zhao Y, et al. Leveraging advances in tuberculosis diagnosis and treatment to address nontuberculous mycobacterial disease. *Emerging Infect Dis*. 2016;22(3):365–369. DOI:10.3201/eid2203.151643
- Cowman S, van Ingen J, Griffith DE, et al. Non-tuberculous mycobacterial pulmonary disease. *Eur Respir J*. 2019;54(1):54. DOI:10.1183/13993003.00250-2019
- Jonsson BE, Gilljam M, Lindblad A, et al. Molecular epidemiology of *Mycobacterium abscessus*, with focus on cystic fibrosis. *J Clin Microbiol*. 2007;45(5):1497–1504. DOI:10.1128/JCM.02592-06
- Esther CR, Esserman DA, Gilligan P, et al. Chronic *Mycobacterium abscessus* infection and lung function decline in cystic fibrosis. *J Cyst Fibros*. 2010;9(2):117–123. DOI:10.1016/j.jcf.2009.12.001
- Catherinot E, Roux A-L, Macheras E, et al. Acute respiratory failure involving an R variant of *Mycobacterium abscessus*. *J Clin Microbiol*. 2009;47(1):271–274. DOI:10.1128/JCM.01478-08
- Adekambi T, Sassi M, van Ingen J, et al. Reinstating *Mycobacterium massiliense* and *Mycobacterium bolletii* as species of the *Mycobacterium abscessus* complex. *Int J Sys Evol Microbiol*. 2017;67(8):2726–2730. DOI:10.1099/ijsem.0.002011
- Richard M, Gutiérrez AV, Kremer L. Dissecting *erm(41)*-mediated macrolide-inducible resistance in *Mycobacterium abscessus*. *Antimicrob Agents Chemother*. 2020;64(2):e01879–19. doi:10.1128/AAC.01879-19.
- Nash KA, Brown-Elliott BA, Wallace RJ. A novel gene, *erm(41)*, confers inducible macrolide resistance to clinical isolates of *Mycobacterium abscessus* but is absent from *Mycobacterium chelonae*. *Antimicrob Agents Chemother*. 2009;53(4):1367–1376. doi:10.1128/AAC.01275-08.
- Nessar R, Cambau E, Reyat JM, et al. *Mycobacterium abscessus*: a new antibiotic nightmare. *J Antimicrob Chemother*. 2012;67(4):810–818. DOI:10.1093/jac/dkr578
- van Ingen J, Boeree MJ, van Soolingen D, et al. Resistance mechanisms and drug susceptibility testing of nontuberculous mycobacteria. *Drug Resist Updat*. 2012;15(3):149–161. DOI:10.1016/j.drug.2012.04.001
- Brown-Elliott BA, Nash KA, Wallace RJ. Antimicrobial susceptibility testing, drug resistance mechanisms, and therapy of infections with nontuberculous mycobacteria. *Clin Microbiol Rev*. 2012;25(3):545–582. doi:10.1128/CMR.05030-11.
- Lopeman R, Harrison J, Desai M, et al. *Mycobacterium abscessus*: environmental bacterium turned clinical nightmare. *Microorganisms*. 2019;7(3):90. DOI:10.3390/microorganisms7030090
- Wu M-L, Aziz DB, Dartois V, et al. NTM drug discovery: status, gaps and the way forward. *Drug Discov Today*. 2018;23(8):1502–1519. DOI:10.1016/j.drudis.2018.04.001.
- \*\* This review details the current status of NTM drug discovery.**
- Luthra S, Rominski A, Sander P. The role of antibiotic-target-modifying and antibiotic-modifying enzymes in *Mycobacterium abscessus* drug resistance. *Front Microbiol*. 2018;9:2179.
- \*\* This review provides an overview of the enzyme-mediated antibiotic resistance mechanisms in M. abscessus.**
- Richard M, Gutiérrez AV, Viljoen A, et al. Mutations in the MAB\_2299c TetR regulator confer cross-resistance to clofazimine and bedaquiline in *Mycobacterium abscessus*. *Antimicrob Agents Chemother*. 2019;63(1):e01316–18. DOI:10.1128/AAC.01316-18
- Griffith DE, Aksamit T, Brown-Elliott BA, et al. An official ATS/IDSA statement: diagnosis, treatment, and prevention of nontuberculous mycobacterial diseases. *Am J Respir Crit Care Med*. 2007;175(4):367–416. DOI:10.1164/rccm.200604-571ST
- Floto RA, Olivier KN, Saiman L, et al. US Cystic Fibrosis Foundation and European Cystic Fibrosis Society consensus recommendations for the management of non-tuberculous mycobacteria in individuals with cystic fibrosis: executive summary. *Thorax*. 2016;71(1):88–90. DOI:10.1136/thoraxjnl-2015-207983
- Daley CL, Iaccarino JM, Lange C, et al. Treatment of nontuberculous mycobacterial pulmonary disease: an official ATS/ERS/ESCMID/IDSA clinical practice guideline. *Eur Respir J*. 2020;56:2000535.
- Wallace RJ, Dukart G, Brown-Elliott BA, et al. Clinical experience in 52 patients with tigecycline-containing regimens for salvage treatment of *Mycobacterium abscessus* and *Mycobacterium chelonae* infections. *J Antimicrob Chemother*. 2014;69(7):1945–1953. DOI:10.1093/jac/dku062
- Roux A-L, Catherinot E, Soismier N, et al. Comparing *Mycobacterium massiliense* and *Mycobacterium abscessus* lung infections in cystic fibrosis patients. *J Cyst Fibros*. 2015;14(1):63–69. DOI:10.1016/j.jcf.2014.07.004
- Dupont C, Viljoen A, Dubar F, et al. A new piperidinol derivative targeting mycolic acid transport in *Mycobacterium abscessus*. *Mol Microbiol*. 2016;101(3):515–529. DOI:10.1111/mmi.13406.
- \*\* First description of a MmpL3 inhibitor in M. abscessus.**
- Degiacomi S, Chiarelli, et al. *Mycobacterium abscessus*, an emerging and worrisome pathogen among cystic fibrosis patients. *Int J Mol Sci*. 2019;20(23):5868. DOI:10.3390/ijms20235868
- Brennan PJ, Nikaido H. The envelope of mycobacteria. *Annu Rev Biochem*. 1995;64(1):29–63. doi:10.1146/annurev.bi.64.070195.000333.
- Bhatt A, Molle V, Besra GS, et al. The *Mycobacterium tuberculosis* FAS-II condensing enzymes: their role in mycolic acid biosynthesis, acid-fastness, pathogenesis and in future drug development. *Mol Microbiol*. 2007;64(6):1442–1454. DOI:10.1111/j.1365-2958.2007.05761.x
- Kozikowski AP, Onajole OK, Stec J, et al. Targeting mycolic acid transport by indole-2-carboxamides for the treatment of *Mycobacterium abscessus* infections. *J Med Chem*. 2017;60(13):5876–5888. DOI:10.1021/acs.jmedchem.7b00582

28. Raynaud C, Daher W, Johansen MD, et al. Active benzimidazole derivatives targeting the MmpL3 transporter in *Mycobacterium abscessus*. *ACS Infect Dis.* 2020;6(2):324–337. DOI:10.1021/acinfed.9b00389
29. Alcaraz M, Roquet-Banères F, Leon-Icaza SA, et al. Efficacy and mode of action of a direct inhibitor of *Mycobacterium abscessus* InhA. *ACS Infect Dis.* 2022;8(10):2171–2186. DOI:10.1021/acinfed.2c00314.
- **Proof-of-concept that direct inhibition of InhA correlates with M. abscessus growth inhibition.**
30. Bansal-Mutalik R, Nikaido H. Mycobacterial outer membrane is a lipid bilayer and the inner membrane is unusually rich in diacyl phosphatidylinositol dimannosides. *Proc Natl Acad Sci, USA.* 2014;111(13):4958–4963. doi:10.1073/pnas.1403078111.
31. Pitarque S, Larrouy-Maumus G, Payré B, et al. The immunomodulatory lipoglycans, lipoarabinomannan and lipomannan, are exposed at the mycobacterial cell surface. *Tuberculosis.* 2008;88(6):560–565. DOI:10.1016/j.tube.2008.04.002
32. Guerin ME, Korduláková J, Alzari PM, et al. Molecular basis of phosphatidyl-myo-inositol mannoside biosynthesis and regulation in mycobacteria. *J Biol Chem.* 2010;285(44):33577–33583. DOI:10.1074/jbc.R110.168328
33. Briken V, Porcelli SA, Besra GS, et al. Mycobacterial lipoarabinomannan and related lipoglycans: from biogenesis to modulation of the immune response: the mycobacterial lipoarabinomannan and related molecules. *Mol Microbiol.* 2004;53(2):391–403. DOI:10.1111/j.1365-2958.2004.04183.x
34. Fukuda T, Matsumura T, Ato M, et al. Critical roles for lipomannan and lipoarabinomannan in cell wall integrity of mycobacteria and pathogenesis of tuberculosis. *MBio.* 2013;4(1):e00472–12. DOI:10.1128/mBio.00472-12
35. Zuber B, Chami M, Houssin C, et al. Direct visualization of the outer membrane of mycobacteria and corynebacteria in their native state. *J Bacteriol.* 2008;190(16):5672–5680. DOI:10.1128/JB.01919-07
36. Daffé M, Marrakchi H, Fischetti VA, et al. Unraveling the structure of the mycobacterial envelope. *Microbiol Spectr.* 2019;7(4):7.4.1. DOI:10.1128/microbiolspec.GPP3-0027-2018
37. Lavollay M, Arthur M, Fourceaud M, et al. The peptidoglycan of stationary-phase *Mycobacterium tuberculosis* predominantly contains cross-links generated by L,D-transpeptidation. *J Bacteriol.* 2008;190(12):4360–4366. DOI:10.1128/JB.00239-08
38. Lavollay M, Fourceaud M, Herrmann J-L, et al. The peptidoglycan of *Mycobacterium abscessus* is predominantly cross-linked by L,d-transpeptidases. *J Bacteriol.* 2011;193(3):778–782. DOI:10.1128/JB.00606-10
39. Jankute M, Cox JAG, Harrison J, et al. Assembly of the mycobacterial cell wall. *Annu Rev Microbiol.* 2015;69(1):405–423. DOI:10.1146/annurev-micro-091014-104121
40. McNeil M, Wallner SJ, Hunter SW, et al. Demonstration that the galactosyl and arabinosyl residues in the cell wall arabinogalactan of *Mycobacterium leprae* and *Mycobacterium tuberculosis* are furanoid. *Carbohydrate Res.* 1987;166(2):299–308. DOI:10.1016/0008-6215(87)80065-4
41. Alderwick LJ, Harrison J, Lloyd GS, et al. The mycobacterial cell wall-peptidoglycan and arabinogalactan. *Cold Spring Harb Perspect Med.* 2015;5(8):a021113. DOI:10.1101/cshperspect.a021113
42. Jackson M. The mycobacterial cell envelope lipids. *Cold Spring Harb Perspect Med.* 2014;4(10):a021105–a021105. doi:10.1101/cshperspect.a021105.
- **This review summarizes the role of lipids in mycobacterial physiology and pathogenicity.**
43. Chiaradia L, Lefebvre C, Parra J, et al. Dissecting the mycobacterial cell envelope and defining the composition of the native mycomembrane. *Sci Rep.* 2017;7(1):12807. DOI:10.1038/s41598-017-12718-4
44. Chatterjee D, Khoo K-H. The surface glycopeptidolipids of mycobacteria: structures and biological properties. *Cell Mol Life Sci.* 2001;58(14):2018–2042. doi:10.1007/PL00000834.
45. Pang L, Tian X, Pan W, et al. Structure and function of mycobacterium glycopeptidolipids from comparative genomics perspective. *J Cell Biochem.* 2013;114(8):1705–1713. DOI:10.1002/jcb.24515
46. Gutiérrez AV, Viljoen A, Ghigo E, et al. Glycopeptidolipids, a double-edged sword of the *Mycobacterium abscessus* complex. *Front Microbiol.* 2018;9:1145. DOI:10.3389/fmicb.2018.01145
47. Gilleron M, Quesniaux VFJ, Puzo G. Acylation state of the phosphatidylinositol hexamannosides from *Mycobacterium bovis* Bacillus Calmette Guérin and *Mycobacterium tuberculosis* H37Rv and its implication in Toll-like receptor response. *J Biol Chem.* 2003;278(32):29880–29889. doi:10.1074/jbc.M303446200.
48. Pawelczyk J, Kremer L, Hatfull GF, et al. The molecular genetics of mycolic acid biosynthesis. *Microbiol Spectr.* 2014;2(4):2.4.24. DOI:10.1128/microbiolspec.MGM2-0003-2013
49. Barry CE, Lee RE, Mdluli K, et al. Mycolic acids: structure, biosynthesis and physiological functions. *Prog Lipid Res.* 1998;37(2–3):143–179. DOI:10.1016/S0163-7827(98)00008-3
50. Di Capua CB, Belardinelli JM, Carignano HA, et al. Unveiling the biosynthetic pathway for short mycolic acids in nontuberculous mycobacteria: *Mycobacterium smegmatis* MSMEG\_4301 and its ortholog *Mycobacterium abscessus* MAB\_1915 are essential for the synthesis of α-mycolic acids. *Microbiol Spectr.* 2022;10(4):e01288–22. DOI:10.1128/spectrum.01288-22
51. Halloum I, Carrère-Kremer S, Blaise M, et al. Deletion of a dehydratase important for intracellular growth and cording renders rough *Mycobacterium abscessus* avirulent. *Proc Natl Acad Sci, USA.* 2016;113(29):E4228–4237. DOI:10.1073/pnas.1605477113.
- **First description of the role of cording in M. abscessus pathogenicity.**
52. George KM, Yuan Y, Sherman DR, et al. The biosynthesis of cyclopropanated mycolic acids in *Mycobacterium tuberculosis*. *J Biol Chem.* 1995;270(45):27292–27298. DOI:10.1074/jbc.270.45.27292
53. Dubnau E, Chan J, Raynaud C, et al. Oxygenated mycolic acids are necessary for virulence of *Mycobacterium tuberculosis* in mice. *Mol Microbiol.* 2002;36(3):630–637. DOI:10.1046/j.1365-2958.2000.01882.x
54. Yuan Y, Zhu Y, Crane DD, et al. The effect of oxygenated mycolic acid composition on cell wall function and macrophage growth in *Mycobacterium tuberculosis*. *Mol Microbiol.* 1998;29(6):1449–1458. DOI:10.1046/j.1365-2958.1998.01026.x
55. Barkan D, Hedhli D, Yan H-G, et al. *Mycobacterium tuberculosis* lacking all mycolic acid cyclopropanation is viable but highly attenuated and hyperinflammatory in mice. *Infect Immun.* 2012;80(6):1958–1968. DOI:10.1128/IAI.00021-12
56. Glickman MS, Cox JS, Jacobs WR. A novel mycolic acid cyclopropane synthetase is required for cording, persistence, and virulence of *Mycobacterium tuberculosis*. *Mol Cell.* 2000;5(4):717–727. doi:10.1016/S1097-2765(00)80250-6.
57. Hunter RL, Olsen M, Jagannath C, et al. Trehalose 6,6'-dimycolate and lipid in the pathogenesis of caseating granulomas of tuberculosis in mice. *Am J Pathol.* 2006;168(4):1249–1261. DOI:10.2353/ajpath.2006.050848
58. Nguyen TKT, d'Aigle J, Chinae L, et al. Mycobacterial Trehalose 6,6'-Dimycolate-Induced M1-Type Inflammation. *Am J Pathol.* 2020;190(2):286–294. DOI:10.1016/j.ajpath.2019.10.006
59. Schweizer E, Hofmann J. Microbial type I fatty acid synthases (FAS): major players in a network of cellular FAS systems. *Microbiol Mol Biol Rev.* 2004;68(3):501–517. table of contents. DOI:10.1128/MMBR.68.3.501-517.2004
60. Elad N, Baron S, Peleg Y, et al. Structure of Type-I *Mycobacterium tuberculosis* fatty acid synthase at 3.3 Å resolution. *Nat Commun.* 2018;9(1):3886. DOI:10.1038/s41467-018-06440-6
61. Kremer L, Nampoothiri KM, Lesjean S, et al. Biochemical characterization of acyl carrier protein (AcpM) and malonyl-CoA: AcpM transacylase (mtFabd), two major components of *Mycobacterium tuberculosis* fatty acid synthase II. *J Biol Chem.* 2001;276(30):27967–27974. DOI:10.1074/jbc.M103687200

62. Choi K-H, Kremer L, Besra GS, et al. Identification and substrate specificity of  $\beta$ -ketoacyl (acyl carrier protein) synthase III (mtFabH) from *Mycobacterium tuberculosis*. *J Biol Chem*. 2000;275(36):28201–28207. DOI:10.1074/jbc.M003241200
63. Marrakchi H, Ducasse S, Labesse G, et al. MabA (FabG1), a *Mycobacterium tuberculosis* protein involved in the long-chain fatty acid elongation system FAS-II. *Microbiology*. 2002;148(4):951–960. DOI:10.1099/00221287-148-4-951
64. Sacco E, Covarrubias AS, O'Hare HM, et al. The missing piece of the type II fatty acid synthase system from *Mycobacterium tuberculosis*. *Proc Natl Acad Sci, USA*. 2007;104(37):14628–14633. DOI:10.1073/pnas.0704132104
65. Banerjee A, Dubnau E, Quemard A, et al. *inhA*, a gene encoding a target for isoniazid and ethionamide in *Mycobacterium tuberculosis*. *Science*. 1994;263(5144):227–230. DOI:10.1126/science.8284673.
- **First demonstration of *InhA* as the target of isoniazid and ethionamide in mycobacteria.**
66. Quemard A, Sacchetti JC, Dessen A, et al. Enzymic characterization of the target for isoniazid in *Mycobacterium tuberculosis*. *Biochemistry*. 1995;34(26):8235–8241. DOI:10.1021/bi00026a004
67. Slayden RA, Barry CE. The role of KasA and KasB in the biosynthesis of meromycolic acids and isoniazid resistance in *Mycobacterium tuberculosis*. *Tuberculosis*. 2002;82(4–5):149–160. doi:10.1054/tube.2002.0333.
68. Kremer L, Dover LG, Carrère S, et al. Mycolic acid biosynthesis and enzymic characterization of the  $\beta$ -ketoacyl-ACP synthase A-condensing enzyme from *Mycobacterium tuberculosis*. *Biochem J*. 2002;364(2):423–430. DOI:10.1042/bj20011628
69. Glickman MS. The *mmaA2* gene of *Mycobacterium tuberculosis* encodes the distal cyclopropane synthase of the  $\alpha$ -mycolic acid. *J Biol Chem*. 2003;278(10):7844–7849. doi:10.1074/jbc.M212458200.
70. Behr MA, Schroeder BG, Brinkman JN, et al. A point mutation in the *mma3* gene is responsible for impaired methoxymycolic acid production in *Mycobacterium bovis* BCG strains obtained after 1927. *J Bacteriol*. 2000;182(12):3394–3399. DOI:10.1128/JB.182.12.3394-3399.2000
71. Portevin D, de Sousa-D'Auria C, Houssin C, et al. A polyketide synthase catalyzes the last condensation step of mycolic acid biosynthesis in mycobacteria and related organisms. *Proc Natl Acad Sci, USA*. 2004;101(1):314–319. DOI:10.1073/pnas.0305439101
72. Lea-Smith DJ, Pyke JS, Tull D, et al. The reductase that catalyzes mycolic motif synthesis is required for efficient attachment of mycolic acids to arabinogalactan. *J Biol Chem*. 2007;282(15):11000–11008. DOI:10.1074/jbc.M608686200
73. Grzegorzewicz AE, Pham H, Gundi VAKB, et al. Inhibition of mycolic acid transport across the *Mycobacterium tuberculosis* plasma membrane. *Nat Chem Biol*. 2012;8(4):334–341. DOI:10.1038/nchembio.794.
- **First demonstration of MmpL3 as the transporter of mycolic acids in mycobacteria.**
74. Belisle JT, Vissa VD, Sievert T, et al. Role of the major antigen of *Mycobacterium tuberculosis* in cell wall biogenesis. *Science*. 1997;276(5317):1420–1422. DOI:10.1126/science.276.5317.1420
75. Jackson M, Raynaud C, Lanéelle MA, et al. Inactivation of the antigen 85C gene profoundly affects the mycolate content and alters the permeability of the *Mycobacterium tuberculosis* cell envelope. *Mol Microbiol*. 1999;31(5):1573–1587. DOI:10.1046/j.1365-2958.1999.01310.x
76. Marrakchi H, Lanéelle M-A, Daffé M. Mycolic acids: structures, biosynthesis, and beyond. *Chem Biol*. 2014;21(1):67–85. doi:10.1016/j.chembiol.2013.11.011.
- **A compelling review on the structure, diversity, biosynthesis and role of mycolic acids in mycobacteria.**
77. North E, Jackson M, Lee R. New approaches to target the mycolic acid biosynthesis pathway for the development of tuberculosis therapeutics. *Curr Pharm Des*. 2013;20(27):4357–4378. doi:10.2174/1381612819666131118203641.
78. Baulard AR, Betts JC, Engohang-Ndong J, et al. Activation of the pro-drug ethionamide is regulated in mycobacteria. *J Biol Chem*. 2000;275(36):28326–28331. DOI:10.1074/jbc.M003744200
79. Vilchèze C, Jacobs WR Jr. The mechanism of isoniazid killing: clarity through the scope of genetics. *Annu Rev Microbiol*. 2007;61(1):35–50. doi:10.1146/annurev.micro.61.111606.122346.
80. Unissa AN, Subbian S, Hanna LE, et al. Overview on mechanisms of isoniazid action and resistance in *Mycobacterium tuberculosis*. *Infect Genet Evol*. 2016;45:474–492. DOI:10.1016/j.meegid.2016.09.004
81. Varela C, Rittmann D, Singh A, et al. *MmpL* genes are associated with mycolic acid metabolism in mycobacteria and corynebacteria. *Chem Biol*. 2012;19(4):498–506. DOI:10.1016/j.chembiol.2012.03.006
82. Degiacomi G, Benjak A, Madacki J, et al. Essentiality of *mmpL3* and impact of its silencing on *Mycobacterium tuberculosis* gene expression. *Sci Rep*. 2017;7(1):43495. DOI:10.1038/srep43495.
- **First demonstration of the essentiality of *mmpL3* in *M. tuberculosis*.**
83. Viljoen A, Dubois V, Girard-Misguich F, et al. The diverse family of MmpL transporters in mycobacteria: from regulation to antimicrobial developments. *Mol Microbiol*. 2017;104(6):889–904. DOI:10.1111/mmi.13675
84. Xu Z, Meshcheryakov VA, Poce G, et al. MmpL3 is the flippase for mycolic acids in mycobacteria. *Proc Natl Acad Sci, USA*. 2017;114(30):7993–7998. DOI:10.1073/pnas.1700062114
85. Li W, Obregón-Henao A, Wallach JB, et al. Therapeutic potential of the *Mycobacterium tuberculosis* mycolic acid transporter, MmpL3. *Antimicrob Agents Chemother*. 2016;60(9):5198–5207. DOI:10.1128/AAC.00826-16
86. Li W, Stevens CM, Pandya AN, et al. Direct inhibition of MmpL3 by novel antitubercular compounds. *ACS Infect Dis*. 2019;5:1001–1012.
87. Li W, Yazidi A, Pandya AN, et al. MmpL3 as a target for the treatment of drug-resistant nontuberculous mycobacterial infections. *Front Microbiol*. 2018;9:1547. DOI:10.3389/fmicb.2018.01547
88. Ballell L, Bates RH, Young RJ, et al. Fueling open-source drug discovery: 177 small-molecule leads against tuberculosis. *ChemMedchem*. 2013;8(2):313–321. DOI:10.1002/cmdc.201200428
89. Ruyck J, Dupont C, Lamy E, et al. Structure-based design and synthesis of piperidinol-containing molecules as new *Mycobacterium abscessus* inhibitors. *ChemistryOpen*. 2020;9(3):351–365. DOI:10.1002/open.202000042
90. Stec J, Onajole OK, Lun S, et al. Indole-2-carboxamide-based MmpL3 inhibitors show exceptional antitubercular activity in an animal model of tuberculosis infection. *J Med Chem*. 2016;59(13):6232–6247. DOI:10.1021/acs.jmedchem.6b00415
91. Lun S, Guo H, Onajole OK, et al. Indoleamides are active against drug-resistant *Mycobacterium tuberculosis*. *Nat Commun*. 2013;4(1):2907. DOI:10.1038/ncomms3907
92. Raynaud C, Daher W, Roquet-Banères F, et al. Synergistic interactions of indole-2-carboxamides and  $\beta$ -lactam antibiotics against *Mycobacterium abscessus*. *Antimicrob Agents Chemother*. 2020;64(5):e02548–19. DOI:10.1128/AAC.02548-19
93. Franz ND, Belardinelli JM, Kaminski MA, et al. Design, synthesis and evaluation of indole-2-carboxamides with pan anti-mycobacterial activity. *Bioorg Med Chem*. 2017;25(14):3746–3755. DOI:10.1016/j.bmc.2017.05.015
94. Pandya AN, Prathipati PK, Hegde P, et al. Indole-2-carboxamides are active against *Mycobacterium abscessus* in a mouse model of acute infection. *Antimicrob Agents Chemother*. 2019;63(3):e02245–18. DOI:10.1128/AAC.02245-18
95. Bhattarai P, Hegde P, Li W, et al. Structural determinants of indole-2-carboxamides: identification of lead acetamides with pan antimycobacterial activity. *J Med Chem*. 2022;66(1):170–187. DOI:10.1021/acs.jmedchem.2c00352
96. Gobis K, Foks H, Serocki M, et al. Synthesis and evaluation of *in vitro* antimycobacterial activity of novel 1H-benzo[d]imidazole derivatives and analogues. *Eur J Med Chem*. 2015;89:13–20. DOI:10.1016/j.ejmech.2014.10.031
97. Korycka-Machała M, Viljoen A, Pawełczyk J, et al. 1 H -Benzo[d] Imidazole derivatives affect MmpL3 in *Mycobacterium tuberculosis*. *Antimicrob Agents Chemother*. 2019;63(10):e00441–19. DOI:10.1128/AAC.00441-19



98. Graham J, Wong CE, Day J, et al. Discovery of benzothiazole amides as potent antimycobacterial agents. *Bioorg Med Chem Lett*. 2018;28(19):3177–3181. DOI:10.1016/j.bmcl.2018.08.026
99. De Groot MA, Jarvis TC, Wong C, et al. Optimization and lead selection of benzothiazole amide analogs toward a novel antimycobacterial agent. *Front Microbiol*. 2018;9:2231. DOI:10.3389/fmicb.2018.02231
100. Ochsner UA, De Groot MA, Jarvis TC, et al. Microbiological profile, preclinical pharmacokinetics and efficacy of CRS0393, a novel antimycobacterial agent targeting MmpL3. *Tuberculosis*. 2023;138:102288. DOI:10.1016/j.tube.2022.102288
101. Williams JT, Haiderer ER, Coulson GB, et al. Identification of new MmpL3 inhibitors by untargeted and targeted screens defines MmpL3 domains with differential resistance. *J Antimicrob Chemother*. 2019;63(Supplement 1):i18–i20. DOI:10.1093/jac/dkp077
102. Zheng H, Williams JT, Coulson GB, et al. HC2091 kills *Mycobacterium tuberculosis* by targeting the MmpL3 mycolic acid transporter. *Antimicrob Agents Chemother*. 2018;62(7):e02459–17. DOI:10.1128/AAC.02459-17
103. Shetty A, Xu Z, Lakshmanan U, et al. Novel acetamide indirectly targets mycobacterial transporter MmpL3 by proton motive force disruption. *Front Microbiol*. 2018;9:2960. DOI:10.3389/fmicb.2018.02960
104. Zhang Y, Heymt B, Young D, et al. The catalase-peroxidase gene and isoniazid resistance of *Mycobacterium tuberculosis*. *Nature*. 1992;358(6387):591–593. DOI:10.1038/358591a0
- **First publication on the role of KatG in activation of INH.**
105. Rozwarski DA, Grant GA, Barton DHR, et al. Modification of the NADH of the isoniazid target (InhA) from *Mycobacterium tuberculosis*. *Science*. 1998;279(5347):98–102. DOI:10.1126/science.279.5347.98
106. Rawat R, Whitty A, Tonge PJ. The isoniazid-NAD adduct is a slow, tight-binding inhibitor of InhA, the *Mycobacterium tuberculosis* enoyl reductase: adduct affinity and drug resistance. *Proc Natl Acad Sci, USA*. 2003;100(24):13881–13886. doi:10.1073/pnas.2235848100.
107. Gagliardi A, Selchow P, Luthra S, et al. KatG as counterscreening marker for nontuberculous mycobacteria. *Antimicrob Agents Chemother*. 2020;64(5):e02508–19. DOI:10.1128/AAC.02508-19
108. Manjunatha UH, Rao SP, Kondreddi RR, et al. Direct inhibitors of InhA are active against *Mycobacterium tuberculosis*. *Sci Transl Med*. 2015;7(269):ra2693–ra2693. DOI:10.1126/scitranslmed.3010597
- **This paper presents for the first time NITD-916 and its activity on M. tuberculosis.**
109. Sánchez-Chardi A, Olivares F, Byrd TF, et al. Demonstration of cord formation by rough *Mycobacterium abscessus* variants: implications for the clinical microbiology laboratory. *J Clin Microbiol*. 2011;49(6):2293–2295. DOI:10.1128/JCM.02322-10
110. Johansen MD, Daher W, Roquet-Banères F, et al. Rifabutin is bactericidal against intracellular and extracellular forms of *Mycobacterium abscessus*. *Antimicrob Agents Chemother*. 2020;64(11):e00363–20. DOI:10.1128/AAC.00363-20
111. Bernut A, Herrmann J-L, Kissa K, et al. *Mycobacterium abscessus* cording prevents phagocytosis and promotes abscess formation. *Proc Natl Acad Sci, USA*. 2014;111(10):E943–952. DOI:10.1073/pnas.1321390111
112. Iakobachvili N, Leon-Icaza SA, Knoops K, et al. Mycobacteria–host interactions in human bronchiolar airway organoids. *Mol Microbiol*. 2022;117(3):682–692. DOI:10.1111/mmi.14824
113. Leon-Icaza SA, Bagayoko S, Vergé R, et al. Druggable redox pathways against *M. abscessus* in cystic fibrosis patient-derived airway organoids. *bioRxiv* 2022.01.03.474765.
114. Richards CJ, Olivier KN. Nontuberculous mycobacteria in cystic fibrosis. *Semin Respir Crit Care Med*. 2019;40(6):737–750. doi:10.1055/s-0039-1693706.
115. Santos DR de S, Lourenço MCS, Coelho FS, et al. Resistance profile of strains of *Mycobacterium fortuitum* isolated from clinical specimens. *J Bras Pneumol*. 2016;42:299–301. DOI:10.1590/s1806-37562016000000073
116. Shen Y, Wang X, Jin J, et al. *In vitro* susceptibility of *Mycobacterium abscessus* and *Mycobacterium fortuitum* isolates to 30 antibiotics. *BioMed Res Int*. 2018;2018:4902941. DOI:10.1155/2018/4902941
117. Roquet-Banères F, Alcaraz M, Hamela C, et al. *In vitro* and *in vivo* efficacy of NITD-916 against *Mycobacterium fortuitum*. *Antimicrob Agents Chemother*. 2023;67(4):e01607–22. DOI:10.1128/aac.01607-22
- **This paper demonstrates the activity of NITD-916 against M. fortuitum in the zebrafish model of infection.**
118. Le Moigne V, Raynaud C, Moreau F, et al. Efficacy of bedaquiline, alone or in combination with imipenem, against *Mycobacterium abscessus* in C3HeB/FeJ Mice. *Antimicrob Agents Chemother*. 2020;64(6):e00114–20. DOI:10.1128/AAC.00114-20
119. Prasad MS, Bhole RP, Khedekar PB, et al. *Mycobacterium* enoyl acyl carrier protein reductase (InhA): a key target for antitubercular drug discovery. *Bioorg Chem*. 2021;115:105242.
- **This review reports many InhA inhibitors identified in drug discovery programs.**
120. Doğan ŞD, Gündüz MG, Doğan H, et al. Design and synthesis of thiourea-based derivatives as *Mycobacterium tuberculosis* growth and enoyl acyl carrier protein reductase (InhA) inhibitors. *Eur J Med Chem*. 2020;199:112402. DOI:10.1016/j.ejmech.2020.112402
121. Sivaraman S, Sullivan TJ, Johnson F, et al. Inhibition of the bacterial enoyl reductase FabI by triclosan: a structure–reactivity analysis of FabI inhibition by triclosan analogues. *J Med Chem*. 2004;47(3):509–518. DOI:10.1021/jm030182i
122. McMurry LM, McDermott PF, Levy SB. Genetic evidence that InhA of *Mycobacterium smegmatis* is a target for triclosan. *Antimicrob Agents Chemother*. 1999;43(3):711–713. doi:10.1128/AAC.43.3.711.
123. Parikh SL, Xiao G, Tonge PJ. Inhibition of InhA, the enoyl reductase from *Mycobacterium tuberculosis*, by triclosan and isoniazid. *Biochemistry*. 2000;39(26):7645–7650. doi:10.1021/bi0008940.
124. Vosátka R, Krátky M, Vinšová J. Triclosan and its derivatives as antimycobacterial active agents. *Eur J Pharm Sci*. 2018;114:318–331. doi: 10.1016/j.ejps.2017.12.013
125. Pan P, Tonge J. Targeting InhA, the FASII enoyl-ACP reductase: SAR studies on novel inhibitor scaffolds. *Curr Top Med Chem*. 2012;12(7):672–693. doi:10.2174/156802612799984535.
126. Stec J, Vilchère C, Lun S, et al. Biological evaluation of potent triclosan-derived inhibitors of the enoyl-acyl carrier protein reductase InhA in drug-sensitive and drug-resistant strains of *Mycobacterium tuberculosis*. *ChemMedchem*. 2014;9(11):2528–2537. DOI:10.1002/cmdc.201402255
127. Am Ende CW, Knudson SE, Liu N, et al. Synthesis and *in vitro* antimycobacterial activity of B-ring modified diaryl ether InhA inhibitors. *Bioorg Med Chem Lett*. 2008;18(10):3029–3033. DOI:10.1016/j.bmcl.2008.04.038
128. Hartkoorn RC, Sala C, Neres J, et al. Towards a new tuberculosis drug: pyridomycin – nature’s isoniazid. *EMBO Mol Med*. 2012;4(10):1032–1042. DOI:10.1002/emmm.201201689
129. Hartkoorn RC, Pojer F, Read JA, et al. Pyridomycin bridges the NADH- and substrate-binding pockets of the enoyl reductase InhA. *Nat Chem Biol*. 2014;10(2):96–98. DOI:10.1038/nchembio.1405
130. Kienle M, Eisenring P, Stoessel B, et al. Synthesis and structure–activity relationship studies of C2-modified analogs of the antimycobacterial natural product pyridomycin. *J Med Chem*. 2020;63(3):1105–1131. DOI:10.1021/acs.jmedchem.9b01457
131. He X, Alian A, Stroud R, et al. Pyrrolidine carboxamides as a novel class of inhibitors of enoyl acyl carrier protein reductase from *Mycobacterium tuberculosis*. *J Med Chem*. 2006;49(21):6308–6323. DOI:10.1021/jm060715y
132. Joshi SD, Dixit SR, Kirankumar MN, et al. Synthesis, antimycobacterial screening and ligand-based molecular docking studies on novel pyrrole derivatives bearing pyrazoline, isoxazole and phenyl thiourea moieties. *Eur J Med Chem*. 2016;107:133–152. DOI:10.1016/j.ejmech.2015.10.047
133. More UA, Joshi SD, Aminabhavi TM, et al. Design, synthesis, molecular docking and 3D-QSAR studies of potent inhibitors of enoyl-acyl carrier protein reductase as potential antimycobacterial agents. *Eur J Med Chem*. 2014;71:199–218. DOI:10.1016/j.ejmech.2013.11.004

134. More UA, Joshi SD, Aminabhavi TM, et al. Discovery of target based novel pyrrolyl phenoxy derivatives as antimycobacterial agents: an *in silico* approach. *Eur J Med Chem.* 2015;94:317–339. DOI:10.1016/j.ejmech.2015.03.013
135. Shirude PS, Madhavapeddi P, Naik M, et al. Methyl-Thiazoles: a novel mode of inhibition with the potential to develop novel inhibitors targeting InhA in *Mycobacterium tuberculosis*. *J Med Chem.* 2013;56(21):8533–8542. DOI:10.1021/jm4012033
136. Šink R, Sosič I, Živec M, et al. Design, synthesis, and evaluation of new thiadiazole-based direct inhibitors of enoyl acyl carrier protein reductase (InhA) for the treatment of tuberculosis. *J Med Chem.* 2015;58(2):613–624. DOI:10.1021/jm501029r
137. El Sawy MA, Elshatanofy MM, El Kilany Y, et al. Novel hybrid 1,2,4- and 1,2,3-triazoles targeting *Mycobacterium tuberculosis* enoyl acyl carrier Protein reductase (InhA): design, synthesis, and molecular docking. *Int J Mol Sci.* 2022;23(9):4706. DOI:10.3390/ijms23094706
138. Pedgaonkar GS, Sridevi JP, Jeankumar VU, et al. Development of 2-(4-oxoquinazolin-3(4H)-yl)acetamide derivatives as novel enoyl-acyl carrier protein reductase (InhA) inhibitors for the treatment of tuberculosis. *Eur J Med Chem.* 2014;86:613–627. DOI:10.1016/j.ejmech.2014.09.028
139. Pauli I, dos Santos RN, Rostirolla DC, et al. Discovery of new inhibitors of *Mycobacterium tuberculosis* InhA enzyme using virtual screening and a 3D-pharmacophore-based approach. *J Chem Inf Model.* 2013;53(9):2390–2401. DOI:10.1021/ci400202t
140. Paz JD, Denise de Moura Sperotto N, Ramos AS, et al. Novel 4-aminoquinolines: synthesis, inhibition of the *Mycobacterium tuberculosis* enoyl-acyl carrier protein reductase, antitubercular activity, SAR, and preclinical evaluation. *Eur J Med Chem.* 2023;245:114908. DOI:10.1016/j.ejmech.2022.114908
141. Ganapathy US, Dick T. Why matter matters: fast-tracking *Mycobacterium abscessus* drug discovery. *Molecules.* 2022;27(20):6948. doi:10.3390/molecules27206948.
- **A review that proposes strategies to screen anti-TB validated compounds to accelerate discovery of anti-Mabs drugs.**
142. Ripoll F, Pasek S, Schenowitz C, et al. Non mycobacterial virulence genes in the genome of the emerging pathogen *Mycobacterium abscessus*. *PLoS ONE.* 2009;4(6):e5660. DOI:10.1371/journal.pone.0005660
143. Choo SW, Wee WY, Ngeow YF, et al. Genomic reconnaissance of clinical isolates of emerging human pathogen *Mycobacterium abscessus* reveals high evolutionary potential. *Sci Rep.* 2014;4(1):4061. DOI:10.1038/srep04061
144. Bernut A, Le Moigne V, Lesne T, et al. *In vivo* assessment of drug efficacy against *Mycobacterium abscessus* using the embryonic zebrafish test system. *Antimicrob Agents Chemother.* 2014;58(7):4054–4063. DOI:10.1128/AAC.00142-14.
- **Validation of a Mabs zebrafish model of infection to assess in vivo drug efficacy.**
145. Dupont C, Viljoen A, Thomas S, et al. Bedaquiline inhibits the ATP synthase in *Mycobacterium abscessus* and is effective in infected zebrafish. *Antimicrob Agents Chemother.* 2017;61(11):61. DOI:10.1128/AAC.01225-17
146. Habjan E, VQT H, Gallant J, et al. An anti-tuberculosis compound screen using a zebrafish infection model identifies an aspartyl-tRNA synthetase inhibitor. *Dis Model Mech.* 2021;14(12):dmm049145. DOI:10.1242/dmm.049145
147. Nicola F, Cirillo DM, Lorè NI. Preclinical murine models to study lung infection with *Mycobacterium abscessus* complex. *Tuberculosis.* 2022;138:102301.
- **A review that summarizes the murine models to study Mabs infection and to test drugs.**
148. Maggioncalda EC, Story-Roller E, Mylius J, et al. A mouse model of pulmonary *Mycobacteroides abscessus* infection. *Sci Rep.* 2020;10(1):3690. DOI:10.1038/s41598-020-60452-1
149. Busatto C, Vianna JS, da Silva LV, et al. *Mycobacterium avium*: an overview. *Tuberculosis.* 2019;114:127–134. DOI:10.1016/j.tube.2018.12.004
150. Qvist T, Gilljam M, Jönsson B, et al. Epidemiology of nontuberculous mycobacteria among patients with cystic fibrosis in Scandinavia. *J Cyst Fibros.* 2015;14(1):46–52. DOI:10.1016/j.jcf.2014.08.002
151. Dupont C, Chen Y, Xu Z, et al. A piperidinol-containing molecule is active against *Mycobacterium tuberculosis* by inhibiting the mycolic acid flippase activity of MmpL3. *J Med Chem.* 2019;294(46):17512–17523. DOI:10.1074/jbc.RA119.010135
152. Pflégr V, Maixnerová J, Stolaříková J, et al. Design and synthesis of highly active antimycobacterial mutual esters of 2-(2-Isonicotinoylhydrazineylidene)propanoic acid. *Pharmaceuticals.* 2021;14(12):1302. DOI:10.3390/ph14121302

Les inhibiteurs directs d'InhA<sub>MTB</sub> présentent donc un fort potentiel à exploiter contre *M. abscessus*, dont notamment le TCS [503] qui présente un intérêt de repositionnement tout particulier à travers les nombreux analogues déjà décrits [504]. Dans cette lignée, notre collaboration avec l'équipe du Pr Vipin Kumar nous a permis d'évaluer l'activité d'adduits azoïques et d'adduits de Mannich et de Glaser à base de TCS vis-à-vis de *M. tuberculosis* et des MNT (soumis pour publication). Nous avons ainsi pu mettre en évidence des analogues présentant une meilleure activité antimycobactérienne que la molécule parentale et présentant des propriétés pharmacologiques favorables telles qu'une toxicité moindre sur les macrophages en culture.

Notre revue présentée précédemment expose également le potentiel d'inhibiteurs de MmpL3 qui ont montré leur efficacité contre *M. abscessus*. En effet, ce transporteur présente également un intérêt croissant pour le développement de nouveaux antituberculeux. Afin d'appuyer ces propos, nous avons mis en place dans l'équipe un système permettant de réaliser une inactivation génique conditionnelle chez *M. abscessus*. Placé sous le contrôle d'un promoteur de type Tet-OFF, nous avons démontré le caractère essentiel de *mmpL3* chez *M. abscessus*. J'ai notamment pu démontrer que la réduction de l'expression du transporteur MmpL3 en présence d'anhydrotétracycline s'accompagnait d'une perte des TDM et des acides mycoliques liés à l'AG avec pour conséquence une chute drastique de la viabilité bactérienne (**Annexe 2**). Ces résultats et l'ensemble des inhibiteurs prometteurs précédemment décrits, ouvrent un nouveau pan de recherche dans la lutte contre les infections à *M. abscessus* sachant qu'aucun antibiotique utilisé en clinique à ce jour ne cible la voie de biosynthèse et de transport des acides mycoliques chez cette bactérie.

Par ailleurs, la recherche de nouveaux inhibiteurs ne se limite pas aux enzymes de la voie de synthèse des lipides de surface. D'autres cibles identifiées précédemment chez *M. tuberculosis* présentent un intérêt tout particulier, telles que l'ATP synthase, inhibée par la BDQ. Pour dépasser le seul concept de repositionnement, nous avons étudié, en collaboration avec l'équipe du Pr Gerhard Grüber (Nanyang Technological University, Singapour) un nouveau dérivé de la BDQ. De la même manière, ce composé cible le domaine F<sub>0</sub> de l'ATP synthase empêchant sa rotation et donc la translocation de protons nécessaires à la production d'ATP (manuscrit soumis). Ce composé montre une très forte activité antimycobactérienne sur différentes MNT, incluant *M. abscessus*, *M. fortuitum* et *M. avium* à très faibles concentrations *in vitro*. J'ai, pour ma part, pu montrer l'action de ce dérivé au sein de macrophages infectés par *M. abscessus* sans pour autant montrer d'effet toxique. De plus, nous avons mis en évidence sa grande efficacité dans un modèle d'infection *in vivo* de poisson zèbre associée à une baisse de la charge bactérienne et des symptômes majeurs de virulence. Ce composé



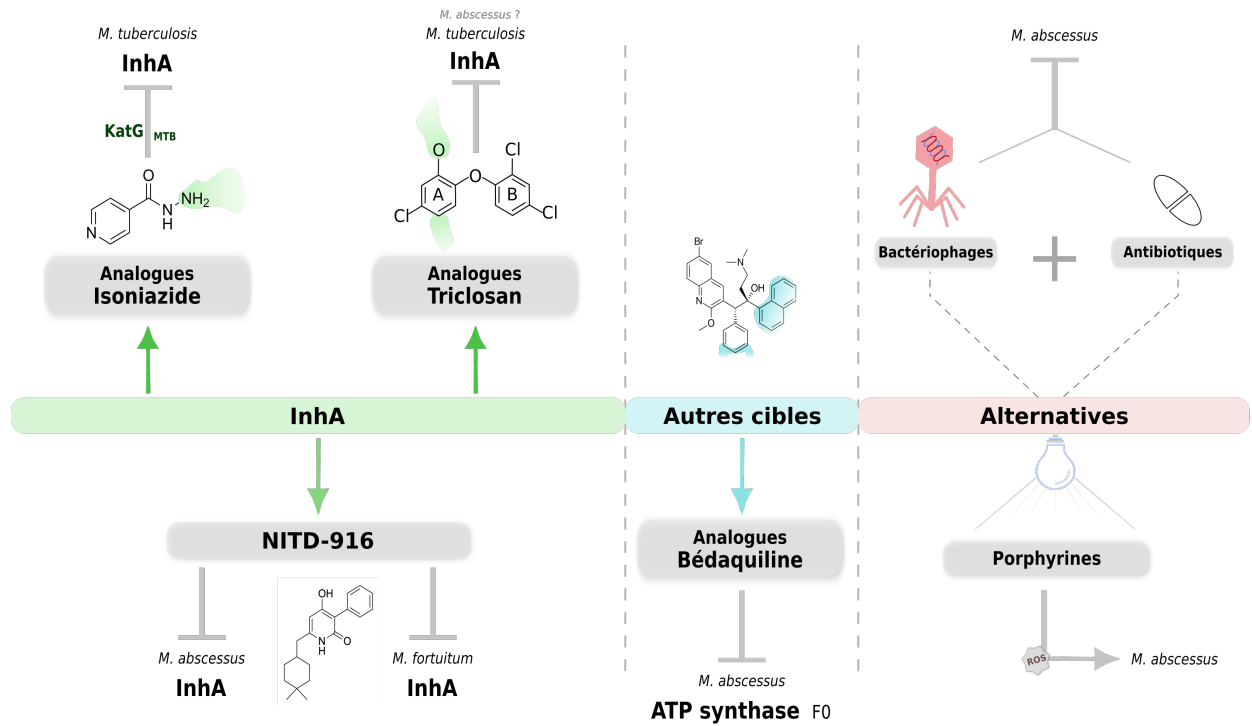
potentialise également l'activité d'autres antimycobactériens ce qui en fait un candidat intéressant à inclure dans les cocktails thérapeutiques actuels même si des études complémentaires précliniques et cliniques doivent être menées afin de le vérifier.

Néanmoins, nous savons que *M. abscessus*, et les mycobactéries en général développent rapidement des résistances contre les antibiotiques, ce qui en fait un frein majeur dans la réussite de la chimiothérapie. Ainsi, de nouvelles alternatives aux antibiotiques se doivent d'être également abordées et étudiées. Dans cette lignée, une alternative prometteuse consiste en l'utilisation de bactériophages (voir **Chapitre II : Antibiothérapie et mécanismes de résistance chez *M. abscessus***, 1.6.2. Les bactériophages : une alternative aux antibiotiques). Si la phagothérapie a pendant longtemps souffert d'une perte d'intérêt devant le succès des antibiotiques, l'utilisation des bactériophages, notamment pour le traitement d'infections causées par des pathogènes multirésistants aux antibiotiques, revient sur le devant de la scène. Bien que les autorités sanitaires ne favorisent pas encore l'utilisation à grande échelle de cette approche, des usages à caractère compassionnel et personnalisé peuvent être autorisés comme cela a été décrit dans plusieurs cas d'utilisation contre des infections mycobactériennes persistantes [292]. Ces cas soulignent les avantages et les inconvénients d'une telle thérapie, ainsi que la nécessité de mieux comprendre les interactions spécifiques entre phages et bactéries et d'optimiser l'efficacité des cocktails phagiques. Néanmoins, leur utilisation nécessite d'être couplée aux antibiotiques, et leur grande spécificité complexifie leur utilisation à grande échelle. En conséquence, j'ai pu démontrer que l'efficacité d'un des phages utilisés dans un traitement compassionnel [291], combiné à des antibiotiques tels que la RFB était supérieure à l'action d'un des deux antibactériens seul *in vitro*. Ce qui a été corroboré au sein d'un modèle *in vivo* de poisson zèbre délétée de la protéine CFTR, soulignant également l'impact de l'immunité dans l'efficacité du traitement phagique (**Annexe 3**). En outre, cette étude met en évidence l'utilisation d'un modèle d'organisme vivant dans le but de pouvoir prédire la fiabilité et le succès d'un traitement phagique avant leur utilisation chez l'Homme.

Une seconde alternative envisageable à l'utilisation des antibiotiques réside dans le développement de molécules photoactivables. En effet, un inconvénient majeur caractéristique de nombreux antibiotiques est l'acquisition rapide de mutations dans le gène codant la cible ou l'activateur. De plus, ces mécanismes de résistance peuvent également survenir par transfert horizontal de gènes entre espèces bactériennes dans un environnement soumis à une pression antibiotique. Dès lors, l'utilisation de molécules à large spectre ne ciblant pas une protéine particulière, mais déstabilisant par exemple la membrane bactérienne, pourrait représenter un recours



Figure 50 : Représentation des différentes stratégies mises en évidence par ces travaux et exploitables dans de futures études envers les infections mycobactériennes



supplémentaire pour éradiquer l'infection. La thérapie photodynamique se base sur l'administration d'un photosensibilisateur irradié à une longueur d'ondes optimale qui, en présence d'oxygène, va produire des ROS permettant des dommages oxydatifs irréversibles au niveau de la membrane et contre des substrats organiques qui vont engendrer la lyse bactérienne [543]. Cette méthode, utilisée contre les cellules cancéreuses, a montré son intérêt contre diverses infections bactériennes. La thérapie photodynamique est site spécifique et ne permet pas aux bactéries de développer une résistance grâce au temps court entre l'administration du photosensibilisateur et la stimulation par la lumière, combiné à un mode d'action très large [544]. Cette méthode permet notamment de contrôler les biofilms bactériens, d'être appliquée à des plaies cutanées locales mais également internes afin d'éliminer un foyer infectieux bien localisé [545]. Une des thérapies antibactérienne photodynamique développées récemment est basée sur l'utilisation de porphyrines [546]. L'action de ces dernières a été démontré *in vitro* contre les MNT [547] mais aussi *in vivo* dans des infections de la peau et des tissus mous [548]. Ainsi, j'ai pu cribler un ensemble de composés dérivés de porphyrines synthétisés par l'équipe du Dr Sébastien Ulrich (Institut des Biomolécules Max Mousseron, Montpellier) et étudier leurs caractéristiques sur *E. coli* et *M. abscessus*. Les résultats obtenus rapportent une excellente activité antibactérienne *in vitro* et dans un modèle de biofilms (données non publiées). De plus, nous avons pu démontrer la désagrégation morphologique de la membrane de *M. abscessus* due à l'action d'un composé photoactivable cationique. Ces résultats sont encourageants dans une perspective d'avenir de traitement contre les infections mycobactériennes multirésistantes aux antibiotiques mais nécessitent encore d'être étayés et validés par d'autres études.

En conclusion, face à l'impasse thérapeutique subie par les patients, il apparaît essentiel de développer de nouveaux traitements contre les infections mycobactériennes. Ainsi, les résultats générés aux cours de cette thèse permettent de proposer de nouvelles molécules et nouvelles cibles d'intérêt à exploiter dans de futurs développements thérapeutiques (**Figure 50**). Ils ouvrent également la voie à de nouvelles approches à envisager et valider ultérieurement dans le but d'améliorer la prise en charge de ces patients.



# Références

- [1] Lehmann KB, Neumann RO. Atlas und Grundriss der Bakteriologie, und Lehrbuch der speziellen bakteriologischen Diagnostik. 1896.
- [2] Ventura M, Canchaya C, Tauch A, et al. Genomics of *Actinobacteria* : Tracing the Evolutionary History of an Ancient Phylum. *Microbiol Mol Biol Rev.* 2007;71:495–548.
- [3] Vilchère C, Kremer L. Acid-Fast Positive and Acid-Fast Negative *Mycobacterium tuberculosis* : The Koch Paradox. Jacobs Jr. WR, McShane H, Mizrahi V, et al., editors. *Microbiol Spectr.* 2017;5:5.2.15.
- [4] Runyon EH. Anonymous Mycobacteria in Pulmonary Disease. *Med Clin North Am.* 1959;43:273–290.
- [5] Johansen MD, Herrmann J-L, Kremer L. Non-tuberculous mycobacteria and the rise of *Mycobacterium abscessus*. *Nat Rev Microbiol.* 2020;18:392–407.
- [6] Koch A, Mizrahi V. *Mycobacterium tuberculosis*. *Trends Microbiol.* 2018;26:555–556.
- [7] Sugawara-Mikami M, Tanigawa K, Kawashima A, et al. Pathogenicity and virulence of *Mycobacterium leprae*. *Virulence.* 2022;13:1985–2011.
- [8] Tortoli E, Fedrizzi T, Meehan CJ, et al. The new phylogeny of the genus *Mycobacterium* : The old and the news. *Infect Genet Evol.* 2017;56:19–25.
- [9] Mignard S, Flandrois J-P. A seven-gene, multilocus, genus-wide approach to the phylogeny of mycobacteria using supertrees. *Int J Syst Evol Microbiol.* 2008;58:1432–1441.
- [10] Bachmann NL, Salamzade R, Manson AL, et al. Key Transitions in the Evolution of Rapid and Slow Growing Mycobacteria Identified by Comparative Genomics. *Front Microbiol.* 2020;10:3019.
- [11] Gupta RS, Lo B, Son J. Phylogenomics and Comparative Genomic Studies Robustly Support Division of the Genus *Mycobacterium* into an Emended Genus *Mycobacterium* and Four Novel Genera. *Front Microbiol.* 2018;9:67.
- [12] Tortoli E, Brown-Elliott BA, Chalmers JD, et al. Same meat, different gravy: ignore the new names of mycobacteria. *Eur Respir J.* 2019;54:1900795.
- [13] Meehan CJ, Barco RA, Loh Y-HE, et al. Reconstituting the genus *Mycobacterium*. *Int J Syst Evol Microbiol* [Internet]. 2021 [cited 2023 Apr 4];71. Available from: <https://www.microbiologyresearch.org/content/journal/ijsem/10.1099/ijsem.0.004922>.
- [14] Daniel TM. Robert Koch and the pathogenesis of tuberculosis. *Int J Tuberc Lung Dis Off J Int Union Tuberc Lung Dis.* 2005;9:1181–1182.
- [15] Morse D, Brothwell DR, Ucko PJ. Tuberculosis in Ancient Egypt. *Am Rev Respir Dis.* 1964;
- [16] Crubézy E, Ludes B, Poveda J-D, et al. Identification of Mycobacterium DNA in an Egyptian Pott's disease of 5400 years old. *Comptes Rendus Académie Sci - Ser III - Sci Vie.* 1998;321:941–951.
- [17] Zimmerman MR. Pulmonary and Osseous Tuberculosis in an Egyptian Mummy. *Bull N Acad Med.* 1979;55.
- [18] Dockrell HM, Smith SG. What Have We Learnt about BCG Vaccination in the Last 20 Years? *Front Immunol.* 2017;8:1134.
- [19] WHO. WHO Global Tuberculosis report 2022 [Internet]. 2022. Available from: <https://www.who.int/teams/global-tuberculosis-programme/tb-reports/global-tuberculosis-report-2022>.
- [20] Brown-Elliott BA, Philley JV. Rapidly Growing Mycobacteria. Schlossberg D, editor. *Microbiol Spectr.* 2017;5:5.1.02.
- [21] Cowman S, van Ingen J, Griffith DE, et al. Non-tuberculous mycobacterial pulmonary disease. *Eur Respir J.*

- 2019;54:1900250.
- [22] Honda JR, Viridi R, Chan ED. Global Environmental Nontuberculous Mycobacteria and Their Contemporaneous Man-Made and Natural Niches. *Front Microbiol.* 2018;9:2029.
- [23] Lee M-R, Sheng W-H, Hung C-C, et al. *Mycobacterium abscessus* Complex Infections in Humans. *Emerg Infect Dis* [Internet]. 2015 [cited 2023 Apr 30];21. Available from: [http://wwwnc.cdc.gov/eid/article/21/9/14-1634\\_article.htm](http://wwwnc.cdc.gov/eid/article/21/9/14-1634_article.htm).
- [24] da Costa Cruz J. *Mycobacterium fortuitum*: um novo bacilo acido-resistente patogenico para o homen (new acid fast bacillus pathogenic for man). *Acta Med.* 1938;
- [25] Runyon EH. Conservation of the Specific Epithet fortuitum in the Name of the Organism Known as *Mycobacterium fortuitum* da Costa Cruz: Request for an Opinion. *Int J Syst Bacteriol.* 1972;22:50–51.
- [26] Falkinham J. Ecology of Nontuberculous Mycobacteria—Where Do Human Infections Come from? *Semin Respir Crit Care Med.* 2013;34:095–102.
- [27] Richards CJ, Olivier KN. Nontuberculous Mycobacteria in Cystic Fibrosis. *Semin Respir Crit Care Med.* 2019;40:737–750.
- [28] Park S, Suh GY, Chung MP, et al. Clinical significance of *Mycobacterium fortuitum* isolated from respiratory specimens. *Respir Med.* 2008;102:437–442.
- [29] Franco-Paredes C, Marcos LA, Henao-Martínez AF, et al. Cutaneous Mycobacterial Infections. *Clin Microbiol Rev.* 2019;32.
- [30] Wallace RJ, Swenson JM, Silcox VA, et al. Spectrum of Disease Due to Rapidly Growing Mycobacteria. *Clin Infect Dis.* 1983;5:657–679.
- [31] Brown-Elliott BA, Nash KA, Wallace RJ. Antimicrobial Susceptibility Testing, Drug Resistance Mechanisms, and Therapy of Infections with Nontuberculous Mycobacteria. *Clin Microbiol Rev.* 2012;25:545–582.
- [32] Santos DR de S, Lourenço MCS, Coelho FS, et al. Resistance profile of strains of *Mycobacterium fortuitum* isolated from clinical specimens. *J Bras Pneumol.* 2016;42:299–301.
- [33] Shen Y, Wang X, Jin J, et al. In Vitro Susceptibility of *Mycobacterium abscessus* and *Mycobacterium fortuitum* Isolates to 30 Antibiotics. *BioMed Res Int.* 2018;2018:1–10.
- [34] Kim S-Y, Moon SM, Jhun BW, et al. Species Distribution and Macrolide Susceptibility of *Mycobacterium fortuitum* Complex Clinical Isolates. *Antimicrob Agents Chemother.* 2019;63:e02331-18.
- [35] Nash KA, Zhang Y, Brown-Elliott BA, et al. Molecular basis of intrinsic macrolide resistance in clinical isolates of *Mycobacterium fortuitum*. *J Antimicrob Chemother.* 2005;55:170–177.
- [36] Griffith DE, Aksamit T, Brown-Elliott BA, et al. An Official ATS/IDSA Statement: Diagnosis, Treatment, and Prevention of Nontuberculous Mycobacterial Diseases. *Am J Respir Crit Care Med.* 2007;175:367–416.
- [37] Medjahed H, Gaillard J-L, Reyrat J-M. *Mycobacterium abscessus*: a new player in the mycobacterial field. *Trends Microbiol.* 2010;18:117–123.
- [38] Gutiérrez AV, Viljoen A, Ghigo E, et al. Glycopeptidolipids, a Double-Edged Sword of the *Mycobacterium abscessus* Complex. *Front Microbiol.* 2018;9:1145.
- [39] Moore M, Frerichs JB. An Unusual Acid-Fast Infection of the Knee with Subcutaneous, Abscess-Like Lesions of the Gluteal Region. *J Invest Dermatol.* 1953;20:133–169.
- [40] Kubica GP, Baess I, Gordon RE, et al. A Co-operative Numerical Analysis of Rapidly Growing Mycobacteria. *J Gen Microbiol.* 1972;73:55–70.
- [41] Adekambi T, Sassi M, van Ingen J, et al. Reinstating *Mycobacterium massiliense* and *Mycobacterium bolletii* as species of the *Mycobacterium abscessus* complex. *Int J Syst Evol Microbiol.* 2017;67:2726–2730.
- [42] Tortoli E, Kohl TA, Brown-Elliott BA, et al. Emended description of *Mycobacterium abscessus*, *Mycobacterium abscessus* subsp. *abscessus* and *Mycobacterium abscessus* subsp. *bolletii* and designation of *Mycobacterium abscessus* subsp.

- massiliense* comb. nov. Int J Syst Evol Microbiol. 2016;66:4471–4479.
- [43] Nash KA, Brown-Elliott BA, Wallace RJ. A Novel Gene, *erm(41)*, Confers Inducible Macrolide Resistance to Clinical Isolates of *Mycobacterium abscessus* but Is Absent from *Mycobacterium chelonae*. Antimicrob Agents Chemother. 2009;53:1367–1376.
- [44] Benwill JL, Wallace RJ. *Mycobacterium abscessus*: challenges in diagnosis and treatment. Curr Opin Infect Dis. 2014;27:506–510.
- [45] Howard ST, Rhoades E, Recht J, et al. Spontaneous reversion of *Mycobacterium abscessus* from a smooth to a rough morphotype is associated with reduced expression of glycopeptidolipid and reacquisition of an invasive phenotype. Microbiology. 2006;152:1581–1590.
- [46] Ripoll F, Deshayes C, Pasek S, et al. Genomics of glycopeptidolipid biosynthesis in *Mycobacterium abscessus* and *M. chelonae*. BMC Genomics. 2007;8:114.
- [47] Sánchez-Chardi A, Olivares F, Byrd TF, et al. Demonstration of Cord Formation by Rough *Mycobacterium abscessus* Variants: Implications for the Clinical Microbiology Laboratory. J Clin Microbiol. 2011;49:2293–2295.
- [48] Bernut A, Herrmann J-L, Kissa K, et al. *Mycobacterium abscessus* cording prevents phagocytosis and promotes abscess formation. Proc Natl Acad Sci. 2014;111:E943–E952.
- [49] Clary G, Sasindran SJ, Nesbitt N, et al. *Mycobacterium abscessus* Smooth and Rough Morphotypes Form Antimicrobial-Tolerant Biofilm Phenotypes but Are Killed by Acetic Acid. Antimicrob Agents Chemother. 2018;62:e01782-17.
- [50] Chakraborty P, Kumar A. The extracellular matrix of mycobacterial biofilms: could we shorten the treatment of mycobacterial infections? Microb Cell. 2019;6:105–122.
- [51] Dokic A, Peterson E, Arrieta-Ortiz ML, et al. *Mycobacterium abscessus* biofilms produce an extracellular matrix and have a distinct mycolic acid profile. Cell Surf. 2021;7:100051.
- [52] Fennelly KP, Ojano-Dirain C, Yang Q, et al. Biofilm Formation by *Mycobacterium abscessus* in a Lung Cavity. Am J Respir Crit Care Med. 2016;193:692–693.
- [53] Roux A-L, Viljoen A, Bah A, et al. The distinct fate of smooth and rough *Mycobacterium abscessus* variants inside macrophages. Open Biol. 2016;6:160185.
- [54] Whang J, Back YW, Lee K-I, et al. *Mycobacterium abscessus* glycopeptidolipids inhibit macrophage apoptosis and bacterial spreading by targeting mitochondrial cyclophilin D. Cell Death Dis. 2017;8:e3012–e3012.
- [55] Rhoades ER, Archambault AS, Greendyke R, et al. *Mycobacterium abscessus* Glycopeptidolipids Mask Underlying Cell Wall Phosphatidyl-*myo*-Inositol Mannosides Blocking Induction of Human Macrophage TNF- $\alpha$  by Preventing Interaction with TLR2. J Immunol. 2009;183:1997–2007.
- [56] Tomaszefski JF, Stern RC, Demko CA, et al. Nontuberculous mycobacteria in cystic fibrosis. An autopsy study. Am J Respir Crit Care Med. 1996;154:523–528.
- [57] Bernut A, Nguyen-Chi M, Halloum I, et al. *Mycobacterium abscessus*-Induced Granuloma Formation Is Strictly Dependent on TNF Signaling and Neutrophil Trafficking. Behr MA, editor. PLOS Pathog. 2016;12:e1005986.
- [58] Catherinot E, Roux A-L, Macheras E, et al. Acute Respiratory Failure Involving an R Variant of *Mycobacterium abscessus*. J Clin Microbiol. 2009;47:271–274.
- [59] Park IK, Hsu AP, Tettelin H, et al. Clonal Diversification and Changes in Lipid Traits and Colony Morphology in *Mycobacterium abscessus* Clinical Isolates. Forbes BA, editor. J Clin Microbiol. 2015;53:3438–3447.
- [60] Pawlik A, Garnier G, Orgeur M, et al. Identification and characterization of the genetic changes responsible for the characteristic smooth-to-rough morphotype alterations of clinically persistent *Mycobacterium abscessus*: Genetic traits of rough mutants of *Mycobacterium abscessus*. Mol Microbiol. 2013;90:612–629.
- [61] Byrd TF, Lyons CR. Preliminary Characterization of a *Mycobacterium abscessus* Mutant in Human and Murine Models

- of Infection. *INFECT IMMUN*. 1999;67:8.
- [62] Catherinot E, Clarissou J, Etienne G, et al. Hypervirulence of a Rough Variant of the *Mycobacterium abscessus* Type Strain. *Infect Immun*. 2007;75:1055–1058.
- [63] Boudehen Y-M, Kremer L. *Mycobacterium abscessus*. *Trends Microbiol*. 2021;29:951–952.
- [64] Prevots DR, Marras TK. Epidemiology of Human Pulmonary Infection with Nontuberculous Mycobacteria. *Clin Chest Med*. 2015;36:13–34.
- [65] Sharma S, Upadhyay V. Epidemiology, diagnosis & treatment of non-tuberculous mycobacterial diseases. *Indian J Med Res*. 2020;152:185.
- [66] Wu M-L, Aziz DB, Dartois V, et al. NTM drug discovery: status, gaps and the way forward. *Drug Discov Today*. 2018;23:1502–1519.
- [67] Gopinath K, Singh S. Non-Tuberculous Mycobacteria in TB-Endemic Countries: Are We Neglecting the Danger? Phillips RO, editor. *PLoS Negl Trop Dis*. 2010;4:e615.
- [68] Shahraki AH, Heidarieh P, Bostanabad SZ, et al. “Multidrug-resistant tuberculosis” may be nontuberculous mycobacteria. *Eur J Intern Med*. 2015;26:279–284.
- [69] Wongkitisophon P, Rattanakaemakorn P, Tanrattanakorn S, et al. Cutaneous *Mycobacterium abscessus* Infection Associated with Mesotherapy Injection. *Case Rep Dermatol*. 2011;3:37–41.
- [70] Moreno-Izquierdo C, Zurita J, Contreras-Yametti FI, et al. *Mycobacterium abscessus* subspecies abscessus infection associated with cosmetic surgical procedures: Case series. *IDCases*. 2020;22:e00992.
- [71] Nagpal R, Vanam HP, Dhingra H, et al. Post Cesarean Surgical Site Infection with *Mycobacterium Abscessus* Sp. *Massiliense*. *J Fam Reprod Health* [Internet]. 2022 [cited 2023 May 10]; Available from: <https://publish.kne-publishing.com/index.php/JFRH/article/view/9486>.
- [72] Kerkemeyer KL, Darby JD, Green J. *Mycobacterium abscessus* infection of a new tattoo in an Australian traveller returning from Bali, Indonesia. *J Travel Med*. 2020;27:taaa014.
- [73] Ricciardo B, Weedon D, Butler G. *Mycobacterium abscessus* infection complicating a professional tattoo: *M. abscessus* infection in a tattoo. *Australas J Dermatol*. 2010;51:287–289.
- [74] Ryu HJ, Kim WJ, Oh CH, et al. Iatrogenic *Mycobacterium abscessus* infection associated with acupuncture: clinical manifestations and its treatment: *M. abscessus* infection associated with acupuncture. *Int J Dermatol*. 2005;44:846–850.
- [75] Chadha R, Grover M, Sharma A, et al. An outbreak of post-surgical wound infections due to *Mycobacterium abscessus*. *Pediatr Surg Int*. 1998;13:406–410.
- [76] Grubbs J, Bowen C. *Mycobacterium abscessus* Infection Following Home Dermabrasion. 2019;
- [77] El Helou G, Hachem R, Viola GM, et al. Management of Rapidly Growing Mycobacterial Bacteremia in Cancer Patients. *Clin Infect Dis*. 2013;56:843–846.
- [78] El Helou G, Viola GM, Hachem R, et al. Rapidly growing mycobacterial bloodstream infections. *Lancet Infect Dis*. 2013;13:166–174.
- [79] Lee M-R, Ko J-C, Liang S-K, et al. Bacteraemia caused by *Mycobacterium abscessus* subsp. *abscessus* and *M. abscessus* subsp. *bolletii*: Clinical features and susceptibilities of the isolates. *Int J Antimicrob Agents*. 2014;43:438–441.
- [80] Hoefsloot W, Van Ingen J, Andrejak C, et al. The geographic diversity of nontuberculous mycobacteria isolated from pulmonary samples: an NTM-NET collaborative study. *Eur Respir J*. 2013;42:1604–1613.
- [81] Zweijpfenning S, Ingen J, Hoefsloot W. Geographic Distribution of Nontuberculous Mycobacteria Isolated from Clinical Specimens: A Systematic Review. *Semin Respir Crit Care Med*. 2018;39:336–342.
- [82] Mougari F, Guglielmetti L, Raskine L, et al. Infections caused by *Mycobacterium abscessus* : epidemiology, diagnostic

- tools and treatment. *Expert Rev Anti Infect Ther*. 2016;14:1139–1154.
- [83] Falkinham JO. Nontuberculous Mycobacteria from Household Plumbing of Patients with Nontuberculous Mycobacteria Disease. *Emerg Infect Dis*. 2011;17:419–424.
- [84] Thomson R, Tolson C, Carter R, et al. Isolation of Nontuberculous Mycobacteria (NTM) from Household Water and Shower Aerosols in Patients with Pulmonary Disease Caused by NTM. *J Clin Microbiol*. 2013;51:3006–3011.
- [85] De Groot MA, Pace NR, Fulton K, et al. Relationships between *Mycobacterium* Isolates from Patients with Pulmonary Mycobacterial Infection and Potting Soils. *Appl Environ Microbiol*. 2006;72:7602–7606.
- [86] Balavoine C, Andréjak C, Marchand-Adam S, et al. Relations entre la BPCO et les infections à mycobactéries non tuberculeuses. *Rev Mal Respir*. 2017;34:1091–1097.
- [87] Morita H, Nakamura A, Kato T, et al. Isolation of nontuberculous mycobacteria from patients with pneumoconiosis. *J Infect Chemother*. 2005;11:89–92.
- [88] Singh UB, Das R, Shrestha P, et al. Compromised longevity due to *Mycobacterium abscessus* pulmonary disease in lungs scarred by tuberculosis. *Access Microbiol* [Internet]. 2019 [cited 2023 May 16];1. Available from: <https://www.microbiologyresearch.org/content/journal/acmi/10.1099/acmi.0.000003>.
- [89] Kim B-G, Choi YS, Shin SH, et al. Risk Factors for the Development of Nontuberculous Mycobacteria Pulmonary Disease during Long-Term Follow-Up after Lung Cancer Surgery. *Diagnostics*. 2022;12:1086.
- [90] Okamoto M, Kim YH, Ouchi A, et al. Exacerbation of nontuberculous mycobacterial pulmonary disease in a patient with advanced non-small-cell lung cancer during treatment with PD-1 inhibitor and chemotherapy. *Respir Med Case Rep*. 2021;34:101529.
- [91] Rodriguez RR, Alhamad K, Ghosh S, et al. Atypical *Mycobacterium Abscessus* Infection in Stable Chronic Lymphocytic Leukemia: A Case Report and Review of the Literature. *Cureus* [Internet]. 2021 [cited 2023 May 16]; Available from: <https://www.cureus.com/articles/80667-atypical-mycobacterium-abscessus-infection-in-stable-chronic-lymphocytic-leukemia-a-case-report-and-review-of-the-literature>.
- [92] Henkle E, Winthrop KL. Nontuberculous Mycobacteria Infections in Immunosuppressed Hosts. *Clin Chest Med*. 2015;36:91–99.
- [93] Jung S-Y, Kim BG, Kwon D, et al. An outbreak of joint and cutaneous infections caused by non-tuberculous mycobacteria after corticosteroid injection. *Int J Infect Dis*. 2015;36:62–69.
- [94] Liao T-L, Lin C-F, Chen Y-M, et al. Risk Factors and Outcomes of Nontuberculous Mycobacterial Disease among Rheumatoid Arthritis Patients: A Case-Control study in a TB Endemic Area. *Sci Rep*. 2016;6:29443.
- [95] Winthrop KL, Chang E, Yamashita S, et al. Nontuberculous Mycobacteria Infections and Anti-Tumor Necrosis Factor- $\alpha$  Therapy. *Emerg Infect Dis*. 2009;15:1556–1561.
- [96] Wetzstein N, Geil A, Kann G, et al. Disseminated disease due to non-tuberculous mycobacteria in HIV positive patients: A retrospective case control study. Yu Q, editor. *PLOS ONE*. 2021;16:e0254607.
- [97] Benwill J, Babineaux M, Sarria JC. Pulmonary *Mycobacterium abscessus* in an AIDS Patient. *Am J Med Sci*. 2010;339:495–496.
- [98] Sungkanuparph S, Sathapatayavongs B, Prachartam R. Infections with rapidly growing mycobacteria: report of 20 cases. *Int J Infect Dis*. 2003;7:198–205.
- [99] Prieto MD, Alam ME, Franciosi AN, et al. Global burden of nontuberculous mycobacteria in the cystic fibrosis population: a systematic review and meta-analysis. *ERJ Open Res*. 2023;9:00336–02022.
- [100] Floto RA, Olivier KN, Saiman L, et al. US Cystic Fibrosis Foundation and European Cystic Fibrosis Society consensus recommendations for the management of non-tuberculous mycobacteria in individuals with cystic fibrosis. *Thorax*. 2016;71:i1–i22.



- [101] Orens JB, Estenne M, Arcasoy S, et al. International Guidelines for the Selection of Lung Transplant Candidates: 2006 Update—A Consensus Report From the Pulmonary Scientific Council of the International Society for Heart and Lung Transplantation. *J Heart Lung Transplant*. 2006;25:745–755.
- [102] Ratjen F, Bell SC, Rowe SM, et al. Cystic fibrosis. *Nat Rev Dis Primer*. 2015;1:15010.
- [103] Hill DB, Long RF, Kissner WJ, et al. Pathological mucus and impaired mucus clearance in cystic fibrosis patients result from increased concentration, not altered pH. *Eur Respir J*. 2018;52:1801297.
- [104] Pezzulo AA, Tang XX, Hoegger MJ, et al. Reduced airway surface pH impairs bacterial killing in the porcine cystic fibrosis lung. *Nature*. 2012;487:109–113.
- [105] Bernut A, Dupont C, Ogryzko NV, et al. CFTR Protects against *Mycobacterium abscessus* Infection by Fine-Tuning Host Oxidative Defenses. *Cell Rep*. 2019;26:1828-1840.e4.
- [106] Bernut A, Herrmann J-L, Ordway D, et al. The Diverse Cellular and Animal Models to Decipher the Physiopathological Traits of *Mycobacterium abscessus* Infection. *Front Cell Infect Microbiol* [Internet]. 2017 [cited 2023 May 21];7. Available from: <http://journal.frontiersin.org/article/10.3389/fcimb.2017.00100/full>.
- [107] Madhvi A, Mishra H, Leisching G, et al. Comparison of human monocyte derived macrophages and THP1-like macrophages as in vitro models for *M. tuberculosis* infection. *Comp Immunol Microbiol Infect Dis*. 2019;67:101355.
- [108] Peyron P, Vaubourgeix J, Poquet Y, et al. Foamy Macrophages from Tuberculous Patients' Granulomas Constitute a Nutrient-Rich Reservoir for *M. tuberculosis* Persistence. Bishai W, editor. *PLoS Pathog*. 2008;4:e1000204.
- [109] Viljoen A, Blaise M, de Chastellier C, et al. *MAB\_3551c* encodes the primary triacylglycerol synthase involved in lipid accumulation in *Mycobacterium abscessus*: TAG accumulation in *Mycobacterium abscessus*. *Mol Microbiol*. 2016;102:611–627.
- [110] Caire-Brändli I, Papadopoulos A, Malaga W, et al. Reversible Lipid Accumulation and Associated Division Arrest of *Mycobacterium avium* in Lipoprotein-Induced Foamy Macrophages May Resemble Key Events during Latency and Reactivation of Tuberculosis. Flynn JL, editor. *Infect Immun*. 2014;82:476–490.
- [111] Santucci P, Bouzid F, Smichi N, et al. Experimental Models of Foamy Macrophages and Approaches for Dissecting the Mechanisms of Lipid Accumulation and Consumption during Dormancy and Reactivation of Tuberculosis. *Front Cell Infect Microbiol* [Internet]. 2016 [cited 2023 May 22];6. Available from: <http://journal.frontiersin.org/article/10.3389/fcimb.2016.00122/full>.
- [112] Drancourt M. Looking in amoebae as a source of mycobacteria. *Microb Pathog*. 2014;77:119–124.
- [113] Lamrabet O, Merhej V, Pontarotti P, et al. The Genealogic Tree of Mycobacteria Reveals a Long-Standing Sympatric Life into Free-Living Protozoa. Manganelli R, editor. *PLoS ONE*. 2012;7:e34754.
- [114] Bakala N'Goma JC, Le Moigne V, Soismier N, et al. *Mycobacterium abscessus* Phospholipase C Expression Is Induced during Coculture within Amoebae and Enhances *M. abscessus* Virulence in Mice. Roy CR, editor. *Infect Immun*. 2015;83:780–791.
- [115] Dubois V, Pawlik A, Bories A, et al. *Mycobacterium abscessus* virulence traits unraveled by transcriptomic profiling in amoeba and macrophages. Behr MA, editor. *PLOS Pathog*. 2019;15:e1008069.
- [116] Laencina L, Dubois V, Le Moigne V, et al. Identification of genes required for *Mycobacterium abscessus* growth in vivo with a prominent role of the ESX-4 locus. *Proc Natl Acad Sci* [Internet]. 2018 [cited 2023 Jun 18];115. Available from: <https://pnas.org/doi/full/10.1073/pnas.1713195115>.
- [117] Kicka S, Trofimov V, Harrison C, et al. Establishment and Validation of Whole-Cell Based Fluorescence Assays to Identify Anti-Mycobacterial Compounds Using the Acanthamoeba castellanii - *Mycobacterium marinum* Host-Pathogen System. Greub G, editor. *PLoS ONE*. 2014;9:e87834.
- [118] Richter A, Shapira T, Av-Gay Y. THP-1 and *Dictyostelium* Infection Models for Screening and Characterization of Anti-

- Mycobacterium abscessus* Hit Compounds. *Antimicrob Agents Chemother.* 2019;64:e01601-19.
- [119] Puissegur M-P, Botanch C, Duteyrat J-L, et al. An in vitro dual model of mycobacterial granulomas to investigate the molecular interactions between mycobacteria and human host cells. *Cell Microbiol.* 2004;6:423–433.
- [120] Saunders BM, Cooper AM. Restraining mycobacteria: Role of granulomas in mycobacterial infections. *Immunol Cell Biol.* 2000;78:334–341.
- [121] Je S, Quan H, Na Y, et al. An *in vitro* model of granuloma-like cell aggregates substantiates early host immune responses against *Mycobacterium massiliense* infection. *Biol Open.* 2016;5:1118–1127.
- [122] Iakobachvili N, Leon-Icaza SA, Knoops K, et al. Mycobacteria–host interactions in human bronchiolar airway organoids. *Mol Microbiol.* 2022;117:682–692.
- [123] Leon-Icaza SA, Bagayoko S, Vergé R, et al. Druggable redox pathways against *Mycobacterium abscessus* in cystic fibrosis patient-derived airway organoids. Boshoff HI, editor. *PLOS Pathog.* 2023;19:e1011559.
- [124] Torraca V, Masud S, Spaink HP, et al. Macrophage-pathogen interactions in infectious diseases: new therapeutic insights from the zebrafish host model. *Dis Model Mech.* 2014;7:785–797.
- [125] Ramakrishnan L. Looking Within the Zebrafish to Understand the Tuberculous Granuloma. In: Divangahi M, editor. *New Paradigm Immun Tuberc* [Internet]. New York, NY: Springer New York; 2013 [cited 2023 May 24]. p. 251–266. Available from: [https://link.springer.com/10.1007/978-1-4614-6111-1\\_13](https://link.springer.com/10.1007/978-1-4614-6111-1_13).
- [126] Varela M, Meijer AH. A fresh look at mycobacterial pathogenicity with the zebrafish host model. *Mol Microbiol.* 2022;117:661–669.
- [127] Bernut A, Dupont C, Sahuquet A, et al. Deciphering and Imaging Pathogenesis and Cording of *Mycobacterium abscessus* in Zebrafish Embryos. *J Vis Exp.* 2015;53130.
- [128] Bernut A, Le Moigne V, Lesne T, et al. *In Vivo* Assessment of Drug Efficacy against *Mycobacterium abscessus* Using the Embryonic Zebrafish Test System. *Antimicrob Agents Chemother.* 2014;58:4054–4063.
- [129] Habjan E, Ho VQT, Gallant J, et al. An anti-tuberculosis compound screen using a zebrafish infection model identifies an aspartyl-tRNA synthetase inhibitor. *Dis Model Mech.* 2021;14:dmm049145.
- [130] Nicola F, Cirillo DM, Lorè NI. Preclinical murine models to study lung infection with *Mycobacterium abscessus* complex. *Tuberculosis.* 2023;138:102301.
- [131] Ordway D, Henao-Tamayo M, Smith E, et al. Animal model of *Mycobacterium abscessus* lung infection. *J Leukoc Biol.* 2008;83:1502–1511.
- [132] Obregón-Henao A, Arnett KA, Henao-Tamayo M, et al. Susceptibility of *Mycobacterium abscessus* to Antimycobacterial Drugs in Preclinical Models. *Antimicrob Agents Chemother.* 2015;59:6904–6912.
- [133] Riva C, Tortoli E, Cugnata F, et al. A New Model of Chronic *Mycobacterium abscessus* Lung Infection in Immunocompetent Mice. *Int J Mol Sci.* 2020;21:6590.
- [134] Kramnik I, Dietrich WF, Demant P, et al. Genetic Control of Resistance to Experimental Infection with Virulent *Mycobacterium tuberculosis*. *Proc Natl Acad Sci U S A.* 2000;97:8560–8565.
- [135] Maggioncalda EC, Story-Roller E, Mylius J, et al. A mouse model of pulmonary *Mycobacteroides abscessus* infection. *Sci Rep.* 2020;10:3690.
- [136] Nessar R, Cambau E, Reytrat JM, et al. *Mycobacterium abscessus*: a new antibiotic nightmare. *J Antimicrob Chemother.* 2012;67:810–818.
- [137] Daley CL, Iaccarino JM, Lange C, et al. Treatment of nontuberculous mycobacterial pulmonary disease: an official ATS/ERS/ESCMID/IDSA clinical practice guideline. *Eur Respir J.* 2020;56:2000535.
- [138] BC CDC. Tuberculosis Physician Manual - Section 12 : Pulmonary Non-Tuberculous Mycobacteria. 2022.
- [139] Griffith DE, Daley CL. Treatment of *Mycobacterium abscessus* Pulmonary Disease. *Chest.* 2022;161:64–75.

- [140] Bunch RL, McGuire JM. Erythromycin, its salt and method of preparation.pdf. US Pat. 1952;
- [141] Lohsen S, Stephens DS. Current Macrolide Antibiotics and Their Mechanisms of Action. In: Capelo-Martínez J, Igrejas G, editors. *Antibiot Drug Resist* [Internet]. 1st ed. Wiley; 2019 [cited 2023 Jun 14]. p. 97–117. Available from: <https://onlinelibrary.wiley.com/doi/10.1002/9781119282549.ch5>.
- [142] Douthwaite S. Structure–activity relationships of ketolides vs. macrolides. *Clin Microbiol Infect*. 2001;7:11–17.
- [143] Kannan K, Mankin AS. Macrolide antibiotics in the ribosome exit tunnel: species-specific binding and action: Species-specific binding and action of macrolides. *Ann N Y Acad Sci*. 2011;1241:33–47.
- [144] Wilson DN. Ribosome-targeting antibiotics and mechanisms of bacterial resistance. *Nat Rev Microbiol*. 2014;12:35–48.
- [145] Luthra S, Rominski A, Sander P. The Role of Antibiotic-Target-Modifying and Antibiotic-Modifying Enzymes in *Mycobacterium abscessus* Drug Resistance. *Front Microbiol*. 2018;9:2179.
- [146] Renna M, Schaffner C, Brown K, et al. Azithromycin blocks autophagy and may predispose cystic fibrosis patients to mycobacterial infection. *J Clin Invest*. 2011;121:3554–3563.
- [147] Catherinot E, Roux A-L, Vibet M-A, et al. Inhaled therapies, azithromycin and *Mycobacterium abscessus* in cystic fibrosis patients. *Eur Respir J*. 2013;41:1101–1106.
- [148] Fleming A. On the antibacterial action of cultures of a penicillium, with special reference to their use in the isolation of *B. Influenzæ*. 1929;
- [149] Chain E, Florey HW, Gardner AD, et al. Penicillin as a chemotherapeutic agent. 1940;The Lancet.
- [150] Notter A. Difficultés d’industrialisation de la pénicilline. *Hist Sci Médicales*. 1991;
- [151] Bush K, Bradford PA.  $\beta$ -Lactams and  $\beta$ -Lactamase Inhibitors: An Overview. *Cold Spring Harb Perspect Med*. 2016;6:a025247.
- [152] Pavelka Jr. MS, Mahapatra S, Crick DC. Genetics of Peptidoglycan Biosynthesis. Hatfull GF, Jacobs Jr. WR, editors. *Microbiol Spectr*. 2014;2:2.4.07.
- [153] Lavollay M, Fourgeaud M, Herrmann J-L, et al. The Peptidoglycan of *Mycobacterium abscessus* Is Predominantly Cross-Linked by L, D -Transpeptidases. *J Bacteriol*. 2011;193:778–782.
- [154] Story-Roller E, Maggioncalda EC, Cohen KA, et al. *Mycobacterium abscessus* and  $\beta$ -Lactams: Emerging Insights and Potential Opportunities. *Front Microbiol*. 2018;9:2273.
- [155] Lavollay M, Dubée V, Heym B, et al. In vitro activity of cefoxitin and imipenem against *Mycobacterium abscessus* complex. *Clin Microbiol Infect*. 2014;20:O297–O300.
- [156] Lefebvre A-L, Dubée V, Cortes M, et al. Bactericidal and intracellular activity of  $\beta$ -lactams against *Mycobacterium abscessus*. *J Antimicrob Chemother*. 2016;71:1556–1563.
- [157] Kumar P, Chauhan V, Silva JRA, et al. *Mycobacterium abscessus* L, D -Transpeptidases Are Susceptible to Inactivation by Carbapenems and Cephalosporins but Not Penicillins. *Antimicrob Agents Chemother*. 2017;61:e00866-17.
- [158] Pandey R, Chen L, Manca C, et al. Dual  $\beta$ -Lactam Combinations Highly Active against *Mycobacterium abscessus* Complex *In Vitro*. Darwin KH, editor. *mBio*. 2019;10:e02895-18.
- [159] Story-Roller E, Maggioncalda EC, Lamichhane G. Select  $\beta$ -Lactam Combinations Exhibit Synergy against *Mycobacterium abscessus In Vitro*. *Antimicrob Agents Chemother*. 2019;63:e02613-18.
- [160] Story-Roller E, Galanis C, Lamichhane G.  $\beta$ -Lactam Combinations That Exhibit Synergy against *Mycobacteroides abscessus* Clinical Isolates. *Antimicrob Agents Chemother*. 2021;
- [161] Story-Roller E, Maggioncalda EC, Lamichhane G. Synergistic Efficacy of  $\beta$ -Lactam Combinations against *Mycobacterium abscessus* Pulmonary Infection in Mice. *Antimicrob Agents Chemother*. 2019;63:e00614-19, /aac/63/8/AAC.00614-19.atom.
- [162] Kresge N, Simoni RD, Hill RL. Selman Waksman: the Father of Antibiotics. *J Biol Chem*. 2004;279:e7–e8.

- [163] Schatz A, Bugle E, Waksman SA. Streptomycin, a Substance Exhibiting Antibiotic Activity Against Gram-Positive and Gram-Negative Bacteria.\*. *Exp Biol Med.* 1944;55:66–69.
- [164] Hinshaw C, M. Pyle M, Feldman WH. Streptomycin in Tuberculosis. 1947;
- [165] WHO. WHO consolidated guidelines on tuberculosis, module 4: Treatment Drug-resistant tuberculosis treatment. 2022.
- [166] Umezawa H, Ueda M, Maeda K, et al. Production and isolation of a new antibiotic, Kanamycin. *J Antibiot (Tokyo).* 1957;
- [167] Kawaguchi H, Naito T, Nakagawa S, et al. BB-K8, A NEW SEMISYNTHETIC AMINOGLYCOSIDE ANTIBIOTIC. *J Antibiot (Tokyo).* 1972;25:695–708.
- [168] Krause KM, Serio AW, Kane TR, et al. Aminoglycosides: An Overview. *Cold Spring Harb Perspect Med.* 2016;6:a027029.
- [169] Serio AW, Keepers T, Andrews L, et al. Aminoglycoside Revival: Review of a Historically Important Class of Antimicrobials Undergoing Rejuvenation. Bush K, editor. *EcoSal Plus.* 2018;8:ecosalplus.ESP-0002-2018.
- [170] Kotra LP, Haddad J, Mobashery S. Aminoglycosides: Perspectives on Mechanisms of Action and Resistance and Strategies to Counter Resistance. *Antimicrob Agents Chemother.* 2000;44:3249–3256.
- [171] Tai PC, Wallace BJ, Davis BD. Streptomycin causes misreading of natural messenger by interacting with ribosomes after initiation. *Proc Natl Acad Sci.* 1978;75:275–279.
- [172] Dudek M, Romanowska J, Witula T, et al. Interactions of amikacin with the RNA model of the ribosomal A-site: Computational, spectroscopic and calorimetric studies. *Biochimie.* 2014;102:188–202.
- [173] Kohanski MA, Dwyer DJ, Collins JJ. How antibiotics kill bacteria: from targets to networks. *Nat Rev Microbiol.* 2010;8:423–435.
- [174] Davis BD. Mechanism of Bactericidal Action of Aminoglycosides. *MICROBIOL REV.* 1987;
- [175] Shen G-H, Wu B-D, Hu S-T, et al. High efficacy of clofazimine and its synergistic effect with amikacin against rapidly growing mycobacteria. *Int J Antimicrob Agents.* 2010;35:400–404.
- [176] Van Ingen J, Totten SE, Helstrom NK, et al. *In Vitro* Synergy between Clofazimine and Amikacin in Treatment of Nontuberculous Mycobacterial Disease. *Antimicrob Agents Chemother.* 2012;56:6324–6327.
- [177] Zhang Z, Lu J, Song Y, et al. *In vitro* activity between linezolid and other antimicrobial agents against *Mycobacterium abscessus* complex. *Diagn Microbiol Infect Dis.* 2018;90:31–34.
- [178] Ferro BE, Meletiadiis J, Wattenberg M, et al. Clofazimine Prevents the Regrowth of *Mycobacterium abscessus* and *Mycobacterium avium* Type Strains Exposed to Amikacin and Clarithromycin. *Antimicrob Agents Chemother.* 2016;60:1097–1105.
- [179] Van N, Degefu YN, Leus PA, et al. Novel Synergies and Isolate Specificities in the Drug Interaction Landscape of *Mycobacterium abscessus*. *Antimicrob Agents Chemother.* 2023;e00090-23.
- [180] Jukes TH. Some Historical Notes on Chlortetracycline. *Clin Infect Dis.* 1985;7:702–707.
- [181] Chopra I, Roberts M. Tetracycline Antibiotics: Mode of Action, Applications, Molecular Biology, and Epidemiology of Bacterial Resistance. *Microbiol Mol Biol Rev.* 2001;65:232–260.
- [182] Tally FT, Ellestad GA, Testa RT. Glycylcyclines: a new generation of tetracyclines. *J Antimicrob Chemother.* 1995;35:449–452.
- [183] Ferro BE, Srivastava S, Deshpande D, et al. Tigecycline Is Highly Efficacious against *Mycobacterium abscessus* Pulmonary Disease. *Antimicrob Agents Chemother.* 2016;60:2895–2900.
- [184] Rudra P, Hurst-Hess K, Lappierre P, et al. High Levels of Intrinsic Tetracycline Resistance in *Mycobacterium abscessus* Are Conferred by a Tetracycline-Modifying Monooxygenase. *Antimicrob Agents Chemother.* 2018;62:e00119-18, /aac/62/6/e00119-18.atom.
- [185] Jenner L, Starosta AL, Terry DS, et al. Structural basis for potent inhibitory activity of the antibiotic tigecycline during protein synthesis. *Proc Natl Acad Sci.* 2013;110:3812–3816.

- [186] Wallace RJ, Brown-Elliott BA, Crist CJ, et al. Comparison of the *In Vitro* Activity of the Glycylcycline Tigecycline (Formerly GAR-936) with Those of Tetracycline, Minocycline, and Doxycycline against Isolates of Nontuberculous Mycobacteria. *Antimicrob Agents Chemother.* 2002;46:3164–3167.
- [187] Wallace RJ, Dukart G, Brown-Elliott BA, et al. Clinical experience in 52 patients with tigecycline-containing regimens for salvage treatment of *Mycobacterium abscessus* and *Mycobacterium chelonae* infections. *J Antimicrob Chemother.* 2014;69:1945–1953.
- [188] Pearce C, Ruth MM, Pennings LJ, et al. Inhaled tigecycline is effective against *Mycobacterium abscessus in vitro* and *in vivo*. *J Antimicrob Chemother.* 2020;75:1889–1894.
- [189] Schedlbauer A, Kaminishi T, Ochoa-Lizarralde B, et al. Structural Characterization of an Alternative Mode of Tigecycline Binding to the Bacterial Ribosome. *Antimicrob Agents Chemother.* 2015;59:2849–2854.
- [190] Yaghoubi S, Zekiy AO, Krutova M, et al. Tigecycline antibacterial activity, clinical effectiveness, and mechanisms and epidemiology of resistance: narrative review. *Eur J Clin Microbiol Infect Dis.* 2022;41:1003–1022.
- [191] Brown-Elliott BA, Wallace RJ. *In Vitro* Susceptibility Testing of Omadacycline against Nontuberculous Mycobacteria. *Antimicrob Agents Chemother.* 2021;65:e01947-20.
- [192] Kaushik A, Ammerman NC, Martins O, et al. *In Vitro* Activity of New Tetracycline Analogs Omadacycline and Eravacycline against Drug-Resistant Clinical Isolates of *Mycobacterium abscessus*. *Antimicrob Agents Chemother.* 2019;63:e00470-19.
- [193] Li A, He S, Li J, et al. Omadacycline, Eravacycline, and Tigecycline Express Anti-*Mycobacterium abscessus* Activity *In Vitro*. Lamichhane G, editor. *Microbiol Spectr.* 2023;11:e00718-23.
- [194] Chew KL, Octavia S, Yeoh SF, et al. *In Vitro* Synergy Testing of Eravacycline in Combination with Clarithromycin and Rifabutin against *Mycobacterium abscessus* Complex. Kumar A, editor. *Microbiol Spectr.* 2021;9:e00045-21.
- [195] Cheng A, Tsai Y-T, Chang S-Y, et al. *In Vitro* Synergism of Rifabutin with Clarithromycin, Imipenem, and Tigecycline against the *Mycobacterium abscessus* Complex. *Antimicrob Agents Chemother.* 2019;63:e02234-18.
- [196] Pryjma M, Burian J, Thompson CJ. Rifabutin Acts in Synergy and Is Bactericidal with Frontline *Mycobacterium abscessus* Antibiotics Clarithromycin and Tigecycline, Suggesting a Potent Treatment Combination. *Antimicrob Agents Chemother.* 2018;62:e00283-18.
- [197] Leshner GY, Froelich EJ, Gruett MD, et al. 1,8-Naphthyridine Derivatives. A New Class of Chemotherapeutic Agents. *J Med Pharm Chem.* 1962;5:1063–1065.
- [198] Andersson MI. Development of the quinolones. *J Antimicrob Chemother.* 2003;51:1–11.
- [199] Petrella S, Capton E, Raynal B, et al. Overall Structures of *Mycobacterium tuberculosis* DNA Gyrase Reveal the Role of a Corynebacteriales GyrB-Specific Insert in ATPase Activity. *Structure.* 2019;27:579-589.e5.
- [200] Conde MB, Efron A, Loredó C, et al. Moxifloxacin versus ethambutol in the initial treatment of tuberculosis: a double-blind, randomised, controlled phase II trial. *The Lancet.* 2009;373:1183–1189.
- [201] Gillespie SH, Crook AM, McHugh TD, et al. Four-Month Moxifloxacin-Based Regimens for Drug-Sensitive Tuberculosis. *N Engl J Med.* 2014;371:1577–1587.
- [202] Pletz MWR, De Roux A, Roth A, et al. Early Bactericidal Activity of Moxifloxacin in Treatment of Pulmonary Tuberculosis: a Prospective, Randomized Study. *Antimicrob Agents Chemother.* 2004;48:780–782.
- [203] Maitre T, Petitjean G, Chauffour A, et al. Are moxifloxacin and levofloxacin equally effective to treat XDR tuberculosis? *J Antimicrob Chemother.* 2017;72:2326–2333.
- [204] Cho EH, Huh HJ, Song DJ, et al. Drug susceptibility patterns of *Mycobacterium abscessus* and *Mycobacterium massiliense* isolated from respiratory specimens. *Diagn Microbiol Infect Dis.* 2019;93:107–111.
- [205] He G, Wu L, Zheng Q, et al. Antimicrobial susceptibility and minimum inhibitory concentration distribution of common

- clinically relevant non-tuberculous mycobacterial isolates from the respiratory tract. *Ann Med*. 2022;54:2499–2509.
- [206] Caballero AR, Marquart ME, O’Callaghan RJ, et al. Effectiveness of Fluoroquinolones Against *Mycobacterium abscessus* *In Vivo*. *Curr Eye Res*. 2006;31:23–29.
- [207] Pacheco PA, Tam PMK. Oral moxifloxacin and topical amikacin for *Mycobacterium abscessus* keratitis after laser in situ keratomileusis. *J Cataract Refract Surg*. 2010;36:843–846.
- [208] Nie WJ, Xie ZY, Gao S, et al. Efficacy of Moxifloxacin against *Mycobacterium abscessus* in Zebrafish Model *in vivo*. *Biomed Environ Sci BES*. 2020;33:350–358.
- [209] Bush NG, Evans-Roberts K, Maxwell A. DNA Topoisomerases. Lovett ST, editor. *EcoSal Plus*. 2015;6:ecosalplus.ESP-0010-2014.
- [210] Bhatt S, Chatterjee S. Fluoroquinolone antibiotics: Occurrence, mode of action, resistance, environmental detection, and remediation – A comprehensive review. *Environ Pollut*. 2022;315:120440.
- [211] Hooper DC. Mechanisms of Action of Antimicrobials: Focus on Fluoroquinolones. *Clin Infect Dis*. 2001;32:S9–S15.
- [212] Choi G-E, Min K-N, Won C-J, et al. Activities of Moxifloxacin in Combination with Macrolides against Clinical Isolates of *Mycobacterium abscessus* and *Mycobacterium massiliense*. *Antimicrob Agents Chemother*. 2012;56:3549–3555.
- [213] Choi WS, Kim MJ, Park DW, et al. Clarithromycin and amikacin vs. clarithromycin and moxifloxacin for the treatment of post-acupuncture cutaneous infections due to *Mycobacterium abscessus*: a prospective observational study. *Clin Microbiol Infect*. 2011;17:1084–1090.
- [214] Foo CS-Y, Pethe K, Lupien A. Oxidative Phosphorylation—an Update on a New, Essential Target Space for Drug Discovery in *Mycobacterium tuberculosis*. *Appl Sci*. 2020;10:2339.
- [215] Yano T, Kassovska-Bratinova S, Teh JS, et al. Reduction of Clofazimine by Mycobacterial Type 2 NADH:Quinone Oxidoreductase. *J Biol Chem*. 2011;286:10276–10287.
- [216] Barry VC, Belton JG, Conalty ML, et al. A New Series of Phenazines (Rimino-Compounds) With High Antituberculosis Activity. *Nature*. 1957;179:1013–1015.
- [217] Yawalkar SJ, Mcdougall AC, Languillon J, et al. Once-Monthly Rifampicin Plus Daily Dapsone in Initial treatment of Lepromatous Leprosy. *The Lancet*. 1982;319:1199–1202.
- [218] Mirnejad R, Asadi A, Khoshnood S, et al. Clofazimine: A useful antibiotic for drug-resistant tuberculosis. *Biomed Pharmacother*. 2018;105:1353–1359.
- [219] Van Deun A, Maug AKJ, Salim MAH, et al. Short, Highly Effective, and Inexpensive Standardized Treatment of Multidrug-resistant Tuberculosis. *Am J Respir Crit Care Med*. 2010;182:684–692.
- [220] Schulthess B, Akdoğan Kittana FN, Hömke R, et al. *In Vitro* Bedaquiline and Clofazimine Susceptibility Testing in *Mycobacterium abscessus*. *Antimicrob Agents Chemother*. 2022;66:e02346-21.
- [221] Adler-Shohet FC, Singh J, Nieves D, et al. Safety and Tolerability of Clofazimine in a Cohort of Children With Odontogenic *Mycobacterium abscessus* Infection. *J Pediatr Infect Dis Soc*. 2020;9:483–485.
- [222] Pinapala A, Koh LJ, Ng K-H, et al. Clofazimine in *Mycobacterium abscessus* peritonitis: A pediatric case report. *Perit Dial Int J Int Soc Perit Dial*. 2021;41:104–109.
- [223] Yang B, Jhun BW, Moon SM, et al. Clofazimine-Containing Regimen for the Treatment of *Mycobacterium abscessus* Lung Disease. *Antimicrob Agents Chemother*. 2017;61:e02052-16.
- [224] Fujiwara K, Aono A, Asami T, et al. *In Vitro* Synergistic Effects of Omadacycline with Other Antimicrobial Agents against *Mycobacterium abscessus*. *Antimicrob Agents Chemother*. 2023;67:e01579-22.
- [225] Singh S, Bouzinbi N, Chaturvedi V, et al. In vitro evaluation of a new drug combination against clinical isolates belonging to the *Mycobacterium abscessus* complex. *Clin Microbiol Infect*. 2014;20:O1124–O1127.
- [226] Lechartier B, Cole ST. Mode of Action of Clofazimine and Combination Therapy with Benzothiazinones against



- Mycobacterium tuberculosis*. Antimicrob Agents Chemother. 2015;59:4457–4463.
- [227] Heikal A, Hards K, Cheung C-Y, et al. Activation of type II NADH dehydrogenase by quinolinequinones mediates antitubercular cell death. J Antimicrob Chemother. 2016;71:2840–2847.
- [228] Brickner SJ, Hutchinson DK, Barbachyn MR, et al. Synthesis and Antibacterial Activity of U-100592 and U-100766, Two Oxazolidinone Antibacterial Agents for the Potential Treatment of Multidrug-Resistant Gram-Positive Bacterial Infections. J Med Chem. 1996;39:673–679.
- [229] Leach KL, Brickner SJ, Noe MC, et al. Linezolid, the first oxazolidinone antibacterial agent: Linezolid, antibacterial agent. Ann N Y Acad Sci. 2011;1222:49–54.
- [230] Hashemian SM, Farhadi T, Ganjparvar M. Linezolid: a review of its properties, function, and use in critical care. Drug Des Devel Ther. 2018;Volume 12:1759–1767.
- [231] Poce G, Cocozza M, Consalvi S, et al. SAR analysis of new anti-TB drugs currently in pre-clinical and clinical development. Eur J Med Chem. 2014;86:335–351.
- [232] Ippolito JA, Kanyo ZF, Wang D, et al. Crystal Structure of the Oxazolidinone Antibiotic Linezolid Bound to the 50S Ribosomal Subunit. J Med Chem. 2008;51:3353–3356.
- [233] Tsai K, Stojković V, Lee DJ, et al. Structural basis for context-specific inhibition of translation by oxazolidinone antibiotics. Nat Struct Mol Biol. 2022;29:162–171.
- [234] Wilson DN, Schluenzen F, Harms JM, et al. The oxazolidinone antibiotics perturb the ribosomal peptidyl-transferase center and effect tRNA positioning. 2008;
- [235] Negatu DA, Aragaw WW, Dartois V, et al. Characterization of *In Vitro* Resistance to Linezolid in *Mycobacterium abscessus*. Lamichhane G, editor. Microbiol Spectr. 2023;e02199-23.
- [236] Alcalá L, Ruiz-Serrano MJ, Pérez-Fernández Turégano C, et al. In Vitro Activities of Linezolid against Clinical Isolates of *Mycobacterium tuberculosis* That Are Susceptible or Resistant to First-Line Antituberculous Drugs. Antimicrob Agents Chemother. 2003;47:416–417.
- [237] Tato M, De La Pedrosa EG-G, Cantón R, et al. In vitro activity of linezolid against *Mycobacterium tuberculosis* complex, including multidrug-resistant *Mycobacterium bovis* isolates. Int J Antimicrob Agents. 2006;28:75–78.
- [238] Lee M, Lee J, Carroll MW, et al. Linezolid for Treatment of Chronic Extensively Drug-Resistant Tuberculosis. N Engl J Med. 2012;367:1508–1518.
- [239] Baker AW, Maziarz EK, Lewis SS, et al. Invasive *Mycobacterium abscessus* Complex Infection After Cardiac Surgery: Epidemiology, Management, and Clinical Outcomes. Clin Infect Dis. 2021;72:1232–1240.
- [240] Chen J, Zhao L, Mao Y, et al. Clinical Efficacy and Adverse Effects of Antibiotics Used to Treat *Mycobacterium abscessus* Pulmonary Disease. Front Microbiol. 2019;10:1977.
- [241] Cremades R, Santos A, Rodríguez JC, et al. *Mycobacterium abscessus* from respiratory isolates: activities of drug combinations. J Infect Chemother. 2009;15:46–48.
- [242] Schaadt R, Sweeney D, Shinabarger D, et al. In Vitro Activity of TR-700, the Active Ingredient of the Antibacterial Prodrug TR-701, a Novel Oxazolidinone Antibacterial Agent. Antimicrob Agents Chemother. 2009;53:3236–3239.
- [243] Shaw KJ, Poppe S, Schaadt R, et al. *In Vitro* Activity of TR-700, the Antibacterial Moiety of the Prodrug TR-701, against Linezolid-Resistant Strains. Antimicrob Agents Chemother. 2008;52:4442–4447.
- [244] Vera-Cabrera L, Gonzalez E, Rendon A, et al. *In Vitro* Activities of DA-7157 and DA-7218 against *Mycobacterium tuberculosis* and *Nocardia brasiliensis*. Antimicrob Agents Chemother. 2006;50:3170–3172.
- [245] Compain F, Soroka D, Heym B, et al. In vitro activity of tedizolid against the *Mycobacterium abscessus* complex. Diagn Microbiol Infect Dis. 2018;90:186–189.
- [246] Wen S, Gao X, Zhao W, et al. Comparison of the in vitro activity of linezolid, tedizolid, sutezolid, and delpazolid against

- rapidly growing mycobacteria isolated in Beijing, China. *Int J Infect Dis*. 2021;109:253–260.
- [247] Tang YW, Cheng B, Yeoh SF, et al. Tedizolid Activity Against Clinical *Mycobacterium abscessus* Complex Isolates—An *in vitro* Characterization Study. *Front Microbiol*. 2018;9:2095.
- [248] Le Run E, Arthur M, Mainardi J-L. *In Vitro* and Intracellular Activity of Imipenem Combined with Tedizolid, Rifabutin, and Avibactam against *Mycobacterium abscessus*. *Antimicrob Agents Chemother*. 2019;63:e01915-18, /aac/63/4/AAC.01915-18.atom.
- [249] Ruth MM, Koeken VACM, Pennings LJ, et al. Is there a role for tedizolid in the treatment of non-tuberculous mycobacterial disease? *J Antimicrob Chemother*. 2020;75:609–617.
- [250] Protopopova M, Bogatcheva E, Nikonenko B, et al. In Search of New Cures for Tuberculosis. *Med Chem*. 2007;3:301–316.
- [251] Andries K, Verhasselt P, Guillemont J, et al. A Diarylquinoline Drug Active on the ATP Synthase of *Mycobacterium tuberculosis*. *Science*. 2005;307:223–227.
- [252] Cohen J. New TB Drug Promises Shorter, Simpler Treatment. *Science*. 2004;306:1872–1872.
- [253] De Jonge MR, Koymans LHM, Guillemont JEG, et al. A computational model of the inhibition of *Mycobacterium tuberculosis* ATPase by a new drug candidate R207910. *Proteins Struct Funct Bioinforma*. 2007;67:971–980.
- [254] Mahajan R. Bedaquiline: First FDA-approved tuberculosis drug in 40 years. *Int J Appl Basic Med Res*. 2013;3:1.
- [255] Brown-Elliott BA, Wallace RJ. *In Vitro* Susceptibility Testing of Bedaquiline against *Mycobacterium abscessus* Complex. *Antimicrob Agents Chemother*. 2019;63:e01919-18.
- [256] Low JL, Wu M-L, Aziz DB, et al. Screening of TB Actives for Activity against Nontuberculous Mycobacteria Delivers High Hit Rates. *Front Microbiol*. 2017;8:1539.
- [257] Viljoen A, Raynaud C, Johansen MD, et al. Verapamil Improves the Activity of Bedaquiline against *Mycobacterium abscessus* *In Vitro* and in Macrophages. *Antimicrob Agents Chemother*. 2019;63:e00705-19.
- [258] Dupont C, Viljoen A, Thomas S, et al. Bedaquiline Inhibits the ATP Synthase in *Mycobacterium abscessus* and Is Effective in Infected Zebrafish. *Antimicrob Agents Chemother*. 2017;61:e01225-17, e01225-17.
- [259] Chan WY-K, Ho P-L, To KK-W, et al. A child with acute myeloid leukemia complicated by calcaneal osteomyelitis due to *Mycobacterium abscessus* infection after induction chemotherapy successfully salvaged with bedaquiline and clofazimine. *Int J Infect Dis*. 2021;103:9–12.
- [260] Lee J, Ammerman N, Agarwal A, et al. Differential *In Vitro* Activities of Individual Drugs and Bedaquiline-Rifabutin Combinations against Actively Multiplying and Nutrient-Starved *Mycobacterium abscessus*. *Antimicrob Agents Chemother*. 2021;65:e02179-20.
- [261] Gao T, Yao C, Shang Y, et al. Antimicrobial Effect of Oxazolidinones and Its Synergistic Effect with Bedaquiline Against *Mycobacterium abscessus* Complex. *Infect Drug Resist*. 2023;Volume 16:279–287.
- [262] Ruth MM, Sangen JJN, Remmers K, et al. A bedaquiline/clofazimine combination regimen might add activity to the treatment of clinically relevant non-tuberculous mycobacteria. *J Antimicrob Chemother*. 2019;74:935–943.
- [263] Le Moigne V, Raynaud C, Moreau F, et al. Efficacy of Bedaquiline, Alone or in Combination with Imipenem, against *Mycobacterium abscessus* in C3HeB/FeJ Mice. *Antimicrob Agents Chemother*. 2020;64:e00114-20.
- [264] Lindman M, Dick T. Bedaquiline Eliminates Bactericidal Activity of  $\beta$ -Lactams against *Mycobacterium abscessus*. *Antimicrob Agents Chemother*. 2019;63:e00827-19.
- [265] Meir M, Barkan D. Alternative and Experimental Therapies of *Mycobacterium abscessus* Infections. *Int J Mol Sci*. 2020;21:6793.
- [266] Aziz DB, Low JL, Wu M-L, et al. Rifabutin Is Active against *Mycobacterium abscessus* Complex. *Antimicrob Agents Chemother*. 2017;61:e00155-17.



- [267] Chen J, Zhang H, Guo Q, et al. In vitro activity of rifabutin against *Mycobacterium abscessus*, clinical isolates. *Clin Exp Pharmacol Physiol*. 2022;49:767–775.
- [268] Dick T, Shin SJ, Koh W-J, et al. Rifabutin Is Active against *Mycobacterium abscessus* in Mice. *Antimicrob Agents Chemother*. 2020;64:e01943-19.
- [269] Ganapathy US, Dartois V, Dick T. Repositioning rifamycins for *Mycobacterium abscessus* lung disease. *Expert Opin Drug Discov*. 2019;14:867–878.
- [270] Lan T, Ganapathy US, Sharma S, et al. Redesign of Rifamycin Antibiotics to Overcome ADP-Ribosylation-Mediated Resistance. *Angew Chem Int Ed [Internet]*. 2022 [cited 2023 Jul 20];61. Available from: <https://onlinelibrary.wiley.com/doi/10.1002/anie.202211498>.
- [271] Paulowski L, Beckham KSH, Johansen MD, et al. C25-modified rifamycin derivatives with improved activity against *Mycobacterium abscessus*. Nelson KE, editor. *PNAS Nexus*. 2022;1:pgac130.
- [272] Viljoen A, Dubois V, Girard-Misguich F, et al. The diverse family of MmpL transporters in mycobacteria: from regulation to antimicrobial developments: MmpL structure and diversity in mycobacteria. *Mol Microbiol*. 2017;104:889–904.
- [273] Xu Z, Meshcheryakov VA, Poce G, et al. MmpL3 is the flippase for mycolic acids in mycobacteria. *Proc Natl Acad Sci*. 2017;114:7993–7998.
- [274] Degiacomi G, Benjak A, Madacki J, et al. Essentiality of mmpL3 and impact of its silencing on *Mycobacterium tuberculosis* gene expression. *Sci Rep*. 2017;7:43495.
- [275] Grzegorzewicz AE, Pham H, Gundi VAKB, et al. Inhibition of mycolic acid transport across the *Mycobacterium tuberculosis* plasma membrane. *Nat Chem Biol*. 2012;8:334–341.
- [276] Li W, Yazidi A, Pandya AN, et al. MmpL3 as a Target for the Treatment of Drug-Resistant Nontuberculous Mycobacterial Infections. *Front Microbiol*. 2018;9:1547.
- [277] Ballell L, Bates RH, Young RJ, et al. Fueling Open-Source Drug Discovery: 177 Small-Molecule Leads against Tuberculosis. *ChemMedChem*. 2013;8:313–321.
- [278] Dupont C, Viljoen A, Dubar F, et al. A new piperidinol derivative targeting mycolic acid transport in *Mycobacterium abscessus*: Inhibiting mycolic acid transport in *M. abscessus*. *Mol Microbiol*. 2016;101:515–529.
- [279] Franz ND, Belardinelli JM, Kaminski MA, et al. Design, synthesis and evaluation of indole-2-carboxamides with pan anti-mycobacterial activity. *Bioorg Med Chem*. 2017;25:3746–3755.
- [280] Kozikowski AP, Onajole OK, Stec J, et al. Targeting Mycolic Acid Transport by Indole-2-carboxamides for the Treatment of *Mycobacterium abscessus* Infections. *J Med Chem*. 2017;60:5876–5888.
- [281] Raynaud C, Daher W, Johansen MD, et al. Active Benzimidazole Derivatives Targeting the MmpL3 Transporter in *Mycobacterium abscessus*. *ACS Infect Dis*. 2020;6:324–337.
- [282] De Groote MA, Jarvis TC, Wong C, et al. Optimization and Lead Selection of Benzothiazole Amide Analogs Toward a Novel Antimycobacterial Agent. *Front Microbiol*. 2018;9:2231.
- [283] Ochsner UA, De Groote MA, Jarvis TC, et al. Microbiological profile, preclinical pharmacokinetics and efficacy of CRS0393, a novel antimycobacterial agent targeting MmpL3. *Tuberculosis*. 2023;138:102288.
- [284] Hatfull GF. Phage Therapy for Nontuberculous Mycobacteria: Challenges and Opportunities. *Pulm Ther*. 2023;9:91–107.
- [285] d'Hérelle F. An invisible microbe that is antagonistic to the dysentery bacillus. *Comptes Rendus L'Academie Sci*. 1917;
- [286] Twort FW. An investigation on the nature of ultra-microscopic viruses. *The Lancet*. 1915;186:1241–1243.
- [287] Campbell A. The future of bacteriophage biology. *Nat Rev Genet*. 2003;4:471–477.
- [288] Hatfull GF, Dedrick RM, Schooley RT. Phage Therapy for Antibiotic-Resistant Bacterial Infections. *Annu Rev Med*. 2022;73:197–211.
- [289] Dufour N, Debarbieux L. La phagothérapie: Une arme crédible face à l'antibiorésistance. *médecine/sciences*.

- 2017;33:410–416.
- [290] Parfitt T. Georgia: an unlikely stronghold for bacteriophage therapy. *The Lancet*. 2005;365:2166–2167.
- [291] Dedrick RM, Guerrero-Bustamante CA, Garlena RA, et al. Engineered bacteriophages for treatment of a patient with a disseminated drug-resistant *Mycobacterium abscessus*. *Nat Med*. 2019;25:730–733.
- [292] Dedrick RM, Smith BE, Cristinziano M, et al. Phage Therapy of *Mycobacterium* Infections: Compassionate Use of Phages in 20 Patients With Drug-Resistant Mycobacterial Disease. *Clin Infect Dis*. 2023;76:103–112.
- [293] Dedrick RM, Freeman KG, Nguyen JA, et al. Potent antibody-mediated neutralization limits bacteriophage treatment of a pulmonary *Mycobacterium abscessus* infection. *Nat Med*. 2021;27:1357–1361.
- [294] Dedrick RM, Freeman KG, Nguyen JA, et al. Nebulized Bacteriophage in a Patient With Refractory *Mycobacterium abscessus* Lung Disease. *Open Forum Infect Dis*. 2022;9:ofac194.
- [295] Skurnik M. Can Bacteriophages Replace Antibiotics? *Antibiotics*. 2022;11:575.
- [296] Banerjee A, Dubnau E, Quemard A, et al. inhA, a Gene Encoding a Target for Isoniazid and Ethionamide in *Mycobacterium tuberculosis*. *Sci New Ser*. 1994;263:227–230.
- [297] Vilchèze C, Jacobs, Jr. WR. The Mechanism of Isoniazid Killing: Clarity Through the Scope of Genetics. *Annu Rev Microbiol*. 2007;61:35–50.
- [298] Gagliardi A, Selchow P, Luthra S, et al. KatG as Counterselection Marker for Nontuberculous Mycobacteria. *Antimicrob Agents Chemother*. 2020;64:e02508-19.
- [299] Telenti A, Philipp WJ, Sreevatsan S, et al. The emb operon, a gene cluster of *Mycobacterium tuberculosis* involved in resistance to ethambutol. *Nat Med*. 1997;3:567–570.
- [300] Xiang X, Gong Z, Deng W, et al. Mycobacterial ethambutol responsive genes and implications in antibiotics resistance. *J Drug Target*. 2021;29:284–293.
- [301] Zhang N, Torrelles JB, McNeil MR, et al. The Emb proteins of mycobacteria direct arabinosylation of lipoarabinomannan and arabinogalactan via an N-terminal recognition region and a C-terminal synthetic region: Two functional domains in Emb proteins. *Mol Microbiol*. 2003;50:69–76.
- [302] Alcaide F, Pfyffer GE, Telenti A. Role of embB in natural and acquired resistance to ethambutol in mycobacteria. *Antimicrob Agents Chemother*. 1997;41:2270–2273.
- [303] Guillemin I, Jarlier V, Cambau E. Correlation between Quinolone Susceptibility Patterns and Sequences in the A and B Subunits of DNA Gyrase in Mycobacteria. *Antimicrob Agents Chemother*. 1998;42:2084–2088.
- [304] Matrat S, Aubry A, Mayer C, et al. Mutagenesis in the  $\alpha 3\alpha 4$  GyrA Helix and in the Toprim Domain of GyrB Refines the Contribution of *Mycobacterium tuberculosis* DNA Gyrase to Intrinsic Resistance to Quinolones. *Antimicrob Agents Chemother*. 2008;52:2909–2914.
- [305] Mwangi Z, Naeku G, Mureithi M, et al. Mutation patterns of resistance genes for macrolides, aminoglycosides, and rifampicin in non-tuberculous mycobacteria isolates from Kenya. 2023;
- [306] Wallace RJ, Meier A, Brown BA, et al. Genetic Basis for Clarithromycin Resistance among Isolates of *Mycobacterium chelonae* and *Mycobacterium abscessus*. *Antimicrob Agents Chemother*. 1996;40:6.
- [307] Bastian S, Veziris N, Roux A-L, et al. Assessment of Clarithromycin Susceptibility in Strains Belonging to the *Mycobacterium abscessus* Group by *erm* (41) and *rrl* Sequencing. *Antimicrob Agents Chemother*. 2011;55:775–781.
- [308] Kim H-Y, Kim BJ, Kook Y, et al. *Mycobacterium massiliense* is differentiated from *Mycobacterium abscessus* and *Mycobacterium bolletii* by erythromycin ribosome methyltransferase gene (*erm*) and clarithromycin susceptibility patterns: Characteristic *erm*(41) of *M. massiliense*. *Microbiol Immunol*. 2010;54:347–353.
- [309] Zhai L, Yang K-W, Liu C-C, et al. Thermokinetic characterization of imipenem hydrolysis with metallo- $\beta$ -lactamase CcrA from *Bacteroides fragilis*. *Thermochim Acta*. 2012;539:67–70.

- [310] Prammananan T, Sander P, Brown BA, et al. A Single 16S Ribosomal RNA Substitution Is Responsible for Resistance to Amikacin and Other 2-Deoxystreptamine Aminoglycosides in *Mycobacterium abscessus* and *Mycobacterium chelonae*. *J Infect Dis*. 1998;177:1573–1581.
- [311] Wu M, Li B, Guo Q, et al. Detection and molecular characterisation of amikacin-resistant *Mycobacterium abscessus* isolated from patients with pulmonary disease. *J Glob Antimicrob Resist*. 2019;19:188–191.
- [312] Kim S-Y, Kim DH, Moon SM, et al. Association between 16S rRNA gene mutations and susceptibility to amikacin in *Mycobacterium avium* Complex and *Mycobacterium abscessus* clinical isolates. *Sci Rep*. 2021;11:6108.
- [313] Zhang Z, Wang W, Wang Y, et al. Inducible Resistance to Amikacin in *Mycobacterium abscessus* Isolated in Beijing, China. *Infect Drug Resist*. 2022;Volume 15:2287–2291.
- [314] Soroka D, Dubee V, Soulier-Escrihuela O, et al. Characterization of broad-spectrum *Mycobacterium abscessus* class A - lactamase. *J Antimicrob Chemother*. 2014;69:691–696.
- [315] Matagne A, Lamotte-Brasseur J, Dive G, et al. Interactions between active-site-serine  $\beta$ -lactamases and compounds bearing a methoxy side chain on the  $\alpha$ -face of the  $\beta$ -lactam ring: kinetic and molecular modelling studies. *Biochem J*. 1993;293:607–611.
- [316] Ung KL, Alsarraf HMAB, Olieric V, et al. Crystal structure of the aminoglycosides *N*-acetyltransferase Eis2 from *Mycobacterium abscessus*. *FEBS J*. 2019;286:4342–4355.
- [317] Dubée V, Bernut A, Cortes M, et al.  $\beta$ -Lactamase inhibition by avibactam in *Mycobacterium abscessus*. *J Antimicrob Chemother*. 2015;70:1051–1058.
- [318] Negatu DA, González Del Río R, Cacho-Izquierdo M, et al. Activity of Oral Tebipenem-Avibactam in a Mouse Model of *Mycobacterium abscessus* Lung Infection. *Antimicrob Agents Chemother*. 2023;67:e01459-22.
- [319] Harrison J, Weaver JA, Desai M, et al. *In vitro* efficacy of relebactam versus avibactam against *Mycobacterium abscessus* complex. *Cell Surf*. 2021;7:100064.
- [320] Le Run E, Atze H, Arthur M, et al. Impact of relebactam-mediated inhibition of *Mycobacterium abscessus* BlaMab  $\beta$ -lactamase on the *in vitro* and intracellular efficacy of imipenem. *J Antimicrob Chemother*. 2019;dkz433.
- [321] Kaushik A, Ammerman NC, Lee J, et al. *In Vitro* Activity of the New  $\beta$ -Lactamase Inhibitors Relebactam and Vaborbactam in Combination with  $\beta$ -Lactams against *Mycobacterium abscessus* Complex Clinical Isolates. *Antimicrob Agents Chemother*. 2019;63:e02623-18.
- [322] Kaushik A, Ammerman NC, Parrish NM, et al. New  $\beta$ -Lactamase Inhibitors Nacubactam and Zidebactam Improve the *In Vitro* Activity of  $\beta$ -Lactam Antibiotics against *Mycobacterium abscessus* Complex Clinical Isolates. *Antimicrob Agents Chemother*. 2019;63.
- [323] Maurer FP, Bruderer VL, Castelberg C, et al. Aminoglycoside-modifying enzymes determine the innate susceptibility to aminoglycoside antibiotics in rapidly growing mycobacteria. *J Antimicrob Chemother*. 2015;70:1412–1419.
- [324] Rominski A, Selchow P, Becker K, et al. Elucidation of *Mycobacterium abscessus* aminoglycoside and capreomycin resistance by targeted deletion of three putative resistance genes. *J Antimicrob Chemother*. 2017;72:2191–2200.
- [325] Ripoll F, Pasek S, Schenowitz C, et al. Non-Mycobacterial Virulence Genes in the Genome of the Emerging Pathogen *Mycobacterium abscessus*. Ahmed N, editor. *PLoS ONE*. 2009;4:e5660.
- [326] Dal Molin M, Gut M, Rominski A, et al. Molecular Mechanisms of Intrinsic Streptomycin Resistance in *Mycobacterium abscessus*. *Antimicrob Agents Chemother*. 2017;62:e01427-17.
- [327] Ramón-García S, Otal I, Martín C, et al. Novel Streptomycin Resistance Gene from *Mycobacterium fortuitum*. *Antimicrob Agents Chemother*. 2006;50:3920–3922.
- [328] Strnad L, Winthrop K. Treatment of *Mycobacterium abscessus* Complex. *Semin Respir Crit Care Med*. 2018;39:362–376.
- [329] Staudinger T, Redl B, Glasgow BJ. Antibacterial activity of rifamycins for *M. smegmatis* with comparison of oxidation

- and binding to tear lipocalin. *Biochim Biophys Acta BBA - Proteins Proteomics*. 2014;1844:750–758.
- [330] Rominski A, Roditscheff A, Selchow P, et al. Intrinsic rifamycin resistance of *Mycobacterium abscessus* is mediated by ADP-ribosyltransferase MAB\_0591. *J Antimicrob Chemother*. 2017;72:376–384.
- [331] Baysarowich J, Koteva K, Hughes DW, et al. Rifamycin antibiotic resistance by ADP-ribosylation: Structure and diversity of Arr. *Proc Natl Acad Sci*. 2008;105:4886–4891.
- [332] Koteva K, Cox G, Kelso JK, et al. Rox, a Rifamycin Resistance Enzyme with an Unprecedented Mechanism of Action. *Cell Chem Biol*. 2018;25:403-412.e5.
- [333] Schäfle D, Selchow P, Borer B, et al. Rifabutin Is Inactivated by *Mycobacterium abscessus* Arr. *Antimicrob Agents Chemother*. 2021;65:e02215-20.
- [334] Combrink KD, Denton DA, Harran S, et al. New C25 carbamate rifamycin derivatives are resistant to inactivation by ADP-ribosyl transferases. *Bioorg Med Chem Lett*. 2007;17:522–526.
- [335] Combrink KD, Ramos AR, Spring S, et al. Rifamycin derivatives active against pathogenic rapidly-growing mycobacteria. *Bioorg Med Chem Lett*. 2019;29:2112–2115.
- [336] Madsen CT, Jakobsen L, Buriánková K, et al. Methyltransferase Erm(37) Slips on rRNA to Confer Atypical Resistance in *Mycobacterium tuberculosis*. *J Biol Chem*. 2005;280:38942–38947.
- [337] Madsen CT, Jakobsen L, Douthwaite S. *Mycobacterium smegmatis* Erm(38) Is a Reluctant Dimethyltransferase. *Antimicrob Agents Chemother*. 2005;49:3803–3809.
- [338] Weisblum B. Erythromycin resistance by ribosome modification. *Antimicrob Agents Chemother*. 1995;39:577–585.
- [339] Buriánková K, Doucet-Populaire F, Dorson O, et al. Molecular Basis of Intrinsic Macrolide Resistance in the *Mycobacterium tuberculosis* Complex. *Antimicrob Agents Chemother*. 2004;48:143–150.
- [340] Nash KA. Intrinsic Macrolide Resistance in *Mycobacterium smegmatis* Is Conferred by a Novel *erm* Gene, *erm(38)*. *Antimicrob Agents Chemother*. 2003;47:3053–3060.
- [341] Richard M, Gutiérrez AV, Kremer L. Dissecting *erm* (41)-Mediated Macrolide-Inducible Resistance in *Mycobacterium abscessus*. *Antimicrob Agents Chemother*. 2020;64:e01879-19.
- [342] Hurst-Hess K, Rudra P, Ghosh P. *Mycobacterium abscessus* WhiB7 Regulates a Species-Specific Repertoire of Genes To Confer Extreme Antibiotic Resistance. *Antimicrob Agents Chemother*. 2017;61:e01347-17, e01347-17.
- [343] Soliveri JA, Gomez J, Bishai WR, et al. Multiple paralogous genes related to the *Streptomyces coelicolor* developmental regulatory gene *whiB* are present in *Streptomyces* and other actinomycetes. *Microbiology*. 2000;
- [344] Halloum I, Carrère-Kremer S, Blaise M, et al. Deletion of a dehydratase important for intracellular growth and cording renders rough *Mycobacterium abscessus* avirulent. *Proc Natl Acad Sci*. 2016;113:E4228–E4237.
- [345] Halloum I, Viljoen A, Khanna V, et al. Resistance to Thiacetazone Derivatives Active against *Mycobacterium abscessus* Involves Mutations in the MmpL5 Transcriptional Repressor MAB\_4384. *Antimicrob Agents Chemother*. 2017;61:e02509-16, e02509-16.
- [346] Nunn' P, Porter' J, Porter J, et al. Thiacetazone—avoid like poison or use with care? *Trans R Soc Trop Med Hyg*. 1993;
- [347] Watkins WM, Mungai M, Muhia DK, et al. Cutaneous hypersensitivity reactions to thiacetazone, HIV infection and thiacetazone concentrations in plasma. *Br J Clin Pharmacol*. 1996;41:160–162.
- [348] Richard M, Gutiérrez AV, Viljoen AJ, et al. Mechanistic and Structural Insights Into the Unique TetR-Dependent Regulation of a Drug Efflux Pump in *Mycobacterium abscessus*. *Front Microbiol*. 2018;9:649.
- [349] Hartkoorn RC, Uplekar S, Cole ST. Cross-Resistance between Clofazimine and Bedaquiline through Upregulation of MmpL5 in *Mycobacterium tuberculosis*. *Antimicrob Agents Chemother*. 2014;58:2979–2981.
- [350] Richard M, Gutiérrez AV, Viljoen A, et al. Mutations in the MAB\_2299c TetR Regulator Confer Cross-Resistance to Clofazimine and Bedaquiline in *Mycobacterium abscessus*. *Antimicrob Agents Chemother*. 2019;63:e01316-18.

- [351] Gutiérrez AV, Richard M, Roquet-Banères F, et al. The TetR Family Transcription Factor MAB\_2299c Regulates the Expression of Two Distinct MmpS-MmpL Efflux Pumps Involved in Cross-Resistance to Clofazimine and Bedaquiline in *Mycobacterium abscessus*. *Antimicrob Agents Chemother*. 2019;63:e01000-19.
- [352] Ye M, Xu L, Zou Y, et al. Molecular Analysis of Linezolid-Resistant Clinical Isolates of *Mycobacterium abscessus*. *Antimicrob Agents Chemother*. 2018;63:e01842-18.
- [353] Vianna JS, Machado D, Ramis IB, et al. The Contribution of Efflux Pumps in *Mycobacterium abscessus* Complex Resistance to Clarithromycin. *Antibiotics*. 2019;8:153.
- [354] Guo Q, Chen J, Zhang S, et al. Efflux Pumps Contribute to Intrinsic Clarithromycin Resistance in Clinical, *Mycobacterium abscessus* Isolates. *Infect Drug Resist*. 2020;Volume 13:447–454.
- [355] Rindi L. Efflux Pump Inhibitors against Nontuberculous Mycobacteria. *Int J Mol Sci*. 2020;21:4191.
- [356] Martin A, Bouyakoub Y, Soumillion K, et al. Targeting Bedaquiline Mycobacterial Efflux Pump to Potentially Enhance Therapy in *Mycobacterium abscessus*. *Int J Mycobacteriology*. 2020;9.
- [357] Vianna JS, Ramis IB, Bierhals D, et al. Tetrahydropyridine derivative as efflux inhibitor in *Mycobacterium abscessus*. *J Glob Antimicrob Resist*. 2019;17:296–299.
- [358] Ramis IB, Vianna JS, Silva Junior L, et al. In silico and in vitro evaluation of tetrahydropyridine compounds as efflux inhibitors in *Mycobacterium abscessus*. *Tuberculosis*. 2019;118:101853.
- [359] Mudde SE, Schildkraut JA, Ammerman NC, et al. Unraveling antibiotic resistance mechanisms in *Mycobacterium abscessus*: the potential role of efflux pumps. *J Glob Antimicrob Resist*. 2022;31:345–352.
- [360] Gram C. The differential staining of Schizomycetes in tissue sections and in dried preparations (Ueber die isolirte Firbung der Schizomyceten iu Schnitt-und Trockenpreparaten). *Fortschritte Med*. 1884;2:185–189.
- [361] Moyes RB, Reynolds J, Breakwell DP. Differential Staining of Bacteria: Gram Stain. *Curr Protoc Microbiol* [Internet]. 2009 [cited 2023 Jul 28];15. Available from: <https://onlinelibrary.wiley.com/doi/10.1002/9780471729259.mca03cs15>.
- [362] Coico R. Gram Staining. *Curr Protoc Microbiol* [Internet]. 2006 [cited 2023 Jul 28];00. Available from: <https://onlinelibrary.wiley.com/doi/10.1002/9780471729259.mca03cs00>.
- [363] Rohde M. The Gram-Positive Bacterial Cell Wall. Fischetti VA, Novick RP, Ferretti JJ, et al., editors. *Microbiol Spectr*. 2019;7:7.3.10.
- [364] Silhavy TJ, Kahne D, Walker S. The Bacterial Cell Envelope. *Cold Spring Harb Perspect Biol*. 2010;2:a000414–a000414.
- [365] Vollmer W, Blanot D, De Pedro MA. Peptidoglycan structure and architecture. *FEMS Microbiol Rev*. 2008;32:149–167.
- [366] Park BS, Lee J-O. Recognition of lipopolysaccharide pattern by TLR4 complexes. *Exp Mol Med*. 2013;45:e66–e66.
- [367] Wang X, Quinn PJ. Lipopolysaccharide: Biosynthetic pathway and structure modification. *Prog Lipid Res*. 2010;49:97–107.
- [368] Jackson M. The Mycobacterial Cell Envelope--Lipids. *Cold Spring Harb Perspect Med*. 2014;4:a021105–a021105.
- [369] Daffé M, Draper P. The Envelope Layers of Mycobacteria with Reference to their Pathogenicity. *Adv Microb Physiol* [Internet]. Elsevier; 1997 [cited 2019 Nov 11]. p. 131–203. Available from: <https://linkinghub.elsevier.com/retrieve/pii/S0065291108600168>.
- [370] Bansal-Mutalik R, Nikaido H. Mycobacterial outer membrane is a lipid bilayer and the inner membrane is unusually rich in diacyl phosphatidylinositol dimannosides. *Proc Natl Acad Sci*. 2014;111:4958–4963.
- [371] Daffé M, Marrakchi H. Unraveling the Structure of the Mycobacterial Envelope. Fischetti VA, Novick RP, Ferretti JJ, et al., editors. *Microbiol Spectr*. 2019;7:7.4.1.
- [372] Guerin ME, Korduláková J, Alzari PM, et al. Molecular Basis of Phosphatidyl-myo-inositol Mannoside Biosynthesis and Regulation in Mycobacteria. *J Biol Chem*. 2010;285:33577–33583.
- [373] Brennan PJ, Nikaido H. The Envelope of Mycobacteria. *Annu Rev Biochem*. 1995;64:29–63.

- [374] Fukuda T, Matsumura T, Ato M, et al. Critical Roles for Lipomannan and Lipoarabinomannan in Cell Wall Integrity of Mycobacteria and Pathogenesis of Tuberculosis. Bishai W, Klugman KP, editors. *mBio*. 2013;4:e00472-12.
- [375] Morita YS, Sena CBC, Waller RF, et al. PimE Is a Polyprenol-phosphate-mannose-dependent Mannosyltransferase That Transfers the Fifth Mannose of Phosphatidylinositol Mannoside in Mycobacteria. *J Biol Chem*. 2006;281:25143–25155.
- [376] Parish T, Liu J, Nikaido H, et al. A *Mycobacterium smegmatis* mutant with a defective inositol monophosphate phosphatase gene homolog has altered cell envelope permeability. *J Bacteriol*. 1997;179:7827–7833.
- [377] Palčeková Z, Gilleron M, Angala SK, et al. Polysaccharide Succinylation Enhances the Intracellular Survival of *Mycobacterium abscessus*. *ACS Infect Dis*. 2020;6:2235–2248.
- [378] Nguyen PP, Kado T, Prithviraj M, et al. Inositol acylation of phosphatidylinositol mannosides: a rapid mass response to membrane fluidization in mycobacteria. *J Lipid Res*. 2022;63:100262.
- [379] Rivera-Calzada A, Famelis N, Llorca O, et al. Type VII secretion systems: structure, functions and transport models. *Nat Rev Microbiol*. 2021;19:567–584.
- [380] Jankute M, Cox JAG, Harrison J, et al. Assembly of the Mycobacterial Cell Wall. *Annu Rev Microbiol*. 2015;69:405–423.
- [381] Mahapatra S, Scherman H, Brennan PJ, et al. N-Glycolylation of the Nucleotide Precursors of Peptidoglycan Biosynthesis of *Mycobacterium* spp. Is Altered by Drug Treatment. *J Bacteriol*. 2005;187:2341–2347.
- [382] Raymond JB, Mahapatra S, Crick DC, et al. Identification of the namH Gene, Encoding the Hydroxylase Responsible for the N-Glycolylation of the Mycobacterial Peptidoglycan. *J Biol Chem*. 2005;280:326–333.
- [383] Alderwick LJ, Harrison J, Lloyd GS, et al. The Mycobacterial Cell Wall—Peptidoglycan and Arabinogalactan. *Cold Spring Harb Perspect Med*. 2015;5:a021113.
- [384] McNeil M, Daffé M, Brennan PJ. Evidence for the nature of the link between the arabinogalactan and peptidoglycan of mycobacterial cell walls. *J Biol Chem*. 1990;265:18200–18206.
- [385] Daffé M, Brennan PJ, McNeil M. Predominant structural features of the cell wall arabinogalactan of *Mycobacterium tuberculosis* as revealed through characterization of oligoglycosyl alditol fragments by gas chromatography/mass spectrometry and by <sup>1</sup>H and <sup>13</sup>C NMR analyses. *J Biol Chem*. 1990;265:6734–6743.
- [386] Wallners S, Hunter H, Brennan NPJ. Demonstration that the galactosyl and arabinosyl residues in the cell wall of *Mycobacterium leprae* and *Mycobacterium tuberculosis* are furanoid. 1987;
- [387] Marrakchi H, Lanéelle M-A, Daffé M. Mycolic Acids: Structures, Biosynthesis, and Beyond. *Chem Biol*. 2014;21:67–85.
- [388] McNeil M, Daffé M, Brennan PJ. Location of the mycolyl ester substituents in the cell walls of mycobacteria. *J Biol Chem*. 1991;266:13217–13223.
- [389] Burbaud S, Laval F, Lemassu A, et al. Trehalose Polyphosphates Are Produced by a Glycolipid Biosynthetic Pathway Conserved across Phylogenetically Distant Mycobacteria. *Cell Chem Biol*. 2016;23:278–289.
- [390] Parmar S, Tocheva EI. The cell envelope of *Mycobacterium abscessus* and its role in pathogenesis. Dehio C, editor. *PLOS Pathog*. 2023;19:e1011318.
- [391] Chatterjee D, Khoo K-H. The surface glycopeptidolipids of mycobacteria: structures and biological properties. *Cell Mol Life Sci*. 2001;58:2018–2042.
- [392] Pang L, Tian X, Pan W, et al. Structure and function of mycobacterium glycopeptidolipids from comparative genomics perspective. *J Cell Biochem*. 2013;114:1705–1713.
- [393] Mishra AK, Driessen NN, Appelmeik BJ, et al. Lipoarabinomannan and related glycoconjugates: structure, biogenesis and role in *Mycobacterium tuberculosis* physiology and host–pathogen interaction. *FEMS Microbiol Rev*. 2011;35:1126–1157.
- [394] Vergne I, Fratti RA, Hill PJ, et al. *Mycobacterium tuberculosis* Phagosome Maturation Arrest: Mycobacterial Phosphatidylinositol Analog Phosphatidylinositol Mannoside Stimulates Early Endosomal Fusion. *Mol Biol Cell*.



- 2004;15:751–760.
- [395] Daher W, Pichler V, Karam J, et al. The molecular basis and downstream immune consequences of mycobacteria–host cell interactions. *FEMS Microbiol Rev.* 2023;47:fuad009.
- [396] Fatima Z, Canaan S. *Biology of mycobacterial lipids*. S.l.: Academic Press; 2022.
- [397] Stodola FH, Lesuk A, Anderson RJ. The chemistry of the lipids of tubercle bacilli. *J Biol Chem.* 1938;126:505–513.
- [398] Asselineau J, Lederer E. Structure of the Mycolic Acids of Mycobacteria. *Nature.* 1950;782–783.
- [399] Barry CE, Lee RE, Mdluli K, et al. Mycolic acids: structure, biosynthesis and physiological functions. *Prog Lipid Res.* 1998;37:143–179.
- [400] Liu J, Barry CE, Besra GS, et al. Mycolic Acid Structure Determines the Fluidity of the Mycobacterial Cell Wall. *J Biol Chem.* 1996;271:29545–29551.
- [401] Pawełczyk J, Kremer L. The Molecular Genetics of Mycolic Acid Biosynthesis. Hatfull GF, Jacobs Jr. WR, editors. *Microbiol Spectr.* 2014;2:2.4.24.
- [402] George KM, Yuan Y, Sherman DR, et al. The Biosynthesis of Cyclopropanated Mycolic Acids in *Mycobacterium tuberculosis*. *J Biol Chem.* 1995;270:27292–27298.
- [403] Yuan Y, Lee RE, Besra GS, et al. Identification of a gene involved in the biosynthesis of cyclopropanated mycolic acids in *Mycobacterium tuberculosis*. *Proc Natl Acad Sci.* 1995;92:6630–6634.
- [404] Barkan D, Hedhli D, Yan H-G, et al. *Mycobacterium tuberculosis* Lacking All Mycolic Acid Cyclopropanation Is Viable but Highly Attenuated and Hyperinflammatory in Mice. Flynn JL, editor. *Infect Immun.* 2012;80:1958–1968.
- [405] Glickman MS, Cox JS, Jacobs WR. A Novel Mycolic Acid Cyclopropane Synthetase Is Required for Cording, Persistence, and Virulence of *Mycobacterium tuberculosis*. *Mol Cell.* 2000;5:717–727.
- [406] Ishikawa E, Ishikawa T, Morita YS, et al. Direct recognition of the mycobacterial glycolipid, trehalose dimycolate, by C-type lectin Mincle. *J Exp Med.* 2009;206:2879–2888.
- [407] Nguyen TKT, d’Aigle J, China L, et al. Mycobacterial Trehalose 6,6’-Dimycolate–Induced M1-Type Inflammation. *Am J Pathol.* 2020;190:286–294.
- [408] Beckman EM, Porcelli SA, Morita CT, et al. Recognition of a lipid antigen by CD1-restricted ap+ T cells. *Nature.* 1994;372.
- [409] Tahiri N, Fodran P, Jayaraman D, et al. Total Synthesis of a Mycolic Acid from *Mycobacterium tuberculosis*. *Angew Chem Int Ed.* 2020;59:7555–7560.
- [410] Yuan Y, Zhu Y, Crane DD, et al. The effect of oxygenated mycolic acid composition on cell wall function and macrophage growth in *Mycobacterium tuberculosis*. *Mol Microbiol.* 1998;29:1449–1458.
- [411] Dubnau E, Chan J, Raynaud C, et al. Oxygenated mycolic acids are necessary for virulence of *Mycobacterium tuberculosis* in mice: Oxygenated mycolic acids in *M. tuberculosis*. *Mol Microbiol.* 2002;36:630–637.
- [412] Vander Beken S, Al Dulayymi JR, Naessens T, et al. Molecular structure of the *Mycobacterium tuberculosis* virulence factor, mycolic acid, determines the elicited inflammatory pattern. *Eur J Immunol.* 2011;41:450–460.
- [413] Savintseva LA, Steshin IS, Avdoshin AA, et al. Conformational Dynamics and Stability of Bilayers Formed by Mycolic Acids from the *Mycobacterium tuberculosis* Outer Membrane. *Molecules.* 2023;28:1347.
- [414] Villeneuve M, Kawai M, Horiuchi K, et al. Conformational folding of mycobacterial methoxy- and ketomycolic acids facilitated by  $\alpha$ -methyl *trans*-cyclopropane groups rather than *cis*-cyclopropane units. *Microbiology.* 2013;159:2405–2415.
- [415] Di Capua CB, Belardinelli JM, Carignano HA, et al. Unveiling the Biosynthetic Pathway for Short Mycolic Acids in Nontuberculous Mycobacteria: *Mycobacterium smegmatis* MSMEG\_4301 and Its Ortholog *Mycobacterium abscessus* MAB\_1915 Are Essential for the Synthesis of  $\alpha'$ -Mycolic Acids. Lamichhane G, editor. *Microbiol Spectr.* 2022;10:e01288-22.

- [416] Trivedi OA, Arora P, Sridharan V, et al. Enzymic activation and transfer of fatty acids as acyl-adenylates in mycobacteria. *Nature*. 2004;428:441–445.
- [417] Minnikin DE, Minnikin SM, Parlett JH, et al. Mycolic acid patterns of some species of *Mycobacterium*. *Arch Microbiol*. 1984;139–139:225–231.
- [418] Lacave C, Laneelle M-A, Daffe M, et al. Etude structurale et métabolique des acides mycoliques de *Mycobacterium fortuitum*. *Eur J Biochem*. 1987;163:369–378.
- [419] Minnikin DE, Minnikin SM, Hutchinson IG, et al. Mycolic Acid Patterns of Representative Strains of *Mycobacterium fortuitum*, “*Mycobacterium peregrinum*” and *Mycobacterium smegmatis*. *Microbiology*. 1984;130:363–367.
- [420] Cronan JE, Waldrop GL. Multi-subunit acetyl-CoA carboxylases. *Prog Lipid Res*. 2002;41:407–435.
- [421] Diacovich L, Peirú S, Kurth D, et al. Kinetic and Structural Analysis of a New Group of Acyl-CoA Carboxylases Found in *Streptomyces coelicolor* A3(2). *J Biol Chem*. 2002;277:31228–31236.
- [422] Gago G, Kurth D, Diacovich L, et al. Biochemical and Structural Characterization of an Essential Acyl Coenzyme A Carboxylase from *Mycobacterium tuberculosis*. *J Bacteriol*. 2006;188:477–486.
- [423] Oh T-J, Daniel J, Kim H-J, et al. Identification and Characterization of Rv3281 as a Novel Subunit of a Biotin-dependent Acyl-CoA Carboxylase in *Mycobacterium tuberculosis* H37Rv. *J Biol Chem*. 2006;281:3899–3908.
- [424] Rodríguez E, Banchio C, Diacovich L, et al. Role of an Essential Acyl Coenzyme A Carboxylase in the Primary and Secondary Metabolism of *Streptomyces coelicolor* A3(2). *Appl Environ Microbiol*. 2001;67:4166–4176.
- [425] Cole ST, Brosch R, Parkhill J, et al. Deciphering the biology of *Mycobacterium tuberculosis* from the complete genome sequence. *Nature*. 1998;393:537–544.
- [426] Pawelczyk J, Viljoen A, Kremer L, et al. The influence of AccD5 on AccD6 carboxyltransferase essentiality in pathogenic and non-pathogenic *Mycobacterium*. *Sci Rep*. 2017;7:42692.
- [427] Bennett M, Högbom M. Crystal structure of the essential biotin-dependent carboxylase AccA3 from *Mycobacterium tuberculosis*. *FEBS Open Bio*. 2017;7:620–626.
- [428] Daniel J, Oh T-J, Lee C-M, et al. AccD6, a Member of the Fas II Locus, Is a Functional Carboxyltransferase Subunit of the Acyl-Coenzyme A Carboxylase in *Mycobacterium tuberculosis*. *J Bacteriol*. 2007;189:911–917.
- [429] Kurth DG, Gago GM, De La Iglesia A, et al. ACCase 6 is the essential acetyl-CoA carboxylase involved in fatty acid and mycolic acid biosynthesis in mycobacteria. *Microbiology*. 2009;155:2664–2675.
- [430] Pawelczyk J, Brzostek A, Kremer L, et al. AccD6, a Key Carboxyltransferase Essential for Mycolic Acid Synthesis in *Mycobacterium tuberculosis*, Is Dispensable in a Nonpathogenic Strain. *J Bacteriol*. 2011;193:6960–6972.
- [431] Bazet Lyonnet B, Diacovich L, Gago G, et al. Functional reconstitution of the *Mycobacterium tuberculosis* long-chain acyl-CoA carboxylase from multiple acyl-CoA subunits. *FEBS J*. 2017;284:1110–1125.
- [432] Lin T-W, Melgar MM, Kurth D, et al. Structure-based inhibitor design of AccD5, an essential acyl-CoA carboxylase carboxyltransferase domain of *Mycobacterium tuberculosis*. *Proc Natl Acad Sci*. 2006;103:3072–3077.
- [433] Portevin D, De Sousa-D’Auria C, Montrozier H, et al. The Acyl-AMP Ligase FadD32 and AccD4-containing Acyl-CoA Carboxylase Are Required for the Synthesis of Mycolic Acids and Essential for Mycobacterial Growth. *J Biol Chem*. 2005;280:8862–8874.
- [434] Schweizer E, Hofmann J. Microbial Type I Fatty Acid Synthases (FAS): Major Players in a Network of Cellular FAS Systems. *Microbiol Mol Biol Rev*. 2004;68:501–517.
- [435] Smith S, Witkowski A, Joshi AK. Structural and functional organization of the animal fatty acid synthase. *Prog Lipid Res*. 2003;42:289–317.
- [436] Elad N, Baron S, Peleg Y, et al. Structure of Type-I *Mycobacterium tuberculosis* fatty acid synthase at 3.3 Å resolution. *Nat Commun*. 2018;9:3886.



- [437] Zimhony O, Vilchère C, Jacobs WR. Characterization of *Mycobacterium smegmatis* Expressing the *Mycobacterium tuberculosis* Fatty Acid Synthase I ( *fasI* ) Gene. *J Bacteriol.* 2004;186:4051–4055.
- [438] Lamichhane G, Zignol M, Blades NJ, et al. A postgenomic method for predicting essential genes at subsaturation levels of mutagenesis: Application to *Mycobacterium tuberculosis*. *Proc Natl Acad Sci.* 2003;100:7213–7218.
- [439] Fernandes ND, Kolattukudy PE. Cloning, sequencing and characterization of a fatty acid synthase-encoding gene from *Mycobacterium tuberculosis* var. *bovis* BCG. *Gene.* 1996;
- [440] Bloch K. Control Mechanisms for Fatty Acid Synthesis in *Mycobacterium Smegmatis*. In: Meister A, editor. *Adv Enzymol - Relat Areas Mol Biol* [Internet]. Hoboken, NJ, USA: John Wiley & Sons, Inc.; 1977 [cited 2023 Aug 16]. p. 1–84. Available from: <https://onlinelibrary.wiley.com/doi/10.1002/9780470122907.ch1>.
- [441] Kikuchi S, Rainwater DL, Kolattukudy PE. Purification and characterization of an unusually large fatty acid synthase from *Mycobacterium tuberculosis* var. *bovis* BCG. *Arch Biochem Biophys.* 1992;295:318–326.
- [442] Schaeffer ML, Agnihotri G, Kallender H, et al. Expression, purification, and characterization of the *Mycobacterium tuberculosis* acyl carrier protein, AcpM. *Biochim Biophys Acta BBA - Mol Cell Biol Lipids.* 2001;1532:67–78.
- [443] Chan DI, Vogel HJ. Current understanding of fatty acid biosynthesis and the acyl carrier protein. *Biochem J.* 2010;430:1–19.
- [444] Chalut C, Botella L, De Sousa-D'Auria C, et al. The nonredundant roles of two 4'-phosphopantetheinyl transferases in vital processes of *Mycobacteria*. *Proc Natl Acad Sci.* 2006;103:8511–8516.
- [445] Zimhony O, Schwarz A, Raitses-Gurevich M, et al. AcpM, the Meromycolate Extension Acyl Carrier Protein of *Mycobacterium tuberculosis*, Is Activated by the 4'-Phosphopantetheinyl Transferase PptT, a Potential Target of the Multistep Mycolic Acid Biosynthesis. *Biochemistry.* 2015;54:2360–2371.
- [446] Kremer L, Nampoothiri KM, Lesjean S, et al. Biochemical Characterization of Acyl Carrier Protein (AcpM) and Malonyl-CoA:AcpM Transacylase (mtFabD), Two Major Components of *Mycobacterium tuberculosis* Fatty Acid Synthase II. *J Biol Chem.* 2001;276:27967–27974.
- [447] Choi K-H, Kremer L, Besra GS, et al. Identification and Substrate Specificity of  $\beta$ -Ketoacyl (Acyl Carrier Protein) Synthase III (mtFabH) from *Mycobacterium tuberculosis*. *J Biol Chem.* 2000;275:28201–28207.
- [448] Marrakchi H, Ducasse S, Labesse G, et al. MabA (FabG1), a *Mycobacterium tuberculosis* protein involved in the long-chain fatty acid elongation system FAS-II. *Microbiology.* 2002;148:951–960.
- [449] Cohen-Gonsaud M, Ducasse S, Hoh F, et al. Crystal Structure of MabA from *Mycobacterium tuberculosis*, a Reductase involved in Long-chain Fatty Acid Biosynthesis. *J Mol Biol.* 2002;320:249–261.
- [450] Küssau T, Flipo M, Van Wyk N, et al. Structural rearrangements occurring upon cofactor binding in the *Mycobacterium smegmatis*  $\beta$ -ketoacyl-acyl carrier protein reductase MabA. *Acta Crystallogr Sect Struct Biol.* 2018;74:383–393.
- [451] Veyron-Churlet R, Zanella-Cléon I, Cohen-Gonsaud M, et al. Phosphorylation of the *Mycobacterium tuberculosis*  $\beta$ -Ketoacyl-Acyl Carrier Protein Reductase MabA Regulates Mycolic Acid Biosynthesis. *J Biol Chem.* 2010;285:12714–12725.
- [452] Sacco E, Covarrubias AS, O'Hare HM, et al. The missing piece of the type II fatty acid synthase system from *Mycobacterium tuberculosis*. *Proc Natl Acad Sci.* 2007;104:14628–14633.
- [453] Molle V, Kremer L. Division and cell envelope regulation by Ser/Thr phosphorylation: *Mycobacterium* shows the way. *Mol Microbiol.* 2010;75:1064–1077.
- [454] Slama N, Leiba J, Eynard N, et al. Negative regulation by Ser/Thr phosphorylation of HadAB and HadBC dehydratases from *Mycobacterium tuberculosis* type II fatty acid synthase system. *Biochem Biophys Res Commun.* 2011;412:401–406.
- [455] Quemard A, Sacchetti JC, Dessen A, et al. Enzymic Characterization of the Target for Isoniazid in *Mycobacterium*

- tuberculosis*. *Biochemistry*. 1995;34:8235–8241.
- [456] Vögeli B, Rosenthal RG, Stoffel GMM, et al. InhA, the enoyl-thioester reductase from *Mycobacterium tuberculosis* forms a covalent adduct during catalysis. *J Biol Chem*. 2018;293:17200–17207.
- [457] Kremer L, Dover LG, Carrère S, et al. Mycolic acid biosynthesis and enzymic characterization of the  $\beta$ -ketoacyl-ACP synthase A-condensing enzyme from *Mycobacterium tuberculosis*. *Biochem J*. 2002;364:423–430.
- [458] Schaeffer ML, Agnihotri G, Volker C, et al. Purification and Biochemical Characterization of the *Mycobacterium tuberculosis*  $\beta$ -Ketoacyl-acyl Carrier Protein Synthases KasA and KasB. *J Biol Chem*. 2001;276:47029–47037.
- [459] Slayden RA, Barry CE. The role of KasA and KasB in the biosynthesis of meromycolic acids and isoniazid resistance in *Mycobacterium tuberculosis*. *Tuberculosis*. 2002;82:149–160.
- [460] Bhatt A, Fujiwara N, Bhatt K, et al. Deletion of *kasB* in *Mycobacterium tuberculosis* causes loss of acid-fastness and subclinical latent tuberculosis in immunocompetent mice. *Proc Natl Acad Sci*. 2007;104:5157–5162.
- [461] Molle V, Brown AK, Besra GS, et al. The Condensing Activities of the *Mycobacterium tuberculosis* Type II Fatty Acid Synthase Are Differentially Regulated by Phosphorylation. *J Biol Chem*. 2006;281:30094–30103.
- [462] Takayama K, Wang C, Besra GS. Pathway to Synthesis and Processing of Mycolic Acids in *Mycobacterium tuberculosis*. *Clin Microbiol Rev*. 2005;18:81–101.
- [463] Phetsuksiri B, Jackson M, Scherman H, et al. Unique Mechanism of Action of the Thiourea Drug Isoxyl on *Mycobacterium tuberculosis*. *J Biol Chem*. 2003;278:53123–53130.
- [464] Singh A, Varela C, Bhatt K, et al. Identification of a Desaturase Involved in Mycolic Acid Biosynthesis in *Mycobacterium smegmatis*. Kremer L, editor. *PLOS ONE*. 2016;11:e0164253.
- [465] Bailo R, Radhakrishnan A, Singh A, et al. The mycobacterial desaturase DesA2 is associated with mycolic acid biosynthesis. *Sci Rep*. 2022;12:6943.
- [466] Dinadayala P, Laval F, Raynaud C, et al. Tracking the Putative Biosynthetic Precursors of Oxygenated Mycolates of *Mycobacterium tuberculosis*. *J Biol Chem*. 2003;278:7310–7319.
- [467] Behr MA, Schroeder BG, Brinkman JN, et al. A Point Mutation in the *mma3* Gene Is Responsible for Impaired Methoxymycolic Acid Production in *Mycobacterium bovis* BCG Strains Obtained after 1927. *J Bacteriol*. 2000;182:3394–3399.
- [468] Yuan Y, Barry CE. A common mechanism for the biosynthesis of methoxy and cyclopropyl mycolic acids in *Mycobacterium tuberculosis*. *Proc Natl Acad Sci*. 1996;93:12828–12833.
- [469] Quémard A. New Insights into the Mycolate-Containing Compound Biosynthesis and Transport in Mycobacteria. *Trends Microbiol*. 2016;24:725–738.
- [470] Barkan D, Rao V, Sukenick GD, et al. Redundant Function of *cmaA2* and *mmaA2* in *Mycobacterium tuberculosis* *cis* Cyclopropanation of Oxygenated Mycolates. *J Bacteriol*. 2010;192:3661–3668.
- [471] Glickman MS. The *mmaA2* Gene of *Mycobacterium tuberculosis* Encodes the Distal Cyclopropane Synthase of the  $\alpha$ -Mycolic Acid. *J Biol Chem*. 2003;278:7844–7849.
- [472] Glickman MS, Cahill SM, Jacobs WR. The *Mycobacterium tuberculosis* *cmaA2* Gene Encodes a Mycolic Acid trans-Cyclopropane Synthetase. *J Biol Chem*. 2001;276:2228–2233.
- [473] Léger M, Gavalda S, Guillet V, et al. The Dual Function of the *Mycobacterium tuberculosis* FadD32 Required for Mycolic Acid Biosynthesis. *Chem Biol*. 2009;16:510–519.
- [474] Gavalda S, Léger M, Van Der Rest B, et al. The Pks13/FadD32 Crosstalk for the Biosynthesis of Mycolic Acids in *Mycobacterium tuberculosis*. *J Biol Chem*. 2009;284:19255–19264.
- [475] Bon C, Cabantous S, Julien S, et al. Solution structure of the type I polyketide synthase Pks13 from *Mycobacterium tuberculosis*. *BMC Biol*. 2022;20:147.

- [476] Gavalda S, Bardou F, Laval F, et al. The Polyketide Synthase Pks13 Catalyzes a Novel Mechanism of Lipid Transfer in Mycobacteria. *Chem Biol*. 2014;21:1660–1669.
- [477] Javid A, Cooper C, Singh A, et al. The mycolic acid reductase Rv2509 has distinct structural motifs and is essential for growth in slow-growing mycobacteria. *Mol Microbiol*. 2020;113:521–533.
- [478] Lea-Smith DJ, Pyke JS, Tull D, et al. The Reductase That Catalyzes Mycolic Motif Synthesis Is Required for Efficient Attachment of Mycolic Acids to Arabinogalactan. *J Biol Chem*. 2007;282:11000–11008.
- [479] Tang X, Deng W, Xie J. Novel Insights into *Mycobacterium* Antigen Ag85 Biology and Implications in Countermeasures for *M. tuberculosis*. *Crit Rev Eukaryot Gene Expr*. 2012;22:179–187.
- [480] Varela C, Rittmann D, Singh A, et al. *MmpL* Genes Are Associated with Mycolic Acid Metabolism in Mycobacteria and Corynebacteria. *Chem Biol*. 2012;19:498–506.
- [481] Fay A, Czudnochowski N, Rock JM, et al. Two Accessory Proteins Govern MmpL3 Mycolic Acid Transport in Mycobacteria. Darwin KH, editor. *mBio*. 2019;10:e00850-19.
- [482] Ung KL, Alsarraf HMAB, Kremer L, et al. The crystal structure of the mycobacterial trehalose monomycolate transport factor A, TtfA, reveals an atypical fold. *Proteins Struct Funct Bioinforma*. 2020;88:809–815.
- [483] Chollet A, Maveyraud L, Lherbet C, et al. An overview on crystal structures of InhA protein: Apo-form, in complex with its natural ligands and inhibitors. *Eur J Med Chem*. 2018;146:318–343.
- [484] Belisle JT, Vissa VD, Sievert T, et al. Role of the Major Antigen of *Mycobacterium tuberculosis* in Cell Wall Biogenesis. *Science*. 1997;276:1420–1422.
- [485] Puech V, Guilhot C, Perez E, et al. Evidence for a partial redundancy of the fibronectin-binding proteins for the transfer of mycoloyl residues onto the cell wall arabinogalactan termini of *Mycobacterium tuberculosis*: Redundancy of fibronectin-binding proteins in *M. tuberculosis*. *Mol Microbiol*. 2002;44:1109–1122.
- [486] Jackson M, Raynaud C, Laneelle M-A, et al. Inactivation of the antigen 85C gene profoundly affects the mycolate content and alters the permeability of the *Mycobacterium tuberculosis* cell envelope. *Mol Microbiol*. 1999;31:1573–1587.
- [487] Prasad MS, Bhole RP, Khedekar PB, et al. Mycobacterium enoyl acyl carrier protein reductase (InhA): A key target for antitubercular drug discovery. *Bioorganic Chem*. 2021;115:105242.
- [488] Shetye GS, Franzblau SG, Cho S. New tuberculosis drug targets, their inhibitors, and potential therapeutic impact. *Transl Res*. 2020;220:68–97.
- [489] Williams JT, Abramovitch RB. Molecular Mechanisms of MmpL3 Function and Inhibition. *Microb Drug Resist*. 2023;29:190–212.
- [490] Massengo-Tiassé RP, Cronan JE. Diversity in enoyl-acyl carrier protein reductases. *Cell Mol Life Sci*. 2009;66:1507–1517.
- [491] Parikh S, Moynihan DP, Xiao G, et al. Roles of Tyrosine 158 and Lysine 165 in the Catalytic Mechanism of InhA, the Enoyl-ACP Reductase from *Mycobacterium tuberculosis*. *Biochemistry*. 1999;38:13623–13634.
- [492] Bell AF, Stratton CF, Zhang X, et al. Evidence from Raman Spectroscopy That InhA, the Mycobacterial Enoyl Reductase, Modulates the Conformation of the NADH Cofactor to Promote Catalysis. *J Am Chem Soc*. 2007;129:6425–6431.
- [493] Molle V, Gulten G, Vilchère C, et al. Phosphorylation of InhA inhibits mycolic acid biosynthesis and growth of *Mycobacterium tuberculosis*: Mycolic acid biosynthesis regulation in *M. tuberculosis*. *Mol Microbiol*. 2010;78:1591–1605.
- [494] Vilchère C, Morbidoni HR, Weisbrod TR, et al. Inactivation of the *inhA*-Encoded Fatty Acid Synthase II (FASII) Enoyl-Acyl Carrier Protein Reductase Induces Accumulation of the FASI End Products and Cell Lysis of *Mycobacterium smegmatis*. *J Bacteriol*. 2000;182:4059–4067.
- [495] Rawat R, Whitty A, Tonge PJ. The isoniazid-NAD adduct is a slow, tight-binding inhibitor of InhA, the *Mycobacterium tuberculosis* enoyl reductase: Adduct affinity and drug resistance. *Proc Natl Acad Sci*. 2003;100:13881–13886.

- [496] Rozwarski DA, Grant GA, Barton DHR, et al. Modification of the NADH of the Isoniazid Target (InhA) from *Mycobacterium tuberculosis*. 1998;279:5.
- [497] Zhang Y, Heymt B, Young D, et al. The catalase-peroxidase gene and isoniazid resistance of. 1992;358:3.
- [498] Unissa AN, Subbian S, Hanna LE, et al. Overview on mechanisms of isoniazid action and resistance in *Mycobacterium tuberculosis*. Infect Genet Evol. 2016;45:474–492.
- [499] Baulard AR, Betts JC, Engohang-Ndong J, et al. Activation of the Pro-drug Ethionamide Is Regulated in Mycobacteria. J Biol Chem. 2000;275:28326–28331.
- [500] Wang F, Langley R, Gulsten G, et al. Mechanism of thioamide drug action against tuberculosis and leprosy. J Exp Med. 2007;204:73–78.
- [501] Sivaraman S, Sullivan TJ, Johnson F, et al. Inhibition of the Bacterial Enoyl Reductase FabI by Triclosan: A Structure–Reactivity Analysis of FabI Inhibition by Triclosan Analogues. J Med Chem. 2004;47:509–518.
- [502] McMurry LM, McDermott PF, Levy SB. Genetic Evidence that InhA of *Mycobacterium smegmatis* Is a Target for Triclosan. Antimicrob Agents Chemother. 1999;43:711–713.
- [503] Parikh SL, Xiao G, Tonge PJ. Inhibition of InhA, the Enoyl Reductase from *Mycobacterium tuberculosis*, by Triclosan and Isoniazid. Biochemistry. 2000;39:7645–7650.
- [504] Vosátka R, Krátký M, Vinšová J. Triclosan and its derivatives as antimycobacterial active agents. Eur J Pharm Sci. 2018;114:318–331.
- [505] am Ende CW, Knudson SE, Liu N, et al. Synthesis and in vitro antimycobacterial activity of B-ring modified diaryl ether InhA inhibitors. Bioorg Med Chem Lett. 2008;18:3029–3033.
- [506] Pan P, J. Tonge P. Targeting InhA, the FASII Enoyl-ACP Reductase: SAR Studies on Novel Inhibitor Scaffolds. Curr Top Med Chem. 2012;12:672–693.
- [507] Stec J, Vilchère C, Lun S, et al. Biological Evaluation of Potent Triclosan-Derived Inhibitors of the Enoyl-Acyl Carrier Protein Reductase InhA in Drug-Sensitive and Drug-Resistant Strains of *Mycobacterium tuberculosis*. ChemMedChem. 2014;9:2528–2537.
- [508] Hartkoorn RC, Sala C, Neres J, et al. Towards a new tuberculosis drug: pyridomycin – nature’s isoniazid. EMBO Mol Med. 2012;4:1032–1042.
- [509] Hartkoorn RC, Pojer F, Read JA, et al. Pyridomycin bridges the NADH- and substrate-binding pockets of the enoyl reductase InhA. Nat Chem Biol. 2014;10:96–98.
- [510] He X, Alian A, Stroud R, et al. Pyrrolidine Carboxamides as a Novel Class of Inhibitors of Enoyl Acyl Carrier Protein Reductase from *Mycobacterium tuberculosis*. J Med Chem. 2006;49:6308–6323.
- [511] Joshi SD, Dixit SR, Kirankumar MN, et al. Synthesis, antimycobacterial screening and ligand-based molecular docking studies on novel pyrrole derivatives bearing pyrazoline, isoxazole and phenyl thiourea moieties. Eur J Med Chem. 2016;107:133–152.
- [512] More UA, Joshi SD, Aminabhavi TM, et al. Design, synthesis, molecular docking and 3D-QSAR studies of potent inhibitors of enoyl-acyl carrier protein reductase as potential antimycobacterial agents. Eur J Med Chem. 2014;71:199–218.
- [513] More UA, Joshi SD, Aminabhavi TM, et al. Discovery of target based novel pyrrolyl phenoxy derivatives as antimycobacterial agents: An in silico approach. Eur J Med Chem. 2015;94:317–339.
- [514] Shirude PS, Madhavapeddi P, Naik M, et al. Methyl-Thiazoles: A Novel Mode of Inhibition with the Potential to Develop Novel Inhibitors Targeting InhA in *Mycobacterium tuberculosis*. J Med Chem. 2013;56:8533–8542.
- [515] Šink R, Sosič I, Živec M, et al. Design, Synthesis, and Evaluation of New Thiadiazole-Based Direct Inhibitors of Enoyl Acyl Carrier Protein Reductase (InhA) for the Treatment of Tuberculosis. J Med Chem. 2015;58:613–624.
- [516] Pedgaonkar GS, Sridevi JP, Jeankumar VU, et al. Development of 2-(4-oxoquinazolin-3(4H)-yl)acetamide derivatives as

- novel enoyl-acyl carrier protein reductase (InhA) inhibitors for the treatment of tuberculosis. *Eur J Med Chem.* 2014;86:613–627.
- [517] Pauli I, dos Santos RN, Rostirolla DC, et al. Discovery of New Inhibitors of *Mycobacterium tuberculosis* InhA Enzyme Using Virtual Screening and a 3D-Pharmacophore-Based Approach. *J Chem Inf Model.* 2013;53:2390–2401.
- [518] Paz JD, Denise de Moura Sperotto N, Ramos AS, et al. Novel 4-aminoquinolines: Synthesis, inhibition of the *Mycobacterium tuberculosis* enoyl-acyl carrier protein reductase, antitubercular activity, SAR, and preclinical evaluation. *Eur J Med Chem.* 2023;245:114908.
- [519] O'Neill J. Tackling drug-resistant infections globally : Final Report and Recommendations. *AMR Rev.* 2016;
- [520] Raju RM, Raju SM, Zhao Y, et al. Leveraging Advances in Tuberculosis Diagnosis and Treatment to Address Nontuberculous Mycobacterial Disease. *Emerg Infect Dis.* 2016;22:365–369.
- [521] Choo SW, Wee WY, Ngeow YF, et al. Genomic reconnaissance of clinical isolates of emerging human pathogen *Mycobacterium abscessus* reveals high evolutionary potential. *Sci Rep.* 2014;4:4061.
- [522] Koul A, Arnoult E, Lounis N, et al. The challenge of new drug discovery for tuberculosis. *Nature.* 2011;469:483–490.
- [523] Meunier B. Hybrid Molecules with a Dual Mode of Action: Dream or Reality? *Acc Chem Res.* 2008;41:69–77.
- [524] Hu Y-Q, Zhang S, Zhao F, et al. Isoniazid derivatives and their anti-tubercular activity. *Eur J Med Chem.* 2017;133:255–267.
- [525] Rani A, Johansen MD, Roquet-Banères F, et al. Design and synthesis of 4-Aminoquinoline-isoindoline-dione-isoniazid triads as potential anti-mycobacterials. *Bioorg Med Chem Lett.* 2020;30:127576.
- [526] Johansen MD, Shalini, Kumar S, et al. Biological and Biochemical Evaluation of Isatin-Isoniazid Hybrids as Bactericidal Candidates against *Mycobacterium tuberculosis*. *Antimicrob Agents Chemother.* 2021;65:e00011-21.
- [527] Sharma B, Kumar S, Preeti, et al. 1 H -1,2,3-triazole embedded Isatin-Benzaldehyde-bis(heteronuclearhydrazones): design, synthesis, antimycobacterial, and cytotoxic evaluation. *Chem Biol Drug Des.* 2022;99:301–307.
- [528] Almeida D, Converse PJ, Li S-Y, et al. Comparative Efficacy of the Novel Diarylquinoline TBAJ-876 and Bedaquiline against a Resistant *Rv0678* Mutant in a Mouse Model of Tuberculosis. *Antimicrob Agents Chemother.* 2021;65:e01412-21.
- [529] Sutherland HS, Tong AST, Choi PJ, et al. 3,5-Dialkoxyppyridine analogues of bedaquiline are potent antituberculosis agents with minimal inhibition of the hERG channel. *Bioorg Med Chem.* 2019;27:1292–1307.
- [530] Huang Z, Luo W, Xu D, et al. Discovery and preclinical profile of sudapyridine (WX-081), a novel anti-tuberculosis agent. *Bioorg Med Chem Lett.* 2022;71:128824.
- [531] Butler MS, Henderson IR, Capon RJ, et al. Antibiotics in the clinical pipeline as of December 2022. *J Antibiot (Tokyo).* 2023;76:431–473.
- [532] Dartois VA, Rubin EJ. Anti-tuberculosis treatment strategies and drug development: challenges and priorities. *Nat Rev Microbiol.* 2022;20:685–701.
- [533] WHO. 2021 antibacterial agents in clinical and preclinical development: an overview and analysis. 2022.
- [534] Kumar S, Sharma B, Mehra V, et al. Recent accomplishments on the synthetic/biological facets of pharmacologically active 1H-1,2,3-triazoles. *Eur J Med Chem.* 2021;212:113069.
- [535] Zhou B, He Y, Zhang X, et al. Targeting mycobacterium protein tyrosine phosphatase B for antituberculosis agents. *Proc Natl Acad Sci.* 2010;107:4573–4578.
- [536] Reddyrajula R, Dalimba U, Madan Kumar S. Molecular hybridization approach for phenothiazine incorporated 1,2,3-triazole hybrids as promising antimicrobial agents: Design, synthesis, molecular docking and *in silico* ADME studies. *Eur J Med Chem.* 2019;168:263–282.
- [537] Agalave SG, Maujan SR, Pore VS. Click Chemistry: 1,2,3-Triazoles as Pharmacophores. *Chem - Asian J.* 2011;6:2696–2718.

- [538] Arun KB, Madhavan A, Abraham B, et al. Acetylation of Isoniazid Is a Novel Mechanism of Isoniazid Resistance in *Mycobacterium tuberculosis*. *Antimicrob Agents Chemother*. 2020;65:e00456-20.
- [539] Hearn MJ, Cynamon MH, Chen MF, et al. Preparation and antitubercular activities *in vitro* and *in vivo* of novel Schiff bases of isoniazid. *Eur J Med Chem*. 2009;44:4169–4178.
- [540] Manjunatha UH, S. Rao SP, Kondreddi RR, et al. Direct inhibitors of InhA are active against *Mycobacterium tuberculosis*. *Sci Transl Med* [Internet]. 2015 [cited 2021 Dec 17];7. Available from: <https://www.science.org/doi/10.1126/scitranslmed.3010597>.
- [541] Dartois V, Dick T. Drug development challenges in nontuberculous mycobacterial lung disease: TB to the rescue. *J Exp Med*. 2022;219:e20220445.
- [542] Ganapathy US, Dick T. Why Matter Matters: Fast-Tracking *Mycobacterium abscessus* Drug Discovery. *Molecules*. 2022;27:6948.
- [543] Kwiatkowski S, Knap B, Przystupski D, et al. Photodynamic therapy – mechanisms, photosensitizers and combinations. *Biomed Pharmacother*. 2018;106:1098–1107.
- [544] Kolarikova M, Hosikova B, Dilenko H, et al. Photodynamic therapy: Innovative approaches for antibacterial and anticancer treatments. *Med Res Rev*. 2023;43:717–774.
- [545] Warriar A, Mazumder N, Prabhu S, et al. Photodynamic therapy to control microbial biofilms. *Photodiagnosis Photodyn Ther*. 2021;33:102090.
- [546] Amos-Tautua B, Songca S, Oluwafemi O. Application of Porphyrins in Antibacterial Photodynamic Therapy. *Molecules*. 2019;24:2456.
- [547] Rossi GG, Guterres KB, Da Silveira CH, et al. Peripheral tetra-cationic Pt(II) porphyrins photo-inactivating rapidly growing mycobacteria: First application in mycobacteriology. *Microb Pathog*. 2020;148:104455.
- [548] Wang X, Wang X, Lei X, et al. Photodynamic therapy: a new approach to the treatment of Non-Tuberculous Mycobacterial skin and soft tissue infections. *Photodiagnosis Photodyn Ther*. 2023;43:103645.



# ANNEXES





**Annexe 1 :**

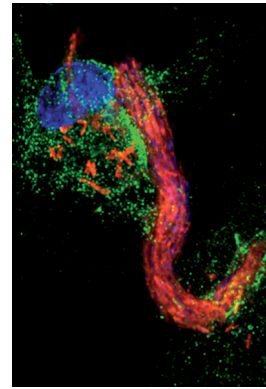
**“Mycobacterium abscessus, un modèle de résistance aux différentes classes d’antibiotiques”**,

Morgane Illouz\*, Matthéo Alcaraz \*, Françoise Roquet-Banères et Laurent Kremer. *Médecine/Sciences (Paris)*, 2021, Vol 37, N°11 Page 993-1001. PMID : 34851275, DOI : 10.1051/medsci/2021164.

> *Mycobacterium abscessus* est une bactérie non tuberculeuse, environnementale, à croissance rapide, qui est responsable d'infections pulmonaires sévères, notamment chez les patients atteints de mucoviscidose. Le traitement actuel combine l'utilisation d'une  $\beta$ -lactamine et d'un aminoglycoside associés à un macrolide. Cette bactérie est polyrésistante à la plupart des antibiotiques utilisés en clinique. Les mécanismes de résistance, innés ou acquis, qu'elle a développés, conduisent fréquemment à des échecs thérapeutiques, ce qui limite considérablement les moyens de lutte disponibles pour le clinicien. Une compréhension globale des mécanismes de résistance de cette bactérie s'avère ainsi nécessaire pour contrer les infections pulmonaires qu'elle provoque. <

## ***Mycobacterium abscessus*, un modèle de résistance aux différentes classes d'antibiotiques**

Morgane Illouz<sup>1,\*</sup>, Matthéo Alcaraz<sup>1,\*</sup>,  
Françoise Roquet-Banères<sup>1</sup>, Laurent Kremer<sup>1,2</sup>



<sup>1</sup>CNRS UMR 9004, Institut de recherche en infectiologie de Montpellier (IRIM), Université de Montpellier, 1919 route de Mende, 34293, Montpellier, France.

<sup>2</sup>Inserm, IRIM, 34293 Montpellier, France.

\*Contribution équivalente  
laurent.kremer@irim.cnrs.fr

*Mycobacterium abscessus* a été isolée pour la première fois en 1950, par Morris Moore et John B Frerichs, chez une patiente de 63 ans ayant consulté pour divers troubles dont un abcès situé au niveau du genou, résultant d'un traumatisme survenu 48 ans plus tôt [1]. Cette mycobactérie non tuberculeuse (MNT) à croissance rapide est classée dans le phylum des Actinobactéries (Figure 1A). *M. abscessus* regroupe en fait trois sous-espèces bactériennes : *M. abscessus* subsp. *abscessus*, *M. abscessus* subsp. *bolletii* et *M. abscessus* subsp. *massiliense*. Celles-là diffèrent par leur profil génétique mais aussi par leur susceptibilité à certains antibiotiques [2]. *M. abscessus* est un pathogène opportuniste intracellulaire (Figure 1B) qui est souvent assimilé à d'autres mycobactéries. Confondue avec ces autres espèces, sa prévalence propre pourrait ainsi être largement sous-estimée. Son mode de transmission reste encore largement incompris. Néanmoins, une étude réalisée en 2016 suggère une transmission interhumaine possible chez les patients atteints de mucoviscidose [3]. *M. abscessus* est responsable de manifestations cliniques très étendues. Outre des infections cutanées, osseuses, disséminées et, voire, dans de rares cas, lorsque la barrière

hémato-encéphalique est altérée, d'atteintes du système nerveux central, *M. abscessus* est responsable d'infections pulmonaires sévères, en particulier chez les patients souffrant de troubles pulmonaires comme la mucoviscidose [4]. On estime en effet que 10 à 20 % de ces patients, qui présentent une susceptibilité accrue aux infections bactériennes, sont infectés par une MNT (principalement *M. abscessus* et *Mycobacterium avium*). L'infection par *M. abscessus* est l'une des infections bactériennes les plus difficiles à traiter : elle est en effet multi-résistante aux antibiotiques, et le taux d'échec des traitements atteint près de 60 % [5]. Sa place de pathogène émergent s'explique par son incidence, qui peut surpasser, dans certains pays industrialisés, celle de *Mycobacterium tuberculosis*, l'agent étiologique de la tuberculose [4]. Le séquençage complet du génome de *M. abscessus* a révélé la présence de plusieurs gènes codant des facteurs de virulence spécifiques de *M. tuberculosis* ainsi que de nombreux facteurs de virulence non mycobactériens, caractéristiques d'autres pathogènes souvent associés à la mucoviscidose, tels que *Pseudomonas aeruginosa* [6, 7]. La grande plasticité du génome de *M. abscessus* et les nombreux mécanismes de résistance aux antibiotiques que déploie cette bactérie témoignent de sa capacité d'adaptation à son environnement.

### ***M. abscessus*, une menace croissante pour les patients atteints de mucoviscidose ?**

La mucoviscidose est une maladie génétique héréditaire causée par une mutation du gène codant la protéine CFTR (*cystic fibrosis transmembrane regulator*) [8] (→).

(→) Voir la Synthèse de C. Ferec, m/s n° 6-7, juin-juillet 2021, page 618

Vignette (Photo © Wassim Daher).

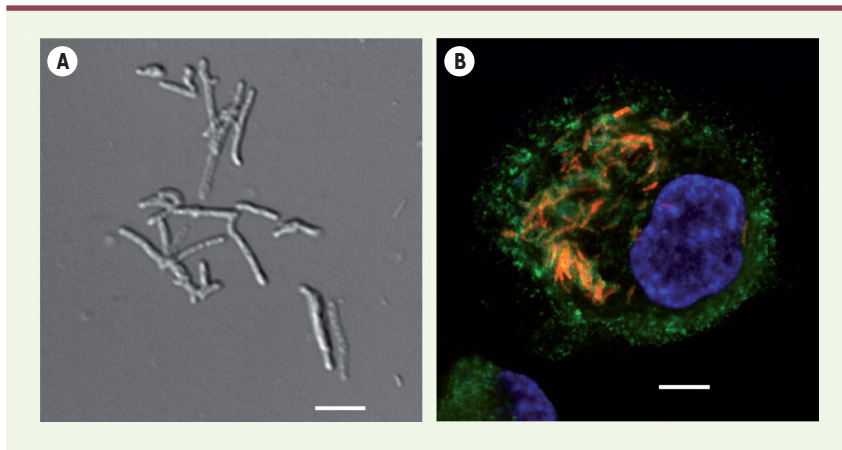


**Figure 1.** *M. abscessus*, un bacille intracellulaire. **A.** Image de microscopie en contraste de phase de *M. abscessus*. L'échelle représente 5  $\mu$ m. **B.** Image d'immunofluorescence d'un macrophage infecté par *M. abscessus* exprimant Tdtomato (rouge). Les macrophages sont détectés grâce à un anticorps anti-CD63 (vert) et les noyaux sont marqués au DAPI (bleu). L'échelle représente 10  $\mu$ m.

Cette maladie autosomique récessive affecte, en particulier, les fonctions digestives et respiratoires. La protéine CFTR est en effet une protéine transmembranaire qui joue un rôle de canal ionique localisé au pôle apical des cellules épithéliales pulmonaires, permettant l'échange d'ions chlorure et sodium au travers de la membrane des cellules [9]. Des mutations du gène *CFTR* entraînent un dysfonctionnement à l'origine d'une mauvaise hydratation du mucus bronchique, qui, de ce fait, devient de plus en plus épais et visqueux, favorisant ainsi l'établissement d'infections polymicrobiennes chroniques. *M. abscessus* représente, avec *M. avium*, la MNT la plus fréquemment retrouvée dans les expectorations de patients atteints de mucoviscidose, pouvant induire un déclin rapide de leurs fonctions pulmonaires [10]. Le dysfonctionnement de CFTR réduit, entre autre, l'activité bactéricide des macrophages en raison d'une diminution de leur production de radicaux oxydants en réponse aux infections [11]. À l'incapacité du système immunitaire inné à contrôler efficacement les infections bactériennes, s'ajoute la difficulté, pour le clinicien, à traiter ces infections et à éradiquer le bacille responsable [12]. La présence de *M. abscessus* peut aussi représenter une contre-indication à la greffe pulmonaire, un recours souvent nécessaire chez les patients atteints de mucoviscidose.

### L'antibiothérapie comme traitement des infections à *M. abscessus*

La majorité des molécules utilisées en clinique dans le traitement contre *M. abscessus* ont un effet bactériostatique : elles ne font que stopper la prolifération bactérienne, sans induire la mort des bactéries. Ces molécules ne montrent également que peu ou pas d'activité vis-à-vis des biofilms, constructions complexes formées de colonies bactériennes, ce qui pourrait expliquer la relative inefficacité des régimes thérapeutiques actuellement appliqués [13]. Pendant plusieurs années, les recommandations thérapeutiques ont été fondées sur une trithérapie, associant une  $\beta$ -lactamine (imipénème ou céfoxitine), un aminoglycoside (amikacine), administrés par voie parentérale pendant 12 mois, et un macrolide (clarithromycine ou azithromycine), par voie orale. Afin d'optimiser cette thérapie chez les personnes atteintes de mucoviscidose, un

consortium regroupant l'*US Cystic Fibrosis Foundation* et l'*European Cystic Fibrosis Society*, préconise maintenant une première phase de thérapie dite intensive (durant au moins un mois), suivie d'une phase de prolongation (de 12 mois) (Figure 2). Cette stratégie prend en compte le profil de résistance aux antibiotiques de la souche à l'origine de l'infection. Il est donc important de différencier les isolats cliniques de *M. abscessus* qui sont sensibles ou résistants aux antibiotiques, dont les macrolides. L'action combinée de plusieurs antibiotiques permet de cibler différentes voies métaboliques utilisées par la bactérie afin de l'éradiquer (Figure 3) [14].

### Les classes d'antibiotiques

Les  $\beta$ -lactamines regroupent une large classe d'antibiotiques (dont les pénicillines, les céphalosporines, les carbapénèmes). Elles agissent en inhibant la synthèse d'un composant essentiel de la paroi des mycobactéries, le peptidoglycane, formé d'une épine dorsale alternant des chaînons N-acétyl glucosamine - acide N-acétyl muramique, et de chaînes tétrapeptidiques (L-Alaninyl-D-isoGlutaminyl-meso-diaminopimétyl-D-Alanine) liées à l'acide muramique. Lors de l'étape finale de la synthèse de cet hétéropolymère, des liaisons covalentes se forment entre les chaînes latérales des peptides monomères qui le composent, produisant la macromolécule qui englobera la membrane plasmique. La réticulation du peptidoglycane est assurée par des transpeptidases bactériennes qui appartiennent à la famille des protéines liant la pénicilline (PBP), les D,D-transpeptidases (DDT) et les L,D-transpeptidases (LDT), qui catalysent respectivement des liaisons de type 4 $\rightarrow$ 3 et 3 $\rightarrow$ 3 entre ces chaînes peptidiques latérales [15]. Les  $\beta$ -lactamines agissent sur ces transpeptidases en entrant en compétition, par mimétisme, avec le substrat de ces enzymes, bloquant ainsi la biosynthèse du peptidoglycane. Les céphalosporines et les

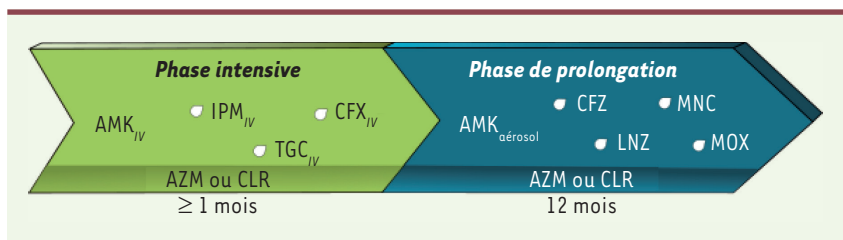


**Figure 2. Régime thérapeutique dans le cadre d'infections à *M. abscessus*.** La phase intensive, d'une durée pouvant excéder un mois, comporte une dose quotidienne d'amikacine injectée par voie intraveineuse (AMK<sub>IV</sub>), d'un antibiotique choisi parmi l'imipénème (IPM), la tigécycline (TGC) ou la céfoxitine (CFX), ainsi qu'un macrolide (azithromycine (AZM)

ou clarithromycine (CLR)). La phase de prolongation, d'une durée d'environ 12 mois, comprend un macrolide, de l'AMK en aérosol ainsi que 2 à 3 antibiotiques choisis parmi la clofazimine (CFZ), le linézolide (LNZ), la minocycline (MNC) ou la moxifloxacine (MOX), dont le choix est dépendant du profil de résistance de chaque isolat clinique.

carbapénèmes présentent des activités différentes sur les deux types de transpeptidases : plus efficaces contre les DDT pour les céphalosporines, supérieures contre les LDT pour les carbapénèmes [16].

Les macrolides représentent une autre classe d'antibiotiques. Ils ciblent, quant à eux, la synthèse protéique en interagissant avec l'ARN ribosomique (ARNr) 23S de la grande sous-unité du ribosome (50S). Ces antibiotiques empêchent ainsi l'allongement de la chaîne peptidique en bloquant le tunnel de sortie par lequel les peptides nouvellement synthétisés s'éloignent du centre peptidyltransférase [17]. Les macrolides, tels que la clarithromycine ou l'azithromycine ont un effet bactériostatique auquel malheureusement *M. abscessus subsp. abscessus* et *M. abscessus subsp. bolletii* sont souvent résistantes [18].

Les aminoglycosides sont des molécules hydrophiles qui inhibent la synthèse des protéines en se liant au site A de l'ARNr 16S constituant la petite sous-unité des ribosomes [19]. Cette interaction est à l'origine d'une mauvaise lecture du codon lors de la délivrance de l'ARN de transfert (ARNt) des aminoacyls et, par conséquent, provoquent une traduction erronée de l'ARN messager (ARNm).

Les tétracyclines inhibent également la synthèse protéique des bactéries mais en prévenant l'association des aminoacyl-ARNt aux ribosomes bactériens [20]. Les membres de cette famille, comme la minocycline, ne présentent généralement qu'une activité modeste contre *M. abscessus*. Dérivée de la minocycline, la tigécycline fait exception. Elle est la seule tétracycline à présenter une chaîne 2-tert-butylglycylamino liée au carbone C-9 du cycle aromatique du squelette de la molécule (Figure 3). Ce substituant augmente l'affinité de la molécule pour le ribosome, lui conférant une forte activité inhibitrice ainsi que la capacité d'échapper aux mécanismes de résistance aux tétracyclines les plus couramment développés par les bactéries [21].

Le traitement de l'infection par *M. abscessus* par ces antibiotiques, dont la durée excède souvent 12 mois, s'accompagne néanmoins d'effets secondaires notoires, ce qui conduit, malgré leur efficacité, à de nombreuses impasses thérapeutiques.

## La polyrésistance de *M. abscessus* aux diverses classes d'antibiotiques

### Une résistance innée de la bactérie

#### *La paroi mycobactérienne, une barrière naturelle*

Si les mécanismes de résistance développés par *M. abscessus* sont nombreux et variés, la paroi mycobactérienne, unique en son genre par

la diversité des lipides qui la constituent, joue le rôle de première barrière à l'encontre de nombreuses molécules exogènes, dont certains antibiotiques. Comme toute cellule, la bactérie est bordée d'une membrane constituée d'une bicouche lipidique : la membrane interne (MI) (Figure 4A). Ancrés dans cette bicouche, se trouvent une grande variété de glycoconjugués : des glycolipides et des lipoglycannes, tels que le phosphatidyl-*myo*-inositol mannoside, le lipomannane ou le lipoarabinomannane [22] (→).

Entourant cette membrane interne, l'espace périplasmique est constitué du peptidoglycane, un hétéropolymère lié de manière covalente à une couche d'arabinogalactane, elle-même estérifiée par des acides mycoliques, des acides gras à longues chaînes carbonées. Ces acides mycoliques, caractéristiques des mycobactéries, constituent le feuillet interne de la mycomembrane. Dans le feuillet externe de cette dernière viennent s'insérer des lipides et glycolipides, tels que le tréhalose monomycolate, le tréhalose dimycolate, le tréhalosepolyphléate mais aussi des glycopeptidolipides [23]. Cette vaste panoplie de lipides participe grandement aux propriétés de résistance de la paroi, par exclusion de taille des molécules exogènes, mais aussi par son caractère hydrophobe, conférant une résistance naturelle aux antibiotiques hydrophiles.

#### *L'export actif à travers la membrane*

Dans la membrane interne, de nombreuses protéines jouant le rôle de pompes à efflux sont insérées (Figure 4B). Parmi celles-ci, les protéines de la famille MmpL (*Mycobacterial membrane protein Large*) [24] permettent de maintenir l'homéostasie de la bactérie. Elles sont également responsables d'une balance physiologique permettant l'export de toxines et de métabolites produits par la bactérie. Ces protéines membranaires ont une grande variété de substrats, comme les facteurs de virulence, mais elles ont aussi un rôle indispensable dans le transport de lipides et dans l'élaboration de la paroi bactérienne. Dans certains cas, les

(→) Voir la Synthèse de L. Kremer et al., m/s n° 6-7, juin-juillet 1999, page 842

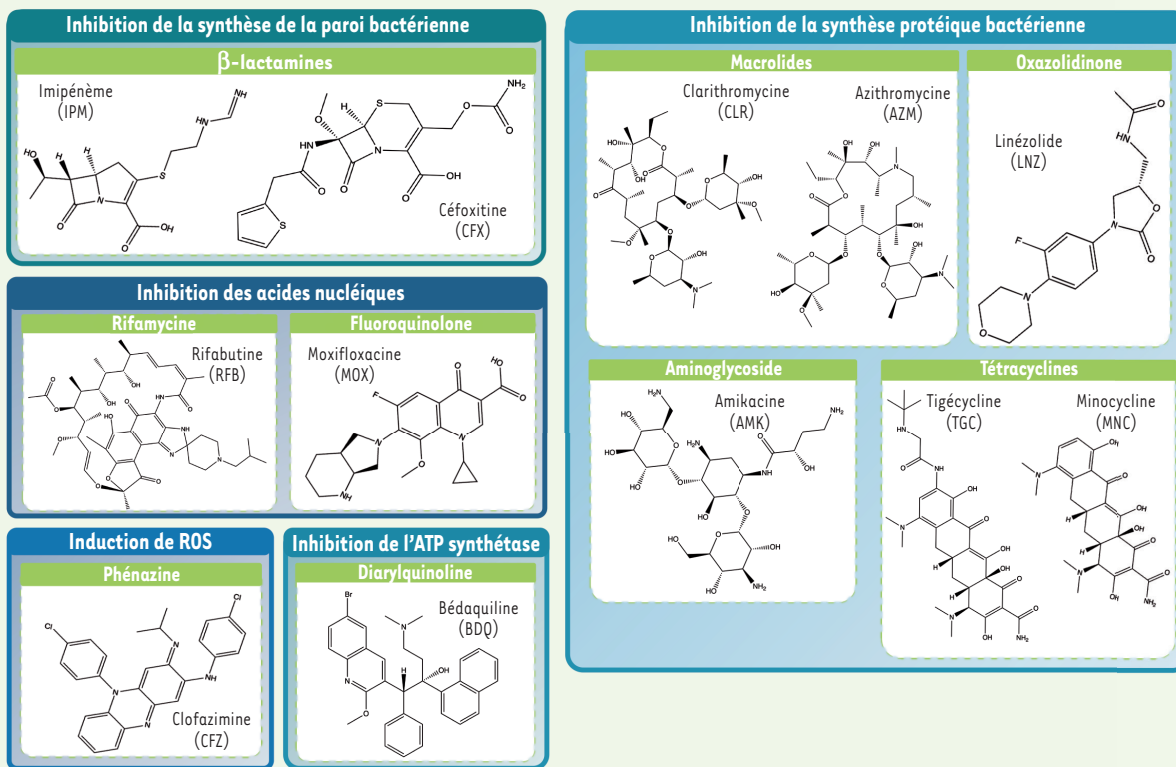


**Figure 3. Structure chimique des principaux antibiotiques utilisés dans le traitement des infections pulmonaires à *M. abscessus*.** Les principales classes d'antibiotiques préconisées dans le traitement ainsi que leur mode d'action sont indiqués. ROS : *reactive oxygen species*.

pompes à efflux peuvent participer à l'export, du cytoplasme vers le milieu extérieur, de substances exogènes (telles que les antibiotiques) qui auraient pénétré dans la cellule. Certaines de ces protéines MmpL agissent de concert avec des protéines MmpS (*Mycobacterial membrane protein Small*), dont les gènes sont adjacents à ceux codant les MmpL. Le cluster de gènes *MAB\_2300/MAB\_2301*, codant les protéines MmpS/MmpL, est ainsi impliqué dans l'export d'antibiotiques comme la bédaquiline (BDQ) et la clofazimine (CFZ) (Figure 4B). Leur capacité d'export n'induit toutefois pas de résistances importantes [25] (Tableau 1). Une protéine apparentée à la pompe à efflux LmrS (*lincomycin resistance protein of Staphylococcus aureus*), ainsi que MmpL9, participent à la résistance au linézolide (LNZ) chez *M. abscessus*. En effet, des niveaux élevés de transcrits du gène codant MmpL9 ont été décrits chez des souches résistantes au linézolide, témoignant de l'implication probable de cette molécule dans l'export de l'antibiotique [26] (Figure 4B). La résistance de *M. abscessus* aux analogues du thiacétazone (TAC) s'explique également par l'export actif de ces antibiotiques par le système *MAB\_4383c/MAB\_4382c*, homologue de *mmpS5/mmpL5* chez *Mycobacterium tuberculosis* [27].

Si l'ensemble de ces transporteurs confèrent une perméabilité ajustable à la paroi bactérienne et représentent ainsi des mécanismes de résistance intrinsèque aux antibiotiques chez *M. abscessus*, nos connaissances sur l'implication d'autres systèmes de transport poten-

tiels dans la résistance aux antibiotiques de la bactérie restent encore limitées. Toutefois, diverses études sont actuellement menées dans le but d'identifier des inhibiteurs spécifiques de ces pompes à efflux afin de potentialiser l'efficacité des traitements [28].

#### *Les enzymes modifiant/inactivant les antibiotiques*

À côté de ces systèmes d'export, *M. abscessus* regorge d'une grande variété d'enzymes capables de modifier chimiquement de nombreux antibiotiques, et ainsi de les rendre inopérants. Ces enzymes, qui limitent donc considérablement les options de traitement, constituent un pan non négligeable du « résistome » de *M. abscessus* (Tableau 1). Parmi celles-là, une seule, ciblant les β-lactamines, a été identifiée chez *M. abscessus* : la β-lactamase  $Bla_{MAB}$  (Figure 4C). Codée par le gène *MAB\_2875*, elle hydrolyse le noyau β-lactame de nombreuses molécules antibiotiques, comme les pénicillines, les carbapénèmes ou les céphalosporines. En clinique, l'utilisation de certains antibiotiques, comme l'imipénème et la céfoxitine, reste néanmoins possible. La  $Bla_{MAB}$  ne les dégradent en effet que très lentement, leur conférant une certaine efficacité [29]. L'avibactam, développé par AstraZeneca, un inhibiteur spéci-



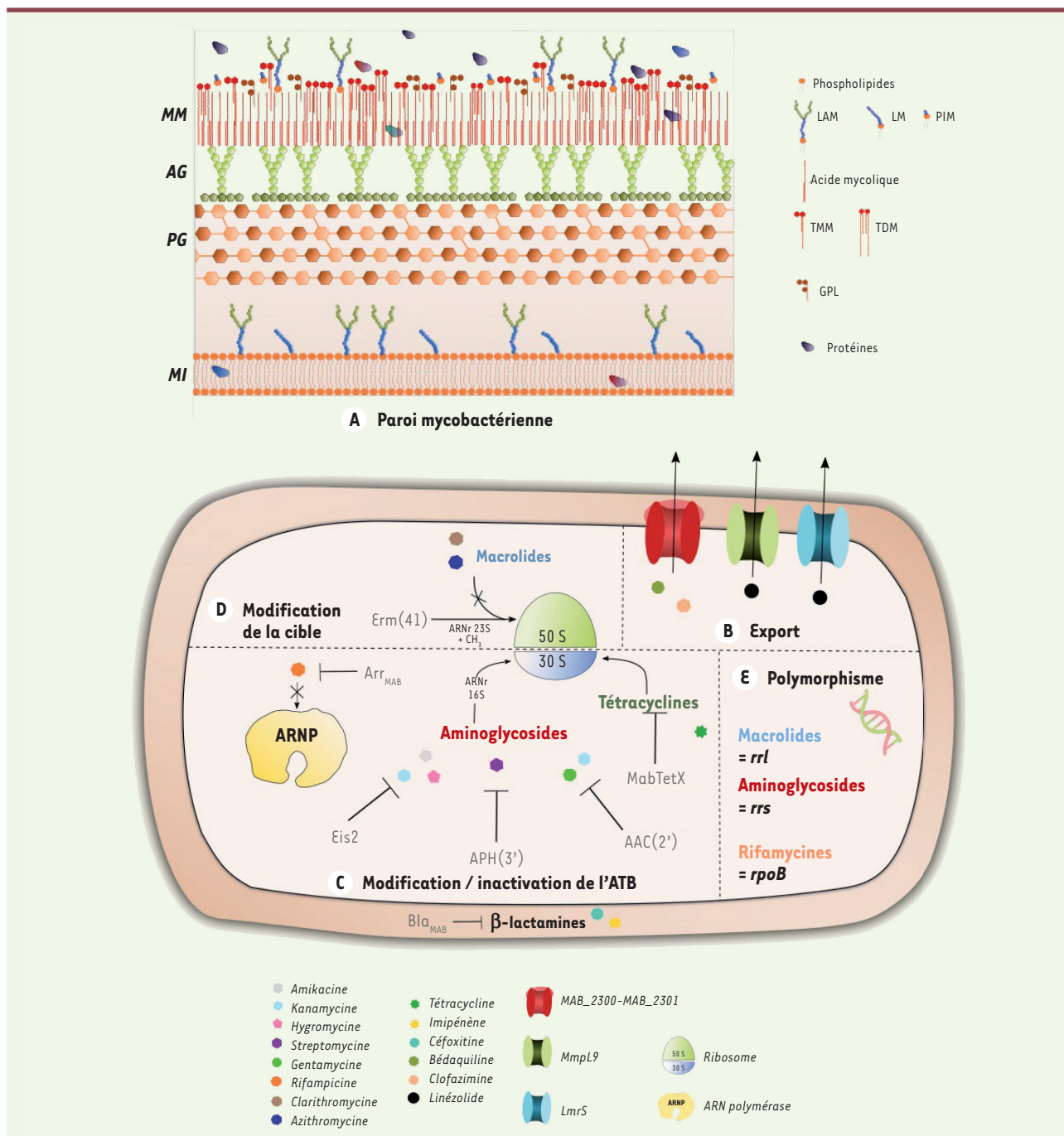


**Figure 4. Mécanismes de résistances innée et acquise chez *M. abscessus* vis-à-vis des principales classes d'antibiotiques.** **A.** La paroi mycobactérienne riche en lipides représente la première ligne de défense contre certains antibiotiques, de par sa forte hydrophobicité et l'exclusion de taille qu'elle provoque. **B.** L'export d'antibiotiques, tels que la bédacouline, la clofazimine ou encore le linézolide, implique des protéines transmembranaires, incluant par exemple les transporteurs de type MmpL. **C.** *M. abscessus* exprime de nombreuses enzymes capables de modifier et d'inactiver directement les antibiotiques. Arr<sub>MAB</sub> (une ADP ribosyltransférase) inhibe l'action de la rifampicine tandis que AAC(2') et Eis2 (des N-acétyltransférases) ainsi que APH(3') (une 3''-O-phosphotransférase) neutralisent l'activité des aminoglycosides. MabTetX (une monoxygénase) inactive l'activité des tétracyclines. **D.** D'autres enzymes modifient la cible des antibiotiques. La méthyltransférase Erm(41) inhibe l'action des macrolides en méthylant l'ARNr 23S de la sous-unité 50S du ribosome, diminuant ainsi l'affinité de l'antibiotique vis-à-vis du ribosome. **E.** Le polymorphisme génétique est impliqué dans la résistance à plusieurs classes d'antibiotiques, incluant notamment les macrolides, les aminoglycosides ou les rifamycines. MM : mycomembrane ; AG : arabinogalactane ; PG : peptidoglycane ; MI : membrane interne ; LAM : lipoarabinomannane ; LM : lipo-mannane ; TMM : tréhalose monomycolate ; TDM : tréhalose dimycolate ; GPL : glycopeptidolipide ; PIM : phosphatidyl-*myo*-inositol mannoside.

Antibiotique	Voie métabolique/cible	Gène(s) impliqué(s)	Réf.
Isoniazide	Synthèse des acides mycoliques /énoyl ACP réductase InhA	Polymorphisme du gène <i>katG</i> codant l'enzyme d'activation de l'INH	[31]
Rifampicine	Transcription/ARN polymérase	ADP-ribosylation de la rifampicine par Arr <sub>MAB</sub>	[35]
Aminoglycosides	Synthèse protéique/ARNr 16S	Inactivation par AAC(2') Inactivation par APH(3'')	[31] [33]
β-lactamines	Synthèse du peptidoglycane/Penicillin-binding protein	Inactivation par Bla <sub>MAB</sub>	[53]
Tétracycline	Synthèse protéique/empêche l'attachement de l'aminoacyl-ARNt au ribosome	Inactivation par MabTetX	[34]
Macrolides	Synthèse protéique/ARNr 23S	Modification de la cible par le produit du gène <i>erm(41)</i>	[18]
Analogues du thiacétazone	Synthèse des acides mycoliques /déshydratases HadABC	Pompe à efflux de type MmpS/MmpL codée par <i>MAB_4383c/4382c</i>	[54]
Bédaquiline	Production d'énergie/ATP synthase	Pompes à efflux de type MmpS/MmpL codées par <i>MAB_2300/2301</i> et <i>MAB_1135c/1134c</i>	[25,55]
Clofazimine	Production de radicaux oxydants produits par la NADH:quinone oxydoréductase de type 2	Pompes à efflux de type MmpS/MmpL codées par <i>MAB_2300/2301</i> et <i>MAB_1135c/1134c</i>	[25,55]

**Tableau I. Résistance innée et acquise aux antibiotiques chez *M. abscessus*.** ACP : acyl carrier protein ; Inh : isoniazid ; KatG : catalase/peroxidase ; MmpL : Mycobacterial membrane protein Large ; MmpS : Mycobacterial membrane protein Small.

fique de la Bla<sub>MAB</sub>, permet, également de réduire considérablement la concentration minimale inhibitrice de certaines β-lactamines. Cette molécule augmente ainsi l'efficacité de ces antibiotiques, ouvrant la voie vers de nouvelles approches thérapeutiques, et donc à l'utilisation de cette famille d'antibiotiques [30].

La résistance de *M. abscessus* aux aminoglycosides s'explique par la présence chez cette bactérie de trois enzymes (deux acétyltransférases et une phosphotransférase) capables de neutraliser cette classe d'antibiotiques. Les deux N-acétyltransférases, AAC(2') et Eis2, sont codées respectivement par les gènes *MAB\_4395* et *MAB\_4532c*. AAC(2') acétyle le groupement amine situé en position 2' de certains aminoglycosides tels que la kanamycine ou la gentamycine [31], deux antibiotiques qui ne sont pas utilisés dans les traitements cliniques. Eis2, quant à elle, inactive l'amikacine, la kanamycine ou l'hygromycine, en acétylant le premier groupement amine de ces molécules [32]. L'inactivation des gènes codant ces enzymes entraîne une sensibilité accrue des bactéries aux aminoglycosides [31]. La 3''-O-phosphotransférase (APH(3'')), codée par le gène *MAB\_2385*, est, elle, déterminante dans la résistance à la streptomycine [33]. Les modifications chimiques que ces enzymes produisent sur les aminoglycosides, diminuent leur affi-

nité pour l'ARNr 16S de la sous-unité 30S du ribosome, ce qui les rend inopérantes (Figure 4C).

Bien qu'efficaces contre *M. tuberculosis*, les tétracyclines n'ont que peu d'effet sur *M. abscessus*. En effet, *M. abscessus* exprime une monoxygénase, la MabTetX [34], qui inactive les tétracyclines (Figure 4C). La délétion du gène *MAB\_1496c* qui code cette enzyme, entraîne chez la souche mutée, une sensibilité accrue à ce type d'antibiotique, vingt fois plus élevée par rapport à la souche parentale, confirmant l'importance de cette enzyme dans la résistance aux tétracyclines.

La rifampicine est une molécule utilisée en première intention pour le traitement de la tuberculose. *M. abscessus* reste cependant insensible à l'action de cet antibiotique. La raison de cette résistance repose sur la présence chez *M. abscessus* d'une ribosyltransférase, l'ADP ribosyltransférase Arr<sub>MAB</sub>, codée par le gène *MAB\_0591*. Cette enzyme est capable d'ADP ribosyler la rifampicine, l'empêchant d'agir au niveau de la sous-unité β de l'ARN polymérase [35] (Figure 4C). La décou-



verte de dérivés de la rifamycine, plus réfractaires à l'ADP-ribosylation par Arr<sub>MAB</sub>, représente néanmoins une piste de recherche prometteuse dans la lutte contre *M. abscessus* [36].

#### Les enzymes protégeant la cible des antibiotiques

*M. abscessus* possède également une enzyme capable de protéger les protéines ciblées par les macrolides (Tableau I). La méthyltransférase Erm(41), codée par le gène *MAB\_2997*, est en effet capable de méthyle l'adénine en position 2058 de l'ARNr 23S de la sous-unité 50S du ribosome [18] (Figure 4D). Par cette méthylation, cette enzyme produit un encombrement stérique qui réduit l'affinité des macrolides pour le tunnel de sortie du polypeptide. Il existe un polymorphisme du gène *erm(41)* codant cette méthyltransférase, sur le nucléotide en position 28 : thymine ou cytosine. Selon ce polymorphisme, les souches cliniques de *M. abscessus* présentent une résistance à la clarithromycine ou à l'azithromycine : le sequevar (ou variant) T28 (correspondant à un résidu tryptophane [Trp] en position 10 de la protéine) est en effet associé à une résistance inductible, alors que le sequevar C28 (correspondant à un résidu arginine [Arg10]) est associé à une sensibilité de la bactérie aux macrolides [37]. Le niveau de résistance de la bactérie, qui augmente progressivement en fonction du temps d'exposition à la clarithromycine ou à l'azithromycine, est inductible et directement lié à l'activateur de transcription WhiB7 [38]. Sachant que les macrolides représentent la pierre angulaire de la thérapie anti-*M. abscessus*, cette résistance aux macrolides inductible, observée dans 40 à 60 % des souches cliniques [37], rend compte du problème majeur de santé publique que représente l'infection par cette bactérie.

### Polymorphisme nucléotidique et résistance acquise

Aux mécanismes de résistance innée que nous avons décrits, s'ajoutent des résistances acquises par *M. abscessus*. Ces résistances, fruit de modifications génétiques qui sont retrouvées dans les isolats cliniques, sont le résultat d'une exposition prolongée de la bactérie aux antibiotiques. Des mutations spontanées surviennent ainsi au sein des gènes codant les cibles protéiques des antibiotiques (Tableau I et Figure 4E), mais d'autres mécanismes additionnels, tels que le transfert génétique entre espèces bactériennes, sont probablement impliqués.

#### Résistance acquise aux macrolides

Des mutations du gène *rml*, qui code l'ARNr 23S [39], touchant les adénines en position 2058 et 2059 de l'ARNr 23S, sont induites au décours des expositions aux antibiotiques. Celles-ci réduisent l'activité des macrolides, et sont retrouvées dans les isolats de *M. abscessus*, comme c'est le cas pour d'autres espèces mycobactériennes, telles que *M. avium* [39].

#### Résistance acquise aux aminoglycosides

Des mutations du gène *rrs*, qui code l'ARNr 16S et qui induisent une résistance aux aminoglycosides, ont été décrites. Quatre mutations, affectant l'ARNr 16S (T1406A, A1408G, C1409T et G1491T)<sup>1</sup>, ont été

associées à de hauts niveaux de résistance de *M. abscessus* aux aminoglycosides [40]. Deux nouvelles mutations (C1496T et T1498A)<sup>2</sup> ont été identifiées récemment [41].

#### Résistance acquise aux rifamycines

*M. abscessus* est réfractaire à l'action de la rifampicine qui est inactivée par l'action de la Arr<sub>MAB</sub>. Toutefois, la rifabutine, de la famille des rifamycines, fait exception. Dans un modèle d'infection chez le poisson-zèbre (*zebrafish*) [42, 43] (→) ainsi que dans un modèle murin d'infection par *M. abscessus* [44], cet antibiotique présente des effets

(→) Voir la Synthèse de A. Bernut et al., m/s n° 6-7, juin-juillet 2015, page 638

bactéricides. Ces données confirment la capacité de la rifabutine à inhiber la transcription chez *M. abscessus*, à l'instar de la rifampicine. Des mutations du gène *rpoB* qui code la sous-unité β de l'ARN polymérase (H447Y, H447D et S452L)<sup>3</sup> sont cependant à l'origine de la résistance de la bactérie à la rifabutine [43].

### Conclusion et perspectives

Les nombreux mécanismes de résistance de *M. abscessus*, conjugués à l'émergence de souches multi-résistantes, limitent considérablement les outils mis à la disposition du clinicien pour traiter les infections pulmonaires causées par cette mycobactérie atypique. Le traitement actuel recommandé ne permet pas, dans la plupart des cas, d'éradiquer des infections à *M. abscessus*. Face à ce problème de santé publique en progression constante, des efforts doivent être faits pour encourager et favoriser des études ayant pour but d'identifier de nouvelles pistes thérapeutiques pour lutter contre les infections persistantes à *M. abscessus*, avec en particulier, l'identification de nouvelles cibles d'intérêt thérapeutique et le développement de molécules auxquelles cette bactérie serait sensible. Depuis plusieurs années, la recherche se concentre sur la découverte et le repositionnement de molécules actives vis-à-vis de *M. abscessus* comme, par exemple, la rifabutine [43, 44], la bédaquiline [45, 46], le tédizolide [47] ou les inhibiteurs du transporteur des acides mycoliques MmpL3 [48, 49] (→). D'autres molécules ou formulations sont actuellement testées dans des essais cliniques, comme l'inhalation d'amikacine liposomale ou le monoxyde d'azote [50]. Des approches

(→) Voir la Nouvelle de C. Raynaud et L. Kremer, m/s n° 8-9, août-septembre 2020, page 691

<sup>1</sup> Thymine 1406 > adénine ; adénine 1408 > guanine ; cytosine 1409 > thymine ; guanine 1491 > thymine.

<sup>2</sup> Cytosine 1496 > Thymine ; thymine 1498 > adénine.

<sup>3</sup> Ou c.1339C>T ; c.1339C>G ; c.1355C>T

alternatives à l'antibiothérapie sont également en cours d'étude. La phagothérapie, par exemple, très utilisée au début du  $xx^e$  siècle, est remise au devant de la scène dans la lutte contre les infections par les MNT [51] (→).

Ainsi, l'administration d'un cocktail de mycobactériophages spécifiques à une souche multirésistante de *M. abscessus*, dans le cadre du traitement d'une infection disséminée chez une jeune patiente atteinte de mucoviscidose, a amélioré l'état clinique de la patiente et a suscité beaucoup d'espoir [52]. Si la phagothérapie reste encore anecdotique dans les pays occidentaux, elle pourrait néanmoins permettre d'établir des traitements personnalisés avec une toxicité moindre, notamment chez les patients particulièrement réfractaires à l'antibiothérapie classique. ♦

## SUMMARY

### *Mycobacterium abscessus*, a model of resistance to multiple antibiotic classes

*Mycobacterium abscessus* is an environmental fast-growing, non-tuberculous mycobacterium responsible for severe lung infections, especially in patients with underlying lung disorders such as cystic fibrosis. The standard chemotherapy combines a  $\beta$ -lactam (imipenem or ceftazidime), an aminoglycoside (amikacin) and a macrolide (clarithromycin or azithromycin). However, resistance of this bacterium to most antibiotic classes, including nearly all anti-tubercular drugs, leads frequently to treatment failure and considerably reduces the therapeutic arsenal available to the clinician. A comprehensive understanding of the innate and acquired resistance mechanisms is thus necessary to counteract *M. abscessus* lung infections. ♦

## REMERCIEMENTS

Morgane Illouz est bénéficiaire d'une bourse de thèse de l'Association Grégory Lemarchal et de Vaincre la Mucoviscidose (RF20200502678). Matthéo Alcaraz bénéficie d'une bourse de thèse du Ministère de l'Enseignement Supérieur, de la Recherche et de l'Innovation.

## LIENS D'INTÉRÊT

Les auteurs déclarent n'avoir aucun lien d'intérêt concernant les données publiées dans cet article.

## RÉFÉRENCES

1. Moore M, Frerichs JB. An unusual acid-fast infection of the knee with subcutaneous, abscess-like lesions of the gluteal region. *J Invest Dermatol* 1953 ; 20 : 133-69.
2. Minias A. Subspecies-specific sequence detection for differentiation of *Mycobacterium abscessus* complex. *Sci Rep* 2020 ; 10 : 16415.
3. Bryant JM, Grogono DM, Rodriguez-Rincon D, et al. Emergence and spread of a human-transmissible multidrug-resistant nontuberculous mycobacterium. *Science* 2016 ; 354 : 751-7.
4. Johansen MD, Herrmann J-L, Kremer L. Non-tuberculous mycobacteria and the rise of *Mycobacterium abscessus*. *Nat Rev Microbiol* 2020 ; 18 : 392-407.
5. Kwak N, Dalcolmo MP, Daley CL, et al. *Mycobacterium abscessus* pulmonary disease: individual patient data meta-analysis. *Eur Respir J* 2019 ; 54 : 1801991.
6. Choo SW, Wee WY, Ngeow YF, et al. Genomic reconnaissance of clinical isolates of emerging human pathogen *Mycobacterium abscessus* reveals high evolutionary potential. *Sci Rep* ; 4 : 4061.
7. Ripoll F, Pasek S, Schenowitz C, et al. Non mycobacterial virulence genes in the genome of the emerging pathogen *Mycobacterium abscessus*. *PLoS One* 2009 ; 4 : e5660.
8. Férec C. La mucoviscidose : du gène à la thérapeutique. *Med Sci (Paris)* 2021 ; 37 : 618-24.
9. Davies JC, Alton EFW, Bush A. Cystic fibrosis. *BMJ* 2007 ; 335 : 1255-9.

(→) Voir la Chronique génomique de B. Jordan, m/s n° 10, octobre 2019, page 806

10. Catherinot E, Roux AL, Macheras E, et al. Acute respiratory failure involving an R variant of *Mycobacterium abscessus*. *J Clin Microbiol* 2009 ; 47 : 271-4.
11. Bernut A, Dupont C, Ogryzko NV, et al. CFTR Protects against *Mycobacterium abscessus* infection by fine-tuning host oxidative defenses. *Cell Rep* 2019 ; 26 : 1828-40.
12. Nessar R, Cambau E, Reytrat JM, et al. *Mycobacterium abscessus*: a new antibiotic nightmare. *J Antimicrob Chemother* 2012 ; 67 : 810-18.
13. Yam YK, Alvarez N, Go ML, et al. Extreme drug tolerance of *Mycobacterium abscessus* persists. *Front Microbiol* 2020 ; 11 : 359.
14. Haworth CS, Banks J, Capstick T, et al. British thoracic society guidelines for the management of non-tuberculous mycobacterial pulmonary disease (NTM-PD). *Thorax* 2017 ; 72 : ii1-64.
15. Lavollay M, Fourgeaud M, Herrmann JL, et al. The peptidoglycan of *Mycobacterium abscessus* is predominantly cross-linked by L,D-transpeptidases. *J Bacteriol* 2011 ; 193 : 778-82.
16. Dubée V, Triboulet S, Mainardi JL, et al. Inactivation of *Mycobacterium tuberculosis* L,D-transpeptidase LdtMt1 by carbapenems and cephalosporins. *Antimicrob Agents Chemother* 2012 ; 56 : 4189-95.
17. Wilson DN. Ribosome-targeting antibiotics and mechanisms of bacterial resistance. *Nat Rev Microbiol* 2014 ; 12 : 35-48.
18. Nash KA, Brown-Elliott BA, Wallace RJ. A novel gene, *erm(41)*, confers inducible macrolide resistance to clinical isolates of *Mycobacterium abscessus* but is absent from *Mycobacterium chelonae*. *Antimicrob Agents Chemother* 2009 ; 53 : 1367-76.
19. Kotra LP, Haddad J, Mobashery S. Aminoglycosides: perspectives on mechanisms of action and resistance and strategies to counter resistance. *Antimicrob Agents Chemother* 2000 ; 44 : 3249-56.
20. Chopra I, Roberts M. Tetracycline antibiotics: Mode of action, applications, molecular biology, and epidemiology of bacterial resistance. *Microbiol Mol Biol Rev* 2001 ; 65 : 232-60.
21. Schedlbauer A, Kaminishi T, Ochoa-Lizarralde B, et al. Structural characterization of an alternative mode of tigeicycline binding to the bacterial ribosome. *Antimicrob Agents Chemother* 2015 ; 59 : 2849-54.
22. Kremer L, Besra G, Brennan P, et al. Le lipoarabinomannane : structure et fonctions d'un glycolipide impliqué dans la pathogénie tuberculeuse. *Med Sci* 1999 ; 15 : 842-50.
23. Brennan PJ, Nikaido H. The envelope of mycobacteria. *Annu Rev Biochem* 1995 ; 4 : 29-63.
24. Viljoen A, Dubois V, Girard-Misguich F, et al. The diverse family of MmpL transporters in mycobacteria: from regulation to antimicrobial developments: MmpL structure and diversity in mycobacteria. *Mol Microbiol* 2017 ; 104 : 889-904.
25. Richard M, Gutiérrez AV, Viljoen A, et al. Mutations in the MAB\_2299c TetR regulator confer cross-resistance to clofazimine and bedaquiline in *Mycobacterium abscessus*. *Antimicrob Agents Chemother* 2019 ; 63 : e01316-18.
26. Ye M, Xu L, Zou Y, et al. Molecular analysis of linezolid-resistant clinical isolates of *Mycobacterium abscessus*. *Antimicrob Agents Chemother* 2018 ; 63 : e01842-18.
27. Halloum I, Viljoen A, Khanna V, et al. Resistance to thiacetazone derivatives active against *Mycobacterium abscessus* involves mutations in the MmpL5 transcriptional repressor MAB\_4384. *Antimicrob Agents Chemother* 2017 ; 61 : e02509-16.
28. Vianna JS, Ramis IB, Bierhals D, et al. Tetrahydropyridine derivative as efflux inhibitor in *Mycobacterium abscessus*. *J Glob Antimicrob Resist* 2019 ; 17 : 296-9.
29. Soroka D, Dubee V, Soulier-Escrihueta O, et al. Characterization of broad-spectrum *Mycobacterium abscessus* class A- $\beta$ -lactamase. *J Antimicrob Chemother* 2014 ; 69 : 691-6.
30. Dubee V, Bernut A, Cortes M, et al.  $\beta$ -Lactamase inhibition by avibactam in *Mycobacterium abscessus*. *J Antimicrob Chemother* 2015 ; 70 : 1051-8.
31. Rominski A, Selchow P, Becker K, et al. Elucidation of *Mycobacterium abscessus* aminoglycoside and capreomycin resistance by targeted deletion of three putative resistance genes. *J Antimicrob Chemother* 2017 ; 72 : 2191-2200.
32. Ung KL, Alsarraf HMAB, Olieric V, et al. Crystal structure of the aminoglycosides N-acetyltransferase Eis2 from *Mycobacterium abscessus*. *FEBS J* 2019 ; 286 : 4342-55.
33. Dal Molin M, Gut M, Rominski A, et al. Molecular mechanisms of intrinsic streptomycin resistance in *Mycobacterium abscessus*. *Antimicrob Agents Chemother* 2017 ; 62 : e01427-17.



**Annexe 2 :****“Silencing essential gene expression in *Mycobacterium abscessus* during infection”,**

Yves-Marie Boudehen, John Jairo Aguilera-Correa, Matthéo Alcaraz et Laurent Kremer. *Microbiology Spectrum*, 2023.

1 **Silencing essential gene expression in *Mycobacterium abscessus* during infection**

2  
3 Yves-Marie Boudehen<sup>1</sup>, Yara Tasrini<sup>1</sup>, John Jairo Aguilera-Correa<sup>1</sup>, Matthéo Alcaraz<sup>1</sup>,  
4 and Laurent Kremer<sup>1,2,\*</sup>

5  
6  
7 <sup>1</sup>Centre National de la Recherche Scientifique UMR 9004, Institut de Recherche en Infectiologie de  
8 Montpellier (IRIM), Université de Montpellier, 1919 route de Mende, 34293, Montpellier, France.

9 <sup>2</sup>INSERM, IRIM, Montpellier, France.

10  
11  
12 \*Corresponding author: Laurent Kremer; Tel: (+33) 4 34 35 94 47; E-mail:  
13 [laurent.kremer@irim.cnrs.fr](mailto:laurent.kremer@irim.cnrs.fr)

14  
15  
16  
17  
18  
19 **Running title:** Essential gene knock-down in *M. abscessus*

20  
21 **Keywords:** Tet-OFF system, gene repression, anhydrotetracycline, infection, *Mycobacterium*  
22 *abscessus*, zebrafish, MmpL3

26 **ABSTRACT**

27 *Mycobacterium abscessus* is a multi-drug resistant non-tuberculous mycobacterial species causing  
28 tuberculosis-like lung infections. The functional characterization of the extensive repertoire of  
29 genes encoding virulence factors and drug targets has been largely restricted by the lack of  
30 powerful genetic tools. In this study, we evaluated the performances of a Tet-OFF system,  
31 previously optimized for *Mycobacterium tuberculosis* and *Mycobacterium smegmatis*.  
32 Fluorescence reporter *M. abscessus* strains were developed where mCherry was under the control  
33 of the Tet-OFF regulatory system on an integrative plasmid. The addition of anhydrotetracycline  
34 (ATc) correlated with a decrease in fluorescence intensity not only in solid and broth medium but  
35 also in colony-biofilms, for both smooth and rough variants of *M. abscessus*. Next, unmarked  
36 *mmpL3* conditional knock-down mutants were engineered in both smooth and rough *M.*  
37 *abscessus*. Biochemical studies indicated that the addition of ATc was associated with a dose-  
38 dependent decrease in i) the production of the MmpL3 protein, ii) the biosynthesis of trehalose  
39 dimycolate and mycolylated arabinogalactan, iii) bacterial viability on agar and liquid medium as  
40 well as in biofilms. Importantly, intravenous injection of ATc in zebrafish embryos infected with  
41 the rough *mmpL3* conditional mutant impeded bacterial growth and correlated with a significant  
42 gain in embryo survival. These results suggest that *mmpL3* is essential for *M. abscessus* growth *in*  
43 *vitro* and in the infected host, thus validating MmpL3 as an attractive drug target. Together, this  
44 study demonstrates the potential of ATc-dependent repression to modulate the expression of *M.*  
45 *abscessus* genes in the infected host.

46

47 **IMPORTANCE**

48 *Mycobacterium abscessus* represents the most common rapidly-growing mycobacterial pathogen  
49 in cystic fibrosis and is extremely difficult to eradicate. Essential genes are required for growth,  
50 often participate in pathogenesis, and encode valid drug targets for further chemotherapeutic  
51 developments. However, assessing the function of essential genes in *M. abscessus* remains  
52 challenging, due to the limited spectrum of efficient genetic tools. Herein, we generated a Tet-  
53 OFF-based system allowing to knock-down the expression of *mmpL3*, encoding the mycolic acid  
54 transporter in mycobacteria. Using this conditional mutant, we confirm the essentiality of *mmpL3*

55 in planktonic cultures, in biofilms and during infection in zebrafish embryos. Thus, in this study, we  
56 developed a robust and reliable method to silence the expression of any *M. abscessus* gene during  
57 host infection.

58

## 59 **INTRODUCTION**

60 *Mycobacterium abscessus* is a non-tuberculous mycobacterium responsible for a large array of  
61 human diseases such as skin and soft tissue infections, disseminated disease or chronic lung  
62 infections (1). It represents also an important pathogen in cystic fibrosis (CF) patients where it  
63 colonizes the lungs, and is often associated with a more rapid decline in pulmonary function (2).  
64 *M. abscessus* can also be associated with biomaterial-related infections, where the main  
65 pathological mechanism involves biofilm formation (3, 4), a feature also reported in CF patients  
66 (5). Biofilm formation contributes also to bacterial persistence in harsh environments (6),  
67 rendering eradication extremely challenging.

68 *M. abscessus* can exist as two different phenotypes, either displaying a smooth (S) or a rough  
69 (R) colony morphotype, typified by the presence or absence of cell surface glycopeptidolipids  
70 (GPL), respectively (7–11). These two variants significantly differ in their virulence potential with  
71 the R strain demonstrating a more pathogenic and aggressive behaviour in mice (12), zebrafish (7–  
72 9) and CF patients (13). *M. abscessus* pulmonary diseases are very difficult to treat, owing to the  
73 intrinsic resistance of this pathogen to most antimicrobials, irrespective of the morphotype (1, 14).  
74 Thus, new chemical entities are urgently needed to populate the *M. abscessus* drug pipeline. This  
75 has recently stimulated *M. abscessus* drug discovery by prioritizing screening of advanced  
76 tuberculosis-active compounds for anti-*M. abscessus* activity (15), among which an inhibitor of the  
77 mycolic acid transporter MmpL3 has been identified (16).

78 Essential genes are central to the activity of most antibacterial agents and are among the most  
79 attractive targets for new therapeutic developments. By definition, essential genes are key players  
80 in bacterial growth and/or infection. While their biological activities remain very difficult to  
81 investigate, this can be achieved through the development of genetic tools permitting to silence  
82 gene expression and to generate conditional knock-down mutants. Gene manipulation has been  
83 widely developed during these last two decades, mainly in *M. smegmatis* and *M. tuberculosis*,

84 through the generation of knock-out mutants and the development of regulated expression  
85 systems, which have been instrumental to our understanding of pathogenic mechanisms and to  
86 demonstrate the essentiality of genes encoding drug targets. However, functional genomics tools  
87 are limited in *M. abscessus*, with mutagenesis tools developed in other species often proving to be  
88 challenging to adopt in *M. abscessus* (17, 18). Despite these difficulties, recent studies have  
89 reported the successful use of CRISPR/Cas-based systems to inducibly silence the expression of  
90 targeted genes in *M. abscessus* (19). A previous study has evaluated the potential interest of a  
91 conditional gene expression approach using the TetR/PipOFF system, allowing to generate a  
92 *fadD32* knock-down mutant in both S and R variants of *M. abscessus* (20). While these systems  
93 have allowed studying the effect of gene down-regulation *in vitro*, they have not been exploited to  
94 investigate the effect of gene silencing in *M. abscessus* during the infection process.

95 TetR-based systems have been widely used in mycobacteria to modulate gene expression and  
96 designed either to induce (Tet-ON) or repress (Tet-OFF) gene expression in the presence of  
97 anhydrotetracycline (ATc) (21–23). That ATc crosses biological membranes allows regulating gene  
98 expression in *M. tuberculosis*-infected cells (21) and in infected mice (24). Whereas similar  
99 regulatory systems are applicable to *M. abscessus* growing either *in vitro* or in the host remains to  
100 be addressed. Herein, a Tet-OFF switch in which transcription of the target gene is turned off by  
101 the addition of ATc, previously optimized for *M. tuberculosis* and *M. smegmatis* (22), was  
102 implemented for use in *M. abscessus* S and R variants. The design of reporter strains in which a  
103 fluorescence marker was placed under the control of the Tet-OFF regulatory system was  
104 successfully used to demonstrate an ATc-dependent reduction of fluorescence intensity, on agar  
105 plates, in planktonic cultures and in colony-biofilms. Subsequently, *mmpL3* conditional mutants  
106 were engineered to assess the essentiality of *mmpL3* in *M. abscessus in vitro*, in colony-biofilms as  
107 well as in infected zebrafish embryos.

108

## 109 **RESULTS**

### 110 **Tet-OFF system-mediated mCherry repression is effective in *M. abscessus*.**

111 Tet systems have originally been developed for modulating gene expression in mycobacteria (23).  
112 To address whether this regulatory system is amenable for use *in M. abscessus*, we first



113 constructed a vector derived from the integrative pMV306 where the *mCherry* gene was cloned  
114 downstream of the *tetO*-4C5G operator region, which is itself under the control of the T38  
115 repressor (25), yielding the pMV306-TetOFF-mCherry. Repression of transcription is mediated by  
116 the addition of ATc, which binds to T38, allowing the T38-ATc complex to recognize the operator  
117 region, subsequently blocking transcription of the *mCherry* gene (**Fig. 1A**). This *mCherry*  
118 repressible plasmid was first introduced into the smooth (S) variant of *M. abscessus* CIP104536<sup>T</sup>.  
119 Growth of the parental (designated CIP S) and the transformed (designated CIP S::*tetOFF-mCherry*)  
120 strains was monitored in the presence of a wide range of ATc concentrations (50 to 1000 ng/mL).  
121 **Fig. 1B** shows that the presence of ATc did not alter bacterial growth, even at the highest  
122 concentration tested (1000 ng/mL). Consecutively, the mCherry expression level was assessed by  
123 measuring the fluorescence intensity of the cultures exposed to the various ATc doses for 6, 24, 48  
124 and 72 hrs (**Fig. 1C**). A dose-dependent reduction in fluorescence intensity was particularly evident  
125 from 24 hrs of incubation with ATc. The median repression rates were 87, 83, 88, 84, and 88% at 6  
126 hrs and 38, 55, 63, 69, and 77% at 24 hrs for 50, 100, 200, 500 and 1000 ng/mL ATc, respectively.  
127 However, longer exposure times to ATc did not further reduce fluorescence intensity, presumably  
128 because the half-life of ATc is around 20 hrs (26).

### 129 **Construction of a dual fluorescent Tet-OFF reporter strain.**

130 To simultaneously follow mycobacterial growth and monitor gene repression in more complex  
131 situations, the *mWasabi* coding sequence placed under the control of the constitutive promoter  
132 P<sub>left\*</sub> (27) was introduced in the pMV306-TetOFF-mCherry (**Fig. 2A**). Following transformation into  
133 the S and R variants of *M. abscessus*, the expression of mWasabi and mCherry was determined by  
134 spotting bacterial cultures on LB agar containing ATc (50, 200, 500, 1000 ng/mL). While bacterial  
135 spots exhibited both red and green fluorescence in the absence of ATc (**Fig. 2B and**  
136 **Supplementary Fig. 1A**), the addition of ATc into the medium was associated with a strong  
137 decrease of red fluorescence, without interfering with green signal. This confirms the ATc-  
138 dependent repression of mCherry expression and the constitutive production of mWasabi in both  
139 S and R variants on standard agar plates.

140 While only the R variant has a high propensity to aggregate *in vitro* and forms serpentine  
141 cords (7, 11), both S and R variants can produce biofilms under particular growth conditions.

142 Biofilms are known to contribute to bacterial persistence and are more tolerant antibacterial  
143 agents (28). We thus monitored colony-biofilm formation (29) using an experimental protocol  
144 illustrated in **Fig. 2C**, based on the rapid quantification of both green and red fluorescence levels.  
145 This approach allowed to determine the level of ATc penetration (reflected by the decline in  
146 mCherry expression) in these biofilm structures over time, while mWasabi expression remained  
147 unaffected by ATc (**Fig. 2D**). Monitoring mWasabi fluorescence indicated that the S variant grew  
148 horizontally and vertically (**Fig. 2E**), which is mirrored by the estimated colony volume for each  
149 concentration of ATc tested (**Fig. 2F**). In contrast, drop in mCherry fluorescence was ATc- and time-  
150 dependent (**Fig. 2G**) with an optimal decrease in mCherry expression observed on day 7 (**Fig. 2H**).  
151 mCherry expression in S biofilms was negatively correlated with the ATc concentration from day 3  
152 to day 7 (**Fig. 2I**) ( $\rho=-0.5486$ ,  $p\text{-value}=0.0184$  for day 3;  $\rho=-0.7744$ ,  $p\text{-value}=0.0002$  for day 5; and  
153  $\rho=-0.9142$ ,  $p\text{-value} < 0.0001$  for day 7). In addition, mCherry levels were also observed on cross-  
154 sections of the height of S biofilms (**Fig. 2J**). Quantification indicates that fluorescence intensity  
155 units (FIU) decreased along the whole height in the presence of increasing ATc doses (**Fig. 2K** and  
156 **2L**).

157 Assessing the evolution of fluorescence intensity in the R strain carrying the dual reporter Tet-  
158 OFF construct, showed that this strain grew mainly horizontally, as compared to the S strain  
159 (**Supplementary Fig. 1B, 1C and Fig. 2C**). Growth was also determined by estimating the colony-  
160 biofilm volume for each tested concentration of ATc over time (**Supplementary Fig. 1D**). The red  
161 fluorescence did show an ATc- and time-dependence (**Supplementary Fig. 1E**). Optimal mCherry  
162 fluorescence decrease was observed at day 7 (**Supplementary Fig. 1F**). The mCherry expression  
163 showed a negative correlation with the ATc concentration at days 3, 5 and 7 (**Supplementary Fig.**  
164 **1G**) ( $\rho=-0.6113$ ,  $p\text{-value}=0.0070$  for day 5; and  $\rho=-0.732$ ,  $p\text{-value}=0.0005$  for day 7).

165

### 166 **Generation and functional validation of an *mmpL3* conditional knock-down mutant.**

167 *MmpL3* conditional mutants using the Tet system were successfully used to demonstrate *mmpL3*  
168 gene essentiality in *M. tuberculosis* ( $\Delta Rv0206c\text{-}mmpL3^{Mtb}$  using the Tet-OFF system) (30) as well as  
169 in *M. smegmatis* ( $\Delta MSMEG0250\text{-}mmpL3^{Msm}$  using Tet-ON system) (31), implying that *MmpL3*  
170 represents an attractive pharmacological target in these species. Subsequent work from various

171 groups identified a wide panel of chemical entities inhibiting MmpL3 in *M. abscessus* (16, 32–36),  
172 although the essentiality of *mmpL3* in *M. abscessus* remains to be established. To do so, the  
173 *mCherry* coding sequence was replaced by a HA-tagged *mmpL3* version into the dual reporter  
174 plasmid, generating the pMV306-TetOFF-*mmpL3*-HA (**Fig. 3A**) and introduced in the wild-type *M.*  
175 *abscessus* S strain. This merodiploid strain was then used to delete the endogenous *mmpL3* gene  
176 (**Fig. 3B**), resulting in a mutant whereby the unique copy of *mmpL3* was under the control of the  
177 Tet-OFF regulatory system. This conditional mutant was designated S  $\Delta$ *mmpL3*::c while the  
178 corresponding mutant in the R background was designated R  $\Delta$ *mmpL3*::c. Essentiality of *mmpL3*  
179 was next investigated by spotting culture droplets of the conditional knock-down mutants onto  
180 agar plates containing range concentrations of ATc. In absence of ATc, the growth of S  $\Delta$ *mmpL3*::c  
181 and R  $\Delta$ *mmpL3*::c strains were similar to their corresponding parental strains (**Fig. 3C and**  
182 **Supplementary Fig. 2A and 2C**). Pronounced growth inhibition was observed in presence of 50  
183 ng/mL ATc, as evidenced by the lack of colonies at the  $10^{-2}$  and  $10^{-3}$  dilutions. At 200 ng/mL ATc  
184 (and higher concentrations), no colonies grew at the  $10^{-1}$  dilution and only residual growth was  
185 observed in the undiluted spots. This indicates that *M. abscessus* is unable to grow upon *mmpL3*  
186 transcriptional repression and suggests that *mmpL3* is essential for *in vitro* growth. These results  
187 were also confirmed in planktonic cultures for both S and R conditional knock-down mutants  
188 exposed for 6 days to increasing ATc concentrations (**Fig. 3D and Supplementary Fig. 2B**). The  
189 planktonic growth showed a negative correlation with the concentration of ATc from day 2  
190 onwards for the S variant ( $\rho=-0.576$ , p-value <0.0001 for day 2;  $\rho=-0.631$ , p-value <0.0001 for  
191 day 3;  $\rho=-0.743$ , p-value <0.0001 for day 4;  $\rho=-0.819$ , p-value <0.0001 for day 5; and  $\rho=-0.824$ ,  
192 p-value <0.0001 for day 6). Similar results were also observed in the R variant ( $\rho=-0.637$ , p-value  
193 <0.0001 or day 2;  $\rho=-0.850$ , p-value <0.0001 for day 3;  $\rho=-0.778$ , p-value <0.0001 for day 4;  $\rho$   
194  $=-0.579$ , p-value <0.0001 for day 5; and  $\rho=-0.321$ , p-value <0.0001 for day 6).

195 Transcriptional repression of *mmpL3*-HA by ATc was next assessed at the protein level by  
196 Western blotting using anti-HA antibodies. MmpL3-HA production declined in an ATc  
197 concentration-dependent manner ( $\rho=-1$ , p-value=0.0028). In the presence of 1000 ng/mL ATc,  
198 MmpL3-HA expression was almost completely abolished, while expression of the antigen 85  
199 (Ag85) remains stable (**Fig. 3E**). Because, MmpL3 transports trehalose monomycolate (TMM)

200 across the inner membrane, where it is used as a substrate by the Ag85 complex to convert TMM  
201 into trehalose dimycolate (TDM) and to esterify arabinogalactan (31, 37), we next investigated the  
202 effect of ATc-mediated loss of MmpL3 production on the synthesis the cell wall lipids. <sup>14</sup>C-acetate  
203 labelled cultures were treated with ATc and apolar lipids were extracted and separated by thin  
204 layer chromatography. **Fig. 3F (left panel)** shows a dose-dependent inhibition of TDM synthesis,  
205 which was nearly abolished in the presence of 1000 ng/mL ATc in *S ΔmmpL3::c* while remaining  
206 unaltered in the parental *S* progenitor. The effect of TDM synthesis inhibition in the ATc-mediated  
207 *mmpL3* knock-down mutant was comparable to chemical inhibition of MmpL3 in the wild-type *S*  
208 strain using the indole-2-carboxamide compound 12 (Cpd12), a known MmpL3 inhibitor (32). As  
209 expected, exposure to ATc of the *mmpL3* knock-down mutant, but not of the parental *S* strain,  
210 resulted in reduced mycolylated-arabinogalactan levels, similarly to the treatment with compound  
211 12 (**Fig. 3F, right panel**). Quantifications of the ATc-dependent decrease in TDM and AG-bound  
212 mycolic acid levels in *S ΔmmpL3::c* are shown in **Fig. 3G**.

213

#### 214 **Effect of *mmpL3* knock-down in rough colony-biofilms.**

215 R colony-biofilms of the *mmpL3* conditional mutant showed an ATc-dependent growth and size  
216 phenotype. The inhibitory effect of ATc is directly reflected by the colony diameter and particularly  
217 evident at day 7 (**Supplementary Fig. 3A**). Indeed, untreated biofilm present a maximal diameter  
218 of ~1500 pixels whereas the diameter of the biofilm treated with 1000 ng/mL ATc was ~1200  
219 pixels (**Supplementary Fig. 3B**). The biofilm growth showed a negative correlation with the  
220 concentration of ATc between day 3 and 7 (**Supplementary Fig. 3C**) ( $\rho=-0.5737$ , p-value =0.0128  
221 for day 3;  $\rho=-0.749$ , p-value =0.0003 for day 5; and  $\rho=-0.826$ , p-value <0.0001 for day 7). The  
222 number of CFU/membrane at day 7 is negatively correlated with the concentration of ATc ( $\rho$   
223 =-0.7054, p-value=0.0011) (**Supplementary Fig. 3D**). Moreover, the colony density at day 7  
224 presents a moderate negative correlation with the concentration of ATc ( $\rho=-0.5988$ , p-  
225 value=0.0086) (**Supplementary Fig. 3E**). However, this effect was not observed with the  
226 *S ΔmmpL3::c* mutant (data not shown).

227

#### 228 ***MmpL3* knock-down impairs bacterial growth and pathogenicity of *M. abscessus* in zebrafish.**

229 Zebrafish embryos have been previously exploited to study the virulence of *M. abscessus* (7, 38,  
230 39). Here, we used this model to determine if we could trigger *mmpL3* knock-down *in vivo* by  
231 treating intravenously infected embryos with ATc to assess the effect on the infection outcome  
232 **(Figure 4A)**. While treatment of zebrafish embryos with compounds is often done by simply adding  
233 the compound to the embryo water, our preliminary data indicate it is more reproducible to  
234 deliver the compound by microinjection instead of immersion (data not shown). Therefore, we  
235 first evaluated the toxicity of ATc microinjection at 2dpf using an increasing dose ranging from 1  
236 ng to 100 ng and monitored treated embryos for 11 days. We found no toxicity signs in embryos  
237 treated from 1 to 10 ng of ATc, as opposed to embryos treated with 20 ng, which started to exhibit  
238 toxicity signs increasing with 50 ng and 100 ng **(Supplementary Fig. 4, Table S4)**. We, thus, opted  
239 for 10 ng of ATc which was the highest safest dose. We then injected 30 hours post-fertilization  
240 (hpf) embryos in the caudal vein with  $355 \pm 18$  CFU of R  $\Delta mmpL3::c$ , which were subsequently  
241 treated at 1 day post-infection (dpi) with 10 ng ATc to repress the expression of *mmpL3* **(Fig. 4A)**.  
242 Daily monitoring of embryo survival showed an increase in mortality over time in the non-treated  
243 group (53% mortality at 12 dpi) as expected, while only 5% of embryos treated with ATc  
244 succumbed to the infection **(Fig. 4B)**. This strongly suggests that the temporal control of *mmpL3*  
245 repression is working *in vivo*. In agreement with the reduced embryo mortality, the bacterial  
246 burden from ATc-treated embryos was linearly decreasing overtime ( $r=-0.9105$ ;  $p\text{-value}<0.0001$ ) at  
247 a rate of  $-0.8418 \log_{10}$  per day ( $p\text{-value}<0.0001$ ), as opposed to the non-treated control group in  
248 which the bacterial burden was linearly increasing over time ( $r=0.9340$ ;  $p\text{-value}<0.0001$ ) at a rate  
249 of  $0.9674 \log_{10}$  per day ( $p\text{-value}<0.0001$ ) **(Fig. 4C)**. Moreover, to corroborate the CFU results, we  
250 took advantage of the transparency of the embryos to monitor the evolution of the mWasabi  
251 fluorescence which reflects the bacterial burden. Real-time imaging of embryos clearly showed in  
252 one hand, an increase of green fluorescence overtime in untreated embryos characterized with  
253 the presence of big infection foci **(Fig. 4D left panels)**, and in another hand, a reduction of green  
254 fluorescence over time between 1 day post-treatment (dpt) and 3dpt in treated embryos with only  
255 small residual infection foci persisting **(Fig. 4D right panels)**.

256 Overall, these results correlate with the *in vitro* growth inhibition upon ATc treatment, confirm  
257 the use of the Tet-OFF system to modulate gene expression in *M. abscessus* in the infected host

258 and support the essential character of MmpL3 as a valuable drug target for the treatment of *M.*  
259 *abscessus* diseases.

260

261

## 262 **DISCUSSION**

263 Deciphering the importance and biological functions of essential determinants in *M. abscessus*  
264 remains challenging, due to the lack of relevant genetic systems to knock-down gene expression,  
265 despite the recent development of CRISPR/Cas-based systems to inducibly silence the expression  
266 of targeted genes in this species (19). In this study, we provided evidence that the Tet-OFF  
267 regulatory system is applicable to *M. abscessus* growing *in vitro* as well as in the infected host.  
268 First, we demonstrated that transcription of the target gene encoding either a fluorescent marker  
269 is turned off in *M. abscessus* by the addition of ATc, as previously shown for *M. tuberculosis* and  
270 *M. smegmatis* (22). The ATc-dependent reduction of fluorescence intensity was directly observed  
271 on bacterial colonies and quantified in broth cultures as well as in colony-biofilms, thus validating  
272 the efficacy and robustness of the method in *M. abscessus*. In addition, we showed that the Tet-  
273 OFF silencing system is functional in both S and R variants, which responded similarly to ATc, thus  
274 indicating that the presence of the outermost GPL layer in the S form did not play a major role in  
275 preventing/limiting the entry of ATc inside the bacilli. This prompted us to design an *mmpL3*  
276 conditional mutant in S and R variants to assess the essentiality of *mmpL3* in *M. abscessus*. In *in*  
277 *vitro* experiments, we found that growth inhibition was ATc dose-dependent, which could be  
278 directly linked to the decreased production of the MmpL3 protein, translating into the blockage of  
279 TMM transport. The lack of TMM export was related to reduced levels of AG mycolylation and  
280 reduced pools of TDM, an expected phenotype relying on the fact that TMM serves as a substrate  
281 for the Ag85 mycolyltransferases. We note that, even at the highest concentrations of ATc tested  
282 (500 and 1000 ng/mL), both S  $\Delta mmpL3::c$  and R  $\Delta mmpL3::c$  grew very slowly in liquid media,  
283 presumably indicating that the promoter is leaky, as judged by the low levels of MmpL3 produced  
284 under these repressive conditions, which translates into a partial inhibition of TDM production and  
285 AG mycolylation. Nevertheless, despite the presence of residual levels of MmpL3 upon ATc-  
286 induced repression, these results highlight the vulnerability of MmpL3 and the ensuing  
287 implications for future chemotherapeutic developments for *M. abscessus* infections, as  
288 exemplified by the wide list of chemotypes inhibiting this transporter in *M. abscessus* (16, 32–36).  
289 Recent sequencing of a saturated transposon library in *M. abscessus* provided a comprehensive  
290 prediction of essential genes in this mycobacterial species (40). However, these essential

291 predictions require now further experimental confirmation. Typically, the Tet-OFF system reported  
292 here can be extended for conditional gene modulation of any essential gene in *M. abscessus*. This  
293 will be particularly useful to confirm these predictions and investigating whether inhibiting  
294 essential proteins can provide therapeutic benefit, particularly warranted in the context of  
295 multiple drug resistance of *M. abscessus* and unmet medical need to control/eradicate *M.*  
296 *abscessus* infections (1, 14).

297 Biofilm development is one crucial pathogenicity factor in *M. abscessus* (41). Here, we  
298 demonstrated that the TetOFF system may be applied to the recently developed *M. abscessus*  
299 colony-biofilm model (42). This biofilm model consists of inducing bacterial colony growth onto a  
300 polycarbonate membrane laying on an agar plate (43), for which nutritional or antibiotic  
301 supplementation can be modified at will (29). We show here that ATc not only penetrates the  
302 different mycobacterial layers that compose the colony-biofilms but that it can also modulate the  
303 expression of mCherry. These results are in line with a previous study reporting the enhanced  
304 accumulation of tetracycline in bacterial biofilms (44). The overexpression of hundreds of genes in  
305 *M. abscessus* biofilms has recently been documented in both minimal medium (45) and synthetic  
306 CF medium (46). Our results support the use of the Tet-OFF system for switching off these genes,  
307 providing a valuable approach to study the consequences of silencing these genes during biofilm  
308 development. Of note, the colony-biofilm model reported here does not recapitulate the cellular  
309 characteristics with respect to cell-substratum and cell-cell adhesion found for instance in  
310 mycobacterial pellicles growing at the liquid/air interface. Therefore, the differences observed in  
311 S and R colony-biofilms may result from the absence of GPL in the R morphotype since their  
312 presence, in *M. smegmatis*, favors biofilm formation by facilitating cellular attachment to the  
313 substratum, sliding motility and intercellular aggregation (47, 48). To illustrate the feasibility of  
314 this method, we monitored the effect of silencing *mmpL3* gene expression during *M. abscessus*  
315 colony-biofilm development using R  $\Delta mmpL3::c$ . Knocking down *mmpL3* gene expression reduced  
316 biofilm growth in an ATc-concentration-dependent manner that could be corroborated at the level  
317 of the relative colony volume over time. Interestingly, the negative correlation between density  
318 (CFU/colony volume) and ATc concentration at day 7 points to a decrease in mycobacterial  
319 viability within the biofilm. These results are reminiscent of the bactericidal effect of an *N*-



320 substituted indolemethylamine (IMA6) targeting MmpL3, previously described on nutrient-starved  
321 and oxygen-depleted non-replicating *M. abscessus* biofilm (49).

322 A major finding of this work relies on the possibility to decrease the transcription level of *M.*  
323 *abscessus* genes during systemic infection in zebrafish embryos and visualize the effect of gene  
324 silencing at a spatiotemporal level in a living vertebrate. In the case of infection with R  $\Delta mmpL3::c$ ,  
325 intravenous injection of ATc at 1 dpi resulted in a rapid and progressive reduction in the bacterial  
326 loads (quantified by determining the CFU over time) and infection foci (observed by fluorescence  
327 imaging of whole embryos). This significantly rescued the survival of embryos, which barely  
328 showed signs of pathology, as compared with the non-treated group of animals. Strikingly, the  
329 phenotypes observed here in zebrafish using the inducible *mmpL3* silencing system were very  
330 similar to those observed following chemical inhibition when exposing *M. abscessus*-infected  
331 embryos to MmpL3 inhibitors, such as PIPD1 (16) or benzimidazole derivatives (34). Overall, these  
332 results are in line with previous work demonstrating that MmpL3 is required for the replication  
333 and viability of *M. tuberculosis*, both under standard laboratory growth conditions and during the  
334 acute and chronic phases of infection in mice (50). While zebrafish embryos recapitulate the acute  
335 stages of *M. abscessus* infection in the sole context of innate immunity (7, 51), adult fish, where  
336 both innate and adaptive immunity are operative, have been shown to be useful to describe *M.*  
337 *abscessus* chronic infection (52). Future studies should address the applicability of ATc-induced  
338 gene silencing in adult zebrafish to investigate the biological role of both essential and non-  
339 essential genes in *M. abscessus* persistence and chronic infections.

340 To conclude, we have described a robust and stable genetic system to down-regulate genes in  
341 *M. abscessus* under *in vitro* laboratory conditions and our data highlight MmpL3 as an essential  
342 lipid transporter in *M. abscessus*, validating MmpL3 as target of therapeutic interest. This provides  
343 a strong incentive for the subsequent developments of new or improved MmpL3 inhibitors in the  
344 fight against *M. abscessus* pulmonary diseases.

345

346

347 **MATERIALS AND METHODS**

348 **Bacterial strains, plasmids and primers**

349 Strains, plasmids and primers are listed in Table S1, Table S2, and Table S3, respectively.

350

351 **Culture conditions**

352 *Escherichia coli* strains Stellar<sup>TM</sup> (Takara bio) were grown at 37°C in Luria-Bertini (LB) medium  
353 (Difco) or on LB agar (Roth) plates supplemented with kanamycin (50 µg/mL), hygromycin (200  
354 µg/mL) or zeocin (50 µg/mL), when required. Smooth (S) and rough (R) variants of *M. abscessus*  
355 subsp. *abscessus* CIP104536<sup>T</sup> (53) and related mutants were grown at 37 °C in Middlebrook 7H9  
356 broth (BD Difco) supplemented with 10% oleic acid, albumin, dextrose, catalase (OADC  
357 enrichment), 0.2% glycerol and 0.025% Tyloxapol (Sigma-Aldrich) ; Mueller Hinton broth  
358 (Millipore) ; in Sauton liquid medium (4 g/L asparagine, 0.5 g/L K<sub>2</sub>HPO<sub>4</sub>, 0.5 g/L MgSO<sub>4</sub>, 2g/L citric  
359 acid, 60 g/L glycerol, 0.05 g/L ferric ammonium citrate, 0.0002% ZnSO<sub>4</sub>, adjusted to pH 7.2 with  
360 NaOH) ; on Middlebrook 7H10 agar supplemented with OADC (7H10<sup>OADC</sup>) or on LB agar (Roth)  
361 plates containing the appropriate antibiotics. When required kanamycin (250 µg/mL), hygromycin  
362 (1 mg/mL) or zeocin (25 µg/mL) or various concentrations of anhydrotetracycline (ATc; Sigma-  
363 Aldrich) (0, 50, 100, 200, 500, 1000 ng/mL) were added to the culture media.

364

365 **Construction of Tet-OFF derived vectors**

366 To control repression of gene expression, we adapted a repressible expression vector based on the  
367 Tet-OFF system, reported previously (23, 25). pEN41A-T38S38 and pEN12A-P766 plasmids were  
368 kindly provided By D. Schnappinger (Addgene plasmid # 9524; <http://n2t.net/addgene:49524>;  
369 RRID: Addgene\_49524). Briefly, the T38 sequences (encoded by *tetR38* with the *Ptb38* promoter  
370 sequence), the *tet* operator sequence (*tetO*-4C5G) and genes of interest – *mCherry*, *mmpL3*  
371 (*MAB\_4508*) fused to an HA-tag – were PCR-amplified using the Q5<sup>®</sup> High-Fidelity DNA Polymerase  
372 (New England Biolabs) using pEN12A-P766, pEN41A-T38S38 and pGMCS-mCherry plasmids and *M.*  
373 *abscessus* genomic DNA as templates. Primers were designed to add introduce a HA-tag at the 3'  
374 end of *mmpL3*. Linear fragments were purified on agarose gels (NucleoSpin Gel and PCR Clean-up,  
375 Macherey-Nagel). Following the manufacturer's instructions, In-Fusion SNAP Assembly Master Mix

376 (Takara) reactions were performed to insert these linear fragments into the integrative pMV306  
377 (insertion at the *attL5* mycobacteriophage insertion site in the *glyV* tRNA gene). The resulting  
378 plasmids were transformed into Stellar<sup>TM</sup> competent cells (Takara Bio) then purified (NucleoSpin  
379 Plasmid, Macherey-Nagel) and verified by sequencing. Plasmids were then electroporated into the  
380 *M. abscessus* S and/or R variants. To monitor the bacteria *in vivo*, green versions of the resulting  
381 plasmids were generated by adding the *mWasabi* coding sequence under the control of the  
382 constitutive P<sub>left\*</sub> promoter using the P<sub>ciI</sub> and XbaI restriction sites. The P<sub>left\*</sub> element is a  
383 derivative from the P<sub>left</sub> promoter from mycobacteriophage L5 (54) associated with a ribosomal  
384 binding site that increases expression levels (27).

### 385 **Generation of an *mmpL3* conditional knock-down mutants**

386 The additional copy of *mmpL3* (under the control of the Tet-OFF system, described above) was  
387 first checked in the wild-type S strain by Western blotting, taking advantage of the HA-tag.  
388 Unmarked deletion of the endogenous *mmpL3* gene was performed in the merodiploid strain  
389 using strategy developed previously (55). Briefly, the pUX1-*katG-mmpL3* was designed to generate  
390 an unmarked deletion of 2982 bp (99.2%) of the open reading frame. After the two steps of  
391 selection of the homologous recombination events, the DNA junctions were PCR amplified and  
392 sequenced to confirm the proper genotype of the mutants using primers listed in Table S3 and to  
393 validate the generation of S  $\Delta mmpL3::c$ . While this strategy failed in the rough morphotype, the R  
394  $\Delta mmpL3::c$  conditional mutant was obtained by deleting the *mmpL4b* gene (*MAB\_4115c*) in S  
395  $\Delta mmpL3::c$  using the pUX1-*katG-mmpL4b*. The unmarked deletion of 2925 bp (98.7%) of the open  
396 reading frame of *mmpL4b* was confirmed by PCR amplification and sequencing. Thus, the R  
397  $\Delta mmpL3::c$  genotype corresponds to S  $\Delta mmpL3::c$ ,  $\Delta mmpL4b$ .

398

### 399 **Growth curves**

400 Potential cytotoxicity of ATc on *M. abscessus* was determined as follows. Pre-cultures in  
401 exponential phase were diluted to reach an optical density at 595 nm (OD<sub>595</sub>) of 0.05 in 15 mL of  
402 7H9 broth supplemented with 10% OADC, 0.2% glycerol and 0.025% Tyloxapol, and containing a  
403 range of ATc concentrations. Cultures were incubated at 37 °C under agitation (80 rpm). OD<sub>595</sub>  
404 measurements were performed on a daily basis for 3 days.

405 Pre-cultures of the  $\Delta mmpL3::c$  mutants in exponential phase were diluted in Mueller-Hinton broth  
406 medium to reach an initial OD<sub>595</sub> of 0.01 and dispensed in 96-well microtiter plates in the presence  
407 of increasing ATc concentrations (200  $\mu$ L/well). Plates were incubated at 37 °C without agitation  
408 and measurements were taken on a daily basis using a spectrophotometer multimode microplate  
409 reader (Tecan Spark 10M; Tecan Group Ltd., Switzerland).

410

#### 411 **Colony-biofilm model**

412 *M. abscessus* biofilms were produced based on a recently developed method (42). *M. abscessus*  
413 cultures were grown in Middlebrook 7H9 broth supplemented with OADC, 0.2% glycerol and  
414 tyloxapol (0.025%) at 37 °C and 100 rpm for 72 hrs. Cultures were centrifuged at 3,500 rpm for 5  
415 min, washed two times with sterile phosphate buffer saline (PBS) and then diluted to an OD of 0.5  
416 ( $\sim 1.5 \times 10^8$  colony-forming units (CFU)/mL). Autoclaved black, polycarbonate membranes  
417 (diameter, 25 mm; pore size 0.2  $\mu$ m, Whatman, Merck, Darmstadt, Germany) were placed on  
418 7H10<sup>OADC</sup> and inoculated with 20  $\mu$ L of the bacterial suspension. The membrane-supported  
419 biofilms were statically incubated for 48 hrs at 37 °C, transferred onto fresh 7H10<sup>OADC</sup> containing  
420 and ATc (50, 100, 200, 500, 1,000 ng/mL) and incubated at 37 °C for an additional 7 days. Every 24  
421 hrs, the membrane-supported biofilms were imaged and processed using a binocular (ZEISS Axio  
422 Zoom.V16, Zeiss, Germany) equipped with a lighting device (Zeiss HXP 200C Zeiss, Germany) at 7 $\times$   
423 zoom, detecting mWasabi and mCherry fluorescence. On biofilm fluorescence pictures, a straight  
424 line was drawn (covering all the diameter of the biofilm) and intensity fluorescence of each pixel  
425 was retrieved to draw fluorescence spectra using the ZEN 2 software (Blue Edition).

426 *MmpL3* conditional mutant biofilms were quantified by CFU counting after taking pictures.  
427 Each membrane-supported biofilm was processed for quantifying the number of CFU per  
428 membrane at day 7. Biofilms were removed from the plates with sterile clamps, deposited in a 50-  
429 mL tube containing 10 mL PBS supplemented with 0.025% tyloxapol and a mixture of 5-mm- and  
430 1-mm-diameter glass beads, vortexed for 15 s and sonicated once for the S variant and twice for  
431 the R variant. The resulting bacterial suspension was diluted in a 10-fold bank dilution and plated  
432 on LB agar. Plates were incubated at 37 °C for 4 days prior to CFU counting.

433

#### 434 **Western blotting**

435 Mycobacterial cultures were grown in Sauton's broth containing tyloxapol (0.025%) and treated or  
436 not with ATc. Bacteria were harvested, centrifuged for 10 min at 3,000 *g* at 4 °C, resuspended in  
437 cold PBS containing protease inhibitor cocktail (Sigma-Aldrich). Bacteria were lysed by the addition  
438 of 1 mm-diameter glass beads followed by four times 60 s cycles pulses at full speed in a bead-  
439 beater device (Mixer Mill MM 301, Retsch). The lysates were collected and protein concentrations  
440 assessed using the BCA Protein Assay Reagent kit (ThermoFisher Scientific), according to the  
441 manufacturer's instructions. Equal amounts of proteins (10 µg) were separated by 10% SDS-PAGE  
442 and transferred to a PVDF membrane (Immobilon®-P, Merck Millipore). Protein detection was  
443 done using rat anti-HA (1:5,000 dilution) antibodies or mouse monoclonal antibodies 32/15,  
444 recognizing the Ag85 complex, (1:10 dilution) (56). Membranes were then incubated with anti-rat  
445 or anti-mouse secondary antibodies conjugated to HRP (1:5,000). Signals were detected using HRP  
446 reaction (SuperSignal West Femto, ThermoFisher Scientific) on a ChemiDoc MP system (Bio-Rad).

447

#### 448 **Whole cell radiolabelling experiments and lipid analysis**

449 To visualize the ATc-induced changes on the lipid profile, cultures were inoculated at OD=0.01 in  
450 the presence of increasing concentrations of ATc or left untreated for 72 hrs at 37 °C under gentle  
451 agitation (100 rpm). As a control, cultures were also treated for 1 hr with the indole-2-  
452 carboxamide compound 12 (32). Subsequently, metabolic labelling of lipids was performed by  
453 adding 1 µCi/mL of [<sup>14</sup>C]acetate (56 mCi/mmol) for an additional 2 hrs at 37 °C. Cells were  
454 harvested, delipidated and further processed to analyze the different lipid fractions, as previously  
455 reported (32). The apolar lipid fraction containing TDM was separated on a one-dimensional thin  
456 layer chromatography (TLC) plate using chloroform/methanol/water (40:8:1, v/v/v). Delipidated  
457 cells were further processed to extract the mycolic acids, analyzed by TLC using petroleum  
458 ether/acetone (95:5, v/v) and exposed to reveal <sup>14</sup>C-labeled mycolic acid methyl esters (MAMEs).

459

#### 460 **Zebrafish maintenance**

461 Zebrafish (*Danio rerio*) were kept and handled in compliance with the guidelines of the European  
462 Union for handling laboratory animals and approved by the Direction Sanitaire et Vétérinaire de

463 l'Hérault for the ZEFIX-CRBM zebrafish facility (Montpellier) (registration number C-34-172-39).  
464 Handling and experiments were approved by "le ministère de l'enseignement supérieur, de la  
465 recherche et de l'innovation" under the reference APAFIS#24406-2020022815234677 V3.  
466 Experiments were conducted using the zebrafish *golden* mutants (57), raised in the ZEFIX-CRBM  
467 zebrafish facility and kept on a 12/12 hours light/dark cycle. Eggs were obtained by natural  
468 spawning, quickly bleached and incubated at 28.5 °C in Petri dishes containing E3 medium (5 mM  
469 NaCl, 0.17 mM KCl, 0.33 mM CaCl<sub>2</sub>, 0.33 mM MgSO<sub>4</sub>).

470  
471 **ATc toxicity assay in zebrafish embryos**  
472 To assess the toxicity of ATc in zebrafish, 2 dpf embryos were injected intravenously with an  
473 increasing dose of ATc ranging from 1 ng to 100 ng (n=20 embryos/dose). Embryos were placed  
474 individually in 48-well plates and monitored daily for 11 days. Clinical signs of toxicity were  
475 examined and quantified based on the following criteria: Edema, yolk opacification, swim bladder  
476 inflation, bent body, heartbeat, blood flow and response to stimuli, each scored from 0 to 2  
477 (0=absence, 1=mild, 2=severe), yielding a disease score ranging from 0 (no toxicity) to 14 (dead  
478 embryo) (**Table S4**). The dose of 10 ng was chosen for further treatments.

479  
480 **Zebrafish infection**  
481 At 24 hours post-fertilization (hpf), embryos were dechorionated manually with fine tweezers and  
482 placed in 60 mm Petri dishes containing E3 at 28.5 °C. At 30 hpf, embryos were anesthetized with  
483 0.02% buffered MS222 (Tricaine; ethyl-3-aminobenzoate methanesulfonate salt) and placed in  
484 1.5% agarose plates molded with 0.7 mm slots containing E3 supplemented with 0.02% buffered  
485 MS222. Borosilicate glass capillaries (O.D.=1 mm; I.D.=0.78 mm; 10 cm length) were pulled using a  
486 micropipette puller (Sutter instruments P-97). Needles were opened with fine forceps and loaded  
487 with 5 µL of the desired inoculum supplemented with 0.05% phenol red for microinjection  
488 visualization. Microinjection was performed as previously described (7, 39). Embryos were injected  
489 in the caudal vein with 1.5 nL of either the R  $\Delta mmpL3::c$  preparation (355 ± 18 CFU) or the PBS  
490 control. Injected embryos were then rinsed twice and transferred in 60 mm small Petri dish

491 containing embryo media at 28.5 °C. Inoculum was checked *a posteriori* by microinjecting a PBS  
492 drop and plating it on 7H10<sup>OADC</sup>.

493

#### 494 **Zebrafish ATc treatment**

495 To repress the activity of the Tet-OFF promoter upon infection, half of the embryos from both  
496 groups (control and infected) were injected at 1 day post-infection (dpi) intravenously with 10 ng  
497 of ATc (4 nL of a 2.5 mg/mL solution in PBS) and the other half with the PBS control. Embryos were  
498 rinsed twice and randomized over survival assays, CFU counts and imaging in 48-well plates  
499 individually. For survival assays, embryos were monitored daily for 11 days (n=24 per group per  
500 experiment). In the absence of a heart beat embryos were marked as dead. To quantify bacterial  
501 burden at 2 dpi-1 day post-treatment (dpt), 3dpi-2dpt and 4dpi-5dpt, 5 embryos from each group  
502 were individually disrupted in 50 µL of PBS supplemented with 0.025% of tyloxapol using pellet  
503 pestles. Lysates were mixed vigorously with 50 µL of PBS 2% Triton-X-100, sonicated for 30 s and  
504 left for 5 min at room temperature. 10 µL of 10-fold serial dilutions were plated on LB agar  
505 supplemented with zeocin (50 µg/mL) and rifampicin (15 µg/mL). Plates were kept at 37 °C for 3  
506 days until colonies were countable.

507

#### 508 **Fluorescence microscopy imaging**

509 Mycobacterial cultures (OD<sub>600</sub>=0.5) expressing fluorescent proteins were ten-fold diluted and 3 µL  
510 of each dilution were spotted on LB agar containing or not ATc and were incubated for 3 days at  
511 37 °C. Pictures of bacterial spots and biofilms expressing fluorescent proteins were taken using a  
512 binocular (ZEISS Axio Zoom.V16) equipped with a lighting device (Zeiss HXP 200C Zeiss) at 7× zoom  
513 detecting the green (mWasabi) and red (mCherry) fluorescence using ZEN 2 (Blue Edition)  
514 software.

515 For zebrafish imaging, embryos were anesthetized with 0.02% buffered MS222 and immobilized  
516 with 0.5% low melting agarose in a lateral position in the microinjection molds. Images were  
517 acquired with an EVOS™ M7000 Imaging System every 24 hrs post-ATc injection for 3 days with  
518 the Olympus™ 2X Objective PlanApo 0.08 NA and the EVOS 10x Objective 0.3NA using the EVOS™

519 Light Cube, GFP 2.0. After imaging, embryos were rinsed and transferred back the 48-well plate  
520 with fresh E3. Image processing was done using ZEISS ZEN3.7 software.

### 521 **Statistical analyses**

522 All analyses were performed using R (R Core Team, 2017) with R commander (58–60) or GraphPad  
523 Prism version 9.0.0 for Windows (GraphPad Software, San Diego, California, United States). The  
524 normality of data was evaluated using a Shapiro-Wilk test. Descriptive data are cited as median  
525 and interquartile range in case of non-normal distribution for each of the variables were  
526 calculated. Spearman's rank correlation coefficient ( $\rho$ ) was calculated to determine potential  
527 relationships between the different concentrations of ATc and the evaluated variables from each  
528 experiment. For absolute values of  $\rho$ , 0–0.19 is regarded as very weak, 0.2–0.39 as weak, 0.40–0.59  
529 as moderate, 0.6–0.79 as strong and 0.8–1 as very strong correlation.

530 Zebrafish survival assays are represented in Kaplan-Meier graphs and analysed with a Log rank  
531 test. For determination of bacterial counts, CFU were  $\log_{10}$  transformed and the significance  
532 between multiple selected groups was determined using one-way ANOVA with Šidák's Multiple  
533 Comparisons test after validating the normality of the data. A significance level *a priori* was set at  
534  $\alpha = 0.05$ . Significance is indicated as: ns, non-significant; \*  $p < 0.05$ ; \*\*  $p < 0.01$ ; \*\*\*  $p < 0.001$ ;  
535 \*\*\*\*  $p < 0.0001$  unless stated otherwise in the figure's legend.

536

### 537 **DATA AVAILABILITY**

538 All data generate in this study are available upon request.

539

### 540 **ACKNOWLEDGMENTS**

541 This project has been funded by the French National Research Agency is supported by the ANR  
542 grants 19-CE15-0012-01 (SUNLIVE) and 20-CE44-0019 (ILlome) and by the Fondation pour la  
543 Recherche Médicale (Equipe FRM EQU202103012588). We acknowledge the Ministère de  
544 l'Enseignement Supérieur, de la Recherche et de l'Innovation for funding the PhD of MA. We are  
545 grateful to M. Plays, P. Richard and C. Hamela for zebrafish husbandry and would like to thank D.  
546 Schnappinger for the generous gift of plasmids and W. Daher for helpful discussions.

547



548 **CONFLICT OF INTEREST**

549 The authors report there are no competing interests to declare.

550 **REFERENCES**

- 551 1. Johansen MD, Herrmann J-L, Kremer L. 2020. Non-tuberculous mycobacteria and the rise of  
552 *Mycobacterium abscessus*. *Nat Rev Microbiol* 18:392–407.
- 553 2. Esther CR, Esserman DA, Gilligan P, Kerr A, Noone PG. 2010. Chronic *Mycobacterium abscessus*  
554 infection and lung function decline in cystic fibrosis. *J Cyst Fibros* 9:117–123.
- 555 3. Martins N, Rodrigues CF. 2020. Biomaterial-related infections. *J Clin Med* 9:722.
- 556 4. Esteban J, García-Coca M. 2018. *Mycobacterium* biofilms. *Front Microbiol* 8:2651.
- 557 5. Hunt-Serracin AC, Parks BJ, Boll J, Boutte CC. 2019. *Mycobacterium abscessus* cells have altered  
558 antibiotic tolerance and surface glycolipids in artificial cystic fibrosis sputum medium. *Antimicrob*  
559 *Agents Chemother* 63:e02488-18.
- 560 6. Johnson LR. 2008. Microcolony and biofilm formation as a survival strategy for bacteria. *J Theor Biol*  
561 251:24–34.
- 562 7. Bernut A, Herrmann J-L, Kissa K, Dubremetz J-F, Gaillard J-L, Lutfalla G, Kremer L. 2014.  
563 *Mycobacterium abscessus* cording prevents phagocytosis and promotes abscess formation. *Proc Natl*  
564 *Acad Sci U S A* 111:E943-952.
- 565 8. Bernut A, Viljoen A, Dupont C, Sapriel G, Blaise M, Bouchier C, Brosch R, de Chastellier C, Herrmann J-  
566 L, Kremer L. 2016. Insights into the smooth-to-rough transitioning in *Mycobacterium bolletii* unravels  
567 a functional Tyr residue conserved in all mycobacterial MmpL family members. *Mol Microbiol* 99:866–  
568 883.
- 569 9. Daher W, Leclercq L-D, Johansen MD, Hamela C, Karam J, Trivelli X, Nigou J, Guérardel Y, Kremer L.  
570 2022. Glycopeptidolipid glycosylation controls surface properties and pathogenicity in *Mycobacterium*  
571 *abscessus*. *Cell Chem Biol* 29:910-924.e7.
- 572 10. Gutiérrez AV, Viljoen A, Ghigo E, Herrmann J-L, Kremer L. 2018. Glycopeptidolipids, a double-edged  
573 sword of the *Mycobacterium abscessus* complex. *Front Microbiol* 9:1145.

- 574 11. Howard ST, Rhoades E, Recht J, Pang X, Alsup A, Kolter R, Lyons CR, Byrd TF. 2006. Spontaneous  
575 reversion of *Mycobacterium abscessus* from a smooth to a rough morphotype is associated with  
576 reduced expression of glycopeptidolipid and reacquisition of an invasive phenotype. *Microbiology*  
577 152:1581–1590.
- 578 12. Catherinot E, Clarissou J, Etienne G, Ripoll F, Emile J-F, Daffé M, Perronne C, Soudais C, Gaillard J-L,  
579 Rottman M. 2007. Hypervirulence of a rough variant of the *Mycobacterium abscessus* type strain.  
580 *Infect Immun* 75:1055–1058.
- 581 13. Catherinot E, Roux A-L, Macheras E, Hubert D, Matmar M, Dannhoffer L, Chinet T, Morand P, Poyart  
582 C, Heym B, Rottman M, Gaillard J-L, Herrmann J-L. 2009. Acute respiratory failure involving an R  
583 variant of *Mycobacterium abscessus*. *J Clin Microbiol* 47:271–274.
- 584 14. Wu M-L, Aziz DB, Dartois V, Dick T. 2018. NTM drug discovery: status, gaps and the way forward. *Drug*  
585 *Discov Today* 23:1502–1519.
- 586 15. Ganapathy US, Dick T. 2022. Why matter matters: Fast-tracking *Mycobacterium abscessus* drug  
587 discovery. *Molecules* 27:6948.
- 588 16. Dupont C, Viljoen A, Dubar F, Blaise M, Bernut A, Pawlik A, Bouchier C, Brosch R, Guérardel Y, Lelièvre  
589 J, Ballell L, Herrmann J-L, Biot C, Kremer L. 2016. A new piperidinol derivative targeting mycolic acid  
590 transport in *Mycobacterium abscessus*. *Mol Microbiol* 101:515–529.
- 591 17. Chimukuche NM, Williams MJ. 2021. Genetic manipulation of non-tuberculosis mycobacteria. *Front*  
592 *Microbiol* 12:633510.
- 593 18. Medjahed H, Reytrat J-M. 2009. Construction of *Mycobacterium abscessus* defined glycopeptidolipid  
594 mutants: comparison of genetic tools. *Appl Environ Microbiol* 75:1331–1338.
- 595 19. Gupta R, Rohde KH. 2023. Implementation of a mycobacterial CRISPRi platform in *Mycobacterium*  
596 *abscessus* and demonstration of the essentiality of *ftsZMab*. *Tuberculosis* 138:102292.
- 597 20. Cortes M, Singh AK, Reytrat J-M, Gaillard J-L, Nassif X, Herrmann J-L. 2011. Conditional gene expression  
598 in *Mycobacterium abscessus*. *PloS One* 6:e29306.

- 599 21. Ehrt S, Guo XV, Hickey CM, Ryou M, Monteleone M, Riley LW, Schnappinger D. 2005. Controlling gene  
600 expression in mycobacteria with anhydrotetracycline and Tet repressor. *Nucleic Acids Res* 33:e21.
- 601 22. Klotzsche M, Ehrt S, Schnappinger D. 2009. Improved tetracycline repressors for gene silencing in  
602 mycobacteria. *Nucleic Acids Res* 37:1778–1788.
- 603 23. Schnappinger D, Ehrt S. 2014. Regulated expression systems for mycobacteria and their applications.  
604 *Microbiol Spectr* 2:mgm2-0018–2013.
- 605 24. Gandotra S, Schnappinger D, Monteleone M, Hillen W, Ehrt S. 2007. *In vivo* gene silencing identifies  
606 the *Mycobacterium tuberculosis* proteasome as essential for the bacteria to persist in mice. *Nat Med*  
607 13:1515–1520.
- 608 25. Kim J-H, O'Brien KM, Sharma R, Boshoff HIM, Rehren G, Chakraborty S, Wallach JB, Monteleone M,  
609 Wilson DJ, Aldrich CC, Barry CE, Rhee KY, Ehrt S, Schnappinger D. 2013. A genetic strategy to identify  
610 targets for the development of drugs that prevent bacterial persistence. *Proc Natl Acad Sci U S A*  
611 110:19095–19100.
- 612 26. Politi N, Pasotti L, Zucca S, Casanova M, Micoli G, Cusella De Angelis MG, Magni P. 2014. Half-life  
613 measurements of chemical inducers for recombinant gene expression. *J Biol Eng* 8:5.
- 614 27. Kolbe K, Bell AC, Prosser GA, Assmann M, Yang H-J, Forbes HE, Gallucci S, Mayer-Barber KD, Boshoff  
615 HI, Barry III CE. 2020. Development and optimization of chromosomally-integrated fluorescent  
616 *Mycobacterium tuberculosis* reporter constructs. *Front Microbiol* 11:591866.
- 617 28. Clary G, Sasindran SJ, Nesbitt N, Mason L, Cole S, Azad A, McCoy K, Schlesinger LS, Hall-Stoodley L.  
618 2018. *Mycobacterium abscessus* smooth and rough morphotypes form antimicrobial-tolerant biofilm  
619 phenotypes but are killed by acetic acid. *Antimicrob Agents Chemother* 62:e01782-17.
- 620 29. Merritt JH, Kadouri DE, O'Toole GA. 2005. Growing and analyzing static biofilms. *Curr Protoc Microbiol*  
621 Chapter 1:Unit 1B.1.
- 622 30. Degiacomi G, Benjak A, Madacki J, Boldrin F, Provvedi R, Palù G, Kordulakova J, Cole ST, Manganelli R.  
623 2017. Essentiality of *mmpL3* and impact of its silencing on *Mycobacterium tuberculosis* gene  
624 expression. *Sci Rep* 7:43495.

- 625 31. Varela C, Rittmann D, Singh A, Krumbach K, Bhatt K, Eggeling L, Besra GS, Bhatt A. 2012. *MmpL* genes  
626 are associated with mycolic acid metabolism in mycobacteria and corynebacteria. *Chem Biol* 19:498–  
627 506.
- 628 32. Kozikowski AP, Onajole OK, Stec J, Dupont C, Viljoen A, Richard M, Chaira T, Lun S, Bishai W, Raj VS,  
629 Ordway D, Kremer L. 2017. Targeting mycolic acid transport by indole-2-carboxamides for the  
630 treatment of *Mycobacterium abscessus* infections. *J Med Chem* 60:5876–5888.
- 631 33. Li W, Yazidi A, Pandya AN, Hegde P, Tong W, Calado Nogueira de Moura V, North EJ, Sygusch J,  
632 Jackson M. 2018. MmpL3 as a target for the treatment of drug-resistant nontuberculous  
633 mycobacterial infections. *Front Microbiol* 9:1547.
- 634 34. Raynaud C, Daher W, Johansen MD, Roquet-Banères F, Blaise M, Onajole OK, Kozikowski AP,  
635 Herrmann J-L, Dziadek J, Gobis K, Kremer L. 2020. Active benzimidazole derivatives targeting the  
636 MmpL3 transporter in *Mycobacterium abscessus*. *ACS Infect Dis* 6:324–337.
- 637 35. Sethiya JP, Sowards MA, Jackson M, North EJ. 2020. MmpL3 inhibition: A new approach to treat  
638 nontuberculous mycobacterial infections. *Int J Mol Sci* 21:6202.
- 639 36. Alcaraz M, Edwards TE, Kremer L. 2023. New therapeutic strategies for *Mycobacterium abscessus*  
640 pulmonary diseases - Untapping the mycolic acid pathway. *Expert Rev Anti Infect Ther* 21:813-829.
- 641 37. Grzegorzewicz AE, Pham H, Gundi VAKB, Scherman MS, North EJ, Hess T, Jones V, Gruppo V, Born  
642 SEM, Korduláková J, Chavadi SS, Morisseau C, Lenaerts AJ, Lee RE, McNeil MR, Jackson M. 2012.  
643 Inhibition of mycolic acid transport across the *Mycobacterium tuberculosis* plasma membrane. *Nat*  
644 *Chem Biol* 8:334–341.
- 645 38. Bernut A, Herrmann J-L, Ordway D, Kremer L. 2017. The diverse cellular and animal models to  
646 decipher the physiopathological traits of *Mycobacterium abscessus* infection. *Front Cell Infect*  
647 *Microbiol* 7:100.
- 648 39. Bernut A, Dupont C, Sahuquet A, Herrmann J-L, Lutfalla G, Kremer L. 2015. Deciphering and imaging  
649 pathogenesis and cording of *Mycobacterium abscessus* in zebrafish embryos. *J Vis Exp* 103: e53130.

- 650 40. Rifat D, Chen L, Kreiswirth BN, Nuermberger EL. 2021. Genome-wide essentiality analysis of  
651 *Mycobacterium abscessus* by saturated transposon mutagenesis and deep sequencing. *mBio*  
652 12:e0104921.
- 653 41. Fennelly KP, Ojano-Dirain C, Yang Q, Liu L, Lu L, Progulske-Fox A, Wang GP, Antonelli P, Schultz G.  
654 2016. Biofilm formation by *Mycobacterium abscessus* in a lung cavity. *Am J Respir Crit Care Med*  
655 193:692–693.
- 656 42. Aguilera-Correa J-J, Boudehen Y-M, Kremer L. 2023. Characterization of *Mycobacterium abscessus*  
657 colony-biofilms based on bi-dimensional images. *Antimicrob Agents Chemother* doi:  
658 10.1128/aac.00402-23.
- 659 43. Anderl JN, Franklin MJ, Stewart PS. 2000. Role of antibiotic penetration limitation in *Klebsiella*  
660 *pneumoniae* biofilm resistance to ampicillin and ciprofloxacin. *Antimicrob Agents Chemother*  
661 44:1818–1824.
- 662 44. Hu X, Zhang Y, Chen Z, Gao Y, Teppen B, Boyd SA, Zhang W, Tiedje JM, Li H. 2023. Tetracycline  
663 accumulation in biofilms enhances the selection pressure on *Escherichia coli* for expression of  
664 antibiotic resistance. *Sci Total Environ* 857:159441.
- 665 45. Dokic A, Peterson E, Arrieta-Ortiz ML, Pan M, Di Maio A, Baliga N, Bhatt A. 2021. *Mycobacterium*  
666 *abscessus* biofilms produce an extracellular matrix and have a distinct mycolic acid profile. *Cell Surf*  
667 7:100051.
- 668 46. Belardinelli JM, Li W, Avanzi C, Angala SK, Lian E, Wiersma CJ, Palčėková Z, Martin KH, Angala B, de  
669 Moura VCN, Kerns C, Jones V, Gonzalez-Juarrero M, Davidson RM, Nick JA, Borlee BR, Jackson M.  
670 2021. Unique features of *Mycobacterium abscessus* biofilms formed in synthetic cystic fibrosis  
671 medium. *Front Microbiol* 12:743126.
- 672 47. Recht J, Kolter R. 2001. Glycopeptidolipid acetylation affects sliding motility and biofilm formation in  
673 *Mycobacterium smegmatis*. *J Bacteriol* 183:5718–5724.
- 674 48. Yang Y, Thomas J, Li Y, Vilchère C, Derbyshire KM, Jacobs WR, Ojha AK. 2017. Defining a temporal  
675 order of genetic requirements for development of mycobacterial biofilms. *Mol Microbiol* 105:794–  
676 809.

- 677 49. Yam Y-K, Alvarez N, Go M-L, Dick T. 2020. Extreme drug tolerance of *Mycobacterium abscessus*  
678 “Persisters.” *Front Microbiol* 11:359.
- 679 50. Li W, Obregón-Henao A, Wallach JB, North EJ, Lee RE, Gonzalez-Juarrero M, Schnappinger D, Jackson  
680 M. 2016. Therapeutic potential of the *Mycobacterium tuberculosis* mycolic acid transporter, MmpL3.  
681 *Antimicrob Agents Chemother* 60:5198–5207.
- 682 51. Bernut A, Nguyen-Chi M, Halloum I, Herrmann J-L, Lutfalla G, Kremer L. 2016. *Mycobacterium*  
683 *abscessus*-induced granuloma formation is strictly dependent on TNF signaling and neutrophil  
684 trafficking. *PLoS Pathog* 12:e1005986.
- 685 52. Kam JY, Hortle E, Krogman E, Warner SE, Wright K, Luo K, Cheng T, Manuneehi Cholan P, Kikuchi K,  
686 Triccas JA, Britton WJ, Johansen MD, Kremer L, Oehlers SH. 2022. Rough and smooth variants of  
687 *Mycobacterium abscessus* are differentially controlled by host immunity during chronic infection of  
688 adult zebrafish. *Nat Commun* 13:952.
- 689 53. Ripoll F, Pasek S, Schenowitz C, Dossat C, Barbe V, Rottman M, Macheras E, Heym B, Herrmann J-L,  
690 Daffé M, Brosch R, Risler J-L, Gaillard J-L. 2009. Non mycobacterial virulence genes in the genome of  
691 the emerging pathogen *Mycobacterium abscessus*. *PloS One* 4:e5660.
- 692 54. Nesbit CE, Levin ME, Donnelly-Wu MK, Hatfull GF. 1995. Transcriptional regulation of repressor  
693 synthesis in mycobacteriophage L5. *Mol Microbiol* 17:1045–1056.
- 694 55. Richard M, Gutiérrez AV, Viljoen A, Rodriguez-Rincon D, Roquet-Baneres F, Blaise M, Everall I, Parkhill  
695 J, Floto RA, Kremer L. 2019. Mutations in the MAB\_2299c TetR regulator confer cross-resistance to  
696 clofazimine and bedaquiline in *Mycobacterium abscessus*. *Antimicrob Agents Chemother* 63:e01316-  
697 18.
- 698 56. Kremer L, Maughan WN, Wilson RA, Dover LG, Besra GS. 2002. The *M. tuberculosis* antigen 85  
699 complex and mycolyltransferase activity. *Lett Appl Microbiol* 34:233–237.
- 700 57. Lamason RL, Mohideen M-APK, Mest JR, Wong AC, Norton HL, Aros MC, Jurynech MJ, Mao X,  
701 Humphreville VR, Humbert JE, Sinha S, Moore JL, Jagadeeswaran P, Zhao W, Ning G, Makalowska I,  
702 McKeigue PM, O’donnell D, Kittles R, Parra EJ, Mangini NJ, Grunwald DJ, Shriver MD, Canfield VA,

- 703 Cheng KC. 2005. SLC24A5, a putative cation exchanger, affects pigmentation in zebrafish and humans.  
704 *Science* 310:1782–1786.
- 705 58. Using the R Commander. <https://socialsciences.mcmaster.ca/jfox/Books/RCommander/>. Retrieved  
706 11 August 2021.
- 707 59. Fox J. 2005. The R Commander: A Basic-Statistics Graphical User Interface to R. 1. *J Stat Softw* 14:1–  
708 42.
- 709 60. R Commander. <https://socialsciences.mcmaster.ca/jfox/Misc/Rcmdr/>. Retrieved 11 August 2021.  
710

711 **FIGURE LEGENDS**

712 **Figure 1. mCherry repression controlled by the presence of ATc is effective in *M. abscessus*.**

713 **(A)** Schematic representation of pMV306 derivative plasmid carrying *mCherry* gene and Tet-OFF  
714 system-mediated controlled by ATc. Absence of ATc allows constitutive gene transcription of  
715 *mCherry* gene (top), whereas transcription is blocked when ATc is present in the medium  
716 (bottom). **(B)** Growth of *M. abscessus* CIP S carrying the tetOFF-mCherry plasmid in the presence  
717 of ATc. Bacteria were grown in 7H9 complete medium supplemented or not with different  
718 concentrations of ATc (50, 100, 200, 500, 1000 ng/ $\mu$ L) and optical densities of the cultures were  
719 recorded at 6, 24, 48 and 72 hrs. **(C)** Validation of mCherry repression in *M. abscessus* CIP S strain  
720 carrying repressible mCherry. Bacteria was grown in 7H9 complete medium supplemented or not  
721 with indicated concentrations of ATc. The fluorescence intensity of mCherry signal in relative  
722 fluorescence units (RFU) were normalized to the cell density and expressed as % of control (0 ATc).

723  
724 **Figure 2. Use of dual fluorescent reporter during *M. abscessus* smooth biofilm growth.**

725 **(A)** Schematic representation pMV306 integrative plasmid encoding dual fluorescence. Nucleotide  
726 sequences of  $P_{left^*}$  promoter and the *mWasabi* gene were introduced on the repressible mCherry  
727 plasmid version. **(B)** *M. abscessus* CIP S strain, expressing repressible mCherry and constitutive  
728 mWasabi markers, was grown in 7H9 medium at OD=1. Culture was spotted onto LB agar plates  
729 supplemented or not with different concentrations of ATc (50, 100, 200, 500, 1000 ng/mL). Plates  
730 were incubated 3 days at 37 °C then fluorescent pictures were taken. **(C)** Representative timeline  
731 used for biofilm growth of *M. abscessus* CIP S expressing the dual fluorescent reporter and tracked  
732 over time. Fluorescent pictures of the biofilms were taken at 1, 3, 5, and 7 days showing **(D)**  
733 mWasabi and **(G)** mCherry expression depending on ATc presence (50, 100, 200, 500, 1000 ng/mL)  
734 or not. Scale, 2mm. **(E)** Relative growth (expressed in percentage) of the untreated biofilm (ATc 0)  
735 measured by taking the average intensity levels of the constitutive mWasabi fluorescent protein  
736 along the diameter of biofilms. 100% of growth is the maximum intensity at day 7. Light colors are  
737 corresponding to error bars for each pixel. **(F)** Green colony volume of S biofilms grown in  
738 presence of different concentrations of ATc. **(H)** Intensity levels of mCherry fluorescent protein  
739 along the diameter of biofilms were retrieved from biofilms growing on different concentration of

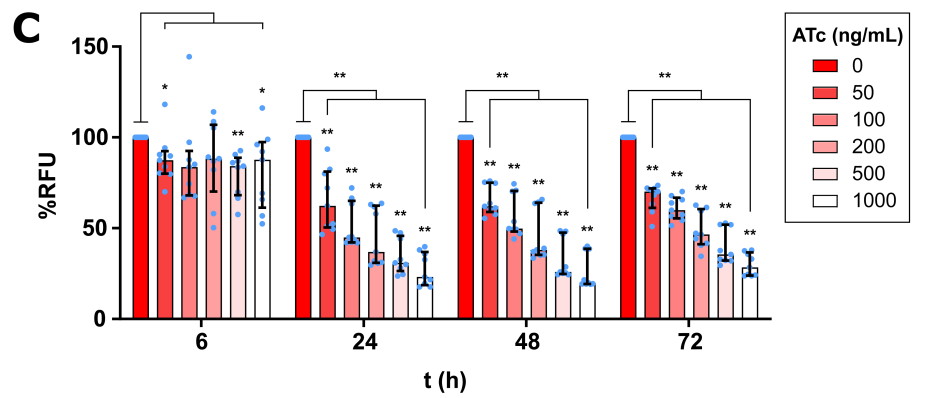
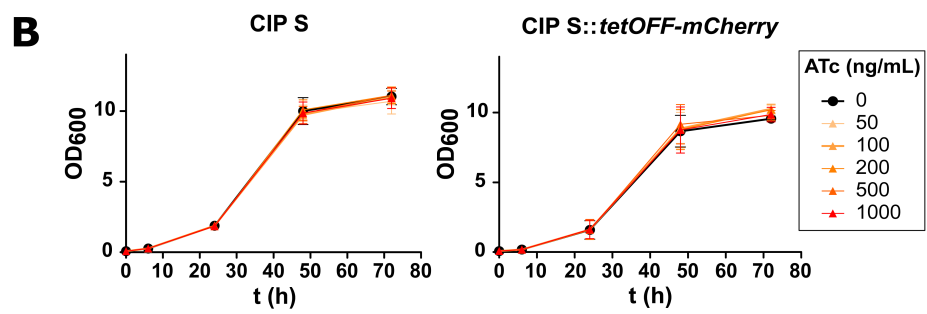
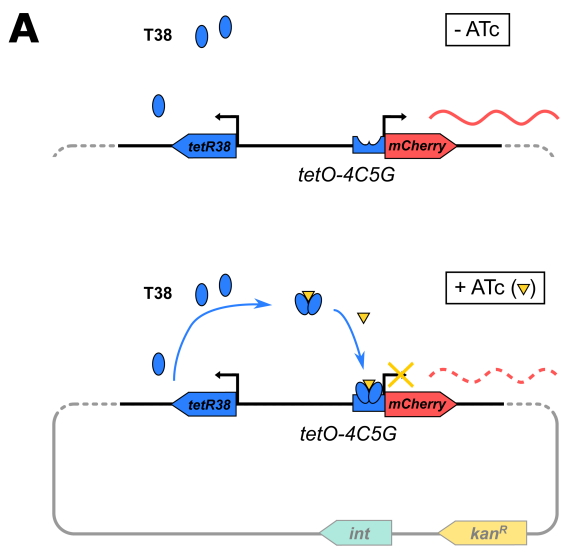


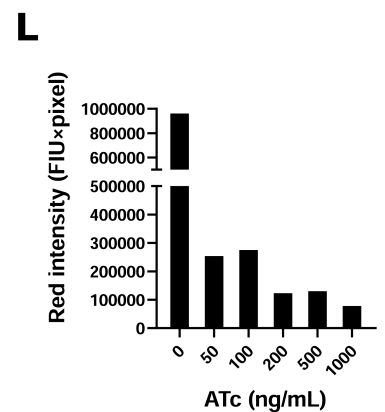
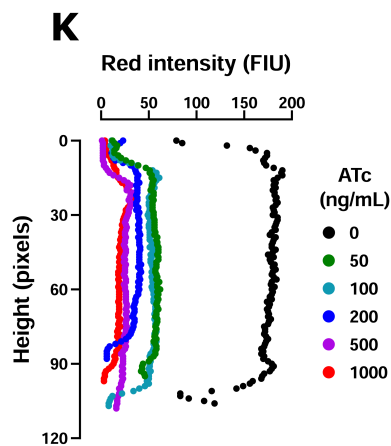
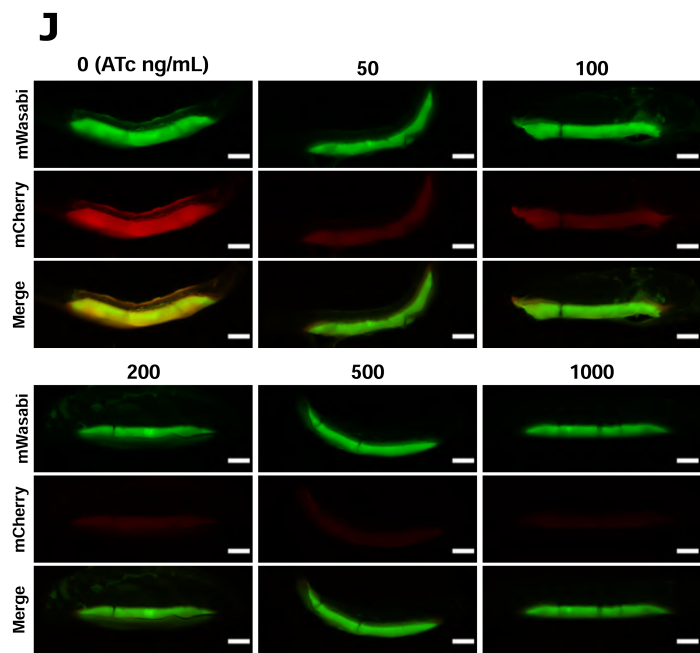
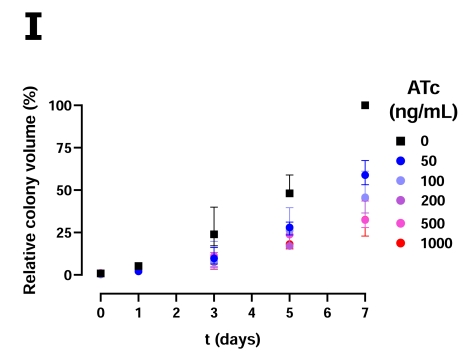
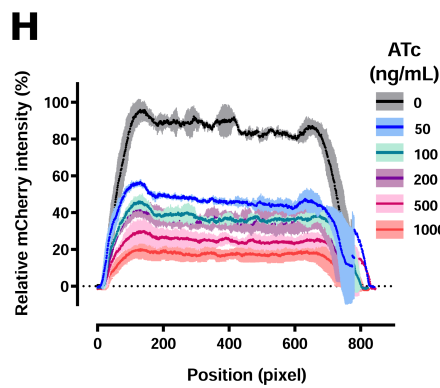
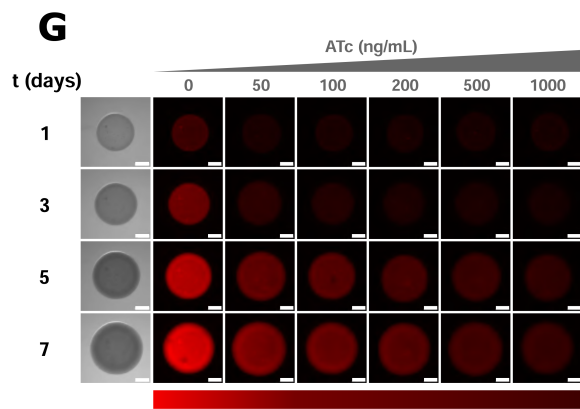
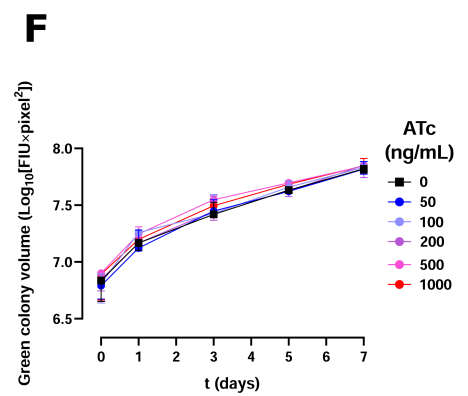
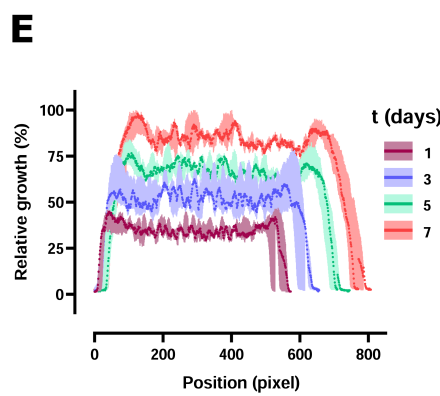
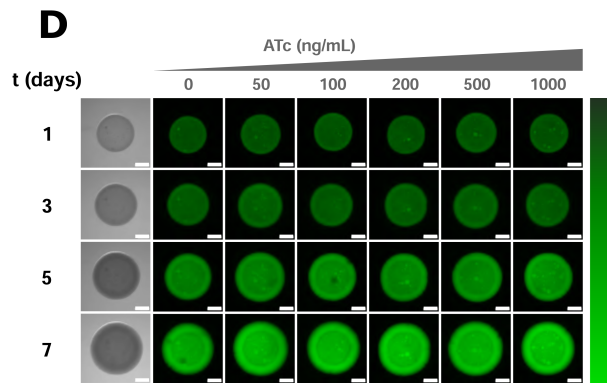
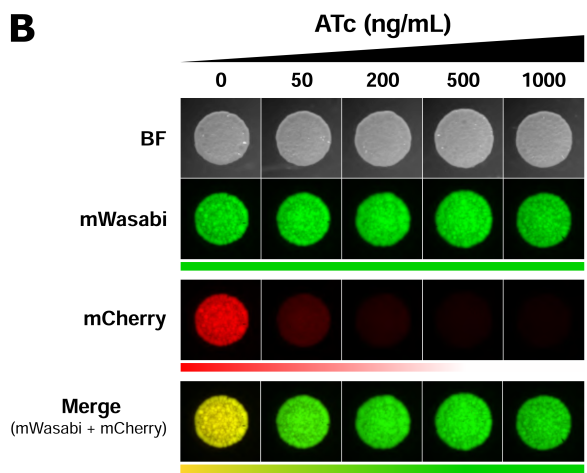
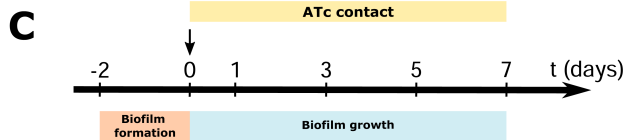
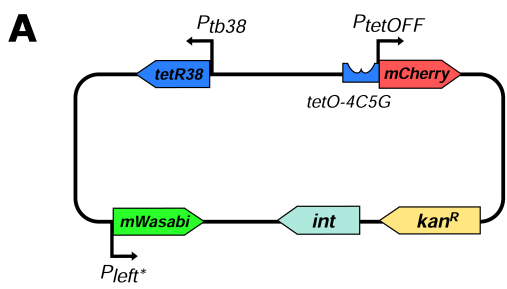
740 ATc at day 7. The mCherry intensity was normalized to the control without drug (ATc 0) and  
741 expressed as %. **(I)** Relative colony volume percentage of *S* biofilms grown in presence of different  
742 concentrations of ATc. Percentages were estimated by considering the red colony volume of *S*  
743 biofilms grown in presence of 0 ng/mL at day 7 as 100%. **(J)** Transversal cuts of *S* biofilms grown in  
744 presence of different concentrations of ATc at day 7. Scale, 2 mm. **(K)** Intensity levels of the  
745 mCherry fluorescent protein along the height of biofilms were retrieved from biofilms growing on  
746 different concentration of ATc. **(L)** Total red fluorescence intensity over colony height.  
747 Fluorescence intensity was estimated the products of each fluorescence intensity (FIU) and its  
748 corresponding height (pixels).

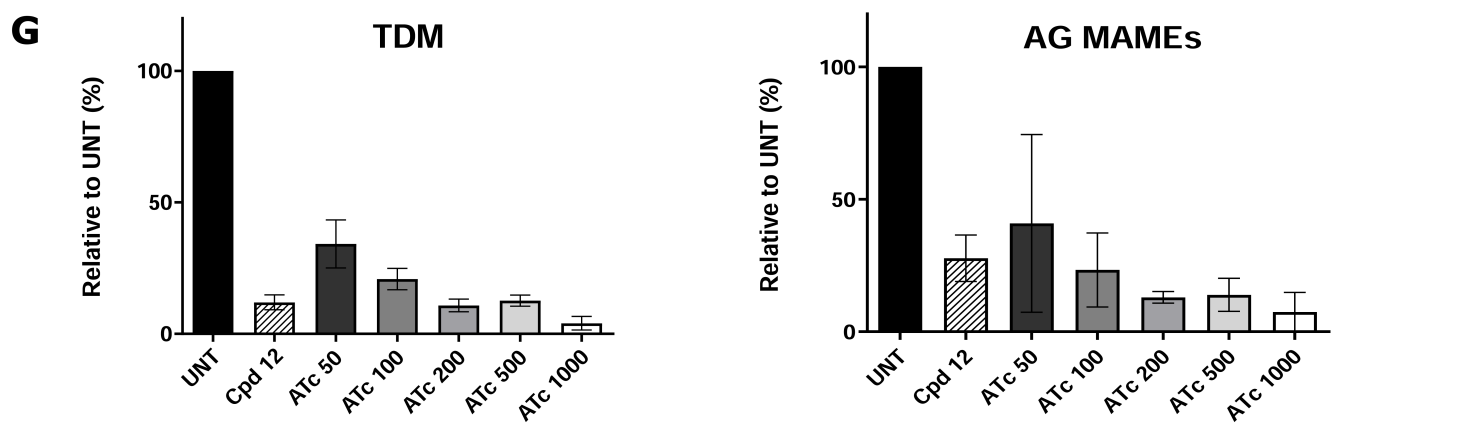
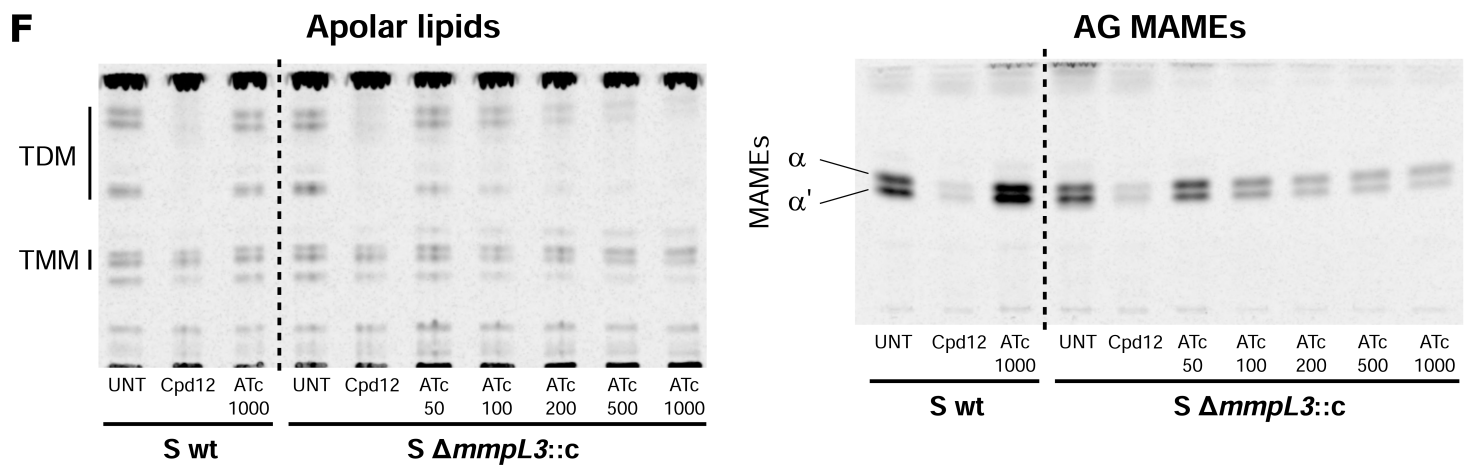
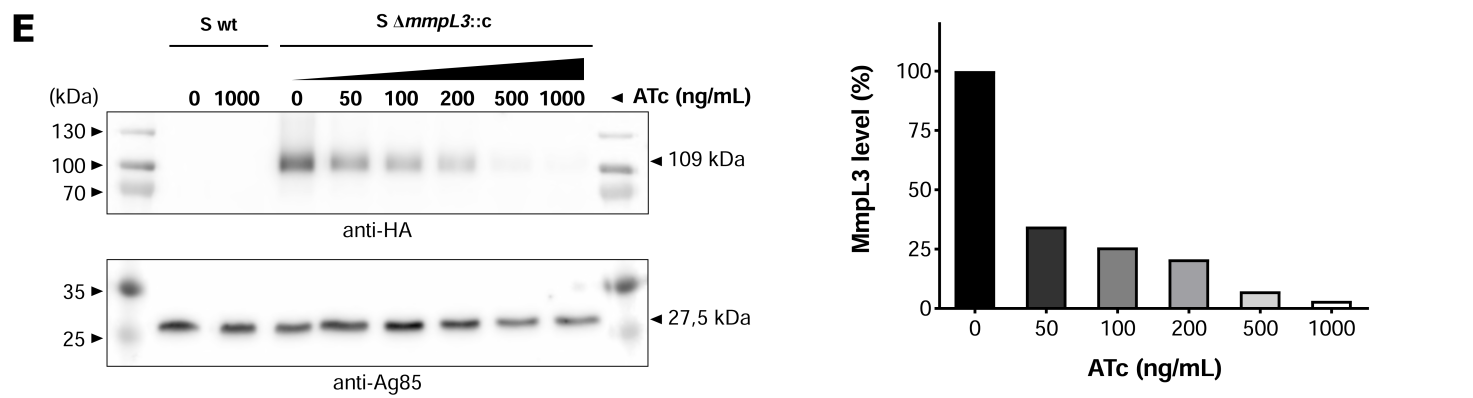
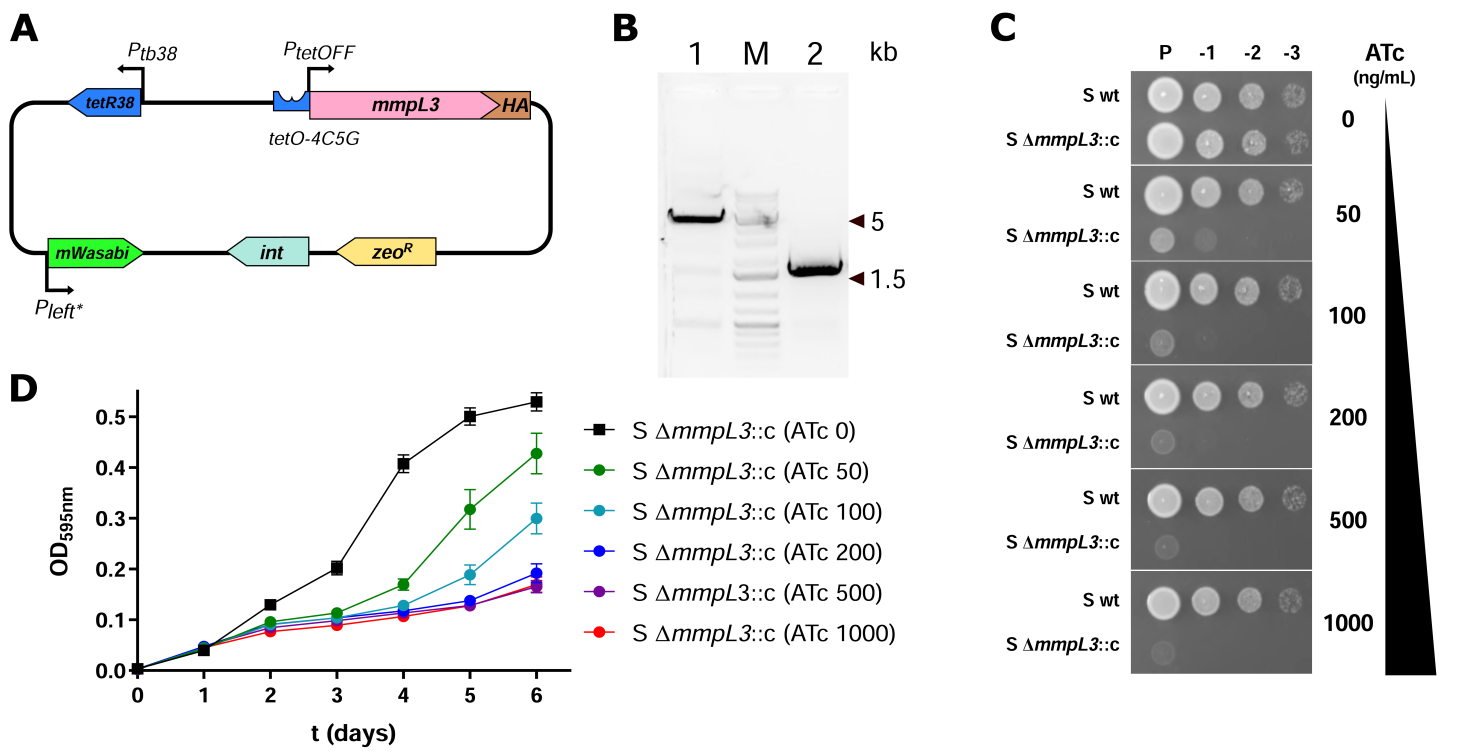
749  
750 **Figure 3. *In vitro* characterization of *M. abscessus mmpL3* conditional knock-down mutant.**  
751 **(A)** Schematic representation of pMV306 derivative plasmid carrying HA-tagged *mmpL3* version  
752 under the control of Tet-OFF system. **(B)** Confirmation of *mmpL3* wild-type locus deletion. PCR was  
753 done with primers producing a 4.5 kb fragment in WT (lane 1), and a 1.5 kb fragment for a  
754 deletion of *mmpL3* (lane 2). The 1.5 kb fragment was verified by Sanger sequencing. M, molecular  
755 size marker. **(C)** Parental (*S* wt) and *mmpL3* conditional mutant (*S*  $\Delta mmpL3::c$ ) cultures were  
756 grown to exponential phase and 3  $\mu$ L of 10-fold serial dilutions were spotted onto LB agar medium  
757 supplemented or not with ATc (50, 100, 200, 500, 1000 ng/mL). Plates were incubated at 37 °C.  
758 Pictures were taken after 3 days. **(D)** Growth curves of the *S mmpL3* conditional mutant (*S*  
759  $\Delta mmpL3::c$ ) facing range of concentrations of ATc during 6 days. Optical density (595 nm)  
760 measurements were taken every day. **(E)** Western blotting analysis of ATc effect on MmpL3  
761 protein level of the *mmpL3* conditional mutant strain **(left panel)**. Bacteria were grown during 72  
762 hrs in Sauton's medium in the presence of increasing concentrations of ATc, as indicated. The  
763 upper membrane was treated for HA immuno-detection and the lower membrane was treated for  
764 Ag85 immuno-detection (loading control). M, molecular size marker. MmpL3 protein levels  
765 quantified from Western blot **(right panel)**. Quantification was normalized and expressed in % of  
766 the non-treated condition (ATc 0). Data are representative of 2 independent experiments. **(F)**  
767 Effect of ATc on mycolic acid transfer in *mmpL3* conditional mutant strain. Apolar lipids were  
768 extracted and loaded to visualize TMM/TDM in the **left panel**. Arabinogalactan (AG)-coupled

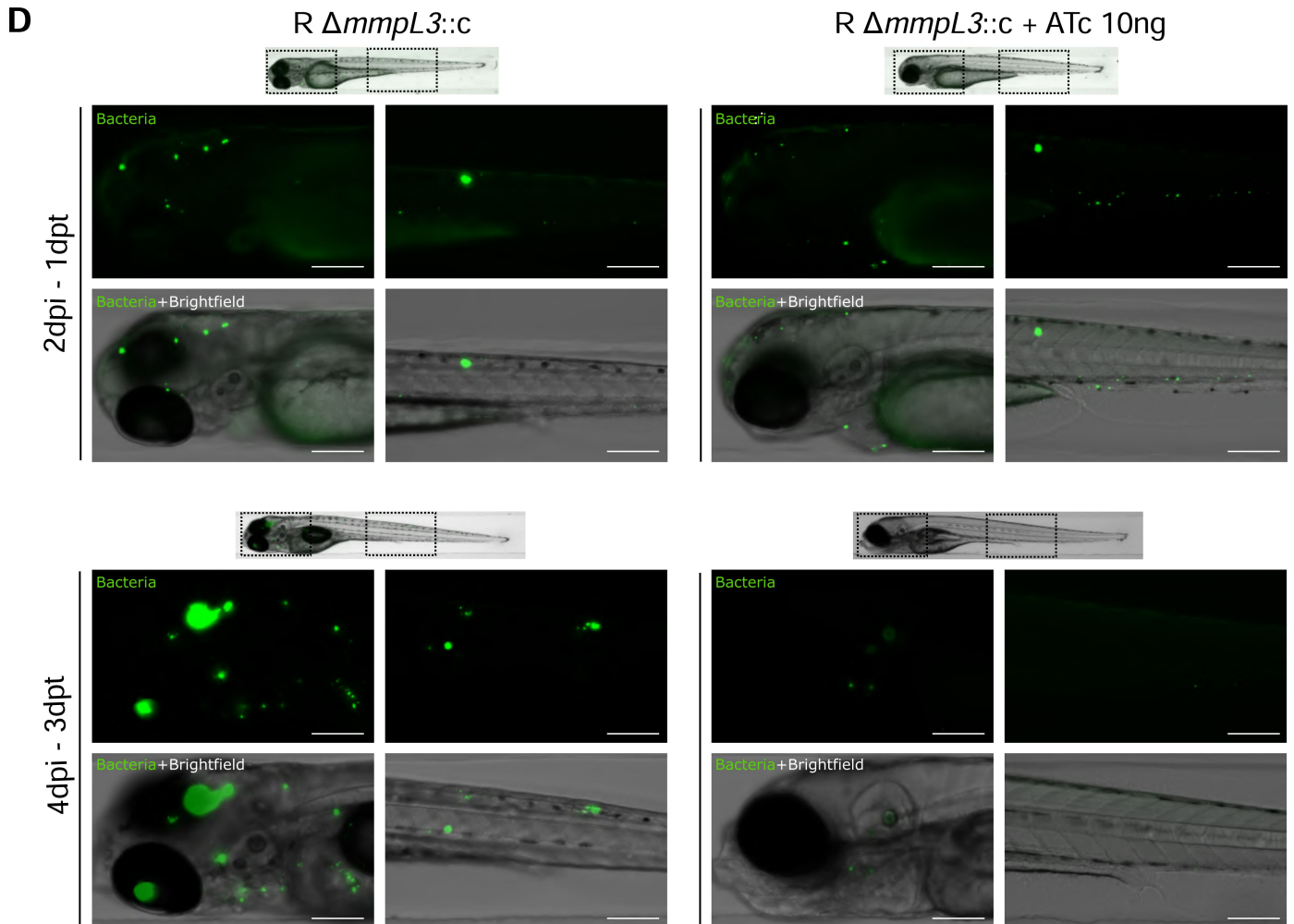
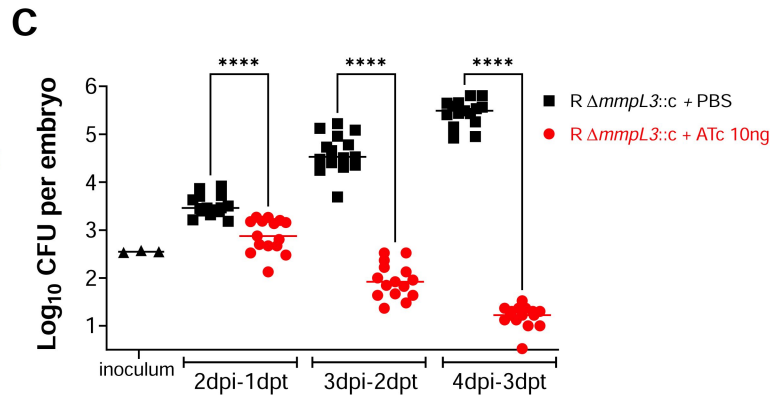
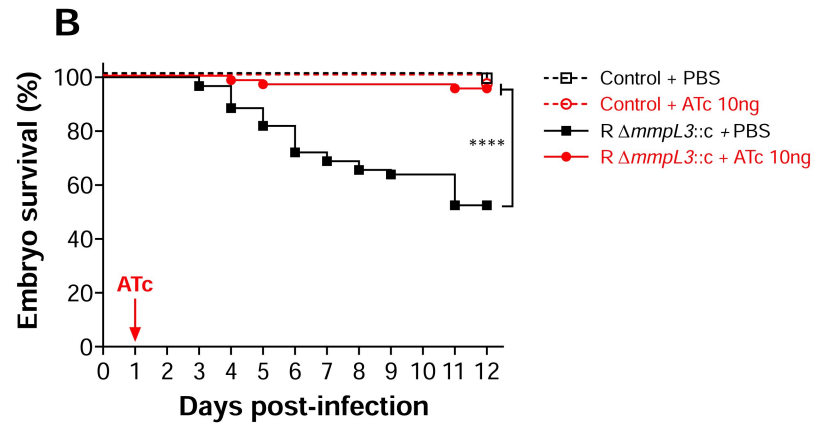
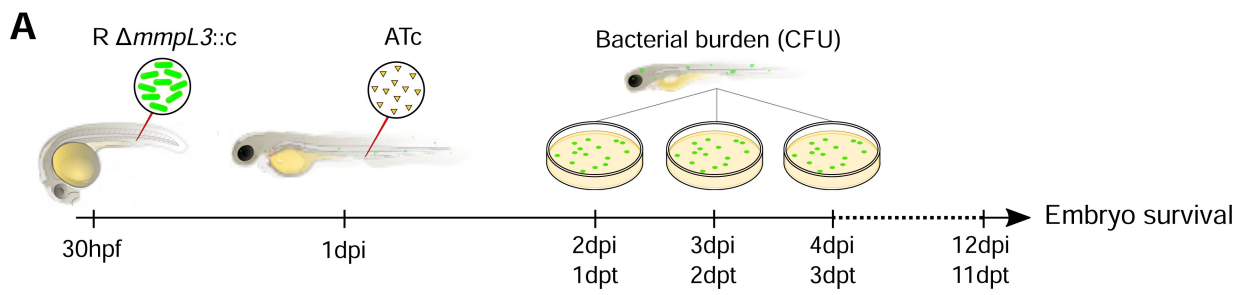
769 mycolic acids are shown in the **right panel**. Culture treated for 1 hr with the indole-2-carboxamide  
770 compound 12 (Cpd12) was used as positive control. The conditional mutant was compared to the  
771 parental strain treated without (UNT) or with the highest ATc concentration (ATc 1000). **(G)**  
772 Densitometric analysis of TDM **(Left panel)** and AG-bound mycolic acids **(right panel)** from the  
773 extracted lipids analyzed by TLC relative to the untreated condition. Results are representative of  
774 3 independent experiments.

775  
776 **Figure 4. Conditional knock-down of *mmpL3* in infected zebrafish embryos leads to reduced**  
777 **bacterial burden and attenuation in virulence. (A)** Schematic representation of the experimental  
778 design. **(B)** Survival of zebrafish embryos upon infection at 1 dpf with an average of  $355 \pm 18$  CFU  
779 of R  $\Delta mmpL3::c$ , and treatment with 10 ng of ATc intravenously at 1 dpi. Embryos were monitored  
780 for 12 days. Pooled results from 3 independent experiments are shown (n=24 per group per  
781 experiment). The red arrow represents the day of ATc injection. For each experiment control  
782 groups were included for the infection as well as the treatment and are represented by dashed  
783 lines. Statistical analysis was performed using a Log rank (Mantel cox) test. **(C)** Bacterial burden  
784 was analysed using CFU counts at 2 dpi, 3 dpi and 4 dpi. Inoculum was determined *a posteriori* and  
785 shown as a triangle. Each point represents an embryo, with rounds corresponding to untreated  
786 embryos and squares to treated embryos. Pooled results from 3 independent experiments are  
787 shown (n=5 per group per time point per experiment). Horizontal lines correspond to the median.  
788 Statistical analysis was performed using one-way ANOVA with Šidák's Multiple Comparisons Test.  
789 **(D)** Real-time imaging of zebrafish embryos infected with R  $\Delta mmpL3::c$  expressing mWasabi,  
790 untreated **(left panels)** or treated with 10 ng of ATc **(right panels)**. Panels show one representative  
791 embryo of each condition at 2dpi-1dpt **(upper panels)** and 4dpi-3dpt **(lower panels)**. For each  
792 embryo, 2 squares with dotted lines indicate the fields imaged with an objective with higher  
793 magnification (head on the left, and tail region on the right). Scale bars represent 200 $\mu$ m.











**Annexe 3 :****“Mycobacteriophage-antibiotic therapy promotes enhanced clearance of drug-resistant *Mycobacterium abscessus*”**

Matt D. Johansen, Matthéo Alcaraz, Rebekah M. Dedrick, Françoise Roquet-Banères, Claire Hamela, Graham F. Hatfull et Laurent Kremer. *Disease Models & Mechanisms*, 2021, Vol 14, N°9 Page dmm049149. PMID : 34530447, DOI : 10.1242/dmm.049159.



## RESEARCH ARTICLE

# Mycobacteriophage–antibiotic therapy promotes enhanced clearance of drug-resistant *Mycobacterium abscessus*

Matt D. Johansen<sup>1,\*</sup>, Matthéo Alcaraz<sup>1</sup>, Rebekah M. Dedrick<sup>2</sup>, Françoise Roquet-Banères<sup>1</sup>, Claire Hamela<sup>1</sup>, Graham F. Hatfull<sup>2</sup> and Laurent Kremer<sup>1,3,‡</sup>

## ABSTRACT

Infection by multidrug-resistant *Mycobacterium abscessus* is increasingly prevalent in cystic fibrosis (CF) patients, leaving clinicians with few therapeutic options. A compassionate study showed the clinical improvement of a CF patient with a disseminated *M. abscessus* (GD01) infection, following injection of a phage cocktail, including phage Muddy. Broadening the use of phage therapy in patients as a potential antibacterial alternative necessitates the development of biological models to improve the reliability and successful prediction of phage therapy in the clinic. Herein, we demonstrate that Muddy very efficiently lyses GD01 *in vitro*, an effect substantially increased with standard drugs. Remarkably, this cooperative activity was retained in an *M. abscessus* model of infection in CFTR-depleted zebrafish, associated with a striking increase in larval survival and reduction in pathological signs. The activity of Muddy was lost in macrophage-ablated larvae, suggesting that successful phage therapy relies on functional innate immunity. CFTR-depleted zebrafish represent a practical model to rapidly assess phage treatment efficacy against *M. abscessus* isolates, allowing the identification of drug combinations accompanying phage therapy and treatment prediction in patients.

This article has an associated First Person interview with the first author of the paper.

**KEY WORDS:** *Mycobacterium abscessus*, Phage therapy, Cystic fibrosis, CFTR, Pathogenesis, Zebrafish

## INTRODUCTION

The incidence of infection with non-tuberculous mycobacteria (NTM) is on the rise, frequently surpassing the infection rate of tuberculosis in many industrialised countries (Johansen et al., 2020a). The *Mycobacterium abscessus* complex is among the

most-relevant NTM affecting humans, and is an acknowledged pathogen infecting a vast array of tissues associated with a broad spectrum of clinical manifestations. Members of this complex are rapid growers, often associated with severe pulmonary diseases, particularly in cystic fibrosis (CF) patients (Cowman et al., 2019; Johansen et al., 2020a). From a taxonomic perspective, the *M. abscessus* complex comprises three subspecies exhibiting different clinical outcomes and susceptibilities to antibiotic treatments: *M. abscessus* subsp. *abscessus* (designated hereafter *M. abscessus*), *M. abscessus* subsp. *bolletii* (designated hereafter *M. bolletii*) and *M. abscessus* subsp. *massiliense* (designated hereafter *M. massiliense*) (Adekambi et al., 2017). These complex subspecies are among the most drug-resistant mycobacteria, harbouring a vast array of innate and acquired drug resistance mechanisms against most antibiotic classes (Johansen et al., 2020a; Nessar et al., 2012). These mechanisms largely rely on the expression of diverse enzymes that inactivate drugs, such as  $\beta$ -lactams (Dubée et al., 2015), tetracyclines (Rudra et al., 2018), rifamycins (Rominski et al., 2017a) and aminoglycosides (Rominski et al., 2017b), and induce the expression of multiple MmpL-based drug efflux pumps (Gutiérrez et al., 2019; Richard et al., 2019).

Conventional therapeutic treatments often require prolonged courses of regimens combining a macrolide (clarithromycin or azithromycin), a  $\beta$ -lactam (cefoxitin or imipenem) and an aminoglycoside (amikacin) (Griffith et al., 2007). Macrolides remain the cornerstone of *M. abscessus* multidrug regimens (Griffith et al., 2007); however, treatment success rates are poor, particularly in macrolide-resistant strains involving an inducible ribosomal methylase encoded by *erm(41)* (Nash et al., 2009; Richard et al., 2020). As such, treatments against *M. abscessus* pulmonary diseases remain extremely challenging, often leading to severe adverse effects and therapeutic failure. New therapeutic interventions are thus required for the treatment and eradication of multidrug-resistant *M. abscessus* strains, particularly in chronically infected patients. In this context, phage therapy may represent a potential antibacterial alternative that involves the administration of phages that infect and lyse bacteria to eradicate or prevent infectious diseases. In the growing era of personalised medicine, phage therapies offer distinct advantages over broad-spectrum antibiotics as they are highly specific toward a particular bacterial pathogen without adversely affecting the host or host commensal microbiota, and ultimately prevent the emergence of antibiotic resistance (Luong et al., 2020). Supporting this view, genetically engineered mycobacteriophages were recently administered to a young CF patient chronically infected with a multidrug-resistant *M. massiliense* strain (GD01) following bilateral lung transplantation. Intravenous phage treatment was well tolerated and associated with significant clinical improvements, representing the first reported therapeutic use of phages for a human mycobacterial infection and

<sup>1</sup>Institut de Recherche en Infectiologie de Montpellier, Centre National de la Recherche Scientifique UMR 9004, Université de Montpellier, Montpellier 34293, France. <sup>2</sup>Department of Biological Sciences, University of Pittsburgh, Pittsburgh, PA 15260, USA. <sup>3</sup>INSERM, Institut de Recherche en Infectiologie de Montpellier, Montpellier 34293, France.

\*Present address: Centre for Inflammation, Centenary Institute and University of Technology Sydney, Faculty of Science, Sydney, NSW, Australia.

‡Author for correspondence (laurent.kremer@irim.cnrs.fr)

id M.D.J., 0000-0001-5553-5270; R.M.D., 0000-0002-3666-711X; F.R.-B., 0000-0003-2636-3734; G.F.H., 0000-0002-6705-6821; L.K., 0000-0002-6604-4458

This is an Open Access article distributed under the terms of the Creative Commons Attribution License (<https://creativecommons.org/licenses/by/4.0>), which permits unrestricted use, distribution and reproduction in any medium provided that the original work is properly attributed.

the first use of engineered mycobacteriophages (Dedrick et al., 2019).

As phage-bacterial pairings are highly specific, there is substantial variation in *M. abscessus* phage susceptibilities, and, thus, phage therapy of large patient cohorts will require expansion of our understanding of mycobacteriophage interactions in the host. In these instances, the development of rapid and reliable pre-clinical models to examine the efficacy of phage therapy against a particular *M. abscessus* clinical isolate would represent a useful predictive marker of successful phage inclusion in a patient prior to clinical application. Moreover, although phage treatment alone is unlikely to be sufficient to clear the infection (Dedrick et al., 2019), an ideal pre-clinical model should allow the identification of top drug candidates that would accompany phage therapy, recapitulating phage-antibiotic cooperation that would facilitate successful eradication in a patient setting.

One of the key steps in drug discovery and phage therapy relies on the evaluation of the *in vitro* and *in vivo* potential of new treatments against *M. abscessus* using adapted animal models. Early studies confirmed that most immunocompetent mouse strains resulted in clearance of *M. abscessus* in the first weeks after infection (Bernut et al., 2014b; Obregón-Henao et al., 2015; Ordway et al., 2008), making these animal models very limited for studying pathogenesis or assaying the *in vivo* efficacy of drug treatments against *M. abscessus*. Comparatively, recent work demonstrated that C3HeB/FeJ mice allow the establishment of a chronic *M. abscessus* infection (Le Moigne et al., 2020). Non-mammalian models of infection have also been developed, including *Drosophila melanogaster*, *Galleria mellonella* larvae (Meir et al., 2018) or zebrafish (*Danio rerio*), offering advantages in terms of speed, cost, technical convenience and ethical acceptability over the mouse model (Bernut et al., 2017). In particular, zebrafish are increasingly recognised as a practical and amenable model to study host-pathogen interactions (Alibaud et al., 2011; Cambier et al., 2014; Clay et al., 2007; Davis et al., 2002; Gomes and Mostowy, 2020; Prajsnar et al., 2008, 2013; van der Sar et al., 2004; Vergunst et al., 2010). Owing to genetic tractability and optical transparency, zebrafish embryos represent an exquisite model to study important aspects of infectious diseases. Although adult zebrafish possess a complex immune system similar to that of humans, comprising both the innate and adaptive arms of immunity, the embryonic stages solely harbour innate immunity (Davis et al., 2002). Critical insights into the *M. abscessus* pathogenesis emerged from a zebrafish infection model, which identified the importance of cording as a mechanism of immune evasion (Bernut et al., 2014a) and the role of TNF signalling in controlling infection and granuloma formation (Bernut et al., 2016b). Zebrafish models of mycobacterial infection recapitulate important bacterial virulence mechanisms and host susceptibility determinants that have been further validated in humans (Bernut et al., 2016b), thus demonstrating their clinical relevance and translatability as an excellent model for human infections. Recently, we reported a CF transmembrane conductance regulator (CFTR)-depleted zebrafish model of *M. abscessus* infection that recapitulates CF immunopathogenesis (Bernut et al., 2019). Loss of CFTR increases susceptibility to *M. abscessus* through impaired NADPH oxidase-dependent restriction of intracellular growth, leading to uncontrolled extracellular multiplication of *M. abscessus* and resulting in abscess formation and lethal infection. Similar phenotypes were also observed in the zebrafish CF model of *Mycobacterium fortuitum* infection (Johansen and Kremer, 2020a), another frequently isolated NTM species that can be isolated from CF patients (Martiniano et al., 2016). Collectively,

these studies highlight the importance of zebrafish infection models as excellent tools to decipher host-pathogen interactions and, for the first time, identified the pivotal role of CFTR in the immunological control of CF-associated NTM infections.

As such, we reasoned that the zebrafish CF model may represent a novel pre-clinical animal model to further understand the complex interplay between phages and bacteria in real time. Furthermore, this model may also provide an effective biological tool to assess the efficacy of mycobacteriophage activity *in vivo*. Herein, we evaluated the selectivity and efficacy of various mycobacteriophages against the *M. massiliense* clinical isolate GD01 *in vitro* and explored the improved activity with leading drug candidates. Importantly, we report the essential contribution of innate immunity in determining phage therapy success and the activity of phages and standard anti-mycobacterial drugs both *in vitro* and *in vivo*. Finally, in the current study, we demonstrate that the zebrafish CF model represents a valuable platform to decipher the lytic activity of mycobacteriophages *in vivo*, which epitomises phage therapy in a clinical setting.

## RESULTS

### High *in vitro* killing activity of phage Muddy against *M. massiliense* GD01

The *M. abscessus* subsp. *massiliense* GD01 strain, with a rough colony morphology, isolated 1 month post-transplantation in a CF patient (homozygous for  $\Delta F508$ ), was originally used to select for potential therapeutic phages by exploiting a collection of >10,000 phages isolated using *Mycobacterium smegmatis*, thanks to the Science Education Alliance-Phage Hunters Advancing Genomics and Evolutionary Science (SEA-PHAGES) program (Jordan et al., 2014). This screen led to the selection of Muddy, which efficiently kills GD01, ZoeJ, from which a lytic derivative was engineered, as well as a lytic derivative of a host range mutant of the phage BPs, designated BPs $\Delta$ 33HTH\_HRM10, and used as a cocktail for treating the CF patient (Dedrick et al., 2019). An additional phage was identified, Gabriela, which infects and kills GD01 very inefficiently compared to Muddy (Fig. 1A) and provides a useful control phage.

We subsequently determined the lowest multiplicity of infection (MOI; corresponding to the phage:GD01 ratio) associated with the highest killing rate. Colony-forming units (CFU) were determined by counting the colonies after incubation of GD01 with either Muddy or Gabriela for 5 days in Middlebrook 7H9 at 37°C by varying the MOI range. As shown in Fig. 1B, even at the MOI of 0.0001, Muddy was able to reduce GD01 CFU numbers by  $\approx 2$  Log compared to the untreated control at Day 5. This lytic activity was further exacerbated at an MOI of 0.01 but remained stable at higher MOI (up to 1). In agreement with the plaque assay (Fig. 1A), Gabriela failed to show substantial killing activity, even at an MOI of 1, the highest MOI tested. Overall, these assays confirmed the differential specificity of the mycobacterial phages tested and high lytic activity of Muddy against GD01 *in vitro*.

### Improved activity between Muddy and antibiotics against GD01 *in vitro*

The CF patient chronically infected with GD01 failed to respond to intensive antibiotic therapies, even after extensive exposure to multidrug chemotherapy (Dedrick et al., 2019). To understand this lack of responsiveness to standard antimicrobial chemotherapy, we determined the drug susceptibility profile of GD01 towards a wide panel of drugs and compared it to that of the *M. abscessus* 104536<sup>T</sup> and *M. massiliense* CIP108297<sup>T</sup> reference strains (both are rough variants). Based on the minimal inhibitory concentration (MIC) and

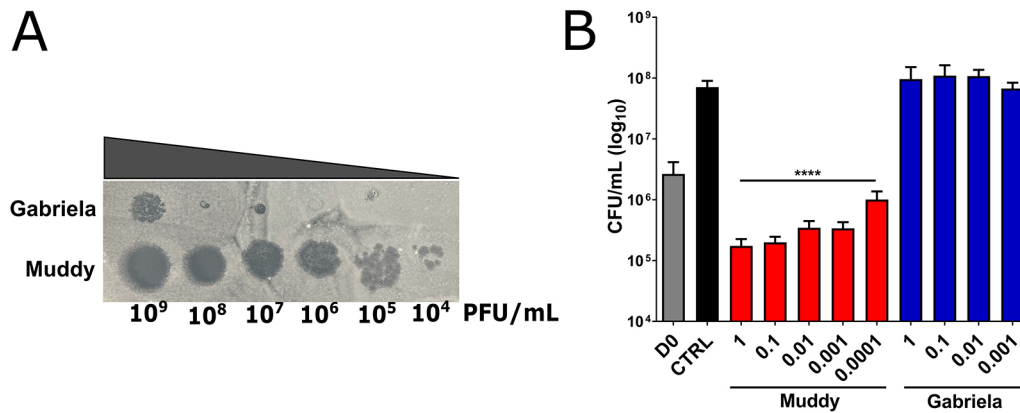


**Fig. 1. Specificity and killing activity of mycobacterial phages against GD01.** (A) Plaque assay. Tenfold serial dilutions of phages Gabriela and Muddy were spotted on a lawn of GD01 grown on 7H10<sup>OADC/CaCl<sub>2</sub></sup>. Lysis was observed after 5 days. PFU, plaque-forming units. (B) Killing assay. GD01 was grown in 7H9<sup>OADC</sup>, incubated with the various phages for 5 days at 37°C and plated on LB agar prior to colony-forming unit (CFU) counting. D0, GD01 inoculum; CTRL, GD01 without phages. \*\*\*\* $P < 0.0001$  (unpaired Student's *t*-test). Data shown are the mean of three independent experiments  $\pm$  s.d.

the Clinical and Laboratory Standards Institute (CLSI) breakpoints (Woods et al., 2011), GD01 shows intermediate susceptibility to imipenem (IPM) and cefoxitin (CFX), and resistance to clarithromycin (CLR), amikacin (AMK), ciprofloxacin (CIP) and linezolid (LNZ) (Table S1). Tigecycline (TGC), clofazimine (CFZ), bedaquiline (BDQ) and MmpL3 inhibitors (the indole-2 carboxamide Cpd12 and the benzimidazole EJMCh-6) are active against GD01 at low concentrations, while rifabutin (RFB) shows a slightly lower activity against GD01 than against the reference strains. Because previous studies have emphasised the increased efficacy of combining phages and antibiotics against *Staphylococcus aureus* (Dickey and Perrot, 2019), we wanted to determine whether phages and antibiotics may cooperate to improve the activity against GD01 *in vitro*. Bacterial cultures were treated for 5 days with either Muddy alone (at an MOI of 0.0001), antibiotics alone (at sub-MIC) or with Muddy plus antibiotics (Fig. 2). As mentioned above, Muddy alone was associated with a nearly 2 to 3 Log decrease in the CFU. Interestingly, although antimicrobial agents such as RFB, IPM, BDQ, CFZ, TGC, AMK, CLR and LNZ were associated with decreased CFU numbers, the addition of Muddy further reduced the CFU levels for most drugs (RFB, IPM, BDQ, CFZ, TGC, AMK) but not for CLR (at 128  $\mu$ g/ml) and LNZ. For instance, the combination of Muddy with RFB, a drug that has recently been shown to inhibit both extracellular and intracellular forms of *M. abscessus* (Aziz et al., 2017; Johansen et al., 2020b), at 3.1  $\mu$ g/ml led to a  $\approx$ 4-5 Log decrease in the CFU compared to the untreated control and a 2 Log reduction compared to RFB alone (Fig. 2G). Interestingly, although GD01 is resistant to AMK (MIC > 128  $\mu$ g/ml; Table S1), with limited CFU reduction, the addition of Muddy to AMK at sub-MIC was accompanied by a striking reduction in the CFU levels (Fig. 2A). Overall, these findings indicate that the addition of a wide panel of antimicrobial drugs potentiates the effect of Muddy and vice versa. In addition, drug/phage combinations can overcome the limited activity of drugs in antibiotic-resistant isolates.

#### Muddy reduces the pathological signs of GD01 infection in wild-type zebrafish

We have previously exploited the optical transparency of zebrafish embryos to describe the increased virulence of rough (R) members of the *M. abscessus* complex over their smooth (S) counterparts, which correlated with the loss of glycopeptidolipid (GPL) production (Bernut et al., 2014a, 2016a). Herein, we exploited

this model to assess whether Muddy exhibits killing activity against GD01 *in vivo* and whether it alters the pathological signs associated with GD01 infection in wild-type embryos. We first addressed whether GD01 induces a typical infection following caudal vein injection with 250-300 CFU of tdTomato-expressing GD01 at 30 h post-fertilisation (hpf). Virulence of GD01 in zebrafish was compared to the virulence of the S and R variants of the *M. massiliense* CIP108297<sup>T</sup> strain as well as T56, an unrelated rough *M. abscessus* clinical isolate. As observed previously for *M. abscessus* and *M. bolletii* (Bernut et al., 2014a, 2016a), daily monitoring of mortality indicated that embryos injected with the S CIP108297<sup>T</sup> survived up until 12 days post-infection (dpi) (Fig. S1A), whereas  $\sim$ 50% of embryos injected with the R CIP108297<sup>T</sup> succumbed to infection by 10 dpi. Infection with T56 showed increased virulence, with nearly 80% embryo mortality at 12 dpi. In contrast, GD01 exhibited a significant delay in embryo killing compared to the other R strains. GD01-infected zebrafish started to succumb to infection 5 days after T56-infected zebrafish, with only 40% embryo mortality by 12 dpi. A possible explanation for this delay may be the slower growth rate of GD01 compared to that of the other strains *in vitro*. This was confirmed by monitoring the growth kinetics of GD01 at both 30°C and 37°C by CFU determination, despite important variations caused by the highly aggregative and clumping properties that typify rough strains (Fig. S2). However, all R strains developed a systemic infection in fish with the presence of the typical growing foci of infection in the larval brain, as shown by whole-embryo imaging (Fig. S1B).

Having established the GD01 infection model in zebrafish, we next tested whether intravenous injection of Muddy or the control phage Gabriela, which infects GD01 inefficiently, would affect the survival and pathology of the infection as outlined in Fig. 3A. We first investigated whether phage treatment increases the survival of GD01-infected larvae. No significant differences in larval survival were observed in the different phage-treated animals compared to the untreated animals (Fig. 3B). We next examined whether phage treatment exerts an effect on the bacterial burden by determining the fluorescent pixel count (FPC) at 6 dpi (Bernut et al., 2015). Fig. 3C clearly shows a significant reduction in the FPC after treatment with Muddy, whereas this effect was less pronounced with Gabriela, thus correlating with the *in vitro* lytic activity of the two phages against GD01. There was no further reduction in bacterial burden when both Muddy and Gabriela were



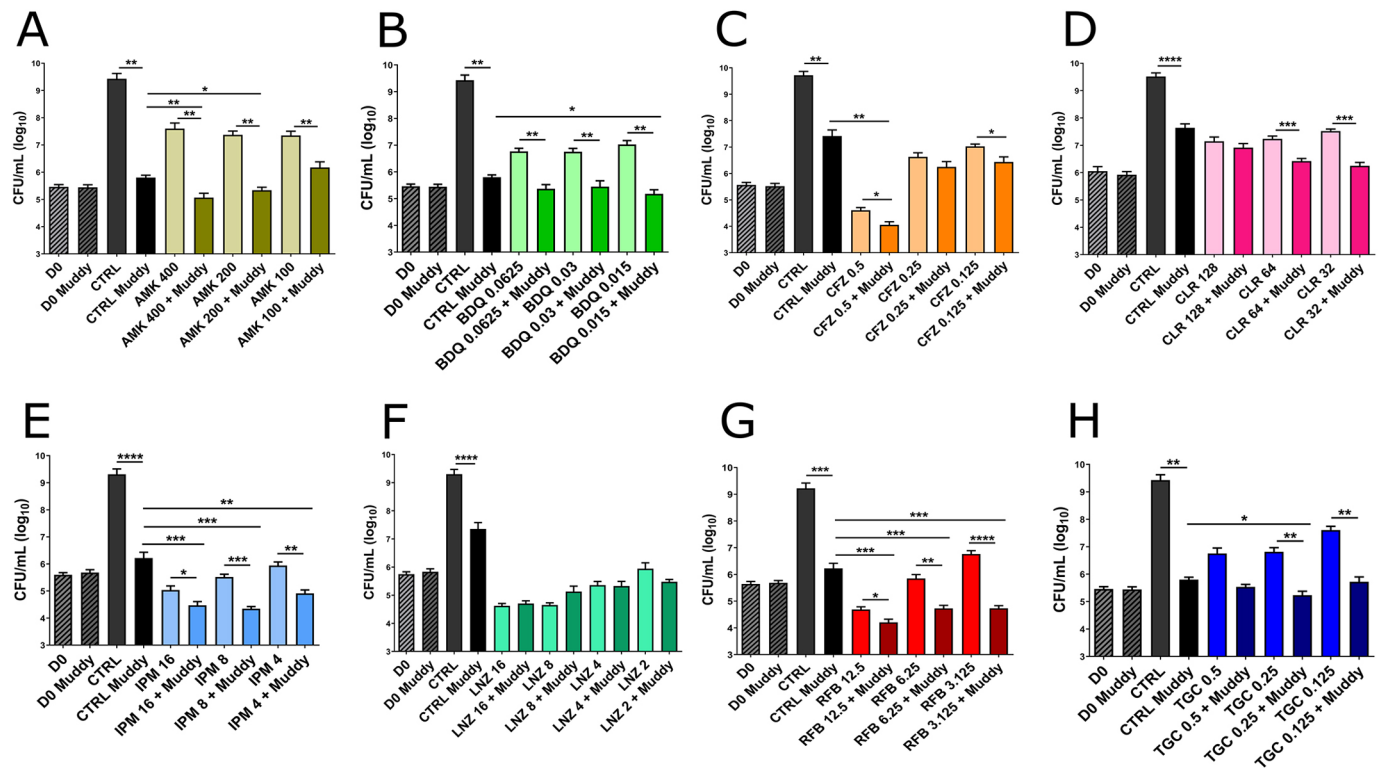


**Fig. 2. *In vitro* killing activity of Muddy and antibiotics against GD01.** (A-H) GD01 was grown in CaMHB at 37°C and incubated with Muddy (MOI=0.0001) in the absence or presence of different antibiotics used in clinical settings. Three drug concentrations were used (in µg/ml) at sub-MIC doses. After 5 days of treatment, bacteria were plated on LB agar prior to CFU counting. D0, GD01 inoculum; CTRL, GD01 without phages. \**P*<0.05; \*\**P*<0.01; \*\*\**P*<0.001; \*\*\*\**P*<0.0001 (unpaired Student's *t*-test). Data shown are the mean of three independent experiments ±s.d.

combined together, suggesting that these phages do not act synergistically *in vivo*.

A noticeable feature of R strains of the *M. abscessus* complex is their high propensity to produce extracellular cords (Bernut et al., 2014a). Owing to their extensive size, cords prevent the bacilli from being phagocytosed by macrophages and neutrophils, thus representing an important mechanism of immune evasion (Bernut et al., 2014a). Therefore, cord formation, often representative of acute infection within the zebrafish embryo, was monitored at different time points after infection. Interestingly, treatment with Muddy was associated with a significant reduction (~2-fold) in the proportion of embryos with cords at 2, 4 and 6 dpi (Fig. 3D). However, no significant changes were observed after treatment with Gabriela alone at 6 dpi, while injection of a cocktail containing both Muddy and Gabriela did not further reduce cording compared to Muddy alone.

Abscess formation often represents loss of infection control and typically occurs following extracellular cord formation and expansion (Bernut et al., 2014a, 2015, 2016a). Abscesses represent a marker of disease severity and are often associated with cellular debris, tissue destruction and acute infection in zebrafish (Bernut et al., 2014a). As such, we wanted to determine whether phage treatment would affect the production of abscesses. As shown in Fig. 3E, treatment with Muddy alone and a phage cocktail of both Muddy and Gabriela showed a significant decrease in the percentage of larvae with abscesses at 4 and 6 dpi. As expected, this was not the case for Gabriela-treated embryos, in which we observed no difference in abscess formation at any time points examined. The decrease in the pathological signs of Muddy-treated larvae correlates with the FPC analysis and whole-embryo imaging (Fig. 3F).

Together, these results suggest that Muddy very efficiently lyses GD01 in wild-type zebrafish embryos, translating into a decreased pathology of the infection. However, this was not sufficient to reduce larval killing. A possible explanation is that, given the delay in larval killing by GD01 compared to other R strains (Fig. S1), a clear effect of phage treatment on larval survival cannot be seen in the 12 dpi-restricted time frame of observation. Moreover, this is further exemplified by the short 5 day phage treatment duration in the zebrafish model, which we postulate may show further reductions in bacterial burden and translationally increased survival.

### Functional innate immunity is essential for efficient activity of Muddy in zebrafish

Macrophages are important immune cells recruited to an infection and are the predominant cell subset involved in the control of *M. abscessus* infection in zebrafish (Bernut et al., 2014a). Importantly, macrophages are required for granuloma formation and controlling mycobacterial growth (Pagán and Ramakrishnan, 2018). Previous studies demonstrated that macrophage ablation results in rapid larval death within several days of infection, underpinning the crucial role of these phagocytes in containing mycobacterial infections (Bernut et al., 2014a; Clay et al., 2007; Johansen and Kremer, 2020b). We observed that injection of liposomal clodronate in the caudal vein had no effect on embryo survival (Fig. S3A) and depleted macrophages for at least 5 days, with macrophages recovering at 7 days post-treatment (Fig. S3B). Following liposomal clodronate treatment and *M. abscessus* infection (Fig. 4A), we observed progressive rapid larval death resulting in 100% of embryo mortality at 8 dpi, compared to standard GD01 infection following liposomal PBS injection prior to infection (Fig. 4B). Unexpectedly, although larval death occurred

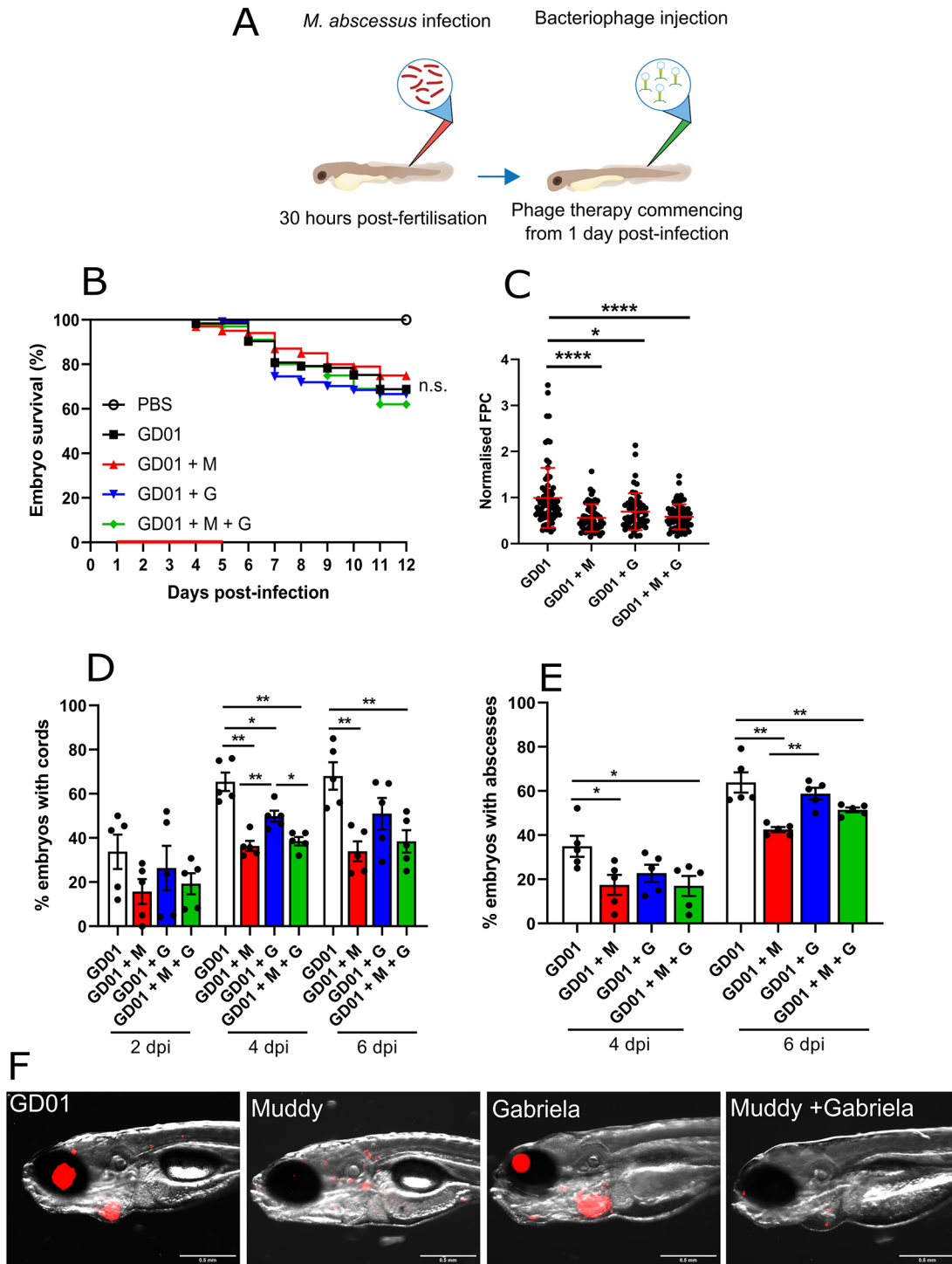


**Fig. 3. Impact of bacteriophage Muddy on GD01 infection in wild-type zebrafish.** At 30 hpf, embryos were infected with 250-300 CFU of GD01 expressing tdTomato via caudal vein injection. At 1 dpi, embryos commenced phage therapy through caudal vein administration at an MOI of 50:1 (phage: bacteria) based on the initial bacterial infection inoculum. Embryos were treated daily from 1 dpi up to and including 5 dpi with either Muddy (M), Gabriela (G) or a phage cocktail containing both Muddy and Gabriela (M+G). (A) A generalised schematic showing the experimental design corresponding to the figure. (B) Embryo survival was monitored over a 12 day period, with embryos counted daily. Survival curves were analysed using the log-rank (Mantel–Cox) statistical test. The red bar across the x-axis indicates the duration of daily phage administration in the current experiment. (C) Bacterial burden [fluorescent pixel count (FPC)] was analysed at 6 dpi using fluorescent microscopy. Fluorescent images were analysed in ImageJ using the ‘Analyze particles’ function. Bacterial burden was analysed using a Kruskal–Wallis one-way ANOVA. (D,E) The proportion of embryos with cords (D) and abscesses (E) was enumerated at 2, 4 and 6 dpi using fluorescent microscopy. Abscess and cord quantification was analysed using a Kruskal–Wallis one-way ANOVA. Data shown are the mean of three independent experiments  $\pm$  s.d. ( $n=20-30$  per group for each experiment). (F) Representative zebrafish images of untreated (GD01) or phage-treated embryos at 6 dpi, showing the presence of extracellular bacterial cords. Red overlay represents GD01 expressing TdTomato. Scale bars: 0.5 mm. n.s., not significant; \* $P<0.05$ ; \*\* $P<0.01$ ; \*\*\* $P<0.0001$ .

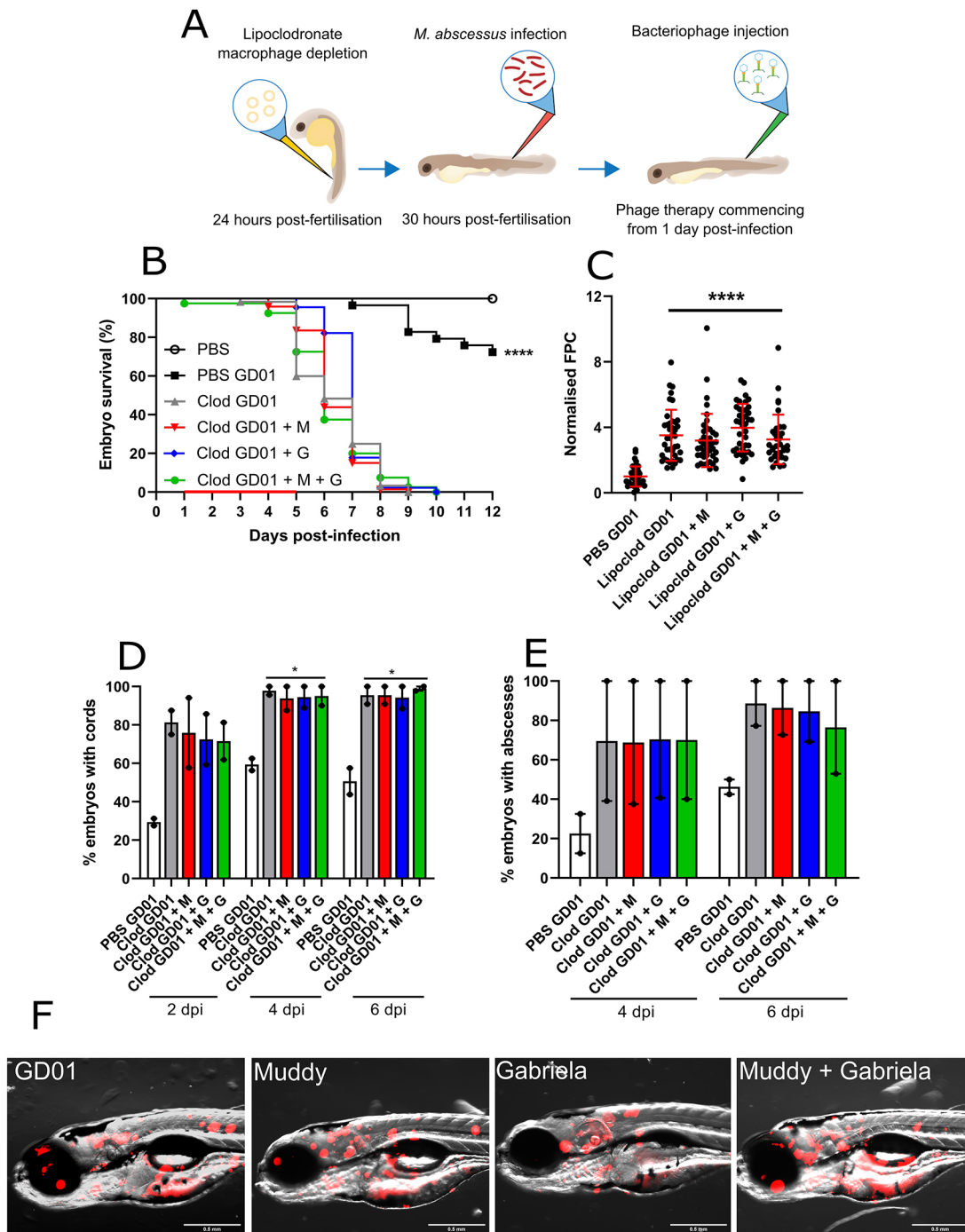


**Fig. 4. Activity of Muddy in GD01-infected zebrafish lacking macrophages.** At 24 hpf, embryos were micro-injected with either PBS liposomes (PBS) or lipoclodronate-filled liposomes (Clod) to achieve macrophage depletion. At 30 hpf, treated embryos were infected with 250–300 CFU of GD01 (PBS GD01 and Clod GD01) via caudal vein injection. At 1 dpi, embryos commenced phage therapy through caudal vein injection at an MOI of 50:1 (phage:bacteria) based on initial bacterial infection inoculum. Embryos were treated daily from 1 dpi, up to and including 5 dpi with Muddy (M), Gabriela (G) or a phage cocktail containing both Muddy and Gabriela (M+G). (A) A generalised schematic showing the experimental design corresponding to the figure. (B) Embryo survival was monitored over a 12 day period, with embryos counted daily. Survival curves were analysed using the log-rank (Mantel–Cox) statistical test. The red bar across the x-axis indicates the duration of daily phage administration in the current experiment. (C) Bacterial burden (FPC) was analysed at 6 dpi using fluorescent microscopy. Fluorescent images were analysed in ImageJ using the ‘Analyze particles’ function. Bacterial burden was analysed using a Kruskal–Wallis one-way ANOVA. (D,E) The proportion of embryos with cords (D) and abscesses (E) was enumerated at 2, 4 and 6 dpi using fluorescent microscopy. Abscess and cord quantification was analysed using a Kruskal–Wallis one-way ANOVA. Data shown are the mean of two independent experiments  $\pm$  s.d. ( $n=20$ –30 per group for each experiment). (F) Representative zebrafish images of untreated (GD01) or phage-treated embryos at 6 dpi, showing the presence of extracellular bacterial cords. Red overlay represents GD01 expressing TdTomato. Scale bars: 0.5 mm. \* $P<0.05$ ; \*\*\*\* $P<0.0001$ .

rapidly and was much more pronounced compared to infection in wild-type fish, treatment with Muddy, Gabriela or Muddy plus Gabriela failed to increase the survival rate of infected embryos (median time to 50% mortality of 6 and 7 days, respectively). We further examined whether there was a change in bacterial burden in macrophage-depleted embryos following phage therapy. Irrespective of individual phages or phage cocktail administration, we saw no change in bacterial burden between any of the macrophage-depleted groups at 6 dpi (Fig. 4C). As anticipated, both cords and abscesses increased drastically within 2 dpi in macrophage-depleted larvae, compared to the control embryos (liposomal PBS) (Fig. 4D,E). However, phage treatment did not reduce the proportion of embryos with cords at 2, 4 and 6 dpi (Fig. 4D), or the percentage of embryos with abscesses at 4 and 6 dpi (Fig. 4E). The presence of large infection foci in the phage-treated fish compared to the untreated fish correlates with the FPC analysis and with whole-embryo imaging (Fig. 4F). Collectively, these results highlight the critical role of macrophages in sustaining the *in vivo* efficacy of Muddy during GD01 infection and emphasise the requirements of a functional innate immunity for establishing a successful phage therapy.

### Validation of phage treatment against GD01 in CFTR-depleted embryos

The *M. abscessus* complex has emerged as an important respiratory pathogen of major concern in CF centres worldwide (Parkins and Floto, 2015). Because our understanding of the particular vulnerability of CF patients to *M. abscessus* complex infection remains limited by the lack of suitable animal models mimicking the immune abnormalities found in the CF population, we have exploited a zebrafish CF model that recapitulates important aspects of CF immunopathogenesis. This allowed us to report a stepwise dissection of *M. abscessus* infection in an animal depleted of CFTR to elucidate the biological implication of CFTR in innate immunity to these infections (Bernut et al., 2019). To address the role of CFTR in GD01 infection, *cfr* loss-of-function experiments were performed in zebrafish using a specific morpholino-modified oligonucleotide (Bernut et al., 2019), which abrogated production of native spliced *cfr* transcripts (Fig. 5A; Fig. S4). We report here that GD01-infected CFTR morphants rapidly succumb to intravenous infection (Fig. 5B), reflecting the hypersusceptibility of the young CF patient to this isolate (Dedrick et al., 2019), providing a first glimpse into CFTR-mediated host defences to GD01 infection. This was associated with an increase in the bacterial burden, as evidenced by FPC determination (Fig. 5C). This early and progressive killing in *cfr* morphants (Fig. 5B) prompted us to investigate whether phage therapy can ameliorate GD01 infection in a CFTR-deficient context.

Treatment with Muddy, Gabriela or Muddy and Gabriela was associated with a slightly delayed survival curve compared to CFTR-depleted embryos infected with GD01 (median time to 50% mortality of 10 days compared to 8 days, respectively) (Fig. 5B). Importantly, although CFTR ablation led to 20% embryo survival in the non-treated group at 12 dpi, ~40% survival was reached in embryos treated with Muddy. Similar to macrophage-depleted embryos, ablation of CFTR was associated with a rapid and pronounced increase in cording (Fig. 5D) and abscesses (Fig. 5E) compared to control morphants. Strikingly, treatment with Muddy alone or in combination with Gabriela led to a severe reduction in the proportion of embryos with cords at 2, 4 and 6 dpi (Fig. 5D), abscesses at 4 and 6 dpi (Fig. 5E) and bacterial loads (Fig. 5C), compared to the untreated controls. The strong decrease in the

pathological signs of Muddy-treated *cfr* morphants correlates with the FPC analysis and whole-embryo imaging (Fig. 5F). As evidenced by increased larval survival and reduced pathological signs, these findings indicate that CFTR-depleted fish are highly susceptible to GD01 infection and respond to phage treatment with Muddy.

### Improved efficacy of combined phage and antibiotic therapy in GD01-infected CFTR zebrafish

Our previous results highlighted the improved activity when combining Muddy and various antibiotics, including RFB (Fig. 2). To enquire whether this therapeutic combination is also effective *in vivo*, GD01-infected CFTR-depleted zebrafish were either treated with RFB alone, Muddy alone or with RFB and Muddy together. The protocol applied is outlined in Fig. 6A. Treatment with RFB alone was associated with a significant increase in the survival rate compared to that of the untreated CFTR morphants (Fig. 6B), in agreement with previous observations performed in wild-type zebrafish infected with *M. abscessus* (Johansen et al., 2020b). In addition, the level of protection conferred by RFB was similar to that of embryos treated with Muddy alone. Importantly, the combined Muddy and RFB treatment further increased the survival rate compared to that of larvae treated with RFB alone or Muddy alone, reaching 70% survival at 12 dpi, almost identical to that seen for GD01 infection in wild-type zebrafish (Fig. 6B). Strikingly, when we compared the median time to 50% mortality between the groups, we observed a median time of 7 days for CFTR embryos infected with GD01, which shifted to 10 days for those treated with RFB or Muddy alone. Importantly, this was beyond the calculation threshold for those embryos treated with RFB and Muddy together, owing to significantly reduced mortality, further reinforcing the relevance of our findings. Similarly, this combination therapy showed markedly reduced bacterial loads compared to untreated *cfr* morphants and showed no differences compared to untreated control morphants (Fig. 6C). Furthermore, combination therapy with Muddy and RFB was also correlated with a substantial reduction in the proportion of embryos with cording at 2, 4 and 6 dpi (Fig. 6D), as well as in the percentage of embryos with abscesses (Fig. 6E). The strong decrease in the pathological signs of Muddy plus RFB-treated *cfr* morphants correlates with the FPC analysis and whole-embryo imaging (Fig. 6F). Together, these findings demonstrate the improved therapeutic efficacy of the combined treatment with Muddy and RFB in a CF animal model with disseminated GD01 infection, characterised by a highly reduced lethality and pathological signs in comparison to embryos treated with either one of the two treatments.

### DISCUSSION

Bacterial pathogens are frequently associated with lung complications and disease progression in CF (Elborn, 2016). These bacteria increasingly show resistance to antibiotics, requiring novel management approaches. Bacteriophage therapy, in which lytic phages are administered to kill target bacterial pathogens, represents one of these strategies (Düzgüneş et al., 2021; Luong et al., 2020). Case reports of phage therapy to treat drug-resistant pulmonary infections in CF have received significant attention in recent years (Chan et al., 2021; Dedrick et al., 2019; Ng et al., 2021). The use of a phage cocktail administered with antibiotics was reported for the treatment of disseminating *M. massiliense* GD01 in a 15-year-old individual with CF who was a post-lung transplant recipient (Dedrick et al., 2019). In this case, the therapy resulted in decreased size of skin lesions and improvement in lung function,



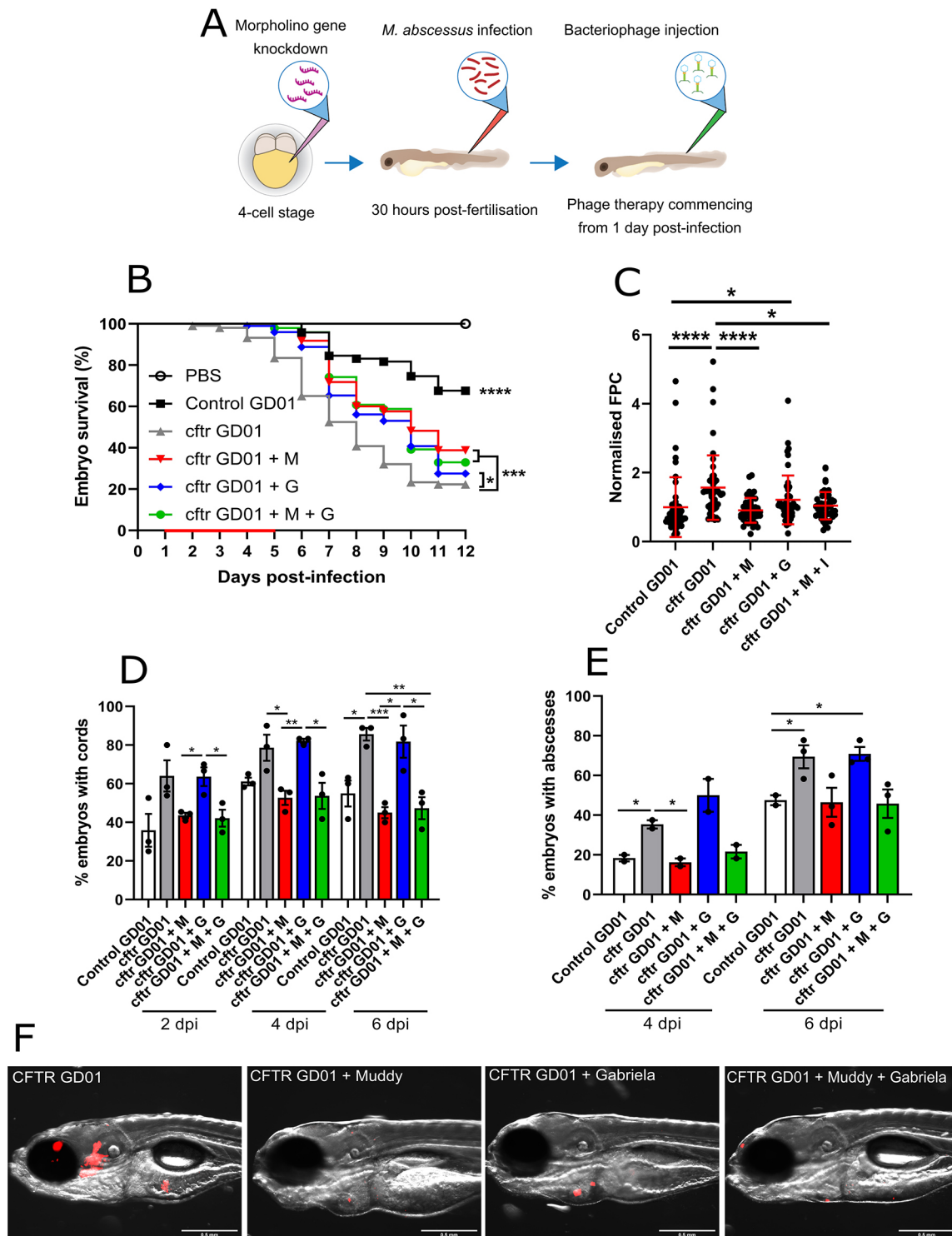


**Fig. 5. Effect of Muddy in GD01-infected *cfr* morphants.** At the one- to four-cell stage, fertilised zebrafish eggs were injected in the nucleus with either control morpholino (control) or *cfr* morpholino (*cfr*). At 30 hpf, embryos were infected with 250–300 CFU of GD01 (control GD01 or *cfr* GD01) via caudal vein injection. At 1 dpi, embryos commenced phage therapy through caudal vein injection at an MOI of 50:1 (phage:bacteria) based on initial bacterial infection inoculum. Embryos were treated daily from 1 dpi, up to and including 5 dpi with Muddy (M), Gabriela (G) or a phage cocktail containing both Muddy and Gabriela (M+G). (A) A generalised schematic showing the experimental design corresponding to the figure. (B) Embryo survival was monitored over a 12 day period, with embryos counted daily. Survival curves were analysed using the log-rank (Mantel–Cox) statistical test. The red bar across the x-axis indicates the duration of daily phage administration in the current experiment. (C) Bacterial burden (FPC) was analysed at 6 dpi using fluorescent microscopy. Fluorescent images were analysed in ImageJ using the ‘Analyze particles’ function. Bacterial burden was analysed using a Kruskal–Wallis one-way ANOVA. (D,E) The proportion of embryos with cords (D) and abscesses (E) was enumerated at 2, 4 and 6 dpi using fluorescent microscopy. Abscess and cord quantification was analysed using a Kruskal–Wallis one-way ANOVA. Data shown are the mean of three independent experiments  $\pm$  s.d. ( $n=20$ –30 per group for each experiment). (F) Representative *cfr* morphant images of untreated (GD01) or phage-treated embryos at 6 dpi, showing the presence of extracellular bacterial cords or localised infection. Red overlay represents GD01 expressing TdTomato. Scale bars: 0.5 mm. \* $P<0.05$ ; \*\* $P<0.01$ ; \*\*\* $P<0.001$ ; \*\*\*\* $P<0.0001$ .



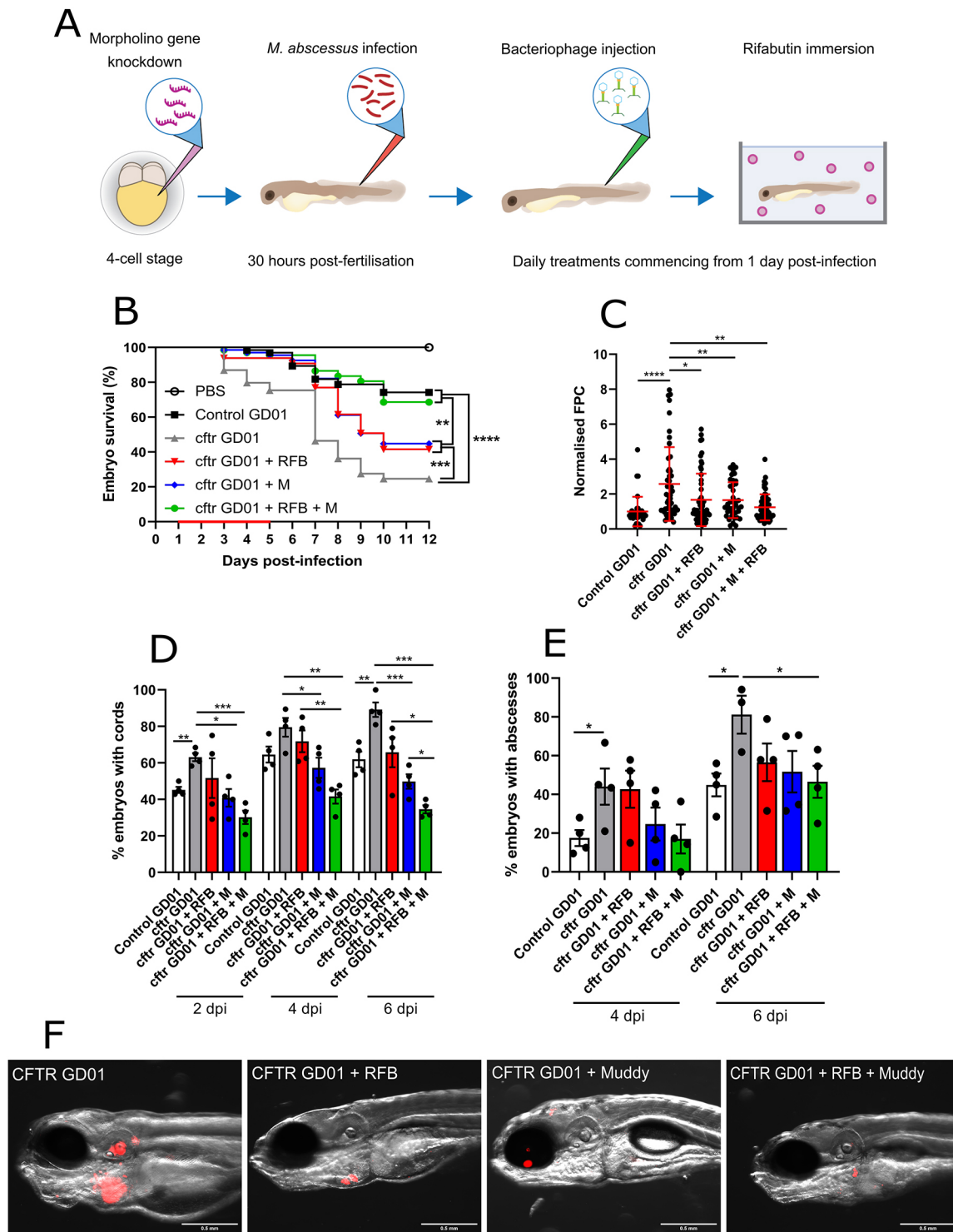


**Fig. 6. Activity of Muddy and rifabutin in GD01-infected *cfr* morphants.** At the one- to four-cell stage, fertilised zebrafish eggs were injected in the nucleus with either control morpholino (control) or *cfr* morpholino via caudal vein injection. At 1 dpi, embryos commenced phage Muddy (M) and/or rifabutin (RFB) therapy through caudal vein injection at an MOI of 50:1 (phage:bacteria) based on initial bacterial infection inoculum. Embryos were treated daily from 1 dpi, up to and including 5 dpi with Muddy. RFB was added to zebrafish water daily at a final concentration of 50  $\mu\text{g}/\text{ml}$ . (A) A generalised schematic showing the experimental design corresponding to the figure. (B) Embryo survival was monitored over a 12 day period, with embryos counted daily. Survival curves were analysed using the log-rank (Mantel–Cox) statistical test. The red bar across the x-axis indicates the duration of daily phage and RFB administration in the current experiment. (C) Bacterial burden (FPC) was analysed at 6 dpi using fluorescent microscopy. Fluorescent images were analysed in ImageJ using the ‘Analyze particles’ function. Bacterial burden was analysed using a Kruskal–Wallis one-way ANOVA. (D,E) The proportion of embryos with cords (D) and abscesses (E) was enumerated at 2, 4 and 6 dpi using fluorescent microscopy. Abscess and cord quantification was analysed using a Kruskal–Wallis one-way ANOVA. Data shown are the mean of three independent experiments  $\pm$  s.d. ( $n=20-30$  per group for each experiment). (F) Representative *cfr* morphant images of embryos left untreated (GD01), treated with Muddy alone, RFB alone or with Muddy plus RFB at 6 dpi, showing the presence of extracellular bacterial cords or localised infection. Red overlay represents GD01 expressing TdTomato. \* $P < 0.05$ ; \*\* $P < 0.01$ ; \*\*\* $P < 0.001$ ; \*\*\*\* $P < 0.0001$ .

liver function, chest imaging and weight gain. Although this illustrates that phage therapy against NTM infections holds vast potential, there is little understanding of phage–host dynamics in disease environments and a clear lack of pre-clinical studies concerning phage therapy of *M. abscessus* infections (Senhaji-Kacha et al., 2021). In this context, we studied the GD01–mycobacteriophage infection dynamics under various physiological and disease-mimicking conditions using a CF zebrafish model of infection.

In general, most findings identified in this biological model paralleled those reported previously in the treated CF patient (Dedrick et al., 2019). First, we found that *cfr* morphants were extremely susceptible (decreased larval survival) to GD01 infection (Fig. 5B), resulting from uncontrolled bacterial multiplication (Fig. 5C) and dissemination, and exacerbation of the pathological features (Fig. 5D,E), as shown previously for *M. abscessus* (Bernut et al., 2019) and *M. fortuitum* (Johansen and Kremer, 2020a). Second, we show the improved activity of phage Muddy (Fig. 2) with a wide panel of antibiotics used in the clinical treatment of *M. abscessus* pulmonary diseases. Although the drugs tested were more or less effective at low concentrations, the addition of Muddy led to a substantial improvement in efficacy, similarly to what has previously been observed when drugs were administered to phages against *S. aureus* or *Pseudomonas aeruginosa* (Dickey and Perrot, 2019; Oechslin et al., 2017). In addition, the adjunct of an antibiotic to phage treatment has also proven effective in reducing the outgrowth of antibiotic- and phage-resistant strains during treatment (Dickey and Perrot, 2019), and this combination could also better help to manage antibiotic-resistant bacterial biofilms. A major drawback of a phage/antibiotic combination is that more complex studies are required to establish effective co-dosing regimens relying on compatible pharmacokinetic and pharmacodynamics properties between the antibiotic and phages. However, the mechanisms underlying potential phage–antibiotic interactions remain largely unknown. Thus, the present study represents a first glimpse into the phage/antibiotic effect in a zebrafish CF model in the context of infection. Indeed, we provide evidence of the improved activity of Muddy when combined with RFB in this animal model (Fig. 6), thus replicating the outcomes observed *in vitro* (Fig. 2) while also reiterating clinical observations associated with phage and antibiotic combination therapies. Whereas Muddy alone was shown to reduce the number of cords and abscesses (Fig. 3D,E and Fig. 5D,E), this effect was further exacerbated when adding RFB to Muddy (Fig. 6D,E). Because mycobacteriophages have limited access to the intracellular compartment of macrophages (Broxmeyer et al., 2002), they are thought to mainly target extracellular bacilli, which, in the case of rough *M. abscessus*, can grow in the form of large serpentine cords (Bernut et al., 2014a). As such, this is likely to explain the decrease in the proportion of embryos with cords and the subsequent proportion of embryos with abscesses. However, it is still not known whether phages have the capacity to lyse the bacilli present on the periphery of the cords, ultimately reducing the size and eventually eradicating cords, or whether they prevent the initiation of cord formation by targeting individual bacilli. Importantly, the proportion of embryos with cords in *cfr* morphants treated with Muddy remained constant at 2, 4 and 6 dpi, suggesting that Muddy does not degrade or modify the bacterial cord structure, but rather prevents the formation of new cords (Fig. 5D).

We previously reported that exposure of *M. abscessus*-infected THP-1 macrophages to RFB was associated with reduced intra- and extracellular cording (Johansen et al., 2020b). Therefore, the net effect of the Muddy plus RFB therapy is likely to result in a

pronounced decrease in both intra- and extracellular cording in zebrafish. Moreover, this significant reduction in cording is particularly interesting, as it may prevent the subsequent formation of abscesses (Bernut et al., 2014a), considered a marker of the severity of the disease. Consistent with this hypothesis, a marked decrease in abscess formation was observed in Muddy-, RFB- and Muddy plus RFB-treated zebrafish embryos (Fig. 6E). Validation of Muddy plus RFB co-treatment against GD01 infection in CFTR-depleted embryos was not only reflected by a strong decrease in the pathophysiological symptoms (abscesses and cords; Fig. 6D,E) but also by a strong reduction in larval mortality (Fig. 6B). Together, the positive outcome of phage plus antibiotic treatment in the infected CF zebrafish reflects those observations identified following treatment of the GD01-infected CF patient, emphasising the usefulness of the zebrafish model as an effective and predictive pre-clinical model. This is particularly justified in the context of an increasing demand for assessing the use of bacteriophages in CF and non-CF patients infected with multidrug-resistant bacteria, including *M. abscessus* (Aslam et al., 2020).

Numerous animal models have recently been developed for the evaluation of phage therapy for infections caused by the ESKAPE group of pathogens (consisting of notable drug-resistant pathogens, such as *Enterococcus faecium*, *S. aureus*, *Klebsiella pneumoniae*, *Acinetobacter baumannii*, *P. aeruginosa* and *Enterobacter* spp.) (Cieřlik et al., 2021). These include *Galleria mellonella*, *Drosophila melanogaster* and various mouse models of sepsis/peritonitis/pneumonia/urinary tract infection or eye infection. In addition, *cfr* zebrafish morphants were used to demonstrate the applicability of phage therapy against *P. aeruginosa* infections (Cafora et al., 2019). However, in this study, phages were injected once in the yolk sac, which does not correspond to a route of administration in humans. In our study, Muddy was administered intravenously several times on a daily basis, similarly to the treatment conditions encountered in the case in the CF patient (Dedrick et al., 2019). It is important to emphasise that, in our study, phages were administered daily to recapitulate clinical implementation; however, we were only able to do this up to 5 days post-infection due to increasing epithelial thickening throughout embryonic development. It is tempting to speculate that we may see further reductions in bacterial burden, cording and abscess formation associated with increased embryo survival if we were able to administer phages for a longer period of time; however, this remains to be further explored.

Noteworthy, despite their unique features for high-throughput therapeutic evaluation, zebrafish embryos display disadvantages over mammals predominantly stemming from stark anatomical differences (gills instead of lungs, haematopoiesis occurring in the anterior kidney instead of the bone marrow, and lack of discernible lymph nodes). In addition, the lack of adaptive immunity early in embryonic development may also influence the outcome of the phage/antibiotic treatment in our study. As such, these factors should be taken into consideration when interpreting the findings from the current study and for determining the suitability of different animal models to examine the efficacy of phage therapy. Although devoid of lungs, which are the main target organs for *M. abscessus* pulmonary disease, zebrafish has recently emerged as a powerful model system to better understand CF as well as the vulnerability of CF patients to *M. abscessus* infection (Bernut et al., 2019), and for assessing the *in vivo* efficacy of multiple drugs against *M. abscessus* (Bernut et al., 2014b; Dubée et al., 2015; Dupont et al., 2016, 2017; Johansen et al., 2020b; Raynaud et al., 2020). From a fundamental

perspective, use of this model allowed us here to assess the contribution of innate immunity in phage therapy. Our results indicate that functional innate immunity is required for efficient activity of Muddy in zebrafish. Using macrophage-depleted embryos, we found that macrophages are critical for successful phage-mediated bacterial clearance. At this stage, we do not know whether the failure of phage therapy was due to the lack of macrophage effector functions such as phagocytosis or the absence of macrophage-dependent activation of other immune effector components participating in GD01 clearance. These findings are in agreement with a previous investigation devoted to studying the effects of host immunity on the efficacy of phage therapy for acute pneumonia caused by multidrug-resistant *P. aeruginosa* using various immune-compromised mouse models, which revealed that neutrophils are required for phages to clear infection (Roach et al., 2017). It is important to recognise that macrophage ablation is known to result in rapid embryo death and significantly enhances susceptibility to mycobacterial infection due to the absence of a major immunological defence (Bernut et al., 2014a). Critically, macrophage ablation led to ineffective phage therapy, suggesting that macrophages may be required to facilitate mycobacterial clearance in the presence of mycobacteriophages. Alternatively, it is also plausible that the phage dose administered to lipoclonate-treated embryos could be below the threshold to observe any improvement in reducing pathophysiological signs of *M. abscessus* infection (Fig. 4). Comparatively, CFTR depletion in zebrafish embryos led to remarkably improved phage responsiveness, recapitulated in improved embryo survival, reduced bacterial burdens and reduced pathophysiological signs such as cords and abscesses (Fig. 5). This is likely due to defective host defences such as reactive oxygen species production, which is known to increase susceptibility to NTM species such as *M. abscessus* and *M. fortuitum* (Bernut et al., 2019; Johansen and Kremer, 2020a), as opposed to being entirely devoid of an immune cell subset, which is essential for infection control. As such, these findings are unsurprising and provide new insight into the requirements for host immunity within the context of phage therapy. Overall, our results suggest that, in animals, phage therapy success not only requires bacterial permissiveness to phage killing but relies also on complex immunophage interactions. This implies the need to explore the patient immunological status as a critical requirement to consider before applying phage therapy, an observation recently emphasised in a patient receiving phage therapy, who rapidly developed a robust humoral response against the therapeutic phages and whereby the phage-neutralising activity correlated with increasing *M. abscessus* bacterial loads (Dedrick et al., 2021). This strongly suggests that the host immune system can represent an important obstacle to phage therapy. Thus, the future of phage therapy will rely on applying optimal treatments adapted to patients and integrating the immune status of each patient into the treatment strategy.

In summary, our easy-to-use *M. abscessus* infection model paves the way for studying the outcomes from the triple partner interactions between the phage, the target bacterial pathogen and host innate immunity. It also supports the development of phage therapies and provides the first framework towards the development of a pre-clinical platform to assess the most successful phage/antibiotic combinations and predictions prior to testing in *M. abscessus* patients.

## MATERIALS AND METHODS

### Mycobacterial strains and culture conditions

*M. abscessus* CIP104536<sup>T</sup> (S and R variants), *M. massiliense* CIP108297<sup>T</sup> (S and R variants) and the clinical strains *M. massiliense* GD01 (rough) and

*M. abscessus* T56 (rough) were routinely grown and maintained at 37°C in Middlebrook 7H9 broth (BD Difco) supplemented with 10% oleic acid, albumin, dextrose, catalase (OADC; BD Difco) and 0.025% Tyloxapol (Sigma-Aldrich) (7H9<sup>OADC/T</sup>), or on Middlebrook 7H10 supplemented with 10% OADC enrichment (7H10<sup>OADC</sup>). Fluorescent GD01 was generated using the pTEC27 expressing tdTomato (Takaki et al., 2013). Red fluorescent colonies were selected on 7H10<sup>OADC/T</sup> supplemented with 1000 µg/ml Hygromycin (Euromedex) and maintained in 7H9<sup>OADC/T</sup> supplemented with 500 µg/ml Hygromycin. Fluorescent *M. abscessus* CIP104536<sup>T</sup> and *M. massiliense* CIP108297<sup>T</sup> strains have previously been described (Bernut et al., 2014a). *M. smegmatis* mc<sup>2</sup>155 was grown at 37°C in Middlebrook 7H9 broth as previously described (Jacobs-Sera et al., 2012).

### Drug susceptibility testing

The MICs were determined according to the CLSI guidelines (Woods et al., 2011). The broth micro-dilution method was used with cation-adjusted Mueller-Hinton broth (CaMHB) with an inoculum of 5×10<sup>6</sup> CFU/ml in exponential growth phase. Each drug dilution was added to the bacterial suspension and incubated for 3–5 days at 30°C. MICs were recorded by visual inspection (Johansen et al., 2020b). Assays were completed in triplicate in three independent experiments.

### Preparation of phage

Phages were grown on *M. smegmatis* mc<sup>2</sup>155 using solid media and recovered by diffusion into phage buffer (68.5 mM NaCl, 10 mM Tris-HCl pH 7.5, 10 mM MgSO<sub>4</sub>, 1 mM CaCl<sub>2</sub>). Phage lysates were filtered through a 0.22 µm filter and used. High-titre cesium chloride-banded phages were prepared and dialysed as previously reported (Dedrick et al., 2019).

### In vitro phage-killing assay

Bacteria grown in 7H9 supplemented with 10% OADC and 2 mM CaCl<sub>2</sub> (7H9<sup>OADC/CaCl<sub>2</sub></sup>) were harvested in the exponential growth phase and pelleted by centrifugation at 3000 g for 10 min. To create single-cell suspensions, bacteria were passed through a 26G needle 20 times and sonicated twice for 10 s to separate large aggregates. Bacteria were made to a concentration of 5×10<sup>6</sup> CFU/ml, and 100 µl bacterial suspension was placed into each well. Mycobacteriophage stock dilutions were added to each corresponding well at the desired MOI (phage:bacteria), mixed well by pipetting and then placed at 37°C for up to 5 days. At the desired time point, bacteria from each corresponding well were 10-fold serially diluted in PBS containing 0.05% Tween 80 to lyse residual extracellular phage, and then plated onto LB agar and placed at 37°C for up to 5 days or until visible colonies emerged.

### Zebrafish maintenance

Zebrafish use was performed in agreement with European Union guidelines for the handling of laboratory animals and was approved by the Direction Sanitaire et Vétérinaire de l'Hérault and Comité d'Ethique pour l'Expérimentation Animale under reference 2020022815234677. All experiments in the current study were performed using the *golden* mutant and macrophage reporter *Tg(mpeg1:mCherry)* lines as previously described (Bernut et al., 2014a, 2015). Zebrafish embryos were obtained and maintained as previously described (Bernut et al., 2015).

### Morpholino injection and *cftr* knockdown

Morpholinos were designed and purchased from GeneTools. A splice-blocking morpholino specifically targeting zebrafish gene *cftr* (ZEBRAFISHIN, ZDB-GENE-050517-20) (5'-GACACATTTTGGCACTCACACCAA-3') was injected into zebrafish embryos at the one- to four-cell stage (1 mM, 2 nl). Furthermore, details of the morpholino efficacy and specificity and *cftr* knockdown were previously validated as described (Bernut et al., 2019).

### Zebrafish microinjection and infection

At 24 hpf, embryos were dechorionated using Pronase (10 mg/ml; Sigma-Aldrich) for up to 5 min at room temperature, followed by extensive washing



in zebrafish water. Following dechlorination, macrophage depletion was achieved by microinjection with either liposomal clodronate or PBS-filled liposomes (Liposoma) (2 nl) via caudal vein injection, as previously described (Bernut et al., 2014a, 2015). At 30 hpf, embryos were anaesthetised in 0.02% tricaine solution and microinjected with fluorescent mycobacteria via caudal vein injection (3 nl containing  $\approx 100$  bacteria/nl). Bacterial inoculum was checked *a posteriori* by injection of 3 nl into sterile PBS and plating onto 7H10<sup>OADC</sup>. Following infection, embryos were transferred to 24-well plates (two embryos/well) and incubated at 28.5°C for the duration of the experiment. Embryo age is expressed as dpi.

### Phage treatment in GD01-infected zebrafish

At 24 h post-infection (hpi), embryos were anaesthetised in 0.02% tricaine solution and microinjected with 10–15 nl mycobacteriophage solutions ( $10^9$  PFU/ml) containing Muddy, Gabriela or a phage cocktail at a final concentration of MOI 50:1 (phage:bacteria) of original bacterial infection inoculum. Control embryos were micro-injected with an identical dilution of phage buffer and PBS, as was performed for the phage-treated embryos. Embryos were microinjected daily between 1 and 5 dpi, with each embryo receiving a total of five phage or PBS injections. Embryos receiving RFB treatment were treated as previously described (Johansen et al., 2020b). Briefly, RFB [stock concentration 10 mg/ml in dimethyl sulfoxide (DMSO)] was diluted to 50  $\mu$ g/ml in zebrafish water, and embryos were immersed in drug-containing water. RFB was replenished daily between 1 and 5 dpi, with each embryo receiving a total of 5 days of RFB treatment. Control embryos were treated with an identical dilution of DMSO and zebrafish water as was performed for the RFB-treated embryos.

### Zebrafish monitoring and live imaging

Embryo survival was monitored daily based on the presence or absence of a heartbeat. Survival curves were determined by counting dead larvae for up to 12 days, or until uninfected embryos begin to die. At designated key time points post-infection, embryos were anaesthetised in 0.02% tricaine solution and mounted on 3% (w/v) methylcellulose solution for live imaging. Images were taken using a Zeiss Axio Zoom.V16 coupled with an AxioCam 503 monochrome camera (Zeiss). FPC measurements were determined using the 'Analyze particles' function in ImageJ. Granulomas were identified based on the co-localisation of fluorescent macrophages and fluorescent GD01. All experiments were completed at least two times independently.

### Statistical analysis

Kill kinetics in the absence or presence of antibiotics were analysed using an unpaired Student's *t*-test. Survival curve analysis was completed using the log-rank (Mantel–Cox) statistical test. Abscess and cord analyses were completed using unpaired Student's *t*-test. Bacterial burden (FPC) analyses were performed using a Kruskal–Wallis one-way ANOVA. All statistical tests were completed using GraphPad Prism (Version 9.0.1).

### Acknowledgements

We thank Deborah Sera-Jacobs for help with prepared phage lysates and Eric Rubin for the gift of the T56 strain. We are grateful to the Montpellier Cell Biology Research Center zebrafish facility, P. Richard and M. Plays for zebrafish husbandry.

### Competing interests

G.F.H. is a compensated consultant for Janssen Inc. The remaining authors have no conflict of interest to declare.

### Author contributions

Conceptualization: M.D.J., G.F.H., L.K.; Methodology: M.D.J., C.H.; Validation: M.D.J., M.A., R.M.D.; Investigation: M.D.J., M.A., F.R.-B.; Resources: R.M.D.; Data curation: M.D.J., M.A., R.M.D., F.R.-B., C.H.; Writing - original draft: M.D.J., L.K.; Writing - review & editing: M.D.J., R.M.D., G.F.H.; Supervision: L.K.; Project administration: L.K.; Funding acquisition: G.F.H., L.K.

### Funding

M.D.J. received a post-doctoral fellowship granted by Laboratoire d'Excellence EpiGenMed, an 'Investissements d'avenir' program (ANR-10-LABX-12-01). This

study was supported by the Association Vaincre la Mucoviscidose (RF20200502678) and the Association Gregory Lemarchal to L.K., and by grants to G.F.H. from the National Institutes of Health (GM131729), the Howard Hughes Medical Institute (GT12053) and the Cystic Fibrosis Foundation (HATFUL19GO).

### References

- Adekambi, T., Sassi, M., van Ingen, J. and Drancourt, M. (2017). Reinstating *Mycobacterium massiliense* and *Mycobacterium boletii* as species of the *Mycobacterium abscessus* complex. *Int. J. Syst. Evol. Microbiol.* **67**, 2726–2730. doi:10.1099/ijsem.0.002011
- Alibaud, L., Rombouts, Y., Trivelli, X., Burguière, A., Cirillo, S. L. G., Cirillo, J. D., Dubremetz, J.-F., Guérardel, Y., Lutfalla, G. and Kremer, L. (2011). A *Mycobacterium marinum* TesA mutant defective for major cell wall-associated lipids is highly attenuated in *Dictyostelium discoideum* and zebrafish embryos. *Mol. Microbiol.* **80**, 919–934. doi:10.1111/j.1365-2958.2011.07618.x
- Aslam, S., Lampley, E., Wooten, D., Karris, M., Benson, C., Strathdee, S. and Schooley, R. T. (2020). Lessons learned from the first 10 consecutive cases of intravenous bacteriophage therapy to treat multidrug-resistant bacterial infections at a single center in the United States. *Open Forum Infect. Dis.* **7**, ofaa389. doi:10.1093/ofid/ofaa389
- Aziz, D. B., Low, J. L., Wu, M.-L., Gengenbacher, M., Teo, J. W. P., Dartois, V. and Dick, T. (2017). Rifabutin is active against *Mycobacterium abscessus* complex. *Antimicrob. Agents Chemother.* **61**, e00155–17. doi:10.1128/AAC.00155-17
- Bernut, A., Herrmann, J.-L., Kissa, K., Dubremetz, J.-F., Gaillard, J.-L., Lutfalla, G. and Kremer, L. (2014a). *Mycobacterium abscessus* cording prevents phagocytosis and promotes abscess formation. *Proc. Natl. Acad. Sci. USA* **111**, E943–E952. doi:10.1073/pnas.1321390111
- Bernut, A., Le Moigne, V., Lesne, T., Lutfalla, G., Herrmann, J.-L. and Kremer, L. (2014b). *In vivo* assessment of drug efficacy against *Mycobacterium abscessus* using the embryonic zebrafish test system. *Antimicrob. Agents Chemother.* **58**, 4054–4063. doi:10.1128/AAC.00142-14
- Bernut, A., Dupont, C., Sahuquet, A., Herrmann, J.-L., Lutfalla, G. and Kremer, L. (2015). Deciphering and imaging pathogenesis and cording of *Mycobacterium abscessus* in zebrafish embryos. *J. Vis. Exp.* 53130. doi:10.3791/53130
- Bernut, A., Viljoen, A., Dupont, C., Sapriel, G., Blaise, M., Bouchier, C., Brosch, R., de Chastellier, C., Herrmann, J.-L. and Kremer, L. (2016a). Insights into the smooth-to-rough transitioning in *Mycobacterium boletii* unravels a functional Tyr residue conserved in all mycobacterial MmpL family members. *Mol. Microbiol.* **99**, 866–883. doi:10.1111/mmi.13283
- Bernut, A., Nguyen-Chi, M., Halloum, I., Herrmann, J.-L., Lutfalla, G. and Kremer, L. (2016b). *Mycobacterium abscessus*-induced granuloma formation is strictly dependent on TNF signaling and neutrophil trafficking. *PLoS Pathog.* **12**, e1005986. doi:10.1371/journal.ppat.1005986
- Bernut, A., Herrmann, J.-L., Ordway, D. and Kremer, L. (2017). The diverse cellular and animal models to decipher the physiopathological traits of *Mycobacterium abscessus* infection. *Front. Cell. Infect. Microbiol.* **7**, 100. doi:10.3389/fcimb.2017.00100
- Bernut, A., Dupont, C., Ogryzko, N. V., Neyret, A., Herrmann, J.-L., Floto, R. A., Renshaw, S. A. and Kremer, L. (2019). CFTR protects against *Mycobacterium abscessus* infection by fine-tuning host oxidative defenses. *Cell Rep.* **26**, 1828–1840.e4. doi:10.1016/j.celrep.2019.01.071
- Broxmeyer, L., Sosnowska, D., Miltner, E., Chacón, O., Wagner, D., McGarvey, J., Barletta, R. G. and Bermudez, L. E. (2002). Killing of *Mycobacterium avium* and *Mycobacterium tuberculosis* by a mycobacteriophage delivered by a nonvirulent *Mycobacterium*: A model for phage therapy of intracellular bacterial pathogens. *J. Infect. Dis.* **186**, 1155–1160. doi:10.1086/343812
- Cafora, M., Deflorian, G., Forti, F., Ferrari, L., Binelli, G., Briani, F., Ghisotti, D. and Pistocchi, A. (2019). Phage therapy against *Pseudomonas aeruginosa* infections in a cystic fibrosis zebrafish model. *Sci. Rep.* **9**, 1527. doi:10.1038/s41598-018-37636-x
- Cambier, C. J., Takaki, K. K., Larson, R. P., Hernandez, R. E., Tobin, D. M., Urdahl, K. B., Cosma, C. L. and Ramakrishnan, L. (2014). Mycobacteria manipulate macrophage recruitment through coordinated use of membrane lipids. *Nature* **505**, 218–222. doi:10.1038/nature12799
- Chan, B. K., Stanley, G., Modak, M., Koff, J. L. and Turner, P. E. (2021). Bacteriophage therapy for infections in CF. *Pediatr. Pulmonol.* **56**, S4–S9. doi:10.1002/ppul.25190
- Cieślak, M., Bagińska, N., Górski, A. and Jończyk-Matysiak, E. (2021). Animal models in the evaluation of the effectiveness of phage therapy for infections caused by Gram-negative bacteria from the ESKAPE group and the reliability of its use in humans. *Microorganisms* **9**, 206. doi:10.3390/microorganisms9020206
- Clay, H., Davis, J. M., Beery, D., Huttenlocher, A., Lyons, S. E. and Ramakrishnan, L. (2007). Dichotomous role of the macrophage in early *Mycobacterium marinum* infection of the zebrafish. *Cell Host Microbe* **2**, 29–39. doi:10.1016/j.chom.2007.06.004
- Cowman, S., van Ingen, J., Griffith, D. E. and Loebinger, M. R. (2019). Non-tuberculous mycobacterial pulmonary disease. *Eur. Respir. J.* **54**, 1900250. doi:10.1183/13993003.00250-2019

- Davis, J. M., Clay, H., Lewis, J. L., Ghori, N., Herbomel, P. and Ramakrishnan, L. (2002). Real-time visualization of *Mycobacterium*-macrophage interactions leading to initiation of granuloma formation in zebrafish embryos. *Immunity* **17**, 693-702. doi:10.1016/S1074-7613(02)00475-2
- Dedrick, R. M., Guerrero-Bustamante, C. A., Garland, R. A., Russell, D. A., Ford, K., Harris, K., Gilmour, K. C., Soothill, J., Jacobs-Sera, D., Schooley, R. T. et al. (2019). Engineered bacteriophages for treatment of a patient with a disseminated drug-resistant *Mycobacterium abscessus*. *Nat. Med.* **25**, 730-733. doi:10.1038/s41591-019-0437-z
- Dedrick, R. M., Freeman, K. G., Nguyen, J. A., Bahadirli-Talbott, A., Smith, B. E., Wu, A. E., Ong, A. S., Lin, C. T., Ruppel, L. C., Parrish, N. M. et al. (2021). Potent antibody-mediated neutralization limits bacteriophage treatment of a pulmonary *Mycobacterium abscessus* infection. *Nat. Med.* **27**, 1357-1361. doi:10.1038/s41591-021-01403-9
- Dickey, J. and Perrot, V. (2019). Adjunct phage treatment enhances the effectiveness of low antibiotic concentration against *Staphylococcus aureus* biofilms in vitro. *PLoS ONE* **14**, e0209390. doi:10.1371/journal.pone.0209390
- Dubée, V., Bernut, A., Cortes, M., Lesne, T., Dorchene, D., Lefebvre, A.-L., Hugonnet, J.-E., Gutmann, L., Mainardi, J.-L., Herrmann, J.-L. et al. (2015).  $\beta$ -Lactamase inhibition by avibactam in *Mycobacterium abscessus*. *J. Antimicrob. Chemother.* **70**, 1051-1058. doi:10.1093/jac/dku510
- Dupont, C., Viljoen, A., Dubar, F., Blaise, M., Bernut, A., Pawlik, A., Bouchier, C., Brosch, R., Guérardel, Y., Lelièvre, J. et al. (2016). A new piperidinol derivative targeting mycolic acid transport in *Mycobacterium abscessus*. *Mol. Microbiol.* **101**, 515-529. doi:10.1111/mmi.13406
- Dupont, C., Viljoen, A., Thomas, S., Roquet-Banères, F., Herrmann, J.-L., Pethe, K. and Kremer, L. (2017). Bedaquiline inhibits the ATP synthase in *Mycobacterium abscessus* and is effective in infected zebrafish. *Antimicrob. Agents Chemother.* **61**, e01225-17. doi:10.1128/AAC.01225-17
- Düzgüneş, N., Sessevmez, M. and Yildirim, M. (2021). Bacteriophage therapy of bacterial infections: the rediscovered frontier. *Pharmaceuticals* **14**, 34. doi:10.3390/ph14010034
- Elborn, J. S. (2016). Cystic fibrosis. *Lancet* **388**, 2519-2531. doi:10.1016/S0140-6736(16)00576-6
- Gomes, M. C. and Mostowy, S. (2020). The case for modeling human infection in zebrafish. *Trends Microbiol.* **28**, 10-18. doi:10.1016/j.tim.2019.08.005
- Griffith, D. E., Aksamit, T., Brown-Elliott, B. A., Catanzaro, A., Daley, C., Gordin, F., Holland, S. M., Horsburgh, R., Huitt, G., Iademarco, M. F. et al. (2007). An official ATS/IDSA statement: diagnosis, treatment, and prevention of nontuberculous mycobacterial diseases. *Am. J. Respir. Crit. Care Med.* **175**, 367-416. doi:10.1164/rccm.200604-571ST
- Gutiérrez, A. V., Richard, M., Roquet-Banères, F., Viljoen, A. and Kremer, L. (2019). The TetR family transcription factor MAB\_2299c regulates the expression of two distinct MmpS-MmpL efflux pumps involved in cross-resistance to clofazimine and bedaquiline in *Mycobacterium abscessus*. *Antimicrob. Agents Chemother.* **63**, e01000-19. doi:10.1128/AAC.01000-19
- Jacobs-Sera, D., Marinelli, L. J., Bowman, C., Brossard, G. W., Guerrero Bustamante, C., Boyle, M. M., Petrova, Z. O., Dedrick, R. M., Pope, W. H., Science Education Alliance Phage Hunters Advancing Genomics and Evolutionary Science (SEA-PHAGES) program. et al. (2012). On the nature of mycobacteriophage diversity and host preference. *Virology* **434**, 187-201. doi:10.1016/j.virol.2012.09.026
- Johansen, M. D. and Kremer, L. (2020a). CFTR depletion confers hypersusceptibility to *Mycobacterium fortuitum* in a zebrafish model. *Front. Cell. Infect. Microbiol.* **10**, 357. doi:10.3389/fcimb.2020.00357
- Johansen, M. D. and Kremer, L. (2020b). Large extracellular cord formation in a zebrafish model of *Mycobacterium kansasii* infection. *J. Infect. Dis.* **222**, 1046-1050. doi:10.1093/infdis/jiaa187
- Johansen, M. D., Herrmann, J.-L. and Kremer, L. (2020a). Non-tuberculous mycobacteria and the rise of *Mycobacterium abscessus*. *Nat. Rev. Microbiol.* **18**, 392-407. doi:10.1038/s41579-020-0331-1
- Johansen, M. D., Daher, W., Roquet-Banères, F., Raynaud, C., Alcaraz, M., Maurer, F. P. and Kremer, L. (2020b). Rifabutin is bactericidal against intracellular and extracellular forms of *Mycobacterium abscessus*. *Antimicrob. Agents Chemother.* **64**, e00363-20. doi:10.1128/AAC.00363-20
- Jordan, T. C., Burnett, S. H., Carson, S., Caruso, S. M., Clase, K., DeJong, R. J., Dennehy, J. J., Denver, D. R., Dunbar, D., Elgin, S. C. R. et al. (2014). A broadly implementable research course in phage discovery and genomics for first-year undergraduate students. *mBio* **5**, e01051-13. doi:10.1128/mBio.01051-13
- Le Moigne, V. L., Raynaud, C., Moreau, F., Dupont, C., Nigou, J., Neyrolles, O., Kremer, L. and Herrmann, J.-L. (2020). Efficacy of bedaquiline, alone or in combination with imipenem, against *Mycobacterium abscessus* in C3HeB/FeJ Mice. *Antimicrob. Agents Chemother.* **64**, e00114-20. doi:10.1128/AAC.00114-20
- Luong, T., Salabarria, A.-C. and Roach, D. R. (2020). Phage therapy in the resistance era: where do we stand and where are we going? *Clin. Ther.* **42**, 1659-1680. doi:10.1016/j.clinthera.2020.07.014
- Martiniano, S. L., Nick, J. A. and Daley, C. L. (2016). Nontuberculous mycobacterial infections in cystic fibrosis. *Clin. Chest Med.* **37**, 83-96. doi:10.1016/j.ccm.2015.11.001
- Meir, M., Grosfeld, T. and Barkan, D. (2018). Establishment and validation of *Galleria mellonella* as a novel model organism to study *Mycobacterium abscessus* infection, pathogenesis, and treatment. *Antimicrob. Agents Chemother.* **62**, e02539-17. doi:10.1128/AAC.02539-17
- Nash, K. A., Brown-Elliott, B. A. and Wallace, R. J. (2009). A novel gene, *erm(41)*, confers inducible macrolide resistance to clinical isolates of *Mycobacterium abscessus* but is absent from *Mycobacterium chelonae*. *Antimicrob. Agents Chemother.* **53**, 1367-1376. doi:10.1128/AAC.01275-08
- Nessar, R., Cambau, E., Reyat, J. M., Murray, A. and Gicquel, B. (2012). *Mycobacterium abscessus*: a new antibiotic nightmare. *J. Antimicrob. Chemother.* **67**, 810-818. doi:10.1093/jac/dkr578
- Ng, R. N., Tai, A. S., Chang, B. J., Stick, S. M. and Kicic, A. (2021). Overcoming challenges to make bacteriophage therapy standard clinical treatment practice for cystic fibrosis. *Front. Microbiol.* **11**, 593988. doi:10.3389/fmicb.2020.593988
- Obregón-Henao, A., Arnett, K. A., Henao-Tamayo, M., Massoudi, L., Creissen, E., Andries, K., Lenaerts, A. J. and Ordway, D. J. (2015). Susceptibility of *Mycobacterium abscessus* to antimycobacterial drugs in preclinical models. *Antimicrob. Agents Chemother.* **59**, 6904-6912. doi:10.1128/AAC.00459-15
- Oechslein, F., Piccardi, P., Mancini, S., Gabard, J., Moreillon, P., Entenza, J. M., Resch, G. and Que, Y.-A. (2017). Synergistic interaction between phage therapy and antibiotics clears *Pseudomonas aeruginosa* infection in endocarditis and reduces virulence. *J. Infect. Dis.* **215**, 703-712. doi:10.1093/infdis/jiw632
- Ordway, D., Henao-Tamayo, M., Smith, E., Shanley, C., Harton, M., Trout, J., Bai, X., Basaraba, R. J., Orme, I. M. and Chan, E. D. (2008). Animal model of *Mycobacterium abscessus* lung infection. *J. Leukoc. Biol.* **83**, 1502-1511. doi:10.1189/jlb.1007696
- Pagán, A. J. and Ramakrishnan, L. (2018). The formation and function of granulomas. *Annu. Rev. Immunol.* **36**, 639-665. doi:10.1146/annurev-immunol-032712-100022
- Parkins, M. D. and Floto, R. A. (2015). Emerging bacterial pathogens and changing concepts of bacterial pathogenesis in cystic fibrosis. *J. Cyst. Fibros.* **14**, 293-304. doi:10.1016/j.jcf.2015.03.012
- Prajsnar, T. K., Cunliffe, V. T., Foster, S. J. and Renshaw, S. A. (2008). A novel vertebrate model of *Staphylococcus aureus* infection reveals phagocyte-dependent resistance of zebrafish to non-host specialized pathogens. *Cell. Microbiol.* **10**, 2312-2325. doi:10.1111/j.1462-5822.2008.01213.x
- Prajsnar, T. K., Renshaw, S. A., Ogrzyzko, N. V., Foster, S. J., Serron, P. and Mesnage, S. (2013). Zebrafish as a novel vertebrate model to dissect enterococcal pathogenesis. *Infect. Immun.* **81**, 4271-4279. doi:10.1128/IAI.00976-13
- Raynaud, C., Daher, W., Johansen, M. D., Roquet-Banères, F., Blaise, M., Onajole, O. K., Kozikowski, A. P., Herrmann, J.-L., Dziadek, J., Gobis, K. et al. (2020). Active benzimidazole derivatives targeting the MmpL3 transporter in *Mycobacterium abscessus*. *ACS Infect. Dis.* **6**, 324-337. doi:10.1021/acscinfed.9b00389
- Richard, M., Gutiérrez, A. V., Viljoen, A., Rodriguez-Rincon, D., Roquet-Baneres, F., Blaise, M., Overall, I., Parkhill, J., Floto, R. A. and Kremer, L. (2019). Mutations in the MAB\_2299c TetR regulator confer cross-resistance to clofazimine and bedaquiline in *Mycobacterium abscessus*. *Antimicrob. Agents Chemother.* **63**, e01316-18. doi:10.1128/AAC.01316-18
- Richard, M., Gutiérrez, A. V. and Kremer, L. (2020). Dissecting *erm(41)*-mediated macrolide-inducible resistance in *Mycobacterium abscessus*. *Antimicrob. Agents Chemother.* **64**, e01879-19. doi:10.1128/AAC.01879-19
- Roach, D. R., Leung, C. Y., Henry, M., Morello, E., Singh, D., Di Santo, J. P., Weitz, J. S. and Debarbieux, L. (2017). Synergy between the host immune system and bacteriophage is essential for successful phage therapy against an acute respiratory pathogen. *Cell Host Microbe* **22**, 38-47.e4. doi:10.1016/j.chom.2017.06.018
- Rominski, A., Roditscheff, A., Selchow, P., Böttger, E. C. and Sander, P. (2017a). Intrinsic rifamycin resistance of *Mycobacterium abscessus* is mediated by ADP-ribosyltransferase MAB\_0591. *J. Antimicrob. Chemother.* **72**, 376-384. doi:10.1093/jac/dkw466
- Rominski, A., Selchow, P., Becker, K., Brülle, J. K., Dal Molin, M. and Sander, P. (2017b). Elucidation of *Mycobacterium abscessus* aminoglycoside and capreomycin resistance by targeted deletion of three putative resistance genes. *J. Antimicrob. Chemother.* **72**, 2191-2200. doi:10.1093/jac/dkx125
- Rudra, P., Hurst-Hess, K., Lappierre, P. and Ghosh, P. (2018). High levels of intrinsic tetracycline resistance in *Mycobacterium abscessus* are conferred by a tetracycline-modifying monooxygenase. *Antimicrob. Agents Chemother.* **62**, e00119-18. doi:10.1128/AAC.00119-18
- Senhaji-Kacha, A., Esteban, J. and Garcia-Quintanilla, M. (2021). Considerations for phage therapy against *Mycobacterium abscessus*. *Front. Microbiol.* **11**, 609017. doi:10.3389/fmicb.2020.609017
- Takaki, K., Davis, J. M., Winglee, K. and Ramakrishnan, L. (2013). Evaluation of the pathogenesis and treatment of *Mycobacterium marinum* infection in zebrafish. *Nat. Protoc.* **8**, 1114-1124. doi:10.1038/nprot.2013.068
- van der Sar, A. M., Appelmelk, B. J., Vandenbroucke-Grauls, C. M. J. E. and Bitter, W. (2004). A star with stripes: zebrafish as an infection model. *Trends Microbiol.* **12**, 451-457. doi:10.1016/j.tim.2004.08.001

- Vergunst, A. C., Meijer, A. H., Renshaw, S. A. and O'Callaghan, D. (2010). *Burkholderia cenocepacia* creates an intramacrophage replication niche in zebrafish embryos, followed by bacterial dissemination and establishment of systemic infection. *Infect. Immun.* **78**, 1495-1508. doi:10.1128/IAI.00743-09
- Woods, G. L., Brown-Elliott, B. A., Conville, P. S., Desmond, E. P., Hall, G. S., Lin, G., Pfyffer, G. E., Ridderhof, J. C., Siddiqi, S. H., Wallace, R. J. et al. (2011). *Susceptibility Testing of Mycobacteria, Nocardiae, and Other Aerobic Actinomycetes*, 2nd edn. Wayne: Clinical and Laboratory Standards Institute.

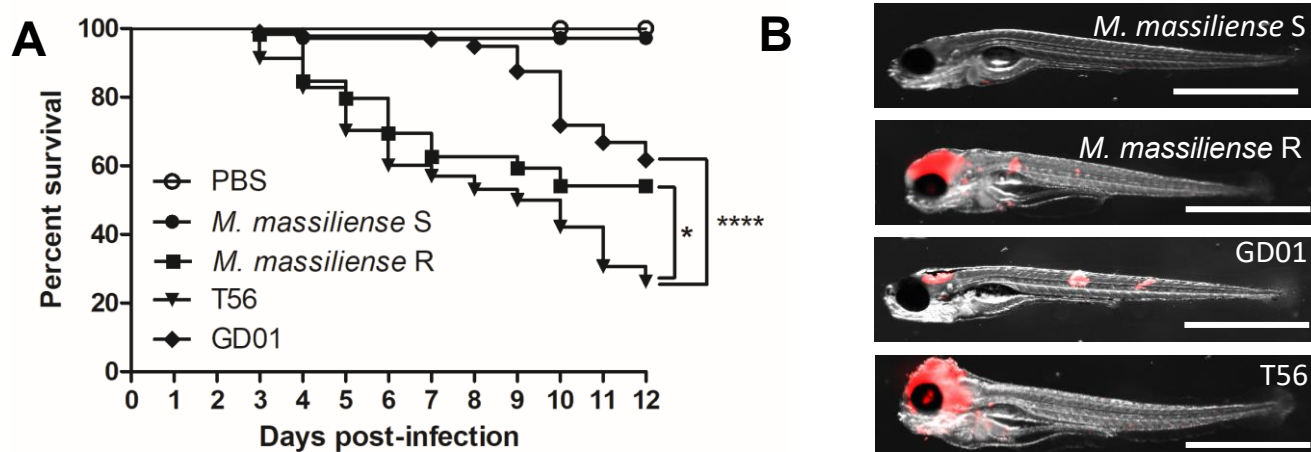


**Fig. S1. Comparative virulence of various *M. massiliense* strains in zebrafish embryos.** (A) Zebrafish embryos at 30 hpf were infected *via* caudal vein injection with approximately 200-250 CFU of each corresponding strain. Embryonic survival was monitored daily over a 12-day period. Represented data is the merged of 4 independent experiments, with approximately 20 embryos per group. \*  $P < 0.05$ , \*\*\*\*  $P < 0.001$ . (B) Representative images taken at 5 dpi, highlighting the heterogeneity in disease phenotypes between the different isolates. Scale bars represent 1 mm. Red areas highlight the bacterial localisation using fluorescence microscopy. Data shown is the merge of three independent experiments ( $n=30/\text{group}$  for each replicate).

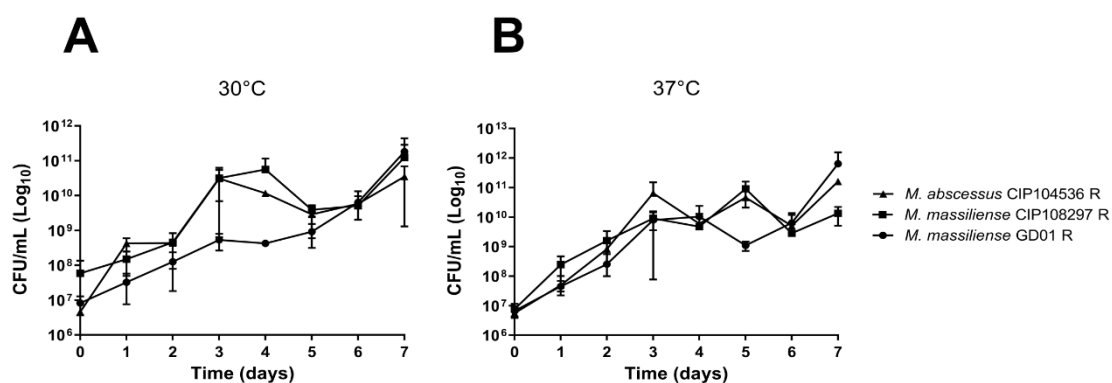
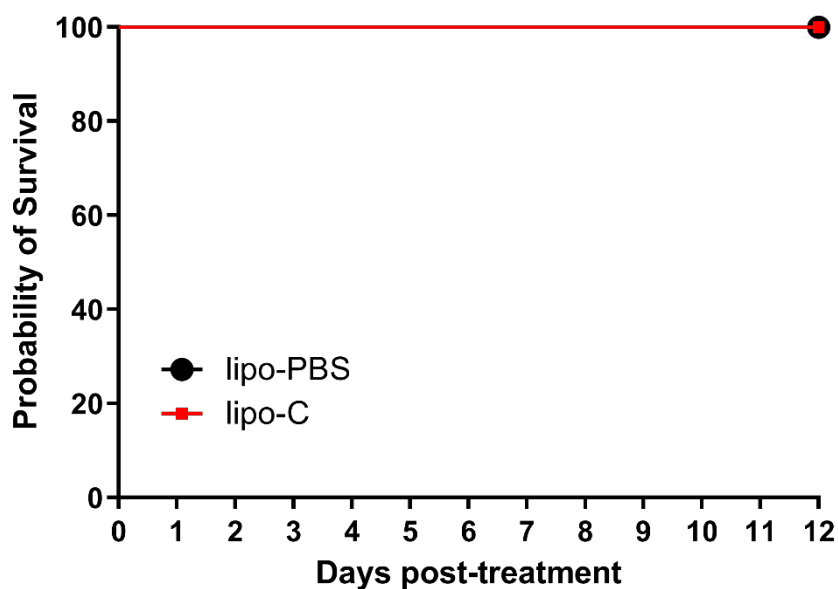


**Fig. S2. Growth curves of rough strains carrying pTEC27 at 30°C and 37°C.** *M. abscessus* CIP104536<sup>T</sup>, *M. massiliense* CIP108297 and GD01 were grown for 7 days in Middlebrook 7H9 supplemented with OADC, 0.025% tyloxapol and 500 µg/ml hygromycin. CFU counts determined by plating serial dilutions onto in Middlebrook 7H10 and enumeration of the colonies after 4 days of incubation at 30°C (**A**) or 37°C (**B**). Data shown is the mean ± standard deviation of two independent experiments run in triplicate.



**A**



**B**

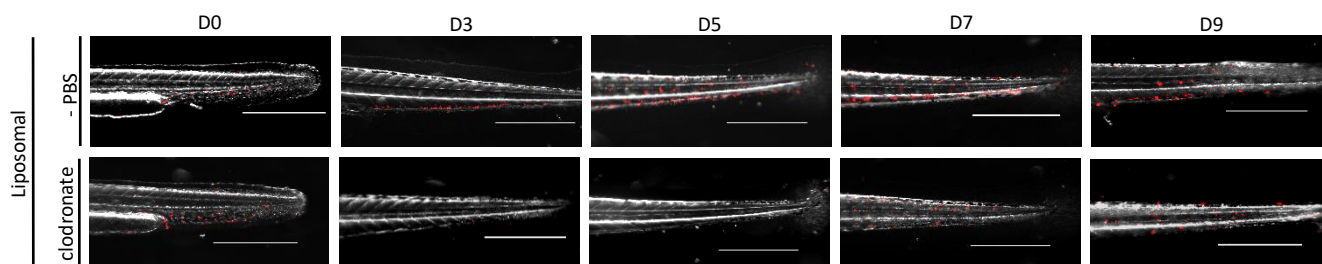


**Fig. S3. Impact of liposomal-clodronate on zebrafish survival and macrophage depletion.** *Tg(mpeg1:mCherry)* embryos harbouring red fluorescent macrophages were injected with 3 nL of either liposomal-PBS (lipo-PBS) or liposomal-clodronate (lipo-C) in the caudal vein at 24 hpf. **(A)** Embryo survival was monitored daily over a 12 day period (n=30/group). **(B)** Representative images of zebrafish tails showing transient macrophage depletion with lipo-clodronate. Macrophages are labelled in red. Scale bars represent 500  $\mu$ m.

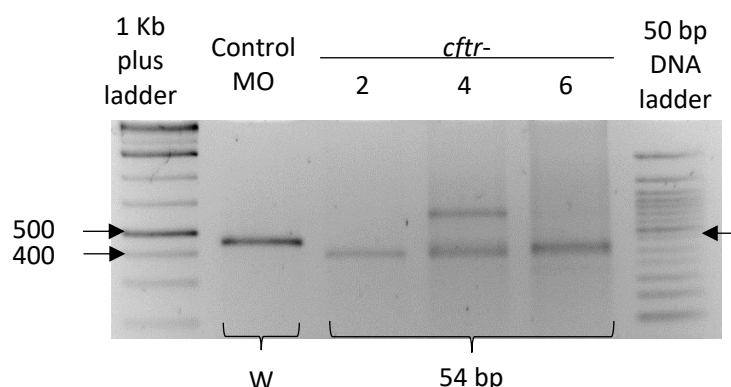


**Fig. S4. Targeted knockdown of *cftr* using splicing morpholino in embryos.** *cftr* specific products were amplified from RNA isolated from whole embryos at 2, 4 and 6 dpf. The *cftr*-MO blocks normal splicing resulting a deletion in exon 3, resulting in a 54 bp deletion in exon 3, and leading to the knockdown of CFTR expression (Bernut et al., 2019; Johansen and Kremer, 2020a).

**Table S1.** Drug susceptibility/resistance profile of *M. massiliense* GD01. Rough *M. abscessus* CIP104536<sup>T</sup> and *M. massiliense* CIP108297<sup>T</sup> were included for comparison. MIC (µg/mL) were determined after 4 days of incubation, following the CLSI guidelines.

Strain (morphotype)	MIC (µg/mL)														
	IPM	CFX	CLR <sup>1</sup>	TGC	CFZ	AMK	CIP	ZEO	KAN	BDQ	LNZ	GEN	RFB	Cpd12	EJMCh-6
<i>M. abscessus</i> (R)	16	64	4	1	1	64	128	32	16	0.03	64	64	12.5	0.06	0.125
<i>M. massiliense</i> (R)	32	64	0.5	2	0.5	32	64	>128	16	0.06	64	64	25	0.06	0.125
GD01 (R)	32	64	>128	2	0.5	>128	64	>128	>128	0.015	64	>128	25-50	0.25	0.125-0.25

IPM, imipenem; CFX, cefoxitin; CLR<sup>1</sup>, clarithromycin; TGC, tigecycline; CFZ, clofazimine; AMK, amikacin; CIP, ciprofloxacin; ZEO, zeocin; KAN, kanamycin; BDQ, bedaquiline; LNZ, linezolid; GEN, gentamycin; RFB, rifabutin; Cpd12, indole-2 carboxamide; EJMCh-6, benzimidazole.

## Nouvelles molécules et cibles thérapeutiques dans le traitement des infections causées par les mycobactéries non-tuberculeuses

La recrudescence des infections mycobactériennes reflète le défi actuel de la lutte contre les micro-organismes pathogènes. Les mycobactéries sont responsables d'infections pulmonaires et extra-pulmonaires sévères, particulièrement chez les patients présentant des comorbidités. De plus, la grande résistance aux antibiotiques de ces espèces bactériennes aboutit à de nombreux échecs et impasses thérapeutiques. Afin d'outrepasser ces derniers, la mise en évidence de nouvelles cibles pharmacologiques et de molécules actives s'avère nécessaire. Les enzymes de la biosynthèse des acides mycoliques, éléments essentiels de la paroi mycobactérienne, représentent des cibles de choix dans le développement de nouveaux antimycobactériens. L'isoniazide, un antituberculeux de première ligne nécessitant une bioactivation par l'enzyme KatG, inhibe l'énoyl-ACP réductase InhA impliquée dans l'élongation des chaînes d'acides mycoliques. Cependant, l'isoniazide et ses analogues partageant le même mode d'action, ne sont pas efficaces vis-à-vis des mycobactéries non-tuberculeuses telles que *Mycobacterium abscessus* ou *Mycobacterium fortuitum*, de par l'incapacité de leur protéine KatG à les activer. Dans ce contexte, l'objectif de ma thèse a été de démontrer l'intérêt de cibler la voie de synthèse des acides mycoliques encore inexploitée contre les mycobactéries non-tuberculeuses. Ainsi, par l'inhibition directe de la protéine InhA chez *M. abscessus* et *M. fortuitum*, mes travaux ont permis de mettre en évidence l'activité antibactérienne robuste de la 4-hydroxy-2-pyridone NITD-916, à la fois *in vitro* ainsi que dans différents modèles cellulaires et animaux. L'ensemble de ces résultats s'inscrivent dans une dynamique de repositionnement de molécules où les inhibiteurs directs d'InhA, et plus largement des autres enzymes impliquées dans la synthèse des acides mycoliques, décrits précédemment chez *M. tuberculosis*, peuvent être transposés à d'autres mycobactéries pathogènes réfractaires à l'antibiothérapie classique. Ces travaux ouvrent la voie à de futures études précliniques et cliniques dans le but d'élargir l'arsenal thérapeutique à la disposition du praticien pour contrer les infections mycobactériennes multirésistantes et persistantes.

## New molecules and therapeutic targets in the treatment of infections caused by non-tuberculous mycobacteria

The resurgence of mycobacterial infections reflects the current challenge in the fight against pathogenic microorganisms. Mycobacteria are responsible for severe pulmonary and extra-pulmonary infections, particularly in patients with co-morbidities. Moreover, the high level of antibiotic resistance in these bacterial species leads to numerous therapeutic failures and dead-ends. To bypass them, it is essential to identify new pharmacological targets and active molecules. Enzymes involved in the biosynthesis of mycolic acids, essential components of the mycobacterial wall, represent attractive candidates for the development of new antimycobacterials. Isoniazid, a first-line anti-tuberculosis drug requiring a bioactivation by KatG enzyme, inhibits the enoyl-ACP reductase InhA involved in the elongation of the mycolic chains. However, isoniazid and its analogs sharing the same mode of action, are inoperant against the non-tuberculous mycobacteria, such as *M. abscessus* or *M. fortuitum*, due to the incapacity of their KatG protein to bioactive them. In this context, the purpose of my thesis was to demonstrate the interest of targeting the so far untapped mycolic acid synthesis pathway in non-tuberculous mycobacteria. Thus, through direct inhibition of the InhA protein in *M. abscessus* and *M. fortuitum*, my work demonstrated the robust antibacterial activity of the 4-hydroxy-2-pyridone NITD-916 both *in vitro* and in various cellular and animal models. Overall, these results are part of a repositioning process in which direct inhibitors of InhA and, more broadly of other enzymes involved in mycolic acid biosynthesis, described earlier in *M. tuberculosis*, can be transposed to others pathogenic mycobacteria refractory to standard chemotherapy. This work paves the way for future preclinical and clinical studies to expand the therapeutic arsenal available to the physician for the treatment of multi-resistant and persistent mycobacterial infections.